SOVIET PHYSICS

JETP

A translation of the Journal of Experimental and Theoretical Physics of the USSR.

SOVIET PHYSICS JETP VOL. 37(10), NO. 4, pp. 637-836 APRIL, 1960

INVESTIGATION OF HIGH-ENERGY NUCLEAR-ACTIVE PARTICLES AT SEA LEVEL

V. A. DMITRIEV, G. V. KULIKOV, and G. B. KHRISTIANSEN

Institute of Nuclear Physics, Moscow State University

Submitted to JETP editor January 26, 1959

J. Exptl. Theoret. Phys. (U.S.S.R.) **37**, 893-905 (October, 1959)

We consider large bursts in an ionization chamber under an absorber that is highly efficient to nuclear interactions. It is shown that at sea level most large bursts ($\geq$ 1000 relativistic particles) are due to interactions of nuclear-active particles with energies $E \geq 10^{12}$ ev in the absorber. The spectrum of the nuclear-active particles and their air accompaniment are given. The accompaniment observed can be attributed to fluctuations in the development of the nuclear shower in the atmosphere. Conclusions are drawn concerning the cross section for the interaction between the nuclei of the atmospheric atoms and particles of energies approximately 10^{13} ev. Cases of high-energy nuclear-active particle beams have been observed.

INTRODUCTION

THE absorption coefficient, the energy spectrum, and the shower accompaniment of high energy nucleons are all connected with the elementary characteristics of nuclear collisions, and their investigation is therefore of considerable interest. Several experiments were recently performed on high mountains, in which nuclear-active particles were investigated by means of bursts in ionization chambers under various absorbers. No analogous work was performed at sea level, and the bursts observed at sea level by Carmichael et al.[1] under layers of lead of different thickness were wholly attributed to μ-meson bursts.

In this connection, we investigated large bursts and their air accompaniment with the aid of apparatus that had a high counting efficiency for nuclear-active high-energy particles. The measurements were performed during 1957 with apparatus, presently in operation at the Moscow State University, intended for an exhaustive investigation of extensive atmospheric showers.

METHOD AND DESCRIPTION OF APPARATUS

The nuclear-active (n.a.) high-energy particles were detected by the electron-nuclear (e.n.) showers that develop in dense matter.[2,3] In a dense medium almost all the energy of the n.a. particles is consumed, in the final analysis, in ionization of the medium and only a small fraction is used for rearrangement of the atomic nuclei. Therefore, by measuring the ionization simultaneously under layers of various thickness, we can determine the n.a. particle energy that gives rise to the shower.[4] However, an approximate measurement of the energy of n.a. particles of high energy ($E \geq 10^{12}$ ev) can also be performed by measuring the ionization under a layer of matter of single thickness, by using an absorber made up of two different substances — a thick layer of a low-Z substance and a thin layer of a high-Z one. (Such an absorber was used earlier.[5]) If the thickness of the low-Z amounts to several nuclear ranges, then a considerable fraction of the energy of the n.a. particles will be converted in it into an electron-photon (e.p.) component; this fraction will change little from

case to case. In the low-Z layer the e.p. cascades due to π^0 mesons will be only weakly developed, since such a layer corresponds to a small number of t-units. In the high-Z layer the electron-photon cascades will develop further and will soon reach a maximum. The number of particles in the cascade maximum is proportional to the energy of the electron-photon component incident on the layer. The depth at which the maximum is reached depends only logarithmically on the initial energy of the photons and electrons, and remains practically constant at large energies. All this makes it possible to measure the energy of high-energy nuclear-active particles incident on such an absorber, by using only a single array of ionization chambers.

We used four ionization chambers, with a total effective area of 1 m^2. A total of 720 Geiger-Müller counters* were used to register the charged-particle currents accompanying the nuclear-active particle showers. This permitted us to determine the thickness of the air accompaniment over a wide range and with a much greater accuracy than previously obtained.[1,6,7] Furthermore, in some experiments we located 48 counters beneath the chambers and inserted 10 centimeters of iron between the counters and the chambers. The arrangement and a section through the nuclear-active particle detector is shown in Fig. 1 of reference 10. The absorber of the nuclear-active particle detector consists of several layers: a layer of lead† 5 cm thick, a layer of graphite (specific gravity 1.68 g/cm^3) 70 cm thick, and a layer of lead 2 cm thick. The first two layers make up approximately 1.8 of the range of nuclear interaction in matter (assuming that the ranges of 160 g/cm^2 for lead and 70 g/cm^2 for graphite, obtained at lower energies, also hold for the energies under consideration here). The detector therefore has high efficiency for nuclear interactions.

It was necessary to cover the graphite from above with lead to reduce the penetration of the electron-photon component of extensive atmospheric showers (e.a.s.) capable of producing large bursts under the graphite layer and in the lower lead layer. The presence of a thick layer of lead greatly softened the energy spectrum of the soft component of the e.a.s. before it entered the graphite, and led to an almost complete screening of the chambers from the soft component of the e.a.s. The apparatus was controlled by pulses from the chambers whenever the amplitudes of the latter exceeded a specified value. The rise time of the chamber pulses was 30 μsec, and therefore the delay in operation of the threshold circuit that segregated the pulses by amplitudes, at pulse amplitudes close to threshold, was not less than 30 microseconds. However, the resolving time of the hodoscope setup was 10 — 12 μsec. The hodoscope was therefore controlled by two circuits, one with a threshold one-tenth that of the other. The pulse rise in the cylindrical chamber was close to linear for nonlocal ionization,[11] and therefore the delay in operation of the first circuit was considerably less. The pulse from the first circuit controlled the hodoscope and the amplitude analyzer, but the data were recorded only when the second threshold circuit was triggered. This insured coordinated operation of the chambers and hodoscopes. The threshold value of the pulse from the chamber needed to operate both circuits corresponded to the passage of 800 relativistic particles along the central chord of the chamber. The nuclear-active particles that produced in the absorber a shower of 1000 particles or more were registered with a probability of 100%.

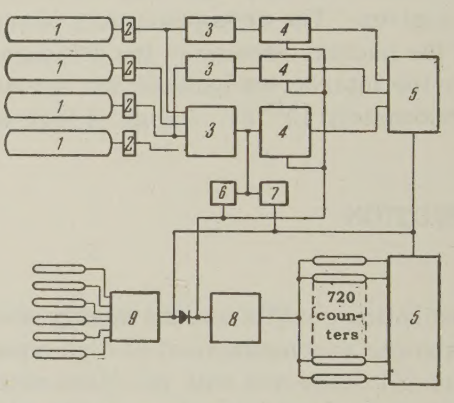

FIG. 1. Block diagram showing connection of chambers and counters. 1 — ionization chambers, 2 — preamplifiers, 3 — amplifiers, 4 — amplitude analyzers, 5 — counting devices, 6 and 7 — threshold circuits, 8 — hodoscope GK-7, 9 — six-fold coincidence circuit.

A block diagram of the apparatus is shown in Fig. 1. The entire apparatus was placed in a special room with a roof made of duraluminum and foamed plastic. The total amount of matter over the apparatus was not less than 2.0 g/cm^2.

RESULTS

During the operating time of the setup (~1300 hours) we registered a total of 948 bursts, each corresponding to the passage of 1000 and more relativistic particles along the central chord of the chamber. The mean frequency of the bursts at $n \geq 1000$ was found to be (0.70 ± 0.04)

*For a detailed description of the arrangement and the apparatus see references 8–10.

†In the case of nuclear-active particles accompanied by a shower with $N \geq 10^5$, the data used have been obtained with a detector in which the upper lead layer has been increased to 8 cm.

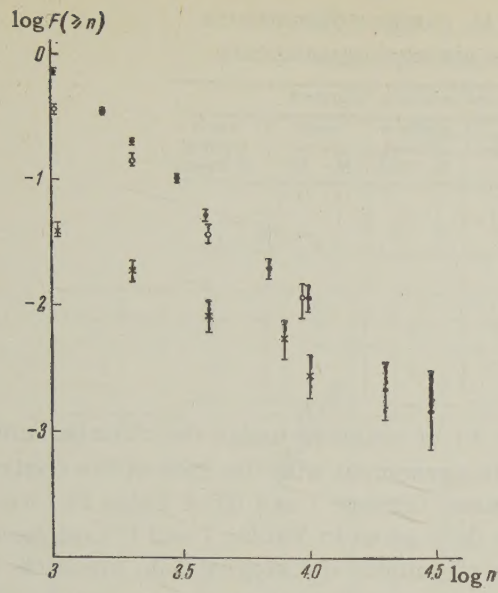

FIG. 2. Spectrum of bursts in chambers at $n \geq 1000$ relativistic particles. Abscissas – logarithm of burst measured in "average" relativistic particles; ordinates – logarithm of number of bursts greater than n/hr-m²; ● – total number of bursts; ○ – burst spectrum at aerial accompaniment of $N \geq 3 \times 10^2$; × – spectrum of bursts in chambers at a shower accompaniment with $N \geq 10^4$.

$hr^{-1}m^{-2}$. The burst spectrum is shown in Fig. 2. The observed bursts could be caused by: 1) the soft component of extensive atmospheric showers, 2) radiation bursts from high-energy muons, 3) strongly ionizing products of nuclear disintegrations of low energy, and finally, 4) nuclear interactions in the absorber between high energy-particles that initiate electron-photon showers.

To verify the role of the bursts due to the soft component of extensive atmospheric showers, we performed preliminary experiments on the determination of the number of bursts with $n \geq 1000$ particles at various thicknesses of the upper layer of lead (2, 4, and 5 cm). With a homogeneous lead absorber, the number of large bursts due the soft component of the e.a.s. begins to diminish at absorber thickness greater than 2 cm.[1] If a layered absorber is used, the burst frequencies at 2 cm of lead differ from those of 4 cm of lead, at a threshold $n \geq 1000$, by a factor of 2.3. At 4 and 5 cm, the burst frequencies become the same (accurate to 10%). This shows that, for the particular filter employed, the role of bursts due to the soft component of e.a.s. is small.

To determine the role of the bursts connected with muons and nuclear disintegrations, we measured bursts with the same apparatus, but without placing a composite absorber over the chamber. The lead shields on the sides and bottoms of the chambers were retained. In this case we registered bursts caused by: 1) e.a.s., 2) nuclear disintegrations, 3) muons traveling at small angles to the horizontal plane. The corresponding experimental data are listed in Table I. Knowledge of the magnitudes of the bursts in the individual chambers, of the number of counters operated under the chambers, and of the number of open counters operated allows us to segregate the bursts due to various processes. (Naturally, such a segregation of bursts is not unique in individual cases, but in each group of Table I the principal part of the bursts is due only to one process.)

From the number of bursts produced by muons traveling at small angles to the horizontal surface we can determine the total number of bursts caused by muons in the composite absorber. Actually, the angular distribution of the muons can be readily obtained by assuming the cosmic radiation to be isotropic, by assuming the pions and the muons to stay

TABLE I. Bursts in chambers without filter above

	Classification of events	Number of events	Number of bursts per hr-m²
I	Bursts in all chambers, accompanied by a nuclear-active shower (minimum number of counters operating in these cases under the chamber is 10).	9	0.07
II	Bursts in one chamber; less than 6 counters operated under the chamber (bursts due to stars in the chamber walls and in the argon)	17	0.13
III	Bursts in three and four chambers. Less than 5 counters operated under the chamber (bursts due to muons traveling at larger angles with the vertical)	10	0.08
IV	Other cases:		
	a) bursts in one chamber; 10 (13) counters operated under the chamber	2	0.02
	b) bursts in three chambers; 9 counters operated under the chamber	1	
	(Aerial accompaniment in these cases amounted to 5–10 counters)		

TABLE II. Distribution of large bursts by number of counters operated under the chambers at various air accompaniments

Number of counters operated under the chambers	Number of aerial-accompaniment counters operated								
	0	1—2	3—4	5—9	10—29	⩾30	medium shower $N \sim 10^4$	large shower $N \sim 10^5$	total number of cases
0	11	3							14
1—2	8	2						1	11
3—4	3	4							7
5—9	3	2							5
10—24	7	8	2	3	7	1	2	3	33
⩾25	1	5	2	3	2	5	4	4	26
Total number of cases	33	24	4	6	9	6	6	8	96

in the direction of the primary particles, and by assuming that the pion-absorption range equals the interaction range.* At sea level, the number of muons with energies E, E+dE, traveling at an angle θ is

$$J^{\mu}(E,\theta) = CA(E)/[1 + (L(E)/Z_0)\cos\theta],$$

where L(E) is the decay range of pions with energy E, $Z_0 = x/\rho$ is a constant relating depth and pressure in the atmosphere, A(E) is the number of pions of energy E along the vertical, and C is a constant.

In calculating the number of bursts we took into account the geometry of our setup and the reduction in effective muon energy with increasing path of particles of the radiation shower in the chambers; the spectrum of the muons was assumed to obey a power law with exponent[13] $\gamma = -2.5$. Assuming that the number of mesons passing through the side walls of the absorber and causing bursts with $n \geq 1000$ is approximately 0.1 $hr^{-1}m^{-2}$, we obtain approximately 0.2 $hr^{-1}m^{-2}$ for the total number of bursts due to muons in the absorber.

Thus, the bulk of the bursts at sea level, under the absorber used, is due to high-energy nuclear-active particles.†

The presence of hodoscopic counters under the chamber during the time of some of the principal measurements also made it possible to segregate, in individual cases, the bursts due to different processes. Data on the accompaniment of large bursts ($n \geq 1000$) with operation of counters under the chambers and air accompaniment of the bursts are listed in Table II.

As can be seen from Table II, the fraction of bursts accompanied by operation of a small number (≤ 5) of counters under the chamber amounts to $\frac{1}{3}$, in agreement with the data of the control experiment (groups I and III of Table I). We note that the data given in Tables I and II exaggerate the role of nuclear disintegrations, since the area of the counters under the chambers equals the area of the chambers, and the distance between chambers is of the order of their linear dimensions. In the case of passage of an electron-photon cascade through the edge of the region occupied by the counters, the number of operated counters decreases and such a case can be classified as a nuclear disintegration.

It is seen also from Table II that among the 40 cases with air accompaniment, equivalent to the operation of three or more counters, only in one case did less than ten counters operate under the chamber. This permits us to state that the role of nuclear disintegration is small in this group. The required presence of air accompaniment allows us to state that the role of bursts due to muons in this group is also small. The bulk of the bursts with such air accompaniment is thus due to high-energy nuclear interactions in the absorber. The spectrum of bursts of this group (Fig. 2) can be represented by a power law with exponent equal to $\gamma = -1.5 \pm 0.2$. The number of bursts with $n \geq 1000$ without air accompaniment, which (as already indicated[9]) is due to a considerable part to nuclear disintegrations, diminishes more steeply (exponentially). From data of other investigations, the spectra of bursts due to muons and strongly-ionizing products of nuclear disintegrations are also characterized by a steep drop.[1,13] The spectrum of bursts due to muons, according to the data of the control experiment, also has a steep drop, corresponding to a power law with exponent $\gamma \simeq -2.6$ (the number of such cases is small). The total burst spectrum (Fig. 2) is characterized by an exponent $\gamma = -1.7 \pm 0.15$. This indicates that the role of nuclear-active particles becomes predominant in the region of large bursts. If we consider the region of bursts with $n \geq 5000$

*Assumptions usually made in calculating the altitude variation of muons (see, for example, reference 12).

†It follows from the data of reference 14 that the number of bursts due to nuclear-active particles of high energy decreases slowly at absorber thicknesses up to 50 cm lead, and more rapidly at 50–80 cm lead. It is therefore erroneous to attribute, as is done in reference 1, a muon origin to large bursts, whose number decreases slowly up to 27 cm lead.

TABLE III. Lateral structure of bursts under differing air accompaniment (bursts in 2 non-adjacent chambers, the smaller comprising a fraction x of the total)

x	Air accompaniment			x	Air accompaniment		
	0—4	5	showers $N \geq 1 \cdot 10^4$		0—4	5	showers $N \geq 1 \cdot 10^4$
~1	3	0	4	≥0.01	5	8	9
≥0.1	7	7	11	<0.01	64	36	6

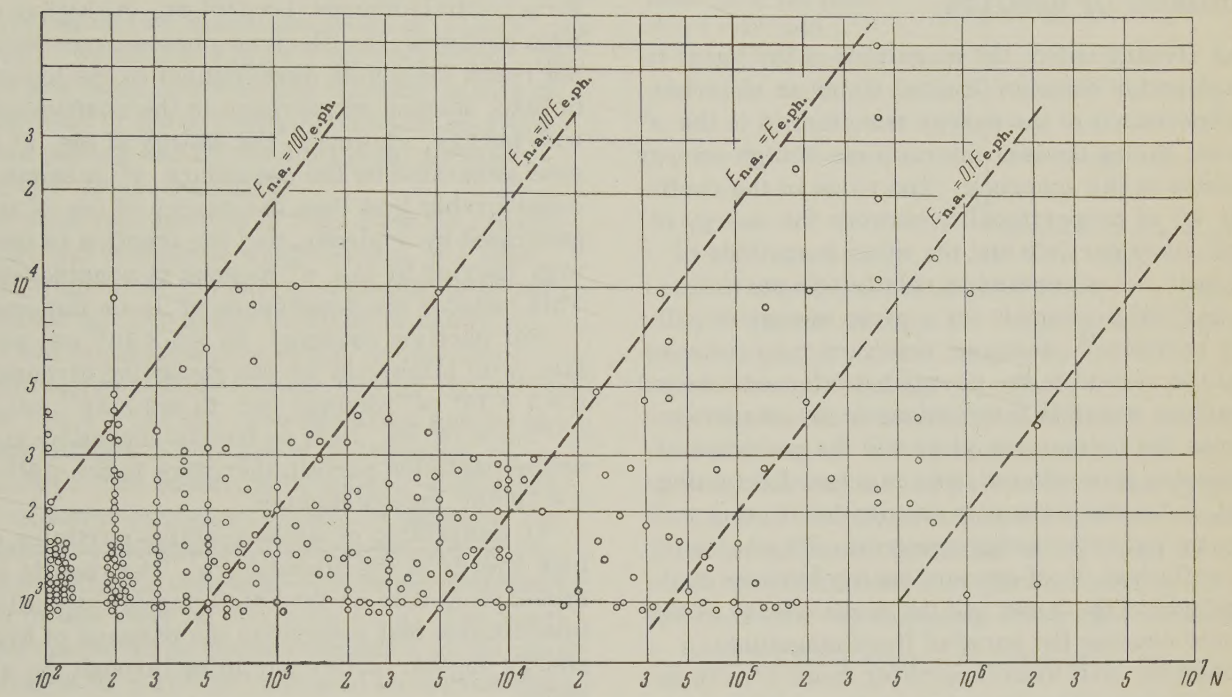

FIG. 3. Magnitude and accompaniment distribution vs. number of particles N in air shower; ordinate – burst measured in "average" relativistic particles, n.

and assume that the spectrum of bursts due to muons and disintegrations is characterized by an exponent $\gamma = -2.5$, the role of such bursts decreases to approximately 10%.

In some cases the burst results from two or more high-energy nuclear-active particles striking the apparatus. Such are cases of large bursts in two non-adjacent chambers and cases of extensive bursts, giving commensurate (differing by a factor of less than 5) bursts in three chambers. The latter cannot be explained by the broad angular distribution of the electrons emitted from the lead.*

Table III gives data pertaining to the structure of the bursts. A fraction of the extensive bursts (one column of the table) is caused by high-energy muons.

The processing of hodoscopic data of a portion of the experiments makes it possible to determine the thickness of the air accompaniment of nuclear-active particles. Figure 3 represents a distribution of the part of the bursts in magnitude and thickness of air accompaniment. Figure 4 shows the

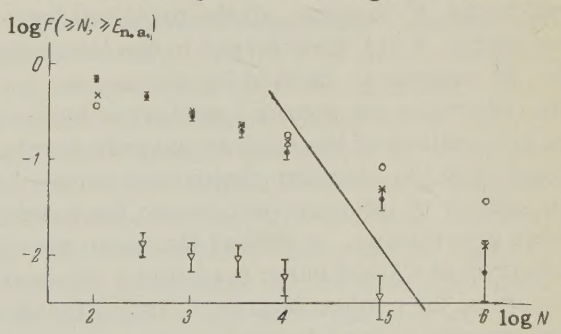

FIG. 4. Nuclear-active particle distribution vs. number of particles N in the accompaniment; ● – bursts with $n \geq 1000$, ▽ – with $n \geq 10{,}000$ relativistic particles. Ordinate – logarithm of the number of nuclear active particles per hr-m², accompanied by a shower with more than N particles. o, × – calculated data, each event results in: o – 7 particles of energy 0.1 E or × – 1 particle of 0.3 E, one particle of 0.2 E, and 1 particle of 0.1 E. Solid curve – shower spectrum.

*We calculated the magnitude of the burst in the chamber assuming isotropic distribution of the particles in the shower under the lead, obviously the limiting case. It was found that even under this assumption the burst in the third chamber was 8% smaller than the summary one, while in the neighboring chamber the burst amounted to 22% of the summary one with the shower axis located at the center of the first chamber.

distribution relative to the number of particles in the shower, accompanying the nuclear-active particles causing a burst with $n \geq 1000$ and with $n \geq 10{,}000$. The spectrum of the bursts of accompaniment by an e.a.s. with $N \geq 1 \times 10^4$ is also shown in Fig. 2. The spectrum can be described by a power law with exponent $\gamma = -1.0 \pm 0.2$.

DISCUSSION OF RESULTS

As already noted, the magnitude of the burst in the ionization chamber located under an absorber is proportional to the energy transferred to the π^0 mesons during nuclear interactions of high-energy particles in the absorber. The value of the coefficient k' of proportionality between the energy of the primary particle and the mean magnitude of the burst n, expressed in relativistic particles, was derived previously for a given energy of primary particle.[10] However, one must take into account the spread in the energy transferred, caused by various possible interactions in the absorber between the primary particle and the particles of successive generations, even in a non-fluctuating event, but in the case of a steeply descending primary-particle energy spectrum. The value of the coefficient k of proportionality between the magnitude of the burst and the mean energy of the particle causing the burst of fixed magnitude in the chamber will therefore differ from k'. To estimate the resultant variation of the coefficient, we have calculated the coefficient k under the following assumptions: a) the incident particle is a nucleon, b) the interaction range of high-energy particles in graphite is independent of the particle energy and equals[15] 70 g/cm^2, c) the fraction of the energy transferred to the mesons in each event is independent of the nucleon energy E_0 and equals $0.4\,E_0$, and $\frac{1}{3}$ of the initial pion energy is transferred to the π^0 mesons, d) the principal faction of the energy (~ 1) transferred in the interactions to the $\pi^{\pm}$ mesons is carried by one meson.

We determine the energy transferred by the first three generations of the nuclear cascade developed in graphite to the electron-photon component, for a given number of interactions between the particles of these generations. In finding the mean energy transferred at a fixed burst magnitude, the energy spectrum of the nuclear-active particles incident on the apparatus was assumed to obey a power law with exponent $\gamma = -1.5$. The development of electron-photon showers in lead was considered on the basis of the data of reference 16. The spectra of the secondary π^0 mesons were not known, and we therefore chose the mean number of particles under lead obtained under the assumption that the shower was due to one γ quantum with energy E_γ, or to the number of γ quanta of equal energy, as expected from the Landau theory (it was assumed that the number of γ quanta equals twice the effective number of mesons[17]). The value thus obtained for the coefficient necessary to convert the number of particles in the burst to the energy of the particle causing the burst, is $k = 8 \times 10^8$ ev for a particle energy 1×10^{12} ev. At higher particle energies, the electron-photon cascades do not reach maximum development in the lower layer of lead, causing an increase in the coefficient k with energy. However, the energy of the π^0 mesons generated by the secondary $\pi^{\pm}$ mesons is considerably less than the energy of the π^0 mesons generated by nucleons, and the fraction of the energy carried by the π^0 mesons is considerable. This reduces the dependence of k on the energy.

For particle energies $E_0 = 4 \times 10^{12}$ ev we obtain, with allowance for the foregoing circumstance, $k = 1 \times 10^9$ ev whereas for $E_0 = 4 \times 10^{13}$ ev we get $k = 1.4 \times 10^9$ ev. Data on bursts caused by nuclear-active particles pertain therefore to the 10^{12}—4×10^{13} ev energy domain.

1) Interaction of nuclear-active particles of high energy in the atmosphere. The results obtained yield data on the character of the nuclear interactions that determine the passage of high-energy nuclear-active particles through the atmosphere.

As already noted, large bursts with $n \geq 5000$ relativistic particles are caused by showers from nuclear-active particles. One can therefore compare our data on the intensities of such bursts with the data pertaining to the level of Pamir (652 g/cm^2),[14] where the relative role of the bursts due to muons is generally small. The apparatus used in reference 14 was similar to ours, the chamber dimensions were almost the same, and the pressure in the chambers was the same. This makes possible a direct comparison of the data obtained with the two setups. It must be taken into account in the comparison that when a composite filter with graphite is used the number of bursts is greater by a factor of approximately 2 than when a solid lead absorber is used.[5] Equipment similar to ours registers the nuclear-active particles within a large angle; assuming therefore that we register the global intensity at both altitudes, we obtain for the connection between the frequency of the bursts, registered at the Moscow level (C_M) and at the Pamir level (C_P) the following expression (see, for example, reference 17):

$$C_M / C_P = 2\,[(\mu x_P + 1)/(\mu x_M + 1)] \exp\{-\mu (x_M - x_P)\},$$

where x_M is the Moscow depth and x_P the Pamir

depth. The absorption range of nuclear-active particles with energies $E \geq 5 \times 10^{12}$ ev, determined from these data, is found to be $\lambda_{abs} = 1/\mu = (124 \pm 14)$ g/cm^2.

The data available[2,18,19] on the intensity of the primary component also make it possible to determine the value of the range for the absorption of nuclear-active particles with energies $E \geq 5 \times 10^{12}$ ev. Averaging the intensities given by Elliott[18] and Cocconi,[19] we obtain $\lambda_{abs} = (120 \pm 6)$ g/cm^2 (the errors are determined by the extreme values of the intensity of the primary component as given in these papers and by the statistical accuracy of our own measurements).

The data represented in Fig. 2 can be recalculated for the domain of larger bursts $n > 5000$, with allowance for the energy dependence of the coefficient k. The graph obtained is shown in Fig. 5 and represents the energy spectrum of nuclear-active particles in the energy range from 5×10^{12} to 5×10^{13} ev. The spectrum can be approximated by a power law with exponent $\gamma = -1.5^{+0.2}_{-0.3}$. The spectrum of nuclear-active particles of lower energies is actually shown in Fig. 2, since at lower energies the coefficient k remains practically constant. The value of the exponent in this case is $\gamma = -1.5 \pm 0.2$. The spectrum of the primary cosmic radiation in the range of energies $E \sim 10^{12}$ ev can also be approximated by a power law with exponent $\gamma = -1.5 \pm 0.1$ (reference 19). Thus, over a broad interval of nuclear-active particle energies, 10^{12}—5×10^{13} ev, the exponent of the energy spectrum at sea level coincides with the exponent of the primary spectrum.

The results obtained indicate that the absorption of the nuclear-active component in the atmosphere is described by a pure exponential curve, i.e., the coefficient of absorption is independent of either the depth of the atmosphere or the particle energy, at least up to $E \simeq 3$ to 5×10^{13} ev, and the exponent of the energy spectrum does not change with depth in the atmosphere.

The fact that λ_{abs} is constant outside of the dependence on the depth in the atmosphere when the exponent γ of the energy spectrum is constant is evidence that the mean characteristics of the elementary act remain unchanged up to energies exceeding, at least by a factor of several times, the energies of the particles registered at sea level (since particles with a given energy at sea level occurred in nuclear collisions of higher-energy particles).

A measurement of the fraction of cases in which the high-energy nuclear-active particle cause a burst not accompanied by a shower in air, as noted

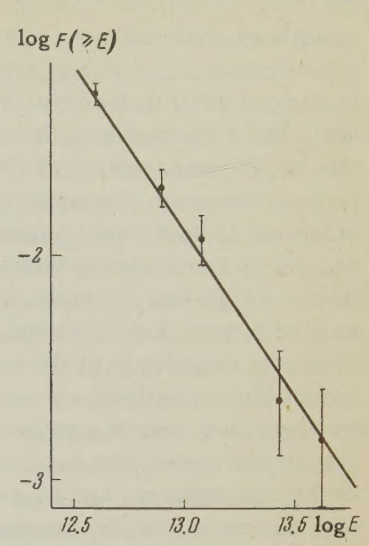

FIG. 5. Energy spectrum of nuclear-active particles at sea level ($E \geq 4 \times 10^{12}$ ev).

in reference 6, makes it possible to determine the effective cross section for inelastic collision between nucleons and the atomic nuclei of air, provided the coefficient of absorption of nuclear-active particles in the atmosphere is known.* Actually the total number M of the registered bursts, caused by a nuclear-active particle with an energy greater than a given value, is connected with the number of bursts M_0, due to particles of the same energy which experience not a single collision in the atmosphere, by the following (average) relation

$$M_0 / M = [(\mu_{abs} x + 1) / (\mu_{int} x + 1)]\, p \exp\{-x(\mu_{int} - \mu_{abs})\},$$

where x is the depth of the point of observation, p the fraction of protons among the primary nuclei, $\lambda_{abs} = 1/\mu_{abs}$ is the range for absorption of nuclear-active particles in the atmosphere, $\lambda_{int} = 1/\mu_{int}$ is the same for the interaction of nuclear-active particles in the atmosphere (assuming that, owing to the great depth of observation, all the nuclei have experienced interactions in the atmosphere). When chambers of large area are used, it is necessary to take into account the possible simultaneous entry of two or several particles of lesser energies, contained in the shower, into the chamber. This increases the total number of bursts M of a given magnitude. An exact determination of the correction for this correlation effect can be obtained from experiments with smaller chambers. An approximate allowance for this factor can be made by introducing a coefficient p_k smaller than unity.

We note that in our setup the area of the counters registering the air accompaniment of the nuclear-active particles was 10.8 m^2. This made it possible to register reliably an accompaniment containing merely several hundred particles. On the other hand, the lead of the absorber in the

*The authors thank G. P. Zatsepin for valuable remarks made in discussing this and other questions.

setup was covered by a layer of low-Z substance (duraluminum, 1 cm) preventing the entrance of scattered particles of electron-photon cascades from the absorber into the counters that registered the air accompaniment of the nuclear-active particles. However, the apparatus did not make it possible, in individual cases, to distinguish bursts caused by muons from bursts caused by interactions of high-energy nuclear-active particles. The role of bursts due to muons diminishes with increasing magnitude of the bursts. Thus, the number of bursts without air accompaniment, which we observed, was due principally to higher-energy particles that experienced no interaction in the atmosphere, and to a small amount to radiation bursts caused by muons. For high-energy particles (large bursts with $n \geq 5000$) this circumstance necessitates a supplementary small term Δ in the foregoing expression

$$M_0 / M = P \exp\{-x(\mu_{int} - \mu_{abs})\} + \Delta,$$
$$\Delta = \delta(\theta) M_\mu / M, \quad P = pp_k;$$

$\delta(\theta)$ is the fraction of muons within a specified angle θ, and M_μ is the number of bursts due to muons. The value of M_μ can be obtained from control-experiment data. The magnitude of $\delta(\theta)$ can be estimated, for mesons of fixed energy, from the formulas given above for the angular distribution of the mesons.

If the number of registered bursts is small, the foregoing formula, which is correct for medium magnitudes, cannot be used. It is necessary to use the expression for the probability of experimentally observing m bursts without air accompaniment from among the observed n bursts, as a function of λ_{int}. Using the Bayes theorem we obtain the distribution for the probability λ_{int} in this case

$$W(\lambda_{int}) = C[P \exp\{-x(\mu_{int} - \mu_{abs})\} + \Delta]^m \times [1 - P \exp\{-x(\mu_{int} - \mu_{abs})\}]^{n-m},$$

where C is a constant.

We registered 26 bursts with $n \geq 5000$, of which only one was not accompanied by a shower. This burst was due to ionization in one chamber only and was accompanied by operation of 9 counters under the chambers. Taking the geometry of the setup into account, we calculated the value of $\delta(\theta)$ for mesons capable of producing bursts with $n \geq 5000$. Figure 6 shows a plot of $W(\lambda_{int})$ for $n \geq 5000$, plotted under the following assumptions: $\lambda_{abs} = 120$ g/cm^2, $p = 0.7$, and $p_k = 0.8$. The dotted curve for $W(\lambda_{int})$ is plotted under the assumption the observed single burst without accompaniment is due to a nuclear-active particle. It follows from the curve that the most probable value is $\lambda_{int} = 90$ g/cm^2, and that $\lambda_{int} = 90 \pm 10$ g/cm^2 if all the bursts are caused by a nuclear-active particle. We note that the value of p_k influences the form of the curve relatively little. The obtained value of λ_{int} agrees with that recently given in other papers for considerably smaller energies (3×10^{10} ev). An analogous value of λ_{int} is also obtained for particles with $E \geq 10^{13}$ ev. We did not register a single particle of this energy without air accompaniment. This makes it possible to state that when $E \geq 10^{13}$ ev, $\lambda_{int} \leq 90$ g/cm^2 with a probability ~ 0.73. Thus, it can be said that the interaction cross section does not decrease at least up to $E \gtrsim 10^{13}$ ev, and that it remains constant up to $E \simeq 5 \times 10^{12}$ ev.

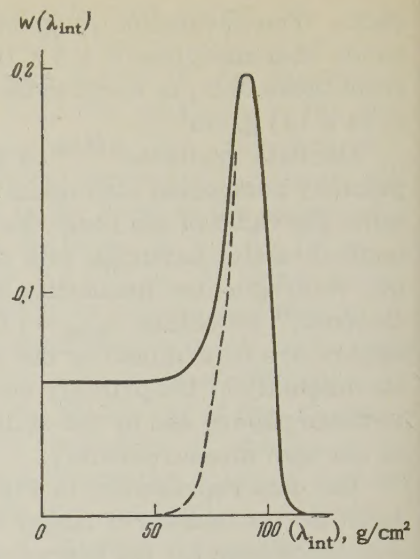

FIG. 6. Probability of various values of λ_{int} for nuclear-active particles of $E \geq 5 \times 10^{12}$ ev (solid curve); dotted – the same under the assumption that the unaccompanied burst is due to a nucleon.

From the observed simultaneous incidence of several particles with $E \gtrsim 10^{12}$ ev on the chamber (see Table III) we can estimate the lateral momentum acquired by a nuclear-active particle in nuclear scattering or generation. It is obvious that for a specified distance between the nuclear-active particles, their effective generation altitude exceeds the nuclear free-path unit. At a range of 500 meters in air, we assume the effective altitude to be 1000 meters. For the observed cases of particles with $E \geq 10^{12}$ ev diverging by a distance ~ 0.5 m, we obtain $p_\perp \gtrsim 5 \times 10^8$ ev/c. We also registered one case where two nuclear-active particles, each with $E \sim 10^{13}$ ev, passed through two non-adjacent chambers. Considering that in this case both particles deviated from the initial direction, we obtain $p_\perp \lesssim 2 \times 10^9$ ev/c.

The accompaniment of nuclear-active particles

shown in Fig. 3 indicates that nuclear-active particles of such energy occur at different frequencies in showers with $N \geq 10^2$ to $N \geq 10^6$ particles.* The accompaniment of nuclear-active particles of a given energy by showers with different number of particles N is determined by the energy spectra of nuclear-active particles in the showers with different N. Vernov et al.[20] calculated the energy spectra of nuclear-active particles from one primary under various very simple assumptions concerning the character of the elementary act. Assuming, like Greisen,[2] that the number of particles in the shower N is proportional to the energy of the primary particle E, and assuming that the spectrum of the number of particles in the shower $\varphi(N)$ is described by a power law with exponent $\gamma = -2.4$ at $10^2 \leq N \leq 10^7$, we obtain curves for the accompaniment of particles with energies greater than a given value $F(\geq E, N)$ for the cases analyzed in reference 20 (see Fig. 4).

Comparison of the experimental data with the theoretical accompaniment curve shows that in the case of particles of given energy, the presence of a broad range of accompaniment intensities ($N \sim 10^2 - 10^6$) is explained by the probabilistic character of the interaction and the finite number of interactions between nuclear-active particles of a nuclear shower and the nuclei of the atmosphere. The relative frequency of differing accompaniments is in sufficiently good agreement with the calculations for different characteristics of the elementary act; at the same time there is no need for making assumptions concerning the presence of two types of interaction, as mentioned in reference 6. To obtain agreement with the experimental data at sea level for different types of acts it is necessary, however, to modify somewhat the interaction cross section. In order to choose a particular model of the act in accordance with the accompaniment curve, it is necessary to have a more rigorous comparison of the air accompaniment (N) and the particle energy (E, E_0), particularly in the range of small N.

Let us note that, as can be seen from Fig. 4, the accompaniment curve of nuclear-active particles with $E \geq 10^{12}$ has the same character as that for $E \geq 10^{13}$ ev.

2) Nuclear-active component in low-density extensive atmospheric showers. The presence of an additional control system enabled us to study simultaneously the extensive atmospheric showers, regardless of whether they contained high-energy nuclear-active particles. Figure 4 shows a line corresponding to the number of particles spectrum of the showers as observed by us. As can be seen from a comparison of the experimental data, nuclear-active particles with $E \geq 10^{12}$ ev are present in showers of low intensity, $N \sim 10^3 - 10^4$, but not in each shower. Since the energy of such nuclear-active particles is of the same order as (or greater than) the energy carried by the electron-photon component of the shower, the role of the nuclear-active component depends substantially on the presence or absence of such particles in an individual shower. This is seen from Fig. 3, which shows the energy and air accompaniment for each individual burst. This circumstance indicates substantial fluctuations in the development of low-intensity showers; the equilibrium between electron-photon and nuclear cascades in showers in which the energy of the nuclear-active component is too large does not exist at the observation level. Such cases can be explained, as indicated by the agreement with the calculation results given above, by a passage of a nuclear shower with weak development through the atmosphere.

From the data on the accompaniment of nuclear-active particles by showers we can also obtain the value of the energy carried by a nuclear-active high-energy particle ($E \geq 10^{12}$ ev and $E \geq 10^{13}$ ev) in a medium shower of different intensity. Actually, in showers with $N < 10^4$ the number of nuclear-active particles of such energies $n(\geq E, N)$ is small, i.e., $n(\geq E, N) < 1$. Then, knowing $F(\geq E, N)$ and $\varphi(N)$, we can find the number of particles with energies greater than a specified value $n(\geq E, N) = F(\geq E, N)/\varphi(N)$ in a medium shower. The form of the energy spectrum of particles in the region $10^{12} - 10^{13}$ ev was obtained by us, and we can therefore determine the energy carried by particles of such energies in the shower. However, the spectrum of low-density showers has not yet been investigated. To estimate the energy we extrapolated our shower spectrum to the region of lower N, using the same spectrum exponent, a fact that can only lead to an overestimate of the number of low-density showers, i.e., to an underestimate of the fraction of high-energy nuclear-active particles. The results on the distribution of energy carried by a high-energy nuclear-active particle are listed below.

Number of particles in the shower:		1×10^3 to 3×10^3	3×10^3 to 1×10^4
Ratio of the energy carried by a nuclear-active particle to the energy of the electron-photon component at the following nuclear-active particle energy:	$E \geq 10^{12}$	6%	7%
	$E \geq 10^{13}$	1%	1.5%

*Strictly speaking, a certain part of the bursts with accompaniment $N \sim 10^2$ can be due to muons.

The energy of the electron-photon component was determined by us as $E_{ep} = 3\beta\bar{N}$, where $\bar{N}$ is the average number of particles in the shower within the considered range of N, and β is the critical energy in air.

To estimate the mean value of the total energy carried by the nuclear-active component of a shower with a specified number of particles it is therefore necessary to take into account the contribution of particles with energies $E \sim 10^{12} - 10^{13}$ ev, which appear in the shower at an average frequency of $\sim 10^{-2}$.

In conclusion, let us estimate the energy carried in a shower by nuclear-active particles that appear at a frequency $\lesssim 1$. For this purpose we extend the spectrum of the nuclear-active particles towards the low-energy region assuming that the integral energy spectrum of such particles has a slope not less than that corresponding* to E^{-1}. For a medium shower with $N \sim 10^3 - 10^4$ particles this gives 40% of the energy carried by the electron-photon component. The value obtained for the energy carried by the nuclear-active component indicates that the latter has a substantial role in the development of showers with $N \sim 10^3 - 10^4$ particles. The estimate given in reference 21 for the energy of the nuclear-active component in the limiting case — equilibrium between the electron-photon and nuclear-active components — allows us to state that for an average shower with $N \sim 10^3 - 10^4$ particles this condition is formally satisfied.

CONCLUSIONS

1. The exponent of the energy spectrum of nuclear-active particles at sea level, in the energy range from 10^{12} to 4×10^{13} ev, remains constant at $\gamma = -1.5 \pm 0.2$ in the $10^{12} - 5 \times 10^{12}$ ev range and $\gamma = -1.5^{+0.3}_{-0.2}$ in the $5 \times 10^{12} - 4 \times 10^{13}$ ev range.

2. The coefficient of absorption of nuclear-active particles with energy $\sim 10^{13}$ ev in the atmosphere corresponds to a range of (120 ± 5.5) g/cm^2.

3. The cross section for the interaction between air nuclei and nuclear-active particles remains constant up to $E = 5 \times 10^{12}$ ev; at any rate, it does not drop until $E \geq 10^{13}$ ev.

4. The presence of a broad range of intensities of air accompaniment for particles with $E \geq 10^{12}$ ev is explained by the different number of interactions between the nuclear-active particles in the atmosphere under unchanged characteristics of the elementary act.

5. Nuclear-active particles of high energy play a substantial role in the development of low-density showers with a total number of particles $N \sim 10^3 - 10^4$. In the development of individual showers of low intensity, one observes large fluctuations in the distribution of energy between the nuclear-active and electron-photon components.

The authors express their gratitude to S. N. Vernov for great help rendered in this work.

*Actually, in showers with $N \geq 10^4$ the energy spectrum of the nuclear-active particles, in the frequency region ~1, is characterized by $\gamma \approx -1.1$. The energy spectra in showers with different N can be expected to be similar when expressed in units of E/E_0.

[1] H. Carmichael and F. Steljis, Phys. Rev. **99**, 1542 (1955). H. Carmichael, Phys. Rev. **107**, 1401 (1957).

[2] K. Greisen, Progress in Cosmic Ray Physics **3**, Amsterdam, 1956.

[3] Veksler, Kurnosova, and Lyubimov, JETP **17**, 1026 (1947). Azimov, Dobrotin, Lyubimov, and Rozhkova, Izv. Akad. Nauk SSSR, Ser. Fiz. **17**, 80 (1953).

[4] Grigorov, Murzin, and Rapoport, JETP **34**, 506 (1958), Soviet Phys. JETP **7**, 348 (1958).

[5] Anishchenko, Zatsepin, Rozental', and Sarycheva, JETP **22**, No. 2, 1952.

[6] Grigorov, Shestoperov, Sobinyakov, and Podgurskaya, JETP **33**, 1099 (1957), Soviet Phys. JETP **6**, 856 (1958).

[7] L. A. Farrow, Phys. Rev. **107**, 1987 (1957).

[8] I. M. Bekkerman, V. A. Dmitriev, et al., Приборы и техника эксперимента (Instrum. and Meas. Engg.) No. 4, 31 (1958).

[9] Dmitriev, Kulikov, and Khristiansen, Paper delivered at Conference on Cosmic Rays, Varenna, 1957.

[10] Abrosimov, Dmitriev, Kulikov, Massal'skiĭ, Solov'ev, and Khristiansen, JETP **36**, 751 (1959), Soviet Phys. JETP **9**, 528 (1959).

[11] V. A. Dmitriev, J. Tech. Phys. (U.S.S.R.) **27**, 205 (1957), Soviet Phys.-Tech. Phys. **2**, 179 (1957).

[12] K. Greisen, Phys. Rev. **73**, 521 (1948).

[13] E. George, Cosmic Ray Physics, vol. 1, 1954.

[14] Zatsepin, Krugovykh, Murzina, and Nikol'skiĭ, JETP **34**, 298 (1958), Soviet Phys. JETP **7**, 207 (1958).

[15] Azimov, Dobrotin, et al., Izv. Akad. Nauk SSSR, Ser. Fiz. **17**, 80 (1953).

[16] I. P. Ivanenko, Dokl. Akad. Nauk SSSR **107**, 819 (1956), Soviet Phys.—Doklady **1**, 231 (1956).

[17] G. T. Zatsepin, Dissertation, Phys. Inst. Acad. Sci., 1953.

[18] L. Elliott, Paper delivered at Conference on Cosmic Rays, Oxford, 1954.

[19] G. Cocconi, Nuovo cimento, VIII, Suppl. No. 2, 1958.

[20] Vernov, Gorchakov, Ivanenko, and Khristiansen, JETP **36**, 1233 (1959), Soviet Phys. JETP **9**, 877 (1959).

[21] Abrosimov, Goryunov, Dmitriev, Solov'eva, Khrenov, and Khristiansen, JETP **34**, 1077 (1958), Soviet Phys. JETP **7**, 746 (1959).

Translated by J. G. Adashko
181

ON THE MEASUREMENT OF THE MOMENTUM OF FAST PARTICLES AND THE INVESTIGATION OF NUCLEAR INTERACTIONS IN THE $10^{10}-10^{12}$ ev ENERGY RANGE

M. I. DAĬON and V. Kh. VOLYNSKIĬ

P. N. Lebedev Physics Institute, Academy of Sciences, U.S.S.R.

Submitted to JETP editor April 10, 1959

J. Exptl. Theoret. Phys. (U.S.S.R.) **37**, 906-909 (October, 1959)

A new method for the direct measurement of the momentum of charged particles in a magnetic field in the $10^{10}-10^{12}$ ev energy range is proposed. The method is based on the simultaneous use of spark counters and nuclear emulsions. The possibility of applying the method to measurements of momentum spectra and to the investigation of nuclear interactions of protons with matter is discussed.

THE method consists of the following procedure: Three spark counters I, II, and III (Fig. 1), triggered by a Geiger-Müller counter system, are placed in the magnet gap. The spark counters make it possible to localize the trajectory of particles in the counter plane with an accuracy of up to ~ 1 mm^2. (At present, counters of 18×80 mm have been constructed for a gap width of 2 mm. The sparks are photographed through transparent electrodes together with a coordinate-grid background.) Nuclear emulsions 1, 2, and 3 ($100-200\,\mu$ thick) are placed under the spark counters.* An approximate localization of the trajectory of the particle is given by the spark counters. (A more accurate determination of the particle-trajectory coordinates is based on the tracks in the emulsion.)

The method, utilizing the tracks in the emulsion, makes it possible to localize the trajectory with a maximum accuracy, and thus to attain a high accuracy in the determination of the curvature of the trajectory and, consequently, of the particle momentum. It should be noted that, in certain cases where the load is small, Geiger counters of a small diameter, Conversi tubes, etc, can be used instead of spark counters. For a study of nuclear interactions, a multiplate cloud chamber, an emulsion stack, or another arrangement for observing the interactions, can be placed under the magnet. The interesting events can then be selected by a suitable triggering method.

*For greater accuracy in the determination of the trajectory and the coordinates (see below), glass plates coated with emulsion on both sides should be used. The direction of the trajectory is determined from the point of intersection of the tracks in the emulsions with the surfaces of the plate.

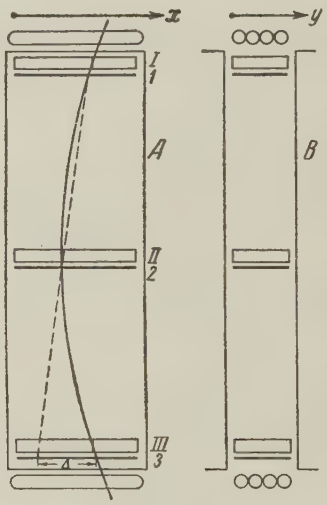

FIG. 1

ACCURACY OF MOMENTUM MEASUREMENTS

Knowing the coordinates of the trajectory x_1, x_2, x_3, we can determine the quantity Δ (Fig. 1), which is related to the particle momentum by the equation

$$p = 300\,HL^2/4\Delta,$$

where p is the particle momentum, L the length of the telescope, H the magnetic field intensity, and

$$\Delta = x_3 + \frac{l_2}{l_1}x_1 - \left(1+\frac{l_2}{l_1}\right)x_2.$$

The error in the momentum is due to the following causes:

1. Errors in the determination of the coordinates x_1, x_2, and x_3, and errors in the determination of l_1 and l_2 (l_1 and l_2 are the distances between the emulsions, and $l_1 + l_2 = L$). We assume that $l_1 = l_2$; we then have $\Delta = x_3 + x_1 - 2x_2$. Let

us denote the standard error in the determination of coordinates x_1, x_2, x_3 by d_0. It can be assumed that $d_0 \approx 2.5 \times 10^{-4}$ cm. The standard error of Δ will then be* $\delta\Delta_{geom} = \sqrt{6}\, d_0 \approx 6 \times 10^{-4}$ cm.

2. The error due to the scattering in the layer of matter inside the gap. The projection of the mean-square scattering angle on the plane A is given by the equation

$$\sqrt{\overline{\theta^2}} = (2 \cdot 10^7 \sqrt{t})/(\sqrt{2}\, p\beta) = (10^7 \sqrt{2t})/(p\beta),$$

where t is the thickness of the scatterer in radiation units. For the large energies that we are dealing with, $\beta \approx 1$. The standard error of the deviation due to the scattering is equal to

$$\delta\Delta_{scat} = (L/2)\sqrt{\overline{\theta^2}} = (L/p)\, 10^7 \sqrt{t/2}.$$

The total error of the deviation is equal to

$$\overline{\Delta^2_{sq}} = 6d_0^2 + 10^{14}(L/p)^2 t/2.$$

Let us consider the value $k = \Delta_M / \sqrt{\overline{\Delta^2_{sq}}}$, where Δ_M is the actual deviation of the particle in the magnetic field

$$k = 300\, HL^2/4p \sqrt{6d_0^2 + 10^{14}(L/p)^2 t/2}.$$

This formula makes it possible to determine the accuracy of the method. Let us put $H = 10^4$ gauss and $t = 1/5$ radiation lengths. The values of momentum for which $k = 1$ and $k = 5$, i.e., those determined with errors of 100 and 20% respectively, are given in Table I.

TABLE I

Telescope length, L, cm	p, ev/c	
	k = 1	k = 5
100	$1.25 \cdot 10^{13}$	$2.5 \cdot 10^{12}$ ($\Delta = 30\ \mu$)
50	$3 \cdot 10^{12}$	$5.7 \cdot 10^{11}$ ($\Delta = 30\ \mu$)
25	$7.5 \cdot 10^{11}$	$8.5 \cdot 10^{10}$ ($\Delta = 55\ \mu$)

Noting that spark counters with a working area 250 × 120 mm can at present be produced, we can calculate the counting rate of protons at an altitude of 3000 m for different solid angles of the telescope. The results are given in Table II (where α is the absolute proton intensity).

From Table II it can be seen that, using small magnets, one can measure the momentum spectrum of protons up to the energy of $\sim 10^{12}$ ev during a comparatively short time. The aperture of the instrument is sufficient for the study of interactions

*We neglect here the errors in l_1 and l_2. Their contribution to the value of Δ depends on the inclination of the trajectory and, for trajectories close to the vertical, is practically negligible.

TABLE II

p, ev/c	α, particles/cm²-sterad-day	Solid angle of the telescope, cm²-sterad		
		25	55	100
		Counting rate, particles/day		
$>10^{10}$	1.3	33	72	132
$>5 \cdot 10^{10}$	0.11	2.7	6.0	10.8
$>10^{11}$	0.04	1	2.2	4
$>5 \cdot 10^{11}$	0.004	0.1	0.22	0.4
$>10^{12}$	0.0013	0.03	0.073	0.13

in the high energy range, since about 50% of the protons will interact in the layer of matter, with a thickness equal to half of the nuclear mean free path, placed under the magnet.

LOADING OF THE EMULSION BY BACKGROUND PARTICLES

A question arises concerning the identification of a given trajectory among trajectories of particles passing through the given area of emulsion (of ~ 1 mm² area) during the total time of exposure.

The identification of an interesting event can be carried out by various methods, as, for instance, in the following way: From the three sparks in counters I, II, and III, we approximately determine the position of the trajectory and calculate the azimuth and the length of the projection of the track in the emulsion on a horizontal plane. These data serve as the basis for the search and identification of the trajectory. For a small intensity of background particles, e.g., in underground experiments, such a method of identification may be sufficient.

In the following, we consider the background problem arising in the detection of protons at an altitude of 3000 m above sea level in the momentum range $\sim 10^{10} - 10^{12}$ ev/c.

Let the total particle flux recorded by the telescope during the exposure time amount to N particles. [We assume a telescope size of $(25^2 \times 12^2) \times (40^2\ \text{cm}^2\text{-sterad})^{-1}$.] If S is the area of one emulsion plate, then the loading is equal to n = N/S. We disregard here the loading due to particles travelling outside the solid angle of the telescope since, owing to the large inclination of their trajectories, they can immediately be excluded from consideration in scanning.

We shall furthermore assume that the error in the determination of the direction of the trajectory in the emulsion in the plane A and in the plane B (Fig. 1) is equal to 0.3° (1/200 rad). (See first footnote.) For a telescope length equal to 40 cm, this gives an inaccuracy of ~ 1 mm in the determination of the corresponding coordinate in the

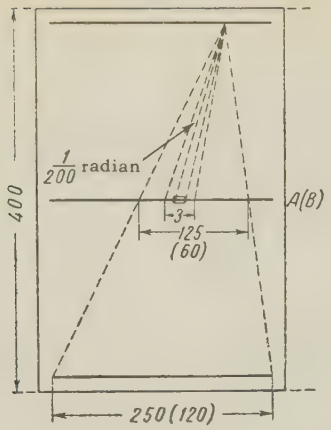

FIG. 2

adjacent row (Fig. 2). If the diameter of the spark is equal to 1 mm, then the probability of a chance coincidence of the direction of the trajectory in the emulsion with a given position of the spark is equal to 3/60 in projection B and to 3/125 in projection A. The total probability of such a chance coincidence is equal to $(3/60) \times (3/125) \approx 1/800$. For three layers of emulsion, this probability is equal to $\sim 3/800$. For a loading n, the probability of a chance coincidence between the direction of the track with the direction given by the sparks is $\sigma = 3n/800$.

Let us evaluate n. From the data on the total intensity of cosmic radiation arriving from the vertical direction and on the intensity of the proton component, we can conclude that ~30,000 particles will traverse the instrument during the time necessary for the detection of one proton with energy $> 10^{11}$ ev. For a proton with energy $> 5 \times 10^{11}$ ev, the number increases to ~300,000 particles. For an emulsion area of 250 × 150 mm, we obtain, respectively, loadings $n_1 = 1$ particle/mm^2 and $n_2 = 10$ particles/mm^2. It should be noted that the actual loadings will be smaller, since the emulsions are placed in a strong magnetic field.

Thus, for the detection of one proton with energy $> 5 \times 10^{11}$ ev, the loading is $n_2 = 10$ particles/mm^2, which gives $\sigma_2 = (3 \times 10)/800 = 3/80$. This means that, in reducing 80 trajectories recorded by the spark telescope, there will be three cases where, in an emulsion region with an area of 1 mm^2, two trajectories may be observed going in the direction of the sparks. It should be noted, however, that the presence of two unresolved trajectories does not represent a danger from the point of view of an error in the momentum determination, since such cases are simply excluded from consideration (3 trajectories out of 80 in this case).

From Table II, it can be seen that the detection frequency of protons with energy $> 5 \times 10^{11}$ ev is equal to ~2 particles in 10 days. It is sufficient to exchange the emulsion every 5 or 10 days to avoid a dangerous loading of the emulsion. For energies $> 10^{12}$ ev, the values obtained should be increased by a factor of three.

The calculation given above is tentative only, since not all the initial data have been accurately determined. For instance, one could expect that the actual localization of the particle trajectories by the spark counter may be a few times better than the value used above (1 mm^2), in which case the loading will play a still smaller role.

Finally, for a large loading, one can use the moving emulsion method for trajectory identification.

On the basis of the above, one can expect that the loading of the emulsion by background particles will not prohibit an application of the proposed method to the study of nuclear interactions of protons.

The authors express their deep gratitude to A. I. Alikhanyan for the interest shown towards our idea and for making its experimental realization possible.

Note received in proof (August 28, 1959): A spark counter telescope in a magnetic field started operation in June 1959.

[1] Gramenitskiĭ, Podgoretskiĭ, and Sharapova, JETP **30**, 277 (1956), Soviet Phys. JETP **3**, 230 (1956).

Translated by H. Kasha
182

ELASTIC PROTON-PROTON SCATTERING AT 8.5 Bev

V. B. LYUBIMOV, P. K. MARKOV, E. N. TSYGANOV, CHENG P'U-YING, and M. G. SHAFRANOVA

Joint Institute of Nuclear Research

Submitted to JETP editor April 17, 1959

J. Exptl. Theoret. Phys. (U.S.S.R.) **37**, 910-916 (October, 1959)

Elastic p-p scattering at 8.5 Bev was studied using photographic emulsions. The geometry of irradiation was such that the incident protons were perpendicular to the plane of the emulsion. Sixty-six cases of elastic scattering were found. Scattering on quasi-free protons and other background effects comprised about 2%. The elastic scattering cross section was (8.4 ± 1.1) mb. The differential cross section down to 2.5° in the c.m.s. was obtained. Near 0° it turned out to be larger than would be expected on the basis of the purely absorbing proton model.

INTRODUCTION

THE study of the elastic scattering of particles at high energy is a convenient way of studying their structure. The optical model, which was first applied to the analysis of scattering of neutrons by nuclei,[1] has been used widely to analyze experimental data on the elastic scattering of π mesons and protons by nuclei at energies of 1 Bev and higher.[2-8] Recently, several authors,[9-11] employing somewhat simplifying assumptions, carried out a phase-shift analysis of experimental data on the elastic scattering of π mesons and protons by protons at various energies. It turned out that the available experimental results could be explained almost completely by diffraction scattering.

In the study of elastic scattering of high-energy π mesons and protons by nucleons, one encounters a series of experimental difficulties. Firstly, the cross section is small (5 — 10 mb). Secondly, the corresponding experiments demand detection of very small scattering angles (~ 1° in the laboratory system, designated l.s.), whereas in the work of references 2 — 8 scatterings through angles up to 5° in the l.s. were missed, and in the work of reference 12 the differential cross section was measured from an angle of 2° in the l.s. (E = 6.15 Bev). Thirdly, in work with photoemulsions, it is hard to segregate cases of scattering by protons bound in the nucleus,[2,3,5] since this requires a very high accuracy in measurement of angles.

An attempt was made in this work to avoid the difficulties indicated above.

EXPERIMENTAL ARRANGEMENT

In this work, the elastic scattering of 8.5 Bev protons by protons was studied using photoemulsions. Usually one scans along the track to find such events. However, with this method of search, the efficiency of detecting cases of scattering through small angles is low.[2] This is especially so for cases in which the scattering plane makes a large angle with the plane of the photoemulsion.[6] An azimuthal asymmetry is also observed in area scanning in the case of irradiation parallel to the plane of the photoemulsion.[13] Estimates using the optical model show that at 8.5 Bev almost all the scattering is concentrated in angles < 3° in the l.s. Therefore, the usual type of scanning along the track would introduce considerable distortion into the results. Also, the accumulation of statistics is exceedingly slow.

In studying elastic scattering at E = 8.5 Bev using photoemulsions, it is advantageous to direct the proton beam perpendicular to the plane of the emulsions and carry out area scanning. Since the recoil proton* in most cases has a small momentum, directed almost perpendicular to the incident proton, i.e., it lies almost in the plane of the photoemulsion, the efficiency of detecting the events of interest is high, and does not depend on the azimuth angle. The beam density employed in perpendicular irradiation can be several times higher than that used in parallel irradiation.[14] This increases the speed of accumulation of statistics. Also, with such geometry it turned out to be possible to measure angles of the scattered proton with high accuracy (~ 3′).

The enumerated advantages of such a method are considerable, and we believe that this method can be successfully used also at somewhat higher energies.

*We call the proton emitted at a large angle the recoil proton, and the one emitted at a small angle (relative to the incident beam) the scattered proton.

The present work was carried out with a camera of dimensions $10 \times 10 \times 2$ cm^3 consisting of layers of emulsion of type NIKFI-BR of thickness $400\,\mu$, irradiated by the internal beam of 8.5 Bev protons from the proton synchrotron of the Joint Institute, perpendicularly to the plane of the photoemulsion. Analysis on hydrogen content was carried out in control layers. It turned out that each cm^3 of irradiated emulsion contained $(2.90 \pm 0.06) \times 10^{22}$ atoms of hydrogen.

Area scanning was carried out with 630-fold magnification in the central part of the layers, of dimensions 2×2 cm. The mean beam density in this zone was $(1.97 \pm 0.05) \times 10^5$ particles/cm^2. In all, 1.53 cm^3 were scanned.

In order to determine the efficiency of detecting the events of interest and the reliability of results, the entire area was scanned twice. Approximately 9000 stars were found, including 451 two-pronged ones. From these two-pronged ones, stars were chosen, which looked like elastic p-p events. These cases were broken down into two groups: 1) cases with a black recoil proton ($I/I_{min} > 4$, $I_{min} \sim 40$ grains per $100\,\mu$), 2) cases with a grey recoil proton ($2 < I/I_{min} \leq 4$).

The detection efficiency in the first scanning turned out to be $(68.7 \pm 2.9)\%$ for events in the first group and $(34.5 \pm 9)\%$ for events in the second group. In the second scanning, the values were (84.0 ± 2.6) and $(56.5 \pm 12)\%$. The overall efficiency as a result of two-fold scanning was equal to (95 ± 1) and $(71 \pm 9)\%$ for events of the first and second groups, respectively. Since it subsequently turned out that the overwhelming majority of cases found (90%) belonged to the first group, the efficiency of detection for events of the second group was not investigated further. With such an efficiency, one scanner was able to scan 12 mm^2 in 6 hours, corresponding to ~ 10 m of track-length of incident protons.

ANALYSIS OF DETECTED EVENTS AND METHOD OF MEASUREMENT

In order to segregate cases of elastic scattering by free hydrogen the following criteria were employed.

1. The relation between the track length of the recoil proton R and its angle with respect to the incident proton φ should satisfy the kinematics of elastic scattering.

2. The angle γ between the direction of the primary proton and the plane defined by the secondary particles should be zero (condition of coplanarity).

3. The relation between the track length of the recoil proton R and the angle ψ of the scattered proton with the direction of the primary particle should satisfy the kinematics of elastic scattering.

4. At the point of scattering there should be no nuclear recoil and no β electron.

When the recoil proton did not stop in the camera and its momentum, determined from ionization measurements, was known only with large error, the relation between the angle of the scattered proton and that of the recoil proton was required to be fulfilled as in elastic scattering. The error in measuring the track length of the recoil proton R did not exceed 5%.

In order to determine the angle of the recoil proton, it is necessary to know the direction of the proton and the direction of the primary particle. Since the angular half-width of the beam of incident particles was $\sim 0.2°$, the direction of the beam was taken as the direction of the incident particle. In order to determine this at a given point in the emulsions, the angle of incident particles was measured from the values of projections along x and y axes. The x and y axes were chosen along lines marked by light, which were parallel to these axes to within $0.1 - 0.2°$. Measurements at a given point were carried out in 37 layers. Because of distortion of the emulsion, these measurements in different layers did not reproduce the same value for the angle, and were distributed with a half-width of $\sim 1°$. The mean value of the angle gave the true direction of the beam through the given point. The beam direction was determined at five such points — on the edges of the working zone and in the middle. The values obtained agreed to within 0.2°, the main error in determining the angle of the recoil proton came from inaccuracies in measuring the angle of dip. This error did not exceed $1 - 1.5°$ on the average, except for cases where the recoil proton had a short track-length ($\lesssim 500\,\mu$).

Measurement of the angle ψ of the scattered proton was carried out in two ways: 1) by measuring the angle between the mean direction of the incident particles and the scattered proton. This method gave an average accuracy of the order of the half-width of the beam, i.e., 0.2°. 2) Near the scattering act, at a distance of $20 - 30\,\mu$, one track of a noninteracting incident proton was chosen for calibration. To determine the scattering angle ψ, four measurements of the projections along the x and y axes in the plane of the photoemulsion of

the line between the calibrating track and the track undergoing scattering were carried out. Two measurements were made before the scattering $\sim 2000\,\mu$ apart (through five plates) and two, at the same distance following the event. The projections were measured to an accuracy of $\sim 1\,\mu$. This made it possible to measure the scattering angle to an accuracy of $2' - 3'$.

In determing the scattering angle ψ, effects of multiple scattering can be neglected. The error in the determination of the thickness of the layers was also small. In order to avoid errors, independent measurements were carried out simultaneously, relative to three calibrating tracks. It is possible to determine the angle of noncoplanarity from these measurements, knowing the direction of the recoil proton. The error in γ is determined mainly by the error in the angle of the scattered proton, and depends on the magnitude of this angle. Thus, $\Delta\gamma = 3°$ for $\psi = 1°$, if $\Delta\psi = 3'$.

Out of 451 two-pronged stars, 170 were discarded, since they obviously did not satisfy the selection criteria. For the remaining events, measurements of the track length R and angle φ of the recoil proton were carried out. All measurements were duplicated. Then the angle of the scattered proton was measured in the first way. These measurements were also duplicated. For a final separation of the elastic scattering cases, the angle ψ was measured in the second way, i.e., to an accuracy of $2' - 3'$.

SELECTION OF CASES OF SCATTERING BY FREE PROTONS

One can try to estimate the expected contribution from quasi-elastic cases which would be counted as scattering by free hydrogen. It is well known[15] that the distribution of protons in the nucleus with momentum is near to $\exp\{-(p_x^2+p_y^2+p_z^2)/p_0^2\}$, where p_0 corresponds to an energy of ~ 20 Mev. The distribution of the projections of the proton momenta on an arbitrary axis will have the same form, with a p_0 corresponding to ~ 7 Mev.

We consider the influence of three mutually perpendicular momentum components on the kinematics of elastic scattering, if the x, y plane coincides with the scattering plane, and x is the direction of the initial proton. A momentum component p_x causes a violation, in the main, of the first criterion (R and φ), a component p_y, of the third criterion (R and ψ) and p_z destroys the coplanarity.

On Fig. 1 is shown the dependence of the angle

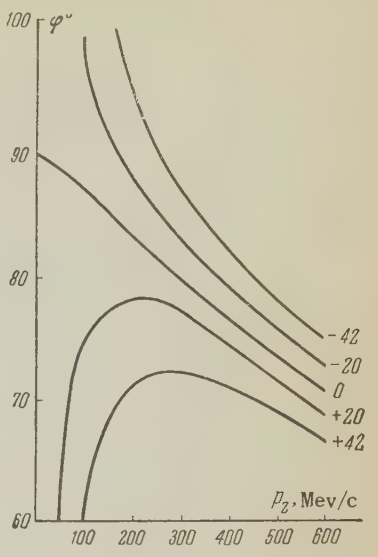

FIG. 1. Dependence of the recoil-proton angle φ (proton scattered through a large angle) on its momentum p_z for various values of the component p_x of momentum of a quasi-free proton, 0; ±20, ±42 Mev/c.

φ of the recoil proton on its momentum for elastic proton-proton scattering, with momentum $p_x = 0$, ± 20, ± 42 Mev/c. Within the intervals $0 - 20$ Mev/c and $0 - 42$ Mev/c, fall 20 and 40%, respectively, of all quasi-free protons. From the figure it is clear that with the given accuracy of 3% in measuring the momentum and of $1 - 1.5\%$ in measuring the angle of the recoil proton, it is possible to segregate at least 80% of the cases of scattering by quasi-free protons using the first criterion. It is easy to show that with the second and third criteria it is also possible to segregate independently $\sim 80\%$ of the cases of scattering on quasi-free protons. Consequently, with the given accuracies of measurement, the contribution from quasi-elastic events will be on the order of a percent in the number of cases selected.

For each case that was measured, the errors in the measurement were estimated, and cases satisfying the kinematics within three standard errors were retained. Distributions for these cases plotted against $|\Delta\varphi|$, $\Gamma = |\gamma/\Delta\gamma|$ and $|\Delta\psi|$ are given on Fig. 2. From Fig. 2a it was found that the root mean square error in the measurement of the angle φ was $\sim 1.5°$. From the distribution of the selected cases with Γ, it is clear that the errors in the angles of noncoplanarity were correctly estimated.

The distribution of cases with $|\Delta\psi|$ is given in Fig. 2c. For this histogram, cases were selected in which the recoil proton stopped and where the kinematics were satisfied to within three root mean square errors in the first two criteria. Cases of scattering on quasi-free protons with momentum p_y fall in this figure, since these cases are not segregated by the first two criteria. A considerable proportion of these cases fall in the region $|\Delta\psi| > 12'$ (i.e., beyond three times the half-width

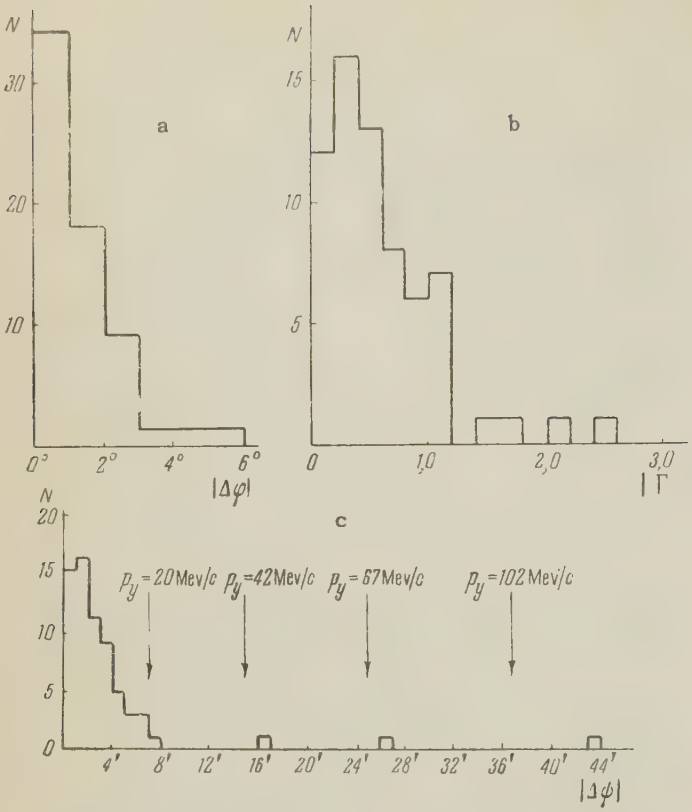

FIG. 2. a: distribution of cases of elastic scattering with $|\Delta\varphi|$, where $\Delta\varphi$ is the difference between the measured angle of the recoil proton and the angle corresponding to its track length according to the kinematics; b: distribution of cases of elastic scattering with Γ, where $\Gamma = |\gamma/\Delta\gamma|$, γ is the angle of noncoplanarity and $\Delta\gamma$, the error in it; c: distribution of cases chosen by the first two criteria (R vs φ and coplanarity) vs $|\Delta\psi|$.

of the distribution), where there are no cases of scattering on free protons. From the number of such cases it is possible to estimate the contribution of quasi-elastic cases of scattering and other cases belonging to the background in the region $|\Delta\psi| \leq 12'$. This contribution was $\sim 2\%$.

RESULTS

The selection criteria were satisfied, within the limits of three rms errors, in 66 cases. Of these, in only two did the recoil proton leave the emulsion camera.

The angular distribution in the center of mass system for the cases in which the angles were $\leq 6.3°$ is given in Fig. 3.

Within the range $0 - 2.5°$ a somewhat smaller number of cases was observed than in the neighboring intervals. This probably resulted from the fact that some of the cases in which the path length of the recoil proton $R \lesssim 10\,\mu$ were missed in the scanning. Therefore, in the angular interval $0 - 2.5°$ a correction of 3.4 ± 1 cases was introduced,

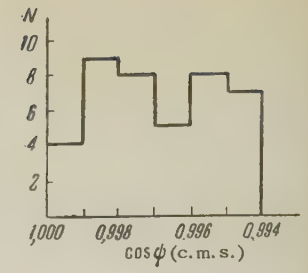

FIG. 3. Angular distribution of cases of elastic scattering for angles <6.3° in the c.m.s.

under the assumption that the differential cross section in this interval is equal to the mean differential cross section in the interval $2.5 - 6.3°$. Calculations show that the influence of Coulomb scattering on the differential cross section for angles larger than 2.5° was negligible. To evaluate the effect of Coulomb scattering for the angles less than 2.5°, much better statistics would be necessary.

On the basis of estimates of the contributions of quasi-elastic cases, omission of cases of scattering through small angles, and efficiency of scanning, the total number of cases of elastic scattering on free protons turned out to be equal to 73.9 ± 9.1. Thus, the cross section for elastic scattering was found equal to

$$\sigma_e = (8.4 \pm 1.1)\ \text{mb}.$$

According to reference 16 the cross section

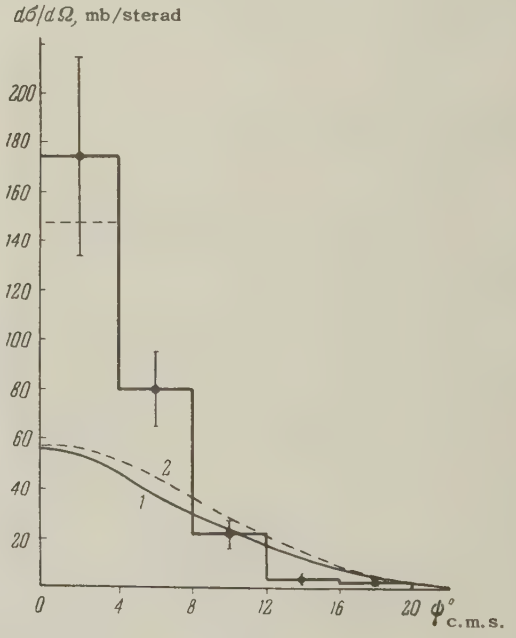

FIG. 4. Differential cross section for elastic scattering of 8.5-Bev protons by protons in the c.m.s. The dashed line in the first interval indicates the differential cross section without correction for the omission of cases at small angles. Curves 1 and 2 were calculated from the optical model for a purely absorbing proton and different assumptions about the dependence of the absorption coefficient on radius.

for elastic scattering at E = 9 Bev is equal to (10 ± 4) mb.

The differential cross section for elastic p-p scattering in the c.m.s. is given on Fig. 4 in the form of a histogram. The solid curve was constructed from the data of Barashenkov and Huang Nen-Ning.[11] In their work the optical model was employed and, for energies of the incident proton greater than 5 Bev, the index of refraction was assumed to be unity, and the dependence of the coefficient of absorption on radius was taken from the work of Grishin.[10] The dashed curve was calculated for the model of a purely-absorbing disc with constant coefficient of absorption. In this, the total proton-proton interaction cross section was taken equal to 30 mb.[17]

The differential cross section obtained cannot, apparently, be made to agree with the model of a purely absorbing proton. According to this model, with neglect of spin, the differential cross section at 0°, as obtained from the optical theorem, is

$$(d\sigma / d\Omega)_{0^\circ} = (k\sigma_t / 4\pi)^2,$$

where k is the wave number of the colliding protons in the c.m.s. and σ_t is the total cross section for p-p interaction. For σ_t = 30 mb, the differential cross section at 0° is equal to 57 mb/sterad, whereas, from Fig. 4 it can be seen that in the region near to 0° the differential cross section is significantly greater.

Optical-model calculations can be made to agree with experimental results if one assumes that the index of refraction is different from unity, i.e., there is potential scattering. It is possible that agreement would also be obtained if the interaction cross section were assumed different in the singlet and triplet states. The present work is being continued, and a more detailed analysis of the experimental data will be made after better statistics have been obtained.

In conclusion, the authors would like to express the gratitude to the entire crew of the proton synchrotron of the Joint Institute for irradiating the emulsion camera, and the photoemulsion processing group of the High-Energy Laboratory of the Joint Institute for the chemical processing of the photoemulsion. The authors are very grateful to Prof. D. I. Blokhintsev, Acad. V. I. Veksler, and to M. Danysh, M. I. Podgoretskiĭ and K. D. Tolstov for valuable remarks in discussions and for interest in the work. We would like to thank M. F. Rodichev for determining the hydrogen content of the dry emulsions, L. G. Kriventsov for determining the moisture content and specific weight of the photoemulsion, and also to the group of laboratory assistants for scanning and measurement.

[1] Fernbach, Serber, and Taylor, Phys. Rev. **75**, 1352 (1949).

[2] W. D. Walker, Phys. Rev. **108**, 872 (1957).

[3] W. D. Walker and J. Crussard, Phys. Rev. **98**, 1416 (1955); **104**, 526 (1956).

[4] Maenchen, Fowler, Powell, and Wright, Phys. Rev. **108**, 850 (1957).

[5] Duke, Lock, March, Gibson, McKeague, Hughes, and Muirhead, Phil. Mag. **46**, 877 (1955).

[6] Duke, Lock, March, Gibson, McEwen, Hughes, and Muirhead, Phil. Mag. **2**, 204 (1957).

[7] Chretien, Leitner, Samios, Schwartz, and Steinberger, Phys. Rev. **108**, 383 (1957). Cester, Hoang, and Kernan, Phys. Rev. **103**, 1443 (1956). Fowler, Shutt, Thorndike, Whittemore, Cocconi, Hart, Block, Harth, Fowler, Garrison, and Morris, Phys. Rev. **103**, 1489 (1956).

[8] Kalbach, Lord, and Tsao, Phys. Rev. **113**, 330 (1959).

[9] S. Z. Belen'kiĭ, JETP **30**, 983 (1956), Soviet Phys. JETP **3**, 813 (1956); JETP **33**, 1248 (1957), Soviet Phys. JETP **6**, 960 (1958). Ito, Minami, and Tanaka, Nuovo cimento **8**, 135 (1958); **9**, 208 (1958). V. G. Grishin and I. S. Saitov, JETP **33**, 1051 (1957), Soviet Phys. JETP **6**, 809 (1958). Grishin, Saitov, and Chuvilo, JETP **34**, 1221 (1958), Soviet Phys. JETP **7**, 844 (1958). Blokhintsev, Barashenkov, and Grishin, JETP **35**, 311 (1958), Soviet Phys. JETP **8**, 215 (1959).

[10] V. G. Grishin, JETP **35**, 501 (1958), Soviet Phys. JETP **8**, 345 (1959).

[11] V. S. Barashenkov and Huang Nen-Ning, JETP **36**, 832 (1959), Soviet Phys. JETP **9**, 587 (1959).

[12] Cork, Wenzel, and Causey, Phys. Rev. **107**, 859 (1957).

[13] Dul'kova, Romanova, Sokolova, Sukhov, Tolstov, and Shafranova, Dokl. Akad. Nauk SSSR **107**, 43 (1956), Soviet Phys.–Doklady **2**, 154 (1956).

[14] Lonina, Tolstov, and Tsyganov, Приборы и техника эксперимента (Instrum. and Meas. Engg.) **2**, 37 (1956).

[15] Cladis, Hess, and Moyer, Phys. Rev. **87**, 425 (1952). J. M. Wilcox and B. J. Moyer, Phys. Rev. **99**, 875 (1955). E. M. Henley, Phys. Rev. **85**, 204 (1952). McEwen, Gibson, and Duke, Phil. Mag. **2**, 231 (1957).

[16] Bogachev, Bunyatov, Merekov, and Sidorov, Dokl. Akad. Nauk SSSR **121**, 617 (1958), Soviet Phys.–Doklady **3**, 785 (1959).

[17] V. S. Barashenkov and Huang Nen-Ning, JETP **36**, 1319 (1959), Soviet Phys. JETP **9**, 935 (1959).

Translated by G. E. Brown
183

THE SPECTRUM OF INTERNAL CONVERSION ELECTRONS ACCOMPANYING ALPHA DECAY OF U^{233}, AND THE LEVEL SCHEME OF Th^{229}

E. F. TRET'YAKOV, M. P. ANIKINA, L. L. GOL'DIN, G. I. NOVIKOVA, and N. I. PIROGOVA

Submitted to JETP editor April 29, 1959

J. Exptl. Theoret. Phys. (U.S.S.R.) 37, 917-927 (October, 1959)

The spectrum of internal conversion electrons emitted by Th^{229} (daughter nucleus of U^{233}) was studied in a β spectrometer with a toroidal magnetic field in conjunction with an $e-\alpha$ coincidence circuit. The existence of a rotational band starting from the ground state of Th^{229} was confirmed. The energies of the rotational levels were determined more accurately. Gamma transitions from some new levels (29.1, 71.4, 320.0, and 366.0 kev, and apparently 131 kev) were discovered and studied. The α spectrum of U^{233} was improved. The level scheme of Th^{229} is discussed.

1. INTRODUCTION

IT is now well known[1,2] that the α decay of U^{233} results in the populating of the whole rotational band of levels of the daughter nucleus Th^{229}, starting from the ground state. Transitions to these levels are enhanced. The intensities of α transitions to the rotational levels of Th^{229} show a very definite anomaly;[2,3] they agree with the theory for the transitions to the first four levels (having spins of the successive levels equal to $5/2$, $7/2$, $9/2$, and $11/2$) and are in marked disagreement with theory for the next two levels ($13/2$? and $15/2$?). The conclusion that the last two levels are rotational then followed only from the agreement of the energy with that calculated from the rotational formula. Such agreement could, of course, be accidental.

The main purpose of the present work was to study the γ transitions between levels of Th^{229}. The study of the intensity and multipolarity of γ transitions enables one to determine the nuclear spin and the parity of the wave function in excited states, and thus to establish whether the level belongs to a particular rotational band.

Investigation of the γ transitions in Th^{229} is also of interest in another connection. The neighboring odd nuclei show a complex system of levels, resulting from the overlap of several rotational bands. In Th^{229} only one band was known, starting from the ground state. It was of interest to find out whether this simple picture is the result of the absence of other independent levels (in the low energy region) or is due to the weakness of α transitions to these other levels. There was every reason to suppose that levels which do not show up (or appear weakly) in the α-decay, will be populated by γ transitions from higher levels.

The investigation was carried out in a β spectrometer with a toroidal magnetic field.[4] The electronic circuit selected electrons emitted immediately following α decay ($e^- - \alpha$ coincidences). We could use pulse height discrimination in the electron channel, and thus lower the counter background. An α spectrometer[1] was used to improve the α-spectrum of U^{233}.

2. PREPARATION OF SOURCES. CHEMICAL PURIFICATION OF URANIUM

The sources were prepared by vacuum deposition of uranium (in the form of the oxide) onto a thin sheet of mica (0.8 mg/cm^2). The deposition was carried out from a tungsten strip, onto which we first baked some tungsten powder. Depending on the intensity of the lines to be studied, the source activity was varied from 0.05 to 1 microcuries.

The first pictures of the conversion electron spectrum showed a large number of lines, which could not be explained on the basis of the known[1,2] α spectrum of U^{233}. The problem arose whether these lines actually belonged to the radiation of Th^{229}, following from α decay of U^{233}. To check this we carried out a purification of the material of possible radioactive impurities. First we knew that the U^{233} sample contained U^{232}, and consequently the whole radioactive series starting from it. It also contained Th^{229}, though in small quantity. We determined the U^{232} activity from the 238.6-kev γ transition which follows the α decay of the Pb^{212} daughter. This transition has been well investigated (cf. for example, reference 5). The activity proved to be extremely small, so that

conversion lines appearing as the result of the α decay of the U^{232} itself could easily be eliminated from the U^{233} spectrum. We first purified the material of Th, and consequently of all its short-lived daughters. The separation of Th from U was done by precipitating the Th in a lanthanum carrier by the fluoride method.[6] Threefold repetition of this cycle gives a purification down to some hundredths of a percent of the initial content of Th in the U. By this same method we simultaneously also rid the U of Ac.[7] The intensity of the K-line of the 238.6-kev transition (Bi^{212}) served as an indicator of the degree of purification of the uranium from thorium. After purification, the intensity of this line was reduced by at least a factor of 20.

Later we carried out a purification of the uranium of protactinium as well as thorium and actinium. The thorium and actinium were separated from the uranium by using a lanthanum carrier by this same method. The protactinium was precipitated with a barium carrier by the following method. A solution of uranyl sulfate was made 1N in H_2SO_4 and 2N in HCl, and then 2 mg of barium carrier were introduced. $BaSO_4$ was precipitated, carrying with it radium and 70 — 80% of the protactinium.[8] After threefold precipitation, only 2 — 3% of the Pa remained in the solution. In order to get rid of all the Pa and to rid the uranium of weighable amounts of iron and aluminum, a Zr carrier was added to a sulfuric acid solution of uranyl sulfate, and a twofold precipitation with cupferron was performed (cf. reference 6). After removal of the zirconium and iron cupferrate from the Pa, the filtrate was steamed several times in concentrated HNO_3 to get rid of organic matter, the uranium was reduced to U^{4+} with amalgamated zinc in a reductor, and precipitated with cupferron.[9] The aluminum remained in the solution. The uranium cupferrate was burned to U_3O_8 and dissolved in nitric acid. The uranyl nitrate was converted to uranyl chloride and used for preparing sources. When the filaments were heated, the chloride was converted to oxide.

Chemical purification of the uranium resulted in no noticeable change in the appearance of the spectrum (except for the disappearance of the 238.6-kev conversion line from Bi^{212}). We thus demonstrated that the remaining electron lines in the spectrum were not part of the radiation associated with the presence in the sample of protactinium, actinium, thorium or the thorium series.

3. RESULTS OF MEASUREMENT

The most intense γ transitions in Th^{229} are in excellent agreement with the principal lines of the α spectrum, as found in references 1 and 2. According to our measurements, the excitation energies of the first three levels of Th^{229} which are known from the α decay are 42.4 ± 0.2, 97.3 ± 0.3, and 163.4 ± 0.4 kev. In measuring the energy, the following electronic lines were used for calibration: the L_{III} line of 51.7 (Pu^{239}); the L_{III} of 43.5 and the L_{II} and L_{III} of 100.0 (Pu^{238}); the L_{III} of 44.1 (Cm^{242}). (The conversion radiation follows the alpha decay of the nucleus listed in parentheses.) We found the following transitions between these levels (the complete list of lines is given in the table)

42.4±0.2(42.4—0)	80%	$M1$+20% $E2$;
54.7±0.5(97.3—42.4)		$M1$+$E2$;
97.3±0.3(97.3—0)		$E2$;
66.0±1.0(163.4—97.3)		—
121.0±0.3(163.4—42.4)		$E2$.

The energies of the levels are in agreement with the rotational formula: the measured values of the energies are 42.4, 97.3, and 163.4 kev; the values calculated from the rotation formula (with $K = 5/2$) are 42.4, 96.8, and 163.5 kev. The energies of these three levels of Th^{229} and the multipolarities of the transitions between them show that together with the ground state they belong to a rotational band with $K = 5/2$.

If the level scheme of Th^{229} were exhausted by the levels found in references 1 and 2, and if all these lines were rotational, then the maximum energy of the conversion electrons would be 170 kev. But there are many lines with greater energy in the spectrum. (the conversion electron spectrum of Th^{229} is shown in Fig. 1). Analyzing this spectrum, we found various transitions which could not be explained by the scheme proposed in reference 2: 29.1, 71.4, 185, 245.3, 248.6, 277.8, 291.5, 317.3, 321, and 366 kev. The K-conversion lines of the 245.3, 291.5, and 317.3 kev transitions have an intensity of the order of 0.01%. From their L/K ratio, these transitions are most likely M1, though we cannot completely exclude E1 or M2, because of the poor statistics.

It is difficult to set up a level scheme for Th^{229} on the basis of these data because the last excited level, which was found in reference 1 and assigned to the ground rotational band in reference 2, has too high an energy (333 ± 5.0). In reference 11, the excitation energy of this level was given as 316 kev. A transition with this energy (317.3 ± 1.0) was also found in our conversion spectrum. The 245.3 and 71.4 γ lines (giving a cascade 71.4 + 245.3 = 316.7) are explained by a transition from this level. It also turned out that the α transition to the 240-kev level (237 kev in reference 2) has an intensity of about 0.007%. A check of our old

data showed that the value of 333 kev[1] was the result of a numerical error. When this error was corrected, the energy became 320 kev.

The intensities of the 317.3 and 245.3 kev transitions (0.01%) are considerably less than the intensity of the 71.4 kev transition (0.3%). It was therefore suggested that the 71.4 kev level is populated mainly by α-decay. In this connection we undertook a new investigation of the α spectrum of U^{233} in the neighborhood of the main α peaks. For this purpose we had to use a very thin source and take long runs. Alpha lines corresponding to the transition to the 71.4 kev level of Th^{229} were actually observed (cf. Fig. 2).

We know from the α spectrum of U^{233} that the population of the 317 kev level is very small and amounts to only 0.04%. In order to find transitions from this level, we had to work with a thick source (~ 100 $\mu g/cm^2$) and reduce the resolving power of the spectrometer. Poor resolution and still insufficient statistics prevented us from determining directly the spin and parity of the 317-kev level from the conversion spectrum. (The ratios of the L and K conversion coefficients for E1, M1, and M2 transitions are not very different.) More definite conclusions concerning spin and parity can be made by comparing the intensities of the transitions with the population of the levels by α decay.

Conversion lines and γ transitions of Th^{229}*

Line Number	Electron energy, kev	Intensity, in % per α decay	Conversion	Energy of γ ray, kev		Multipolarity	Intensity, in % per α decay	Transition between levels
2	9.2	0.51	Auger					
3	12.0	0.51	L-2M					
4	12.75	0.42						
5	15.35	0.21	L-2N					
6	18.40	<0.05						
1	8.5	0.54	partly L_1	29.0				
9	24.2	0.27	M	29.3	29.1±0.2	$M1$?	0.7±0.4	29.1—0
11	28.1	0.15	N	29.4				
7	21.8	2.3	L_I	42.3				
8	22.6	4.5	L_{II}	42.4				
10	26.1	4.3	L_{III}	42.4	42.4±0.2	80% $M1$ 20% $E2$	16.0	42.4—0
13	38.0	4.0	M	42.5				
14	41.2	1.2	N	42.5				
12	34.6	0.6	L_I+L_{II}	54.7				
15	49.5	0.32	M	—	54.7±0.5	$M1+E2$	1.0±0.3	97.3—42.4
17	53.2	0.12	N	—				
19	61.6	—0.01	M	—	66.0±1.0		0.05	163.4—97.3
16	51.7	0.12	L_I+L_{II}?	71.4				
18	55.0	0.08	L_{III}	71.3	71.4±0.6		0.30	71.4—0
20	66.5	0.07	M	71.0				
21	70.8	0.03	N	71.9				
23	77.5	0.25	L_{II}	97.2				
24	81.0	0.18	L_{III}	97.3	97.3±0.3	$E2$	0.6	97.3—0
27	92.8	0.12	M	97.4				
28	95.7	0.03	N	96.8				
22	73.5	<0.005						

Conversion lines and γ transitions of Th^{229}* (continued)

Line Number	Electron energy, kev	Intensity, in % per α decay	Conversion	Energy of γ ray, kev		Multipolarity	Intensity, in % per α decay	Transition between levels
25	83.5	<0.005	L_{II}	103.2	103.0±1.0		0.01	(131—29.1) ?
26	86.6	<0.005	L_{III}	102.9				
29	101.2	0.012	L_{II}	120.9				
30	104.7	0.010	L_{III}	121.0	121.0±0.3	$E2$	0.03	163.4—42.4
31	116.4	0.007	M	120.9				
32	120.8	0.003	N	121.9				
33	124.7	0.001						
34	135.7	0.01	K	245.3	245.3±0.5	$M1$	0.015	317.0—71.4
42	225.2	0.003	L	245.7				
35	139.0	0.004	K		248.6±0.8	$M1$?	0.008	320—71.4
36	151.7	0.001						
37	168.2	0.002	K		277.8±1.5	$M1$?	0.005	320—42.4
38	181.9	0.008	K	291.5	291.5±0.5	$M1$	0.012	320—29.1
44	271.0	0.002	L	291.5				
39	198.0	<0.001						
40	207.7	0.012	K	317.3	317.0±1.5	$M1$	0.02	317.0—0
45	298.0	0.003	L	318.5				
41	212.0	0.004	K		321.0±1.5	$M1$?	0.008	320 - 0
43	256.5	0.0015	K	366.1	366.0±2.0	$M1$?	0.005	366—0
48	348.0	<0.001	L	368.0				
46	313.0	0.0015						
47	325.0	<0.001						

*Intensities of lines with energies below 30 kev are corrected for counter sensitivity.

The intensity of the transitions from the 317 kev level is 0.03%. This immediately excludes the possibility of an E1 transition, because of the smallness of the conversion coefficients ($e_K/\gamma = 0.05$). The only remaining possibilities are M1 or M2.

If we assume that the 317.3-kev transition is M2, then the level must have spin $\frac{1}{2}$ and parity opposite to that of the ground state. If the spin value were large, E1 transitions would be possible with greater intensity than the 317.3 kev transition (0.02% for M2), and the population of the level, as computed from the conversion spectrum, would exceed that obtained from the α spectrum by several times ten. We cannot ascribe a spin of $\frac{1}{2}$ to the 317-kev level because of considerations related to the intensity of α decay. In this case the α transition to the 317-kev level would be very highly forbidden, since the forbiddenness associated with the change of parity would be added to the forbiddenness associated with the large amount of angular momentum carried off by the α particle ($l \geq 3$). However experiment shows that the decay coefficient to this level is not too small ($F = 0.03$), while the coefficient for the known favored transition to the ground state is $F = 0.5$. Thus the additional forbiddenness amounts to 17. (For comparison we note that, for the α decay of Am^{241} the transition with change of parity and $l = 1$ is suppressed by a factor around 400.)

Therefore it is most probable that the parity of the 317-kev level is the same as that of the ground state of U^{233} and Th^{229}, and that the transition from this level to the ground state is M1.

In the conversion electron spectrum, only one

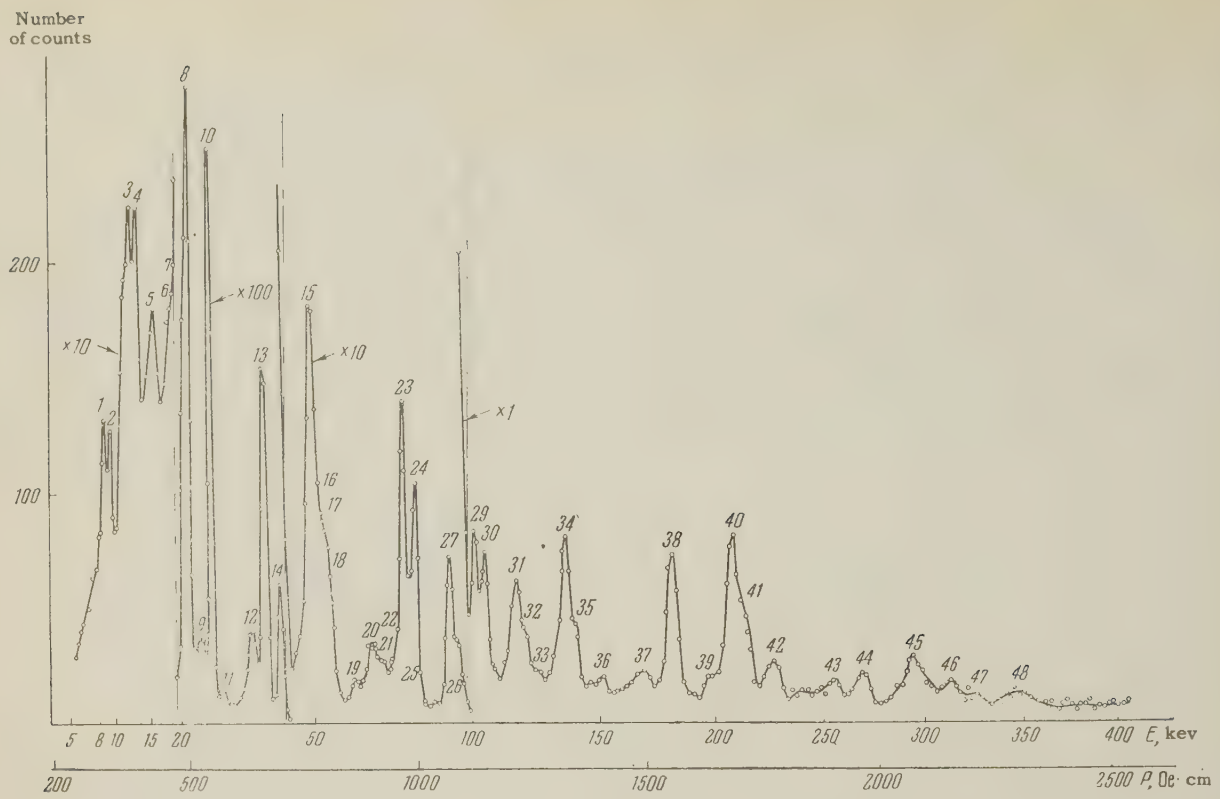

FIG. 1. Spectrum of conversion electrons of Th^{229}.

strong transition from the 317-kev level to a level of the rotational band was observed, namely the transition to the $5/2^+$ ground state. This should be the case if the spin of the 317-kev level is $3/2$. In this case the transitions to other levels of the rotational band will be E2, and their absence from the spectrum is not surprising (because of the lower probability of E2 transitions compared to M1, and their lower conversion coefficient).

In the conversion electron spectra, the K lines of the 245.3- and 317.3-kev transitions are broadened on the high energy side. We suggest that this broadening is caused by the presence of a level with excitation energy 320 kev, near to the 317-kev level. The following transitions are observed from this level: 1) 321.0 ± 1.5 kev; 2) 277.8 ± 1.5; 3) 248.6 ± 0.8; 4) 291.5 ± 0.5 kev, with a total intensity of about 0.02%. From the same arguments as for the 317-kev level, the parity of this level is positive. Just as for the 317-kev level, we can assert on the basis of the intensities of the conversion lines that the 321.0-, 248.6-, and 277.8-kev transitions are M1. The most probable value of the spin of the 320-kev level is $5/2$. The intensities of M1 transitions to the ground and first excited states of the rotational band should then be in the ratio 1 : 0.4.[10] This is in good agreement with our data on the intensities of the 321-kev (320 — 0) and 277.8-kev (320 — 42.4) transitions.

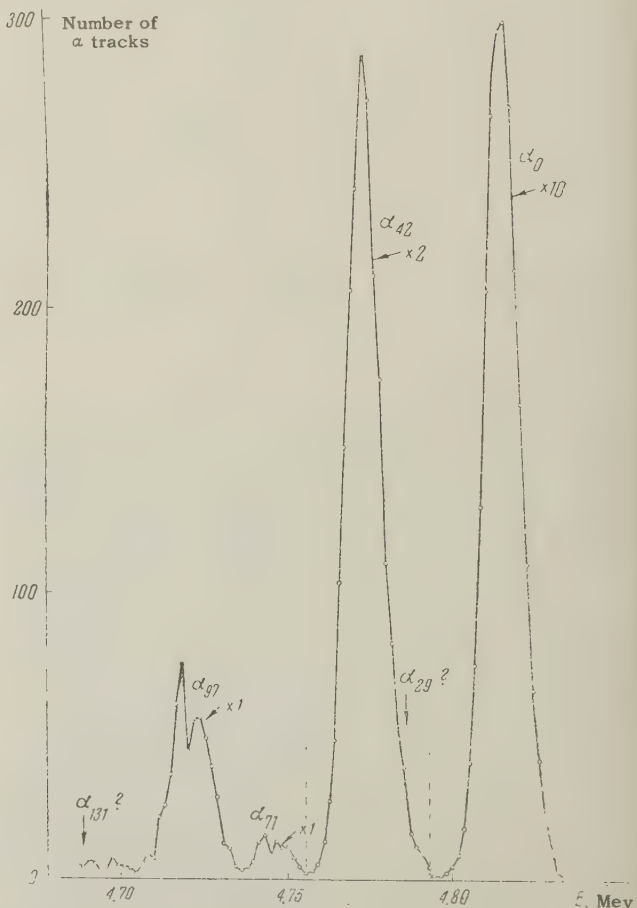

FIG. 2. Alpha spectrum of U^{233} in the region of the principa peaks.

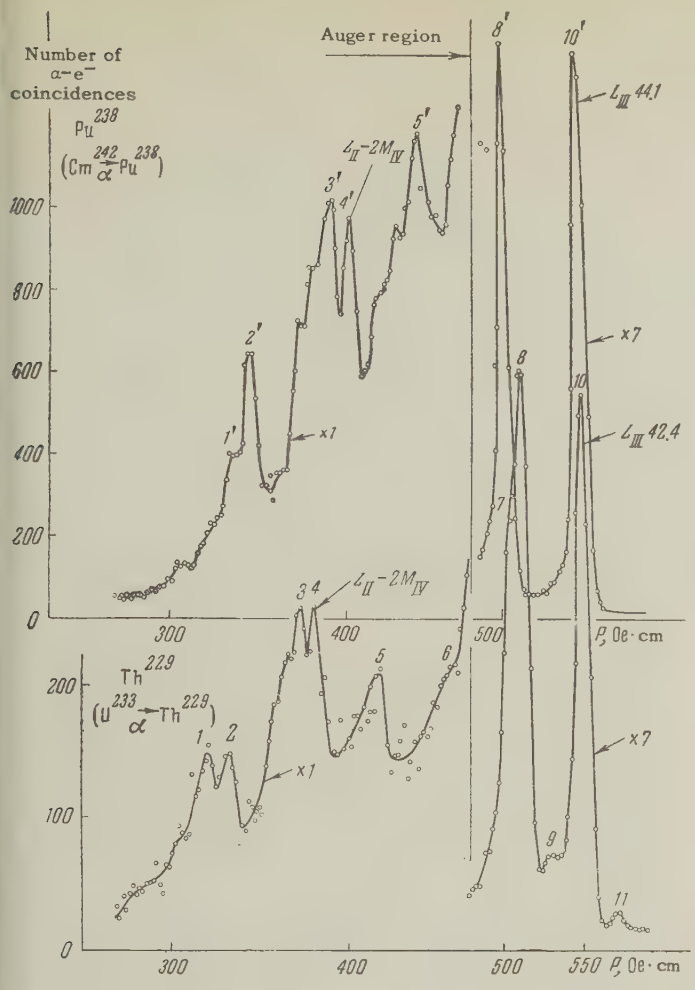

FIG. 3. Electron spectra of Th^{229} and Pu^{238} in the region of Auger transitions.

In the conversion electron spectrum there are relatively strong lines with energies 181.9 kev (0.008%) and 271.0 kev (0.002%). They are interpreted by us as K and L conversion of the 291.5-kev γ transition from the 320-kev level to the 29.1-kev level. The transition energy of 29.1 kev was determined from the electron lines (cf. Fig. 3): 1) L_I, 8.5 kev (0.5%); 9) M, 24.0 kev (0.27%); 11) N, 27.7 kev (0.15%). Line 1 at 8.5 kev lies in the region of the (L-2M) Auger electrons and could easily be interpreted incorrectly. To clarify the picture we made a comparison of the Auger spectra of the parent nuclei U^{233} and Cm^{242}. The corresponding spectra are shown in Fig. 3. As we see from the figure, the spectra are very similar everywhere, except in the region where line 1 is found, and there the intensity is considerably greater than at the corresponding line 1′ in Cm^{242}.

The intensity of the 29.1 transition is 0.7% as calculated from line 1, and is somewhat greater than 1% as calculated from lines 9 and 11. It is possible that there are γ transitions of 44.5 or 48.2 (M1), whose L lines increase the intensity of peaks 9 and 11. The shape of the α spectrum (cf. Fig. 2) also supports such a reduction in intensity of the 29.1-kev transition. Judging from the line α_{42}, the α decay intensity to the 29.1-kev level can hardly be greater than 0.5%. The transition at 48.2 kev (or 44.5) with an intensity no greater than 0.2% could be a transition from the first rotational satellite of the level with energy 71.4 kev. (The 71.4 kev level may be only the ground level of a band, since there is a strong transition going from it to the lowest state.)

Now we discuss possible assignments of spin and parity of the 71.4- and 29.1-kev levels. The parity of the 71.4- and 29.1-kev levels must be the same as the parity of the levels at 317 and 320 kev. In fact, the transitions from the 317 level to 71.4, and from 320 to 71.4 and 29.1 kev can only be M1 or M2 (from the intensities of the conversion lines). M2 transitions, which involve a change in parity, could not compete with the M1 transition to the ground state, and would simply not be seen. But in the experiment they have intensities of the same order as the transitions to the ground state.

The spin of the 71.4-kev level cannot be determined uniquely on the basis of our data. Transitions of type M1 go to the 71.4-kev level from the levels at 317 ($I = {}^3/_2{}^+$) and 320 kev ($I = {}^5/_2{}^+$). Thus the spin of the 71.4-kev level can be ${}^3/_2{}^+$ or ${}^5/_2{}^+$.

Transitions to the 29.1-kev level occur only from the 320 level. The energy of the transition is 291.5 kev (0.012%) and its multipolarity is M1. The spin of the 29.1-kev level must be great enough to forbid an M1 transition from the 317 kev level, for example, ${}^7/_2{}^+$.

The electron lines 43 and 48 are explained on the basis of the 366-kev transition with intensity 0.005% (for M1). Recently we received a report[11] that a line was observed in the α-spectrum of U^{233}, corresponding to a transition to the 364-kev level, and having an intensity of the order of 0.004%. This level is probably the rotational satellite of the 320 or 317 kev level. In this case, the spin of the 366 kev level should be either ${}^7/_2{}^+$ or ${}^5/_2{}^+$.

We also made measurements of the electron spectra for electron energies below 6 kev. (An accelerating voltage of 4 kev was applied to the source.) No difference from the usual Auger spectrum (M − 2N) could be detected.

In the α spectrum of the principal lines there is an indication of a level with excitation energy 130 kev and intensity about 0.05%. The existence of such a level is entirely possible. Electron lines

25 and 26 can be interpreted as the L_{II} and L_{III} conversion lines of the transition from the 131 level to the 29.1-kev level. Part of the intensity of line 37 at 168.2 kev could be interpreted as the L conversion line of a 185-kev transition from the 317 level to the level at 131 kev.

4. CONCLUSION

1. A study of the conversion electrons emitted by Th^{229} has shown that the levels: 0, 42.4, 97.3, and 163.4 kev belong to a rotational band with K equal to $5/2$. As pointed out in reference 3, the intensities of these lines are in good agreement with the theory of α decay. We found no γ transitions from the level at 240 kev (given as 237 kev in reference 2), which could be assigned to this same rotational band. The population of this level was apparently badly overestimated. According to the data of reference 11, it amounts to only around 0.007%. If this level is actually rotational and belongs to the main rotational band, the absence in our spectrum of transitions from this level is not surprising. The transitions would have energies of 77 kev (240 – 163) and 143 kev (240 – 97). To confirm or deny the presence of transitions with such low energy and so small an intensity (of the order of 0.001%) is not possible for us. According to our data, the levels at 317 and 320 kev do not belong to the main rotational band.

Thus the discrepancy between the calculated and experimental values of the intensity of α transitions to the levels at 237 and 317 (given as 333 in reference 2), which was pointed out in references 2 and 3, has been cleared up.

2. The level scheme of Th^{229} has proved to be much richer in excited levels than was apparent at first. A large number of the excited states of Th^{229} appear weakly in the α decay, since transitions to such levels must compete with the enhanced transitions to levels of the main rotational band.

3. A comparison of data from α and γ spectrometry enabled us to establish the energy, spin, and parity of various levels of Th^{229}. The excitation energies of levels in Th^{229} are: 29.1 ± 0.2, 42.4 ± 0.2, 71.4 ± 0.5, 97.3 ± 0.3, (131.0 ± 2.0)?, 163.4 ± 0.4, 240 (from reference 11), 317.0 ± 1.0, 320.0 ± 1.5, and 366 ± 2 kev. The level scheme is shown in Fig. 4.

The authors consider it their duty to express their deep gratitude to their co-workers who took part in the work of investigating the conversion spectrum of Th^{229}: G. I. Grishchuk, L. N. Kondrat'ev, Yu. N. Chernov, V. F. Konyaev, and S. V. Kalashnikov.

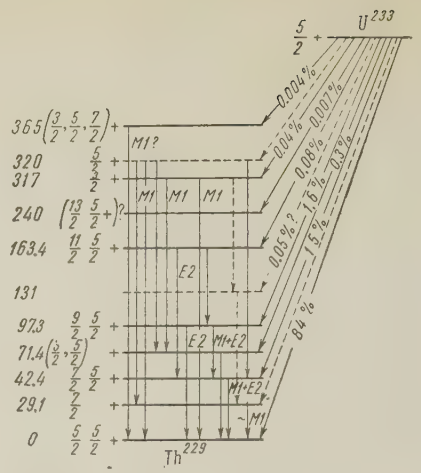

FIG. 4. Level scheme of Th^{229}.

[1] Gol'din, Tret'yakov, and Novikova, Сессия АН СССР по мирному использованию атомной энергии (U.S.S.R. Academy of Sciences Sessions on Peaceful Uses of Atomic Energy), 1956, p. 226.

[2] Gol'din, Novikova, and Tret'yakov, Izv. Akad. Nauk SSSR, Ser. Fiz. **20**, 868 (1956), Columbia Tech Trans. p. 789.

[3] Gol'din, Novikova, and Ter-Martirosyan, JETP **36**, 512 (1959), Soviet Phys. JETP **9**, 356 (1959).

[4] Tret'yakov, Gol'din, and Grishchuk, Приборы и техника эксперимента (Instrum. and Meas. Engg.) **1**, 22 (1957).

[5] Zhernovoĭ, Krisyuk, et al., JETP **32**, 682 (1957) Soviet Phys. JETP **5**, 563 (1957).

[6] Hillebrand, Lundell, Bright, and Hoffman, Applied Inorganic Analysis, (Russ. Transl.) p. 568.

[7] S. E. Bresler, Die Radioaktiven Elemente, VEB Verlag Technik, Berlin, 1957.

[8] F. L. Moore and S. A. Reynolds, Anal. Chem. **29**, 1596 (1957).

[9] Analytical Chemistry of the Manhattan Project, ed. C. J. Rodden, McGraw-Hill, 1950, p. 25. [Russ. Transl., p. 36].

[10] Alaga, Alder, Bohr, and Mottelson, Kgl. Danske Videnskab. Selskab, Mat.-fys. Medd. **29**, No. 9, 1955

[11] Dzhelepov, Ivanov, Nedovesov, and Chumin, Izv. Akad. Nauk SSSR, Ser. Fiz. **23**, 782 (1959), Columbia Tech. Transl., in press.

Translated by M. Hamermesh
184

RADIOACTIVE DECAY OF Ac^{227} *AND EXCITED LEVELS OF* Fr^{223} *AND* Th^{227}

G. I. NOVIKOVA, E. A. VOLKOVA, L. L. GOL' DIN, D. M. ZIV, and E. F. TRET' YAKOV

Submitted to JETP editor April 29, 1959

J. Exptl. Theoret. Phys. (U.S.S.R.) **37**, 928-937 (October, 1959)

The radioactive decay of Ac^{227} was investigated. Alpha decay was studied by means of an alpha-particle spectrometer. A beta-ray spectrometer in conjunction with an alpha-beta coincidence circuit was employed to study beta decay and the spectra of conversion electrons accompanying the alpha and beta decays of Ac^{227}. Fine structure was detected in the Ac^{227} alpha-particle spectrum. The energies of seven new lines and the intensities of the corresponding transitions were determined. A number of gamma transitions between levels of the Fr^{223} daughter nucleus were detected. A level scheme for Fr^{223} is proposed. Three levels were detected in the spectrum of Th^{227} that results from the beta decay of Ac^{227}. The energies of the levels and the intensities of beta decay to them were measured.

1. INTRODUCTION

ESSENTIAL differences are known to exist between nuclear level schemes depending upon the relative completion of nucleon shells in different nuclei. Nuclei possessing a large number of nucleons not included in closed shells are considerably deformed in their equilibrium states. Low-lying levels of such nuclei are, as a rule, associated with collective rotational motion. Because of the simple laws that govern the rotational motion of deformed nuclei it is relatively easy to detect rotational levels and to determine their quantum characteristics (spin, parity etc.). A large number of such nuclei have already been studied. In the case of nuclei with closed shells or with a small number of additional nucleons the stable equilibrium shape is a sphere, and rotational levels cannot appear. The single-particle and vibrational levels are relatively high-lying. As the number of nucleons in unfilled shells increases the energies of these levels are lowered.

Nuclei in the vicinity of closed shells with Z = 82, N = 126 and nuclei with a large number of nucleons in addition to these shells have been studied relatively thoroughly, but the intermediate region is still relatively unexplored. It is usually assumed that the boundary between spherical and deformed heavy nuclei is near A = 225. Even-even nuclei in this region reveal levels that are characterized by the vibrational properties of the nuclear surface. However, the level schemes of odd nuclei near this value of A (in the few instances when they have been studied) are much more complicated and unclear than those of the adjacent even-even nuclei. For example, the alpha-particle spectrum of Th^{227} contains 15 groups of alpha particles,[1] but quantum numbers have not been determined for even a single excited level of the daughter nucleus.

We have studied the radioactive decay of Ac^{227}, which is also in the intermediate region and contains an odd number (7) of protons outside of the shell Z = 82. Ac^{227} decays with 1.2% emission of alpha particles and ~ 99% emission of beta rays, with a half-life of 21.6 years. Although this isotope has been known for a long time its radioactive decay has remained practically uninvestigated. Concerning the alpha decay of Ac^{227} there are only unpublished studies (mentioned in reference 1) which indicate that in its alpha-particle emission Ac^{227} decays only to the ground level of Fr^{223}. Papers concerning the beta decay of Ac^{227} contain conflicting information about the levels of Th^{227}. Reference 2 states that 85% of the decays go to the ground level of Th^{227} and 15% to a 37-kev excited level. More recently[3] the measured end-point energy of the Ac^{227} beta-ray spectrum was found to be 45.5 ± 1.0 kev, but the existence of excited Th^{227} levels was not confirmed. Reference 4 contains indications that the beta decay of Ac^{227} is accompanied by gamma-ray emission with energy > 16 kev.

The absence of reliable experimental data on the decay of Ac^{227} results from the great difficulties encountered in the study of this nucleus. The beta decay of Ac^{227} results in the rapid accumulation of a number of short-lived isotopes: Th^{227} ($T_{1/2}$ = 18.6 days), Ra^{223} ($T_{1/2}$ = 11.2 days), Em^{219} ($T_{1/2}$ = 3.92 sec), Po^{215} ($T_{1/2} = 1.8 \times 10^{-3}$ sec), Bi^{211} ($T_{1/2}$ = 2.6 min), etc. The existence of short-lived emanation and its daughters among the products of Ac^{227} beta decay results in a strong background of random alpha particles, which greatly hinders the

study of the relatively weak Ac^{227} alpha activity. The study of Ac^{227} beta decay is hampered by the large number of conversion electrons emitted by the daughter nuclei; it is quite impossible to distinguish conversion lines associated with Ac^{227} alpha decay against this background. The first problem in the investigation of Ac^{227} decay was therefore the thorough chemical removal of Th^{227} and Ra^{223}. The other products of Ac^{227} decay possess very short half-lives and accumulate only in proportion to the accumulation of Th^{227} and Ra^{223}.

2. CHEMICAL PURIFICATION OF ACTINIUM

Th^{227} and Ra^{223} were separated chromatographically from Ac^{227} by means of a procedure which Peterson[5] and Hagemann[6] had used to separate actinium from irradiated Ra^{226}. In reference 5 Ac was separated from Ra using the Amberlite IR-1 ion-exchange resin. The eluant for Ac was 0.25 M ammonium citrate, while the eluant for Ra was 3N HCl. In reference 6 Ra was eluted from the Dowex-50 cation-exchange resin by means of 2N nitric acid, while 4N nitric acid was used for the Ac. In the latter reference the procedure was indicated very briefly without a description of the conditions for separating these elements.

We separated Ac^{227} from Th^{227} and Ra^{223} using ion-exchange resin KU-2 in hydrogenous form. Nitric acid in different concentrations was the eluant. The resin was first finely divided and shaken together with water. For column filling we required a fraction that would settle at the rate of 0.2 — 0.5 cm/min. 5N HNO_3 and 5% NH_4OH were passed through the columns successively in order to remove the impurities in the resin.

The actinium used as the starting material contained no appreciable amount of radioactive impurities other than its own decay products. The weight of inactive impurities in the actinium sample did not exceed the weight of actinium oxide. Doubly-distilled HNO_3 with a specific gravity of 1.38 was used to prepare the nitric acid eluant. All solutions were kept in quartz flasks.

In developing our technique we had two purposes: 1) to determine HNO_3 concentrations for eluting Ra^{223}, Ac^{227}, and Th^{227}; 2) to determine the conditions for separating these elements which would enable us to reduce the volume of eluant to a minimum.

The first trials showed that the bulk of the Ra^{223} is eluted with 2N HNO_3, Ac^{227} with 4N HNO_3, and Th^{227} with 5N HNO_3. In these experiments an actinium fraction amounting to 50 cm^3 contained ~ 80% of the original amount of Ac together with 3% of the equilibrium amount of Ra^{223} and 1 to 2% of the equilibrium amount of Th^{227}.

The following optimum experimental conditions were determined: column length $l = 8 - 10$ cm, diameter d = 0.2 cm and elution rate v = 0.15 cm^3/min. These conditions enabled us to reduce to 15 or 20 cm^3 the volume of the actinium fraction containing the bulk of the Ac, together with 2 or 3% of the equilibrium amounts of Ra^{223} and Th^{227}. The use of thoroughly purified ion-exchange resin and solutions insured the required purity of the final solution; evaporation and further heating of a 25 cm^3 actinium fraction left a residue weighing no more than 0.01 mg.

The final trials to obtain an actinium solution free of Ra^{223} and Th^{227}, which would be used in preparing sources, were conducted under these same conditions. In trials 1, 2, and 3 the original solution contained 31, 19, and 570 microcuries of Ac^{227} respectively; the results are shown in Table I.

TABLE I

Number of sample	HNO_3 concentration	volume of eluate, cm^3	Ac^{227} content in sample, microcuries		
			Trial 1	Trial 2	Trial 3
1	2 N	50	—	—	—
2	4 N	1	0.7	0.7	8.0
3	4 N	20	20.0	14.3	430
4	4 N	15	7.5	1.4	35
5	4 N	15	0.1	0.1	7.5
6	5 N	50	2.5	1.7	74

For our subsequent work we used samples 3 and 4, which in all three trials contained the bulk of Ac^{227}. The solutions were boiled down to a small volume in quartz dishes and were then transferred to conical quartz test tubes in which they were evaporated almost to dryness before being diluted with 1N HNO_3 to a volume of 0.05 cm^3.

3. EXPERIMENTAL PROCEDURE

The alpha-particle spectrum of Ac^{227} was investigated by means of an alpha-particle spectrometer.[7] The sources were prepared by vacuum evaporation of actinium (that had been purified of decay products) from a tantalum filament. Additional separation of Ac and its daughter isotopes during evaporation was achieved through the proper choice of filament temperature. The chemical purification combined with purification during sublimation yielded sources that were practically free of Ra^{223}, Em^{219}, and all decay products of Em^{219}. At the beginning of the readings the Th^{227} content of the sources amounted to 3 — 6% of the Ac^{227}, as determined from the total activity. With such small

Th^{227} content the ratio of the number of all alpha particles to the number of Ac^{227} alpha particles per unit time varied from 3:1 to 6:1 and became larger in the course of time. Therefore no source could be used for longer than 100 hours, after which period the background of random alpha particles became too large. The actinium activity of the sources amounted to 1 — 3 microcuries.

The spectrum of conversion electrons accompanying the alpha and beta decays of Ac^{227} was investigated by means of an alpha-beta coincidence spectrometer.[8] Even though the sources were carefully purified of Ac^{227} decay products the background of Th^{227} and Ra^{223} conversion electrons accumulating during readings was still too large. Therefore in order to distinguish the conversion electrons accompanying Ac alpha decay we introduced an additional channel for coincidences between conversion electrons and alpha particles discriminated according to their energies. We thus simultaneously registered three curves: 1) the total beta-ray count, 2) the count of alpha-beta coincidences and 3) the count of β-α_{discr} coincidences.

In the β-α_{discr} channel alpha particles were detected by a scintillation counter with a thin CsI(Tl) crystal. The counter resolution was 8%. Alpha particles were discriminated by means of a single-channel pulse-height analyzer with a window of variable width. The transmission of the apparatus was ~ 2% for the recording of β-α coincidences and 0.5% in the β-α_{discr} channel.

A shortcoming of the technique used to study beta-ray and coincidence spectra was the use of a scintillation counter with a stilbene crystal to detect electrons. The sensitivity of such counters declines rapidly as the energy rises. To determine the sensitivity the Ac^{227} spectrum was recorded with accelerating, zero and retarding potentials applied to the source. The sensitivity curve was established according to the variation of relative peak intensities. With calibration performed in this manner the errors in determining conversion line intensities in the soft part of the spectrum may amount to 30%.

4. MEASUREMENT RESULTS

Figures 1 and 2 show the alpha-particle spectrum of Ac^{227} with the ordinate axis representing n_{av}, the average number of alpha-particle tracks in a strip of photographic emulsion. Figure 1 shows alpha lines representing transitions to the ground state and to three low-lying excited levels of Fr^{223}, which were registered during a period of 11 hours and 45 minutes. Figure 2 shows alpha lines corresponding to higher excited levels of Fr^{223}, which were registered in 45 hours and 20 minutes. A

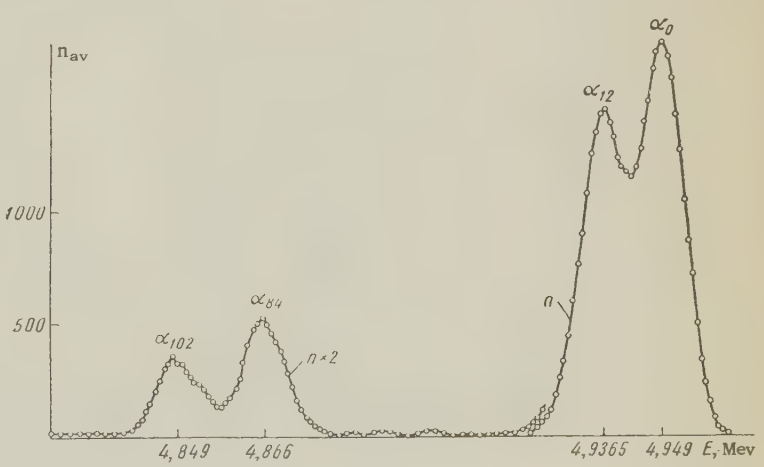

FIG. 1. Alpha-ray spectrum of Ac^{227} in the 4825–4975 kev region.

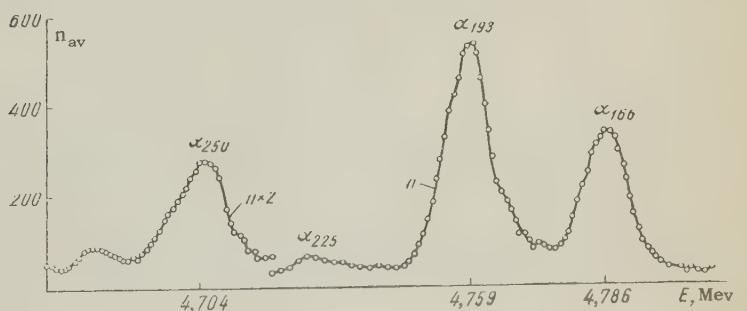

FIG. 2. Alpha-ray spectrum of Ac^{227} in the 4650–4800 kev region.

weak 225-kev line is observed, but the intensity of the corresponding transition is only 0.1% of the alpha activity and the existence of a 225-kev level cannot be regarded as proven. The energy intervals from 4950 to 5050 kev and from 4450 to 4650 kev were also investigated. The 4450-4650 kev region revealed a line with ~ 0.2% intensity corresponding to a 440-kev level, the existence of which also requires confirmation. No alpha line with intensity greater than 0.1% was detected in the 4950 — 5050 kev region.

The results of our investigation of the Ac^{227} alpha-particle spectrum are summarized in Table II.

TABLE II

Line	Alpha-particle energy, kev	Energy level, kev	Alpha-transition intensity, %	Hindrance factor η
α_0	4949±2	0	48.7±3	6.7
α_{12}	4936.5±3	12.7	36.1±3	8
α_{84}	4866±3	84.5	6.9±1	14
α_{102}	4849±3	102	5.5±1	14
α_{166}	4786±5	166	1.0±0.5	40
α_{193}	4759±5	193	1.8±0.5	17
α_{225}?	4728±8	225	~0.1	—
α_{250}	4704±8	250	0.4±0.2	38
α_{440}	4517±10	440	~0.2	—

The Ac^{227} spectra of beta rays and coincidences of conversion electrons with alpha particles are shown in Fig. 3. Curve 1 in the upper part represents the total beta-ray count, while curve 2 represents the β-α coincidence count. Curve 1 clearly shows 9.3-, 15.2-, and 24.5-kev conversion

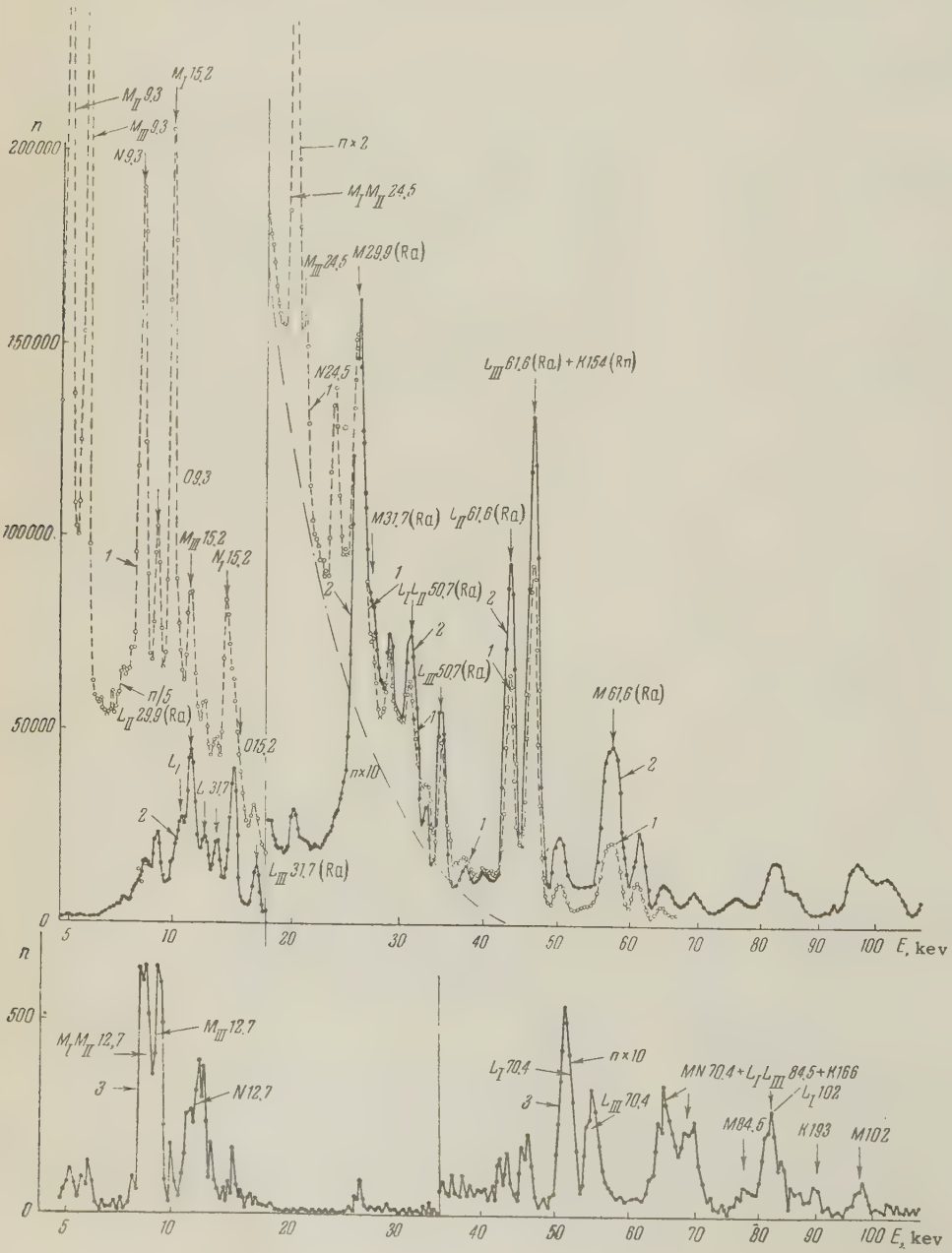

FIG. 3. Beta-ray spectrum of Ac^{227} and spectrum of conversion electrons accompanying the alpha and beta decays of Ac^{227}. 1) total count of electron detector; 2) e—α coincidence count; 3) e—α coincidence count with discrimination in the α-particle channel. The ordinate axis represents the number of beta-counter pulses. Each curve is plotted on two scales as indicated in the figure. The beta line near the end-point is plotted with a dot-dashed line.

transitions, which are not present on the coincidence curve (curve 2). The intensities of these lines do not increase as Ac^{227} decay products accumulate in the source. These energies are therefore associated with the beta decay of Ac and represent transitions between levels of the Th^{227} daughter nucleus. The dashed line below the total-count curve represents the part of the continuous beta-ray spectrum near the end-point.

The β-α_{discr} coincidence curve is shown in the lower part of the figure. A comparison with curve 2 shows that the background of accidental coincidences is small and that all conversion lines can be assumed to represent transitions accompanying Ac^{227} alpha decay. An analysis of results obtained with the same source during different time intervals shows that the intensities of these lines do not increase. This provides additional proof that the corresponding transitions take place in the Fr^{223} nucleus which results from Ac^{227} alpha decay.

Table III summarizes the measurements of conversion electrons accompanying the alpha and beta decays of Ac^{227}.

5. LEVEL SCHEME OF Fr^{223}

The scheme of Ac^{227} alpha decay and Fr^{223} levels is shown in Fig. 4 together with the observed

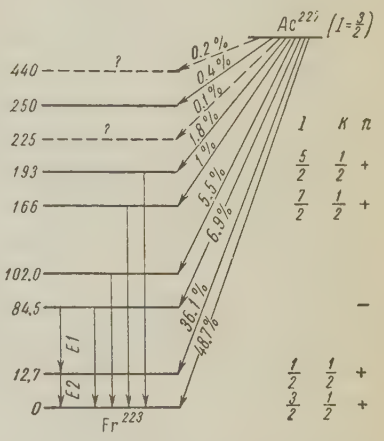

FIG. 4. Scheme of Ac^{227} alpha decay and Fr^{223} levels.

gamma transitions. The 12.7-kev transition (Table III) goes from the first excited level to the ground level; this is an E2 transition [as determined from the $(M_I + M_{II})/M_{III}$ ratio]. 70.4-kev gamma radiation results from a transition between the 84.5-

TABLE III

	Conversion-electron energy, kev	Relative line intensity, arb. units	Line origin	Gamma-ray energy, kev	Transition energy, kev
		Conversion electrons of Th^{227} (curve 1)			
1	4.46	1425	M_{II}	9.27	
2	5.24	1545	M_{III}	9.27	
3	8.28	720	N	~9.33	9.3±0.1
4	9.23	200	O	9.50	
5	10.04	400	M_I	15.20	
6	11.50	40	M_{III}	15.16	15.2±0.1
7	13.98	130	N_I	15.29	
8	15.02		O	15.29	
9	19.5	50	$M_I + M_{II}$	~24.5	
10	20.6	8	M_{III}	24.63	24.5±0.2
11	23.4	15	N	~24.45	
12	24.3		O	24.6	
		Conversion electrons of Fr^{223} (curve 3)			
1	8.47	130	$M_I + M_{II}$	~12.8	
2	9.04	130	M_{III}	12.70	12.7
3	11.90	80	N	~12.7	
4	51.76	11	L_I	70.39	70.4
5	55.38	6	L_{III}	70.40	
6	65.69		L_I	84.32	84.5
7	65.69	7	M	70.0	70.4
8	65.69		K	166.7	166
9	69.6	4	L_{III}	84.6	84.5
10	78.6	1	M	~83	
11	82.4	5	L_I	101.0	101
12	89	1	K	190	190
13	96.6	1.5	M	101	101

and 12.7-kev levels and may be of multipolarity E1 or M2, as shown by an analysis of L-conversion line intensities. In addition, the β-α_{discr} coincidence spectrum includes lines which may be attributed to 84.5-, 101-, 166-, and 190-kev gamma transitions, whose multipolarities could not be determined.

The Ac^{227} ground state has been shown experimentally to have spin $3/2$.[9] According to Nilsson's scheme[10] a nucleus with $Z = 89$ will have $K = 3/2$ and even parity (level [651]). It can therefore be assumed that the ground state of Ac^{227} has $K = 3/2$, $I = 3/2$ and even parity. The spin of Fr^{223} was not measured; if this is a spheroidal nucleus, according to Nilsson's scheme the ground state most probably has $K = 1/2$ and even parity (level [660]). The hindrance factor for decay to the ground state of Fr^{223} is small ($\eta = 6.7$), and it is reasonable to assume that the level scheme should contain rotational levels belonging to the ground-state band. An E2 ground-state transition takes place from the 12.7-kev level. If it is assumed that this level is the first rotational satellite of the ground level, it follows from their small separation that for these two levels $K = 1/2$, which agrees with the value of K for the Fr^{223} ground state in Nilsson's scheme. Higher levels of this band should, like the lower levels, form doublets. The Fr^{223} level scheme clearly shows two doublets in addition to the lower one. However the 84.5-kev level in the lower one of these additional doublets has parity opposite to that of the still lower levels. Moreover, the energies of the four lower levels are not given by the familiar formula[11] for rotational levels with $K = 1/2$:

$$E_{rot} = (\hbar^2/2J)\{I(I+1) - 3/4 - a + a(-1)^{I+1/2}(I+1/2)\}. \quad (1)$$

However this formula accurately represents the energies of the two lower levels and of the 166- and 193-kev levels (within experimental error). We here have $\hbar^2/2J = 17.4$, which agrees with the values that can be expected in this region. We therefore conclude that the 0-, 12.7-, 166-, and 193-kev levels are very probably rotational levels belonging to a single band with the spins given in Fig. 4. We have assigned spin $I = 3/2$ to the ground state and $I = 1/2$ to the first excited level. Inverted spin values have also been assigned to the two upper levels, because of the existing ground-state transition from the 193-kev level. This transition should not be observed if the 193-kev and ground levels have spins $7/2$ and $1/2$ respectively. For the given spin sequence the splitting factor in (1) is $a = -1.25$.

The existence of rotational levels in a nucleus belonging to the intermediate region between deformed and spherical nuclei is significant and merits more thorough discussion. It may be assumed that the nuclear shape and the positions and characteristics of the levels depend essentially on an odd nucleon. It is therefore interesting to compare the level schemes of Fr^{223} and Fr^{221}, which are in the same region of A and have the same number of odd nucleons outside of closed shells. The Fr^{221} levels are known from the alpha-decay spectrum of Ac^{225}, which contains nine alpha lines, while seven gamma transitions have been observed between levels of the Fr^{221} daughter nucleus.[1] As in the case of other investigations of nuclei in this region the literature contains no attempts to identify the observed levels. The lower levels of Fr^{221} are shown in Fig. 5 together with the known gamma transitions.

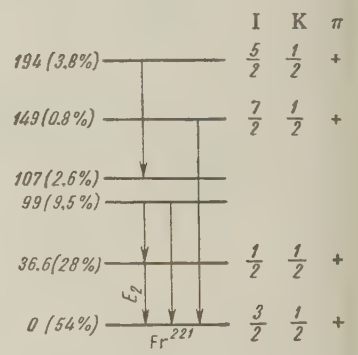

FIG. 5. Lower-lying level scheme of Fr^{221}

The conversion-line intensities associated with the ground-state transition from the first excited level indicate clearly that this is an E2 transition. This multipolarity as well as the relatively small level separation may, just as in the case of Fr^{223}, indicate that these two levels belong to a single band with $K = 1/2$. The next excited levels of the ground-state band may be the 107- and 194-kev levels, which together with the two lower levels are accurately represented by (1). We now have $\hbar^2/2J = 13.3$, which does not differ too much from the corresponding value for Fr^{223}.

The question as to whether the band formed by these four levels has a normal or inverted spin sequence cannot be answered unambiguously without additional investigation of the conversion electron spectrum. We select an inverted sequence by analogy with Fr^{223}. In this case $a = -1.93$, in satisfactory agreement with the value of a for Fr^{223}. Analysis thus shows that the structures of the Fr^{223} and Fr^{221} levels are similar, thus providing additional confirmation of the aforementioned view that the Fr^{223} and Fr^{221} nuclei are deformed. The (nearly) resolved character of the Ac^{227} ($K = 3/2$) alpha decay to the ground state of Fr^{223}

($K = 1/2$), in which K undergoes change, seems at first glance to be a contradiction. But it must be remembered that with diminished deformation we may expect a weakening of K-forbiddenness, and that we at present have no information concerning the magnitude of K-forbiddenness in the given region. It may be small, being represented by $\eta = 6.7$.

Fr^{223} and Fr^{221} may be regarded as deformed nuclei, if the foregoing reasoning is correct. The boundary between deformed and spherical nuclei is then somewhat lower than was previously supposed, at least for odd nuclei.

6. LEVEL SCHEME OF Th^{227}

Table III shows that Ac^{227} beta decay is accompanied by the emission of gamma rays with the energies 9.3 ± 0.1, 15.2 ± 0.1, and 24.5 ± 0.2 kev. The 9.3-kev transition is most likely of the electric quadrupole type, possibly mixed with a considerable amount of magnetic dipole radiation. The multipolarities of the 15.2- and 24.5-kev transitions were determined more accurately: 99.8% M1 + 0.2% E2 for 15.2 kev and 99% M1 + 1% E2 for 24.5 kev. The multipolarities of the transitions were determined from the ratio $(M_I + M_{II})/M_{III}$.

The fact that the sum of two transition energies practically equals the third transition energy indicates that the observed transitions take place between two excited levels at 9.3 and 24.5 kev respectively and the ground state of Th^{227}. Figure 6

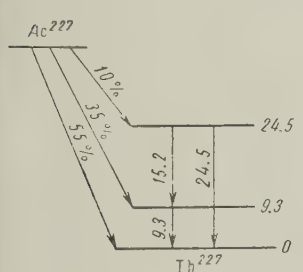

FIG. 6. Scheme of Ac^{227} beta decay and Th^{227} levels.

shows the scheme of Ac^{227} beta decay and Th^{227} levels. For the reasons mentioned above we were unable to determine the intensities of beta decays to Th^{227} levels; approximate intensities are indicated in Fig. 6. The beta-transition intensities were used in calculating log ft. For the ground-state transition log ft = 7.0; for the transition to the 9.3-kev level log ft = 6.9; for the transition to the 24.5-kev level log ft = 6.8. The striking similarity of these values results naturally from the identical parity of the levels. Gamma transitions between these levels are of types M1 and E2. We obtained 42 — 45 kev as the end-point energy of the beta spectrum (Fig. 3), which does not disagree with the result given in reference 3.

Our results are quite insufficient for determining the quantum characteristics of Th^{227} levels. For this purpose we would require information concerning higher levels, which may, of course, not be occupied through Ac^{227} beta decay because of the low end-point energy.

The authors are greatly indebted to G. I. Grishuk, V. F. Konyaev, Yu. N. Chernov and S. V. Kalashnikov for their assistance with the measurements of Ac^{227} alpha and beta spectra.

[1] Strominger, Hollander, and Seaborg, Table of Isotopes, Revs. Modern Phys. **30**, 585 (1958).

[2] Lecoin, Perey, Riou, and Teillac, J. phys. radium **11**, 227 (1950).

[3] W. Beekmann, Z. Physik **142**, 585 (1955).

[4] Bouchez, Michalowicz, Riou, and Teillac, J. phys. radium **16**, 344 (1955).

[5] S. Peterson in The Transuranium Elements (Seaborg, Katz, and Manning, editors), McGraw-Hill Book Co., New York, 1949, Vol. 2, p. 1393.

[6] F. Hagemann in The Actinide Elements (G. T. Seaborg and J. J. Katz, editors), McGraw-Hill Book Co., New York, 1953; Russ Transl. IIL, 1955, p. 15.

[7] L. L. Gol'din and E. F. Tret'yakov, Izv. Akad. Nauk SSSR, Ser. Fiz. **20**, 859 (1956); Columbia Tech. Transl. p. 781.

[8] Tret'yakov, Gol'din and Grishuk, Приборы и техника эксперимента (Instruments and Measurement Engineering) **6**, 22 (1957).

[9] Tomkins, Fred, and Meggers, Phys. Rev. **84**, 168 (1951).

[10] S. G. Nilsson, Kgl. Danske Videnskab. Selskab, Mat.-fys. Medd. **29**, No. 16 (1955).

[11] Bohr, Froman, and Mottelson, Kgl. Danske Videnskab.Selskab, Mat.-fys. Medd. **29**, No. 10 (1955).

Translated by I. Emin
185

ANOMALIES IN INTERNAL FRICTION AND MODULUS OF ELASTICITY IN FERROMAGNETICS NEAR THE CURIE POINT

K. P. BELOV, G. I. KATAEV, and R. Z. LEVITIN

Moscow State University

Submitted to JETP editor May 5, 1959

J. Exptl. Theoret. Phys. (U.S.S.R.) 37, 938-943 (October, 1959)

The temperature dependence of Young's modulus and internal friction has been measured for alloys of the elinvar and coelinvar types and also in nickel and nickel-zinc ferrite. An internal-friction peak, a jump in Young's modulus and an effect of the magnetic field on the dynamic Young's modulus have been detected near the Curie point in alloys possessing the large paraprocess magnetostriction. It is shown that these phenomena are due to redistribution of spins within the domains induced by elastic stresses. The results are treated thermodynamically.

1. Until now the study of the elastic properties of ferromagnetics has been devoted to anomalies in the elastic moduli and internal friction (or absorption of sound) produced by redistributions of the magnetic moments of the domains. The chief aspects of these phenomena are sufficiently well described in the literature.[1] The present work is concerned with elasticity anomalies of a different kind, brought about by a redistribution of spins within a domain on application of elastic strains ("mechano-paraprocess"[2]). These anomalies have not been much studied before, while measurement of them for several ferromagnetics seems essential. The appearance of anomalies of this kind follows from thermodynamic considerations; the theory of second order phase transitions shows that on passing through the Curie point ferromagnetics with a large spontaneous lattice deformation or (which comes to the same thing) a large magnetostriction by the paraprocess, must show a jump in the elastic modulus. It also follows from these thermo-dynamic relations[3] that there must be an anomalous absorption of sound at the Curie point, i.e., a maximum in internal friction. Neither phenomenon has been observed in ferromagnetics so far.

We have measured the temperature dependence of the modulus of elasticity and internal friction near the Curie point in the alloys Fe-Ni-Cr (elinvar), Fe-Co-Cr (coelinvar), nickel, and nickel-zinc ferrite. The measurements were made with a precision apparatus described previously by one of us,[4] utilizing the damping of $\sim 10^3$ cps waves in the specimen. The accuracy in the elastic modulus was 0.004% and about 1% for the decrement.

2. Figure 1a shows the temperature variation of Young's modulus for elinvar of composition 36% Ni, 12% Cr, and 52% Fe, which has a large paraprocess magnetostriction. Alloys of this type have a spread-out magnetic transition, so that the Curie point was determined by using the thermodynamic coefficients.[5] For the alloy used, the Curie point was 74°C. The modulus was measured on the unmagnetized specimen and in an applied field of 252 oe, which is larger than the field for saturation. This makes it possible to exclude a trivial ΔE effect produced by redistribution of the magnetic moments of the domains. The spread-out jump in modulus on passing through the Curie point can be seen on Fig. 1a and is equal to 0.3% of the value of the modulus. A small reduction of modulus in the field relative to the unmagnetized specimen can also be seen in the immediate neighborhood of the Curie point. Figure 1b shows the results for a specimen of composition 33.1% Ni, 7.4% Cr, and 59.5% Fe, which has a larger paraprocess magnetostriction. There is, correspondingly, a larger jump of modulus than in Fig. 1a. The effect of a field in the neighborhood of the Curie point can also be seen.

The temperature dependence of the logarithmic decrement for the first alloy in various fields is shown in Fig. 2a. There is a sharp internal friction peak near the Curie point. This becomes smaller for increasing field and moves slightly to higher temperatures, becoming less sharp. An alloy 53.5% Co, 8.7% Cr, and 37.8% Fe belonging to the coelinvar class (see Fig. 2b) has an even larger and sharper maximum in internal friction near the Curie point and an extremely large paraprocess magnetostriction.[6] Measurements on pure nickel and on nickel-zinc ferrite, in which the paraprocess magnetostriction is negligible, showed that

the maximum in internal friction and the jump in elastic modulus do not occur. This indicates that in elinvar and coelinvar alloys the anomalies are related to magnetoelastic effects produced by redistribution of spins within the domains.

3. These results can be explained qualitatively on the basis of the theory of second-order phase transitions,[7] with the inclusion of relaxation effects. The specific thermodynamic potential of an isotropic single domain ferromagnetic near the Curie point can be expressed by the relation

$$\Phi = \Phi_0(T) + \frac{\alpha(T)}{2}\sigma^2 + \frac{\beta(T)}{4}\sigma^4 + \frac{\gamma(T)}{2}\sigma^2 p - \frac{p^2}{2E_0(T)} - H\sigma, \quad (1)$$

where α and β are thermodynamic coefficients, σ the specific magnetization, γ the magnetostriction constant (we are concerned with the paraprocess magnetostriction), E_0 Young's modulus at constant magnetization, and p the unidirectional elastic stress (we consider the simplest case, when the field and magnetization directions coincide with the direction of the stress). If elastic waves are excited in a ferromagnetic, the time dependence of

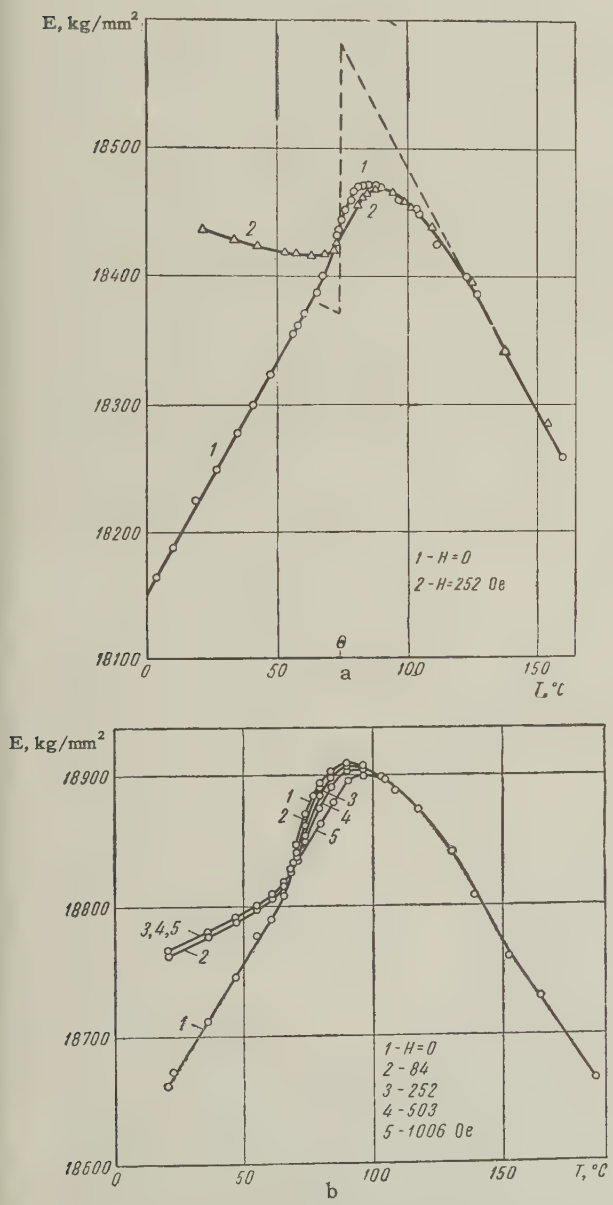

FIG. 1. Dependence of Young's modulus on temperature: a – alloy 36% Ni, 12% Cr, 52% Fe; b – alloy 33.1% Ni, 7.4% Cr, 59.5% Fe.

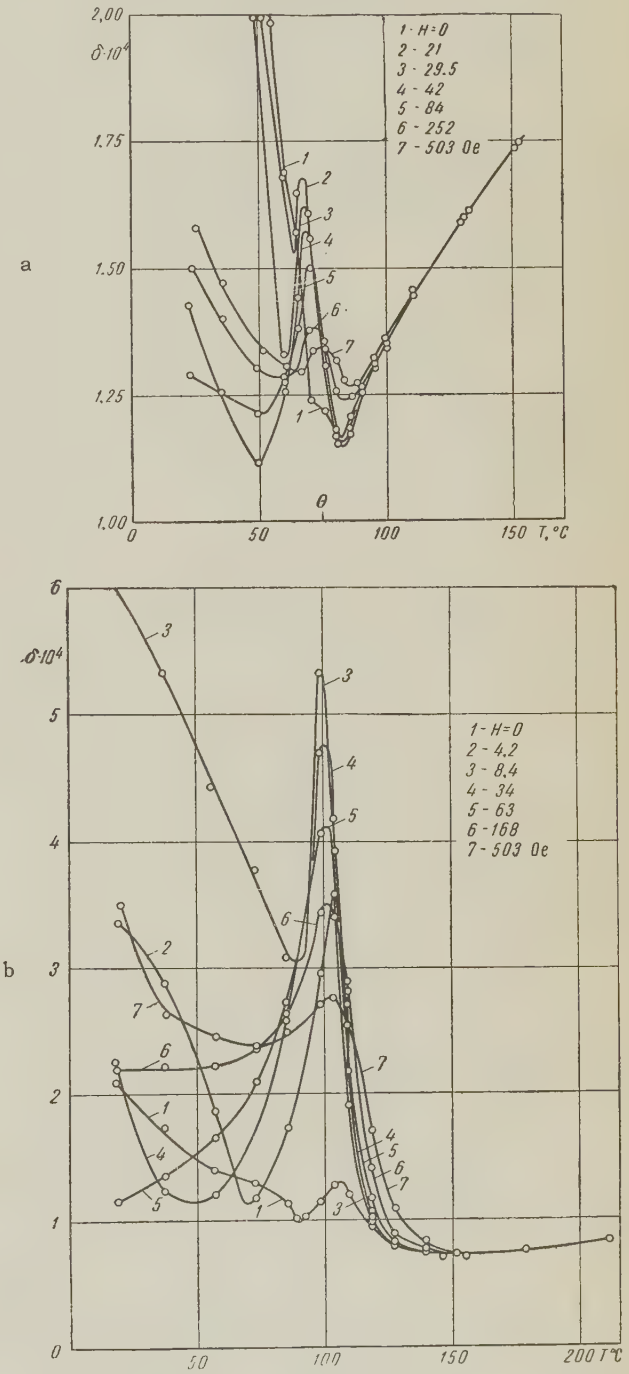

FIG. 2. Dependence of logarithmic decrement on temperature: a – alloy 36% Ni, 12% Cr, 52% Fe; b – alloy 53.5% Co, 8.7% Cr, 37.8% Fe.

magnetization is given by the kinetic equation[3]

$$d\sigma / dt = -k\,\partial\Phi / \partial\sigma, \tag{2}$$

where k is the kinetic coefficient.

The magnetization σ can be considered as the sum of the equilibrium magnetization σ_0, determined from (1), and the equilibrium conditions $(\partial\Phi/\partial\sigma)_{p,T} = 0$, $(\partial^2\Phi/\partial\sigma^2)_{p,T} > 0$, together with an additional magnetization σ_p, produced by the small stresses p of the elastic waves. From (1) and (2) and the equilibrium conditions we obtain (assuming $\sigma_p \ll \sigma_0$):

$$-d\sigma_p / dt = k(H/\sigma_0 + 2\beta\sigma_0^2)\,\sigma_p + k\gamma\sigma_0 p. \tag{3}$$

If we assume $\sigma_p \sim e^{i\omega t}$ and use the thermodynamic relation $\Delta l/l = -\partial\Phi/\partial p$, we obtain from (1) and (3) the relation between the stress p and the deformation produced:

$$\frac{\Delta l}{l} = p\left[\frac{1}{E_0} + \frac{k\gamma^2\sigma_0^2}{k(H/\sigma_0 + 2\beta\sigma_0^2) + i\omega}\right]. \tag{4}$$

Since $\Delta l/lp = E^{-1}(1 - i\delta/\pi)$,[9] where δ is the logarithmic decrement, we obtain, taking $\gamma^2 E_0 \ll 2\beta$, the relaxation relation for Young's modulus and the decrement of a ferromagnetic near the Curie point

$$E = E_0\left(1 - \frac{\Delta_E}{1 + \omega^2\tau^2}\right), \tag{5}$$

$$\delta = \pi\Delta_E\omega\tau / (1 + \omega^2\tau^2), \tag{6}$$

where τ, the relaxation time and Δ_E, the degree of relaxation are given by

$$\tau = 1 / k(H/\sigma_0 + 2\beta\sigma_0^2), \tag{7}$$

$$\Delta_E = E_0\gamma^2\sigma_0^2 / (H/\sigma_0 + 2\beta\sigma_0^2). \tag{8}$$

It can be seen that τ and Δ_E are expressed in terms of purely magnetic quantities.

4. In the simplest case H = 0, when (see reference 8)

$$\begin{aligned} &\sigma_0^2 = \sigma_s^2 = -\alpha/\beta = \alpha'_\Theta(\Theta - T)/\beta, && T \leqslant \Theta; \\ &\sigma_0 = \sigma_s = 0, && T \geqslant \Theta \end{aligned} \tag{9}$$

(σ_S is the spontaneous magnetization), we obtain for the static Young's modulus ($\omega = 0$)

$$E_{T<\Theta} = E_0(1 - E_0\gamma^2/2\beta); \qquad E_{T>\Theta} = E_0.$$

From this it is evident that the jump in elastic modulus at the Curie point is determined by the square of the magnetostriction constant γ:

$$\Delta E / E_0 = (\gamma^2/2\beta)\,E_0. \tag{10}$$

Substituting our measured values for magnetization and magnetostriction for the alloy 36% Ni, 12% Cr, and 52% Fe at the Curie point ($\gamma = 7.4 \times 10^{-8}$ g^2/gauss^2 cm^6, $\beta = 0.43$ g^3/gauss^2 cm^9) we find $\Delta E/E_0 = 1.1\%$. This "ideal" jump is shown by the dashed curve in Fig. 1. In practice the jump obtained is smaller and is spread out in temperature, probably because non-uniformities in the alloy spread out the ferromagnetic transition. In addition, for measurements at frequencies $\omega \neq 0$ one must take relaxation effects into account. If H = 0, then from (7) and (9) the relaxation time is

$$\begin{aligned} \tau_{T\leqslant\Theta} &= -1/2k\alpha = 1/2k\alpha'_\Theta(\Theta - T), \\ \tau_{T\geqslant\Theta} &= \infty. \end{aligned} \tag{11}$$

Therefore on approaching the Curie point, E approaches E_0 because of the increase in τ [see Eq. (5)] and this spreads out the jump in modulus.

It follows from (6) that for

$$\omega\tau = 1 \tag{12}$$

there must be a maximum in the internal friction. The temperature of the maximum is determined (H = 0) by (11) and (12):

$$\Theta - T_{max} = \omega / 2k\alpha'_\Theta. \tag{13}$$

5. We now examine the influence of a magnetic field on the elastic modulus and internal friction. Near the Curie point we can put[8] $\sigma_0 = \beta^{-1/3} H^{1/3}$. Using this relation, we deduce from (8) that the degree of relaxation Δ_E for $T \approx \Theta$ is independent of field. The field will consequently only affect τ. It is easy to see from (5) and (7) that an applied field will reduce the modulus by an amount δE. The calculation shows that in the immediate neighborhood of the Curie point δE depends on H in the following way:

$$1/\delta E = 3\beta/\gamma^2 E_0^2 + (\omega^2\beta^{1/3}/3\gamma^2 k^2 E_0^2)\,H^{-4/3}. \tag{14}$$

Figure 3 shows the dependence of $(\delta E)^{-1}$ on $H^{-4/3}$ for the alloy 53.5% Co, 8.7% Cr, and 37.8% Fe at the Curie point. The experimental points fall satisfactorily on a straight line.

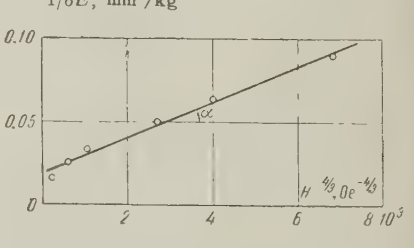

FIG. 3. Dependence of decrease in Young's modulus on magnetic field (coordinates $(\delta E)^{-1}$, $H^{-4/3}$) for alloy 53.5% Co, 8.7% Cr, 37.8% Fe, near the Curie point (109.1°C).

It can be seen from (6), (7), and (8) that an increase in field moves the internal friction peak nearer to the Curie point, reduces its value and spreads it over a wider temperature interval. This is all found experimentally (see Figs. 2a and 2b). We should point out that the experimentally determined peak height is lower than calculated from

(6) and (8). It is also contrary to the theory that the lowest maximum is obtained in the unmagnetized state; it is possible that the domain structure of the specimen has some effect here.

It follows from (13) that the damping maximum should move towards low temperatures with increasing frequency. In fact, measurement of δ for coelinvar at a frequency of 100 kcs shows the maximum displaced to 77° C. It is interesting to note that we could not obtain a maximum for the absorption of sound in such an alloy at 5 Mcs over the whole range from room temperature to the Curie point.

6. The kinetic coefficient k in (2) determines the rate at which the equilibrium magnetic state is reached in a single-domain ferromagnetic. We calculated this quantity in two ways: (a) from (14) and the slope of the straight line in Fig. 3, and (b) from (13) and the experimental $\Theta - T_{max}$, which is 2 to 4° (Fig. 2a). It is difficult to determine T_{max} more accurately because of the background in the $\delta(T)$ curve, due to the domain structure as well as other causes. Both calculations gave the same results: $k \approx 10^2$ cm^3/g-sec.

[1] R. Becker and W. Döring, Ferromagnetismus, Berlin 1939. N. S. Akulov, Ферромагнетизм (Ferromagnetism), ONTI, 1939. R. M. Bozorth, Ferromagnetism, Van Nostrand, N.Y., 1951 (Russ. Transl. IL, M., 1956).

[2] K. P. Belov, Упругие, тепловые и электрические явления в ферромагнетиках, (Elastic, Thermal, and Electrical Properties of Ferromagnetics) Gostekhizdat, 1957.

[3] L. D. Landau and I. M. Khalatnikov, Dokl. Akad. Nauk SSSR **96**, 469 (1954). V. T. Shmatov, Физика металлов и металловедение (Phys. of Metals and Met. Res.) **6**, 570, 984 (1958).

[4] G. I. Kataev, Заводская лаборатория (Plant Laboratory) **24**, 1258 (1958).

[5] K. P. Belov and A. N. Goryaga, Физика металлов и металловедение (Phys. of Metals and Met. Res.) **2**, 441 (1956).

[6] K. P. Belov and G. I. Kataev, Вестник МГУ (Bulletin, Moscow State University) **1**, 73 (1956).

[7] L. D. Landau and E. M. Lifshitz, Статистическая физика, (Statistical Physics) Gostekhizdat, 1951.

[8] K. P. Belov, Физика металлов и металловедение (Phys. of Metals and Met. Res.) **2**, 447 (1956).

[9] A. S. Nowick, Progress in Metal Physics **4**, London, 1953.

Translated by R. Berman
186

POTENTIAL BARRIER CRITERION AND STARS IN EMULSIONS

P. I. FEDOTOV

Radium Institute, Academy of Sciences, U.S.S.R.

Submitted to JETP editor May 11, 1959

J. Exptl. Theoret. Phys. (U.S.S.R.) 37, 944-949 (October, 1959)

Nuclear emulsions were bombarded with 660-Mev protons and the resulting disintegrations of nuclei in the emulsions studied. The nuclei investigated were carbon, introduced as diamond specks, the light nuclei (C, N, O) of the emulsion and the heavy ones (Ag, Br). Analysis of disintegrations in carbon indicates that there is no significant difference in the mechanisms associated with the production of stars which do or do not contain slow ($R \leq 50\mu$) particles. It was found that if the potential barrier criterion were used to pick out stars due to C, N and O nuclei, there would be a 19% admixture of stars due to Ag and Br.

1. INTRODUCTION

In studying disintegrations of nuclei in emulsions when these are bombarded by various particles, one of the first questions to arise concerns the nature of the disintegrated nucleus.

Disintegrations in emulsions can be divided into two fundamental classes: those in light (C, N, O) nuclei and those in heavy ones (Ag, Br). This division can be made using the potential barrier criterion, as follows. If, after the cascade process in the initial nucleus, the remaining intermediate nucleus is a heavy one, then the potential barrier inhibits the emission of particles with energy less than a certain threshold (9 Mev for particles with $Z = 2$ and 4.5 Mev for particles with $Z = 1$). Hence all stars containing a track less than 50μ long (which corresponds to an α particle with energy 9 Mev) must correspond to the disintegration of a light nucleus. It is very unlikely that a heavy nucleus would emit such a low energy particle.

The fundamental work on the disintegration of light nuclei in emulsions has been carried out using this potential barrier criterion. However, a careful analysis of whether this criterion is actually justifiable leads to serious objections.

1. At high excitation energies, deformation of the nuclear surface can lead to lowering of the potential barrier. On the other hand, in principle such a nucleus could decay into unstable fragments, which then decay like a light nucleus, i.e., with the emission of low energy α particles.

2. In a nucleon-bound nucleon collision, the residual nucleus is not highly excited. In interactions of this sort, on light nuclei, slow particles will not be emitted.

3. At sufficiently high excitation energies of light nuclei there is no reason to suppose that low energy particles would be emitted during the disintegration; the higher the energy of the incident particle, the more likely it will be that the decay will not produce low energy particles.

In view of the above, it becomes desirable to take a critical look at the potential barrier criterion, together with experimental data based on it, especially at high energies of the bombarding particles (several hundred Mev and higher).

2. DISINTEGRATIONS OF LIGHT NUCLEI SUCH THAT THERE ARE NO TRACKS SHORTER THAN 50μ

To study the interaction of 660-Mev protons with carbon, we introduced[1] a suspension of diamond dust into a nuclear emulsion. The diamond particles are transparent, so that the interesting disintegrations could easily be picked out.

Analysis of carbon nucleus disintegrations[2] leads to the conclusion that 51% of the disintegrations are not accompanied by tracks of length $R \leq 50\mu$. (In the following, disintegrations unaccompanied by short tracks will be called L_2 disintegrations, while those which do have tracks of length $R \leq 50\mu$ will be called L_1 disintegrations.) In his study of C, N, and O due to protons with energy 1 Bev, Philbert[3] found that 55% of the disintegrations were L_2. Comparing this number with the fraction of L_2 disintegrations that we observed, we find support for the conjecture made above that the fraction of L_2 disintegrations increases with increasing energy of the bombarding particle.

Thus the potential barrier criterion eliminates more than half of the disintegrations of light nuclei.

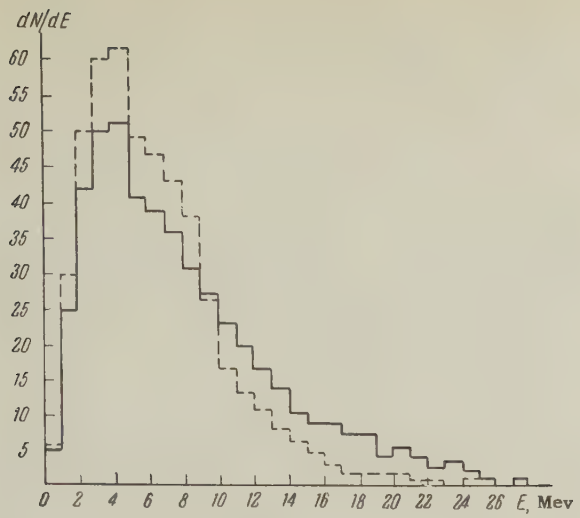

FIG. 1. Energy distribution of α particles from the disintegration of C^{12}. Solid curve – all disintegrations, dotted curve – L_1 disintegrations.

It is interesting to compare the results for the groups L_1 and L_2.

The energy distributions of α particles and protons from C^{12} stars are shown in Figs. 1 and 2. The solid line refers to all stars, while the dotted one refers only to the group L_1. The spectra in each group are normalized to the same total number of particles. Both the α particle and the proton spectra differ somewhat for the two groups. This difference is apparently due to the way the L_1 group is defined, and does not reflect a real difference between the mechanisms for disintegration in the groups L_1 and L_2. This conclusion is supported by the angular distributions in Figs. 3 and 4. The angular distributions are for the same particles, α's and protons, whose energy distributions were given in Figs. 1 and 2. Figures 3 and 4 show that the angular distributions for groups L_1 and $L_1 + L_2$, and hence for L_1 and L_2, are the same.

Our conclusion, that there is no real difference between the mechanisms for formation of stars with short tracks and those which do not have short tracks, is directly opposite to the conclusion drawn

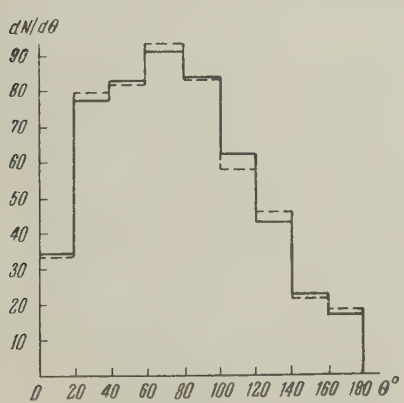

FIG. 3. Angular distribution of α particles from disintegration of C^{12}. Solid curve – all disintegrations, dotted curve – L_1 disintegrations.

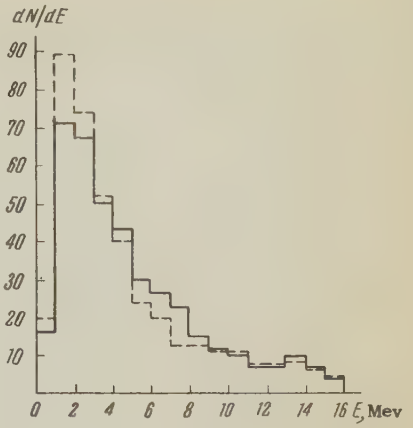

FIG. 2. Energy distribution of protons from disintegration of C^{12}. Solid curve – all disintegrations, dotted curve – L_1 disintegrations.

by Philbert and Vigneron,[4] who studied stars made by 1-Bev protons. In their work, L_2 stars were those having a number of tracks $n \leq 8$, total charge $Z \leq 9$, not containing the recoil nucleus. For L_1 disintegrations, the forward/backward ratio for black tracks was 1.91, while for L_2 disintegrations the corresponding number was 1.35. It was on this basis that Philbert and Vigneron drew their conclusion that there was a difference between the disintegration mechanisms in the two groups. However, their method for defining the L_2 disintegrations raises doubts, since this group will certainly contain stars on heavy nuclei, not containing the recoil nucleus. That this admixture to the group L_2 existed may be shown by the fact that the forward/backward ratio for heavy nuclei is 1.36. In the case of the interaction of 660 Mev protons with light and heavy nuclei in emulsions, the preliminary results presented in Sec. 3 show that, using the definition of L_2 disintegrations adopted by the author, the number of disintegrations of Ag and Br is 1.5 to 2 times greater than the number of disintegrations of light nuclei.

On the other hand, it is possible that the difference between the conclusion drawn in reference 4 and the one drawn here is due to the difference in proton energy. At 1 Bev, meson production is more important than at 660 Mev, and it is by the absorption of mesons that Philbert and Vigneron explain their results.

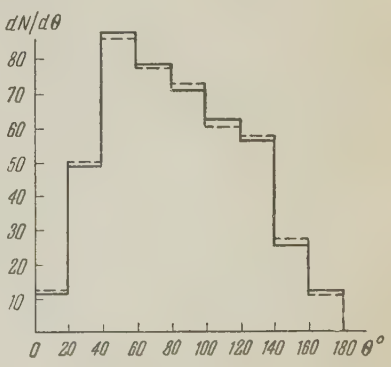

FIG. 4. Angular distribution of protons from disintegration of C^{12}. Solid curve – all disintegrations, dotted curve – L_1 disintegrations.

In addition to comparing the energy and angular distributions in the groups L_1 and L_2, we also compared the types of reactions. The results are shown in the table.

Type of disintegration*	Percent disintegrations	
	L_1	L_2
$2p2\alpha$	50±8.0	38±6.0
$4p\alpha$	18.7±4.5	14.3±3.7
3α	13.8±4.0	2.4±1.5
$p\alpha$ Li	7.5±2.5	14.3±3.7
$2p$ Be	6.2±2.3	11.9±3.4
$6p$	0	9.5±3.0
$2p2\alpha\pi^+$	2.5±1.5	2.4±1.5
$3p$ Li	1.3±1.0	4.8±2.2
$5p$Li π^-	0	2.4±1.5

*Reactions leading to C^{10}, C^{11}, B^{10}, and B^{11} are not considered. The cross sections for these reactions are given in reference 2.

From this table, it appears that there is no difference between the groups L_1 and L_2 as far as types of reaction are concerned, except for stars of type 6p, which appear only in group L_2, and stars 3α, which belong primarily to L_1.

The mean excitation energies for disintegrations in groups L_1 and L_2 are 37 Mev and 55 Mev respectively. The mean excitation energy of 43 Mev is in good agreement with the 42 Mev given by Monte Carlo calculations on the interaction of 660 Mev protons with carbon.

The difference between the mean excitation energies in groups L_1 and L_2 is due to the uneven distribution of 6p and 3α stars over the two groups and the substantial difference between the mean nuclear excitation energies for these two types of stars.

3. ADMIXTURE OF HEAVY-NUCLEUS STARS HAVING TRACKS OF LENGTH $R \leq 50\mu$

The use of the potential barrier criterion to pick out disintegrations of light nuclei introduces a certain admixture of heavy nucleus disintegrations (Ag and Br). To estimate the magnitude of this effect, we studied the disintegration of light and heavy nuclei induced by 660 Mev protons incident on a NIKFI-R type emulsion, registering particles of minimum ionization. All disintegrations were divided into two classes: those with track lengths $5\mu \leq R \leq 50\mu$, and all other (tracks of length $R < 5\mu$ were due to recoil nuclei). Disintegrations of C, N, or O and disintegrations of Ag or Br entered into both of these groups.

Let T_1 be the number of heavy-nucleus stars which do have tracks of length $5\mu \leq R \leq 50\mu$, and T_2 be the number which do not. As mentioned above, L_1 and L_2 are the corresponding numbers for light nuclei. To find T_1, T_2, L_1 and L_2 we can use the following system of equations:

$$L_1/L_2 = C_1, \quad L_1 + T_1 = C_2, \quad L_2 + T_2 = C_3,$$
$$\frac{L_1 + L_2}{T_1 + T_2} = \frac{\sigma_{aC} n_C + \sigma_{aN} n_N + \sigma_{aO} n_O}{\sigma_{a\,Br} n_{Br} + \sigma_{a\,Ag} n_{Ag}}, \qquad (1)$$

where C_1, C_2 and C_3 are experimental constants, σ_{aC}, σ_{aN}, σ_{aO}, σ_{aBr}, σ_{aAg} are the cross sections for absorption of 660 Mev protons by C, N, O, Br and Ag, while n_C, n_N, n_O, n_{Br} and n_{Ag} are the numbers of C, N, O, Br and Ag atoms per unit volume of emulsion.

Analysis of C^{12} disintegrations gives the ratio $L_1/L_2 = 0.96$. C_2 and C_3 were obtained by counting the number of disintegrations having short tracks, and those where all the tracks were longer than 50μ. Since the plates were scanned in two dimensions, all one prong stars and most two prong stars with "gray" tracks were not counted. Hence the number of stars we found in the emulsion must be corrected for the unobserved stars corresponding to the reactions (p, pxn) and (p, 2pxn) on the nuclei C, N, O, Ag, and Br. Taking into account unobserved one and two prong stars, we had 2190 disintegrations. Of these, 450 had tracks with length $5\mu \leq R \leq 50\mu$ while 1740 had only tracks with $R > 50\mu$. The absorption cross section for the various nuclei in the emulsion were taken from a curve of σ_a against atomic number for 650 Mev protons, as constructed from the data of Moskalev and Gavrilovskiĭ.[5] Substituting our values of C_1, C_2 and C_3 into (1), and the values of σ_a and n for the nuclei in the emulsions, we obtain the following values for the numbers of stars in the sub-groups L_1, L_2, T_1 and T_2:

Number of disintegrations with short tracks and on light nuclei	$L_1 = 264$
Number of disintegrations without short tracks and on light nuclei	$L_2 = 276$
Number of disintegrations with short tracks and on heavy nuclei	$T_1 = 186$
Number of disintegrations without short tracks and on heavy nuclei	$T_2 = 1264$

Comparing T_1 and T_2, we find that the potential barrier criterion breaks down in 12.8% of Ag and Br disintegrations. However, we are mostly interested in how many heavy nuclei are admixed to the group of light nuclei with short tracks.

The following is the distribution of the short track distributions $L_1 + T_1$ by number of prongs:

Number of prongs	2	3	4	5	6	7	8	9	10	11	12	13
Number of disintegrations	12	68	90	108	58	42	38	12	12	4	4	2

All stars with 9 or more prongs we consider to belong to Ag and Br, since all tracks with $5\mu \leq R \leq 50\mu$ we take to belong to α particles, except of course for the case $Z > 2$ (over a short range it is impossible to distinguish between singly and doubly charged particles).

For carbon, we found that 10% of the disintegrations of type L_1 have tracks with length $R < 5\mu$. If the same fraction holds for C, N, and O (it is at least not less than 10%), then the number of L_1 disintegrations having tracks with length $R < 5\mu$ is 26. There are 110 tracks in the group $L_1 + T_1$ with tracks of length $R < 5\mu$. Then 84 of the disintegrations with tracks of length $R < 5\mu$ must be due to the nuclei Ag and Br. Furthermore, of the 332 stars remaining in the group $L_1 + T_1$, having $n \leq 8$ prongs and not containing tracks with $R < 5\mu$, 20 have total charge $Z > 9$ and hence must be disintegrations of heavy nuclei.

Hence we conclude that the number of light nuclei disintegrations satisfying the potential barrier criterion and having total charge $Z \leq 9$ is 312 [450 − (84 + 34 + 20)]. Actually, (1) gives 264 as the number of L_1 disintegrations. Hence, application of the potential barrier criterion for picking out disintegrations of light nuclei would have included 48 stars satisfying the criterion $\Sigma Z \leq 9$ but due to Ag and Br. The admixture, 19%, so obtained may be an under-estimate since we assumed that the fraction of C, N, and O disintegrations with track lengths $R < 5\mu$ is the same as for C^{12}. Actually, the number of such disintegrations in a mixture of C, N, and O nuclei might be somewhat larger.

Our value, 12.8%, for the fraction of Ag and Br disintegrations which do not satisfy the potential barrier criterion is in good agreement with the value (15%) obtained by Philbert[3] for 1-Bev protons. As is to be expected, increasing the energy of the incident particle makes it more likely that the heavy nucleus emit a slow α particle.

In conclusion the author would like to express his deep gratitude to A. P. Zhdanov for his constant interest in this work, to L. I. Shur and I. V. Ryzhkova who invested much time and effort in preparing the emulsions for the experiment with carbon and to G. M. Subbotina for help in working over the experimental material.

[1] A. P. Zhdanov and P. I. Fedotov, Приборы и техника эксперимента (Instrum. and Meas. Engg.) **3**, 133 (1959).

[2] A. P. Zhdanov and P. I. Fedotov, JETP **37**, 392 (1959), Soviet Phys. JETP **10**, 280 (1960).

[3] G. Philbert, J. phys. radium **18**, 75 (1957).

[4] G. Philbert and L. Vigneron, Compt. rend. **247**, 290 (1958).

[5] V. I. Moskalev and B. V. Gavrilovskiĭ, Dokl. Akad. Nauk SSSR **110**, 972 (1956); Soviet Phys.–Doklady **1**, 607 (1956).

Translated by R. Krotkov
187

ON THE CRITICAL MODE IN EXPERIMENTS WITH AN OSCILLATING DISK IN HELIUM II*

G. A. GAMTSEMLIDZE

Tbilisi State University

Submitted to JETP editor May 12, 1959

J. Exptl. Theoret. Phys. (U.S.S.R.) **37**, 950-955 (October, 1959)

The results of measurement of the damping of an oscillating disk immersed in helium II are given. The onset of the critical mode and the motion of the disk at supercritical velocities were investigated, and also the dependence of critical velocity on temperature and period of oscillation. The critical velocity was found to be influenced by the cleanliness of the surface. In this connection, the dependence of critical velocity on the number and size of small particles deposited on the disk surface, and also on the radius of the region covered by the particles, was studied. The dependence of the damping in the supercritical regime on temperature, particle concentration, and radius of the contaminated region was also examined.

It was established by Andronikashvili and Kaverkin,[1] Osborne,[2] Hollis-Hallett,[3] Benson and Hollis-Hallett,[4] and others that in the supercritical mode the superfluid fraction of helium II partakes both in rotational and in oscillatory motion.

The onset of the critical mode for rotational oscillations of a disk is characterized by a critical amplitude, Φ_k above which an extra damping appears, $\Delta\gamma = \gamma' - \gamma_n$ where γ_n is the damping of the oscillating system in the subcritical mode, determined by the action of the normal component of helium II on the disk, and γ' is the damping in the supercritical mode.

Andronikashvili[5] and Smith[6] first studied the amplitude dependence of the logarithmic decrement of a pile of disks and of a single disk immersed in helium II, and oscillating about its axis. In both experiments the damping was found to be independent of amplitude at $\Phi = 0.2$ radians (maximum velocity 0.6 cm/sec for the pile and 0.25 cm/sec for the disk).

The critical phenomena were first studied by Hollis-Hallett,[3] who found the onset of the critical mode for motion of a single disk at a velocity $v_k = 0.1$ cm/sec ($T = 1.46°K$, period 11 sec), giving rise to an increase in damping decrement. For a pile of disks the minimum value of the critical velocity was determined as $v_k = 0.05$ cm/sec and at this value both the decrement and the density of the normal component increased. In view of the discrepancy between the results of Andronikashvili[5] and Smith,[6] on the one hand, and of Hollis-Hallett[3] on the other, we thought it appropriate to investigate the conditions for the onset of the critical regime in experiments with oscillating disks.

APPARATUS

The smooth polished disk 20 (see Fig. 1) of radius $R = 1.60$ cm was hung, by means of a glass rod 17 and a clamp 12, on a phosphor bronze thread 10, of diameter 50 μ and length 150 mm (in some experiments a 100 μ thread was used). The other end of the thread was fixed by clamp 9 to the rod 6 which was joined to the head A by means of screw 4. The head was screwed to the end of tube 5 of the stuffing box 8. By turning the head 1 the screw 2 was screwed out of the plate 3 and the whole suspension system, together with the plate, was lowered. When the small rod 13 rested on the brass ring 14, fixed between the plated rods 11, the balance was freed from the tension and the system came to rest.

The upper part of the suspension system was contained in the glass cylinder 7, while the lower part (the glass rod 17 and the disk 20) was surrounded by the glass tube 18 and the beaker 19, fitted to it by the ground glass join to protect the oscillating system from external disturbing influences. The glass cylinder 7 was sealed with picein near tube 5 and cone 16.

Observation of large amplitude oscillations was made with the help of a light spot focussed onto a circular scale after reflection from the mirror 15. The scale had its center on the axis of rotation and was of 18 cm radius. Small amplitudes were meas-

*Presented at the Fifth All Union Low Temperature Physics Conference, Tbilisi, October 1958.

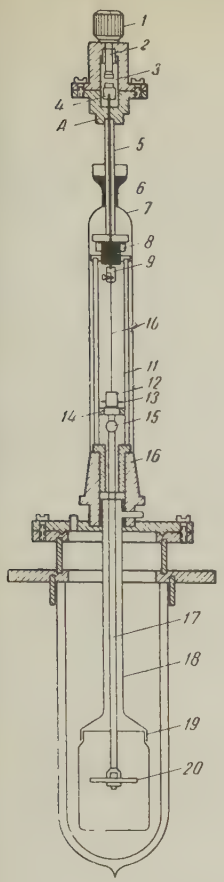

FIG. 1. Diagram of apparatus.

ured by a mirror (not shown in the figure) and light pipe PS-35. Both mirrors were fixed to the glass rod by cement BF-4 in such a way that their planes passed through the axis of the rotating system.

The system was set into oscillation by bringing a permanent magnet up to the rod 13.

The period of oscillation Θ was determined by timing a large number of swings (50 to 150).

STATEMENT OF THE PROBLEM

It follows from the definition of the critical amplitude that above it a dependence of damping on amplitude must appear, i.e., the linear relation between $\ln \Phi$ and the number of oscillations, n, must break down. By finding the amplitudes corresponding to this departure on $\ln \Phi = f(n)$ plots at different temperatures, the temperature dependence of the critical amplitude can be found.

In our experiments the amplitudes of oscillation of the disk, Φ_n, were determined from the swing, A, of the light spot along the circular scale of radius r, from the equation

$$\Phi_n = A / 4r = (a_n + a_{n+1}) / 4r, \qquad (1)$$

where a_n and a_{n+1} are the values of the extreme positions of the spot on the scale. (The dependence of log A on the number of oscillations, n, at different temperatures is shown in Fig. 2). The damping, γ, is derived from the relation

$$\gamma = (2.302 / \Theta)\, d(\lg A_n) / dn. \qquad (2)$$

The well-known relation between v and Φ:

$$v_k = (2\pi / \Theta)\, \Phi_k R, \qquad (3)$$

was used to calculate the critical velocity, where R is the radius of the oscillating disk.

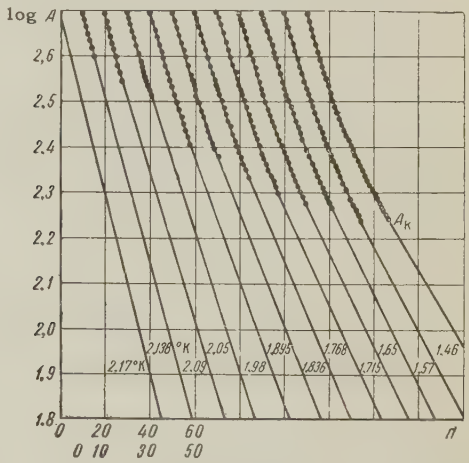

FIG. 2. Dependence of the logarithm of the full amplitude of oscillation of the light spot on the number of oscillations, at the different temperatures shown on the curves in °K (disk radius R = 1.605 cm and Θ = 8.95 sec). The points show the transition to the supercritical mode. The origin of the abscissa scale moves by n = 10 to the right for each succeeding curve relative to the previous one.

DESCRIPTION OF THE EXPERIMENTS

Determinations of critical velocities were made with several disks of different thicknesses and the period of oscillation varied between 3.4 and 14.5 sec. For disks with the cleanest surfaces we obtained the temperature dependence of critical velocity shown in Fig. 3. Bearing in mind the experimental errors, which reached 6 to 7% in these experiments, we can conclude that the critical velocity is independent of the period of oscillation for periods between 6.85 and 14.5 sec (lower curve of Fig. 3).

The data of Hollis-Hallett are shown in the figure for comparison. Our values of critical velocity are 1.5 to 3 times larger, and at some temperatures even 4 times larger than his corresponding results. Our data also differ from those of Hollis-Hallett in that the critical velocities measured on a 3.42-sec period disk (the upper curve of Fig. 3), lie above the curve for the larger periods, and almost join it. In Hollis-Hallett's work the 3.78 and 3.15 sec oscillations give twice the value obtained with a period of 11 sec. We should remark that

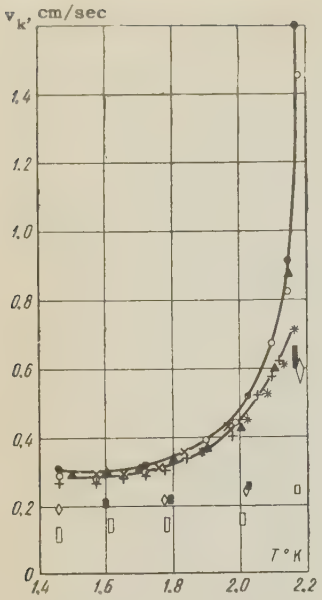

FIG. 3. Temperature dependence of critical velocity for smooth disks with radius R = 1.605 cm for periods of oscillation: ○, ●—3.42 sec, *—6.85 sec, +— —8.95 sec, ×— 14.45 sec, ▲—values derived from Eq. (4). Hollis-Hallett's data[3] for a single disk of radius R = 1.572 cm and period: ■—3.15 sec, ◇—3.78 sec, □—11 sec: The height of the points corresponds to the experimental uncertainty.

our critical velocities are close to those found by Andronikashvili in his experiments on a pile of oscillating disks when laminar flow was not destroyed.

An empirical relation between v_k and temperature leads to the conclusion that

$$v_k = 0{,}105/\sqrt{\rho_s} \text{ cm/sec}, \qquad (4)$$

while from Hollis-Hallett's work it follows that $v_k \sim \rho_s^{-1/3}$. The triangles in Fig. 3 show the critical velocities calculated from (4).

During observations of torsional oscillations of a disk we noticed that the critical mode is reached at considerably lower amplitudes if the surface of the disk is contaminated, even very little, by granules of solid air. We made some measurements with contaminated surfaces to investigate this phenomenon, and deposited particles 0.05, 0.1, and 0.2 mm in size on the surface. Figure 4 shows the relation $\Phi_k = f(T)$ for various sizes of contaminating grains. The value of the critical velocities for rough surfaces also depends on the concentration, c, of particles (Fig. 5) and it can be seen that the critical velocity falls by a factor of at least 3 as the concentration of particles increases from 0 to 250 particles per

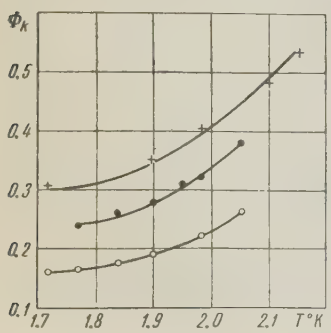

FIG. 4. Temperature dependence of critical amplitude for different contaminating grain sizes: +—0.05 mm, ●—0.1 mm, ○—0.2 mm. in all cases there were 250 particles per cm².

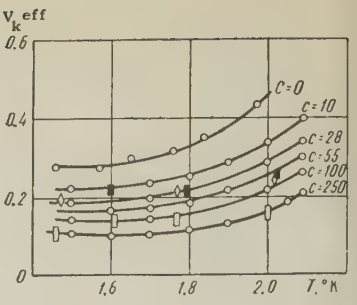

FIG. 5. Temperature dependence of effective critical velocity for different particle concentrations (c is the number per cm²). ■, ◇, □ —data of Hollis-Hallett (see Fig. 3).

cm². The dimensions of all the grains we used were considerably smaller than the penetration of viscous waves in the normal component of the liquid, so that they did not affect the damping until the critical mode was reached.

We show Hollis-Hallett's data (rectangles) together with our own (points) on the curves of temperature dependence of critical velocity for rough surfaces (Fig. 5). It can be seen that his results agree with ours for rough surfaces so that there was evidently contamination present in his experiments.

As the radius of the contaminated region, R_c, decreases, the critical amplitude increases so that the product $\Phi_k R_c$ stays constant (Fig. 6). In our experiments R_c varied from 16 to 6 mm.

An analysis of the temperature dependence of the extra damping $\Delta\gamma$ confirms Hollis-Hallett's conclusion that $\Delta\gamma \sim \rho_s$. All the increase in damping is therefore, in fact, connected with the superfluid component taking part in the motion of the disk.

Besides the magnitude of the critical amplitude, the decrement, γ', in the supercritical mode also depends on the degree of contamination. The dependence of $\Delta\gamma$ in the supercritical region on particle concentration is shown in Fig. 7. It follows from Fig. 8 that $\Delta\gamma$ is proportional to the area of contaminated surface.

Figure 9 shows the amplitude dependence of the total damping, at different temperatures, for a disk with period $\Theta = 8.95$ sec. It can be seen that the transition region, where the superfluid component does not take full part, gradually narrows as the λ-point is approached (see also Fig. 2).

DISCUSSION OF THE RESULTS

1. The temperature dependence of critical velocity [Eq. (4)] is apparently connected with the quantization of energy of a vortex, and indicates that the critical mode is attained with the expenditure of a given amount of energy.

2. The reduction of critical velocity for contaminated surfaces seems apparent. This reduction can be explained by the fact that one is measuring

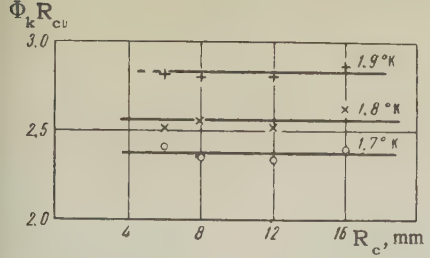

FIG. 6. Dependence of critical amplitude on the radius of the contaminated region, R_c, at different temperatures.

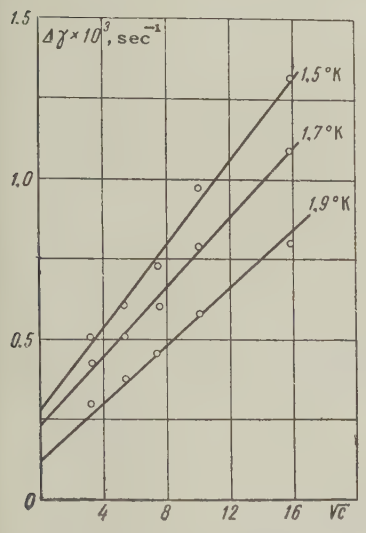

FIG. 7. Dependence of extra damping, $\Delta\gamma$, on particle concentration, c, at different temperatures.

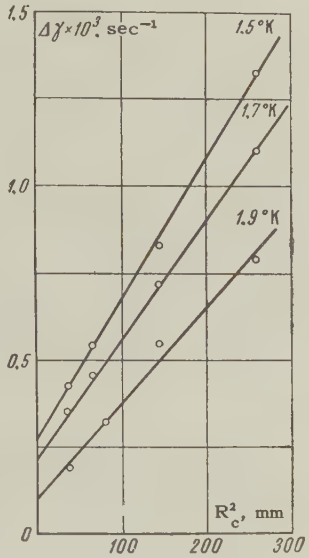

FIG. 8. Dependence of extra damping on the radius of the contaminated region.

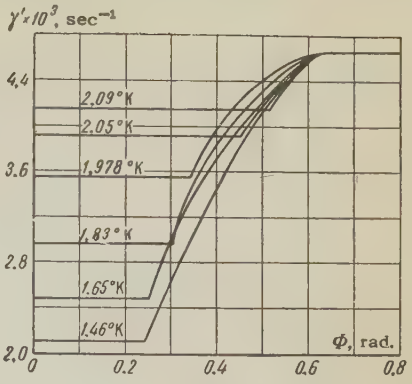

FIG. 9. The amplitude dependence of total damping γ' at different temperatures. Disk radius R = 1.605 cm and Θ = 8.95 sec.

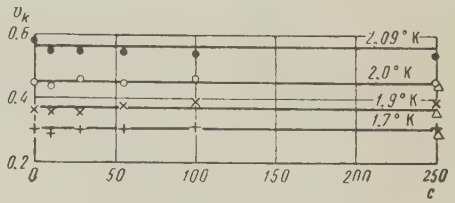

FIG. 10. Independence of the true critical velocity of the concentration at different temperatures and for different grain sizes: ●, ○, +—0.2 mm, △—0.1 mm.

the speed of motion of the disk, and when contamination is present this does not coincide with the speed of the motion of the liquid relative to the oscillating surface. The difference between these is due to the increase in effective path of the superfluid component while the time for the motion, determined by the period of oscillation, remains the same.

The increase in path is determined by the concentration and size of the particles. Making the correction for the increase in flow velocity we obtain the following relation for the critical velocity:

$$v_k = v_k^{\text{eff}}(1 + k\pi d\sqrt{c}), \qquad (5)$$

where v_k^{eff} is the effective critical velocity, i.e., the velocity of the disk, $v_k^{\text{eff}} = (2\pi/\Theta)\,\Phi_k^{\text{eff}} R$, d is the mean linear dimension of the grains, c is their concentration and k = 1.75 is a constant. Figure 10 shows the values of v_k calculated from (5). These values are independent both of concentration and of size of particles and agree well with the results obtained with smooth disks.

3. The constancy of the product $\Phi_k R_c$ found for radii of the particle-covered region from 16 to 6 mm, shows that the critical velocity is independent of radius. Apparently the critical mode is always reached on the periphery of the contaminated region at the same value of the velocity.

4. The dependence of the extra damping on the degree of contamination (Fig. 7) can also be explained by an increase in the mean velocity of the liquid, which must lead to an increase in the number of vortices.

It is a pleasure to thank Prof. É. L. Andronikashvili and Yu. G. Mamaladze for discussion of the results and for valuable advice. I also thank R. A. Bablidze, G. A. Udzulashvili, and N. G. Baazov for help in carrying out this work.

[1] É. L. Andronikashvili and I. P. Kaverkin, JETP **28**, 126 (1955); Soviet Phys. JETP **1**, 174 (1955).

[2] D. V. Osborne, Proc. Phys. Soc. **A63**, 909 (1950).

[3] A. C. Hollis-Hallett, Proc. Roy. Soc. **A210**, 404 (1952).

[4] C. B. Benson and A. C. Hollis-Hallett, Canad. J. Phys. **34**, 668 (1956).

[5] É. L. Andronikashvili, Thesis, Institute for Physical Problems, Moscow (1948).

[6] P. L. Smith, Physica **16**, 808 (1950).

Translated by R. Berman
188

INELASTIC SCATTERING AND ABSORPTION OF (195 ± 15)-Mev POSITIVE PIONS BY CARBON AND LITHIUM NUCLEI

N. I. PETROV, V. G. IVANOV, and V. A. RUSAKOV

Joint Institute for Nuclear Research

Submitted to JETP editor May 13, 1959

J. Exptl. Theoret. Phys. (U.S.S.R.) **37**, 957-965 (October, 1959)

The inelastic scattering and absorption of (195 ± 15) Mev π^+ mesons with carbon and lithium nuclei were investigated using the method of the Wilson cloud chamber in a magnetic field. The total and differential cross sections for inelastic scattering and the summed total cross section for charge exchange scattering and pion absorption were determined. A comparison of the experimental data obtained with the results of the cascade calculation in the carbon nucleus was made, and it was shown that the inelastic scattering of mesons is satisfactorily described on the basis of the pair collision hypothesis. It was established that only two nucleons in the nucleus take part actively in the absorption of (195 ± 15) - Mev pions; here the probability of meson capture by n, p pairs is 2 or 3 times greater than that of capture by pairs of like nucleons.

THE experimental data relating to the inelastic scattering of pions with complex nuclei is in satisfactory agreement with the pair interaction model developed in the papers of Serber and Goldberger.[1,2] Of special interest from the point of view of verifying this model are the processes of inelastic scattering of incident pions in their first interaction with the nucleons in the nucleus (called afterward the primary processes of inelastic scattering) in which the scattered pion and the recoil nucleon leave the nucleus without further collisions. However, as a result of the fact that the majority of the experiments previously carried out studied the interaction of negative pions with heavy nuclei, the experimental material on the primary inelastic scattering processes is very scanty.

In the present work with positive pions, thanks to the use of the light nuclei carbon and lithium as targets, such processes of the interaction were detected with a measurable probability, so that the values of the cross sections and angular distributions for them could be determined. Besides this, observations of the positive pion capture processes in which fast nucleons formed left the nucleons without undergoing collisions made it possible to construct a picture of the absorption of fast pions by light nuclei.

The experimental data obtained were compared with the results of a cascade calculated for the carbon nucleus which included 560 separate trials.* In that calculation the carbon nucleus was considered as a degenerate Fermi gas of nucleons with a maximum kinetic energy E = 25 Mev contained in a square well potential 34 Mev deep; the well radius was 3.2×10^{-13} cm. Pion absorption was treated on the basis of a quasi-deuteron model, where the coefficient connecting the pion capture cross section by n, p pairs in the nucleus and by free deuterons was chosen such that the calculated inelastic scattering cross section was equal to the experimental cross section. The value of this coefficient was 5. The initial energy of the pions in the cascade calculation was taken as 230 Mev, applicable to the data in the work of V. P. Dzhelepov et al.[3] with negative pions.*

The work was carried out on the synchrocyclotron of the Joint Institute for Nuclear Research by bombarding carbon and lithium targets set in a Wilson cloud chamber with (195 ± 15) - Mev positive pions. The experimental procedure has been described in a separate communication,[4] in which data are given on the inelastic scattering of positive pions by the same nuclei.

RESULTS OF THE EXPERIMENT

In the bombardment of the chamber by the pion beam 693 acts of an inelastic interaction with carbon and 508 with lithium were detected. The meas-

*The cascade calculation for the carbon nucleus was carried out by Yu. A. Budagov, V. G. Ivanov, and N. I. Petrov.

*Although the calculated data refer to an initial meson energy of 230 Mev, the majority of them are reasonable for 195-Mev mesons. In some cases, where unavoidable, the calculated data are related to the 195 Mev initial energy.

TABLE I

Nucleus	Sign of pion	Energy, Mev	Total cross sections, 10^{-27} cm²		
			Inelastic scattering	Stars and stoppings	All inelastic processes
C	+	195	122±13	203±22	325±26
Li	+	195	62±9	164±16	226±18

ured total cross sections are given in Table I.

The inelastic scattering data refer to the angular interval 10 — 180°. The measurement errors include only the statistical deviation and the errors in separating the elastic and inelastic scattering.

Inelastic scattering. In Figs. 1 and 2 are given the experimental angular distributions of inelastic scattering for both nuclei and also the calculated distribution for carbon nuclei and the angular distribution for the elastic scattering of 200 Mev positive pions from free protons;[5] here the two last distributions were normalized to the value of the experimental total cross section for inelastic scattering by a carbon nucleus. Comparing these figures we see that on going over from free to bound nucleons a change takes place in the form of the angular distribution, included in the increase of the scattering cross section in the angular region near 180°. The general character of this change is correctly shown by the calculated distribution. The calculation also shows that the effect of the increase of the backward scattering cross section should become weaker in direct proportion to the growth of the energy (as long as the range of the mesons in the nuclear substance increases). This conclusion is strengthened by the experimental data for 250 — 270 Mev positive pions,[6] according to which the inelastic scattering distribution for carbon differs little from the corresponding elastic scattering from free nucleons. It must be noted, however, that there is no rigorous quantitative correspondence between the experimental and the calculated angular distributions: in comparison with experiment the calculation underestimates the value of the cross sections in the large-

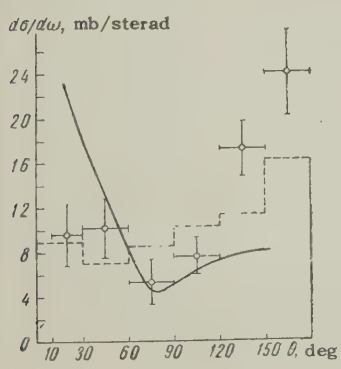

FIG. 1. Angular distribution of inelastic scattering of mesons on carbon nuclei. The dotted line shows the calculated angular distribution for inelastic scattering of positive pions with initial energy E_0 = 230 Mev on carbon nuclei; the solid line shows the angular distribution for the elastic scattering of positive pions with energy E = 200 Mev from free protons.

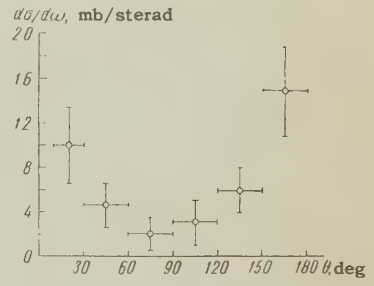

FIG. 2. Angular distribution for positive pion inelastic scattering from lithium nuclei.

and small-angle scattering regions. This circumstance can be looked at as an indication of the difference between the angular distributions for pion scattering from free and bound nucleons, which, according to the work of Watson and Zemach,[7] can depend on the influence of the potential that describes the interaction of particles with atomic nuclei in the framework of the optical model on the pion-nucleon collision in the nucleus.

The calculated and observed energy distributions of the mesons inelastically scattered in the angular intervals 0 — 60° and 120 — 180° are shown in Figs 3 and 4. Since the average energies (see Table II) of the scattered particles for carbon and

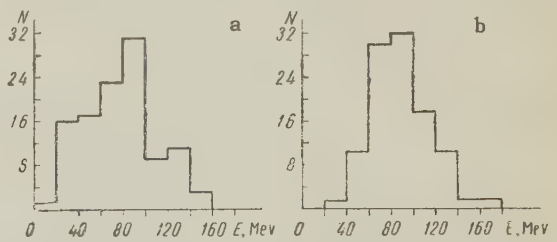

FIG. 3. Energy spectrum of positive pions inelastically scattered in the angular interval $\Delta\theta$ = 120–180°. a — total experimental spectrum. b — calculated spectrum for E_0 = 230 Mev mesons.

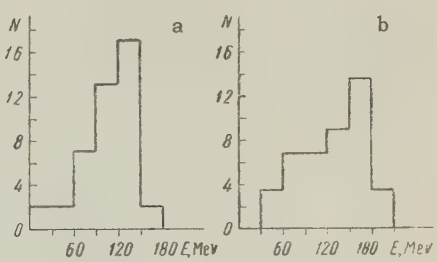

FIG. 4. Energy spectrum of positive pions inelastically scattered in the angular interval $\Delta\theta$ = 0–60°. a — total experimental spectrum. b — calculated spectrum for E_0 = 230 Mev mesons.

TABLE II

Nucleus	Initial energy and meson sign	Average energy, Mev			
		$\Delta\theta = 0$—$60°$		$\Delta\theta = 120$—$180°$	
		Experiment	Calculation	Experiment	Calculation
C	195 (+)	107	—	74	84
Li	195 (+)	104	—	78	—
C[3]	230 (—)	107	128	88	94

lithium practically coincide, the sum of the data has been used in constructing the histogram.

As can be seen from Figs 3 and 4 and Table II, there is satisfactory agreement between the distributions and the corresponding values of the average energy. This testifies that energy exchange from the incident pions to the nucleons in the nucleus proceeds essentially via quasi-elastic collisions with individual nuclei. Our data on the acts of the primary inelastic scattering of positive pions constitute further and more descriptive proof of this energy-exchange mechanism. Altogether 44 primary inelastic scattering acts were observed, out of which 25 were from carbon and 19 from lithium. As a criterion for selection we used the requirement that the sum of the energies of the scattered pion and of the recoil proton was not more than 30 — 35 Mev smaller than the energy of the incident pion. In Figs 5, 6, and 7 the distributions of the indicated interaction events (corrected for efficiency of observation) are given by meson scattering angle, by angle of separation, and by the difference in azimuthal angle of the scattered pion and the recoil proton. The corresponding calculated distributions are also given. The average values of the noncoplanarity of the angles, observed and calculated, are respectively 15° and 13°. The agreement between the calculation and the experimental data is satisfactory, considering the poor statistics. This shows that the collision of a pion with a nucleon in the nucleus proceeds in approximately the same way as with a free but moving nucleon. On this basis one finds, in particular, an explanation of the fact that the curve of the angular distribution for the selected primary inelastic scattering processes drops faster, beginning at a scattering angle of 180°, than the corresponding curve for the entire inelastic scattering. In fact, together with the decrease of the scattering angle, the energy given to the proton and correspondingly the length of its path in the nuclear substance decreases. This fact leads to a fall in the probability of the emission of a proton from the nucleus without collision, and so to a corresponding decrease in the cross section for primary inelastic scattering processes accompanied by the emission of energetic protons. However, even here, as for the entire inelastic scattering, the experimental scattering cross sections diverge significantly from those calculated in the angular region close to 180° (see Fig. 5). The indicated discrepancy is lessened if the calculated distributions are corrected for the influence of the optical potential, using the results of reference 7.

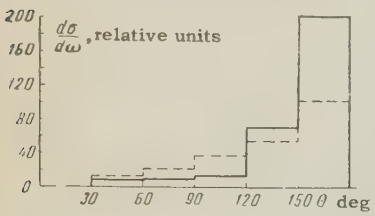

FIG. 5. Angular distribution of pions of primary quasi-elastic scattering processes. The calculated distribution is shown dotted.

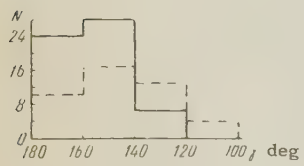

FIG. 6. Distribution of primary quasi-elastic scattering processes by angle of separation of the scattered pion and the recoil proton. The calculated distribution is shown dotted.

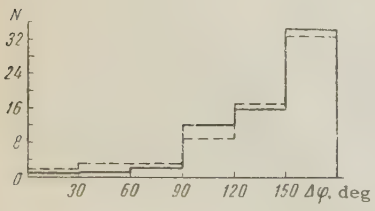

FIG. 7. Distribution of primary quasi-elastic scattering processes by difference of azimuthal angle between the scattered pion and the recoil proton. The calculated distribution is shown dotted.

Table III shows the values of the calculated and experimental probabilities* for the selected events of primary inelastic scattering in relation to the total number of inelastic interactions and also in relation to the total number of inelastic scatterings. The satisfactory agreement between the experimental and calculated probabilities indicates not only that the hypothesis of quasi-inelastic collisions is useful but also that the scattering cross sections for pions with bound nucleons do not differ greatly from the scattering cross sections for these particles with free nucleons. In this connection it is interesting to compare the data on inelastic scattering from carbon for positive and

*The calculated probabilities are corrected for the stoppings of recoil protons in the target.

TABLE III

Nucleus	Probability, %			
	In relation to the inelastic scattering cross section		In relation to the cross section for inelastic interactions	
	Experiment	Calculation	Experiment	Calculation
C	16	21	5,5	7,5
Li	25	—	7	—

TABLE IV

Nucleus	Energy in Mev and meson sign	N_1	N_2	Ratio N_2/N_1, %	
				Calculation	Experiment
C	230 (—)	64	10	16	23
C	195 (+)	91	50	55	50

negative pions. A comparison of the quantity (N_2) of inelastic scattering processes accompanied by the emission of a recoil proton from the target relative to the total inelastic scatterings (N_1) for the scattering angle interval 120 — 180° is given in Table IV.*

Considering that the calculated ratio changes little in going from 230 Mev to 195 Mev, we see that there is good agreement between the data for positive and negative pions. This fact also confirms the qualitative agreement between the experimental and calculated data obtained by Fry and Takeda[8,9] for the primary quasi-elastic scattering of 220-Mev pions by photoemulsion nuclei. For additional confirmation we can point out the agreement between the calculated and experimental cross sections for exchange scattering. The calculated exchange scattering cross section for carbon nuclei is (15 ± 3)%, and the experimental cross section for the same reaction, found for the elements contained in freon,[10] is (10 ± 3)% for a wide range of energies. To these numbers can be added the experimental estimate of the contribution of the exchange scattering of 125-Mev negative pions by carbon nuclei, obtained by Kessler and Lederman.[11] The data on the average number of pion collisions in the nucleus also testify to the usefulness of the hypothesis that the pion scattering cross sections for free and bound nucleons are not greatly different from each other. According to the calculation, the average number of pion collisions in a carbon nucleus is 1.5. This means that more than half of the inelastically scattered pions undergo only one collision in the nucleus. An estimate of the relative contribution of single scattering in the angular interval 120 — 180°, made for primary scattering acts (in which energy balance holds), is 60%. This obviously agrees with the calculated estimate and, in particular, strengthens the conclusion stated in reference 3 that the inelastic scattering of 230-Mev negative pions from carbon nuclei in the angular interval 120 — 180° proceeds predominantly as the result of single collisions of incident pions with nucleons in the nucleus. To end this section we indicate that the value of the momenta of the residual nuclei formed in the primary inelastic scattering of pions (determined for each process as the difference between the vectors of the initial momenta and of the total momentum of the scattered pion and the recoil proton) are included in the limits 0 to 400 Mev/c and are predominantly directed into the forward hemisphere. It must also be noted that, among all the primary inelastic scattering acts for pions from carbon and lithium nuclei, only one was found which could be interpreted as the direct knocking out of a deuteron by an incident pion.

Absorption of Pions. In investigating the mechanism of the absorption of pions in the low energy region from 0 to 60 Mev, it was found that small complexes of nucleons inside the nucleus, consisting mainly of one neutron and one proton, take part in the act of absorption. For example, according to the data of Byfield, Kessler, and Lederman[12] and Tenney and Tinlot,[13] 60 — 70% of the total absorption is contributed by the capture of pions by n, p pairs in the nucleus. Lately two papers[6,10] appeared in which the process of pion absorption was studied for the energy region 80 to 300 Mev; however, contradictory results were obtained for

*The geometry of the experiment is the same for both cases, and the number of inelastic scattering processes is therefore given without corrections for efficiency of observation.

TABLE V

Reaction	Pion energy	Number of protons, $\Delta\theta$ = 0–60°			Number of protons, $\Delta\theta$ = 120–180°		
		Total	With measured energy	$E>100$ Mev	Total	With measured energy	$E>100$ Mev
$\pi^+ + C$	195	365	213	67	96	63	3
$\pi^+ + Li$	195	254	180	48	40	27	5
$\pi^- + C$	230	71	54	17	11	8	5

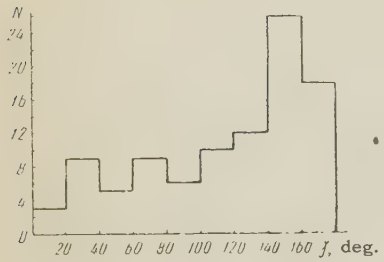

FIG. 8. Distribution of two-pronged stars by emission angle of the protons, for carbon nuclei.

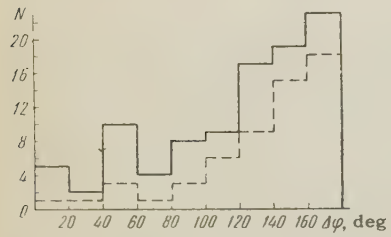

FIG. 9. Distribution of two-pronged stars by the difference of the proton azimuthal angles for carbon nuclei. The distribution for stars with $\gamma > 120°$ is shown dotted.

the mechanism of the capture reaction. In particular, to explain the observed distribution of stars by number of prongs, reference 6 draws on the hypothesis that the nucleus as a whole took part in the capture of 250 — 270 Mev pions in carbon.

In the present experiment 432 stars were detected in carbon and 344 stars in lithium.* As a basis for analysis of these data we determined the relative cross sections for the capture of positive pions by pairs of like and unlike nucleons and also found the relative contribution to the absorption by these particles in the first interaction with the nucleons in the nucleus. Table V shows the numbers of fast protons in the scattering angle interval 0 — 60° and 120 — 180°, including the formerly unpublished data from the experiments with negative pions.

It is evident from this table that a sharp anisotropy is seen in the angular distribution of fast protons, which is hard to explain from the point of view of the many-nucleon mechanism of pion absorption. A direct qualitative estimate of the contribution of pion capture by n, p pairs in the nucleus does not agree either with the supposition of the predominant role of the many-nucleon absorption mechanism.

When a positive pion is captured by a proton and neutron, producing fast protons scattered at an angle close to 180°, the difference of their azimuthal angles is also close to 180°, but the angle of noncoplanarity lies in a relatively narrow angular interval about 0°. In Figs. 8 and 9 are given the distributions of the protons by scattering angle and by the difference in their azimuthal angles for 97 two-pronged stars observed in carbon.* They show that among all the stars there are a considerable number (called by us, from here on, primary) both of whose protons leave the nucleus without experiencing collisions with other nucleons. It can also be seen from the distributions that the contribution of primary stars begins at the angle of emission $\gamma > 120°$ and at the azimuthal difference $\Delta\varphi > 120°$, where the average value of the angle of noncoplanarity is 12°. (A calculation taking account of the intranuclear motion of nucleon pairs gives identical regions of the distribution for the angles indicated.) To determine the true quantity of primary stars in the distribution of Fig. 9, all the stars with $\Delta\varphi \leq 120°$ can be looked at as a background of nonprimary stars which have to be subtracted from the number of two-pronged stars with $\Delta\varphi > 120°$. If the indicated selection rule for primary stars (one of whose prongs is included in the interval 120 — 180°)† is used and the calculated probability of counting primary stars, the correction for stars with prongs below the angle considered, and the contribution to the stars from the pion exchange scattering (equal to 32, 40, and 15%, respectively) are taken into account, we get that 65% of all the carbon stars and 44% of all the lithium ones depend on the absorption of pions by n, p pairs in the nucleus. The value of the cross section obtained for lithium nuclei is probably underestimated, since for them the exchange scattering contribution to the stars may be greater than for carbon nuclei because of the relative abundance of neutrons. Here, however, the possibility is not excluded that some decrease in the cross section for pion absorption by n, p pairs in lithium is connected with the increase of the relative contribu-

*For the analysis here all observed stars are used regardless of their distribution in the exposed region.

*The distribution is analogous for lithium nuclei.

†The emission angle interval 120–180° is excluded from the examination because the true proton spectrum is distorted there by ionization braking in the target.

tion of pion absorption by n, n pairs and by more complicated complexes of nucleons. The observation of one pion capture process by a deuteron and a neutron in lithium serves as an indication of the last situation.

We made an estimate of the contribution to meson absorption by pairs of identical nucleons by comparing the energy spectra of protons in stars formed by positive and negative pions in carbon.* The observed and calculated ratios for the number of fast protons in stars for negative pions and the analogous number for positive pions is given below for the emission angle interval 0 — 60°.

Energy of protons E, Mev	>70	>100	>120	>150
Experimental ratio, %	24	25	22	19
Calculated ratio for 100% absorption by n, p pairs, %	14	12	11	5
Calculated ratio for 70% absorption by n, p pairs and 30% absorption by pairs of identical nucleons, %	29	28	27	26

From this it is evident that pion absorption by pairs of identical nucleons takes place in carbon, but it takes place with a probability 2 — 3 times less than capture by pairs of unlike nucleons. It is obvious that the presence of a many-nucleon absorption mechanism exercises an influence on the size of this estimate especially in the case when the energy realized by the capture of the pion is divided very unevenly between the nucleons. However, if this mechanism were responsible for 30 — 40% of the whole absorption, a group of very fast, isolated protons would appear in the energy spectrum: at the same time, a difference between the energies of the fast particles from one- and two-pronged stars was not observed. Besides, for positive pions in the emission angle interval 120 — 180°, out of 65 protons whose momenta were measured, only two particles with energies greater than 120 Mev were found. Therefore, the contribution of the many-nucleon absorption mechanism is not great and so cannot markedly change the value of the estimate made.

An answer to the question about the relative contribution to the positive pion scattering by the first interaction with nucleons was obtained from the data on the measured total energies of the protons in the primary two-pronged stars. For example, for the carbon nucleus, out of 27 primary stars where the total momenta of both protons were measured, ten stars had a total energy of the protons as an average of 60 Mev less than the total energy of the incident pion. Keeping in mind that the emission of an n, p pair from a carbon nucleus necessarily takes up not less than 30 Mev, these facts must relate to the absorption of a pion in the first interaction. According to the calculation, the relative part of the absorption coming from the first interaction (in which one of the protons falls in the interval 120 — 180°) is 50%; the experimental ratio, 37%, is evidently in agreement with it. The same result is got by comparing the number of energetic protons in stars (by experiment and by calculation) for the interval 0 — 60°, applied to the identical number of stars. For example, the number of protons with energy E > 150 Mev, related for the greatest part to the first interaction, was observed to be 64 in the experiment, while calculated to be 80.

*For negative pions we used the data we got in 1956.

CONCLUSION

1. A comparison of the experimental data obtained with the results of a cascade calculation for the carbon nucleus shows that the inelastic scattering of (195 ± 15)-Mev positive pions from carbon is satisfactorily explained, within the limits of experimental error, by the hypothesis of pair collisions. This is expressed in the following:

a) the calculation gives correctly the general character of the change of the angular distribution of the elastic scattering of pions by free nucleons in the transition to the inelastic scattering of these particles by atomic nuclei;

b) the experimental energy distributions for inelastic scattering and the average values of the energy of inelastically scattered pions is in satisfactory agreement with the corresponding calculated data;

c) the relative cross sections for the primary inelastic scatterings accompanied by fast outgoing recoil protons is equal to the relative cross sections found in the calculations, within the limits of experimental error;

d) the kinematics for the experimentally observed processes of primary inelastic scattering (the angular distribution, and also the distribution by separation angle and difference of azimuthal angles of the scattered mesons and recoil protons) agree with the calculated kinematics for quasi-elastic pion scattering by moving nucleons.

2. A basic mechanism of the absorption of pions at 195 Mev is their capture by n, p pairs of nucleons. For carbon, this mechanism gives a contribution of 60 — 70%.

The contribution to the absorption cross section from meson capture by pairs of identical nucleons is $\frac{1}{3}$ to $\frac{1}{2}$ that from capture by pairs of unlike nucleons.

3. The proportion of captures of incident pions in the first interaction is not less than 35 — 40%

of the whole absorption.

The authors express their thanks to V. P. Dzhelepov for his constant interest in the work and his criticism of the results, to M. S. Kozodaev for his assistance in preparing the work, to A. M. Rozanova, I. M. Rudnevskaya, and P. I. Zhabin for their help in processing the exposures, to Yu. A. Budagov and G. P. Dolya for their help in making the nuclear cascade calculation, and to B. A. Nikol'skiĭ for acquainting us with a nomogram technique for the calculations. The authors also express their profound thanks to V. T. Osipenkov, who gave a great deal of assistance in the first part of the work.

[1] R. Serber, Phys. Rev. **72**, 1114 (1947).

[2] M. L. Goldberger, Phys. Rev. **74**, 1269 (1947).

[3] Dzhelepov, Ivanov, Kozodaev, Osipenkov, Petrov, and Rusakov, JETP **31**, 923 (1956), Soviet Phys. JETP **4**, 864 (1957).

[4] Ivanov, Osipenkov, Petrov, and Rusakov, JETP **37**, 863 (1959), Soviet Phys. JETP **10**, 615 (1960).

[5] Mukhin, Ozerov, and Pontecorvo, JETP **31**, 371 (1956), Soviet Phys. **4**, 237 (1957).

[6] Wang, Wang, Ding, Dubrovskiĭ, Kladnitskaya, and Solov'ev, JETP **35**, 899 (1958), Soviet Phys. JETP **8**, 625 (1959).

[7] K. M. Watson and C. Zemach, Nuovo cimento **10**, 452 (1958).

[8] W. F. Fry, Phys. Rev. **93**, 845 (1954).

[9] G. Takeda, Phys. Rev. **93**, 848 (1954).

[10] Blinov, Lomanov, Shalamov, Shebanov, and Shchegolev, JETP **35**, 880 (1958), Soviet Phys. JETP **8**, 609 (1959).

[11] J. O. Kessler and L. M. Lederman, Phys. Rev. **94**, 689 (1954).

[12] Byfield, Kessler, and Lederman, Phys. Rev. **86**, 17 (1952).

[13] F. N. Tenney and J. Tinlot, Phys. Rev. **92**, 974 (1953).

Translated by W. Ramsay
189

DIRECTED EMISSION OF PARTICLES FROM A COPPER SINGLE CRYSTAL SPUTTERED BY BOMBARDMENT WITH IONS UP TO 50 kev ENERGY

V. E. YURASOVA, N. V. PLESHIVTSEV, and I. V. ORFANOV

Moscow State University

Submitted to JETP editor May 18, 1959

J. Exptl. Theoret. Phys. (U.S.S.R.) **37**, 966-972 (October, 1959)

Sputtering of the (100) plane of a copper single crystal was studied for various energies and angles of incidence of argon and hydrogen ions. It is shown that the particles of the sputtered matter retain a favored direction of emission along some crystallographic directions ([100], [110], etc.) when the energy of the bombarding ions is raised up to 50 kev. Thus a deposit in the form of separate patches is formed on a screen parallel to the (100) face of the copper. The pattern of the deposit changes with increasing ion energy, but is practically independent of the angle of incidence of the particles. The density distribution law of the patches corresponding to the [110] and [100] directions has been studied. The spot material is distributed according to a cosine law. The relief of the (100) copper plane produced through sputtering by A^+ and H_2^+ ions with energies up to 50 kev was also studied. The data obtained cannot be reconciled with existing theoretical papers on cathode sputtering.

INTRODUCTION

THE sputtering of a substance by ion bombardment is a complex process, usually accompanied by many supplementary phenomena which make its investigation difficult. Therefore, in spite of the extensive material already accumulated on cathode sputtering,[1,2] the mechanism by which the ions interact with the sputtered substance is not yet clearly understood.[3-9]

We note that until recently only sputtering of polycrystalline samples in gas-discharge plasma was studied. This yielded averaged values for the measured quantities and made the interpretation of the results difficult. Many phenomena connected with the crystalline structure of the sputtered substance dropped out of view in this method. Consequently, the dependence of the sputtering coefficient and sputtering threshold of single crystals on the crystallographic direction was not formulated with sufficient rigor and was not investigated. Not until 1955 did Wehner[10] show that a metallic single crystal is sputtered most intensely in the close-packed crystallographic directions, if the bombarding-ion energy does not exceed 200 or 300 ev. It was proposed in reference 10 and other papers[7,8] that the preferred sputtering of a single crystal in particular directions would disappear if faster ions were used. However, in later experiments[11] the energy of the bombarding ions was raised to 5 kev and copper single crystals nevertheless were observed to sputter preferably in the close-packed [110] directions. In addition, it was noted that when the ion energy exceeded 1 kev, copper single crystals were intensely sputtered also in the [100] directions, which follow the [110] directions in the order of close packing.

It was deemed interesting to ascertain whether the sputtering coefficient of a metallic single crystal depended on the crystallographic direction at higher bombarding-ion energies (up to several times ten kev). We therefore investigated the sputtering of copper single crystals by beams of argon and hydrogen ions with energies up to 50 kev.

The use of an ion beam[12-15] offers many advantages over sputtering in gas-discharge plasma, where the number, energy, and angle of incidence of the ions cannot be determined accurately. The use of an ion beam has allowed us in the present investigation to study the sputtering of a single crystal copper by ions incident at various angles on the investigated (100) face.

EXPERIMENTAL SETUP

The experimental setup is illustrated in Fig. 1. The ion beam was produced by an ion gun, the principal element of which was an Ardenne-type[16] ion source with double contacting of the plasma, improved by several investigators.[17]

The ion gun produced a well focused beam (6 — 12 mm in diameter) of argon and hydrogen ions,

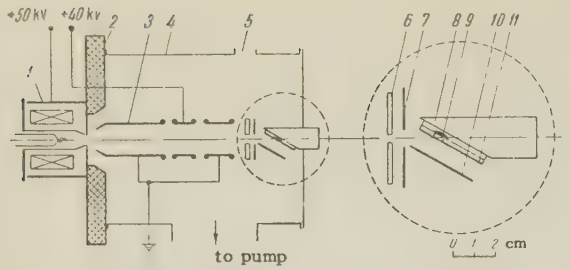

FIG. 1. Diagram of experimental setup: 1 – ion source, 2 – insulator, 3 – single electrostatic lens, 4 – container, 5 – viewing window, 6 – quartz screen, 7 and 10 – glass collectors, 8 – copper holder, 9 – copper single crystal, 10 – mica diaphragm.

the currents being 3 and 20 ma respectively at an accelerating voltage of 50 kv.

The ion beam, accelerated and focused by the single electrostatic lens, passed through an opening (4 – 8 mm in diameter) in a quartz screen and struck the specimen. The sputtered particles were deposited on a mica or glass collector, placed in front of the specimen parallel to its working surface. The collector used at normal ion incidence ($\alpha = 0°$), was a glass disk (7, Fig. 1) 80 mm in diameter with an opening 5 – 10 mm in radius for the ion beam. The collector for inclined beams ($\alpha = 45$ and $60°$) was a rectangular glass plate measuring 30×40 or 40×60 mm. The distance between the sputtered plane and the collector ranged from 16 to 20 mm.

The object was a single crystal of copper $15 \times 15 \times 5$ mm attached with low-melting point cadmium solder to a heavy water-cooled copper holder, so that the sample temperature did not exceed 100 – 200° C during the experiments. Before starting a series of experiments, the (100) face of the single crystal intended for the sputtering was ground and washed with alcohol. The dimensions of the sputtered surface were limited by a mica diaphragm with round hole of 5 to 6 mm diameter, placed over the working surface of the specimen.

The vacuum maintained in the container during the time of the experiments was $1 - 2 \times 10^{-5}$ mm Hg. The sputtering time and the ion-current density were adjusted experimentally until sufficiently sharp and contrasting sputtered patches were obtained, suitable for observation in transmitted light.

EXPERIMENTAL RESULTS

Beamed emission of particles at different energies, angles of incidence, and masses of the bombarding ions. We first investigated the sputtered substance deposited on the collector at normal incidence of argon ions on the target ($\alpha = 0$). Figure 2a shows the pattern produced on the collector when the (100) plane of single-crystal copper is bombarded with 8-kev ions. The photographs show that sputtering takes place essentially in four close-packed [110] directions from the (100) face, so that four symmetrical patches are produced on the collector (the distance between centers of the diagonal spots is twice the distance from the sample to the screen). The sputtered patches were elliptical, since the conical beams of sputtered material struck the collector at 45°. Figure 2a does not show the patch corresponding to the [100] direction since the atoms emitted from the target normal to the sputtered surface pass through the hole in the collector and fall on the quartz screen. Pictures similar to Fig. 2a were obtained also with 12, 20, 30, and 50 kev argon ions.

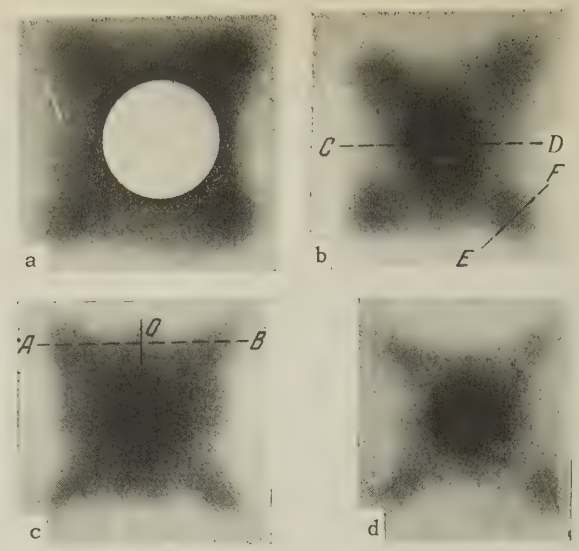

FIG. 2. Pictures of sputtered patches formed on the collectors under the following bombarding conditions:
a) A^+, E = 8 kev, $\alpha = 0°$, j = 0.02 ma/cm², τ = 55 min;
b) A^+, E = 10 kev, $\alpha = 60°$, j = 0.5 ma/cm², τ = 15 min;
c) A^+, E = 40 kev, $\alpha = 60°$, j = 0.6 ma/cm², τ = 20 min;
d) H_2^+, E = 40 kev, $\alpha = 60°$, j = 0.8 ma/cm², τ = 50 min.

The presence of a hole in the center of the collector for the passage of the ion beam did not permit us to investigate the central portion of the deposit at normal ion incidence. This became possible, however, when the investigated crystal plane and the collector plate parallel to it (on which the sputtered substance was deposited) were placed at a certain angle to the ion beam so that the latter passed beyond the collector and struck the specimen at an angle α. The most favorable angle for this purpose was 60° (the distance from the specimen to the collector being 16 mm).

Experiments have shown that when single-crystal copper was sputtered with an inclined beam of argon ions ($\alpha = 60$ and 45°), beamed emission of sputtered particles also takes place. The patterns

of the deposits on the collector are analogous to those obtained at normal incidence ($\alpha = 0$) on the target. In addition, it becomes possible in this case to observe the central maximum corresponding to the [100] direction (Figs. 2b and 2c). The intensity of sputtering increases greatly with increasing angle α. Thus, to obtain a deposit of equal intensity the specimen had to be sputtered by normal-incidence ions several times longer than at $\alpha = 60°$ (other conditions being equal).

The overall view of the deposit changes with increasing ion energy. Starting with an argon-ion energy of ~ 10 kev ($\alpha = 60°$) the central patch increases sharply, possibly because of the appearance of four new spots, due to sputtering of substance near the [113] and [112] directions. Figure 3 shows curves obtained by measuring the density

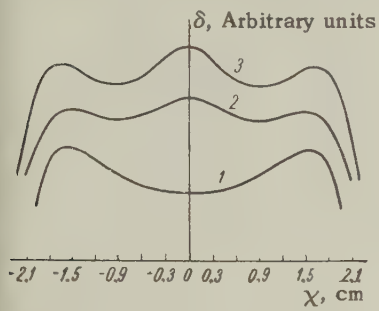

FIG. 3. Curves obtained by photometry of the sputtered deposit along the line AB of Fig. 2c, at the following ion energies: 1 – 1.5 kev, 2 – 10 kev, 3 – 40 kev.

of the deposits in the direction AB (see Fig. 2c) at various ion energies. At a bombarding-ion energy of only 1.5 or 2 kev (curve 1), no maximum was observed in the intensity of single-crystal sputtering near the directions [113] and [112]. On the other hand, sputtering ions with energies 10 kev or more (curves 2 and 3) produced a clearly pronounced maximum in the deposit density, corresponding to directions close to [113] and [112]. This phenomenon can be observed most clearly when the argon ion energy reaches 30–40 kev (see Fig. 2c). At small ion energies (near 10 kev) the increase in sputtering intensity near the [112] and [113] directions could be detected only by photometry of the deposit picture.

We compared the density of the sputtered copper in the individual patches by suitable photometer measurements. The result was that the maximum density P_c in the central patch ([100] direction) relative to the maximum density P_s in the side patches ([110] direction) increases with increasing energy of the bombarding ions. Thus, as the energy is changed from 1.5 to 50 kev, the ratio $p = P_c/P_s$ more than doubles, from 1.5 to 3.75 (Fig. 4). The patches obtained by sputtering single-crystal copper at argon ion energies of 20 and 40 kev and $\alpha = 45°$, and at 6, 10, 20, 30, 38,

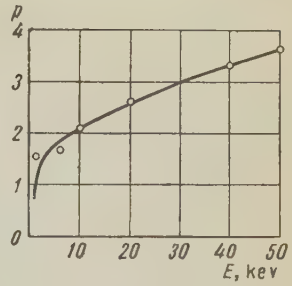

FIG. 4. Ratio of maximum density of deposit P_c in the central patch (corresponding to the [100] direction) to the maximum density of the positive P_s in the side patches (corresponding to the [110] directions) as a function of the energy of bombarding ions, E.

45, and 50 kev and $\alpha = 60°$ were analogous to those shown in Fig. 2.

The preferred emission of particles from the (100) plane of copper in the close-packing directions was observed not only in sputtering with argon ions, when the best ratio of gas-ion mass to metal-atom mass is obtained,[4] but also in sputtering by the much lighter hydrogen ions (Fig. 2d).

Distribution of deposit density in individual patches. It is seen from Fig. 2 that the density in an individual patch of the deposit increases from the center towards the periphery. By photometry of the deposit we can establish the law of distribution of the density of the sputtered substance inside an individual patch. For this purpose we plotted, with a recording microphotometer MF-4, curves of the intensity of light transmitted by the investigated deposit. Examples of such curves (for the central and side patches) are shown in Fig. 5. The horizontal axis represents the ratio $r = x/d$, where x is the distance from the center of the patch to the investigated point, measured in the photometry direction, and d is the distance between the sample and the collector. The vertical axis represents the quantity

$$J(r) = [S_0 - S(r)]/[S_0 - S_{min}]. \qquad (1)$$

Here $S(r)$, S_0, and S_{min} are the intensities of light passing through the collector plate at the investigated point, in a section free of deposit, and in the center of the patch (densest section) respectively.

Let us assume now that the density of the central spot ([100] direction) obeys the "cosine law,"[18] i.e., the amount of matter per unit solid angle, emitted from the sputtered surface at an angle φ to the normal from the plane of the sample is proportional to $\cos\varphi$.

Let a plane surface of radius R be sputtered. It can be shown that in this case the distribution of the density of matter deposited on a plane collector parallel to the sputtered surface is given by the relation

$$P(r) = P_0 \frac{1+r_1^2}{2r_1^2}\left\{1 - \frac{1-r_1^2+r^2}{\sqrt{1+2(r^2+r_1^2)+(r^2-r_1^2)^2}}\right\}, \qquad (2)$$

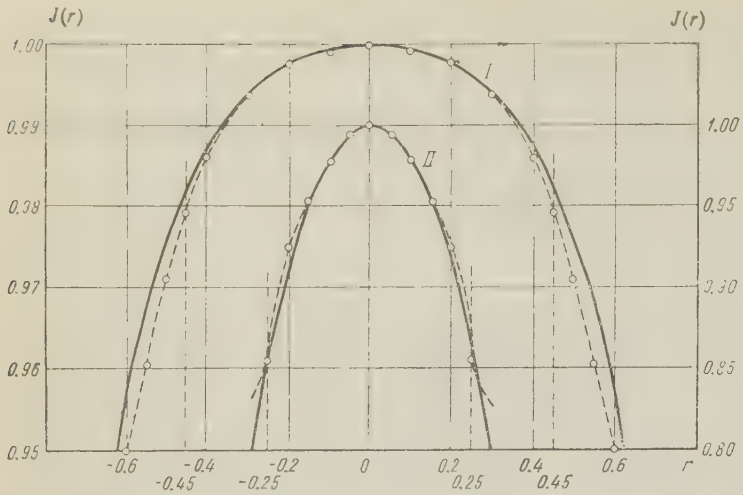

FIG. 5. Comparison of the experimental curves obtained by photometry (solid curves) with the theoretical ones, obtained from the "cosine law" (dotted): I – for the central patch [100] (photometry along the line CD, Fig. 2b), II – for the side patch [110] (photometry along the line EF, Fig. 2b).

where $r_1 = R/d$ and P_0 is the density of the deposit at the center of the patch. However, Eq. (2) is unwieldy, and it is more convenient to use in the calculations the approximate expression

$$P(r) = P_0 / (1 + r^2)^2, \qquad (3)$$

which gives results that agree within 2.5% with those obtained with (1), provided $r_1 = 0.2$ and r ranges from 0 to 0.45; these conditions are satisfied in our experiment.

Inasmuch as the density in this section of the deposit is connected with the intensity of light transmitted through it by the logarithmic law

$$\lg (S_0 / S(r)) = kP(r) \qquad (4)$$

(k is a proportionality factor), we can readily obtain from (1), (3), and (4) the following relation

$$J(r) = \{1 - 10^{-kP_0 (1+r^2)^{-2}}\} : \{1 - 10^{-kP_0}\}, \qquad (5)$$

which should be compared with the experimental curves to verify whether the "cosine law" is satisfied for the density distribution of the sputtered matter near the [100] direction (within the limits of a central patch of $x_c = 7$ mm corresponding to $\varphi \approx 24°$). The quantity kP_0 can be determined graphically if one point of a plot of (5) is made to coincide with the experimental curve.

The points computed from Eq. (5) are plotted in Fig. 5 (curve 1) and coincide within 0.15% with the experimental curve (within a single patch, $r = x_c/d = 0.45$). This means that the density distribution of the sputtered matter in the space near the preferred direction [100] obeys the cosine law with accuracy to 1.5%. The photometer error and the error due to the use of an approximate formula amount to 3%. Equally good agreement was obtained for the central patch ([100] direction) in sputtering of the (100) plane of copper by ions of various energies: 1.5, 40, and 50 kev.

The distribution of the deposit in the side patch in the [110] direction was plotted with a photometer along the line EF of Fig. 2b. In this case the cosine law $P = P_0 \cos \psi$ (where ψ is the angle of deviation from the [110] direction), for comparison with the experimental curves, is expressed approximately by a formula analogous to (5). The comparison of the experimental and computed curves for the side patch ([100] direction) is shown in Fig. 5 (curve II). In this case the cosine law also holds accurate to 1 – 2% within the confines of a single spot ($r = x_s/d = 0.25$), the radius of which is $x_s = 4$ mm, corresponding to $\psi \approx 10°$.

We can thus state that the density of a discrete patch on the picture is distributed in space in accordance with the cosine law.

Microrelief of the surface after sputtering. The anisotropy in the sputtering of a single crystal relative to the different crystallographic directions, at ion energies up to 50 kev, indicates that the mechanism of evaporation of matter from local molten sections of the surface is no longer applicable even for high ion energies. This is also corroborated by the absence of molten sections on the surface of a sample sputtered by fast ions.

Figure 6 shows a relief of the (100) face of copper, formed by sputtering with argon and hydrogen ion beams at 40 kev and an angle of incidence of 60°. We see the tetrahedral pyramidal recesses, characteristic of this plane, similar to those produced by sputtering with slow ions.[11] Oblique incidence of the ions on the (100) plane causes, in addition, the formation of less regular figures, stretched out in the direction of ion incidence (Fig. 6b). The outlines of these figures, as well as of the more detailed relief, are sufficiently clear, without visible traces of melting.

In conclusion, the authors thank Professor B. K. Shembel' and V. A. Teplyakov for providing the ion gun for these experiments, Professor G. V.

FIG. 6. Relief of the surface of the (100) face of copper after sputtering first with an inclined beam ($\alpha = 60°$) of argon ions at E = 40 kev, j = 0.4 ma/cm², τ = 60 min, and then with hydrogen ions at E = 40 kev, j = 0.8 ma/cm², and τ = 75 min. a – (×1000), b – (×3000).

Spivak for continuous interest in the work and for a discussion of its results, and B. K. Kondrat'ev for the preparation and performance of several experiments.

[1] N. D. Morgulis, Usp. Fiz. Nauk **28**, 202 (1946).

[2] G. K. Wehner, Advances in Electronics and Electron Optics **7**, 239 (1955).

[3] C. H. Townes, Phys. Rev. **65**, 319 (1944).

[4] F. Keywell, Phys. Rev. **97**, 1611 (1955).

[5] E. Harrison, Phys. Rev. **102**, 1473 (1956).

[6] E. B. Henschke, J. Appl. Phys. **28**, 411 (1957); Phys. Rev. **106**, 737 (1956).

[7] E. Langberg, Phys. Rev. **111**, 91 (1958).

[8] R. H. Silsbee, J. Appl. Phys. **28**, 1246 (1957).

[9] D. T. Goldman and A. Simon, Bull. Am. Phys. Soc. ser. II, **3**, 40 (1958); Phys. Rev. **111**, 383 (1958).

[10] G. K. Wehner, J. Appl. Phys. **26**, 1056 (1955); Phys. Rev. **102**, 690 (1956).

[11] V. E. Yurasova, J. Tech. Phys. (U.S.S.R.) **28**, 1966 (1958), Soviet Phys.–Tech. Phys. **3**, 1806 (1959); Yurasova, Spivak, and Kushnir, Izv. Akad. Nauk SSSR, Ser. Fiz. **23**, 744 (1959), Columbia Tech. Transl. in press.

[12] L. N. Dobretsov and N. M. Karnaukhova, Dokl. Akad. Nauk SSSR **85**, 745 (1952).

[13] M. A. Ermeev and Ya. K. Éstrinov, J. Tech. Phys. (U.S.S.R.) **22**, 1552 (1952).

[14] M. I. Guseva, Приборы и техника эксперимента (Instrum. and Meas. Engg.) No. 5, 112 (1957).

[15] N. V. Pleshivtsev, Report, Inst. Chem. Phys. U.S.S.R. Acad. Sci., 1958.

[16] M. Ardenne, Technik **2**, 65 (1958).

[17] I. V. Orfanov and V. A. Teplyakov, Приборы и техника эксперимента (Instrum. and Meas. Engg.) in press.

[18] R. Seeliger and K. Sommermeyer, Z. Physik **93**, 692 (1935).

Translated by J. G. Adashko
190

CROSS SECTION FOR PRODUCTION OF Cm^{240} BY IRRADIATION OF Th^{232} WITH C^{12} AND C^{13} IONS

L. I. GUSEVA, B. F. MYASOEDOV, N. I. TARANTIN, and K. V. FILIPPOVA

Submitted to JETP editor May 19, 1959

J. Exptl. Theoret. Phys. (U.S.S.R.) 37, 973-977 (October, 1959)

The dependence of the cross sections for the reactions $Th^{232}(C^{12}, 4n)Cm^{240}$ and $Th^{232}(C^{13}, 5n)Cm^{240}$ on the energy of the bombarding particles was determined by the irradiation of a stack of thin foils followed by radiochemical analysis of the reaction products. The curves of the reaction cross sections exhibit the pronounced peaks that characterize the evaporation of neutrons from an excited compound nucleus. The peak cross sections for the two reactions are 8×10^{-29} cm^2 and 18×10^{-29} cm^2, respectively. It is evident from a comparison with the cross sections for other nuclear reactions that cross sections for neutron evaporation do not depend on Z^2/A in a simple manner.

THE present paper presents results obtained from the investigation of nuclear reactions induced through the irradiation of thorium with accelerated carbon ions. These experiments comprise part of a broader program for the study of the laws of the nuclear reactions that occur when heavy nuclei are bombarded with multiply-charged ions. Specifically, these studies are intended to determine how the cross sections for the formation of different reaction products depend on the atomic number and mass of both the irradiated element and the bombarding particle.

EXPERIMENTAL PROCEDURE

The cross sections for the reactions $Th^{232}(C^{12}, 4n)Cm^{240}$ and $Th^{232}(C^{13}, 5n)Cm^{240}$ were determined as a function of incident-particle energy. We irradiated a stack of thin foils, which were then subjected to radiochemical analysis of the reaction products.

The Th^{232} metal foils, which were rolled to a thickness of $3-4$ mg/cm^2, were bombarded at the terminal radius of the 150-cm cyclotron of the U.S.S.R. Academy of Sciences by monoenergetic beams of $^{+4}C^{12}$ and $^{+4}C^{13}$ ions accelerated to 80 and 82 Mev, respectively. After passing through the target the ions entered a collector which was electrically connected to a current integrator. In order to avoid possible overheating and destruction of the target the ion current was limited to a maximum level of $0.2\,\mu$a. The integrated current in all experiments was $0.7-1.0\,\mu$a per hour.

A curium fraction was extracted chromatographically from each irradiated foil and was then analyzed by means of an ionization chamber and a 50-channel pulse-height analyzer. Cm^{240} was identified by the energy of the emitted α particles (6.25 Mev) and its half-life (26.8 days). Since the products of Th^{232} decay include Rn^{220} and Bi^{212}, which emit α particles whose energies (6.28 and 6.05 Mev) are close to the energy of α particles from Cm^{240}, the chemical separation of the curium from the thorium had to be accompanied by a sufficiently complete separation from the decay products that could produce an undesirable background. A special technique was developed to separate and purify curium from bombarded thorium. The curium was separated chromatographically from thorium and its decay products. Each bombarded thorium foil was dissolved in concentrated (10.7 N) hydrochloric acid to which a specific amount of Am^{241} had been added, from which the chemical yield of Cm^{240} could be determined. The solution was boiled down to $3-5$ drops which were adsorbed in a chromatograph column containing a Dowex-50 cation-exchange resin brought into equilibrium with the concentrated hydrochloric acid. The columns used were 90 mm high and $2-3$ mm in diameter. The columns were subsequently washed with concentrated hydrochloric acid, separate fractions of which were collected on platinum plates and analyzed by means of an ionization chamber. The elution curve is shown in Fig. 1.

Measurements of the half-life (~ 10 hours) and energies (6.05 and 8.8 Mev) of the α particles show that the activity eluted with drops Nos. 10 to 40 belongs to products of the thorium series, Bi^{212} and Po^{212}, which are related genetically to Pb^{212}. Curium was eluted with drops Nos. 20 to 100. Thorium and some of its decay products begin to be eluted with the 80th drop. For measurements in

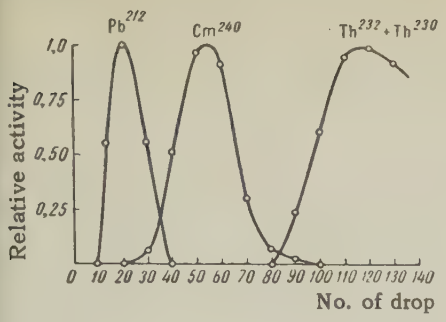

FIG. 1. Chromatographic elution curve.

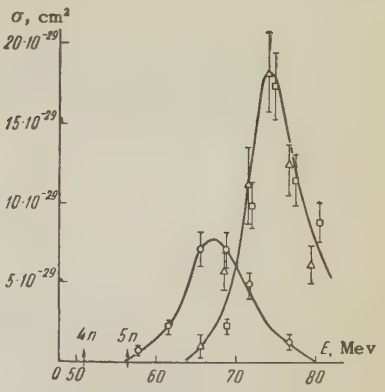

FIG. 2. Reaction cross sections as a function of carbon ion energy. Reaction thresholds are indicated by arrows. o – $Th^{232}(C^{12}, 4n)Cm^{240}$; Δ, □ – $Th^{232}(C^{13}, 5n)Cm^{240}$ (two seperate experiments).

the ionization chamber we selected the fraction in drops Nos. 20 to 80, which contained more than 80% of the curium. The α activity of the Bi^{212} and Po^{212} partially contained in this fraction dropped practically to zero in a few days and did not interfere with measurements of the Cm^{240} content. Purity of the separation of Cm^{240} from thorium was controlled by the content of the thorium-related products Po^{216} and Po^{212}, which emit 6.8- and 8.8-Mev α particles. The counts of 6.8- and 8.8-Mev α particles and consequently also of undesired α particles from Rn^{220} and Bi^{212} did not as a rule exceed 0.2 pulses per minute. This represented ~0.001 of the initial amount of thorium and its decay products in the curium fraction. At the peak of the reaction cross section the initial α particle count in the energy range 6.2 – 6.3 Mev was 4 or 5 pulses per minute. The intensity of Cm^{240} α emission was thus 20 – 25 times as great as the background of Rn^{220} α particles. The reaction product Cm^{240} could thus be reliably identified over a broad range of cross-section variation. It was not possible in these experiments to determine the cross sections for the reactions $Th^{232}(C^{12}, 2n)Cm^{242}$ and $Th^{232}(C^{13}, 3n)Cm^{242}$ from the yield of 162-day Cm^{242}, which emits 6.10-Mev α particles. The count of 6.10-Mev α particles in the curium fraction did not appreciably exceed the background of Bi^{212} α particles.

EXPERIMENTAL RESULTS AND DISCUSSION

The cross sections for $Th^{232}(C^{12}, 4n)Cm^{240}$ and $Th^{232}(C^{13}, 5n)Cm^{240}$ as a function of bombarding energy are shown in Fig. 2. The initial carbon-ion energy and the monoenergetic definition of the beam were determined with the aid of an aluminum absorber. The differential distribution curves of C^{12} and C^{13} ion ranges in aluminum are symmetrical Gaussian curves with ~3% rms deviation from the mean range. The small spread of carbon-ion ranges indicates sufficient energy homogeneity of the beam, especially if we consider the possible instrumental effects, such as nonuniform aluminum absorber thickness, which would increase the natural range fluctuations. An experimental range-energy curve[1] was used to determine the initial C^{12} ion energy. The initial C^{13} ion energy and the energy variation during passage through the thorium foils were determined from calculations of the C^{13} range in aluminum and the stopping power of thorium.

The indicated experimental errors take into account the statistical errors of Cm^{240} α particle counts and the possible errors in determining the chemical yield of curium, the thickness of the irradiated thorium foils and the integral of ingoing current.

The cross section curves in Fig. 2 exhibit the pronounced peaks that characterize neutron evaporation from excited compound nuclei. The $Th^{232}(C^{12}, 4n)Cm^{240}$ maximum is found at 67 Mev and that of $Th^{232}(C^{13}, 5n)Cm^{240}$ at 74 Mev, with half-widths of 9 and 8 Mev, respectively. The $Th^{232}(C^{13}, 5n)Cm^{240}$ peak is 2.3 times higher than that of $Th^{232}(C^{12}, 4n)Cm^{240}$, as a result of increased cross section for the formation of a compound nucleus when the ion energy rises from 67 to 74 Mev. This effect outweighs the reduction in the yield of the final product for the case of the 5n reaction as a result of the fact that the emission of an additional neutron again involves the competition between nuclear fission and neutron evaporation.

It is interesting to compare the peak cross sections for the evaporation of five neutrons from different nuclides bombarded with heavy particles. In this way an approximate picture is obtained of the way in which the ratio between the neutron-evaporation and fission probabilities varies as a function of Z and A for the compound and intermediate nuclei. Although the cross section for neutron evaporation depends on the cross section for compound-nucleus formation, this factor is unimportant when the cross sections for the evaporation of five neutrons are compared. At the maximum of the 5n-reaction cross section (~65 – 70 Mev) the cross section for compound-nucleus

formation has reached a very appreciable fraction of its possible maximum and is approximately independent of the ions used as projectiles.

We present a table of the peak cross sections for the evaporation of five neutrons from gold, thorium and uranium irradiated with carbon and nitrogen ions:

Reaction	σ_{max}, cm²	Reaction	σ_{max}, cm²
$Au^{197}(N^{14}, 5n)Ru^{206}$	$2.75 \cdot 10^{-25}$ [2]	$U^{238}(C^{13}, 5n)Cf^{246}$	$1.25 \cdot 10^{-28}$ [3]
$Th^{232}(C^{13}, 5n)Cm^{240}$	$1.80 \cdot 10^{-28}$	$U^{238}(C^{12}, 5n)Cf^{245}$	$9.0 \cdot 10^{-29}$ [3]

The same data are shown in Fig. 3 as a function of Z^2/A for the compound nucleus. The ratio of the cross sections of gold and thorium is seen to be considerably larger than in the case of thorium compared with uranium. A similar comparison reported by Flerov at the Second International Conference on the Peaceful Uses of Atomic Energy[4] indicated that the neutron-evaporation cross sections decrease monotonically by a factor of about 15 for each unit increase in the value of Z^2/A for the compound nucleus. However, this law was based on data for the evaporation of four neutrons, which is less closely related than the 5n reaction to the competition between neutron evaporation and fission.

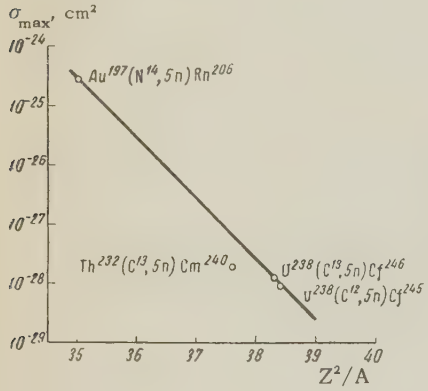

FIG. 3. Cross section for the evaporation of five neutrons as a function of Z^2/A for the compound nucleus.

The comparison of neutron-evaporation cross sections with values of Z^2/A for the compound nucleus[4] was the first attempt to discover a law governing the competition between neutron evaporation and fission in heavy nuclei. It was thus found basically that the cross section decreases as Z increases. The new data obtained from the study of five-neutron evaporation have revealed a more complicated dependence on Z and A than a simple exponential reduction of the cross section as Z^2/A increases.

The competition between neutron evaporation and fission as a function of nuclear parameters can be investigated in greater detail by comparing the values of Γ_n/Γ_f (the ratio of neutron-emission probability to the fission probability of the compound nucleus) for different nuclides. This has been done by Tarantin,[5] using the results presented here and an investigation of certain other nuclear reactions induced by heavy ions.

In conclusion the authors wish to thank Professor G. N. Flerov for directing this investigation, and Professor N. N. Tunitskiĭ and M. V. Tikhomirov for preparing highly enriched C^{13}.

[1] Yu. Ts. Oganesyan, JETP **36**, 936 (1959), Soviet Phys. JETP **9**, 661 (1959).

[2] Gerlit, Karamyan and Myasoedov, Ядерные реакции при малых и средних энергиях (Symp. Nuclear Reactions at Low and Medium Energies), U.S.S.R. Acad. Sci., Moscow, 1958, p. 503.

[3] Volkov, Guseva, Pasyuk, Tarantin, and Filippova, JETP **36**, 762 (1959), Soviet Phys. JETP **9**, 536 (1959).

[4] G. N. Flerov, Second International Conference on the Peaceful Uses of Atomic Energy, Report No. 2299, Geneva, 1958.

[5] N. I. Tarantin, JETP, in press.

Translated by I. Emin
191

INELASTIC INTERACTIONS OF π^+ MESONS WITH LIGHT NUCLEI IN THE ENERGY REGION 80—300 Mev

A. G. MESHKOVSKIĬ and Ya. Ya. SHALAMOV

Submitted to JETP editor May 21, 1959

J. Exptl. Theoret. Phys. (U.S.S.R.) **37**, 978-982 (October, 1959)

The cross sections for the inelastic interactions of π^+ mesons with a mixture of C, F, and Cl nuclei were measured at ten values of the pion energy in the 80 — 300 Mev region. The results are compared with curves calculated by the optical model assuming alternately a uniform charge density distribution in the nucleus and a Fermi-type distribution. It is shown that the experimental results satisfy the second assumption. The pion inelastic scattering cross sections were measured.

A paper by Blinov and others[1] described experiments on the interaction of 80 — 300 Mev π^+ mesons with the mixture of the elements C, F, and Cl which made up the working liquid in a 17-liter freon bubble chamber.[2] The analysis of the photographs taken with the aid of this chamber in π^+-meson beams from the synchrocyclotron of the Joint Institute for Nuclear Research determined the cross sections for exchange scattering and for star formation and the sum of the π^+-meson elastic and inelastic scattering cross sections.

In the present work an analysis of the photographs was done for the purpose of separating out all the inelastic interaction processes from the elastic. We found and analyzed 7400 events of various forms of interaction.

RESULTS OBTAINED

The numbers of events counted of the different interactions are given in Table I as a function of energy.

The number N_1 includes not only the stars seen on the exposures but also the positive-pion stoppings not accompanied by tracks of products from a pion-nucleus interaction. Such events can be related either to stars with outgoing neutrons or to stars with low-energy protons, since protons with energy less than about 10 Mev did not make visible tracks in our chamber. Since not only positive-pion absorption but also charge exchange ($\pi^+ \rightarrow \pi^0$) can take place in star formation, the number N_1 includes also the detected charge exchange events, that is, star events accompanied by an electron-positron pair pointing toward the point of interaction (conversion of a γ quantum from π^0 decay).

TABLE I. Number of events found

π^+-meson energy in Mev, E_π	Absorption of π^+ mesons and charge exchange, N_1	π^+-meson scattering		
		Inelastic, N_2	without visible tracks for nuclear transformation products	
			forward, N_3	back, N_4
67—91	98	14	58	33
91—115	150	29	143	38
120—144	178	108	165	24
144—165	267	120	266	35
165—185	327	191	348	45
185—205	447	286	447	37
210—230	226	138	224	18
230—251	251	171	308	17
251—273	341	218	434	13
273—291	399	281	439	16

We attributed to the inelastic scattering (N_2), first, those events where the positive-pion scattering was accompanied by charged particles (visible on the plate) outgoing from the nucleus and, second, those scattering events without accompanying particles when a noticeable decrease of the pion energy after scattering could be established. An estimate of the π^+ energy after scattering, in these cases, was carried out from the range or from the characteristic formation of ions along the track.

The number of pion forward scattering events without visible charged particle tracks (N_3) was obtained only in scatterings where the sum of the scattering angle projections for two stereoscopic exposures was greater than 10°. These events were fundamentally related to the elastic scattering of positive pions on a nucleus. Obviously the number N_3 includes also pion inelastic forward scattering events not accompanied by visible tracks of nuclear transformation products.

As will be shown below, the pion elastic back-

ward scattering was relatively small in our energy region. Therefore the number of events N_4 is fundamentally attributed to the pion inelastic backward scattering, although tracks of interaction products were not visible on the plate.

Calculation of the cross section for all inelastic processes σ_u was carried out using the number of interactions $n = N_1 + N_2 + (1+\alpha)N_4$ where α is the forward/backward ratio calculated in each energy region for pion inelastic scattering. It is evident that αN_4 is the number of inelastic events which are included in the number N_3 if it is taken that the quantity α is the same for scattering with and without visible interaction tracks.

The value of the cross section σ_u calculated with n included a small correction connected with the fact that N_4 actually included elastic scatterings, since backward elastic scattering always gave some contribution, even though small. This contribution could be estimated with enough accuracy for our purposes from the results of recent work by other authors. For π energies of 80 Mev there exist data for elastic scattering on carbon and aluminum at angles up to 110° (reference 3). Elastic scattering on carbon at 150 Mev has been measured up to 140° (reference 4). One can judge from the results of these two papers that the backward elastic scattering cross section comprises about 5% of the inelastic processes cross section at a pion energy of 80 Mev and fall to 1% at 150 Mev.

The results of the calculation of σ_u are given in Table II. The results of calculating the inelastic cross section σ_i according to the number of interactions $N_2 + (1+\alpha)N_4$, with a correction for elastic backward scattering are also given there. All cross sections are calculated for the mixture of C, F, and Cl which we had in our chamber (20% carbon, 49% fluorine, 31% chlorine). The average geometrical cross section of this mixture is 485 mb, assuming that the nuclear radius is $1.4\,A^{1/3}\,10^{-13}$ cm.

Let us compare the data we obtained with the

TABLE II

π^+-meson energy, Mev	σ_u, mb	σ_u in units of the average geometrical cross section	σ_i, mb	σ_i in units of the average geometrical cross section
79	344±44	0.71±0.09	125±32	0.26±0.07
103	415±44	0.86±0.09	140±30	0.29±0.06
132	525±49	1.08±0.10	229±36	0.47±0.07
154	568±48	1.17±0.10	223±33	0.46±0.07
175	567±43	1.17±0.09	255±34	0.53±0.07
195	573±40	1.18±0.08	250±31	0.52±0.06
220	505±43	1.04±0.09	215±30	0.44±0.06
241	464±37	0.96±0.08	206±27	0.42±0.06
262	462±34	0.95±0.07	191±23	0.49±0.05
282	442±31	0.91±0.06	196±24	0.40±0.05

results of other authors. The cross sections for the inelastic interactions of π^+ and π^- mesons at energies close to ours have been measured for light elements, chiefly carbon, by the methods of scintillation telescopes,[5,6] Wilson chambers in a magnetic field,[7] and propane bubble chambers.[8] The comparison of the data for total inelastic scattering cross sections is given in Table III.

TABLE III

Pion energy, Mev	Element	σ_u in millibarns	σ_u in units of the geometrical cross section	Reference
216	C	350±24	1.08±0.07	[5]
225	C	346±21	1.07±0.07	[6]
225	Al	596±30	1.07±0.05	[6]
230	C	307±37	0.95±0.11	[7]
256	C	326±31	1.01±0.10	[5]
260	C	296^{+35}_{-28}	$0.92^{+0.11}_{-0.09}$	[8]
290	C	269±26	0.83±0.08	[5]

Comparing the cross sections given in Table III with our data for nearby energy points (Table II), we see a good agreement of the results for the total cross sections for inelastic interactions as expressed in units of the geometrical cross section. In the work of Wang Kan-Chang et al.[8] there was also measured the cross section for inelastic scattering for carbon at a pion energy of 260 Mev, which turned out to be 120^{+38}_{-19} mb or $(0.37^{+0.12}_{-0.06})\sigma_g$ (σ_g is the geometrical cross section). This quantity agrees within the limits of error with our value, $\sigma_i = (0.49 \pm 0.05)\sigma_g$ measured at 262 Mev (Table II).

COMPARISON OF THE EXPERIMENTAL RESULTS WITH THEORY

To compare our results with theory we shall use the optical model of the nucleus. Here one must bear in mind that in the basic work on the optical model,[9] the expressions for the cross sections of inelastic and elastic processes were obtained under the assumption of a uniform distribution of charge in the nucleus. It is well known, however, that experiments on high-energy electron scattering[10] agree best with the nuclear model in which the charge density ρ is described by the Fermi function

$$\rho(r) = \rho(0) \Big/ \left[1 + \exp\left(\frac{r-c}{z}\right)\right], \qquad (1)$$

where $c = 1.08\,A^{1/3}\,10^{-13}$ cm and $z = 0.53 \times 10^{-13}$ cm. Expressions for the interaction cross sections using distribution (1) were obtained in the work of Cronin et al.[11] It is evidently interesting; in com-

paring the experimental values of the cross sections with theory, to carry out calculations for the two cases: for a homogeneous distribution and for the Fermi distribution.

For a homogeneous charge distribution in the nucleus we have[9]

$$\sigma_u = \pi R^2 \left[1 - \frac{1-(1+2kR)\,e^{-2kR}}{2k^2R^2} \right], \qquad (2)$$

where R is the radius of the nucleus and k is the coefficient of absorption. For positive pions the quantity k is connected with the cross sections for the interaction of pions with nucleons in the following way (without taking into account the Pauli principle)

$$k = \frac{\rho}{A} [Z\sigma^+_{\pi p} + (A-Z)\,\sigma^-_{\pi p}], \qquad (3)$$

where $\sigma^+_{\pi p}$ and $\sigma^-_{\pi p}$ are the total cross sections for the interaction of positive and negative pions with protons.

If the charge density in the nucleus follows the Fermi distribution, we get the expression[11]

$$\sigma_u = 2\pi \int_0^\infty \{1 - \exp[-2\bar{\sigma}\rho\,(0)\,S\,(b)]\}\, bdb, \qquad (4)$$

where $\bar{\sigma} = [Z\sigma^+_{\pi p} + (A-Z)\sigma^-_{\pi p}]/A$, and the function S(b) is calculated in the paper by Cronin et al. for various values of the parameter c.

The experimental values of the cross sections $\sigma^+_{\pi p}$ and $\sigma^-_{\pi p}$, necessary to calculate k and $\bar{\sigma}$, were taken by us from the work of Anderson.[12] In calculating σ_u by (2) we set $R = 1.4\,A^{1/3}\,10^{-13}$ cm; σ_u was calculated by (4) with the parameter value $c = 1.08\,A^{1/3}\,10^{-13}$ cm, which follows from the electron scattering experiments.[10] In addition, the values of σ_u were increased by the factor $(1 - Ze^2/RE_\pi)$ in order to take into account the Coulomb interaction of the π^+ mesons with the protons inside the nucleus.[13]

The results of the σ_u calculations are shown in the figure. The experimental values of σ_u found in our work (Table II) are also shown there. As follows from the figure, these values satisfy the theoretical curve I, using the Fermi distribution, much better than curve II, calculated assuming a homogeneous charge density in the nucleus.

In conclusion, we express our deep gratitude to V. A. Shebanov for much valuable advice, to I. Yu. Kobzarev and N. I. Petrov for examining the results, to I. S. Bruk for making it possible to do the computations on the electronic calculator M-2 of the Institute of Electronic and Control Machines of the U.S.S.R. Academy of Sciences, and to R. A. Ioffe for carrying out the calculations.

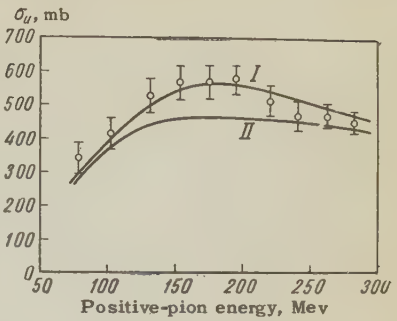

Dependence of the positive-pion inelastic scattering cross section on energy. Theoretical curves: I – Fermi distribution, II – homogeneous charge distribution.

[1] Blinov, Lomanov, Shalamov, Shebanov, and Shchegolev, JETP **35**, 880 (1958), Soviet Phys. JETP **8**, 609 (1959).

[2] Blinov, Lomanov, Meshkovskiĭ, Shalamov, and Shebanov, Приборы и техника эксперимента (Instrum. and Meas. Engg.) **1**, 35 (1958).

[3] Baker, Rainwater, and Williams, Phys. Rev. **112**, 1763 (1958).

[4] T. A. Fujii, Preprint (The Enrico Fermi Institute for Nuclear Studies, Report No. 300) (1958).

[5] Ignatenko, Mukhin, Ozerov, and Pontecorvo, JETP **31**, 546 (1956), Soviet Phys. JETP **4**, 351 (1957).

[6] Ivanov, Osipenkov, Petrov, and Rusakov, JETP **31**, 1097 (1956), Soviet Phys. JETP **4**, 922 (1957).

[7] Dzhelepov, Ivanov, Kozodaev, Osipenkov, Petrov, and Rusakov, JETP **31**, 923 (1956), Soviet Phys. JETP **4**, 864 (1957).

[8] Wang, Wang, Ding, Dubrovskiĭ, Kladnitskaya, and Solov'ev, JETP **35**, 899 (1958), Soviet Phys. JETP **8**, 625 (1959).

[9] Fernbach, Serber, and Taylor, Phys. Rev. **75**, 1352 (1949).

[10] R. Hofstadter, Revs. Modern Phys. **28**, 214 (1956).

[11] Cronin, Cool, and Abashian, Phys. Rev. **107**, 1121 (1957).

[12] H. L. Anderson, Proceedings of the Sixth Annual Rochester Conference, pp. 1-22 (1956).

[13] R. M. Sternheimer, Phys. Rev. **101**, 384 (1955).

Translated by W. Ramsay
192

SMALL ANGLE RAYLEIGH SCATTERING OF Co^{60} GAMMA RAYS

S. A. BEL'SKIĬ and S. V. STARODUBTSEV

Leningrad Physico-Technical Institute, Academy of Sciences, U.S.S.R.

Submitted to JETP editor May 22, 1959

J. Exptl. Theoret. Phys. (U.S.S.R.) **37**, 983-990 (October, 1959)

The integral cross sections for the Rayleigh scattering of Co^{60} γ rays from U, Pb, W, Ta, Sn, Cu and Ni have been measured for the angular intervals 15′ to 1°00′ and 15′ to 2°30′. The results confirm the prediction of the Debye-Franz theory that at small angles the cross section for Rayleigh scattering is proportional to the square of the atomic number of the scatterer. It is further shown that at the angles considered, the experimental values of the Rayleigh cross sections are greater than the theoretically predicted ones, and that with decreasing Z the angular dependence of the cross section becomes more pronounced than that indicated by theory.

1. INTRODUCTION

FOR energies of order 1 Mev, γ rays can interact elastically with matter through Rayleigh scattering from bound electrons, resonance scattering from nuclei, Thomson scattering from nuclei as charges, and potential scattering with the formation of virtual pairs in the field of the nucleus (the so-called Delbrück scattering). Rayleigh scattering at x-ray frequencies has long been known, but the other effects, together with Rayleigh scattering at high γ-ray energies, has not been studied experimentally.

There are two fundamental difficulties in the experimental investigation of elastic scattering of γ rays of about 1 Mev energy. The first is that the cross section for elastic scattering is much less than that for inelastic Compton scattering. The second difficulty is that the elastically scattered photons are masked by a hard component of the bremsstrahlung from Compton and photo-electrons, together with radiation from the annihilation of positrons. Using scintillation techniques, the inelastic Compton component can be discriminated against at large angles, but the hard bremsstrahlung remains troublesome.

Of the four processes for elastic scattering, Rayleigh scattering has the biggest cross section. There are several reasons why an experimental study of Rayleigh scattering is of interest. According to the non-relativistic theory of Debye and Franz,[1,2] which is based on the Thomas-Fermi approximation to the distribution of electron charge in an atom, at large scattering angles the cross section is proportional to the cube of the atomic number of the scatterer. Bethe and Levinger[3] carried out relativistic calculations, using Dirac wave functions for the K electrons, and at large angles obtained somewhat lower cross sections than those predicted by Debye and Franz, and a variation of the cross section with atomic number given by $Z^8 - Z^{10}$. More exact relativistic calculations of the cross section for Rayleigh scattering, with several terms of the Born expansion into a sum over intermediate states being taken into account, have been carried out recently[4-7] for γ-ray energies 0.32, 0.64, 1.28 and 2.56 mc^2. At all angles the cross sections so obtained are lower than those given by the Debye-Franz theory and vary with the atomic number as Z^5.

In resonance scattering experiments, Rayleigh scattering gives rise to a background whose magnitude must be known before a reliable value for the resonance scattering cross section can be obtained. In recent years, resonance scattering has become one of the fundamental methods for measuring the lifetimes of excited states as short as 10^{-11} sec. The resonance scattering technique is useful in solving other important problems, too. Finally, although it has now become possible to measure Rayleigh scattering, the existence of Delbrück and Thomson scattering has not yet been demonstrated experimentally. Since these compete with Rayleigh scattering, it is important in studying them to have reliable theoretical and experimental data on the cross section and angular distribution of the Rayleigh scattering, together with its dependence on the energy of the γ rays and the atomic number of the scatterer.

Rayleigh scattering has a strong angular dependence, as predicted by theory. At large angles,

the cross section for Rayleigh scattering is several orders of magnitude less than that for Compton scattering, while at small angles it is considerably larger than Compton scattering. Hence there are two convenient regions for experimental studies of Rayleigh scattering: 1) large angles, where the soft Compton component can be discriminated against; 2) small angles, where Compton scattering is negligible compared to Rayleigh scattering.

There have been a number of experiments carried out in recent years[8-17] at larger scattering angles ($> 30°$). These experiments measured the magnitude of the Rayleigh cross section, its angular dependence, and variation with Z, for γ-ray energies in the range 0.41 — 2.76 Mev. The results of various authors do not agree, which can be explained by the difficulty of allowing for the secondary hard component contained in the measured elastic scattering.

In the work now being reported we studied the Rayleigh scattering of Co^{60} rays at small angles ($< 3°$) and the behavior of the cross section as a function of the atomic number of the scatterer. The results are compared with the Debye-Franz theory.

2. THEORY

According to Debye,[1] the cross section for Rayleigh scattering on the electron cloud of an atom is, at x ray energies, given by the formula

$$\sigma = \frac{4\pi e^4 Z^2}{E_0^2}\left(\frac{\lambda}{b}\right)^2 \int_0^{b/\lambda} \left(\frac{A}{Z}\right)^2 u\,du, \qquad (1)$$

where E_0 is the electron rest mass, λ is the γ-ray wavelength, Z the atomic number of the scatterer, $b = 5.9 \times 10^{-8} Z^{-1/3}$ cm, $u = (b/\lambda)\sin(\theta/2)$, and θ is the scattering angle. The electron structure factor $f = A/Z$ is determined by the expression

$$f = \int_0^\infty x^{-1/2}\varphi^{3/2}\frac{\sin ux}{u}\,dx, \qquad (2)$$

where $\varphi(x)$ is the Fermi function, $x = r/a$ (r = distance from the nucleus, $a = b/4\pi$ is a characteristic radius). Debye carried out this integration graphically for the range $0 \le u \le 2\pi$. Franz[2] extended Debye's calculations to the range $u \ge 2\pi$, the function $f = A/Z$ being obtained in analytic form as a series

$$f = \frac{1}{u}\sqrt{\frac{\pi}{2u}}\left(1 - \frac{1.19}{u} + \cdots\right). \qquad (3)$$

Over the Debye range ($0 \le u \le 2\pi$), the value of the integral in (1) is 0.6, while over Franz' range ($2\pi \le u \le b/\lambda$) it is $0.2 - \pi\lambda/2b$. Hence, the total cross section for Rayleigh scattering is

$$\sigma = 4\pi e^4 Z^2 E_0^{-2}(\lambda/b)^2(0.8 - \pi\lambda/2b). \qquad (4)$$

The γ rays from Co^{60} have mean energy $\overline{E}_\gamma = 1.25$ Mev; for lead the cross section becomes $\sigma = 3.71 \times 10^{-25}$ cm^2. Since $0.6/[0.8 - \pi\lambda/2b] > 0.75$, more than 75% of the radiation will be scattered through an angle smaller than some angle θ_0.

From the relation $u = 2\pi = b/\lambda \sin(\theta_0/2)$ and for $E_\gamma = 1.25$ Mev we find, for lead, $\theta_0 \approx 5.3°$, while for aluminum $\theta_0 \approx 2.8°$. From this it is evident that Rayleigh scattering is predominantly through small angles. From (1) we can easily derive an expression for the differential cross section for Rayleigh scattering:

$$S(\theta) = (e^4 Z^2/2E_0^2)(A/Z)^2 = 3.971 \cdot 10^{-26} \cdot Z^2 (A/Z)^2. \qquad (5)$$

For $\theta \to 0$ ($(A/Z)^2 \to 1$) the cross section for Rayleigh scattering is proportional to Z^2, and reaches a maximum, independent of the γ-ray energy, given by

$$S(\theta)_{max} = 3.971 \cdot 10^{-26} Z^2. \qquad (6)$$

3. EXPERIMENTAL TECHNIQUE

Figure 1 shows a diagram of the experiment. The lead blocks $Pb_1 - Pb_4$ were arranged so that the holes through their centers (hole diameter 5 mm) were lined up. The Co^{60} source was a metal cylinder 10 mm long, diameter 5 mm, and had an activity 1.8 C. The detection system consisted of a scintillation counter with a NaI(Tl) crystal and an integral discriminator. The electronics operated stably, as indicated by the fact that over 12 — 15 hours the counting rate did not change by more than 2 or 3 statistical errors. The statistical error $\pm\sqrt{N}/N$ in a single measurement was ±0.3%. As scatterers we used U, Pb, W, Ta, Sn, Cu, and Ni discs with diameter 25 mm and thickness $l_Z = 2/\mu_Z$, where μ_Z is the

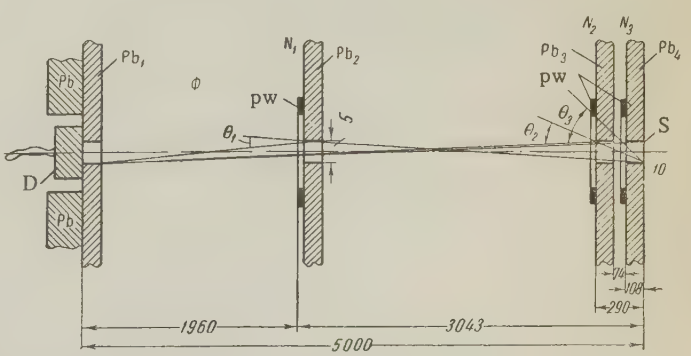

FIG. 1. Schematic diagram of the experimental set up. S — source, D — detector, pw — plexiglas washer for mounting the scatterers, θ_1, θ_2, and θ_3 — maximum scattering angles in the scatterer positions N_1, N_2, and N_3.

linear absorption coefficient for Co^{60} γ rays in the element used.

The Rayleigh-scattered radiation was measured as a small addition to a background provided by the direct beam. The magnitude of this increase depends on the solid angles subtended by the scatterer at the source and detector and the corresponding linear angle θ_{max}. The number of scattered γ quanta is given by the formula

$$I_{sc} = I_{pri} N_a x \int_0^{\theta_{max}} 2\pi S(\theta) \sin\theta \, d\theta = I_{pri} N_a x \sigma_0(\theta_{max}), \quad (7)$$

where N_a is the number of atoms per cc in the scatterer, x is the thickness of the scatterer and $\sigma_0(\theta_{max})$ is the scattering cross section for the interval 0° to θ_{max}.

It is clear that the amount of scattered radiation adding to the primary beam will depend on θ_{max}. The scatterer was successively placed in positions N_1, N_2, and N_3 (Fig. 1), in which positions the maximal scattering angles θ_1, θ_2, and θ_3 were as given in Table I. The maximal scattering angle θ_{max} depends on the maximal linear angles α_{max} and β_{max} subtended by the scatterer at the source and detector respectively. The angles β_3 and β_2 were each equal to 0° 04′, while β_1 was 0° 09′. The finite thickness of the scatterer gave rise to an uncertainty in the scattering angles, also shown in Table I.

Knowing the difference in γ counts between two positions of the scatterer, for instance N_1 and N_3, we can calculate the total scattering cross section $(\sigma_t)_1^3$ corresponding to the interval θ_1 to θ_3, the calculation being done according to the formula

$$(\sigma_t)_1^3 = (I_3 - I_1)/I_1 N_a x. \quad (8)$$

This method obviously is useful only for scattering processes whose differential cross section is sufficiently large at small angles. According to theory, in the angle interval 0 — 2° 30′ Rayleigh scattering of γ rays with E_γ = 1.25 Mev from heavy elements amounts to 1.5% of the direct beam.

4. COMPTON SCATTERING AND THE UNEQUAL CONTRIBUTIONS OF DIFFERENT SCATTERING ANGLES

The cross section determined from experiment using formula (8) is the sum of the Rayleigh cross section and all the other possible elastic and inelastic processes. We need correct only for Compton scattering because the contribution of all the other processes is negligibly small. At small angles, Compton and Rayleigh scattered quanta have practically the same energy and cannot be separated from each other. Hence the contribution of Compton scattering was computed theoretically. The Rayleigh cross section was then obtained as the difference between the total, measured, cross section and the contribution from Compton scattering: $(\sigma_R)_{exp} = (\sigma_t)_{exp} - (\sigma_C)_{theor}$. Theoretical values for the Rayleigh scattering were computed graphically. $S_R(\theta)$ was calculated from formula (5); the quantity $f(\theta) = 2\pi S_R(\theta) \sin\theta$ is shown in Fig. 2.

In calculating the theoretical Rayleigh and Comp-

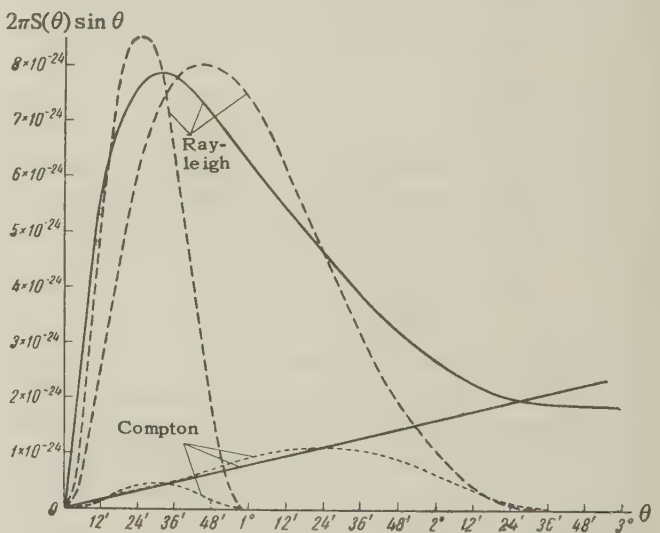

FIG. 2. Angular distribution of Rayleigh and Compton scattered γ rays from uranium. Solid curve — without taking the function F(φ) into account; dashed curves — taking F(φ) into account.

TABLE I. Maximal scattering angles

Z	α_3	θ_3	α_2	θ_2	α_1	θ_1
U	2°35′±12′	2°38′±12′	0°58′±2′	1°02′±2′	0°06′	0°15′
Pb	2°27′±19′	2°31′±19′	0°56′±2′	0°59′±2′	0°06′	0°15′
W	2°33′±13′	2°37′±13′	0°58′±2′	1°02′±2′	0°06′	0°15′
Ta	2°32′±14′	2°36′±14′	0°58′±2′	1°02′±2′	0°06′	0°15′
Sn	2°18′±29′	2°21′±29′	0°55′±5′	0°59′±5′	0°06′	0°15′
Cu	2°22′±25′	2°26′±25′	0°56′±4′	1°0′±4′	0°06′	0°15′
Ni	2°33′±24′	2°27′±24′	0°56′±4′	1°0′±4′	0°06′	0°15′

ton scattering cross sections, it is necessary to take account of the fact that different angles in the range 0° to θ_{max} contribute differently. The angular distribution function for particles emitted by the source and falling on the scatterer was, at our request, graciously furnished by Prof. G. A. Grinberg. This function was calculated for our special case, where $l \gg a$ (a being the diameter of the source and scatterer, while l is the distance between them) and has the form

$$F(\varphi) = (\varphi - \sin\varphi)\sin\varphi, \qquad (9)$$

where

$$\varphi = 2 \arccos(l\theta/2a).$$

From the plot of F vs. φ (Fig. 3) it follows that large scattering angles (small φ) and small scattering angles (large φ) contribute relatively little as compared with intermediate angles.

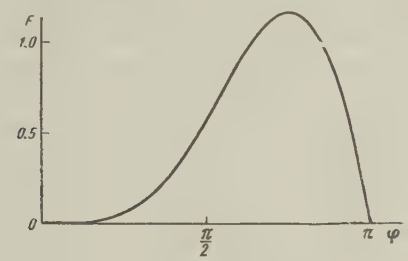

FIG. 3. Dependence of F on φ.

To correct for the unequal weight of different scattering angles, the function $f(\theta) = 2\pi S(\theta)\sin\theta$ for Rayleigh and Compton scattering was multiplied by the function $F(\varphi)$, for our values of the parameter $2a/l$ and the result integrated graphically. The product of these functions is shown in Fig. 2 for uranium. The theoretical values for the Rayleigh and Compton cross sections are shown in Table II, which also gives the corresponding cross sections without this correction (indicated by *).

5. MEASUREMENTS AND RESULTS

The measurements were carried out in the following way. The scatterer was placed first in one position, then in another, for example N_1 and N_3. In these positions, counts I_1 and I_3 were collected for five minutes each. In a single measurement, lasting five minutes, about 128,000 counts were collected, the background being about 500.

Several series of measurements were made on each scatterer; in a series, the counting rate for each position of the scatterer was determined 40 — 50 times. The arithmetic mean and mean square deviation of the differences in counting rates between the two scatterer positions was determined, the average being taken over several series, and the total scattering cross section determined from (8). The experimental data obtained are shown in Table II.

Figure 4 shows, in a semi-logarithmic plot, the theoretical and experimental dependence of the Rayleigh scattering cross section on the atomic number of the scatterer for the two intervals 15′ to 1°00′ and 15′ to 2°30′.

The following conclusions can be drawn from an analysis of the experimental data.

TABLE II

Angle Interval	$\theta_1-\theta_3$					
Cross section in barns (per nucleus)	$(\sigma_P)_{exp}$	$(\sigma_C^*)_{theor}$	$(\sigma_C)_{theor}$	$(\sigma_R^*)_{theor}$	$(\sigma_R)_{theor}$	$(\sigma_R)_{exp}$
Uranium	0.217 ±0.011	0.047	0.027	0.198	0.166	0.180 ±0.011
Lead	0.175 ±0.012	0.038	0.021	0.144	0.120	0.154 ±0.012
Tungsten	0.126 ±0.011	0.036	0.020	0.112	0.095	0.106 ±0.010
Tantalum	0.151 ±0.009	0.036	0.020	0.107	0.090	0.131 ±0.009
Tin	0.0468 ±0.0028	0.0193	0.0111	0.0392	0.0318	0.0357 ±0.0028
Copper	0.0175 ±0.0012	0.0130	0.0069	0.0102	0.0085	0.0106 ±0.0012
Nickel	0.0131 ±0.0018	0.0128	0.0068	0.0093	0.0077	0.0062 ±0.0018

Angle Interval	$\theta_1-\theta_2$					
Cross section in barns (per nucleus)	$(\sigma_P)_{exp}$	$(\sigma_C^*)_{theor}$	$(\sigma_C)_{theor}$	$(\sigma_R^*)_{theor}$	$(\sigma_R)_{theor}$	$(\sigma_R)_{exp}$
Uranium	0.085 ±0.010	0.007	0.004	0.098	0.069	0.081 ±0.010
Lead	0.074 ±0.050	0.006	0.003	0.072	0.050	0.071 ±0.005
Tungsten	0.058 ±0.013	0.006	0.003	0.058	0.041	0.055 ±0.013
Tantalum	0.083 ±0.014	0.006	0.003	0.055	0.040	0.080 ±0.014
Tin	0.0310 ±0.0012	0.0035	0.0015	0.0220	0.0152	0.0295 ±0.0012
Copper	0.0127 ±0.0015	0.0021	0.0010	0.0059	0.0045	0.0117 ±0.0015
Nickel	0.0053 ±0.0012	0.0020	0.0010	0.0055	0.0041	0.0043 ±0.0012

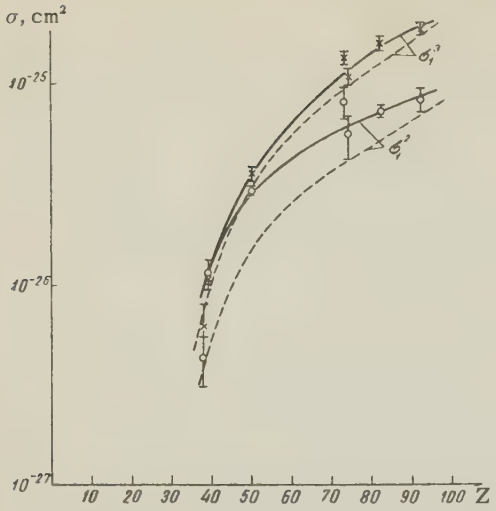

FIG. 4. Dependence of the Rayleigh scattering cross section on the atomic number of the scatterer. Dashed curve – theoretical, solid curve – experimental. × – experimental points for the angle interval θ_1–θ_3; ○ – for the interval θ_1–θ_2.

1. The cross section for Rayleigh scattering at small angles is greater than that predicted by the Debye-Franz theory. The experimental cross section becomes ever bigger than the theoretical one as the scattering angle decreases.

2. The experimental curves for σ_1^3 and σ_1^2 tend to come together as Z decreases. It follows that the experimental scattering cross section varies more strongly with decreasing Z than does the theoretical one. The experimental values of σ_1^3 and σ_1^2 coincide for Cu and Ni, i.e., for these elements we did not see Rayleigh scattering, within the limits of experimental error, at angles greater than 1°.

3. According to theory, about half the Rayleigh scattered radiation should be scattered through angles $\theta_1 = 15'$ to $\theta_2 = 2°30'$. The agreement between the general trend of the experimental and theoretical curves for σ_1^3 over this range of angles confirms the theoretical prediction that the Rayleigh scattering cross section should be proportional to the square of the atomic number of the scatterer.

The experimental points for Ta and Ni are anomalous. The scattering cross section for Ta turned out to be significantly greater than for its neighbor W, while for Ni the state of affairs is reversed, its cross section being markedly less than that for Cu. In this connection, it should be noted that a smooth variation of the angular distribution can be interrupted by diffraction effects. For Co^{60} γ rays, with energy $E_\gamma = 1.25$ Mev, the wave length is 10^{-10} cm, while interatomic distances are of order 10^{-8} cm. From the relation $n\lambda = 2d \sin\theta$ it follows that the first diffraction maximum will be at an angle 30′.

It should also be noted that elastic resonance scattering can occur in Ni; this will be out of phase with the Rayleigh scattering[17] and will compete with it. The observed decrease in the amplitude for elastic scattering can be explained by a strong resonance scattering peak at small angles, the mean differential cross section in the interval $\theta_1 - \theta_2$ being of order 1.37×10^{-24} cm²/sterad.

In conclusion, the authors would like to thank Prof. G. A. Grinberg for his help in making the calculations.

[1] P. Debye, Physik. Z. **31**, 348 (1930).
[2] W. Franz, Z. Physik **98**, 314 (1935).
[3] J. S. Levinger, Phys. Rev. **87**, 656 (1952).
[4] Brown, Peierls, and Woodward, Proc. Roy. Soc. (London) **A227**, 51 (1954).
[5] Brenner, Brown, and Woodward, Proc. Roy. Soc. (London) **A227**, 59 (1954).
[6] G. E. Brown and D. F. Mayers, Proc. Roy. Soc. (London) **A234**, 387 (1956).
[7] G. E. Brown and D. E. Mayers, Proc. Roy. Soc. (London) **A242**, 89 (1957).
[8] E. Pollard and D. E. Alburger, Phys. Rev. **74**, 926 (1948); D. E. Alburger, Phys. Rev. **73**, 344 (1948).
[9] A. Storruste, Proc. Phys. Soc. (London) **A63**, 1197 (1950).
[10] R. R. Wilson, Phys. Rev. **82**, 295 (1951); **90**, 720 (1953).
[11] W. G. Davey, Proc. Phys. Soc. (London) **A66**, 1059 (1953).
[12] T. D. Strickler, Phys. Rev. **92**, 923 (1953).
[13] J. R. Cook, Proc. Phys. Soc. (London) **A68**, 1170 (1955).
[14] S. Messelt and A. Storruste, Proc. Phys. Soc. (London) **A69**, 381 (1956).
[15] A. K. Mann, Phys. Rev. **101**, 4 (1956).
[16] A. M. Bernstein and A. K. Mann, Phys. Rev. **110**, 805 (1958).
[17] J. S. Levinger, Phys. Rev. **84**, 523 (1951).

Translated by R. Krotkov
193

MEASUREMENT OF THE LIFETIME OF THE FIRST EXCITED STATE OF Ne^{21}

A. G. KHABAKHPASHEV and É. M. TSENTER

Submitted to JETP editor May 26, 1959

J. Exptl. Theoret. Phys. (U.S.S.R.) **37**, 991-993 (October, 1959)

The lifetime of the first excited state of Ne^{21} was measured using a 50-channel time analyzer. The measurements gave the value $T_{1/2} = (6.2 \pm 6.2) \times 10^{-11}$ sec. A brief description of the time analyzer is given.

THE lifetime of the first excited state of Ne^{21}, at 0.35 Mev, has been measured with a Po-O^{18} neutron source. The source was a solution of Po^{210} nitrate in water enriched to 24% in O^{18}. The $O^{18}(\alpha, n)Ne^{21}$ reaction in the source is accompanied by the 1.38 — 0.35-Mev gamma cascade. The intensity of the direct transition from the second excited state to the ground state is lower by at least a factor of ten than the cascade transition.

The lifetime was measured using a multichannel time analyzer. The use of multichannel analyzers has various advantages over delayed coincidence methods. In multichannel analyzers, the whole time distribution of the pulses is taken simultaneously. This enables one to shorten the measuring time, reduce the effect of instability of the apparatus, and improve the statistical accuracy of the measurement. Green and Bell[1] used a multichannel analyzer successfully to measure the lifetime of positrons in quartz crystals.

Our analyzer was built following the time-to-pulse height conversion scheme proposed by Neilson and James.[2] A block diagram of the apparatus is shown in Fig. 1. The detectors of the radiation were 40 × 40 mm crystals of NaI(Tl) and FEU-1V photomultipliers. The output signals from the anode of each multiplier pass through the broadband amplified UR-3 to a pulse-shaping circuit. The positive rectangular pulses after shaping have an amplitude ~1.5 v and a duration of 2×10^{-8} sec. The time-to-pulse-height conversion circuit was built like the one described in the paper of Neilson and James.[2] The converter element was a 6A3P tube, cut off by a pair of grids. When the positive rectangular pulses are applied to both grids of the tube, a charge is produced in the anode circuit which is proportional to the time of overlap of the input pulses. The output pulses from the converter are amplified and pass through a gating circuit to an AI-50 50-channel pulse analyzer. The gating circuit is opened by pulses from a slow coincidence circuit.

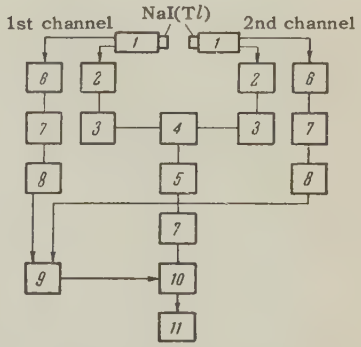

FIG. 1. Block diagram of multichannel time analyzer. 1 — FEU-1V; 2 — 200 Mcs amplifier; 3 — pulse-shaping circuit; 4 — converter circuit; 5 — delay line; 6 — preamplifier; 7 — linear amplifier; 8 — single-channel pulse analyzer; 9 — coincidence circuit with $\tau = 2 \times 10^{-7}$ sec; 10 — gating circuit; 11 — 50-channel pulse analyzer.

Amplitude discrimination on the pulses from each detector is accomplished by using single-channel analyzers in a slow coincidence circuit with a resolving time of 2×10^{-7} sec. The single channel analyzers enable one to select gamma lines of definite energy in each detector, and enable one to improve the resolution of the time analyzer. A calibration curve taken using self-coincidences showed that the analyzer linearity is good in the range from 3×10^{-9} to 18×10^{-9} sec. The width of the analyzer channels was 4.6×10^{-10} sec.

After calibrating the analyzer, we introduced a fixed delay line with a delay of 11×10^{-9} sec into the second channel between the anode of the multiplier and the UR-3 amplifier. In this way the "null" of the time analyzer was shifted to the middle of the linear region of the calibration curve. The single-channel discriminator of the first counter was set to record γ quanta with energy 0.35 Mev, the discriminator of the second counter was set to record γ quanta with energy 1.38 Mev. The channel width of each discriminator was set equal to the width of the photopeak.

With this setup, we used a Co^{60} source to measure the resolution of the time analyzer. The first

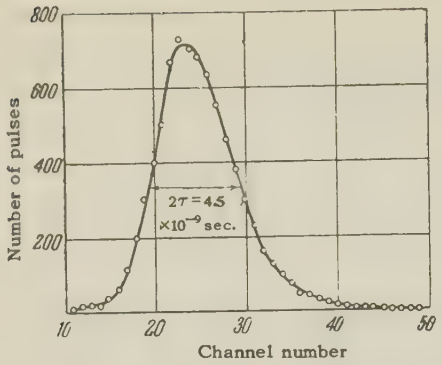

FIG. 2. Resolution curve of time analyzer.

counter recorded part of the Compton distribution from the 1.17-Mev line, the second counter recorded the photopeak of the 1.33-Mev line. Since the lifetime of the first excited state of Ni^{60} is[3] 1.1×10^{-12} sec, we could assume for our measurements that the 1.17- and 1.38-Mev quanta are emitted simultaneously. The resolving time was $2\tau = 4.5 \times 10^{-9}$ sec (see Fig. 2). The asymmetry of the distribution curve is due to the difference of excitation energy in the first and second crystal.

The operation of the analyzer was checked on a source with an artificial "lifetime." For this purpose the Co^{60} source was placed between the detectors, and the time distribution curve of artificially delayed pulses was measured. This curve was determined from the sum of ten measurements, made with different delay times of $t_1 = \Delta t/2$, $t_2 = t_1 + \Delta t$, etc. A step delay line with $\Delta t = 4 \times 10^{-10}$ sec was introduced into the first channel of the analyzer. The time of the measurement for each delay t_n was determined from the expression $T_n = \text{const} \cdot \exp(-t_n/\Theta)$, where Θ is the "lifetime." The distribution curve of the delayed pulses was compared with the prompt curve of the distribution (Fig. 2), using Bay's[4] method. For a source with an artificial "lifetime" $\Theta = 1 \times 10^{-9}$ sec, we found experimentally a value $(1.1 \pm 0.1) \times 10^{-9}$ sec.

The lifetime of Ne^{21} was measured by comparing the distributions from the $Po\text{-}O^{18}$ and Co^{60} sources. The data were treated by Bay's method[4] and Newton's method.[5] The half-life, found from an average of nine measurements, is $T_{1/2} = (6.2 \pm 6.2) \times 10^{-11}$ sec (where we give the mean square error of the average). A correction for internal conversion is not necessary in this case, since it is 8×10^{-5}.

Thus the upper limit on the half-life of the first excited state of Ne^{21} is 1×10^{-10} sec.

Middleton and Tai[6] have shown that the spins and parity of the ground and first excited states of Ne^{21} are $3/2^+$ and $5/2^+$. From measurements of γ-γ angular correlation[7] for Ne^{21} it follows that the 0.35-Mev transition is dipole. The single particle model[8] gives a half life for a magnetic dipole transition of $T_{1/2} = 6 \times 10^{-13}$ sec.

[1] R. Green and R. Bell, Nucl. Instr. **3**, 127 (1958).

[2] G. Neilson and D. James, Rev. Sci. Instr. **26**, 1018 (1955).

[3] F. Metzger, Phys. Rev. **103**, 983 (1956).

[4] Z. Bay, Phys. Rev. **77**, 419 (1950).

[5] T. Newton, Phys. Rev. **78**, 490 (1950).

[6] R. Middleton and C. Tai, Proc. Phys. Soc. (London) **A65**, 752 (1952).

[7] A. G. Khabakhpashev and É. M. Tsenter, Izv. Akad. Nauk SSSR, Ser. Fiz. **23**, 883 (1959), Columbia Tech. Transl., in press.

[8] S. A. Moszkowsky, Theory of Multipole Radiation, in Beta and Gamma Spectroscopy, (ed. Siegbahn), North-Holland, Amsterdam 1955.

Translated by M. Hamermesh
194

SCATTERING OF A PHOTON BY A NUCLEON IN THE ONE-MESON APPROXIMATION

E. D. ZHIZHIN

Submitted to JETP editor March 24, 1959

J. Exptl. Theoret. Phys. (U.S.S.R.) 37, 994-999 (October, 1959)

Photon-nucleon scattering due to strong interactions is treated taking into account the exchange of a single π meson. The scattering matrix is computed for values of angular momentum up to $J = 7/2$. The angular distributions for reactions involving polarized particles are presented.

1. SCATTERING MATRIX IN THE ONE-MESON APPROXIMATION

As was shown by Okun' and Pomeranchuk[1] in peripheral interactions, when in effect the particles exchange the smallest possible number of pions, it is possible to use contemporary meson theory to calculate processes involving large orbital angular momenta.

Photon-nucleon scattering in the one-meson approximation is described by the diagram shown in the figure. The matrix element for this process may be written as

$$M = \frac{\Gamma g \sqrt{\pi}}{(2\pi)^2 \omega} \frac{(\bar{u}_2 \gamma_5 u_1)\, m}{[(k_2 - k_1)^2 - \mu^2]\, E_1} \times \{\xi_2 \cdot [(\mathbf{n}_1 - \mathbf{n}_2) \times \xi_1]\}\ \delta^{(4)}(k_1 + p_1 - k_2 - p_2), \quad (1)$$

where ξ is the photon unit polarization vector, $\mathbf{k}$ and $\mathbf{p}$ are the photon and nucleon momenta, ω and E are the photon and nucleon energies, $\mathbf{n}_1$ and $\mathbf{n}_2$ are unit vectors in the direction of motion of the initial and final photon, μ is the pion mass, Γ is the vertex function $(\gamma\gamma\pi^0)$, the subscripts 1 and 2 refer to initial and final particles and units are used such that $\hbar = c = 1$. The expression is written in the center of mass coordinate system, hence $\mathbf{k}_1 = -\mathbf{p}_1 = \omega \mathbf{n}_1$, $\mathbf{k}_2 = -\mathbf{p}_2 = \omega \mathbf{n}_2$; the z axis is chosen in the direction of $\mathbf{n}_1$ and u_1, u_2 are unit spinor amplitudes.

The scattering amplitude which determines the probability for the transition from the initial state (when the photon has momentum $\mathbf{k}_1$ and prescribed polarization and the nucleon has momentum $\mathbf{p}_1$ and prescribed spin projection onto the z axis) to the final state (when the photon has momentum $\mathbf{k}_2$ and prescribed polarization and the nucleon has momentum $\mathbf{p}_2$ and prescribed spin projection onto the z axis) is given by the expression

$$f(\theta, \varphi) = C\, \{v_2^* \sigma (\mathbf{n}_1 - \mathbf{n}_2)\, v_1\}\, \{\xi_2 \cdot [(\mathbf{n}_1 - \mathbf{n}_2) \times \xi_1]\} / (x - \cos\theta),$$
$$C = \Gamma g \sqrt{\pi} / 8\pi\omega (E_1 + \omega), \qquad x = 1 + \mu^2 / 2\omega^2, \quad (2)$$

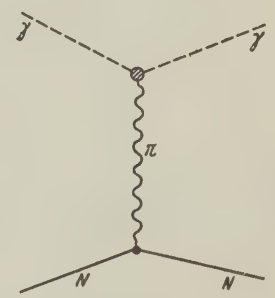

Here θ is the angle between $\mathbf{n}_1$ and $\mathbf{n}_2$ in the center-of-mass system, and v_1, v_2 are unit spinors.

To separate out large angular momenta we go over to the angular momentum representation. In this representation the state of a system consisting of a photon and a nucleon is specified by the total angular momentum L and parity λ of the photon, by the spin of the nucleon, and by the conserved quantities J, M_J and Π. Here J is the total angular momentum of the entire system, M_J is its projection on the z axis, and $\Pi = (-)^{L_1+\lambda_1} = (-)^{L_2+\lambda_2}$ is the parity of the entire system. The scattering amplitude in this representation $R(L_2\lambda_2; L_1\lambda_1; J\Pi)$ is related to the scattering amplitude $f(\theta, \varphi)$ by:[2]

$$f(\theta, \varphi) = C \sqrt{\frac{\pi}{2}} \sum_{JL_2\lambda_2L_1\lambda_1} R(L_2\lambda_2; L_1\lambda_1; J\Pi)\, i^{L_1+\lambda_1-L_2-\lambda_2} \times \sqrt{2L_1+1} \times \sum_{M_1\mu_1} (-M_1)^{1+\lambda_1} C^{JM_J}_{L_1M_1{}^1/_2\mu_1} (-1)^{\lambda_1+\lambda_2} (\chi^*_{M_1}\xi_1) \times (v^*_{\mu_1} v_1)\, (v^*_2 \xi_2 \Psi_2(JM_JL_2\lambda_2)), \quad (3)$$

where $\Psi_2(JM_JL_2\lambda_2)$ is the function describing the state of the system with total angular momentum J and z component M_J. Since J is determined by the vector addition $\mathbf{J} = \mathbf{L}_2 + \mathbf{S}_2$ where $\mathbf{S}_2$ is the spin of the final nucleon we have

$$\Psi_2(JM_JL_2\lambda_2) = \sum_{\mu_2} C^{JM_J}_{L_2M_2{}^1/_2\mu_2}\, Y^{\lambda_2}_{L_2M_2}(\mathbf{n}_2)\, v_{\mu_2}. \quad (4)$$

In (3) and (4), $C^{\cdots}_{\cdots}$ are Clebsch-Gordan coefficients and $Y^{\lambda}_{LM}(\mathbf{n})$ are vector spherical harmon-

ics (defined, for example, in reference 3).

Using the orthogonality properties of the spherical harmonics and the Clebsch-Gordan coefficients the following expression for the scattering matrix may be obtained from (2) and (3) after some simple calculations:

$$R(L_2\lambda_2;\ L_1\lambda_1;\ J\Pi) = -\frac{2}{2J+1} i^{L_2+\lambda_2-L_1-\lambda_1}(-1)^{\lambda_1+\lambda_2} \times \sum_{\mu_1\mu_2M_1} C^{JM_J}_{L_2M_2 1/2\mu_2} C^{JM_J}_{L_1M_1 1/2\mu_1} \times \int \frac{\{v^*_{\mu_2}\sigma\cdot(\mathbf{n}_1-\mathbf{n}_2)\,v_{\mu_1}\}\{Y^{\lambda_2}_{L_2M_2}(\mathbf{n}_2)\cdot[(\mathbf{n}_1-\mathbf{n}_2)\times Y^{\lambda_1}_{L_1M_1}(\mathbf{n}_1)]\}}{x-\cos\theta}\,do \tag{5}$$

In order to obtain the final expressions we use the formulas

$$[\mathbf{n}\times Y^{\lambda}_{LM}(\mathbf{n})] = i\,Y^{1-\lambda}_{LM}(\mathbf{n}), \qquad (\sigma\cdot\mathbf{n})\,v_\mu = -\sqrt{4\pi}\,\Omega_{1/2 1\mu}(\mathbf{n}), \tag{6}$$

where $\Omega_{1/2 1\mu}(\mathbf{n})$ is a spherical spinor (defined in reference 3). After some simple but tedious calculations we obtain the following expression for the scattering matrix:

$$\begin{aligned} R(L_2\lambda_2;\ L_1\lambda_1;\ J\Pi) = {} & -i\,(4\sqrt{2L_1+1}/(2J+1))\,i^{L_2+\lambda_2-L_1-\lambda_1} \\ & \times \Big\{ \sum_{l_2} C^{l_2 0}_{l_2-111}\,\delta(l_2\lambda_2)\sqrt{2l_2+1}\Big[C^{L_2 1}_{l_2 011}Q_{l_2}(x)\,b(JL_2L_1) \\ & - \sum_f C^{f0}_{l_2 010}Q_f(x)\,(C^{f0}_{l_2 010}C^{L_2 1}_{l_2 011}b(JL_2L_1) \\ & + \sqrt{2}\,C^{f0}_{l_2 11-1}d_{l_2}(JL_2L_1))\Big] - \sum_{l_2} C^{l_2 0}_{l_2-111}\,\delta(l_2 1-\lambda_2) \\ & \times \sqrt{2l_2+1}\Big[C^{L_2 1}_{l_2 011}Q_{l_2}(x)\,b(JL_2L_1) - \sum_f C^{f0}_{l_2 010}Q_f(x) \\ & \times (C^{f0}_{l_2 010}C^{L_2 1}_{l_2 011}b(JL_2L_1) + \sqrt{2}\,C^{f0}_{l_2 11-1}d_{l_2}(JL_2L_1))\Big]\Big\}. \end{aligned} \tag{7}$$

Here we have introduced the following abbreviations:

$$b(JL_2L_1) = C^{J1/2}_{L_2 1^1/_2-1/_2}C^{J1/2}_{L_1 1^1/_2-1/_2} - C^{J3/2}_{L_2 1^1/_2 1/_2}C^{J3/2}_{L_1 1^1/_2 1/_2},$$

$$d_{l_2}(JL_2L_1) = C^{J1/2}_{L_1 1^1/_2-1/_2}C^{J1/2}_{L_2 0^1/_2 1/_2}C^{L_2 0}_{l_2-111} - C^{J3/2}_{L_1 1^1/_2 1/_2}C^{J3/2}_{L_2 2^1/_2-1/_2}C^{L_2 2}_{l_2 111};$$

$\delta(l_2\lambda_2)$ indicates that in the sum over l_2 only the term with $l_2 = L_2$ enters if $\lambda_2 = 0$, and only the terms with $l_2 = L_2 \pm 1$ if $\lambda_2 = 1$; $Q_l(x)$ are the Legendre functions of the second kind (for an analytic expression for $Q_l(x)$ see reference 4; for a table of values see reference 5).

Values of $R(L_2\lambda_2;\ L_1\lambda_1;\ J\Pi)$ up to $J = 7/2$ are given in the table.

2. ANGULAR DISTRIBUTIONS

The angular distribution may be expressed in the form

$$d\sigma/do = \mathrm{Sp}\,[\rho_2 f \rho_1 f^+], \tag{8}$$

where

$$\rho_1 = \tfrac{1}{4}(1+\xi_1\omega)(1+\zeta_1\sigma), \qquad \rho_2 = \tfrac{1}{4}(1+\xi_2\omega)(1+\zeta_2\sigma) \tag{9}$$

are density matrices describing the initial and final states respectively of the nucleon-photon system. Here ξ_1 and ξ_2 are photon polarization vectors, ζ_1 and ζ_2 are nucleon polarization vectors, σ are the Pauli matrices and $\omega_1 = \sigma_Z$, $\omega_2 = \sigma_X$, $\omega_3 = \sigma_Y$. We follow here the definitions given by Tolhoek.[6]

Let us write the angular distribution as a sum of sixteen terms:

$$\begin{aligned} d\sigma/do = {} & \Phi_0 + \Phi_1(\xi_1) + \Phi_1(\xi_2) + \Phi_1(\zeta_1) + \Phi_1(\zeta_2) \\ & + \Phi_2(\xi_1,\ \xi_2) + \Phi_2(\zeta_1,\ \zeta_2) + \Phi_2(\xi_1,\ \zeta_1) + \Phi_2(\xi_1,\ \zeta_2) \\ & + \Phi_2(\xi_2,\ \zeta_1) + \Phi_2(\xi_2,\ \zeta_2) + \Phi_3(\xi_1,\ \xi_2,\ \zeta_1) + \Phi_3(\xi_1,\ \xi_2,\ \zeta_2) \\ & + \Phi_3(\xi_1,\ \zeta_1,\ \zeta_2) + \Phi_3(\xi_2,\ \zeta_1,\ \zeta_2) + \Phi_4(\xi_1,\ \xi_2,\ \zeta_1,\ \zeta_2). \end{aligned} \tag{10}$$

To average over the polarization states of an initial particle we remove from (10) the terms containing the corresponding polarization vector and multiply the cross section by 2; to sum over the polarization states of a final particle we simply remove the corresponding terms from the total cross section (10).

In Eq. (8) we write f in the form of a matrix whose elements represent the scattering amplitude with prescribed polarizations for the photon and nucleon

$$f = \frac{C}{x-\cos\theta}\,a(\alpha,\beta)\,b(\lambda,\mu), \tag{11}$$

where $a(\alpha, \beta)$, $b(\lambda, \mu)$ depend on the polarizations of the nucleon and photon and are given by (see Goertzel)[7]

$$a(1/2;\ 1/2) = (1-\cos\theta), \qquad a(-1/2;\ -1/2) = -(1-\cos\theta),$$
$$a(1/2;\ -1/2) = -\sin\theta e^{-i\varphi}, \qquad a(-1/2;\ 1/2) = -\sin\theta e^{i\varphi}; \tag{12}$$

$$b(1;1) = b(-1;-1) = 0, \qquad b(1;-1) = ie^{-i\varphi}(1-\cos\theta),$$
$$b(-1;1) = -ie^{i\varphi}(1-\cos\theta). \tag{13}$$

From (11), (12), and (13) we find.

$$\Phi_0 = \tfrac{1}{2}C^2(1-\cos\theta)^3/(x-\cos\theta)^2,$$

$$\Phi_1(\xi_1) = \Phi_1(\zeta_1) = \Phi_1(\xi_2) = \Phi_1(\zeta_2) = 0, \tag{14}$$

$$\Phi_2(\xi_1,\xi_2) = \frac{1}{2}C^2\frac{(1-\cos\theta)^3}{(x-\cos\theta)^2}\{-\xi_{21}\xi_{11} + (\xi_{23}\xi_{13} - \xi_{22}\xi_{12})\cos 2\varphi - (\xi_{23}\xi_{12} + \xi_{22}\xi_{13})\sin 2\varphi\}, \tag{15}$$

Values of the coefficients $D(L_2\lambda_2; L_1\lambda_1; J) = -iR(L_2\lambda_2; L_1\lambda_1; J\Pi)$

D^* \ ω, Mev	68 5	97	116	137	154	217	308
$D(1,0;\ 1,0;\ 1/2)$	0.7726	1.099	1.262	1.402	1.487	1.696	1.830
$D(1,1;\ 1,1;\ 3/2)$	0.3863	0.5493	0 6307	0.7012	0.7433	0.8480	0.9152
$D(1,0;\ 2,1;\ 3/2)$	—0.3022	—0.4065	—0.4522	—0.4877	—0.5069	—0.5470	—0.5657
$D(2,0;\ 2,0;\ 3/2)$	$3.739\cdot10^{-2}$	$7.986\cdot10^{-2}$	$1.085\cdot10^{-1}$	0.1380	0.1580	0.2164	0.2620
$D(2,1;\ 2,1;\ 5/2)$	$2.493\cdot10^{-2}$	$5.324\cdot10^{-2}$	$7.237\cdot10^{-2}$	$9.203\cdot10^{-2}$	0.1054	0.1443	0.1747
$D(2,0;\ 3,1;\ 5/2)$	$-3.079\cdot10^{-2}$	$-6.072\cdot10^{-2}$	$-7.863\cdot10^{-2}$	$-9.527\cdot10^{-2}$	—0,1056	—0,1309	—0.1457
$D(3,0;\ 3,0;\ 5/2)$	$3.157\cdot10^{-3}$	$1.031\cdot10^{-2}$	$1.677\cdot10^{-2}$	$2.467\cdot10^{-2}$	$3.072\cdot10^{-2}$	$5.168\cdot10^{-2}$	$7.170\cdot10^{-2}$
$D(3,1;\ 3,1;\ 7/2)$	$2.368\cdot10^{-3}$	$7.732\cdot10^{-3}$	$1.258\cdot10^{-2}$	$1.850\cdot10^{-2}$	$2.304\cdot10^{-2}$	$3.876\cdot10^{-2}$	$5.377\cdot10^{-2}$
$D(3,0;\ 4,1;\ 7/2)$	$-3.942\cdot10^{-3}$	$-1.174\cdot10^{-2}$	$-1.802\cdot10^{-2}$	$-2.500\cdot10^{-2}$	$-2.989\cdot10^{-2}$	$-4,424\cdot10^{-2}$	$-5.454\cdot10^{-2}$
$D(4,0;\ 4,0;\ 7/2)$	$0.3320\cdot10^{-3}$	$1.671\cdot10^{-3}$	$0.3270\cdot10^{-2}$	$0.5592\cdot10^{-2}$	$0.7610\cdot10^{-2}$	$1.592\cdot10^{-2}$	$2.561\cdot10^{-2}$

*The $D(L_2, \lambda_2; L_1, \lambda_1; J)$ satisfy the following relations: $D(1,1;\ 1,1;\ 1/2) = -D(1,0;\ 1,0;\ 1/2)$; $D(1,0;\ 1,0;\ 3/2) = -D(1,1;\ 1,1;\ 3/2)$; $D(2,1;\ 2,1;\ 3/2) = -D(2,0;\ 2,0;\ 3/2)$; $D(2,0;\ 2,0;\ 5/2) = -D(2,1;\ 2,1;\ 5/2)$; $D(3,1;\ 3,1;\ 5/2) = -D(3,0;\ 3,0;\ 5/2)$; $D(3,0;\ 3,0;\ 7/2) = -D(3,1;\ 3,1;\ 7/2)$; $D(4,1;\ 4,1;\ 7/2) = -D(4,0;\ 4,0;\ 7/2)$; $D(a, \alpha; b, \beta; J) = D(b,\alpha; a,\beta; J) = D(a,\beta; b,\alpha; J) = D(b,\beta; a,\alpha; J)$, where a and b are values of the angular momenta L_2 and L_1; α, β are values of the photon parities λ_1 and λ_2 respectively, and $a = b \pm 1$ $\alpha = 1 - \beta$.

$$\Phi_2(\xi_1, \zeta_1) = \Phi_2(\xi_1, \zeta_2) = \Phi_2(\xi_2, \zeta_1) = \Phi_2(\xi_2, \zeta_2) = 0,$$

$$\Phi_2(\zeta_1, \zeta_2) = \frac{1}{2} C^2 \frac{(1-\cos\theta)^2}{(x-\cos\theta)^2}$$

$$\times \{(\zeta_2(\mathbf{n}_1 - \mathbf{n}_2))(\zeta_1(\mathbf{n}_1 - \mathbf{n}_2)) - (\zeta_1\zeta_2)(1-\cos\theta)\},$$

$$\Phi_3(\xi_1, \xi_2, \zeta_1) = \Phi_3(\xi_1, \xi_2, \zeta_2)$$

$$= \Phi_3(\xi_1, \zeta_1, \zeta_2) = \Phi_3(\xi_2, \zeta_1, \zeta_2) = 0, \qquad (16)$$

$$\Phi_4(\xi_1, \xi_2, \zeta_1, \zeta_2) = \frac{1}{2} C^2 \frac{(1-\cos\theta)^2}{(x-\cos\theta)^2}$$

$$\times \{-\xi_{21}\xi_{11} + (\xi_{23}\xi_{13} - \xi_{22}\xi_{12})\cos 2\varphi - (\xi_{23}\xi_{12} + \xi_{22}\xi_{13})\sin 2\varphi\}$$

$$\times \{(\zeta_1(\mathbf{n}_1 - \mathbf{n}_2))(\zeta_2(\mathbf{n}_1 - \mathbf{n}_2)) - (\zeta_1\zeta_2)(1-\cos\theta)\}. \qquad (17)$$

To separate out large angular momenta it is necessary to express the amplitude in terms of the scattering matrix. Making use of (3), we obtain the desired expressions for the angular distributions.

a) Angular distribution for unpolarized particles. Using the formulas[8,9]

$$\sum_\beta C^{l\alpha+\beta}_{a\alpha b\beta} C^{c\gamma}_{l\alpha+\beta d\gamma-\alpha-\beta} C^{f\gamma-\alpha}_{b\beta d\gamma-\alpha-\beta}$$

$$= \sqrt{(2l+1)(2f+1)}\, C^{c\gamma}_{a\alpha f\gamma-\alpha} W(abcdef)$$

and

$$Y_{lm}(\mathbf{n}) Y^*_{l'm'}(\mathbf{n}) = (-1)^{m'} \sum_\nu \sqrt{\frac{(2l+1)(2l'+1)}{4\pi(2\nu+1)}}$$

$$\times C^{\nu 0}_{l'0l0} C^{\nu\sigma}_{l'-m'lm} Y_{\nu\sigma}(\mathbf{n}),$$

we obtain (see Morita et al.[2])

$$\frac{d\sigma_0}{do} = 4\Phi_0 = (C^2/16) \sum R(L_2\lambda_2; L_1\lambda_1; J\Pi)$$

$$\times R^*(L_2'\lambda_2'; L_1'\lambda_1'; J'\Pi')\, i^{L_1+\lambda_1-L_2-\lambda_2+L_2'+\lambda_2'-L_1'-\lambda_1'}$$

$$\times a_\nu(JL_2J'L_2')\, a_\nu(JL_1J'L_1')\, P_\nu(\cos\theta), \qquad (18)$$

where

$$a_\nu(JLJ'L') = \sqrt{(2L+1)(2J+1)(2L'+1)(2J'+1)}$$

$$\times C^{\nu 0}_{L1L'-1} W(LJL'J'\,1/2\,\nu). \qquad (19)$$

The summation is over all values of the angular momenta, their projections and ν, W(a, b, c, d, e, f) is the Racah coefficient.

b) Photon polarized before and after the reaction, nucleon unpolarized

$$d\sigma(\xi_1, \xi_2)/do = \{1 - \xi_{21}\xi_{11} + (\xi_{23}\xi_{13} - \xi_{22}\xi_{12})\cos 2\varphi$$

$$- (\xi_{23}\xi_{12} + \xi_{22}\xi_{13})\sin 2\varphi\} \quad (C^2/32) \sum R(L_2\lambda_2; L_1\lambda_1; J\Pi)$$

$$\times R^*(L_2'\lambda_2'; L_1'\lambda_1'; J'\Pi')\, i^{L_1+\lambda_1-L_2-\lambda_2+L_2'+\lambda_2'-L_1'-\lambda_1'}$$

$$\times a_\nu(JL_2J'L_2')\, a_\nu(JL_1J'L_1')\, P_\nu(\cos\theta). \qquad (20)$$

c) Nucleon polarized before and after the reaction, photon unpolarized

$$d\sigma(\zeta_1, \zeta_2)/d\sigma = \left\{1 + \frac{(\zeta_2(n_1 - n_2))/(\zeta_1(n_1 - n_2))}{1 - \cos\theta} - (\zeta_1\zeta_2)\right\}(C^2/32)\sum R(L_2\lambda_2; L_1\lambda_1; J\Pi) \times R^*(L_2'\lambda_2'; L_1'\lambda_1'; J'\Pi')\, i^{L_1+\lambda_1-L_2-\lambda_2+L_2'+\lambda_2'-L_1'-\lambda_1'} \times a_\nu(JL_2J'L_2')\, a_\nu(JL_1J'L_1')\, P_\nu(\cos\theta). \quad (21)$$

The expressions for $R(L_2\lambda_2; L_1\lambda_1; J\Pi)$ calculated in the first section are valid only for sufficiently large angular momenta. Therefore, as was done for nucleons by Grashin,[10] the terms corresponding to small values of angular momenta may be separated from the sum over angular momenta in (18), (20), and (21) and treated as adjustable parameters to be determined by experiment or by a future exact theory.

In conclusion I wish to express gratitude to V. B. Berestetskiĭ, L. B. Okun', and I. Ya. Pomeranchuk for suggesting this research and for their interest in the work. I also wish to thank V. P. Ignatenko for useful discussions.

[1] L. B. Okun' and I. Ya. Pomeranchuk, JETP **36**, 300 (1959), Soviet Phys. JETP **9**, 207 (1959).

[2] Morita, Sugie, and Yoshida, Progr. Theoret. Phys. **12**, 713 (1954).

[3] A. I. Akhiezer and V. B. Berestetskiĭ, Квантовая электродинамика (Quantum Electrodynamics), Gostekhizdat, 1953 [AEC Tr. 2876].

[4] M. M. Ryzhik and I. S. Gradshteĭn, Таблицы интегралов, сумм, рядов и произведений, (Tables of Integrals, Sums, Series and Products), Gostekhizdat, 1951.

[5] Tables of Associated Legendre Functions, Columbia Univ. Press, N.Y., 1954.

[6] H. A. Tolhoek, Revs. Modern Phys. **28**, 277 (1956).

[7] G. Goertzel, Phys. Rev. **70**, 897 (1946).

[8] Biedenharn, Blatt, and Rose, Revs. Modern Phys. **24**, 249 (1952).

[9] J. Blatt and V. Weisskopf, Theoretical Nuclear Physics, Wiley, N.Y., 1952 (Russ. Transl., IIL, 1954).

[10] A. F. Grashin, JETP **36**, 1717 (1959), Soviet Phys. JETP **9**, 1223 (1959).

Translated by A. M. Bincer
195

ABSORPTION OF SOUND AND THE WIDTH OF SHOCK WAVES IN RELATIVISTIC HYDRODYNAMICS

M. T. ZHUMARTBAEV

Institute of Nuclear Physics, Academy of Sciences, Kazakh S.S.R.

Submitted to JETP editor March 26, 1959

J. Exptl. Theoret. Phys. (U.S.S.R.) **37**, 1000-1004 (October, 1959)

The absorption coefficient of sound due to viscosity and heat conduction is derived in relativistic hydrodynamics. The structure of relativistic low-intensity shock waves is considered.

INTRODUCTION

IF a relativistic liquid possesses viscosity and heat conduction, then this leads to the gradual dissipation of the energy of the sound waves, i.e., to the absorption of the sound. The energy dissipated per unit time E_{mech} can be found by making use of the equation for the entropy increase, and also the expression for the maximum work performed in the transition from a given non-equilibrium state to a state of thermodynamic equilibrium (see reference 1).

The expression for the maximum work is

$$E_{mech} = E_0 - E(S). \tag{1}$$

Here the energy $E(S) = \int \epsilon(s)\, dV_0$; integration is carried out over the volume of the liquid, dV_0 is the element of volume in the proper system of the observer; E_0 is the initial energy, and $E(S)$ is the energy of the body in the equilibrium state with the same entropy S which the body had initially. Starting out from (1), we can write the expression for the dissipated energy in the following form:

$$\dot{E}_{mech} = -T_0 c \int \frac{dS}{ds}\, dV. \tag{2}$$

Here $T_0 = \partial\epsilon/\partial s$ is the temperature which the body would have had in the state of thermodynamic equilibrium; $ds = c\,d\tau$, where $d\tau$ is the differential of proper time; dV is the volume element in the laboratory system of the observer. The expression under the integral in Eq. (2) is determined by the equation for the growth of the entropy:[2]

$$\frac{dS}{ds} = \frac{S}{n}\frac{dn}{ds} + \frac{w}{T}\frac{\partial \nu^k}{\partial x^k} + \frac{1}{T} u^k \frac{\partial \tau_k^l}{\partial x^l}. \tag{3}$$

Here S is the entropy density, n is the density of number of particles per unit volume, while w is the heat function referred to a single particle; ν_i is the additional term in the four vector of the density of material flow n_i and τ_{ik} is the four-tensor of the viscosity (see reference 2).

CALCULATION OF THE SOUND ABSORPTION COEFFICIENT

For calculation of the dissipation of energy in the sound wave we make use of the fact that the velocity of motion of the particles of the liquid v in the sound wave is small, and that the motion takes place adiabatically. Then, taking it into account that the temperature at an infinitely distant surface tends to a constant limit, we obtain

$$E_{mech} \approx -T_0 \int \frac{s}{n}\left(v\frac{\partial n}{\partial x} + \frac{\partial n}{\partial t}\right) dV + T_0 \varkappa \int \left[-\frac{2}{w^2}\left(\frac{\partial w}{\partial x}\right)^2 + \frac{2}{wT}\frac{\partial T}{\partial x}\frac{\partial w}{\partial x} + \frac{1}{w}\frac{\partial^2 w}{\partial x^2} - \frac{1}{T^2}\left(\frac{\partial T}{\partial x}\right)^2\right] dV - T_0 \frac{4\eta/3 + \zeta}{c}\int \frac{1}{T}\left(\frac{\partial v}{\partial x}\right)^2 dV. \tag{4}$$

(Here η and ζ are the two coefficients of viscosity, while κ is the coefficient of heat conduction, taken in correspondence with its nonrelativistic value.)

For the determination of the integrals entering into (4), we make use of a series of relations which hold for a sound wave and also of a number of thermodynamic relations between arbitrary thermodynamical quantities. It is not difficult to show (see reference 2) that the following relations hold:

$$p' = (\partial p/\partial \varepsilon)_\sigma\, \varepsilon' = (W/c^2)\, c_0 v,$$
$$w' = (\partial w/\partial p)_\sigma\, p' = (W/nc^2)\, c_0 v,$$
$$T' = (\partial T/\partial p)_\sigma\, p' = (W/c^2)\, c_0 (\partial T/\partial p)_\sigma\, v \tag{5}$$

(c_0 is the sound velocity, W is the heat function per unit volume). The primed quantities in these relations refer to small increments in the sound wave, the derivatives are taken at constant entropy σ per single particle, and the velocity $v = \partial\varphi/\partial x$, where φ is the velocity potential. The mean energy density of the sound wave in relativistic hy-

drodynamics in the laboratory system is given by the expression

$$\bar{v}^2(\varepsilon + 2p)/c^2. \tag{6}$$

If we denote by

$$c_p = T(\partial\sigma/\partial T)_p, \qquad c_V = T(\partial\sigma/\partial T)_V \tag{6a}$$

the heat capacity per single particle at constant pressure and constant volume $1/n = mV$, respectively, then, if we make use of the thermodynamical identities

$$d\varepsilon = nTd\sigma - n^2 w d(1/n), \qquad dw = Td\sigma + (1/n)dp,$$
$$d\mu = -\sigma dT + (1/n)dp, \tag{7}$$

we can obtain the following formulas:

$$c_V - c_p = T\left[\frac{\partial}{\partial T}\left(\frac{1}{n}\right)\right]_p^2 \Big/ \frac{\partial}{\partial p}\left(\frac{1}{n}\right)_T, \tag{8}$$

$$\left(\frac{\partial T}{\partial p}\right)_\sigma = \frac{T}{c_p}\frac{\partial}{\partial T}\left(\frac{1}{n}\right)_p, \tag{9}$$

$$\left[\frac{\partial(1/n)}{\partial p}\right]_\sigma = \frac{c_V}{c_p}\left[\frac{\partial(1/n)}{\partial p}\right]_T. \tag{10}$$

Making use of (9), and the value of the derivatives

$$\frac{\partial p}{\partial(1/n)_\sigma} = -Wnc_0^2/c^2, \tag{10a}$$

we write out Eq. (8) in the form

$$c_V - c_p = -\frac{c_V T W c_0^2}{c_p n c^2}\left[n\frac{\partial(1/n)}{\partial T}\right]_p^2. \tag{11}$$

The integrals entering into (4) will be computed for a plane wave of the form $v = v_0\cos(kx - \omega t)$, the time average energy of such a wave in a volume V_0 of liquid being, in accord with (6),

$$\bar{E} = \tfrac{1}{2}v_0^2 V_0(\varepsilon + 2p)/c^2. \tag{12}$$

The first integral in Eq. (4) vanishes in the mean; the same also applies to the integral of $(\partial^2 w/\partial x^2)/w$. Using (8) – (12) and

$$\left(\frac{\partial T}{\partial p}\right)_\sigma = \frac{T\beta}{c_p n}, \qquad \beta = n\frac{\partial}{\partial T}\left(\frac{1}{n}\right)_p \tag{12a}$$

(β is the coefficient of thermal expansion), the sound absorption coefficient

$$\gamma = |\bar{E}_{\text{mech}}|/2c_0\bar{E} \tag{13}$$

takes the following final form in relativistic hydrodynamics:

$$\gamma = \frac{\omega^2 c^2}{2(\varepsilon + 2p)c_0^2}\left[\frac{1}{c}\left(\frac{4}{3}\eta + \zeta\right) + \varkappa\left(\frac{W}{nc^2}\right)\left(\frac{1}{c_V} - \frac{1}{c_p}\right)\right.$$
$$\left. - \frac{2\varkappa}{c^2}\left(\frac{1}{c_V} - \frac{1}{c_p}\right)\frac{c_p}{\beta}\left(1 - \frac{c_p}{\beta w}\right)\right] \tag{14}$$

(where $k = \omega/c_0$). In the nonrelativistic limit, (14) goes over into the usual expression for the sound absorption coefficient.

THICKNESS OF SHOCK WAVES

It is well known that a weak shock wave in nonrelativistic hydrodynamics has a finite thickness which is inversely proportional to the amplitude of the wave.

The distribution of thermodynamical quantities over the thickness of the shock wave is found with the help of the usual hydrodynamical laws of conservation of mass, energy and momentum, with account of streaming produced by viscosity and heat conduction. In relativistic hydrodynamics, the corresponding conservation laws have the following form:

$$\frac{\bar{n}\bar{v}}{(1 - \bar{v}^2/c^2)^{1/2}} - \frac{\varkappa}{1 - \bar{v}^2/c^2}\left(\frac{T}{w}\right)^2\left[\frac{\partial}{\partial x}\left(\frac{\bar{\mu}}{T}\right) + \frac{\bar{v}}{c^2}\frac{\partial}{\partial t}\left(\frac{\bar{\mu}}{T}\right)\right]$$
$$= \frac{nv}{\sqrt{1 - v^2/c^2}} = j, \tag{15}$$

$$\bar{n}\bar{w}\frac{\bar{v}^2}{c^2(1 - \bar{v}^2/c^2)} + \bar{p} - \left(\frac{4}{3}\eta + \zeta\right)\frac{1}{c(1 - \bar{v}^2/c^2)^{5/2}}\left[\frac{\partial\bar{v}}{\partial x} + \frac{\bar{v}}{c^2}\frac{\partial\bar{v}}{\partial t}\right]$$
$$= nw\frac{v^2}{c^2(1 - v^2/c^2)} + p, \tag{16}$$

$$\bar{n}\bar{w}\frac{\bar{v}}{c(1 - \bar{v}^2/c^2)} - \left(\frac{4}{3}\eta + \zeta\right)\frac{\bar{v}}{c^2(1 - \bar{v}^2/c^2)^{5/2}}\left[\frac{\partial\bar{v}}{\partial x} + \frac{\bar{v}}{c^2}\frac{\partial\bar{v}}{\partial t}\right]$$
$$= nw\frac{v}{c^2(1 - v^2/c^2)} \tag{17}$$

(the shock wave moves from the right to the left, the state in front of the shock wave is denoted without bars).

Proceeding in the usual fashion, we expand the values of all quantities on the shock wave in a series of powers of the entropy jump $\Delta\sigma = \bar{\sigma} - \sigma$ and the pressure jump $\Delta p = \bar{p} - p$. Taking the thermodynamic identities (7) into account, we have

$$\bar{w} - w = T\Delta\sigma + \frac{1}{n}\Delta p + \frac{1}{2}\frac{\partial}{\partial p}\left(\frac{1}{n}\right)_\sigma \Delta p^2,$$
$$\bar{n} - n = -n^2\frac{\partial}{\partial\sigma}\left(\frac{1}{n}\right)_p \Delta\sigma - n^2\frac{\partial}{\partial p}\left(\frac{1}{n}\right)_\sigma$$
$$\times \Delta p - n^2\left[\frac{1}{2}\frac{\partial^2}{\partial p^2}\left(\frac{1}{n}\right)_\sigma - n\left(\frac{\partial}{\partial p}\left(\frac{1}{n}\right)_\sigma\right)^2\right]\Delta p^2. \tag{18}$$

Here we have neglected terms in $\Delta\sigma$ and Δp higher than the first and third, because $\Delta\sigma$ (as we shall see below) has an order of smallness not higher than second. Further, we express the derivatives in (15) in terms of derivatives of p and σ. In this case, it is necessary to recall that differentiation with respect to x and t increases the order of smallness of quantities per unit value (since the width of the shock wave is inversely proportional to the amplitude of the wave). Therefore, the derivatives $\partial p/\partial x$ and $\partial p/\partial t$ are quantities of second order of smallness, while the derivatives $\partial\sigma/\partial x$ and $\partial\sigma/\partial t$ are third order. Thus, on the

whole, the mass flow brought about by the thermal conductivity has a second order of smallness in Eq. (15). As a result we obtain (15) in the form

$$\frac{\bar{n}\bar{v}}{(1-\bar{v}^2/c^2)^{1/2}} = \varkappa\left(\frac{T}{w}\right)^2 \frac{1}{T}\left(\frac{\partial w}{\partial p_\sigma} - \frac{w}{T}\frac{\partial T}{\partial p_\sigma}\right)\left[\left(1+\frac{j^2}{n^2c^2}\right)\frac{\partial p}{\partial x} + \frac{j}{nc^2}\left(1+\frac{j^2}{n^2c^2}\right)^{1/2}\frac{\partial p}{\partial t}\right] + j. \quad (19)$$

It is then easy to find the expansion for $\bar{v}$. Hence, substituting the resultant expansions in (16), we find an equation which connects the pressure and entropy jumps (this relation is too cumbersome to write down here).

To determine the energy jump $\Delta\sigma$ on the discontinuity, it is necessary to make use of both Eqs. (16) and (17), first subtracting the second, multiplied by $\bar{v}/c$, from the first. Carrying out a number of transformations of the thermodynamical derivatives, we finally obtain the following expression of second order relative to Δp:

$$\left[\left(1+\frac{j^2}{n^2c^2}\right)+\frac{j^2}{n^2c^2}wn^2\frac{\partial}{\partial p}\left(\frac{1}{n}\right)\right]\Delta p + \left[\frac{3}{2}\frac{j^2}{n^2c^2}n\frac{\partial}{\partial p}\left(\frac{1}{n}\right) + \frac{1}{2}\frac{j^2}{n^2c^2}wn^2\frac{\partial^2}{\partial p^2}\left(\frac{1}{n}\right)\right]\Delta p^2 = j\left(1+\frac{j^2}{n^2c^2}\right)\frac{\partial}{\partial p}\left(\frac{1}{n}\right)_\sigma\left[\frac{\partial p}{\partial x} + \frac{j}{nc^2(1+j^2/n^2c^2)^{1/2}}\frac{\partial p}{\partial t}\right]a_1, \quad (20)$$

where

$$a = \frac{1}{c}\left(\frac{4}{3}\eta+\zeta\right) + \varkappa\left(\frac{W}{nc^2}\right)\left(\frac{1}{c_V}-\frac{1}{c_p}\right) - \frac{2\varkappa}{c^2}\left(\frac{1}{c_V}-\frac{1}{c_p}\right)\frac{c_p}{\beta}\left(1-\frac{c_\rho}{\beta w}\right). \quad (20a)$$

The right side of Eq. (20) vanishes along with $\partial\bar{p}/\partial x$ and $\partial\bar{p}/\partial t$ at great distances on both sides of the surface of discontinuity (a replacement of $\partial p/\partial x$ by $\partial\bar{p}/\partial x$ is valid with accuracy up to terms of third order of smallness). At these distances, the pressure is equal to p and p_1, respectively. In other words, the quadratic (in p) expression on the left side of (20) has the roots $\bar{p} = p$ and $\bar{p} = p_1$. Therefore Eq. (20) can be represented in the form

$$\left[\frac{3}{2}\frac{j^2}{n^2c^2}n\frac{\partial}{\partial p}\left(\frac{1}{n}\right)+\frac{1}{2}\frac{j^2}{n^2c^2}wn^2\frac{\partial^2}{\partial p^2}\left(\frac{1}{n}\right)\right](\bar{p}-p)(\bar{p}-p_1) = a_1 j\left(1+\frac{j^2}{n^2c^2}\right)\frac{\partial}{\partial p}\left(\frac{1}{n}\right)_\sigma\left[\frac{\partial\bar{p}}{\partial x}+\frac{j}{nc^2(1+j^2/n^2c^2)^{1/2}}\frac{\partial\bar{p}}{\partial t}\right]. \quad (21)$$

From the system of ordinary differential equations which correspond to Eq. (21), we find, by integrating with respect to x,

$$\bar{p} - \frac{p_1+p}{2} = \frac{p_1-p}{2}\tanh\frac{x}{\delta_x}, \quad (22)$$

where

$$\delta_x = \frac{8a(\varepsilon+2p)/n^2W}{(p_1-p)\left[\frac{3}{nc^2}\frac{\partial}{\partial p}\left(\frac{1}{n}\right)+\left(\frac{W}{nc^2}\right)\frac{\partial^2}{\partial p^2}\left(\frac{1}{n}\right)\right]\left(1-\frac{c_0^2}{c^2}\right)^{1/2}}. \quad (23)$$

Here it is taken into account that the velocity of the weak shock wave in zeroth approximation is equal to the sound velocity c_0^3 and therefore can be expanded to the same approximation:

$$j/n = c_0/\sqrt{1-c_0^2/c^2}. \quad (23a)$$

As expected, the quantity a is related to the sound absorption coefficient (14), namely $\gamma = a\omega^2$.

The quantity δ_x determines the width of the shock wave in relativistic hydrodynamics. We see that even here the width of the shock wave is inversely proportional to the amplitude of the wave. In the nonrelativistic limit, the first term in the square brackets in the denominator can be neglected in comparison with the second; then, (23) reduces to the well-known nonrelativistic expression.

Integration over t gives

$$\bar{p} - \frac{p_1+p}{2} = \frac{p_1-p}{2}\tanh\frac{t}{\delta_t}, \quad (24)$$

where

$$\delta_t = \frac{8a(\varepsilon+2p)c_0/n^2Wc^2}{(p_1-p)\left[\frac{3}{nc^2}\frac{\partial}{\partial p}\left(\frac{1}{n}\right)+\left(\frac{W}{nc^2}\right)\frac{\partial^2}{\partial p^2}\left(\frac{1}{n}\right)\right]\left(1-\frac{c_0^2}{c^2}\right)^{1/2}}; \quad (25)$$

δ_t determines the variation of the pressure over the thickness of the shock wave as a function of time. In the nonrelativistic limit, δ_t tends to zero.

For the variation of the entropy inside the discontinuity, we have the following results:

$$\Delta\sigma = \frac{\varkappa n}{16c_0aT}\left(\frac{\partial T}{\partial p}\right)_\sigma\left[\frac{3}{nc^2}\frac{\partial}{\partial p}\left(\frac{1}{n}\right)+\left(\frac{W}{nc^2}\right)\frac{\partial^2}{\partial p^2}\left(\frac{1}{n}\right)\right](p_1-p)^2 \times\left(\cosh^{-2}\frac{x}{\delta_x}+\cosh^{-2}\frac{t}{\delta_t}\right)\left(1-\frac{T}{nw\partial T/\partial p_\sigma}\right). \quad (26)$$

The entropy reaches a maximum inside the discontinuity (for $x = 0$ and $t = 0$). At large distances on both sides of the shock wave, for $x \to \pm\infty$ and $t \to \pm\infty$, this formula gives $\bar{\sigma} = \sigma$. This is connected with the fact that in relativistic hydrodynamics, as well as in nonrelativistic, the total discontinuity in the entropy is a quantity of third order in Δp, while $\bar{\sigma} - \sigma$ is of second order.

[1] L. D. Landau and E. M. Lifshitz, Статистическая физика. (Statistical Physics) (English translation, Pergamon Press, 1958).

[2] L. D. Landau and E. M. Lifshitz, Механика сплошных сред (Mechanics of Continuous Media) (Gostekhizdat, 1954).

[3] I. M. Khalatnikov, JETP **27**, 529 (1954).

Translated by R. T. Beyer
196

INCOMPATIBILITY OF THE CONDITIONS OF ANALYTICITY AND UNITARITY IN THE LEE MODEL

K. A. TER-MARTIROSYAN

Submitted to JETP editor April 1, 1959; resubmitted July 6, 1959

J. Exptl. Theoret. Phys. (U.S.S.R.) **37**, 1005-1009 (October, 1959)

It is shown that outside the framework of the Hamiltonian formalism, and when one takes into account only the selection rules that are characteristic of the Lee model, the conditions of analyticity lead (even in the simplest $N + \theta$ sector) to a contradiction with the condition of unitarity. Owing to the existence of crossing symmetry this contradiction does not arise in the usual meson theories (at any rate for a static nucleon in the one-meson approximation, which in the Lee model is analogous to the case of the $N + \theta$ sector).

QUITE recently there have been[1,2] a number of interesting attempts to construct a theory of the strong interactions on the basis of a combination of the conditions of unitarity and analyticity. In this connection it is interesting to examine what such an approach gives in the simple case of the Lee model.[3] As is well known, in the usual Hamiltonian formalism of quantum field theory unphysical states appear in the Lee model,[4] and the theory is found to be self-contradictory.

It is shown below that outside the framework of the Hamiltonian formalism, and when we take into account only the selection rules that are characteristic of the Lee model (and which, as is well known, destroy the crossing symmetry of the theory), even in the simplest $N + \theta$ sector the condition of unitarity is incompatible with the condition of analyticity of the scattering amplitude. Thus, independently of the formalism used, just the assumption that the selection rule $V \rightleftarrows N + \theta$ holds, with the theory nonrelativistic in particles V and N, leads to clearly unphysical results. Unlike the Lee model, the usual meson theories, characterized by crossing symmetry, do not lead to a similar contradiction,* in any case for a static nucleon in the simplest one-meson approximation, which is analogous to the case of the $N + \theta$ sector in the Lee model.

Let us first examine in detail the case of meson theories that have crossing symmetry as a characteristic feature; this case has been studied in earlier papers.[5,6] For definiteness we shall speak of the theory of scalar charged mesons with scalar coupling and a static nucleon. In this case for $\mu/M \ll 1$, $\omega/M \ll 1$, where $\omega = (\mu^2 + k^2)^{1/2}$ is the energy of the meson, the meson-nucleon scattering amplitude depends only on ω. For a point

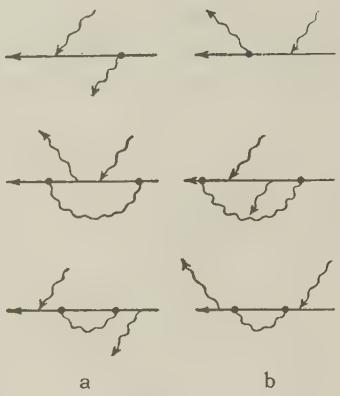

FIG. 1

interaction it is given by an analytic function $A(\omega)$, such that $A_+(\omega) = A(\omega + i\tau)$ for the scattering of π^+ mesons by protons and $A_-(\omega) = A(-\omega - i\tau)$ for the scattering of π^- [where $\tau \to 0$; these relations hold in the physical region $|\omega| \geq \mu$; in the region $|\omega| < \mu$ the function $A(\omega)$ is a real quantity]. The relation $A_-(\omega) = A_+^*(-\omega)$ expresses the crossing symmetry of the theory; it is not hard to see that this is a consequence of the fact that in the whole set of diagrams for the scattering of a meson by a nucleon each diagram, for example any of those of Fig. 1a, can be paired with another, as in Fig. 1b, in which the incident and scattered mesons are interchanged.

The function $A(\omega)$ satisfies the conditions of unitarity ($\omega > \mu$)

$$\operatorname{Im} A(\omega + i\tau) = \sqrt{\omega^2 - \mu^2}\,|A(\omega)|^2 + \ldots \quad (1)$$

$$\operatorname{Im} A(-\omega - i\tau) = \sqrt{\omega^2 - \mu^2}\,|A(-\omega)|^2 + \ldots \quad (2)$$

(where in the right members we have neglected terms corresponding to the occurrence of two or more mesons), and a condition of analyticity, which, on the assumption that for $\omega \to \infty$ the quantity $|A|^2$ falls off sufficiently rapidly, can be written in the

*A similar statement is contained in a paper by Mandelstam.[1]

form of the well known dispersion relation

$$A(\omega) = \frac{g^2}{\omega} + \frac{1}{\pi}\int_{\mu}^{\infty} \frac{\operatorname{Im} A(\omega' + i\tau)\, d\omega'}{\omega' - \omega}$$

$$- \frac{1}{\pi}\int_{-\infty}^{-\mu} \frac{\operatorname{Im} A(\omega' - i\tau)\, d\omega'}{\omega' - \omega} \qquad (3)$$

(here g is the coupling constant, normalized in a definite way).

As is well known, the appearance of the last term in the right member of Eq. (3) is due to the crossing symmetry, since because of the equation $A(\omega - i\tau) = A_-(-\omega)$ the function $A(\omega)$ has a branch point not only at $\omega = +\mu$ [where the amplitude $A_+(\omega)$ has a branch point] but also at $\omega = -\mu$, since here the amplitude $A_-(-\omega)$ has a branch point. Substitution of (1) and (2) in (3) leads to the Low equations, whose general solution has been found by Castillejo, Dalitz, and Dyson.[5] These authors remarked that the most general form of an analytic function satisfying the unitarity relations (1) and (2), having a pole with residue g^2 at $\omega = 0$, and having two branches for $|\omega| > \mu$, is

$$A(\omega) = -\frac{1}{\omega}\,\frac{1}{H(\omega)}, \qquad (4)$$

where

$$H(\omega) = -\frac{1}{g^2} + \frac{1}{\pi}\int_{\mu}^{\infty} \frac{\operatorname{Im} H(\omega' + i\tau)\, \omega d\omega'}{\omega'(\omega' - \omega)}$$

$$- \frac{1}{\pi}\int_{-\infty}^{-\mu} \frac{\omega}{\omega'}\,\frac{\operatorname{Im} H(\omega' - i\tau)\, d\omega'}{\omega' - \omega} + R(\omega), \qquad (5)$$

with

$$R(\omega) = \sum_n \frac{\omega}{\omega_n}\,\frac{R_n}{\omega_n - \omega} + \omega R_\infty. \qquad (6)$$

Here R_n and R_∞ are real positive numbers, and the ω_n are also real quantities, namely the values of ω at which $A(\omega)$ is zero. It follows immediately from (1), (2), and (4) that

$$\operatorname{Im} H(\omega' \pm i\tau) = \pm \frac{\sqrt{\omega'^2 - \mu^2}}{\omega'}, \qquad (7)$$

for $\omega' > \mu$ and $\omega' < -\mu$, respectively; therefore both the integrals in (5) [the integral $J_1(\omega)$ from μ to ∞ and the integral $J_2(\omega)$ from $-\infty$ to $-\mu$] can be calculated immediately:

$$J(\omega) = J_1(\omega) + J_2(\omega)$$

$$= \frac{2\omega}{\pi}\int_{\mu}^{\infty} \frac{\sqrt{\omega'^2 - \mu^2}\, d\omega'}{\omega'(\omega'^2 - \omega^2 - i\tau)} = \frac{\mu - \sqrt{\mu^2 - \omega^2}}{\omega} \qquad (8)$$

[for $\omega > \mu$, in the regions $\pm(\omega \pm i\tau)$ the root $(\mu^2 - \omega^2)^{1/2}$ is defined so that it takes the value $+i(\omega^2 - \mu^2)^{1/2}$]. Therefore, by (4), (5), and (8)

$$A(\omega) = \frac{g^2}{\omega}\{1 - g^2[J(\omega) + R(\omega)]\}^{-1}. \qquad (9)$$

This function will satisfy the relation (3) if the curly bracket in (9) does not vanish for any value of ω, i.e., if $A(\omega)$ has no other poles besides the pole at the point $\omega = 0$. It follows directly from (9), (8), and (6) that this requirement can be satisfied if all $|\omega_n| > \mu$ (except just one value $|\omega_{n_0}|$, which can be less than μ), and if

$$g^2 < \frac{1}{1 + R(\mu)} \qquad (10)$$

[if $R(\omega) \equiv 0$, i.e., for that solution for which $\omega A(\omega)$ vanishes nowhere it is enough if $g^2 < 1$].

Thus from these results, obtained by Castillejo, Dalitz, and Dyson, it follows that in the case of the meson theories the unitarity and analyticity conditions (1) — (3) are compatible and determine the scattering amplitude in the form (9).

The situation is quite different in the case of the Lee model. Let us consider the simplest $N + \theta$ sector and denote by $a(\omega)$ the analytic function whose value at the point $\omega + i\tau$ $(\omega > \mu)$ determines the amplitude of the scattering $N + \theta$. Instead of Eqs. (1) — (3), the unitarity and analyticity conditions are now written in the form

$$\operatorname{Im} a(\omega + i\tau) = \sqrt{\omega^2 - \mu^2}\,|a(\omega)|^2, \qquad (11)$$

$$a(\omega) = \frac{g^2}{\varepsilon_0 - \omega} + \frac{1}{\pi}\int_{\mu}^{\infty} \frac{\operatorname{Im} a(\omega' + i\tau)}{\omega' - \omega}\, d\omega', \qquad (12)$$

where $\varepsilon_0 = M_V - M_N$, and from the condition of stability of the V particle it follows that $\varepsilon_0 < \mu$. Unlike (1), Eq. (11) is exact, because transitions from the $N + \theta$ sector into other sectors are forbidden. There is no term in (12) analogous to the last term in (3), since now the values of the function $a(\omega)$ for negative ω (more exactly, for any $\omega < \mu$) do not have the physical meaning of the amplitude of some process, as they could in the meson theories.

Just as in the preceding case of the meson theories we can see that the most general form of the analytic function $a(\omega)$ that satisfies the unitarity condition (11), and that has a pole at $\omega = \varepsilon_0$ and a branch point at $\omega = \mu$,* is

$$a(\omega) = -\frac{1}{\omega - \varepsilon_0}\,\frac{1}{h(\omega)}, \qquad (13)$$

where

$$\operatorname{Im} h(\omega + i\tau) = \frac{\sqrt{\omega^2 - \mu^2}}{\omega - \omega_0}, \qquad (14)$$

*The general form of the analytic function satisfied the condition, also satisfied by $A(\omega)$, that for complex ω the sign of $\operatorname{Im}\omega A(\omega)$ is the same as that of $\operatorname{Im}\omega$. This requirement follows from the analyticity condition (12) [and from Eq. (3) for $A(\omega)$].

$$h(\omega) = \frac{1}{g^2} + J_1(\omega) + \rho(\omega), \tag{15}$$

$$J_1(\omega) = \frac{1}{\pi}\int_{\mu}^{\infty} \frac{(\omega - \varepsilon_0)}{(\omega' - \varepsilon_0)^2} \frac{\sqrt{\omega'^2 - \mu^2}}{\omega' - \omega} d\omega', \tag{16}$$

and, in analogy with Eq. (6),

$$\rho(\omega) = \sum_n \frac{\omega - \varepsilon_n}{\omega_n - \varepsilon_0} \frac{R_n}{\omega_n - \omega} + (\omega - \varepsilon_0) R_\infty. \tag{17}$$

All the R_n and R_∞ are real and positive, and the ω_n are real.

The value of $a(\omega)$, that follows from (13) — (17)

$$a(\omega) = \frac{g^2}{\varepsilon_0 - \omega} \{1 + g^2 [J_1(\omega) + \rho(\omega)]\}^{-1} \tag{18}$$

coincides for $\rho(\omega) \equiv 0$ with the well known exact solution of the usual Hamiltonian equations of the Lee model in quantum field theory.

The analyticity relation (12) will be satisfied if $a(\omega)$ has no poles other than that at $\omega = \epsilon_0$. In particular, the curly brackets in (18) must not vanish for any real $\omega < \mu$ [in the case of the meson theories, owing to the crossing symmetry, it was enough to require that the curly brackets in (9) be nonvanishing only in the range $-\mu \leq \omega \leq \mu$; for $|\omega| > \mu$, in particular, and for $\omega < -\mu$, the integral $J(\omega)$ contained an imaginary part known to be different from zero]. This, however, can be so only for $g^2 = 0$. In other words, for any $g^2 \neq 0$ $(g^2 > 0)$ and for any choice of the numbers ω_n and R_n in (17), there is always a real value $\omega < \mu$ for which the curly brackets in (18) vanish.

What has been said follows immediately from (18) if we take into account the fact that, according to (16) and (17), $J_1'(\omega) > 0$ and $\rho'(\omega) > 0$, i.e., both these functions, $J_1(\omega)$ and $\rho(\omega)$, are increasing functions. Besides this it follows from (16) that at $\omega = \mu$ the integral $J_1(\omega)$ has a certain finite positive value, and for $\omega \to -\infty$ it increases without limit in absolute value, while remaining a negative quantity:

$$J_1(\omega) \approx -\frac{1}{\pi} \ln \frac{|\omega|}{\mu}, \quad \omega \to -\infty.$$

Therefore if we choose all the ω_n larger than μ the expression in curly brackets in (18) will be a a positive quantity at $\omega = \mu$ and a negative number of arbitrarily large absolute value for $\omega \to -\infty$. It is clear that at some value of ω this expression vanishes. If, on the other hand, we choose one (or several) ω_n smaller than μ and note that near such an ω_n the behavior of $\rho(\omega)$, by Eq. (17), is given by a discontinuous curve of the type shown in Fig. 2, it is all the more clear that at some value of ω in the region $\omega < \mu$ the curly brackets in (18) will have a (possibly multiple) zero.

Since (18) is the most general form of an analytic function that satisfies the condition of unitarity (11), it is clear that no solution of (11) and (12) exists. In other words, in the Lee model the conditions of unitarity and analyticity are not compatible.

In conclusion we shall demonstrate the incompatibility of Eqs. (11) and (12) by a different method. Let us set $\omega \to \omega + i\tau$ in Eq. (12) and write

$$a(\omega + i\tau) = (u(\omega) + iv(\omega))/2(\varepsilon_0 - \omega - i\tau)$$

$$[v(\omega) \neq 0, \text{ for } \omega > \mu].$$

Then from Eq. (11) we have

$$v(\omega) = \frac{\varepsilon_0 - \omega}{\sqrt{\omega^2 - \mu^2}} \left\{1 - \sqrt{1 - \frac{\omega^2 - \mu^2}{(\omega - \varepsilon_0)^2} u^2(\omega)}\right\}.$$

Substitution of this in Eq. (12) leads to an integral equation for the function $u(\omega)$:

$$u(\omega) = g^2 + \frac{1}{\pi} P \times \int_{\mu}^{\infty} \frac{\omega - \varepsilon_0}{\omega - \omega'} \left\{1 - \sqrt{1 - \frac{\omega'^2 - \mu^2}{(\omega' - \varepsilon_0)^2} u^2(\omega')}\right\} \frac{d\omega'}{\sqrt{\omega'^2 - \mu^2}}$$

(the symbol P means that the integral is taken in the sense of the principal value). As can easily be seen, this equation cannot have any solution (real by definition) if $g^2 \neq 0$. In fact, for $\omega \to \infty$ it gives

$$u(\infty) = g^2 + \frac{1}{\pi}\int_{\mu}^{\infty} \left\{1 - \sqrt{1 - \frac{\omega' - \mu^2}{(\omega' - \varepsilon_0)^2} u^2(\omega')}\right\} \frac{d\omega'}{\sqrt{\omega'^2 - \mu^2}}. \tag{19}$$

Since the integral in the right member is positive, $u(\infty)$ cannot be equal to zero. But for $u(\infty) \neq 0$ the integral in the left member diverges logarithmically, and it then follows from the equation that $u(\infty) \to \infty$. On the other hand, $u(\infty)$ cannot exceed unity; otherwise, in the region $\omega' \to \infty$ the square root in the integrand becomes imaginary and the right side of (19) is a complex number.

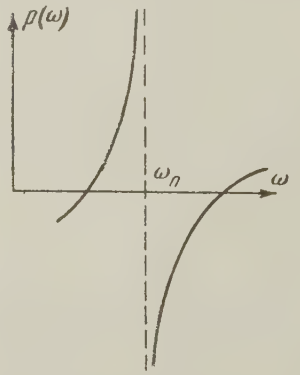

FIG. 2

The writer expresses his gratitude to B. L. Ioffe for several helpful discussions.

[1] S. Mandelstam, Phys. Rev. **112**, 1344 (1959).
[2] G. F. Chew and S. Mandelstam, preprint.
[3] T. D. Lee, Phys. Rev. **95**, 1329 (1954).
[4] G. Källén and W. Pauli, Kgl. Danske Videnskab. Selskab. Mat.-fys. Medd. 30, No. 7 (1955).
[5] Castillejo, Dalitz, and Dyson, Phys. Rev. **101**, 453 (1956).
[6] G. F. Chew and F. Low, Phys. Rev. **101**, 1570 (1956).

Translated by W. H. Furry
197

EFFECT OF MULTIPLE SCATTERING ON PAIR PRODUCTION BY HIGH-ENERGY PARTICLES IN A MEDIUM

F. F. TERNOVSKIĬ

Moscow State University

Submitted to JETP editor April 11, 1959

J. Exptl. Theoret. Phys. (U.S.S.R.) 37, 1010-1016 (October, 1959)

The effect of multiple scattering on the process of pair production by a fast particle going through a medium is considered. Calculations are carried out using a method developed previously by Migdal.

1. INTRODUCTION

LANDAU and Pomeranchuk[1,2] have shown that radiation processes in media are cut down considerably at high energies because of multiple scattering. Taking this effect into account, Migdal[3-5] obtained cross sections for bremsstrahlung and pair production by γ rays.

In this work, the influence of the medium on pair production by charged particles is considered. With this in mind, following Migdal,[5] we establish the connection between the transition probability and the density matrix, and then use the equations for the density matrix, averaged over the coordinates of the scattering atoms.

Expressions (16) — (19) obtained for the cross section go over at low energies into those from the theory neglecting the influence of the medium, and at high energies give a substantially reduced probability for the process considered.

2. EFFECT OF MULTIPLE SCATTERING ON PAIR PRODUCTION BY CHARGED PARTICLES IN THE MEDIUM

We denote systems of electron and positron solutions to the Dirac equation in the medium by Ψ_S and Φ_S, respectively, defining them by

$$\Psi_s(\mathbf{r}, t) = e^{-iHt} u^{\lambda s}_{\mathbf{p}_s} e^{i\mathbf{p}_s\mathbf{r}},$$

$$\Phi_s(\mathbf{r}, t) = e^{-iHt} v^{\lambda s}_{\mathbf{p}_s} e^{-i\mathbf{p}_s\mathbf{r}},$$

where $v^{\lambda}_{\mathbf{p}}$ and $u^{\lambda}_{\mathbf{p}}$ are unit spin amplitudes,

$$H = H_0 + \sum_n V(\mathbf{r} - \mathbf{r}_n)$$

is the Dirac Hamiltonian in the external field of the scatterers.*

Taking into account the fact that at high energies the scattering leaves the spin state and absolute value of the momentum almost unchanged, we obtain

$$\Psi_s(\mathbf{r}, t) \approx \sum_{p=p_s} u^{\lambda s}_{\mathbf{p}} e^{i\mathbf{p}\mathbf{r}} (e^{-iHt})^{+}_{p,\,\mathbf{p}_s},$$

$$\Phi_s(\mathbf{r}, t) \approx \sum_{p=p_s} v^{\lambda s}_{\mathbf{p}} e^{-i\mathbf{p}\mathbf{r}} (e^{-iHt})^{-}_{-p,\,-\mathbf{p}_s}, \qquad (1)$$

where the signs + and − remind us that the matrix element does not depend on the orientation of the spin, but does depend on the sign of the energy.

Processes of first and second order (see reference 6) contribute to the effect considered. The largest term in the integral cross section comes from the second-order process in which the effects of the external field on the wave functions of the resulting electron and positron are taken into account, but the initial particle is viewed as free. The corresponding matrix element has the form*

$$M = \tfrac{1}{2} e^2 \int I_\mu(x) (\overline{\Psi}(x') \gamma_\mu \Phi(x')) D(x' - x)\, dx\, dx', \qquad (2)$$

where

$$I_\mu = P_\mu \exp\{i(\mathbf{p} - \mathbf{p}')\mathbf{r} - i(E - E')t\}$$

is the transition current of initial particles. If the latter have zero spin, then

$$P_\mu = (p + p')_\mu / 2EE',$$

and for spin $\frac{1}{2}$

$$P_\mu = (\bar{u}^{\lambda}_{\mathbf{p}'} \gamma_\mu u^{\lambda_0}_{\mathbf{p}}).$$

Using Eq. (1), the matrix element (2) takes the form:

$$M = \frac{e^2 P_\mu}{\omega^2 - k^2} \int_0^{t_0} dt\, e^{-i\omega t} \sum_{\mathbf{p}_1} (\bar{u}^{\lambda_1}_{p_1} \gamma_\mu v^{\lambda_2}_{\mathbf{k}-\mathbf{p}_1}) (e^{iHt})^{+}_{p_-,\,\mathbf{p}_1} (e^{-iHt})^{-}_{p_1-\mathbf{k},\,-\mathbf{p}_+}.$$

Here t_0 is the time of motion in the medium,

*We employ the system of units in which $\hbar = c = m_e = 1$.

*The notation is that used in the book of Akhiezer and Berestetskiĭ.[7]

$\mathbf{k} = \mathbf{p} - \mathbf{p}'$, $\omega = E - E'$. The quantity $\langle |M^2| \rangle$, where $\langle \ldots \rangle$ denotes an average over the coordinates of the scatterers, enters into the transition probability. In the future it will be convenient to integrate the quantity $\langle |M|^2 \rangle$ over the angle of emission of the positron, since, as is easily seen from Eq. (1), this is practically equivalent to integration over $d^3\mathbf{p}_+$. We obtain

$$\int \langle |M|^2 \rangle d^3\mathbf{p}_+ = \mathrm{Re} \frac{2e^4 P_\mu P_\nu^*}{(\omega^2 - k^2)^2} \int_0^{t_0} dt \int_0^{t_0} dt' e^{i\omega(t'-t)} \cdot$$

$$\times \int \frac{d^3\mathbf{p}_1}{(2\pi)^3} \frac{d^3\mathbf{p}_2}{(2\pi)^3} (\bar{u}^{\lambda_1}_{\mathbf{p}_1} \gamma_\mu v^{\lambda_2}_{\mathbf{k}-\mathbf{p}_1}) (\bar{v}^{\lambda_2}_{\mathbf{k}/2-\mathbf{p}_2} \bar{\gamma}_\nu u^{\lambda_1}_{\mathbf{k}/2+\mathbf{p}_2})$$

$$\times \langle (e^{iHt})^+_{\mathbf{p}_-, \mathbf{p}_1} [e^{iH(t'-t)}]^-_{\mathbf{p}_1-\mathbf{k}, \mathbf{p}_2-\mathbf{k}/2} (e^{-iHt'})^+_{\mathbf{p}_2+\mathbf{k}/2, \mathbf{p}_-} \rangle. \quad (3)$$

Employing the equality

$$(e^{-iHt'})^+_{\mathbf{p}_2+\mathbf{k}/2, \mathbf{p}_-} = \sum_{\mathbf{p}'} [e^{-iH(t'-t)}]^+_{\mathbf{p}_2+\mathbf{k}/2, \mathbf{p}'} (e^{-iHt})^+_{\mathbf{p}', \mathbf{p}_-},$$

denoting $t' - t = \tau$ and using the fact that one can average independently over the coordinates of the scatterers which enter through the factors $e^{\pm iHt}$ and $e^{\pm iH\tau}$, we can put (3) into the form

$$\int \langle |M|^2 \rangle d^3\mathbf{p}_+ = \frac{2e^4}{(\mathbf{k}^2 - \omega^2)^2} \mathrm{Re}\, P_\mu P_\nu^* \int_0^{t_0} dt \int_0^{t_0 - t} d\tau e^{i\omega\tau}$$

$$\times \int \frac{d^3\mathbf{p}_1}{(2\pi)^3} \frac{d^3\mathbf{p}_2}{(2\pi)^3} (\bar{u}^{\lambda_1}_{\mathbf{p}_1} \gamma_\mu v^{\lambda_2}_{\mathbf{k}-\mathbf{p}_1}) (\bar{v}^{\lambda_2}_{\mathbf{k}/2-\mathbf{p}_2} \bar{\gamma}_\nu u^{\lambda_1}_{\mathbf{k}/2+\mathbf{p}_2})$$

$$\times f_0^{++}(\mathbf{p}_-, \mathbf{p}_1, t) f_{\mathbf{k}}^{+-}(\mathbf{p}_1, \mathbf{p}_2, \tau),$$

$$\langle (e^{iHt})^+_{\mathbf{p}_-, \mathbf{p}_1} (e^{-iHt})^+_{\mathbf{p}', \mathbf{p}_-} \rangle = \delta_{\mathbf{p}_1, \mathbf{p}'} f_0^{++}(\mathbf{p}_-, \mathbf{p}_1, t)$$

$$\langle (e^{-iH\tau})^+_{\mathbf{p}_2+\mathbf{k}/2, \mathbf{p}_1} (e^{iH\tau})^-_{\mathbf{p}_1-\mathbf{k}, \mathbf{p}_2-\mathbf{k}/2} \rangle = f_{\mathbf{k}}^{+-}(\mathbf{p}_1, \mathbf{p}_2, \tau). \quad (4)$$

The functions f_0 and $f_{\mathbf{k}}$ were introduced by Migdal.[5] They obey the same equation as the averaged density matrix (see reference 4).

We now sum the expression (4) over the spins of the final state and average over those of the initial state, obtaining

$$I = \frac{1}{2} \sum_{\lambda_1, \lambda_2} \int \langle |M|^2 \rangle d^3\mathbf{p}_+ = e^4 \mathrm{Re} \Lambda_{\mu\nu}(\mathbf{p}, \mathbf{p}') \int_0^{t_0} dt \int_0^{t_0 - t} d\tau e^{i\omega\tau}$$

$$\times \int \frac{d^3\mathbf{p}_1}{(2\pi)^3} \frac{d^3\mathbf{p}_2}{(2\pi)^3} \frac{G_{\mu\nu}(\mathbf{p}_1, \mathbf{p}_2)}{(k^2 - \omega^2)^2} f_0^{++}(\mathbf{p}_-, \mathbf{p}_1, t) f_{\mathbf{k}}^{+-}(\mathbf{p}_1, \mathbf{p}_2, \tau), \quad (5)$$

where

$$G_{\mu\nu}(\mathbf{p}_1, \mathbf{p}_2) = \sum_{\lambda_1, \lambda_2} (\bar{u}^{\lambda_1}_{\mathbf{p}_1} \gamma_\mu v^{\lambda_2}_{\mathbf{k}-\mathbf{p}_1}) (\bar{v}^{\lambda_2}_{\mathbf{k}/2-\mathbf{p}_2} \bar{\gamma}_\nu u^{\lambda_1}_{\mathbf{k}/2+\mathbf{p}_2}),$$

$$\Lambda_{\mu\nu}(\mathbf{p}, \mathbf{p}') = \begin{cases} (p + p')_\mu (p + p')^*_\nu / 2EE' & \text{for spin } 0, \\ \frac{1}{4EE'} \mathrm{Sp}\, \gamma_\mu (i\hat{p} - m) \bar{\gamma}_\nu (i\hat{p}' - m) & \text{for spin } \frac{1}{2}. \end{cases} \quad (6)$$

In so far as we are interested in only the integral cross sections, we can make the following replacements (compare reference 6)

$$G_{\mu\nu}\Lambda_{\mu\nu} \to \tfrac{1}{2} G_\perp \Lambda_\perp \cdot$$

$$+ (1 - k^{-2}\omega_1\omega)(1 - k^{-2}\omega_2\omega) G_{44}\Lambda_{44}, \quad (7)$$

where

$$G_\perp = G_{11} + G_{22}, \qquad \Lambda_\perp = \Lambda_{11} + \Lambda_{22}.$$

The further transformation of (5) and calculation of quantities entering into (7) is carried out just as in the work of Migdal.[5] Introducing the notation

$$\mathbf{p} = \mathbf{n}p(1 - \theta^2/2) + p\boldsymbol{\theta}, \qquad \mathbf{p}' = \mathbf{n}(p - k - p\theta^2/2) + p\boldsymbol{\theta},$$

$$\mathbf{p}_1 \approx \mathbf{n}q + g\boldsymbol{\eta}_0, \qquad \mathbf{p}_2 \approx \mathbf{n}g + g\boldsymbol{\eta},$$

$$q = |\mathbf{p}_-|, \qquad g = |q - k/2|, \quad (8)$$

we have

$$G_{\mu\nu}\Lambda_{\mu\nu} \to \frac{1}{2}\Lambda_\perp \left\{ \frac{k^2}{q^2(k-q)^2} + \frac{[q^2 + (k-q)^2] g^2 \eta\eta_0}{q^2(k-q)^2} \right\}$$

$$+ \frac{1}{2}\Lambda_{44} \left[\frac{1 + g^2\eta^2}{q(k-q)} - \frac{m^2 + p^2\theta^2}{p(p-k)} \right] \left[\frac{1 + g^2\eta_0^2}{q(k-q)} - \frac{m^2 + p^2\theta^2}{p(p-k)} \right]. \quad (9)$$

Here, for scalar particles

$$\tfrac{1}{2}\Lambda_\perp = p^2\theta^2/p(p-k), \qquad \tfrac{1}{2}\Lambda_{44} = (p - k/2)^2/p(p-k),$$

and for spin-$\frac{1}{2}$ particles

$$\tfrac{1}{2}\Lambda_\perp = \frac{m^2k^2 + [p^2 + (p-k)^2] p^2\theta^2}{2p^2(p-k)^2}, \qquad \tfrac{1}{2}\Lambda_{44} = 1.$$

Further we find

$$I = e^4 \mathrm{Re} \int_0^{t_0} dt \int_0^{t_0 - t} d\tau e^{i\omega\tau}$$

$$\times \int d\vartheta\, d\boldsymbol{\eta} v_0(\vartheta, t) v(\boldsymbol{\eta}, \tau) \frac{\Lambda_{\mu\nu} G_{\mu\nu}}{(k^2 - \omega^2)^2}, \quad (10)$$

where we have set

$$\vartheta = \mathbf{p}_-/p_- - \mathbf{p}_1/p_1,$$

$$f_0^{++}(\mathbf{p}_-, \mathbf{p}_1, t)\, d^3p_1/(2\pi)^3 \approx \delta(p_- - p_1)\, dp_1 v_0(\vartheta, t)\, d\vartheta,$$

$$f_{\mathbf{k}}^{+-}(\mathbf{p}_1, \mathbf{p}_2, \tau)\, d^3p_2/(2\pi)^3 \approx \delta(p_2 - g)\, dp_2 v(\boldsymbol{\eta}, \tau)\, d\boldsymbol{\eta}.$$

Here the function $v_0(\vartheta, t)$ is normalized by

$$\int v_0(\vartheta, t)\, d\vartheta = 1. \quad (11)$$

In addition, we use $\boldsymbol{\xi}$ to denote the vector angle between $\mathbf{k}$ and $\mathbf{p}_-$. Then

$$\vartheta = \mathbf{p}_-/p_- - \mathbf{n} + \mathbf{n} - \mathbf{p}_1/p_1 = \boldsymbol{\xi} - \boldsymbol{\eta}_0 g/q. \quad (12)$$

The probability of pair production with summed energy between k and $k + dk$ and electron energy

between q and q+dq, per unit distance in the medium, can now be written in the form

$$w(p, k, q)\, dk\, dq = \frac{k^2\, dk q^2\, dq}{(2\pi)^6} \int \frac{dI}{dI_0}\, d\vartheta\, d\xi.$$

Using (11) and (12) and the equality $d\xi d\theta = (g/q)^2 d\xi d\eta_0$, we obtain

$$w(p, k, q) = \frac{k^2 g^2 e^4}{(2\pi)^6} \mathrm{Re} \int_0^{t_0} d\tau e^{i\omega\tau} \int d\vartheta\, d\boldsymbol{\eta}\, d\boldsymbol{\eta}_0 \frac{\Lambda_{\mu\nu} G_{\mu\nu}}{(k^2 - \omega^2)^2} v(\boldsymbol{\eta}, \tau), \tag{13}$$

where

$$k^2 - \omega^2 = k^2 (m^2 + p^2\vartheta^2) / p (p - k),$$

and $\Lambda_{\mu\nu} G_{\mu\nu}$ is given by (9).

The integrals in (13) have the same form as those in the work of Migdal. The only difference consists in the fact that in our case $k \neq \omega$, in so far as we are dealing with virtual quanta. This can be taken into account by simply redefining the parameter α which enters into the equation for the function $e^{i\omega\tau} v(\boldsymbol{\eta}, \tau)$ (see reference 5). We have

$$\alpha = \frac{k (M^2 + p^2\vartheta^2)}{4Qp (p - k)}, \qquad \beta = \frac{kg^2}{4Qq (k - q)},$$

$$M^2 = m^2 + \frac{p (p - k)}{q (k - q)}.$$

The meaning of the parameters α and β is clear from the expansion

$$[\varepsilon_{p_z + k/2} - \varepsilon_{p_z - k/2} - \omega] / 2Q = \alpha + \beta\eta^2 / 2. \tag{14}$$

In our notation

$$Q = Z^2 e^4 nL / 8\pi g^2,$$

where $L = \ln (\vartheta_{max}/\vartheta_{min})$. In order of magnitude, Q corresponds to the root mean square scattering angle per unit track length. We discuss the choice of angles ϑ_{max} and ϑ_{min} below.

As shown in reference 5, the effect of multiple scattering is determined by the size of the parameter

$$\tilde{s} = \frac{\alpha}{2\sqrt{2\beta}} = \frac{q (k - q) (M^2 + p^2\vartheta^2)}{8p (p - k)} \sqrt{\frac{k}{q (k - q) Qg^2}}.$$

For $\tilde{s} > 1$, the effect of multiple scattering vanishes. We note now that, in so far as the time is concerned, times $\tau \lesssim t_k = s/\alpha Q(1 + s)$ are essential, so that for $t_0 \gg t_k$, the integration over $d\tau$ can be extended to infinity. Then one obtains

$$\mathrm{Re} \int_0^\infty e^{i\omega\tau} d\tau \int d\boldsymbol{\eta}\, d\boldsymbol{\eta}_0\, v(\boldsymbol{\eta}, \tau) = \frac{\pi}{6Q\alpha^2} G(\tilde{s}),$$

$$\mathrm{Re} \int_0^\infty e^{i\omega\tau} d\tau \int d\boldsymbol{\eta}\, d\boldsymbol{\eta}_0 (\boldsymbol{\eta}\boldsymbol{\eta}_0)\, v(\boldsymbol{\eta}, \tau) = \frac{2\pi}{3\alpha\beta Q} \Phi(\tilde{s}),$$

$$\mathrm{Re} \int_0^\infty e^{i\omega\tau} d\tau \int \eta^2\, d\boldsymbol{\eta}\, d\boldsymbol{\eta}_0\, v(\boldsymbol{\eta}, \tau)$$

$$= \mathrm{Re} \int_0^\infty e^{i\omega\tau} d\tau \int \eta_0^2\, d\boldsymbol{\eta}\, d\boldsymbol{\eta}_0\, v(\boldsymbol{\eta}, \tau) = -\frac{\pi G(\tilde{s})}{3\alpha\beta Q},$$

$$\mathrm{Re} \int_0^\infty e^{i\omega\tau} d\tau \int \eta^2\eta_0^2\, d\boldsymbol{\eta}\, d\boldsymbol{\eta}_0\, v(\boldsymbol{\eta}, \tau) = \frac{2\pi}{3Q\beta^2} G(\tilde{s}). \tag{15}$$

The first of two of these equations were obtained by Migdal. The remaining are derived analogously.

Now, employing (13) – (15), we finally obtain for spin-$\frac{1}{2}$ particles, after integration over $d\vartheta$,

$$w_{1/2}(p, k, q) = \frac{2r_0^2 nZ^2}{3\pi (137)^2 k^2}$$

$$\times L \left\{ \frac{p^2 + (p - k)^2}{p^2} \left[A(s, x) + 2\frac{q^2 + (k - q)^2}{k^2} B(s, x) \right] \right.$$

$$+ \frac{k^2}{p^2} \left[C(s, x) + 2\frac{q^2 + (k - q)^2}{k^2} D(s, x) \right]$$

$$\left. + \frac{8q (k - q)}{k^2} \frac{p - k}{p} E(s, x) \right\}, \tag{16}$$

and for particles with zero spin

$$w_0(p, k, q) = \frac{4r_0^2 nZ^2}{3\pi (137)^2 k^2}$$

$$\times L \left\{ \frac{p - k}{p} \left[A(s, x) + 2\frac{q^2 + (k - q)^2}{k^2} B(s, x) \right] \right.$$

$$\left. + \frac{4q (k - q)}{k^2} \frac{(p - k/2)^2}{p^2} E(s, x) \right\}. \tag{17}$$

Here

$$A(s, x) = \int_{1+x}^\infty \frac{(z - x - 1)\, G(sz)\, dz}{z^2 (z - 1)^2},$$

$$B(s, x) = \int_{1+x}^\infty \frac{(z - x - 1)\, \Phi(sz)\, dz}{z (z - 1)^2}, \quad C(s, x) = x \int_{1+x}^\infty \frac{G(sz)\, dz}{z^2 (z - 1)^2},$$

$$D(s, x) = x \int_{1+x}^\infty \frac{\Phi(sz)\, dz}{z (z - 1)^2}, \tag{18}$$

$$E(s, x) = \int_{1+x}^\infty \frac{G(sz)\, dz}{z^2} \qquad s = \tfrac{1}{8} [k / q (k - q)\, Qg^2]^{1/2},$$

$$x = m^2 q (k - q) / p (p - k), \tag{19}$$

and Φ and G are functions introduced by Migdal.[5] For $s > 1$

$$\Phi(s) \approx G(s) \approx 1,$$

and for $s \ll 1$:

$$\Phi(s) \approx 6s, \qquad G(s) \approx 12\pi s^2 \approx (6s)^2.$$

In the intermediate region $0.1 < s < 1$, these functions can be approximated, to within a reasonable accuracy, by the following simple expressions

$$\Phi(s) \approx 6s/(6s+1), \quad G(s) \approx (6s)^2/[(6s)^2+1]. \quad (20)$$

The error from using these expressions oscillates from 10% at the edges of the interval to 20% in the middle of it.

The integrals (18) are easy to find by using expressions (20). We will not give the very lengthy formulae which result here, but consider only limiting cases.

1. $s \gg 1/(1+x)$. Then, in complete agreement with the results of the theory[6] neglecting effects of the medium, we obtain

$$A(s, x) = (1+2x)\ln\left(1+\frac{1}{x}\right) - 2,$$

$$B(s, x) = (1+x)\ln\left(1+\frac{1}{x}\right) - 1,$$

$$C(s, x) = \frac{1+2x}{1+x} - 2x\ln\left(1+\frac{1}{x}\right),$$

$$D(s, x) = 1 - x\ln\left(1+\frac{1}{x}\right),$$

$$E(s, x) = 1/(1+x). \quad (21)$$

2. $s \ll 1/(1+x)$. Then

$$A(s, x) \approx 36s^2\ln\frac{1}{6sx}, \quad B(s, x) \approx 6s\ln\frac{1}{6sx},$$

$$C(s, x) \approx 36s^2, \quad D(s, x) \approx 6s, \quad E(s, x) \approx 3\pi s. \quad (22)$$

We turn now to understanding the magnitudes of the angles θ_{max} and θ_{min}, which enter into L. The quantity $\theta_{min} = q_{min}/g = Z^{1/3}/137\,g$ is determined by the minimum momentum transfer; θ_{max} is of the same order of magnitude as the mean angle of particle emission. For $s > 1$, the latter is determined by Eq. (14), giving

$$\theta_{max} \sim \sqrt{\eta_1^2} \sim \sqrt{\alpha/\beta} \sim \sqrt{1+x}/g \equiv \theta_0.$$

The multiple scattering has the effect of broadening the angular distribution. As shown in reference 5, for $s \ll 1$ we obtain $\eta^2 \sim \theta_0^2/s$, so that

$$\theta_{max} \sim \theta_0/\sqrt{s} = \sqrt{(1+x)/sg^2}.$$

At high energies, the quantity $\theta_0/\sqrt{s}$ can exceed the angle of diffraction on the nucleus, $\theta_1 = 1/Rg$, where $R = 0.5\,r_0Z^{1/3}$. Then one should take $\theta_{max} = \theta_1$. Thus, we find

$$L = \begin{cases} \ln(190\ Z^{-1/3}\sqrt{1+x}) & \text{for } s>1,\ \sqrt{1+x} < 190\ Z^{-1/3} \\ 2\ln(190\ Z^{-1/3}) & \text{for } s>1,\ \sqrt{1+x} > 190\ Z^{-1/3} \\ \ln(190\ Z^{-1/3}\sqrt{(1+x)/s}) & \text{for } s<1,\ \sqrt{(1+x)/s} < 190\ Z^{-1/3} \\ 2\ln(190\ Z^{-1/3}) & \text{for } s<1,\ \sqrt{(1+x)/s} > 190\ Z^{-1/3} \end{cases} \quad (23)$$

One knows the numerical factor in the argument of the logarithm only to within order of magnitude. The number 190 was only a convenient choice.

Through the use of Eqs. (22) and (23) for $k \ll p/m$, $x \ll 1$, $s \ll 1$, Eqs. (16) and (17) assume the same form

$$w(p, k, q) \approx \frac{16r_0^2nZ^2}{\pi(137)^2k^2} L\,\frac{q^2+(k-q)^2}{k^2}\,s\ln\frac{1}{6sx}. \quad (24)$$

The condition $s \ll 1$, according to Eq. (19), means

$$s \approx 1400\,[kt/q(k-q)]^{1/2} \ll 1, \quad (25)$$

where t is the radiation length in centimeters, and k and q are in units of m_ec^2.

Multiple scattering will have a substantial effect on the integral cross section if Eq. (25) is fulfilled for values of q and $k-q \ll p/m$, i.e., for energies of the initial particle $p \gg 2\cdot 10^6\,t\mu c^2$.

The theory described here is applicable to electrons when the energies of the pair particles are much less than the energy of the electron.

3. DISCUSSION OF RESULTS

We considered the effect of multiple scattering, only on second-order processes. If the initial particle is an electron, the effect of the medium will also substantially decrease the contribution of the first-order processes, so that, as in the usual theory, they can be completely neglected in the region $k \ll p$. If $m \gg 1$, the medium has little effect on the first-order processes, and their contribution is given by formulae obtained previously.[6]

We note, further, that at high energies, when the multiple scattering (or the effect of polarization of the medium) cuts down substantially the probability of bremsstrahlung with emission of soft quanta, direct production of pairs may become the main source of low-energy particles appearing in showers. In fact, according to Eq. (25), the effect of the medium on pair production is appreciable only for $k > 10^{12}$ ev, whereas its effect on bremsstrahlung becomes important already for $p^2/k > 10^{12}$ ev (see reference 5). Take, for example, $p = 5 \times 10^{11}$ ev. Then, already for $p/k > 200$, the production of pairs is more important than emission of bremsstrahlung. This situation should be taken into account in analysis of shower processes, especially when the showers have penetrated only small depths.

In conclusion, I would like to express my deep gratitude to Prof. A. B. Migdal for his interest in the work and valuable discussions.

[1] L. D. Landau and I. Yu. Pomeranchuk, Dokl. Akad. Nauk SSSR 92, 535 (1953).

[2] L. D. Landau and I. Yu. Pomeranchuk, Dokl. Akad. Nauk SSSR **92**, 735 (1953).

[3] A. B. Migdal, Dokl. Akad. Nauk SSSR **96**, 49 (1954).

[4] A. B. Migdal, Dokl. Akad. Nauk SSSR **105**, 77 (1955).

[5] A. B. Migdal, JETP **32**, 633 (1957), Soviet Phys. JETP **5**, 527 (1957).

[6] F. F. Ternovskiĭ, JETP (in the press).

[7] A. I. Akhiezer and V. B. Berestetskiĭ, Квантовая электродинамика (Quantum Electrodynamics) M., 1953 (AEC Tr. 2876, 1957).

Translated by G. E. Brown
198

THE DYNAMICAL CHARACTER OF THE JAHN-TELLER EFFECT AND ITS INFLUENCE ON THE PARAMAGNETIC RESONANCE OF Cu^{2+}

V. I. AVVAKUMOV

Kazan' Branch, Academy of Sciences, U.S.S.R.

Submitted to JETP editor April 14, 1959

J. Exptl. Theoret. Phys. (U.S.S.R.) 37, 1017-1025 (October, 1959)

We consider copper complexes $Cu^{2+}Y_6$ for which there are, in contradistinction to other paramagnetic complexes, in first approximation an infinite number of geometries within a certain manifold corresponding to the minimum energy, instead of one well-defined geometry. Using crystal field theory we establish the connection between the geometry of the complex and the electron density distribution of the Cu^{2+} ion. "Geometrical degeneracy" leads to the result that the latter may experience finite (permanent) distortions; it is shown that the changes in the "crystalline" field corresponding to these distortions should lead to oscillations of the electron cloud of the Cu^{2+} ion relative to the nucleus. We also consider the influence of the interactions which lead to a partial stabilization of the complex. It is shown that even when these interactions are taken into account the electron cloud continues to oscillate but at a lower frequency, and the frequency depends on the mass of the corner atoms. We have considered the influence of the effect considered on the hyperfine structure and g-factors in free complexes.

1. INTRODUCTION

IT is well established that in copper salts in which the crystalline electrical field at the position of the Cu^{2+} ion has a symmetry higher than a tetragonal one[1] and, as an exception, in copper Tutton salts[2] where the crystalline field is tetragonal, the magnitudes of the g-factors and of the hyperfine-structure (hfs) constants are temperature dependent: they are strongly anisotropic at low temperatures and become isotropic at high temperatures, while the hfs constant is considerably decreased at high temperatures. Aqueous solutions of copper salts have a peculiar behavior.

The behavior of a Cu^{2+} ion in salts with a trigonal (or higher) symmetry was explained by the dynamic character of the Jahn-Teller effect which occurs in these salts.[3] The behavior of a copper ion in Tutton salts[2] and also in aqueous solutions[4,5] has not yet been adequately explained.

There are grounds for assuming that the Jahn-Teller effect is also responsible for the decrease and isotropy of the hfs constant in aqueous solutions of copper salts (and, apparently, as an exception, in Tutton salts). This is indicated by the fact that both in a free $Cu^{2+}Y_6$ complex and also in the complex situated in a force field with trigonal symmetry, the ground state of the Cu^{2+} ion is two-fold degenerate, if the Jahn-Teller effect is not taken into account, while in both cases the degeneracy is lifted thanks to the Jahn-Teller effect. Since the Jahn-Teller effect in $Cu^{2+}Y_6$ complexes in a trigonal field has a dynamic character, it follows from the above analogy that it must also have a dynamic character in free complexes.

It is the aim of the present paper to consider from the same point of view all peculiarities of paramagnetic resonance of copper ions which, according to one consideration or another, may be ascribed to the dynamical character of the normal Jahn-Teller effect.

General considerations about the nature of the effect are given in Sec. 2. A theory of the phenomenon in free (not fixed in a lattice) $Cu^{2+}Y_6$ complexes is offered in Sec. 3. A general discussion is given in Sec. 4 of the influence of the effect on the paramagnetic resonance of Cu^{2+} in complexes with different corner atoms Y.

2. THE JAHN-TELLER EFFECT IN FREE COPPER COMPLEXES

The Jahn-Teller theorem[6] applied to XY_6 complexes proves that the octahedral configuration formed by such complexes is unstable, if the atom (ion) X is in a degenerate state.

The Hamiltonian leading to a Jahn-Teller effect can be written in the form[7,8]

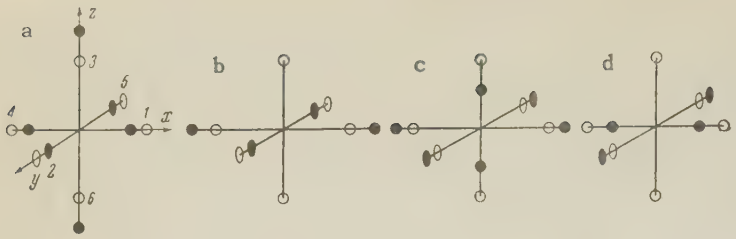

FIG. 1. Static distortions of an octahedral complex of symmetry Q_3 and Q_2 (a: for $\theta = 0$, b: for $\theta = \pi/2$, c: for $\theta = \pi$, d: for $\theta = 3\pi/2$). ● – initial geometry, o – structure arising due to the static Jahn-Teller effect

$$\hat{\mathcal{H}} = \hat{\mathcal{H}}_{\text{cub}} + (\hat{V}_2 Q_2 + \hat{V}_3 Q_3) + \tfrac{1}{2} k (Q_2^2 + Q_3^2). \qquad (1)$$

The term $\hat{\mathcal{H}}_{\text{cub}}$ is the energy of the ion in a crystalline field of cubic symmetry and is considered as the unperturbed Hamiltonian; the second and third terms are perturbations. For our purpose it is sufficient to consider only the influence of the perturbation on the lowest orbital cubic doublet (for the sake of brevity we indicate by this term the lowest two-fold degenerate orbital state of the Cu^{2+} in the field of cubic symmetry).

The Jahn-Teller effect as such is connected with the term linear in Q_2 and Q_3, where

$$\hat{V}_3 = 18\,C\,(3z^2 - r^2)/\sqrt{3}, \qquad \hat{V}_2 = -\,18\,C\,(x^2 - y^2)$$

are operators with matrix elements

$$\langle \psi_1 | \hat{V}_3 | \psi_1 \rangle = -\langle \psi_2 | \hat{V}_3 | \psi_2 \rangle$$

$$= \langle \psi_1 | \hat{V}_2 | \psi_2 \rangle = \langle \psi_2 | \hat{V}_2 | \psi_1 \rangle = -a,$$

and $\mathbf{r}(x, y, z)$ is the radius vector taken from the nucleus to the electron of the incomplete shell of the Cu^{2+} ion. If the corner atoms Y are electric dipoles with moment $\bar{\mu}$, $C = e'\mu/R^5$ where e' is the electron charge and R the equilibrium distance between Cu^{2+} and Y in a regular octahedral complex.

For our further calculations we put $Q_3 = \rho \cos\theta$, $Q_2 = \rho \sin\theta$. The notation of the variables Q_2 and Q_3 in (1) is the same as the notation for the two-fold degenerate vibrational coordinates of a regular octahedral complex XY_6 (of the type E_g), although they characterize in the given case static distortions of the complex. These variables can be expressed as follows in terms of displacements in a Cartesian system of coordinates (see Fig. 1):

$$Q_3 = [z_3 - z_6 - \tfrac{1}{2}(x_1 - x_4 + y_2 - y_5)]/\sqrt{3},$$

$$Q_2 = \tfrac{1}{2}(x_1 - x_4 - y_2 + y_5).$$

Expression (1) determines the energy of the Cu^{2+} ion as a function of the geometrical parameters Q_2 and Q_3 (or ρ and θ). On the other hand, the energy of the $Cu^{2+}Y_6$ "molecule" as a function of the same variables is equal to*

$$\hat{\mathcal{H}} = U_0 + V_2 Q_2 + V_3 Q_3 + \tfrac{1}{2} k (Q_2^2 + Q_3^2), \qquad (1a)$$

where U_0 is the potential energy of the $Cu^{2+}Y_6$ "molecule" when it has the symmetry of a regular octahedron.

In order to find the stable geometry it is necessary first to diagonalize (1a) and then to impose a minimum condition.[7] We get (see Fig. 2)

$$E = -a^2/2k, \qquad \Delta E = 2a\rho_0,$$

$$\rho_0 = (Q_2^2 + Q_3^2)^{1/2} = |a|/k. \qquad (1b)$$

The eigenfunctions of the Cu^{2+} ion are of the form

$$\varphi_1 = \{(1 + \cos\theta)^{1/2}\psi_1 + (1 - \cos\theta)^{1/2}\psi_2\}/\sqrt{2}, \qquad (2a)$$

$$\varphi_2 = \{(1 - \cos\theta)^{1/2}\psi_1 - (1 + \cos\theta)^{1/2}\psi_2\}/\sqrt{2}, \qquad (2b)$$

where ψ_1 and ψ_2 are the functions of the lowest orbital cubic doublet of the copper ion.

It is clear from (1b) that neither the energy of the Cu^{2+} ion (the eigenvalues of the ground-state energy and the magnitude of the level splitting) nor the energy of the $Cu^{2+}Y_6$ "molecule" (equal to $U_0 - E$) depend on the parameter θ, which characterizes the geometry of the complex and the form of the eigenfunction of the ground state of the Cu^{2+} ion.

The fact that the energy of the complex is independent of the deformation (within the limits $Q_2^2 + Q_3^2 = \rho_0^2 = \text{const}$) leads to a situation where the usual Jahn-Teller effect has a dynamic character. The complex can, namely, go over freely (as long as we do not take into account interactions leading

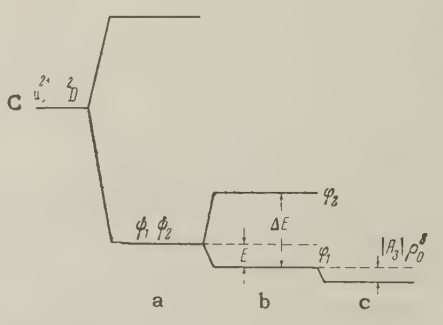

FIG. 2. Energy level splitting for the ion: a – in a field of cubic symmetry, b – thanks to the Jahn-Teller effect, c – thanks to the Jahn-Teller effect, taking the third order approximation in the displacements of the corner atoms Y from the position corresponding to a regular octahedral configuration into account.

*Since we are interested in the connection between the geometry of the complex and the electron density distribution we have omitted from Eq. (1a) third order displacement terms caused by the interaction between the corner atoms Y and the effective charge of the Cu^{2+} nucleus.

to a suppression of the effect, see Sec. 3) from one geometrical arrangement to another one with a sufficiently high frequency, determined by external conditions; the latter is caused by the fact that all these arrangements correspond to the same energy.

We shall now consider what influence is exerted by this phenomenon on the electron density distribution of the Cu^{2+} ion. The external force changes the geometry of the complex, causing a change in the distribution in the electron cloud of the magnetic ion (and a change in the ground-state eigenfunction of Cu^{2+}). This explains the fact that although there are no nondiagonal perturbation matrix elements which can be responsible for a mixing of the cubic eigenfunctions of the ion, nevertheless, in this complex, the eigenfunctions of the ground state of the ion are superpositions of the eigenfunctions of the orbital cubic doublet with, generally speaking, arbitrary coefficients that are subject to the conditions of orthogonality and normalization [see (2a), where θ is arbitrary].

The geometry of a complex with a degenerate ion in a solid is determined by the crystal lattice, so that the distribution of the electron cloud of the magnetic ion is fixed, thanks to the stability of the complex. The given effect can therefore take place in a solid containing a copper complex only in the special cases mentioned above (Sec. 1).

To elucidate the influence of the dynamic character of the Jahn-Teller effect in free complexes with other paramagnetic ions we need a special consideration. We can point here, however, to the essential difference between the copper ion and the other ions in that not one of the latter possesses the aforementioned degeneracy with respect to the geometry of the complex (with the exception of Cr^{2+} and Mn^{3+}, which have an even number of electrons).

The first to introduce the idea of the dynamic nature of the Jahn-Teller effect in copper complexes were Abragam and Pryce[3] in order to explain the small magnitude and the isotropy of the hyperfine structure constant and the isotropy of the g-factor in copper salts with trigonal symmetry. In accordance with the dynamic character of the effect, they used in their calculations eigenfunctions of the ground state of Cu^{2+} in the form $\varphi = \psi_1 \cos\theta + \psi_2 \sin\theta$, and assumed that θ was a cyclic coordinate. After averaging over θ they obtained g-factors and hfs constants that agreed with experiment. The ideal case where the energy of the complex is independent of the character of the deformation (within the limits $Q_2^2 + Q_3^2 = \text{const}$) is, however, in actual fact not realized. It has been established (see, for instance, reference 8) that in reality the $Cu^{2+}Y_6$ complexes have structures with a D_{4b} symmetry. The change in potential energy of the complex is equal to $A_3\rho^3 \cos 3\theta$ ($A_3 \sim$ constant, $|A_3|\rho^3 \sim 600\ \text{cm}^{-1}$, $A_3 < 0$)[9] (see Fig. 2), if we use polar coordinates ρ, θ in the Q_2, Q_3 plane. Thus, there is no free "rotation" of the complex in the Q_2, Q_3 plane. All the same, experiment shows that in some cases the hfs constant is averaged, and this averaging cannot be ascribed to exchange interactions.[5] It is therefore expedient to consider the connection between the Jahn-Teller effect and the vibrational motion of the complex.

3. THE JAHN-TELLER EFFECT, TAKING THE THIRD ORDER APPROXIMATION IN THE DISPLACEMENTS INTO ACCOUNT

If one considers the energy of the Cu^{2+} ion as a function of the parameters Q_2 and Q_3 which characterize the change in the geometry of the complex, the Hamiltonian of the problem becomes

$$\hat{\mathcal{H}} = \hat{\mathcal{H}}_{\text{cub}} + \hat{V}_2 Q_2 + \hat{V}_3 Q_3 + \tfrac{1}{2} k (Q_2^2 + Q_3^2) + A_3\rho^3 \cos 3\theta. \tag{3}$$

Its eigenvalues are

$$E = \pm a\rho_0' + \tfrac{1}{2} k\rho_0'^2 + A_3\rho_0^3 \cos 3\theta. \tag{4a}$$

From this we get, from the requirement that the energy of the system be a minimum,

$$E_1 = -a\rho_0' + \tfrac{1}{2} k\rho_0'^2 + A_3\rho_0'^3, \qquad \Delta E = 2a\rho_0',$$

$$\rho_0' = (k - \sqrt{k^2 - 12a|A_3|})/6|A_3|, \tag{4b}$$

where E_1 is the energy eigenvalue of the Cu^{2+} ion corresponding to the ground state. At the same time, E_1 characterizes the change in potential energy of the $Cu^{2+}Y_6$ complex, considered as a molecule, when the complex goes over from an unstable octahedral configuration to a stable bipyramidal one. Thanks to the presence of a term linear in Q_2 and Q_3 in the Hamiltonian (3), the regular octahedral configuration of the $Cu^{2+}Y_6$ is therefore again unstable, but now both the energy of Cu^{2+} and the energy of $Cu^{2+}Y_6$ as a molecule depend on the angle θ, and their minimum is realized at $\theta = \theta_0 = 0$, $2\pi/3$, and $4\pi/3$.

Our problem will now consist of establishing the dependence of the electron density in Cu^{2+} on the vibrations of the deformed complex. To do this we consider $Cu^{2+}Y_6$ as a vibrational system. The Hamiltonian of the problem has in that case the form

$$\hat{\mathcal{H}} = U_0 + \hat{V}_2 Q_2 + \hat{V}_3 Q_3 + \tfrac{1}{2} k (Q_2^2 + Q_3^2) + A_3\rho^3 \cos 3\theta, \tag{5}$$

where U_0 is the potential energy of a complex that has octahedral symmetry. Before we evaluate the normal vibrations of the system, the Hamiltonian of which is given by (5), it is necessary to find the form of the potential function of the complex when it has the symmetry corresponding to the energy minimum.

Let Q_j; Q_2, Q_3 ($j = 1, \ldots, 13$) be the displacements of the regular octahedral complex, which have the symmetry of the vibrational coordinates $\widetilde{Q}_j$, $\widetilde{Q}_2$, $\widetilde{Q}_3$. The potential function of the bipyramidal complex can in these variables be written in the form

$$U(Q_j^0 = 0;\ Q_2^0,\ Q_3^0) = U_0 - E, \tag{6}$$

where Q_2^0 and Q_3^0 are the displacements of the corner atoms Y. Expanding (6) in a Taylor series in the vicinity of $Q_j = Q_2 = Q_3 = 0$ we get

$$U(Q_j^0 = 0;\ Q_2^0,\ Q_3^0,) = U(0) + \sum_n U_{Q_2}^{(n)}(0)\, Q_2^{0n}/n! + \sum_n U_{Q_3}^{(n)}(0)\, Q_3^{0n}/n!\,, \tag{7}$$

where $U(0) = U_0$ is the potential function of the regular octahedral complex. The function $U(Q_j^0 = 0;\ Q_2^0,\ Q_3^0)$ expressed in this form is identical with

$$U(Q_j^0 = 0;\ \rho_0,\ \theta) = U_0 + U(\rho_0,\ \theta), \tag{8}$$

where $U(\rho, \theta)$ is (4a).

We do not consider it our task to calculate the normal vibrations of the deformed bipyramidal complex and to discuss at the same time the peculiar nature of the vibrations which may occur in this case because the metallic ion is not in an S-state. Our aim is to show that among the normal vibrational coordinates of the bipyramidal complex there will be coordinates of the kind $q = \rho_0 - \rho$ and $\gamma = \theta_0 - \theta$ which will have the symmetries $\widetilde{Q}_3$ and $\widetilde{Q}_2$ respectively; this follows from the relations $\rho = (Q_2^2 + Q_3^2)^{1/2}$, $\theta = \arctan(Q_2/Q_3)$ if we take into account that $Q_2^0 = 0$ and $Q_3^0 = \rho_0$. We shall in particular be interested in vibrations of the type γ, because they influence essentially the electronic density of Cu^{2+}.

Expanding (8) in q and γ in the neighborhood of ρ_0, θ_0 we get

$$U(\rho, \theta) = U(\rho_0, \theta_0) + \tfrac{1}{2}(k - 6\,|\,A_3\,|\,\rho_0 \cos 3\theta_0)\, q^2 + \tfrac{1}{2}(k + 9\,|\,A_3\,|\,\rho_0^3 \cos\ 3\theta_0)\, \gamma^2. \tag{9}$$

Apart from this, we must take into account the contribution from the linear term.[9] We have

$$E^{(2)} = -|\langle \varphi_1^0 | \hat{V}_2 Q_2 + \hat{V}_3 Q_3 | \varphi_2^0 \rangle|^2 / \Delta E,$$

where ΔE is the magnitude of the shift of the lowest orbital doublet of Cu^{2+} (see Fig. 2); one must take the matrix element with respect to the unperturbed wave functions of the copper ion $\varphi_1^0 = \varphi_1(\theta_0)$ and $\varphi_2^0 = \varphi_2(\theta_0)$ [(2a), (2b)].

If we consider $E^{(2)}$ as a correction of the second order to the energy of the ion, we must take the matrix element with respect to wave functions of Cu^{2+}, where the complex is in the vibrational ground state. One sees easily that $E^{(2)} = 0$, since

$$\langle \varphi_1(\theta) | \hat{V}_2 \rho \sin\theta + \hat{V}_3 \rho \cos\theta | \varphi_2(\theta) \rangle = 0$$

for the values ρ_0 and $\theta = 0$. We are, however, interested in the contribution of the linear term to the vibrational energy of the complex and not to the energy of the Cu^{2+} ion, i.e., we must find

$$U'(q_2, q_3) = E^{(2)}(Q_2^0 + q_2, Q_3^0 + q_3) - E^{(2)}(Q_2^0, Q_3^0),$$

where Q_2^0 and Q_3^0 are the values of Q_2 and Q_3 at the minimum of the potential energy of the deformed complex, and $q_2 = \widetilde{Q}_2$, $q_3 = \widetilde{Q}_3$ are the vibrational coordinates. The calculation shows that

$$U'(q_2,\ q_3) \approx -\tfrac{1}{2} k q_2^2 = -\tfrac{1}{2} k \rho_0^2 \gamma^2,$$

so that

$$U(\rho, \theta) = U(\rho_0, \theta_0) + \tfrac{1}{2}(k - 6\,|\,A_3\,|\,\rho_0 \cos 3\theta_0)\, q^2 + \tfrac{9}{2}\,|\,A_3\,|\,\rho_0^3 \cos 3\theta_0 \cdot \gamma^3. \tag{9a}$$

It is necessary to note that vibrations of the type γ possess a peculiar spatial degeneracy: in some fixed system of coordinates identical vibrations may occur when the complex is stretched along the x, y, or z axis; it is essential for this that for the transition, let us say from x to y, the system must overcome a relatively high potential barrier (see Fig. 3).

We shall now consider the connection between the vibrations of the complex of the type γ and the form of the eigenfunctions of the copper ground state. If the complex is in the vibrational ground

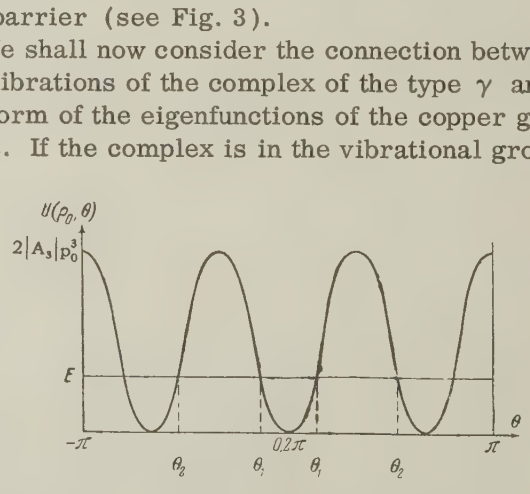

FIG. 3. Curve of the potential energy $U(\rho_0, \theta)$ of the complex.

state as far as the coordinate γ is concerned, the eigenfunction $\varphi_1^{(1)}$ of the copper ground state is a pure ψ_1 [see (2a) and (2b)]. The combinations $\varphi_1^{\{2,3\}} = \frac{1}{2}\psi_1 + (\sqrt{3}/2)\psi_2$ correspond to a change in the configuration of the complex; in some fixed system of xyz coordinates, namely, the functions $\varphi_1^{(2)}$ and $\varphi_1^{(3)}$ may be the eigenfunctions of the Cu^{2+} ion when the complex is stretched along the x and the y axis respectively, if $\varphi^{(1)}$ is defined relative to the z axis.

If the complex performs vibrations of type γ with some frequency, the cubic eigenfunction ψ_2 will be mixed with the same frequency into the eigenfunction φ_1 of the ground state of the ion. The amplitude with which ψ_2 is present in the superposition $\varphi_1(\psi_1, \psi_2)$ is determined by the expression $(1-\cos\theta)^{1/2}/\sqrt{2}$ [see (2a)].

The interdependence of the eigenvibrations of the complex and the form of the function φ_1 of the ground state of Cu^{2+} is a consequence of the connection, already noted by us, of the geometry of the complex and the distribution of the electron cloud of the magnetic ion. In the equilibrium state of the complex at a temperature T, the eigenfunction ψ_2 will be present in φ_1 with some average intensity $\alpha^2 = \frac{1}{2}\langle(1-\cos\theta)\rangle_{av}$ (time average) so that the eigenfunctions will be of the form*

$$\varphi_1 = (1-\alpha^2)^{1/2}\psi_1 + \alpha\psi_2. \qquad (10)$$

An arbitrary physical quantity L obtained by quantum mechanical averaging over the ground state of the system (such as the g-factor, the hfs constants, and so on) will therefore be of the form

$$L = L_1 - \alpha^2(L_1 - L_2), \quad L_1 = \langle\psi_1|\hat{L}|\psi_1\rangle,$$
$$L_2 = \langle\psi_2|\hat{L}|\psi_2\rangle. \qquad (11)$$

This mechanism was considered by us. It gives a qualitatively correct dependence of the g-factors and the hfs constants on the temperature, but under the given conditions it is not unique and is, apparently, not the main mechanism.

Indeed it is well known[10] that if a quantum particle with momentum p is in a potential well U(x) of the form depicted in Fig. 4, while U(x) satisfies the condition for quasi-classical behavior: $m\hbar F/p^3 \ll 1$, $F = -\partial U/\partial x$, the probability (per unit time) for the overcoming of the barrier is equal to

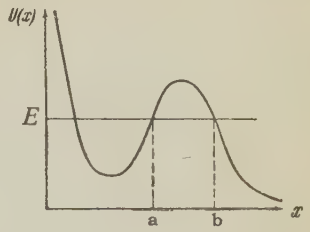

FIG. 4. Curve of the potential energy U(x).

$$w = (\omega_0/2\pi)\exp\left[-2\hbar^{-1}\left|\int_a^b p\,dx\right|\right],$$

since during a unit time interval a particle performing classical vibrations inside the well impinges $\omega_0/2\pi$ times on the barrier.

The considerations given here are applicable in our case to vibrations of type γ if the condition for quasi-classical behavior is satisfied for the potential curve $U(\rho_0, \theta)$ (see Fig. 3). Calculation shows that the condition for quasi-classical behavior is satisfied for $U(\rho_0, \theta)$ so that we get

$$w(E) = (\omega_0/\pi)\exp\left[-2\hbar^{-1}\left|\int_{\theta_1}^{\theta_2} M(\theta)\,d\theta\right|\right], \qquad (12a)$$

where

$$U(\rho_0, \theta) = U_0(1-\cos 3\theta), \quad U_0 = |A_3|\rho_0^3,$$

and $M(\theta)$ is found from the equation

$$M^2/2J + U(\rho_0, \theta) = E.$$

J is the moment of inertia for the "rotation" of the complex along the circle $Q_2^2 + Q_3^2 = \text{const}$; for the hydrated complex $J \sim 7.8\times10^{-40}$ g-cm^2 (for $\rho_0 = 0.3\times10^{-8}$ cm);[9] E is the energy.

It is clear that if the vibrations have large amplitudes they will no longer be harmonic, but for $2|A_3|\rho_0^3 \gg E$ we can restrict ourselves to the harmonic-oscillator approximation for a rough estimate of the frequency ω_0 of the vibrations. For hydrated complexes $\omega_0 \approx 5\times10^{13}$ sec^{-1} ($\hbar\omega_0 \approx 300$ cm^{-1}).

Since $J\omega_0^2 = 9|A_3|\rho_0^3$,

$$w(E) = \frac{\omega_0}{\pi}\exp\left[-\frac{2U_0}{\hbar\omega_0}\left|\int_{\delta_1}^{\delta_2}\sqrt{2[E/U_0 - (1-\cos\delta)]}\,d\delta\right|\right]. \qquad (12b)$$

It is unfortunately difficult to perform the thermodynamic averaging (12b) and to find $\tilde{w}(T; M, U_0)$ explicitly (M is the mass of the corner atoms Y, and $2U_0$ the height of the potential barrier). Indeed, for such an averaging it is assumed that E changes from 0 to ∞. For a sufficiently large increase of E the theory of small vibrations becomes, however, inapplicable so that $\omega_0 = \omega_0(E)$.

It is well known that an exchange interaction of the order of $I \sim 1$ cm^{-1} ($I/\hbar = \omega_{exch} \sim 2$

*The eigenfunctions ψ_1 and ψ_2 taken by us in the $LMSS_z$ representations are arbitrary spin and orbital functions. This is connected with the fact that $\langle\psi_1|\lambda(\mathbf{L}\cdot\mathbf{S})|\psi_2\rangle = 0$, where $\lambda(\mathbf{L}\cdot\mathbf{S})$ is the spin-orbit interaction.

$\times 10^{11}$ sec^{-1}) leads practically to a complete removal of hfs in copper. The given mechanism will thus be essential for the averaging of the hfs and g-factor, only if the frequency of the "rotation" of the electron density $2\pi\tilde{w} \sim 10^{11}$ sec^{-1}.

In addition to the tunnel effect, another factor contributing to the "rotation" of the electron density is the classical mechanism of overcoming the potential barrier through energy fluctuations. This mechanism is not considered in the present paper.

4. DISCUSSION

The decrease in the hfs constant, which is observed in a number of cases in solid salts of elements of the iron group and in particular in copper salts, is usually explained either by exchange interactions or by a partial covalent bond between the magnetic ion and the corner atoms.

We propose still another mechanism for solutions of copper salts, which under well defined conditions may lead to both isotropy and a decrease of the hfs constants and at the same time to isotropy of the g-factor; this mechanism predicts, generally speaking, a temperature dependence of the hfs constants and of the g-factors.

If there occurs a "rotation" of the electron density, as discussed in Sec. 3, the eigenfunction of the ground state can be written in the form

$$\varphi_1 = [1 - \alpha^2(\tilde{\omega})]^{1/2}\psi_1 + \alpha(\tilde{\omega})\psi_2,$$

$$\alpha(\tilde{\omega}) = (1 - \cos 2\pi\tilde{\omega}t)^{1/2}/\sqrt{2},$$

and the magnitude of L is equal to the time average

$$L = \langle\varphi_1|L|\varphi_1\rangle_{av} = L_1 - \langle\alpha^2(\tilde{\omega})\rangle_{av}(L_1 - L_2).$$

For such an average the ratio of $2\pi\tilde{w}$ and the frequency of the Larmor precession ω_{res} is an important quantity. If the barrier is sufficiently low so that $2\pi\tilde{w} \gg \omega_{res}$ one may put the period T equal to $2\pi/\omega_{res}$. We have then

$$\langle\alpha^2(\tilde{\omega})\rangle_{av} = 1/2, \qquad \tilde{L} = \tfrac{1}{2}(L_1 + L_2).$$

This corresponds to a complete averaging of the quantity L.

In the other extreme case, when the barrier is so high that $2\pi\tilde{w} = \omega_{res}$, one cannot average the quantity L by taking the overcoming of the barrier into account. Only the eigenvibrations of the complex can in that case influence the magnitude of L; however, calculation shows that the influence of these vibrations is unimportant.

When $2\pi\tilde{w} \sim \omega_{res}$ the magnitude of L will be temperature dependent. As was mentioned already it is difficult to get an explicit expression for this dependence.

In hydrated complexes $Cu^{2+}(H_2O)_6$ in solutions and also in copper salts with a trigonal symmetry, complete averaging apparently does take place. Bearing in mind that*

$$g_x^{(1)} = g_y^{(1)} \approx 2.28, \quad g_z^{(1)} \approx 2.0,$$

$$|A^{(1)}| = 85 \cdot 10^{-4}\text{cm}^{-1}, \quad |B^{(1)}| = 78 \cdot 10^{-4}\text{cm}^{-1};$$

$$g_x^{(2)} = g_y^{(2)} \approx 2.11, \quad g_z^{(2)} \approx 2.46,$$

$$|A^{(2)}| \approx 110 \cdot 10^{-4}\text{cm}^{-1}, \quad |B^{(2)}| \approx 30 \cdot 10^{-4}\text{cm}^{-1},$$

we get

$$\tilde{g}_x = \tilde{g}_y \approx 2.19, \quad \tilde{g}_z \approx 2.23,$$

$$|\tilde{A}| \approx 17 \cdot 10^{-4}\text{cm}^{-1}, \quad |\tilde{B}| \approx 24 \cdot 10^{-4}\text{cm}^{-1}.$$

In evaluating $|\tilde{A}|$ and $|\tilde{B}|$ we have taken into account the theoretical considerations about the signs of the constants A and B.[11]

In the framework of the given theory there is also an explanation for the experimental fact that some copper complexes, as a rule with heavy corner atoms,[12] have a hyperfine structure. Indeed, the theoretical considerations involve the three parameters J, ω_0, and $|A_3|\rho_0^3$ which are connected by the relation $J\omega_0^2 = 9|A_3|\rho_0^3$. A change in the corner atoms may lead both to a change in $|A_3|\rho_0^3$ and to a change in J due to a change in the effective mass of the complex ($J \approx \frac{1}{2}M\rho_0^2$): one must understand by M not the total mass of the corner atoms, but some effective mass, since the corner atoms Y do not take part in the vibrations of the complex as a whole. If we assume that $|A_3|\rho_0^3$ does not change appreciably when we make a substitution of the corner atoms, we obtain all the same an important dependence of $\tilde{w}$ on the mass of the corner atoms, as follows from Eq. (12b) ($\omega_0 = \sqrt{9|A_3|\rho_0^3/J}$). We have not enough data about the character of the change of the quantities mentioned at our disposal to make concrete calculations.

In conclusion the author expresses his deep gratitude to B. M. Kozyrev for a discussion of his results and to S. A. Al'tshuler for his interest in the work.

[1] B. Bleaney and K. D. Bowers, Proc. Phys. Soc. (London) A65, 667 (1952).

*The data are taken for Tutton salts of copper[2] where the ground state (in the $LMSS_z$ representation) is $\psi_1 = \psi_{2,0}\psi_\alpha(S_z)$ and for the fluorosilicate of copper (at T = 20°K)[1] where the ground state is $\psi_2 = \psi_\alpha(S_z)(\psi_{2,2} + \psi_{2,-2})/\sqrt{2}$.

[2] D. M. S. Bagguley and J. H. E. Griffiths, Proc. Phys. Soc. (London) **A65**, 594 (1952).

[3] A. Abragam and M. H. L. Pryce, Proc. Phys. Soc. (London) **A63**, 409 (1950).

[4] B. M. Kozyrev, Dokl. Akad. Nauk SSSR **103**, 53 (1955); Discussions Faraday Soc. **19**, 135 (1955).

[5] B. M. Kozyrev, Izv. Akad. Nauk SSSR, Ser. Fiz. **21**, 828 (1957), Columbia Tech. Transl. p. 828.

[6] H. A. Jahn and E. Teller, Proc. Roy. Soc. (London) **A161**, 220 (1937).

[7] J. H. Van Vleck, J. Chem. Phys. **7**, 72 (1939).

[8] Bjerrum, Ballhausen, and Jørgensen, Acta Chem. Scand. **8**, 1275 (1954).

[9] U. Öpik and M. H. L. Pryce, Proc. Roy. Soc. (London) **A238**, 425 (1957); Longuet-Higgins, Öpik, Pryce, and Sack, Proc. Roy. Soc. (London) **A244**, 1 (1958).

[10] L. D. Landau and E. M. Lifshitz, Квантовая механика (Quantum Mechanics), OGIZ, 1948, p. 206 [Engl. Transl., Pergamon, 1958].

[11] A. Abragam and M. H. L. Pryce, Proc. Roy. Soc. (London) **A205**, 135 (1951); **A206**, 164 (1951).

[12] B. R. McGarvey, J. Phys. Chem. **61**, 1232 (1957).

Translated by D. ter Haar
199

ON THE NUCLEON + CORE MODEL OF THE NUCLEUS WITH A VIBRATIONAL EXCITATION SPECTRUM OF THE CORE

D. P. GRECHUKHIN

Moscow State Pedagogical Institute

Submitted to JETP editor April 23, 1959

J. Exptl. Theoret. Phys. (U.S.S.R.) **37**, 1026-1033 (October, 1959)

The nucleon + core model with intermediate coupling between the nucleon and the phonon excitations of the core has been considered in a number of papers[1-5] as a possible way of describing the spectra of odd nuclei in the atomic weight region where even-even nuclei have level spectra similar to that of the vibrational quadrupole excitations of the nuclear surface (phonons). The state of the nucleon + core system is a superposition of nucleon states and core states with various numbers of phonons. The energy levels and the wave functions of the system have been determined approximately by diagonalizing the energy matrix, which is cut off at a certain number of phonons, N. The convergence of the approximations for various cutoff values N is investigated on the simple model of spinless photons, which leads to an energy matrix which retains the main features of the matrix for phonons with spin.

INTRODUCTION

THE level spectrum of even-even nuclei in the regions $60 \leq A \leq 150$ and $190 \leq A \leq 214$ has the characteristic features of the vibrational spectrum of the quadrupole excitations of the nucleus:[1] 1) the ratio of the energies of the second and first excited states, E_2/E_1, is close to the value 2; 2) the reduced probabilities for E2 transitions exhibit a collective character; 3) the intensities of the M1 transitions are below the estimates given by the single-particle model; 4) the reduced probabilities for the "crossing" E2 transitions are smaller than the probabilities for E2 transitions between adjacent levels.

The model of vibrational quadrupole excitations of the nucleus predicts three degenerate states with spins I = 0, 2, and 4 for the second excited level. If the conditions of adiabatic motion of the nucleons of the core and collective motion of the core are violated, this degeneracy is removed. At present three levels are known for Cd_{48}^{110} and Hg_{80}^{198}.

For the case of the adjacent odd nuclei it is natural to try to apply the nucleon + core model for the description of the level spectrum of the nucleus. This model has been considered earlier by a number of authors[1-6] and is now regarded as one of the possible descriptions of the odd nuclei.[7]

In the framework of this model the state of the nucleon + core system is given by a solution of the Schrödinger equation with Hamiltonian[1,3]

$$\hat{H} = \hat{H}_{\text{vibr}} + \hat{H}_{\text{single}} + \hat{H}_{\text{cplg}}. \quad (1)$$

Here

$$\hat{H}_{\text{vibr}} = \tfrac{1}{2}\sum_{\mu} B_2 (-1)^{\mu} \dot{\alpha}_{2\mu}\dot{\alpha}_{2-\mu} + \tfrac{1}{2}\sum_{\mu} C_2 (-1)^{\mu}\alpha_{2\mu}\alpha_{2-\mu}, \quad (2)$$

$$\hat{H}_{\text{cplg}} = -k\sum_{\mu}\alpha_{2\mu}Y_{2\mu}(\theta, \varphi),$$

$$\hat{H}_{\text{single}} = -(\hbar^2/2M)\Delta + U(r) \quad (3)$$

$\hat{H}_{\text{single}}$ is the Hamiltonian of the nucleon in the field of the nuclear core, U(r). For U(r) one takes either the radially symmetric potential of the Nilsson type[8] or the optical model potential. $\alpha_{2\mu}$ are the deformation parameters of the surface of the nucleus,

$$R(\theta, \varphi) = R_0[1 + \alpha_0 + \sum_{\mu}\alpha_{2\mu}Y_{2\mu}].$$

k is the coupling constant of the interaction of the nucleon with the nuclear surface; it can only be estimated within a particular model of the motion of the nucleon in the deformed nucleus. Thus we have, for a nucleon in a rectangular potential well with depth U_0 and with a deformed surface,[1]

$$\hat{H}_{\text{cplg}} = -U_0 R_0 \delta(r - R_0)\sum_{\mu}\alpha_{2\mu}Y_{2\mu}(\theta, \varphi),$$

after averaging over the state of the nucleon with quantum numbers $nj\mu_j$, we obtain

$$\langle \hat{H}_{\text{cplg}} \rangle = -U_0 R_0^3 \,|\, R_{nj}(R_0) \,|^2 \sum_{\mu} \alpha_{2\mu} Y_{2\mu}(\theta, \varphi).$$

Hence

$$k = U_0 R_0^3 \,|\, R_{nj}(R_0) \,|^2 = 40 \text{ to } 50 \text{ Mev}.$$

It follows that the dimensionless coupling parameter $\kappa = k\sqrt{\hbar\omega\ 2C_2}/\hbar\omega$ is not small, and that perturbation theory with respect to κ cannot be applied if $\hbar\omega$ and the stiffness C_2 are small: $C_2 \sim 20 \div 60$ Mev, $\hbar\omega \approx 0.2$ to 0.8 Mev.

One usually seeks the solution of the Schrödinger equation for the system in the form of an expansion in terms of core states $\chi^{\nu}_{\lambda\mu_\lambda}$ (ν is the number of phonons, and λ and μ_λ are the angular momentum and its projection on the axis of quantization):

$$\Psi_{IM} = \sum_{nj\lambda\nu} a^{Inj}_{\nu\lambda} \sum_{\mu_j \mu_\lambda} C^{IM}_{I\mu_j\lambda\mu_\lambda} \psi_{j\mu_j n} \chi^{\nu}_{\lambda\mu_\lambda} \qquad (4)$$

[$\psi_{j\mu_j n}$ is the function of the nucleon in the spherically symmetric field $U(r)$]. The amplitudes $a^{\cdots}_{\cdots}$ are then determined by diagonalizing the energy matrix.

Approximate solutions of the equation $H\psi = E\psi$ were found in references 1, 3, and 5 by cutting off the energy matrix at a certain number of phonons and assuming that the nucleon moment j is a good quantum number. The cut-off was carried out at the values N = 1, 2, and 3. Since the validity of the model depends on the comparison of the experimental data with the results of the model, there naturally arises the question of the accuracy of these approximations and to what extent the obtained results can be used in the analysis of the experimental data.

THE NUCLEON + CORE MODEL WITH SPINLESS PHONONS

The investigation of the convergence with respect to N for matrices with phonons with spin is difficult, because the state ψ_{IM} for a given number of phonons ν has contributions from several states with different λ. The rank of the matrix is, therefore, considerably greater than N. For this reason we consider the process of approximation on the simple model of spinless phonons. The energy matrix in this model, however, retains the basic features of the matrix for phonons with spin. As model Hamiltonian we take

$$\hat{H}_0 = \tfrac{1}{2}(\hat{q}\hat{q}^+ + \hat{q}^+\hat{q}) - \varkappa(\hat{q}^+ + \hat{q}), \qquad (5)$$

i.e., we assume that the state of the "nucleon" does not change. This is equivalent to the assumption that n and j are good quantum numbers. Here $\hat{q}^+$ and $\hat{q}$ are the creation and annihilation operators of the "phonons" and κ is a dimensionless parameter which characterizes the coupling of the nucleon degree of freedom with the "phonons". The exact solution for the Hamiltonian (5) is known: we introduce the new phonon operators $\hat{p} = \hat{q} - \kappa$ and $\hat{p}^+ = \hat{q}^+ - \kappa$, and obtain

$$\hat{H}_0 = \tfrac{1}{2}(\hat{p}^+\hat{p} + \hat{p}\hat{p}^+) - \varkappa^2, \qquad E_i = \hbar\omega\varepsilon_i = \hbar\omega[i + \tfrac{1}{2} - \varkappa^2].$$

We are, however, not interested in the exact value of the energy level E_i, but in the process of approximating E_i by cutting off the energy matrix at the number of phonons N.

We therefore expand the Ψ_i function of the system into a series in terms of states of the core:

$$\Psi_i = \sum_{\nu} a^i_{\nu}\chi_{\nu}, \text{ where } \chi_{\nu} = (\hat{q}^+)^{\nu}\chi_0/\sqrt{\nu!},$$

χ_0 is the "vacuum" wave function.

Substituting the series $\Psi = \sum_{\nu} a_{\nu}\chi_{\nu}$ in the Schrödinger equation $H_0\Psi = E\Psi$, we obtain the energy matrix

$$(\nu - \varepsilon)a_{\nu} - \varkappa\sqrt{\nu+1}\ a_{\nu+1} - \varkappa\sqrt{\nu}\,a_{\nu-1} = 0; \qquad (6)$$

here the factor $\frac{1}{2}$ is included in ϵ, so that for $\kappa = 0$ (free oscillator), $\epsilon_\nu = \nu$. We regard equation (6) as a recurrence relation for the coefficients a_ν. Choosing a_0 as the independent coefficient, we find all a_ν successively in terms of a_0:

$$a_{\nu} = a_0 f_{\nu}(\varepsilon)/(-\varkappa)^{\nu}\sqrt{\nu!}, \qquad (7)$$

where

$$f_{\nu+1}(\varepsilon) = (\varepsilon - \nu) f_{\nu} - \nu\varkappa^2 f_{\nu-1};$$
$$f_1(\varepsilon) = \varepsilon. \qquad (8)$$

Cutting off the matrix (6) at a certain phonon number N corresponds to the equation $a_{N+1} = 0$ or $f_{N+1} = 0$. From this we find N+1 roots, $\epsilon_i(N)$, which are the eigenvalues of the Hamiltonian in the given approximation. For each root $\epsilon_i(N)$ we find the set of amplitudes $a^i_\nu(N)$ which determines the wave function of the i-th state. As is seen from (8), the essential coupling parameter is not κ, but κ^2; we therefore carried out calculations for $\kappa^2 = 0.5$, 1, 2, and 3. The roots $\epsilon_i(N)$ for each κ^2 were found graphically by constructing the corresponding polynomial $f_{N+1}(\epsilon)$. The results of the calculation of the energy levels for the ground and first three excited levels are given in the figure.

To illustrate the convergence process with respect to N, we list in Tables I to IV the amplitudes of the wave functions of the system in the first excited and ground states for the parameter values $\kappa^2 = 1$ and $\kappa^2 = 3$. The calculations were

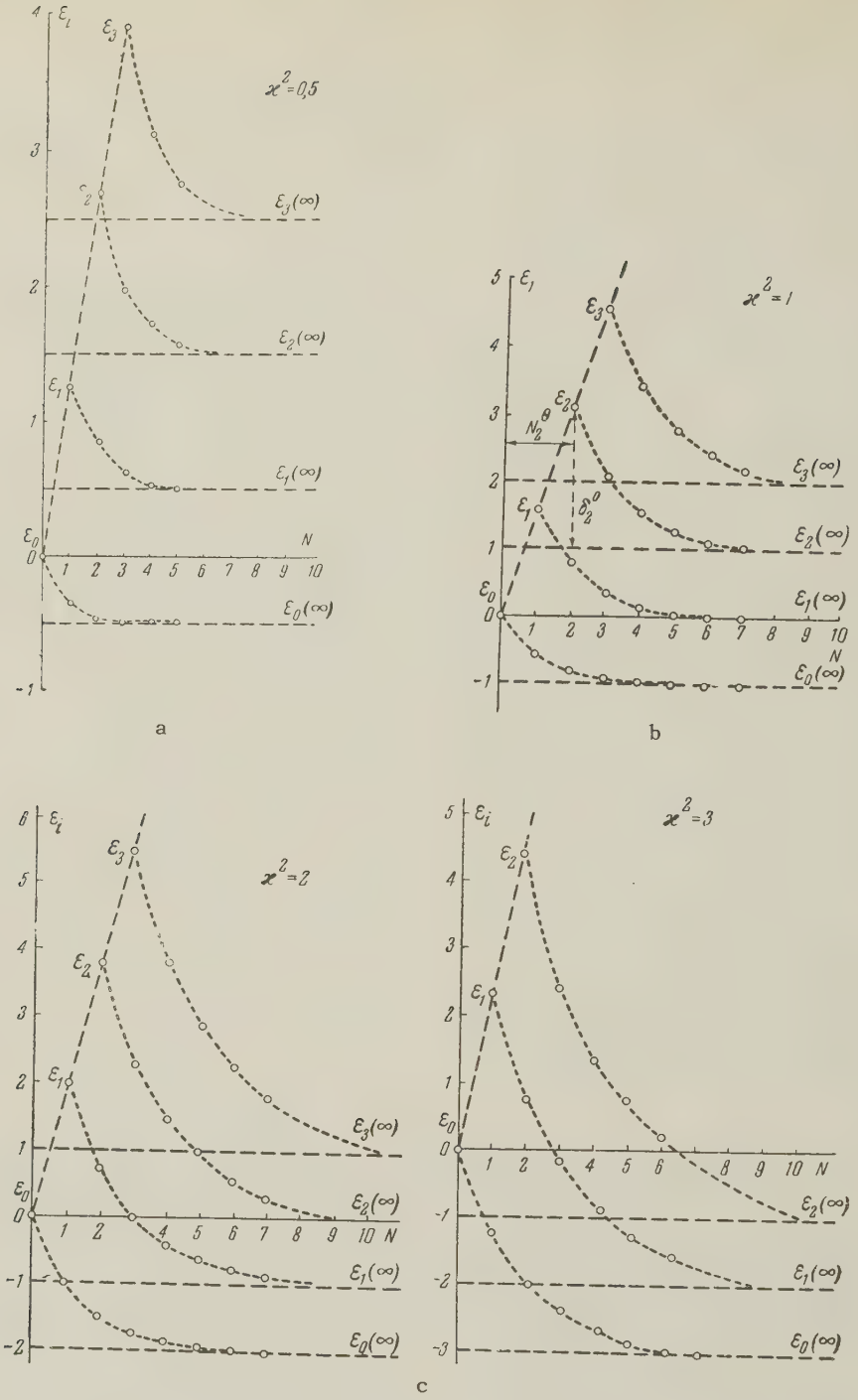

Dependence of the energy levels ε_i on the number of phonons N for various values of κ^2.

carried out with slide rule accuracy. As is seen from the tables, the coefficients of the wave functions have appreciable magnitudes in the interval N = 1 to 5. The $a_\nu^i(N)$ become smaller by an order of magnitude only for $\nu \approx 5$. The solution given by the cut-off matrix can therefore only be close to the actual solution for $N \approx 5$ or 6. The errors in the calculation of the matrix elements of operators with functions obtained from an energy matrix cut off at $N \leq 3$ may be large, especially in the case of operators which are proportional to $\hat{q}\hat{q}$, $\hat{q}^+\hat{q}^+$, $\hat{q}\hat{q}^+$ and higher powers of the operators $\hat{q}$ and $\hat{q}^+$.

The approximation $\epsilon_i(N)$ to the exact value $\epsilon_i(\infty)$ can, at least in the region $\Delta N \leq 5$, be expressed by the exponential function

$$\varepsilon_i(N) - \varepsilon_i(\infty) = \delta_i(N) = \delta_i^0 \exp\{-\alpha_i(N - N_i^0)\}; \quad (9)$$

N_i^0 and δ_i^0 are indicated in the figure for $\kappa^2 = 1$. For δ_i^0 we have the relation

TABLE I. Amplitudes $a_\nu^0(N)$ for ϵ_0 with $\kappa^2 = 1$

N	ε_0	a_0	a_1	a_2	a_3	a_4	a_5
1	—0.62	0.85	0.53	—	—	—	—
2	—0.86	0.72	0.62	0.31	—	—	—
3	—0.96	0.65	0.62	0.40	0.17	—	—
4	—0.99	0.63	0.62	0.42	0.22	0.067	—
5	—1.0	0.60	0.60	0.43	0.25	0.12	0.054

TABLE II. Amplitudes $a_\nu^0(N)$ for ϵ_1 with $\kappa^2 = 1$

N	ε_1	a_0	a_1	a_2	a_3	a_4	a_5	a_6
1	1.62	0.53	—0.85	—	—	—	—	—
2	0.77	0.66	—0.51	—0.56	—	—	—	—
3	0.32	0.68	—0.22	—0.58	—0.39	—	—	—
4	0.14	0.66	—0.09	—0.52	—0.49	—0.25	—	—
5	0.05	0.63	—0.03	—0.47	—0.50	—0.33	—0.13	—
6	0.013	0.61	—0.008	—0.47	—0.50	—0.37	—0.22	—0.095

TABLE III. Amplitudes $a_\nu^0(N)$ for ϵ_0 with $\kappa^2 = 3$

N	ε_0	a_0	a_1	a_2	a_3	a_4	a_5	a_6
1	—1.3	0.91	0.40	—	—	—	—	—
2	—2.0	0.81	0.54	0.19	—	—	—	—
3	—2.44	0.73	0.59	0.31	0.13	—	—	—
4	—2.70	0.68	0.61	0.37	0.17	0.054	—	—
5	—2.86	0.62	0.60	0.39	0.20	0.084	0.025	—
6	—2.92	0.62	0.60	0.42	0.23	0.10	0.04	0.012

TABLE IV. Amplitudes $a_\nu^1(N)$ for ϵ_1 with $\kappa^2 = 3$

N	ε_1	a_0	a_1	a_2	a_3	a_4	a_5	a_6
1	2.3	0.79	—0.61	—	—	—	—	—
2	0.70	0.94	—0.22	—0.24	—	—	—	—
3	—0.20	0.96	0.065	—0.21	—0.12	—	—	—
4	—0.86	0.95	0.27	—0.10	—0.13	—0.06	—	—
5	—1.30	0.91	0.39	0.00	—0.11	—0.08	—0.03	—
6	—1.54	0.87	0.44	0.061	—0.16	—0.14	—0.07	—0.02

TABLE V

κ^2	α_0	α_1	α_2	α_3	$\bar{\alpha}$	tg φ
1.0	0.80	0.75	0.70	0.60	~0.70	1.50
1.5	0.75	0.65	0.55	0.50	~0.60	1.75
2.0	0.70	0.55	0.45	0.40	~0.50	1.90
3.0	0.55	0.40	0.40	—	~0.45	2.20

$$\delta_i^0 = \varkappa^2 + N_i^0 \tan \varphi(\varkappa^2). \qquad (10)$$

The values of $\alpha_i(\kappa^2)$ and $\tan \varphi(\kappa^2)$ are listed in Table V ($\bar{\alpha}$ is the average value of the parameter α_i over the four energy levels). In view of the crudeness of the calculation of the energy levels, the values of α_i and $\tan \varphi$ reflect only qualitatively the behavior of the energy matrix.

It follows from Table V that the convergence of the energy matrix with respect to the number of included phonons, N, becomes worse as κ^2 and the index of the level, i, increase, since the exponent $\alpha_i(\kappa^2)$ decreases while δ_i^0 becomes larger (the error in the term E_0 of the energy reaches the order $\hbar\omega/2$ for cutoff at $N = 3$ and $\kappa^2 = 3$).

This simple model of phonons without spin permits us to make some qualitative remarks about the more realistic model with phonons with spin

as well, since the energy matrix retains its oscillatory character even in this case.

For simplicity we restrict ourselves to a model in which the state of the nucleon does not change, i.e., the principal quantum number n and the total angular momentum j of the nucleon are good quantum numbers. The state of the system is described by the function

$$\Psi_{IM} = \sum_{\nu\lambda} a_{\nu\lambda}^{Ijn} \sum_{\mu_j \mu_\lambda} C_{j\mu_j \lambda\mu_\lambda}^{IM} \phi_{jn\mu_j} \chi_{\lambda\mu_\lambda}^{\nu}. \quad (11)$$

For the matrix elements of the operator $\hat{H}_{cplg}$ of (3) (see, for example, reference 3) we have, after some transformations,

$$\langle j,\ \nu\lambda,\ IM | \hat{H}_{cplg} | j, \nu'\lambda',\ IM\rangle$$

$$= -k \sqrt{\frac{\hbar\omega}{2C_2} \frac{5}{4\pi}} [C_{20l0}^{l0} u(2lj^1/_2;\ lj)]$$

$$\times \{\langle \nu\lambda \| \beta \| \nu'\lambda' \rangle u(Ij\lambda' 2;\ \lambda j)\} \sqrt{\nu+1}\, \delta_{\nu+1,\ \nu'}. \quad (12)$$

Here $u(\alpha\beta\gamma\delta;\ \epsilon\varphi)$ is the Racah function (see, for example, reference 9). The reduced matrix element $\langle \nu\lambda \| \beta \| \nu'\lambda' \rangle$ has the order of magnitude $\sim \frac{1}{2}$ to 1.

The effective coupling constant between the phonons and the nucleon is given by

$$\varkappa_{eff} = \varkappa \{C_{20l0}^{l0} u(2lj^1/_2;\ lj)\}, \quad (13)$$

where

$$\varkappa = k \sqrt{(5/4\pi)(\hbar\omega/2C_2)}/\hbar\omega,$$

$$\{C_{20l0}^{l0} u(2lj^1/_2;\ lj)\}^2$$

$$= \begin{cases} l(l+2)(2l-1)/(2l+3)(2l+1)^2 & \text{for } j = l + 1/_2, \\ (l^2-1)/(2l+1)^2 & \text{for } j = l - 1/_2. \end{cases}$$

Introducing the matrices

$$\{\hat{\gamma}_{\nu,\nu+1}\}_{\lambda\lambda'} = \langle \nu\lambda \| \beta \| \nu+1\lambda' \rangle u(Ij\lambda' 2;\ j\lambda),$$

$$\{\hat{\gamma}_{\nu\nu-1}\}_{\lambda\lambda''} = \langle \nu-1\lambda'' \| \beta \| \nu\lambda \rangle u(Ij\lambda 2;\ j\lambda'')$$

and the state vector a_ν with components $a_{\nu\lambda}$, we write the energy matrix in a form similar to equation (6):

$$(\nu - \varepsilon) a_\nu - \varkappa_{eff} \sqrt{\nu+1}\, \hat{\gamma}_{\nu,\nu+1} a_{\nu+1}$$

$$- \varkappa_3 \sqrt{\nu}\, \hat{\gamma}_{\nu,\nu-1} a_{\nu-1} = 0. \quad (14)$$

The analysis of this matrix is considerably more difficult than in the case (6). However, utilizing the similarity in the forms of the matrices (14) and (6), we can apply the results obtained earlier for qualitative estimates in this case.

Let us consider the particular nucleus Cd_{48}^{111} (reference 6). For the even-even nucleus Cd_{48}^{110} we have $\hbar\omega = 0.656$ Mev and $C_2 = 58$ Mev; the odd nucleon can be in the states $3s_{1/2}$, $2d_{3/2}$, $2d_{5/2}$, $1g_{7/2}$, and $1h_{11/2}$. The corresponding constants κ_{eff}^2 are equal to:

States:	$3s^1/_2$	$2d^3/_2$	$2d^5/_2$	$1g^7/_2$	$1h^{11}/_2$
κ_{eff}^2	0	1.60	1.80	2.5	2.7

The number of phonons, N, to be included in the energy matrix is determined by the accuracy required for the position of the energy terms.

If the admissible error in the position of the term is equal to Δ, the required number of phonons can be estimated from the relation

$$\Delta/\hbar\omega \geqslant \kappa_{eff}^2 \exp(-\bar{\alpha}N). \quad (15)$$

For κ_{eff}^2 we must take the largest among all possible values.

If j is not a good quantum number, all nucleon states with the same parity are combined into a single energy matrix. The convergence of this matrix with respect to the included number of phonons is determined by the largest value of the coupling constant for nucleon states with the same parity. In the case of Cd_{48}^{111} the largest coupling constant for even states is $\kappa_{eff}^2 = 2.5$. This constant corresponds to the exponent $\bar{\alpha} \approx 0.5$. If the spectrum is to have an accuracy of the distance to the first excited level, $E_1 = 0.247$ Mev, we must include at least four phonons.

If the accuracy is increased ($\Delta = 80$ kev, $N \geq 6$; and for $\Delta = 20$ kev, $N \geq 9$), the number of phonons is higher.

In the case of $Cd^{110,111}$ we used the values for $\hbar\omega$ and C_2 quoted in the well known review article of Bohr, Mottelson, et al.[6] These values were obtained by fitting the experimental data on the Coulomb excitation of the nuclei in the framework of the hydrodynamic theory of vibrational excitations of the nucleus. On the whole, the hydrodynamic theory contradicts the experimental results, so that the question of the structure of the vibrational excitations of the nuclei remains open. The abovementioned example of $Cd^{110,111}$ must, therefore, be regarded only as an illustration of the convergence process for the energy matrix with respect to the number of phonons.

In conclusion I sincerely thank S. T. Belyaev, B. T. Geĭlikman, and L. A. Sliv for their interest in this work.

[1] A. Bohr and B. Mottelson, Kgl. Danske Videnskab. Selskab, Mat.-fys. Medd. **27**, No. 16 (1953).

Russ. Transl. Проблемы совр. физ. (Prob. Modern Phys.) No. 9, 1955.

[2] K. W. Ford, Phys. Rev. **90**, 29 (1953), Russ. Transl. ibid. No. 1, 1956.

[3] D. C. Choudhury, Kgl. Danske Videnskab. Selskab, Mat.-fys. Medd. **28**, No. 4 (1954).

[4] A. K. Kerman, Phys. Rev. **92**, 1176 (1953).

[5] F. J. Milford, Phys. Rev. **93**, 1297 (1953).

[6] Alder, Bohr, Huus, Mottelson, and Winther, Revs. Modern Phys. **28**, 432 (1956).

[7] A. M. Korolev, Report at the Ninth Annual Conference on Nuclear Spectroscopy, Khar'kov (1959).

[8] S. G. Nilsson, Kgl. Danske Videnskab. Selskab, Mat.-fys. Medd. **29**, No. 16 (1955).

[9] H. A. Jahn, Proc. Roy. Soc. **A205**, 192 (1951).

Translated by R. Lipperheide
200

PARITY NONCONSERVATION IN STRONG INTERACTIONS OF STRANGE PARTICLES

S. G. MATINYAN

Institute of Physics, Academy of Sciences, Georgian S.S.R.

Submitted to JETP editor April 25, 1959

J. Exptl. Theoret. Phys. (U.S.S.R.) 37, 1034-1040 (October, 1959)

A modification of Lee and Yang's theory of strange-particle parity doublets is considered in which parity conjugation invariance is extended to weak interactions. As a result parity nonconservation in weak interactions is found to be closely related to a change in strangeness.

Results of the analysis pertaining to the "forward-backward" asymmetry of the hyperon decay products are compared with the corresponding consequences due to parity nonconservation in strange particle production and interaction processes. Both interpretations are found to yield the same results as far as particles with odd strangeness are concerned. The two approaches can be distinguished by studying processes involving Ξ hyperons.

1. INTRODUCTION

THE question of parity nonconservation in strong interactions of elementary particles has recently come to hold considerable interest.[1-7]

Starting from a renormalizable Yukawa interaction for elementary particles, Solov'ev[1-4] has shown that the requirement of CP invariance for the Lagrangian together with the laws of charge conservation and isotopic invariance results in space parity conservation for electromagnetic and strong interactions of ordinary particles. On the other hand CP invariance and isotopic invariance do not lead to space parity conservation for strong interactions involving strange particles — isotopic-invariant additions to the usual Lagrangian, which violate parity conservation, are possible.

Parity nonconservation in strong interactions involving strange particles should lead to the appearance of a component of the polarization vector in the plane of their production and should result in a "forward-backward" ("right-left") asymmetry in the distribution of the decay products. So far experiments have given no evidence for the existence of such an asymmetry,[6] although one cannot exclude the possibility that the angular dependence of the longitudinal polarization is such that a vanishing asymmetry results after averaging over the angle of emission of the hyperons. It is also possible that this polarization will become detectable as the energy of strange particle production increases.

In this paper we wish to show that effects arising from parity nonconservation in strong interactions of strange particles, in particular the above-mentioned asymmetry, would also arise in a parity-conserving theory, namely, a modification of the parity-doublets theory of Lee and Yang[8,9] which would not contradict any other experimental facts.

2. STATEMENT OF THE PROBLEM

We amplify the Lee and Yang parity-doublets hypothesis by the requirement that all weak (and electromagnetic) as well as strong interactions of elementary particles be invariant under the CP operation of parity conjugation $\theta \longleftrightarrow \tau$, $\Lambda_1 \longleftrightarrow \Lambda_2$, etc. In this way parity doubling of all particles with odd strangeness is introduced.

It is easy to see that this requirement automatically leads to parity nonconservation in weak interactions of strange particles whenever strangeness changes by an odd number.* Indeed in such cases we have strange particles with odd strangeness before (Λ-, Σ- and K-decays) or after (Ξ-decay) the decay. The requirement that the decay process be invariant under parity conjugation then results in either the decay of particles of opposite parities into ordinary particles in the same orbital states or (in the Ξ-decay case) the decay of a strange particle of definite parity into a strange particle of one or the other intrinsic parity, the decay products being in the same orbital states in both cases. As a result, parity nonconservation in the decay is closely related to the change in strangeness.

Extending CP invariance to the decays causes the parity doublets to have the same lifetime and

*It is interesting to note that the decay $\Xi \to n + \pi$ for which $\Delta S = 2$, would be parity conserving were it to exist.

not to differ from each other in either weak or strong interactions. Consequently the question of the existence of a long-lived component of the Σ-hyperon parity doublet, not found in the experiments of Alvarez,[10] does not arise.

It is obvious that all known experimental facts which can be explained by the theory with parity nonconservation in decays without doubling the number of particles can also be explained by the present approach.

The existence of K-particle doublets permits the introduction in a natural way of a strong $KK\pi$ interaction, which leads to a number of experimentally-confirmed consequences. However this interaction may also be introduced in Solov'ev's theory, where there is no need for parity doublets, since the conservation of combined parity permits the Lagrangian of a strong (parity violating) local $KK\pi$ interaction to be written in the form

$$L_{K\pi} = ig_{K\pi}\{K^+K_0\Phi + KK_0^+\Phi^+\},$$

where Φ is the wave function of the π meson.

However this Lagrangian is not invariant under rotations in isotopic spin space. Consequently it is possible in principle to verify the K-particle doublet hypothesis by studying the universality of isotopic invariance in strong interactions and the existence of a strong $KK\pi$ interaction. (In this connection we should mention the work of Taylor[11] in which very general considerations based on a method of Chew[12] are used to show, by comparing the theory with the experimental results on the production of strange particles, that a strong $KK\pi$ interaction is necessary.) It is true that one must keep in mind the hypothesis advanced by Pais[13,14] according to which the K^+ and K^0 mesons have opposite parity. Here there are two possibilities: the $KK\pi$ interaction conserves parity but isotopic invariance is violated,[13] or the alternative — isotopic spin is conserved but parity conservation is violated.[14]

It is seen that the question of K-meson doublets can hardly be solved in the framework discussed above. A real possibility for verifying the parity doublets hypothesis will be indicated below.

Before passing on to a study of the consequences of the hypothesis of strange particle doubling on the processes of their interaction and production we note the following circumstance.

The revival in this paper of the parity doublets hypothesis is connected with the fact that, as will be seen later, the existence of a "forward-backward" ("right-left") asymmetry in processes involving strange particles may be explained not only by giving up space parity conservation in strong interactions of strange particles but also on the basis of the above introduced hypothesis. Also it is possible to find experimental tests to determine whether the "forward-backward" ("right-left") asymmetry in processes involving Λ and Σ particles is due to parity nonconservation in strong interactions or not.

3. INTERACTION AND PRODUCTION OF STRANGE PARTICLES

Turning now to effects resulting from the hypothesis discussed above we use the notation of Lee and Yang.[9]

Let us consider first the process of K^--particle capture by protons leading to formation of Σ^--hyperon doublets which subsequently decay, with the K^- beam consisting of a coherent mixture of θ^- and τ^- particles with amplitudes a_θ and a_τ. The density matrix describing the Σ^--hyperon beam at the instant of production (t = 0) is given by

$$D(0) = \begin{pmatrix} I_1(0) + \mathbf{P}_1(0)\,\sigma & J(0) + \mathfrak{P}_1(0)\sigma \\ J^+(0) + \mathfrak{P}_2^+(0)\sigma & I_2(0) + \mathbf{P}_2(0)\sigma \end{pmatrix}. \qquad (1)$$

The diagonal terms in Eq. (1) correspond to the usual density matrix for a beam of intensity I and polarization $\mathbf{P}$, the off-diagonal terms result from interference effects between the doublet components of opposite parity: J is a pseudoscalar, $\mathfrak{P}$ is a polar vector. The time dependence of these quantities is given by the exponential factor $e^{-\lambda t}$ where λ^{-1} is the lifetime of the Σ^- particles (it is the same for Σ_1^- and Σ_2^- in the model under consideration).

For the capture process I_i, J_i, $\mathbf{P}_i$ and $\mathfrak{P}_i$ are given by

$$I_1(0) \equiv I_1(t)|_{t=0} = |\alpha_\theta|^2|a|^2 + |\alpha_\tau|^2|b|^2,$$
$$I_2(0) = |\alpha_\theta|^2|b|^2 + |\alpha_\tau|^2|a|^2$$
$$J(0) = \alpha_\theta\alpha_\tau^+|a|^2 + \alpha_\tau\alpha_\theta^+|b|^2, \quad \mathbf{P}_1(0) = \mathrm{Re}\,[\alpha_\theta\alpha_\tau^+ ab^+]\,\mathbf{k}_\Sigma/k_\Sigma,$$
$$\mathbf{P}_2(0) = \mathrm{Re}\,[\alpha_\theta\alpha_\tau^+ ba^+]\,\mathbf{k}_\Sigma/k_\Sigma,$$
$$\mathfrak{P}(0) = [|\alpha_\theta|^2 ab^+ + |\alpha_\tau|^2 ba^+]\,\mathbf{k}_\Sigma/k_\Sigma, \qquad (2)$$

where $\mathbf{k}_\Sigma$ is the momentum of the Σ^- hyperon. In Eq. (2) a and b denote the amplitudes for the processes $\theta^- + p \to \Sigma_1^- + \pi^+$ ($\tau^- + p \to \Sigma_2^- + \pi^+$) and $\theta^- + p \to \Sigma_2^- + \pi^+$ ($\tau^- + p \to \Sigma_1^- + \pi^+$) respectively. These processes are dynamically different since they lead to final states with different orbital angular momenta, so that $a \neq b$.

The Σ^--hyperon decay process is described by the column (cf. reference 9)

$$M = \begin{pmatrix} A_0[1 + \mathbf{x}\mathbf{\sigma}\mathbf{k}] \\ B_0[\mathbf{x} + \mathbf{\sigma}\mathbf{k}] \end{pmatrix}, \qquad (3)$$

where κ is the degree of parity nonconservation in the decay, and $\mathbf{k}$ is a unit vector along the direction of the decay nucleon (in the hyperon rest frame).* A_0 and B_0 are related to the probabilities λ_i of the Σ_1 of the Σ_2 decay by

$$|A_0|^2[1+\varkappa^2]=\lambda_1, \qquad |B_0|^2[1+\varkappa^2]=\lambda_2. \tag{4}$$

(Of course, in our model expression (3) must commute with the parity conjugation operator C_p so that $A_0 = \pm B_0$ and $\kappa = \pm 1$. However we find it convenient in the following to use this general notation for purposes of comparison and only to impose the above equalities in the final expressions.)

We obtain for the angular distribution of the nucleons relative to the direction of emission of the Σ^- hyperons (in the hyperon rest frame):

$$W = \mathrm{Sp}\,(MDM^+) = N + Q\cos\theta, \tag{5}$$

$$N = \lambda[|a|^2+|b|^2]\,|\alpha_\theta+\alpha_\tau|^2,$$

$$Q = \pm\lambda[|\alpha_\theta|^2+|\alpha_\tau|^2+\mathrm{Re}\,\alpha_\theta\alpha_\tau^+]\,2\,\mathrm{Re}\,ab^+, \tag{5'}$$

where the upper sign corresponds to $\kappa = 1$ and the lower sign to $\kappa = -1$.

A characteristic of the "forward-backward" asymmetry formula obtained here, as distinct from the results of Lee and Yang,[9] is the coherence of the θ and τ particles in the K^--capture process. This fact is obviously related to parity nonconservation in the act of decay.

The circumstance that no "forward-backward" asymmetry has been observed in K^- captures may be explained by assuming that one of the amplitudes a, b is small in comparison with the other at energies of the order of the energy available in the K^- capture process. Of course, neither here nor below do we obtain any changes in lifetime characteristic of the Lee and Yang work, since $\lambda_1 = \lambda_2 = \lambda$ and the masses of the components of the doublet are strictly equal.

Let us consider next production of Λ and Σ hyperons in π-N or N-N collisions. In this case, after "averaging" over all remaining particles involved in the reaction, we get[9]

$$I_1 = I_2 = I, \qquad \mathbf{P}_1 = \mathbf{P}_2 = \mu\mathbf{n}, \qquad J = 0,$$
$$\mathfrak{P} = \mathfrak{P}^+ = \nu_1\mathbf{k}_{\mathrm{inc}} + \nu_2\mathbf{k}_\Lambda, \tag{6}$$

where $\mathbf{P}_i$ are the usual polarization vectors, $\mathbf{n} = \mathbf{k}_{\mathrm{inc}} \times \mathbf{k}_\Lambda$; μ, ν_1, ν_2 are constants depending on the dynamics of the process; $\mathbf{k}_{\mathrm{inc}}$ and $\mathbf{k}_\Lambda$ are unit vectors in the direction of the incident particle and of the hyperon in the center of mass system.

For the angular distribution of the decay nucleons in the rest frame of the hyperon we find the expression

$$W = [|A_0|^2+|B_0|^2][(1+\varkappa^2)I + 2\varkappa\mu\mathbf{nk}]$$
$$+ (1+\varkappa^2)\,2\,\mathrm{Re}\,A_0B_0^+(\nu_1\mathbf{k}_{\mathrm{inc}}+\nu_2\mathbf{k}_\Lambda)\,\mathbf{k}. \tag{7}$$

Here $\mathbf{k}$ is a unit vector in the direction of the nucleon momentum; we do not as yet consider our specific model and therefore use expression (3). This corresponds to the fact that parity nonconservation is not connected with the invariance of weak interactions under the $\theta \leftrightarrow \tau$ conjugation.

The term proportional to κ and intrinsically connected with parity nonconservation in the decay gives rise to the "up-down" asymmetry. The "forward-backward" ("right-left") asymmetry, expressed by the second term in (7) could also arise if parity were conserved in the decay process. In that case the "effective" asymmetry coefficients in the decay would be, generally speaking, different in the direction $\mathbf{n}$ and $\nu_1\mathbf{k}_{\mathrm{inc}} + \nu_2\mathbf{k}_\Lambda$. This is an example of the independence of effects due to parity nonconservation in the decay from those due to the parity doublets in the conventional treatment, as was pointed out in the past by Arnowitt and Teutsch.[15]

On the other hand, if parity is not conserved in the strange particle production process then the density matrix for the hyperon beam will have the following structure:*

$$I + \sigma\,\mathbf{P} + \sigma\mathfrak{P},$$

and for the decay $M = A_0(1+\kappa\sigma\mathbf{k})$.

For the corresponding angular distribution we find

$$W = |A_0|^2[I(1+\varkappa^2) + 2\varkappa(\mathbf{P}+\mathfrak{P})\,\mathbf{k}] \tag{8}$$

with the same asymmetry coefficients. However it is not difficult to see that Eq. (7) also gives equal asymmetry coefficients if we take into account the equalities $A_0 = \pm B_0$, $\kappa = \pm 1$, which hold in our approach. In that case

$$W = \lambda[I \pm (\mathbf{P}+\mathfrak{P})\,\mathbf{k}] \tag{9}$$

and the consequences due to parity nonconservation

*We assume here for simplicity that the degree of parity nonconservation $\varkappa$ is the same in the decay of Σ_1 and Σ_2, although from the invariance of expression (3) under the $\theta \to \tau$ conjugation one can deduce only that $\varkappa_1\varkappa_2 = 1$. This however does not affect results connected with maximal parity nonconservation in the decay when $\varkappa^2 = 1$.

*Let us note the difference in the formal apparatus in our case and in the case of parity nonconservation in strong interactions. In the latter case the density matrix for particles produced in strong interactions has on the diagonal pseudoscalar terms, whereas in our case the pseudoscalars appear only for the off-diagonal elements of the density matrix.

are the same as the consequences arising from our model.

Let us consider one more interesting example of a process involving strange particles*

$$\Sigma^0 + p \to \Lambda^0 + p, \tag{10}$$

in which the capture takes place from the S-state of the continuous spectrum. If parity is not conserved in this process the Λ^0 particle should be produced in S as well as P states, so that the transition amplitude has the form (compare reference 16):

$$a_1\Pi_t + a_2\Pi_s + \chi\,[(3/2)^{1/2}b_1\mathbf{k}_\Lambda\mathbf{S} + 3^{1/2}b_2\mathbf{k}_\Lambda\mathbf{S}'\,\Pi_t + b_3\mathbf{k}_\Lambda\cdot\mathbf{S}'\Pi_s], \tag{11}$$

where a_i and b_k are amplitudes for the $S \to S$ and $S \to P$ transitions respectively,

$$\Pi_t = \tfrac{1}{4}(3 + \sigma_1\sigma_2), \qquad \Pi_s = \tfrac{1}{4}(1 - \sigma_1\sigma_2),$$

$$\mathbf{S} = \tfrac{1}{2}(\sigma_1 + \sigma_2), \qquad \mathbf{S}' = \tfrac{1}{2}(\sigma_1 - \sigma_2),$$

and χ is the degree of parity nonconservation in the process (10). The subscript 1 in the spin matrices refers to the strange particles, subscript 2 to the proton. For the angular distribution of π mesons from the Λ^0 decay we obtain the following expression:

$$W = \lambda I\,[\beta + 4\mathrm{Re}\,(\chi\alpha)\,\mathbf{k}_\pi\mathbf{k}_\Lambda\varkappa/(1 + \varkappa^2)], \tag{12}$$

where I is the intensity of the Σ^0 beam,

$$\alpha = \tfrac{1}{2}\,[\sqrt{3/2}\,a_1^+(b_1 + b_2/\sqrt{2}) + \tfrac{1}{2}\,a_2^+b_3],$$

$$\beta = \tfrac{1}{4}\,[3\,|a_1|^2 + |a_2|^2 + 3\,|b_1|^2 + 9\,|b_2|^2 + 3\,|b_3|^2].$$

Let us now discuss the same process from the point of view of the parity doublets hypothesis advanced here. The density matrix of the incident Σ^0-hyperon beam consisting of Σ_1^0 and Σ_2^0 has the form (for hyperons of low kinetic energy):

$$\rho_i = \begin{pmatrix} I_1 & J \\ J^+ & I_2 \end{pmatrix}. \tag{13}$$

We assume, without loss of generality, that the relative parity of Σ_1 and Λ_1 is positive. Then the reaction corresponds to $S \to S$ transitions. and the existence of doublets of the Σ and Λ particles will result in the $S \to P$ transitions: $\Sigma_{1,2} + p \to \Lambda_{2,1} + p$. In this case the transition amplitude is in the form of a 2×2 matrix

$$\begin{pmatrix} S \to S & S \to P \\ S \to P & S \to S \end{pmatrix} \tag{14}$$

where $S \to S$, $S \to P$ represent symbolically the amplitudes of the corresponding transitions of the strange particle + proton system, taken from the work of Pais and Treiman.[16]

After some calculations we find for W the following expression:

$$W = \lambda\,\{[I \pm \mathrm{Re}\,J]\,\beta + 2\,\mathrm{Re}\,(I \pm J)\,\alpha\mathbf{k}_\pi\mathbf{k}_\Lambda\}, \tag{15}$$

where we have already set $\kappa = \pm 1$, as well as $I_1 = I_2 = I$.

4. DISCUSSION OF RESULTS

From a comparison of (8) and (9) with (12) and (15) the conclusion follows that if parity nonconservation in the decay is the maximum possible (as is in agreement with experimental data) then the consequences due to parity nonconservation in the strong interactions of strange particles are the same, as far as production of particles with odd strangeness is concerned, as the consequences due to the hypothesis of invariance of all interactions under the $\theta \longleftrightarrow \tau$ conjugation.

The two approaches (should the "forward-backward" asymmetry be definitely proven) may, however, be distinguished by studying, for example, reactions producing Ξ particles:

$$\pi^- + p \to \Xi^- + K^+ + K^0,$$

$$\pi^+ + n \to \Xi^- + K^+ + K^+. \tag{16}$$

If the "forward-backward" ("right-left") asymmetry in processes involving Λ and Σ particles is connected with invariance of the interactions under the $\theta \longleftrightarrow \tau$ conjugation then there should be no "forward-backward" ("right-left") asymmetry in the distribution of the Λ^0 particles (π^- mesons) from the Ξ^- decay because the Ξ^- particle is not a parity doublet and consequently will have zero longitudinal polarization (in our model parity is conserved in strong interactions). If, however, the indicated asymmetry is due to parity nonconservation in the strange particle production process then the asymmetry of Λ^0 particles (π^- mesons) from Ξ^- decay will, generally speaking, be different from zero.

Indeed, in the framework of parity nonconservation for processes involving K mesons and hyperons, the reactions (16) may be caused by the following renormalizable parity-conserving interactions (we assume here for simplicity that the parity of all fermions and K mesons is positive);

$$g_5\,[\bar{N}\theta\Lambda + \bar{\Lambda}\theta^+N], \qquad g_7\,[\bar{\Xi}\tau_2\theta^+\Lambda + \bar{\Lambda}\theta\tau_2\Xi]$$

and the following CP and charge-invariant but parity nonconserving interactions:

$$ig_5'\,[\bar{N}\gamma_5\Lambda\theta - \bar{\Lambda}\theta^+\gamma_5N], \qquad ig_7'\,[\bar{\Xi}\gamma_5\tau_2\theta^+\Lambda + \bar{\Lambda}\theta\gamma_5\tau_2\Xi].$$

*It is in this reaction that a nonvanishing "forward – backward" asymmetry of π^- mesons from Λ^0 decay was observed, although the results are not definitive.

The effective matrix element for the process, including interferences between the interactions with primed and unprimed constants, will contain pseudoscalar terms and, generally speaking, the Ξ^- particle will be longitudinally polarized.

The same conclusions follow from Sakata's[17] model in which the interaction $(\bar{\Lambda}\Lambda)(\bar{N}N)$ responsible for the production of strange particles of any strangeness does not, generally speaking, conserve parity.[7]

In connection with all that has been said a study of reactions of the type (16) becomes of great interest.

In conclusion we might venture the hypothesis that the various kinds of asymmetries of physical processes are not a consequence of an asymmetry of space but are due to specific properties of the neutrino and of the strange particles. It is possible that invariance of all interactions under the "θ-τ conjugation" is a formal expression of some peculiar intrinsic properties of strange particles.

I take this opportunity to express appreciation to G. E. Chikovani, in conversation with whom arose the idea expressed in this paper; and to sincerely thank T. I. Kopaleĭshvili, V. I. Mamasakhlisov, M. E. Perel'man, G. R. Khutsishvili, and O. D. Cheishvili for their interest in the work and discussion of results.

[1] V. G. Solov'ev, JETP **33**, 537 (1957), Soviet Phys. JETP **6**, 419 (1958).

[2] V. G. Solov'ev, JETP **33**, 796 (1957), Soviet Phys. JETP **6**, 613 (1958).

[3] V. G. Solov'ev, Nucl. Phys. **6**, 618 (1958).

[4] V. G. Solov'ev, JETP **34**, 1335 (1958), Soviet Phys. JETP **7**, 921 (1958).

[5] S. N. Gupta, Canad. J. Phys. **35**, 1309 (1957).

[6] Crawford, Cresti, Good, Solmitz, and Stevenson, Phys. Rev. Lett. **1**, 209 (1958).

[7] C. Iso, Progr. Theoret. Phys. (Japan) **20**, 410 (1958).

[8] T. D. Lee and C. N. Yang, Phys. Rev. **102**, 290 (1956).

[9] T. D. Lee and C. N. Yang, Phys. Rev. **104**, 822 (1956).

[10] Alvarez, Bradner, Falk-Variant, Gow, Rosenfeld, Solmitz, and Tripp, Nuovo cimento **5**, 1026 (1957).

[11] J. G. Taylor, Nucl. Phys. **9**, 357 (1958/59).

[12] G. Chew, Phys. Rev. **112**, 1380 (1958).

[13] A. Pais, Phys. Rev. **112**, 624 (1958).

[14] A. Pais, Phys. Rev. Lett. **1**, 418 (1958).

[15] R. Arnowitt and W. Teutsch, Phys. Rev. **105**, 285 (1957).

[16] A. Pais and S. B. Treiman, Phys. Rev. **109**, 1759 (1958).

[17] S. Sakata, Progr. Theoret. Phys. (Japan) **16**, 686 (1956).

Translated by A. M. Bincer
201

CALCULATION OF PHASE INTEGRALS IN THE COVARIANT FORMULATION OF THE THEORY OF MULTIPLE PRODUCTION OF PARTICLES

L. G. YAKOVLEV

Uzbek State University

Submitted to JETP editor April 27, 1959

J. Exptl. Theoret. Phys. (U.S.S.R.) 37, 1041-1045 (October, 1959)

A method is proposed for the exact calculation of integrals over momentum space in the covariant statistical theory of the multiple production of particles. The method can be applied in other types of theory, though the calculations become more complicated. Approximate and exact calculations are carried out.

SRIVASTAVA and Sudarshan[1] have proposed a covariant formulation of the statistical theory of the multiple production of π mesons. In this formulation the probability of the production of n particles of arbitrary masses m_i is proportional to an integral over energy-momentum space,

$$I=\int\prod_{i=1}^{n} d^4k_i\,\delta(k_i^2+m_i^2)\,\delta^4\Big(\sum_{i=1}^{n}k_i-P\Big), \qquad (1)$$

where k is the four-momentum of a meson ($k_4 = i\epsilon$) and P is the momentum of the system (in the center-of-mass system $\mathbf{P}=0$, $P_4 = i\mathcal{E}$).* We shall discuss a method for performing the integration of Eq. (1).

After integrating over all the k_{4i} we get

$$I=2^{-n}\int\prod_{i=1}^{n}\frac{d^3k_i}{\varepsilon_i}\,\delta^3\Big(\sum_{1}^{n}\mathbf{k}_i\Big)\,\delta\Big(\sum_{1}^{n}\varepsilon_i-\mathcal{E}\Big). \qquad (2)$$

(A similar form is found in the integral that appears in the quantum-field treatment of the process, if the wave functions are normalized to $\epsilon_i^{-1/2}$. We have under the integral sign the remaining part of the matrix element, but at high energies it is obviously almost constant.[2]) The integration in (2) can be carried out by a method similar to that devised by Lepore and Stuart.[3] Using the Fourier representation for the δ function, we bring (2) to the form†

$$I=2^{-n}(2\pi)^{-4}\int d^3r\,dt\,e^{i\mathcal{E}t}$$

$$\times\Big[\int_0^\infty dk\int_\Omega d\varphi\,d(\cos\theta)\,\frac{k^2}{\varepsilon}\,e^{i(kr\cos\theta-\varepsilon t)}\Big]^n. \qquad (3)$$

After the integrations over the angles and some simple transformations we get

$$I=2^{-(2+n)}\pi^{n-3}\mathcal{E}^{2n-4}\int_0^\infty dz\int_{-\infty}^{\infty}d\alpha\cdot z^{2-n}e^{i\alpha}I_1^n, \qquad (4)$$

where

$$I_1=\int_\mu^\infty \sin(z\sqrt{y^2-\mu^2})\,e^{i\alpha y}\,dy,$$

$$y^2=\mu^2(k^2+1),\quad \mu=1/\mathcal{E},\quad \alpha=t\mathcal{E},\quad z=r\mathcal{E}. \qquad (5)$$

Obviously y represents the total energy, and μ the rest energy, of a meson. Consequently $y\geq\mu$, and for $y\leq\mu$ the integrand can be set equal to zero, after which the integration can be extended from 0 to ∞, and we can use the formulas of the Laplace transformation,[4] defining the original function as

$$f(\mu)=\begin{cases}\sin(z\sqrt{y^2-\mu^2}), & y\geq\mu,\\ 0, & y\leq\mu.\end{cases}$$

Then

$$I_1=\frac{z\mu}{\sqrt{z^2-\alpha^2}}K_1(\mu\sqrt{z^2-\alpha^2}), \qquad (6)$$

where $K_1(x)$ is the Macdonald cylinder function [$K_1(x)=-\frac{1}{2}\pi H_1^{(1)}(ix)$].

Thus the calculation of the quantity (1) reduces to the calculation of the integral

$$I_2=\int_0^\infty dz\int_{-\infty}^{\infty}d\alpha\,\frac{z^2e^{i\alpha}}{(z^2-\alpha^2)^{n/2}}[K_1(\mu\sqrt{z^2-\alpha^2})]^n. \qquad (7)$$

The calculation of integrals of this form encounters difficulties[5] and is usually done approximately. In the extreme relativistic case the calculations can be carried through to the end. For this case we can set $\mu^2=0$; then

$$I_2=\frac{1}{2}\int_{-\infty}^{\infty}dz\int_{-\infty}^{\infty}d\alpha\,\frac{z^2e^{i\alpha}}{(z^2-\alpha^2)^n}. \qquad (8)$$

*We are setting $\hbar = c = m_\pi = 1$ (m_π is the mass of the π meson).

†In (3)–(7) it is assumed for simplicity that all the particles are π mesons.

By displacing the poles in a suitable way, we can perform the integration by the method of residues. Integrating first over z and then over α, we get finally

$$I = [2^{1-n}\pi^{n-1}/(n-1)!\,(n-2)!]\,\mathcal{E}^{2n-4}. \qquad (9)$$

Thus for $n = 2$ the integral I does not depend on the energy, for $n = 3$ we have $I \sim \mathcal{E}^2$, and so on. Exact computations show that for $n = 2$ the approximate value (9) is useful for practical purposes for arbitrary energy, and for $n = 3$ it is good for energies $\mathcal{E} > 2.5 \times 10^9$ ev (i.e., for kinetic energies in the laboratory system larger than 1.45×10^9 ev). For $n = 4$, 5, and so on, the threshold for the usefulness of (9) increases, so that exact computation is necessary.

The exact calculation can be carried out in the following way.[2] Integrating over $\mathbf{k}_1$ in (2) and taking account of the δ function of the momentum we get

$$I = 2^{-n}\int \varepsilon_1^{-1}\prod_{i=2}^{n}\varepsilon_i^{-1}\,d^3k_i\,\delta\Big(\sum_2^n \varepsilon_i + \varepsilon_1 - \mathcal{E}\Big). \qquad (10)$$

Here

$$\varepsilon_1 = (k_1^2+1)^{1/2} = [p_{n-2} + k_2 + 2(\mathbf{p}_{n-2}\,\mathbf{k}_2) + 1]^{1/2},$$

where

$$\mathbf{p}_{n-r} = \sum_{r+1}^{n}\mathbf{k}_i, \qquad p_{n-r} = [p_{n-r-1}^2 + k_{r+1}^2 + 2(\mathbf{p}_{n-r-1}\,\mathbf{k}_{r+1})]^{1/2}.$$

For the further integration over $\mathbf{k}_2$ we go over to spherical coordinates, taking the polar axis along the momentum $\mathbf{p}_{n-2}$. After the integrations over the polar angle θ_2 and the azimuth φ_2 we get

$$I = 2^{-n}(2\pi)\int d\varepsilon_2 \prod_{i=4}^{n}\frac{d^3k_i}{\varepsilon_i}\,\frac{d^3k_3}{\varepsilon_3 k_3 p_{n-2}}. \qquad (11)$$

For the integration over $\mathbf{k}_3$ we take the axis of spherical coordinates along $\mathbf{p}_{n-3}$; using the fact that

$$p_{n-2} = \sqrt{p_{n-3}^2 + k_3^2 + 2p_{n-3}k_3\cos\theta_3},$$

we integrate first over $\cos\theta_3$ (we take the integral in the sense of the principal value, since p_{n-2} can pass through the value zero). It is not hard to show in this way that in any case the integral (11) reduces to the form

$$I = \frac{1}{4}(2\pi)^{n-1}\int\prod_{i=4}^{n}(\varepsilon_i^2 - m_i^2)^{1/2}\,d\varepsilon_i\,d\varepsilon_3\,d\varepsilon_2. \qquad (12)$$

Here the π-meson mass ($m_\pi = 1$) has been replaced by masses m_i; thus the formula holds for the production of particles of arbitrary masses.

It is convenient to go over to the kinetic energies $x_i = \epsilon_i - m_i$. The expression (12) then takes the form

$$I = \frac{1}{4}(2\pi)^{n-1}\int\prod_{i=4}^{n}(x_i^2 + 2m_i x_i)^{1/2}\,dx_i\,dx_2\,dx_3. \qquad (13)$$

In Eq. (13) we must perform $(n-1)$ successive integrations. Let us find the region of integration, taking account of the existence of a maximum energy for each of the particles.[6]

The kinetic energies of the particles lie in the ranges

$$0 \leqslant x_i \leqslant t_i, \qquad (14)$$

where

$$t_i = \frac{\mathcal{E}}{2} - \frac{M^2 - m_i^2}{2\mathcal{E}} - m_i = \frac{T}{2}\Big(1 + \frac{M - m_i}{T + M + m_i}\Big). \qquad (15)$$

Here M is the sum of the rest masses of all the particles except the one in question, and T is the kinetic energy of the system:

$$T = \mathcal{E} - \sum_{i=1}^{n} m_i = \sum_{i=1}^{n} x_i.$$

From these equations there follow the relations

$$T - t_i \leqslant \sum_2^n x_i \equiv T_{n-1} \leqslant T,$$
$$T - T_{n-3} - t_1 \leqslant x_2 + x_3 \leqslant T - T_{n-3}. \qquad (16)$$

Let us consider for simplicity the case in which $m_1 = m_2 = m_3$. Simple arguments show that the integral over x_2, x_3 is equal to the area of the entire triangle shown in Fig. 1 for $T_{n-3} \geq T - t_1$,

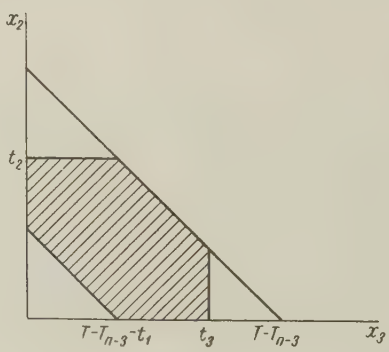

FIG. 1

and for $T_{n-3} \leq T - t_1$ it is equal to the area of the shaded region. The areas in question are easily calculated, and the further analysis of the limits of integration in terms of the relations (14) — (16) also presents no difficulty.

For $n = 3$ we have $T_{n-3} = 0$, and because $t_1 \leq T$ we find that I is simply equal to the area of the shaded region multiplied by π^2; that is,

$$I = \frac{1}{2}\pi^2\Big[T^2 - \sum_{i=1}^{3}(T - t_i)^2\Big] \qquad (17)$$

[for $n = 2$ we have $I = \pi(\frac{1}{4} - \mathcal{C}^{-2})^{1/2}$].

For $n = 4$ we have $T_{n-3} = x_4$, and the expression (13) breaks up into two terms* ($x_4 \geq T - t$ or $x_4 \leq T - t$), in which the integrand contains the product of $(x_4^2 + 2m_4x_4)^{1/2}$ by the value of the corresponding area (as a function of x_4). Thus, on making some transformations, we get

$$I = \pi^3\Big[\int_0^t (T - x_4)^2 (x_4^2 + 2x_4)^{1/2}\, dx_4 - 3\int_0^{T-t} (T - t - x_4)^2 (x_4^2 + 2x_4)^{1/2}\, dx_4\Big]$$

$$= \pi^3 \{[\tfrac{5}{4}(T-t)^3 + \tfrac{9}{4}(T-t)^2 - \tfrac{1}{2}(T-t) - \tfrac{15}{8}] \times [(T-t)^2 + 2(T-t)]^{1/2} - [(\tfrac{2}{3}T - \tfrac{1}{4}t + \tfrac{5}{12})(t^2 + 2t) - (\tfrac{1}{2}T^2 + T + \tfrac{5}{8})(t+1)][t^2 + 2t]^{1/2} + \tfrac{1}{2}\left(T^2 + 2T + \tfrac{5}{4}\right)\ln[t + 1 - (t^2 + 2t)^{1/2}] - \tfrac{3}{2}[(T-t)^2 + 2(T-t) + \tfrac{5}{4}] \times \ln[T - t + 1 - ((T-t)^2 + 2(T-t))^{1/2}]\}. \qquad (18)$$

For $n = 5$, $T_{n-3} = x_4 + x_5$; the integral over x_2 and x_3 will be equal to the area of the triangle or the truncated triangle (Fig. 1), depending on whether $x_4 + x_5 \geq T - t$ or $x_4 + x_5 \leq T - t$. As can be seen from Fig. 2, in the first case the region of

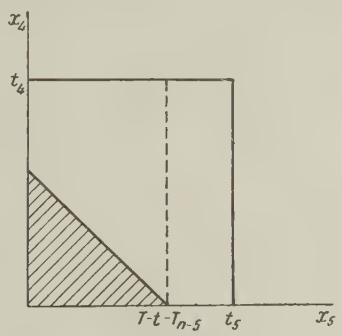

FIG. 2

integration over x_5 and x_4 is the unshaded part of the rectangle, and in the other case it is the shaded part (in this case $T_{n-5} = 0$; we always have $T - t - T_{n-5} < t_5$). For I we get the expression ($m_i = 1$):

$$I = 2\pi^4 \int_0^{t_5} dx_5 (x_5^2 + 2m_5x_5)^{1/2} \int_0^{t_4} (x_4^2 + 2m_4x_4)^{1/2} (T - x_4 - x_5)^2\, dx_4 - 2\pi^4 \sum_{i=1}^{3} \int_0^{T-t} dx_5 (x_5^2 + 2m_5x_5)^{1/2} \times \int_0^{T-t-x_5} dx_4 (x_4^2 + 2m_4x_4)^{1/2} (T - x_4 - x_5 - t_i)^2. \qquad (19)$$

It is obvious that a similar analysis of the limits of integration can be extended without difficulty to the case of large values of n.

The limits of the integrations can thus be found for arbitrary n and for arbitrary concrete types of particles. The integration itself, however, becomes steadily more complicated. This method of integration over the momentum space can also be applied in other theories of multiple production, but the integration itself is more complicated because of the changes of the forms of the integrands.

It must be noted that in the covariant statistical theory the angular distribution is symmetrical. The matrix element, which has not been taken into account, is obviously responsible for the experimentally observed unsymmetrical distribution.

The writer thanks Professor D. D. Ivanenko for his interest in this work and for a discussion of the results.

*We consider for simplicity the case $m_1 = m_2 = m_3 \neq m_4$ ($m_4 = 1$).

[1] P. Srivastava and G. Sudarshan, Phys. Rev. **110**, 765 (1958).

[2] L. Yakovlev, Dissertation. Moscow State University, 1958.

[3] J. V. Lepore and R. N. Stuart, Phys. Rev. **94**, 1724 (1954).

[4] I. Ryzhik and I. Gradshteĭn, Таблицы интегралов (Tables of Integrals), Moscow-Leningrad, 1951.

[5] Belen'kiĭ, Maksimenko, Nikishev, and Rozental', Usp. Fiz. Nauk **62**, No. 2, 1 (1957).

[6] L. Yakovlev, JETP **31**, 142 (1956), Soviet Phys. JETP **4**, 141 (1957).

Translated by W. H. Furry
202

ON THE THEORY OF THE PASSAGE OF THE NUCLEAR CASCADE THROUGH THE ATMOSPHERE

I. P. IVANENKO

Nuclear Physics Institute, Moscow State University

Submitted to JETP editor May 9, 1959

J. Exptl. Theoret. Phys. (U.S.S.R.) 37, 1046-1049 (October, 1959)

A method for the solution of the equations describing the passage of the nuclear cascade through the atmosphere is proposed. The boundary conditions can be prescribed at any arbitrary depth. The proposed method makes it possible to obtain the solution in a form similar to the one obtained by the usual method of successive generations with boundary conditions prescribed at the top of the atmosphere. The form of the solution is discussed for various boundary conditions.

A number of methods for calculating the characteristics of the nuclear cascade process in the atmosphere have been developed in recent years.[1-3] Of these, the method of successive generations[3] has been found to be a convenient and efficient one for the calculation of the required characteristics. In all calculations, it was assumed that the boundary conditions are given at the top of the atmosphere, at $x = 0$.

In experiments on extensive air showers (EAS), the energy of the primary particle initiating the shower is usually not known, and neither is the depth of the initiation of the shower. In general, various characteristics of different EAS components are known at a certain depth of the atmosphere. Therefore, for an estimate of the influence of the decay processes on the development of EAS in the depth of the atmosphere, and also for the calculation of the various development schemes of the shower,[4] it is necessary to find a solution of the nuclear cascade equations, the boundary conditions being given at a certain arbitrary depth x_n in the atmosphere.

Zatsepin, Nikol'skiĭ, and Pomanskiĭ[5] proposed to solve the problem by the method of successive approximations. It was shown that, for a certain specific choice of the zero generation, the i-th term of the series gives the depth and energy distribution of the particles of the i-th generation. However, the form of the solution given in reference 5 needs to be integrated over x and E for the determination of each consecutive generation. This makes it difficult to use this method of solution in practice.

In the present article, a method is presented for the solution of the nuclear-cascade equation with boundary conditions prescribed at a given depth of the atmosphere, which is analogous to the general method of successive generations with boundary conditions prescribed at the top of the atmosphere, at $x_n = 0$.

We shall solve the one-dimensional problem neglecting, for the time being, the ionization loss, and assuming an isothermal atmosphere. We shall use a system of notation similar to that used by Zatsepin and Rozental'.[3]

A system of nuclear-cascade equations, describing the atmospheric-depth dependence of the number of particles of type η having an energy E can be written in the form

$$\frac{dP^{(\eta)}(E,x)}{dx} = -P^{(\eta)}(E,x) + \sum_{\zeta}\int_{E}^{\infty} P^{(\zeta)}(E',x)\,W_{\eta}^{(\zeta)}(E',E)\,dE' - \frac{K_{\eta}(E)}{x}P^{(\eta)}(E,x) + \frac{1}{x}\sum_{\varkappa}\int_{E_1}^{E_2} P^{(\varkappa)}(E',x)\,K_{\varkappa}(E')\,D_{\eta}^{(\varkappa)}(E',E)\,dE. \quad (1)$$

We assume that, in the energy range under consideration, $\sigma_{\eta}^{(\kappa)}(E) = \sigma_0$.

The boundary conditions at the atmospheric depth x_n are given by the values of the function $P^{(\eta)}(x_n, E)$, $P^{(\zeta)}(x_n, E)$, $P^{(\kappa)}(x_n, E)$ etc. We are looking for the solution of Eqs. (1) in the form

$$P^{(\eta)}(x,E) = e^{-(x-x_n)}\sum_{i=0}^{\infty}\frac{(x-x_n)^i}{i!}P_i^{(\eta)}(x,E,x_n). \quad (2)$$

Substituting (2) into (1), and equating the coefficients of identical powers of $(x - x_n)$, we obtain the following system of equations for the determination of the functions $P_i^{(\eta)}$:

$$P_{i+1}^{(\eta)}(x, E, x_n) = -\frac{\partial P^{(\eta)}(x, E, x_n)}{\partial x}$$

$$+\sum_{\zeta}\int_{E}^{\infty} P_i^{(\zeta)}(x, E', x_n)\, W_{\eta}^{(\zeta)}(E', E)\, dE' - \frac{K_{\eta}(E)}{x} P_i^{(\eta)}(x, E, x_n)$$

$$+\frac{1}{x}\sum_{\varkappa}\int_{E_1}^{E_2} P_i^{(\varkappa)}(x, E', x_n)\, K_{\varkappa}(E')\, D_{\eta}^{(\varkappa)}(E', E)\, dE'. \qquad (3)$$

$P_0(x, E, x_n)$ has to be suitably defined to insure a rapid convergence of the series (2). From Eq. (2), for $x = x_n$, we have

$$P(x_n, E) = P_0(x_n, E, x_n).$$

Hence it follows that $P_0(x, E, x_n)$ should be defined as the zero generation (i.e., primary particles).

We shall consider the following types of primary particles: a) stable nuclear-active particles which cannot be produced in the decay of any other particles, b) stable particles which can be produced in the decay of other particles, and c) and d) unstable particles analogous to a) and b). It is easy to obtain the dependence of $P_0(x, E, x_n)$ on all arguments. In case a),

$$P_0(x, E, x_n) = P(x_n, E). \qquad (4a)$$

In case b),

$$P_0(x, E, x_n) = P(x_n, E)$$

$$+\sum_{\varkappa}\int_{x_n}^{x}\frac{e^{x-x_n}}{x}\,dx\int_{E_1}^{E_2} P_0^{(\varkappa)}(E', x, x_n)\, K_{\varkappa}(E')\, D_{\eta}^{(\varkappa)}(E', E)\, dE' \qquad (4b)$$

In case c),

$$P_0(x, E, x_n) = P(x_n, E)\,(x_n/x)^{E_{\eta}/E} \qquad (4c)$$

In case d),

$$P_0(x, E, x_n) = P(x_n, E)\,(x_n/x)^{E_{\eta}/E}$$

$$+(x_n/x)^{E_{\eta}/E}\sum_{\varkappa}\int_{x_n}^{x}\frac{e^{x-x_n}}{x}\,(x/x_n)^{E_{\eta}/E}\,dE$$

$$\times\int_{E_1}^{E_2} P_0^{(\varkappa)}(E', x, x_n)\, K_{\varkappa}(E')\, D_{\eta}^{(\varkappa)}(E', E)\, dE'. \qquad (4d)$$

Thus, Eqs. (2), (3), and (4) fully determine the solution of Eq. (1) with boundary conditions prescribed at the depth x_n. The solution is in the form of an infinite power series in $(x - x_n)$. It can be shown, however, that, in cases most interesting in practice, the series converges rapidly, and the sum of the terms from $i = 0$ to $i \leq (x - x_n)$ represents the solution with an acceptable accuracy.

We shall determine the depth and energy dependence of nuclear-passive mesons of type ρ. For these particles, Eq. (1) can be written in the form

$$\frac{dP^{(\eta)}(E, x)}{dx} = -\frac{K_{\eta}(E)}{x} P^{(\eta)}(E, x)$$

$$+\frac{1}{x}\sum_{\varkappa}\int_{E_1}^{E_2} P^{(\varkappa)}(E', x)\, K_{\varkappa}(E')\, D_{\eta}^{(\varkappa)}(E', E)\, dE'. \qquad (1')$$

Its solution is easy to find:

$$P^{(\eta)}(E, x) = \left(\frac{x_n}{x}\right)^{E_{\eta}/E} P(E, x_n) + x^{-E_{\eta}/E}\sum_{\varkappa}\int_{x_n}^{x} x^{E_{\eta}/E}\,dx$$

$$\times\int_{E_1}^{E_2} P^{(\varkappa)}(E', x)\,\frac{E_{\varkappa}}{E'}\, D_{\eta}^{(\varkappa)}(E', E)\, dE', \qquad (5)$$

Thus, to calculate the number of nuclear-passive mesons it is first necessary to find, according to Eqs. (2) — (4), the depth and energy distributions of the mesons whose decay results in the mesons under consideration.

The above discussion can easily be generalized to take the ionization loss into account. The ionization-loss term can be written in the form $\beta\partial P^{(\eta)}(E, x)/\partial E$, where β is the ionization loss per mean free path, assumed to be independent of the energy. As before, we shall look for a solution in the form of Eq. (2). It should be noted that the series represented by Eq. (2) will converge rapidly only if the ionization loss is not the main process that determines the passage of nuclear-active particles through the matter. Consequently, the particle energy E should be markedly greater than βx. In analogy to Eq. (3), we obtain the following system of equations for the function $P_i^{(\eta)}$:

$$P_{i+1}^{(\eta)}(x, E, x_n) = -\frac{\partial P_i^{(\eta)}(x, E, x_n)}{\partial x}$$

$$+\sum_{\zeta}\int_{E}^{\infty} P_i^{(\zeta)}(x, E', x_n)\, W_{\eta}^{(\zeta)}(E', E)\, dE'$$

$$-\frac{E_{\eta}}{Ex} P_i^{(\eta)}(x, E, x_n)$$

$$+\frac{1}{x}\sum_{\varkappa}\int_{E_1}^{E_2} P_i^{(\varkappa)}(x, E', x_n)\,\frac{E_{\varkappa}}{E'}\, D_{\eta}^{(\varkappa)}(E', E)\, dE'$$

$$+\beta\frac{\partial P_i^{(\eta)}(x, E, x_n)}{\partial E};\quad i \geqslant 1. \qquad (3')$$

In this case, the dependence of $P_0(x, E, x_n)$ on all arguments is also given by Eqs. (4a) — (4d), where, on the right-hand side, we should substitute for E the value $E + \beta_{\chi} - \beta x_0$. In this way, the above formulae give the most complete solution of nuclear cascade equations by the method of successive generations. Formulae for the remaining components of the nuclear cascade do not differ from the corresponding formulae given by Zatsepin and Rozental'.[3]

[1] H. Messel and H. S. Green, Proc. Phys. Soc. **A66**, 1009 (1953).
[2] S. Olbert and R. Stora, Ann. Phys. (USA) **1**, 247 (1957).
[3] G. T. Zatsepin and I. L. Rozental', Dokl. Akad. Nauk SSSR **99**, 369 (1954).
[4] N. L. Grigorov and V. Ya. Shestoperov, JETP **34**, 1539 (1958), Soviet Phys. JETP **7**, 1061 (1958).
[5] Zatsepin, Nikol'skiĭ, and Pomanskiĭ, JETP **37**, 197 (1959), Soviet Phys. JETP **10**, 138 (1960).

Translated by H. Kasha
203

CLASSIFICATION OF MOLECULAR TERMS WITH RESPECT TO TOTAL NUCLEAR SPIN

E. G. KAPLAN

Institute of Chemical Physics, Academy of Sciences, U.S.S.R.

Submitted to JETP editor May 12, 1959

J. Exptl. Theoret. Phys. (U.S.S.R.) **37**, 1050-1053 (October, 1959)

A method is proposed for finding nuclear multiplicities of molecular terms, for nuclei of arbitrary spin. The relation between Young tableaus and total spin, on the one hand, and between the permutation group and the point symmetry group of the molecule, on the other, is used.

1. FORMULATION OF THE PROBLEM

THOUGH the nuclear spin has a negligible direct influence on molecular term values, it has a significant indirect effect on their symmetry. Namely, only those types of point symmetry groups of the molecule occur which correspond to the permutation symmetry of the nuclear spins. Existing methods enable one to find these allowed symmetry types together with their nuclear statistical weights.[1] However, each type of symmetry of the terms occurs only for definite values of the total nuclear spin. It is of interest to find this relation. The solutions of the analogous problem for electronic terms are very complicated, and have been achieved[2,3] only for spin $\frac{1}{2}$. The method presented in this paper allows one relatively easily to assign to terms the value of the total nuclear spin, for nuclei with arbitrary spin i, and at the same time automatically gives the allowed terms and their statistical weights.

2. BASIS OF THE METHOD

Let us consider a system of n identical nuclei, each having spin i. The permutation symmetry of the coordinate wave function of the system is determined by the Young tableaus which are consistent with the given spin value i.[1] Each Young tableau defines an irreducible representation of the group of permutations of n particles, whose characters are given in the tables of characters of the symmetric groups[4,5]. However, this representation may be reducible with respect to the point group of the molecule. By resolving into irreducible representations of the point group, we find the relation between symmetry types of the molecule and its coordinate Young tableaus. On the other hand, there is a one-to-one correspondence between the coordinate and spin Young tableaus, which is determined by the Pauli principle. But each spin Young tableau corresponds to definite values of the total spin of the particles. Thus we find the relation between the total nuclear spin and the molecular terms. Terms which do not appear in the representations of the coordinate Young tableaus are forbidden.

3. YOUNG TABLEAUS AND TOTAL SPIN

In the general case of arbitrary spin i, a single Young tableau may correspond to several values of the total spin of the system. This connection can be found by adding cells to Young tableaus which have already been investigated, and corresponds to successive vector addition of spins.[6] The permutation symmetry of the state corresponding to the product of two Young tableaus is given by Littlewood's theorem (reference 5, p. 94).*

The results of the calculation for n = 3, 4, and i = 1, $\frac{3}{2}$, are given in the table.

Young tableau*	Dimensionality of representation	i = 1	i = 3/2 †
$[1^3]$	1	0	3/2
[2,1]	2	1; 2	1/2; 3/2; 5/2; 7/2
[3]	1	1; 3	3/2; 5/2; 9/2;
$[1^4]$	1	—	0
$[2,1^2]$	3	1	1; 2; 3
$[2^2]$	2	0; 2	0; 2 (2); 4
[3,1]	3	1; 2; 3;	1 (2); 2; 3 (2); 4; 5
[4]	1	0; 2; 4	0; 2; 3; 4; 6

*$[\lambda_1^{(a)}, \lambda_2^{(b)}, \cdots]$ denotes a Young tableau in which the first a rows contain λ_1 boxes, the next b rows have λ_2 boxes, etc.

†The numbers in parentheses give the number of times a given total spin occurs, if this number is greater than unity.

*The formulation of Littlewood's theorem is also in reference 6, p. 527.

We note that to check the results we can make use of the fact that the total number of states of a system of n particles which give total spin I is equal to the sum of the dimensionalities of the irreducible representations of those Young tableaus which occur for the given value of I. On the other hand this same number can be found from the vector addition diagrams used by Van Vleck for electronic configurations.[7] The figure shows the diagram for $i = 3/2$. The numbers in circles given the total number of states for given I and n.

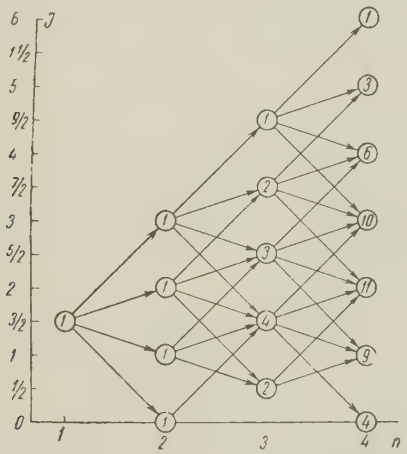

4. MOLECULES WITH A TOTAL SPIN WHICH IS DETERMINED BY IDENTICAL NUCLEI

Let us consider molecules whose nuclei can be divided into two groups. In the one group there are identical nuclei with $i \neq 0$, while the nuclei of the other group have $i = 0$. Then the total spin of the molecule will be determined by the total spin of the group of nuclei with $i \neq 0$.

Suppose that a molecule of type YX_4 ($i(Y) = 0$) has point symmetry T_d.* Any symmetry operation of the molecule can be considered as a permutation of the nuclei. Thus we can associate with each class of the point symmetry group the corresponding class of the permutation group:

Classes of group T_d	E	C_3	C_2	σ_d	S_4
Classes of the permutation group	$[1^4]$	[1,3]	$[2^2]$	$[1^2,2]$	[4]

Next, resolving the characters of the irreducible representations of the coordinate Young tableaus in characters of the point group, we find the correspondence between symmetry types of the molecule and coordinate Young tableaus. In the case of symmetry T_d, there is a one-to-one correspondence, since the group T_d is isomorphic to the group of permutations of four objects:

$$[4] \leftrightarrow A_1, \quad [1^4] \leftrightarrow A_2, \quad [2^2] \leftrightarrow E, \quad [2, 1^2] \leftrightarrow F_1, \quad [3, 1] \leftrightarrow F_2.$$

*We shall use the notation of reference 1.

a) $C^{12}H_4^1$; $i(C^{12}) = 0$, $i(H^1) = 1/2$. The allowed spin tableaus are [4], $I = 2$; [3,1], $I = 1$; $[2^2]$, $I = 0$. The corresponding coordinate tableaus are $[1^4]$, $[2,1^2]$, $[2^2]$. Consequently, the possible levels are $^5A_2$, $^3F_1$, ^1E.

b) $C^{12}H_4^2$; $i(H^2) = 1$. The spin and coordinate tableaus have the same symmetry. The allowed spin patterns are [4], [3,1], $[2^2]$, $[2,1^2]$. The corresponding values of total spin are given in the table. Thus the possible levels are $^{9,5,1}A_1$; $^{5,1}E$; $^{7,5,3}F_2$; $^3F_1$. The sum of the multiplicities of each level gives its nuclear degeneracy (statistical weight).

c) $C^{12}Cl_4^{35}$; $i(Cl^{35}) = 3/2$. All spin patterns for $n = 4$ are allowed. Using the fact that the coordinate patterns are dual to the spin patterns, and taking the total spin values from the table, we find the following level multiplicities:

$$^1A_1; \ ^{13,9,7,5,1}A_2; \ ^{9,5(2),1}E; \ ^{11,9,7(2),5,3(2)}F_1; \ ^{7,5,3}F_2.$$

As another example we consider the benzene molecule $C_6^{12}H_6^1$, with point symmetry D_{6h}. Since the molecule is planar, inversion is equivalent to a rotation, so we can restrict ourselves to the symmetry D_6. We have a system of six identical nuclei with $i = 1/2$. The allowed coordinate patterns are $[1^6]$, $[2.1^4]$, $[2^2, 1^2]$, $[2^3]$, with total spins of 3, 2, 1, and 0 respectively. Resolution into irreducible representations of the point group gives the following term multiplicities:

$$^{5,1(2)}A_1; \ ^3A_2; \ ^{7,3(2)}B_1; \ ^1B_2; \ ^{5,3(2)}E_1; \ ^{5,3,1}E_2.$$

5. MOLECULES CONSISTING OF SEVERAL GROUPS OF IDENTICAL NUCLEI WITH $i \neq 0$.

In this case we can find the total spin of each of the groups for each molecular term. We then construct direct products of the irreducible representations of each of the groups. The resolution of these direct products into irreducible parts gives the allowed symmetry types. The total statistical weight of a term is given by the sum of the statistical weights of the direct products (in whose resolution the particular term occurs), multiplied by the number of times the term appears in the direct product. We note that if we want only to find the total statistical weights of the terms, this can be done more simply for complicated molecules by the method of reference 1.

If the molecule has one group of identical nuclei, while all the other nuclei with $i \neq 0$ are different, the allowed terms can be found by considering the permutation symmetry of the identical nuclei. To

find the total statistical weight we must multiply the multiplicity found in this way by the number of different projections of spin of the remaining nuclei.

Let us consider, as an example, the molecule $C^{13}H^{1}Cl_3^{35}$, $i(C^{13}) = 1/2$; symmetry group C_{3v}. From the character tables, we find the correspondence $[3] \leftrightarrow A_1$; $[2,1] \leftrightarrow E$; $[1^3] \leftrightarrow A_2$. Noting that the spin patterns for $i = 3/2$ must be dual to the coordinate patterns, we find that to a level of symmetry A_1 there correspond total spins of the chlorine nuclei equal to $3/2$; to A_2 the spins $3/2$, $5/2$, $9/2$; to E — $1/2$, $3/2$, $5/2$, $7/2$. We find the total statistical weight by multiplying the statistical weight due to the chlorine nuclei by four. As a result we get: $16\,A_1$, $80\,A_2$, $80\,E$.

In conclusion I thank E. M. Lifshitz for discussion of the results of this work.

[1] L. D. Landau and E. M. Lifshitz, Квантовая механика (Quantum Mechanics) Gostekhizdat, 1948 [Transl., Pergamon Press, 1958].

[2] M. Kotani, Proc. Phys. Math. Soc. Japan **19**, 460 (1937).

[3] E. M. Corson, Perturbation Methods in the Quantum Mechanics of n-Electron Systems, London, 1951.

[4] G. Ya. Lyubarskiĭ, Теория групп и ее применение в физике (Group Theory and its Application to Physics), Gostekhteorizdat, 1957.

[5] D. E. Littlewood, The Theory of Group Characters and Matrix Representation of Groups, Oxford, 1940.

[6] H. A. Jahn, Proc. Roy. Soc. (London) **A201**, 516 (1950).

[7] J. H. Van Vleck, Phys. Rev. **45**, 405 (1934).

Translated by M. Hamermesh
204

ON TWO TYPES OF NEUTRINOS; THE ISOTOPIC SPIN OF LEPTONS, AND THE UNIVERSAL FOUR-FERMION INTERACTION

É. M. LIPMANOV

Stalingrad State Pedagogical Institute

Submitted to JETP editor May 19, 1959

J. Exptl. Theoret. Phys. (U.S.S.R.) **37**, 1054-1057 (October, 1959)

The hypothesis is suggested that there exist in nature two types of neutrinos ν_1 and ν_2, which have the same longitudinal polarization but different leptonic charges, and which form, together with the electron and the μ meson, two isotopic leptonic doublets $(\nu_1 e)$ and $(\nu_2 \mu)$. The leptonic charges of the electron and the μ meson are also opposite. The laws of conservation of isotopic spin, leptonic charge, and chirality uniquely determine the character of the μ decay and give selection rules that forbid various unobserved reactions involving leptons.

1. The discovery of the noninvariance of the laws of nature under mirror imaging has led to a revision of the properties of one of the most interesting of the elementary particles, the neutrino. The result has been the development of the theory of the two-component neutrino,[1-3] whose wave function is an eigenfunction of the chirality operator γ_5. The problem of the neutrino, however, cannot yet be regarded as solved. Ya. B. Zel'dovich[4] has pointed out the interesting possibility of describing the weak interactions involving leptons in terms of isotopically invariant couplings between the particle-pairs electron-neutrino (νe) (a doublet in isotopic space, denoted hereafter as l_1), muon-neutrino $(\nu\mu)$ (the doublet l_2), and proton-neutron (the doublet B). Without including hyperons* in our discussion, let us make the assumption that the Hamiltonian of the four-fermion interactions has the following form:

$$\begin{aligned} H &= g\,[(\bar{B}\tau O B) + (\bar{l}_1\tau O l_1) + (\bar{l}_2\tau O l_2)]^2 \\ &= g\,[(\bar{B}\tau O B)(\bar{B}\tau O B) + (\bar{l}_1\tau O l_1)(\bar{l}_1\tau O l_1) + (\bar{l}_2\tau O l_2)(\bar{l}_2\tau O l_2)] \\ &+ 2g\,[(\bar{B}\tau O B)(\bar{l}_1\tau O l_1) + (\bar{B}\tau O B)(\bar{l}_2\tau O l_2) \\ &+ (\bar{l}_1\tau O l_1)(\bar{l}_2\tau O l_2)], \end{aligned} \tag{1}$$

where τ is the vector matrix of the isotopic spin, and $O = \gamma_\mu(1 \pm \gamma_5)$. The expression (1) for the Hamiltonian excludes the unobserved decay of the μ meson into three electrons, satisfies the requirements of Lorentz and isotopic invariance and of the conservation of chirality in the weak interactions,[5] and is invariant with respect to any interchanges of the types $l_1 \rightleftarrows l_2$, $l_{1,2} \rightleftarrows$ B. The expression (1) leads to the following interactions:

$$\begin{aligned} H &= g\,[(\bar{p}ON)(\bar{e}O\nu) + (\bar{N}Op)(\bar{\nu}O\mu) \\ &+ (\bar{\nu}O\mu)(\bar{e}O\nu) + \text{Herm. c.} \\ &+ (g/2)\,[(\bar{N}Op)(\bar{p}ON) + (\bar{e}Oe)(\bar{\mu}O\mu) + 2(\bar{p}Op)(\bar{\nu}O\nu) \\ &- 2(\bar{N}ON)(\bar{\nu}O\nu) - (\bar{p}Op)(\bar{e}Oe) - (\bar{p}Op)(\bar{\mu}O\mu) \\ &+ (\bar{N}ON)(\bar{e}Oe) + (\bar{N}ON)(\bar{\mu}O\mu)] \\ &+ (g/4)[(\bar{e}Oe)(\bar{e}Oe) + (\bar{\mu}O\mu)(\bar{\mu}O\mu) + 4(\bar{\nu}O\nu)(\bar{\nu}O\nu) \\ &+ (\bar{p}Op)(\bar{p}Op) + (\bar{N}ON)(\bar{N}ON)]. \end{aligned} \tag{2}$$

In addition to the first-order parity-nonconservation effects considered by Zel'dovich,[4] the Hamiltonian (2) leads to other analogous effects, for example to parity nonconservation in the scattering of electrons by electrons and positrons, to a displacement of levels of different parities in positronium, etc. A characteristic feature is that Eq. (2) does not contain the terms for scattering of neutrinos by electrons,* $(\bar{e}O\nu)(\bar{\nu}Oe)$, which were proposed by Gell-Mann and Feynman.[6] It also follows from Eq. (2) that in the four-fermion interaction there are three different constants for the three types of coupling terms, those containing four different fermions (g), two different fermions (g/2), and just one single fermion (g/4). An exception to this rule is seen in the terms containing neutrinos.

*The question of the possibility of including the hyperons in the general scheme of four-fermion interactions will be considered in another place.

*Such terms could be kept if we were to change the sign of the third term $(\bar{l}_2\tau O l_2)$ in the first expression (1). Then, however, Eq. (2) would lack the terms for scattering of neutrinos by nucleons and by neutrinos themselves, and the symmetry of the interaction would be destroyed.

2. How plausible is the assumption of the existence of the isotopic doublets (νe) and $(\nu\mu)$? Clearly the strangest thing about this is that the same particle ν occurs in two isotopic doublets. Let us assume that we have here two different neutrinos ν_1 and ν_2, so that what we are speaking of is the two pairs $l_1 \equiv (\nu_1 e^-)$ and $l_2 \equiv (\nu_2 \mu^-)$. Instead of Eqs. (2) and (1) we then have:

$$
\begin{aligned}
H = {} & g\,[(\bar{p}ON)(\bar{e}O\nu_1) + (\bar{N}Op)(\bar{\nu}_2 O\mu) \\
& + (\bar{\nu}_2 O\mu)(\bar{e}O\nu_1) + \text{Herm. c.}] \\
& + (g/2)\,[(e O\nu_1)(\bar{\nu}_1 Oe) + (\bar{\mu}O\nu_2)(\bar{\nu}_2 O\mu) - (\bar{e}Oe)(\bar{\nu}_2 O\nu_2) \\
& - (\bar{\mu}O\mu)(\bar{\nu}_1 O\nu_1) + (\bar{N}Op)(\bar{p}ON) + (\bar{e}Oe)(\bar{\mu}O\mu) \\
& + (\bar{N}ON)(\bar{e}Oe) + (\bar{N}ON)(\bar{\mu}O\mu) - (\bar{p}Op)(\bar{e}Oe) \\
& - (\bar{p}Op)(\bar{\mu}O\mu) + (\bar{p}Op)(\bar{\nu}_1 O\nu_1) + (\bar{p}Op)(\bar{\nu}_2 O\nu_2) \\
& - (\bar{N}ON)(\bar{\nu}_1 O\nu_1) - (\bar{N}ON)(\bar{\nu}_2 O\nu_2) + (\bar{\nu}_1 O\nu_1)(\bar{\nu}_2 O\nu_2)] \\
& + (g/4)\,[(\bar{e}Oe)(\bar{e}Oe) + (\bar{\mu}O\mu)(\bar{\mu}O\mu) + (\bar{p}Op)(\bar{p}Op) \\
& + (\bar{N}ON)(\bar{N}ON) + (\bar{\nu}_1 O\nu_1)(\bar{\nu}_1 O\nu_1) + (\bar{\nu}_2 O\nu_2)(\bar{\nu}_2 O\nu_2)]. \qquad (3)
\end{aligned}
$$

Unlike the expression (2), the Hamiltonian (3) contains no exceptions to the rule state above, and there is scattering of neutrinos by electrons and by μ mesons. By what do ν_1 and ν_2 differ? A theoretically permissible assumption is that they differ in the value of the chirality $(\gamma_5 \nu_{1,2} = \pm \nu_{1,2})$ while having the same leptonic charge.* This assumption, however, leads to a contradiction with the experimental data on the spectrum of the electrons from μ decay (it gives the Michel parameter $\rho = 0$).

We shall show that the existing experimental data do not contradict the alternative theoretical hypothesis, namely that while having the same chirality ν_1 and ν_2 have different leptonic charges. In this case the leptonic charges will also be opposite for the electron and μ meson when the electric charges are the same.* The properties of the leptons are conveniently shown in a table.

	I_z	l	γ_5	e	S
e^-	−1/2	−1	+1	−1	0
ν_1	1/2	−1	+1	0	0
μ^-	−1/2	+1	+1	−1	−2
ν_2	1/2	+1	+1	0	−2
e^+	1/2	+1	−1	+1	0
$\tilde{\nu}_1$	−1/2	+1	−1	0	0
μ^+	1/2	−1	−1	+1	+2
$\tilde{\nu}_2$	−1/2	−1	−1	0	+2

Here I_Z is the isotopic spin projection, l is the leptonic charge, γ_5 is the chirality in the weak interactions,[5] e is the electric charge, and S is the "strangeness" calculated by the formula $e = I_Z + l/2 + S/2$. A particularly significant fact is that the data of this table, together with the requirements of conservation of electric charge, leptonic charge, and chirality, uniquely determine the character of the μ decay, $\mu^- \to e^- + \tilde{\nu}_1 + \nu_2$, and give rigorous selection rules that forbid various unobserved reactions involving leptons:*

$$
\mu \to e + \gamma,\ \mu \to e + 2\nu,\ \mu \to e + e^+ + e^-,
$$
$$
K \to \pi + e^- + \mu^+,\ p + e \to p + \mu,\ \Lambda^0 \to n + \mu + e
$$

and so on. The reaction $n + \nu \to p + e$ is impossible with the neutrino produced in μ capture. Since leptons can occur in all the interactions only in the isotopic pairs $(\nu_1 e)$ and $(\nu_2 \mu)$, it is impossible for the neutrinos produced in the μ decay of $\pi^\pm$ mesons $(\pi^\pm \to \mu^\pm \pm \nu_2)$ to react with nucleons (or nuclei) to produce electrons; that is, the reactions $p + \tilde{\nu}_2 \to n + e^+$, $n + \nu_2 \to p + e^-$ are impossible.[6]† The fact that μ^+ mesons do not annihilate with atomic electrons finds a natural explanation.

If we start with our classification of leptons into isotopic doublets, the expression for the Hamiltonian of the four-fermion interactions involving only leptons and nucleons is uniquely determined in the form (1), on the basis of the requirements of Lorentz and isotopic invariance, conservation of chirality, conservation of the leptonic charge, and invariance of the interaction with respect to any interchanges of the type $l_1 \rightleftarrows l_2$, $l_{1,2} \rightleftarrows B$ (universality of the interaction).‡

In conclusion we point out the following. In a paper by Goldhaber[9] the hypothesis is suggested that fermions have a "doublet" character, and that

*The concept of leptonic charge was first introduced in a paper by Konopinski and Mahmoud.[7]

†The assumption that electrons and μ mesons of the same electric charge differ in their values of another ("neutrino") charge was suggested by Zel'dovich in 1953.[8]

*It is not hard to verify that all five of the reactions

$$
\mu \to e + 2\nu_{1,2},\ \mu \to e + 2\tilde{\nu}_{1,2},\ \mu \to e + \nu_1 + \tilde{\nu}_2.
$$

are forbidden.

†It is not hard to show that interactions between nucleons (or nuclei) and the neutrinos produced in the decay of slow π mesons cannot lead to the production of observable leptons (electrons or μ mesons).

‡For the choices of "particles" and "antiparticles," and also for the choice of the sign of the operator O, we appeal to experiment. The experimental value of the Michel parameter forces us to take simultaneously as "particles" $(\nu_1 e^-)$ and $(\nu_2 \mu^-)$.[6] The left-hand screw neutrino in β decay corresponds to the sign "+" in the operator O.

"doublets" of the type $(e\mu)$ (the electron and μ meson were regarded as two states of the same particle) can also occur in the case of the heavy fermions. Accordingly, it was suggested that there be an experimental search for the heavier component of the proton doublet. From the point of view of the theory presented here, with two neutrinos, this question is obviously settled in the sense that the situation in the lepton case cannot be repeated, since it is due to the peculiarities of the neutrinos: in this sense the existence of the μ meson is a direct consequence of parity nonconservation.*

The writer is deeply grateful to Ya. B. Zel'dovich for his attention and interest in this work, to I. S. Shapiro and L. B. Okun' for discussion and criticism, and to V. A. Yakovlev for support.

*If we put in correspondence with the "ordinary" lepton doublet $(\nu_1 e)$ a nucleonic isotopic doublet $(\tilde{n}\tilde{p})$, then the analogue of the "strange" lepton doublet will be $(\Xi^0\Xi^-)$.

[1] A. Salam, Nuovo cimento **5**, 299 (1957).

[2] L. D. Landau, JETP **32**, 405 (1957), Soviet Phys. JETP **5**, 336 (1957).

[3] T. D. Lee and C. N. Yang, Phys. Rev. **105**, 1671 (1957).

[4] Ya. B. Zel'dovich, JETP **36**, 964 (1959), Soviet Phys. JETP **9**, 682 (1959).

[5] E. Sudarshan and R. Marshak, Proc. Padua-Venice Conference on Mesons, 1957.

[6] M. Gell-Mann and R. P. Feynman, Phys. Rev. **109**, 193 (1958).

[7] E. J. Konopinski and H. M. Mahmoud, Phys. Rev. **92**, 1045 (1953).

[8] Ya. B. Zel'dovich, Dokl. Akad. Nauk SSSR **91**, 1317 (1953).

[9] M. Goldhaber, Phys. Rev. Letters **1**, 467 (1958).

Translated by W. H. Furry
205

EFFECT OF VISCOSITY IN MULTIPLE PRODUCTION ON THE ENERGY DISTRIBUTION OF SECONDARY PARTICLES

A. A. EMEL' YANOV and D. S. CHERNAVSKIĬ

P. N. Lebedev Physical Institute, Academy of Sciences, U.S.S.R.

Submitted to JETP editor May 14, 1959

J. Exptl. Theoret. Phys. (U.S.S.R.) **37**, 1058-1061 (October, 1959)

The effect of viscosity on processes taking place in a simple wave is considered in the hydrodynamical theory of multiple production of particles. It is shown that the effect of viscosity on the energy distribution of the fastest particles may be significant at sufficiently high energies.

In most researches on the hydrodynamical theory of multiple production of particles, the equations of a relativistic ideal liquid are used without consideration of viscosity. The effect of viscosity can be of a two-fold nature. In the first place, the viscosity increases the energy dissipation, raises the entropy, and, consequently, the number of secondary particles. In the second place, the appearance of new particles can bring about a significant change in the energy distribution, particularly in that region in which the number of particles is small while the energy possessed by them is large (for example in a simple wave[1]).

The problem of the role of viscosity was considered by Emel'yanov.[2] It was found that in the region of the fundamental solution (see reference 3) in the case in which the viscosity coefficient is not large, the number of secondary particles that owe their origin to the viscosity is small in comparison with N_0 and increases slightly with increase in the primary energy E_L (while the number of secondary particles N_0 formed in the initial stage upon passage of the shock waves increases significantly with the energy $N_0 \sim E_L^{1/4}$).

In the present work we compute the change ΔN in the number of particles which arise as a result of the viscosity in the region of the simple wave. This region is of interest, first, because even an increase that is small in absolute value can appreciably change the energy distribution, and second, because the velocity gradients in the region of the simple wave are larger than in the region of the fundamental solution, and therefore the role of the viscous terms is much more significant.

It should be noted that it is not immediately possible to determine the coefficient of viscosity of a relativistic liquid, in view of which the results here are of a qualitative character. Much more important from our point of view is the character of the dependence of ΔN on the energy of the primary particle E_L.

To estimate the number of particles formed in a simple wave because of viscosity, we make use of the expression for the 4-divergence of the entropy flux:[4]

$$\frac{\partial}{\partial x^i}(\sigma u^i) = -\frac{\tau_l^k}{T}\frac{\partial u^i}{\partial x^k}, \tag{1}$$

where σ is the entropy density, u^i is the velocity of an element of volume, T is the temperature, τ_{ik} is the viscous part of the energy momentum tensor, equal[4] to

$$\tau_{ik} = -\eta'\left(\frac{\partial u_i}{\partial x^k} + \frac{\partial u_k}{\partial x^i} + u_i u^l \frac{\partial u_k}{\partial x^l} + u_k u^l \frac{\partial u_i}{\partial x^l}\right) + \left(\frac{2}{3}\eta' - \zeta\right)\frac{\partial u^l}{\partial x^l}(g_{ik} + u_i u_k). \tag{2}$$

Equation (1) takes the form

$$\frac{\partial}{\partial x^i}(\sigma u^i) = \frac{4}{3}\frac{\eta}{T}\left(\frac{\partial u^i}{\partial x^i}\right)^2, \tag{3}$$

after substitution of the expression for τ_{ik}. Here $\eta = \eta' + \frac{3}{4}\zeta$. Further, we shall carry out the calculation under the assumption that the coefficient of viscosity η is small. Then quantities entering into the right hand side (T and u^i), we express in the form

$$T = T_0 + \eta T', \qquad u^i = u_0^i + \eta u'^i, \tag{3a}$$

where we shall assume that

$$\eta T' \ll T_0, \qquad \eta u^i \ll u_0^i. \tag{4}$$

Taking into account the assumptions made above, we can find the total increase in the entropy in first order in the coefficient of viscosity, making use of the one-dimensional solution for the simple wave

$$T_0 = T_0^*[(t-x)(1-c_0)/(t+x)(1+c_0)]^{c_0/2},$$

$$u_0^0 = (t+c_0x)/\sqrt{(1-c_0^2)(t^2-x^2)},$$

$$u_0^1 = (x+c_0t)/\sqrt{(1-c_0^2)(t^2-x^2)},$$

$$u_0^2 = u_0^3 = 0, \tag{5}$$

where $c_0 = 1/\sqrt{3}$ is the velocity of sound.

The increase in momentum in the simple wave will be

$$\Delta S = \int_\Omega dx^4 \frac{\partial \sigma u^i}{\partial x^i} = \frac{4\eta}{3}\int_\Omega dx^4 \left(\frac{\partial u^i}{\partial x^i}\right)^2 \frac{1}{T}. \tag{6}$$

The region of integration Ω here encloses the entire simple wave with the exception of those of its parts where the temperature is less than critical $T_k = \mu$. Relative to these parts, we have assumed (as is usually done in hydrodynamical theory) that the interaction between particles is completely absent. Furthermore, a region of the order of the mean free path of the particles λ around the point $t = x = 0$ has been discarded. This point represents the state of the system at the moment when the shock wave reaches the edge of the nucleon, and therefore a discontinuity of temperature takes place in it. The region of integration Ω is shown in the drawing. Integration has resulted in*

$$\Delta S = \frac{2\sqrt{3}\,\pi a^2\eta}{\mu}\left\{\ln\frac{l(1-c_0)}{2c_0\lambda}\left(\frac{T_0^*}{\mu}\right)^{(1+c_0)^2/2c_0^2} - \frac{\mu}{T_0^*}\ln\frac{l(\sqrt{3}-1)}{2\lambda} - \frac{(1+c_0)^2}{2c_0^2}\left(1-\frac{\mu}{T_0^*}\right)\right\}, \tag{7}$$

where πa^2 is the cross section of the interaction and l is the initial longitudinal dimension of the system. It is evident from this expression that the additional number of particles, $\Delta N \sim \Delta S$, formed in a simple wave increases logarithmically with the energy. However, the ratio of the increase of entropy to its initial value $\Delta S/S_0$ remains very small and falls off with the energy (inasmuch as $S_0 \sim E_L^{1/4}$). Thus the effect of viscosity on the total number of secondary particles is not large.

We now compute the number of secondary particles which are formed in the simple wave and remain in it to the moment of its decay. For this purpose we need to take the integral of (6) not over the entire region Ω, but over a flow tube of particles remaining in the simple wave, Ω_1. The region of integration Ω_1 is shown in the drawing.*

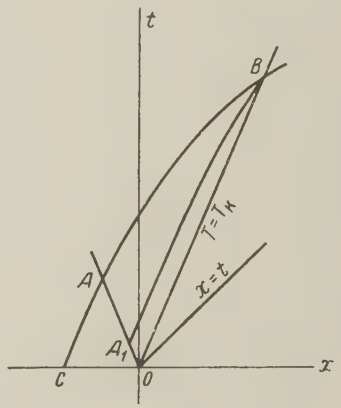

AB is the boundary with the region of the general solution, COA is the region at rest, OA_1B is the region Ω_1, OAB is the region Ω.

As a result of the integration, we obtain

$$\Delta S_1 = \frac{2\sqrt{3}\,\pi a^2\eta}{\mu}\left\{\ln\frac{l(1-c_0)}{2\lambda c_0}\left(\frac{T_0^*}{\mu}\right)^{(1+c_0)^2/2c_0^2} - \frac{\mu}{T_0^*}\ln\frac{l(1+c_0)}{2\lambda c_0} - \frac{1+c_0}{c_0^2}\left(1-\frac{\mu}{T_0^*}\right)\right\}. \tag{8}$$

It is seen here that the quantity ΔS_1 differs from ΔS only by terms which are independent of the energy of the primary particle; the role of these terms decreases with energy. Consequently, at sufficiently high energy, practically none of the particles created in the simple wave emerge from it. This means on the other hand that the new formation of the particles takes place at the boundary $T = \mu$, which is natural, since the effect of viscosity is greater the lower the temperature.

*In the integration it is convenient to transform to the new variables $\tau = t + x$ and $\xi = t - x$. In these variables, Eq. (6) has the form

$$\Delta S = \frac{2\pi}{3T_0^*}\int\int\int\int [\tau(1+c_0)]^{(c_0-2)/2}[\xi(1-c_0)]^{-(c_0+2)/2}\,d\tau\,d\xi\,dydz.$$

The equations for the limits of integration are the following: For the boundary $T = \mu$:

$$\tau = [(1-c_0)/(1+c_0)](T_0^*/\mu)^{2c_0}\xi;$$

the boundary of the rarefaction wave with the general solution:

$$\tau = \tau_k(\xi/\xi_k)^{(1+c_0)^2/(1-c_0)^2},$$

where τ_k and ξ_k are the critical values of the variables τ and ξ corresponding to the temperature $T = \mu$. They are equal to

$$\tau_k = {}^1/_2\, l(\sqrt{3}-1)(T_0^*/\mu)^{(1+c_0)^2/2c_0^2},$$

$$\xi_k = {}^1/_2\, l(\sqrt{3}+1)(T_0^*/\mu)^{(1-c_0)^2/2c_0^2}.$$

*The region Ω_1 differs from Ω only in that the boundary with the fundamental solution is replaced by the equation of the flow line passing through the point (τ_k, ξ_k). In the coordinates τ, ξ, this equation has the form

$$\tau = \tau_k(\xi/\xi_k)^{(1+c_0)/(1-c_0)}.$$

We estimate the absolute number of particles remaining in the simple wave under the assumption that these are pions. Then, in accord with reference 3,

$$\Delta N_1' = 0.2\Delta S_1 \approx 0.4\pi a^2 \gamma_1 \mu^{-1} [\ln (E_L/\mu) - (1 + c)/c_0^2]. \quad (9)$$

In spite of the fact that $\Delta N_1 \ll N_0$ always, the value of ΔN_1 can, with increase in energy, be compared with the number of particles remaining in the simple wave without account of viscosity (according to reference 1, this number does not depend on the energy and is equal to unity in order of magnitude), or can even surpass it. This can materially change the character of the interaction, since in the region where the greatest amount of energy is concentrated there will be found not a single particle but several, and the fraction of the energy remaining with a single particle will be much less. The energy for which $\Delta N_1 \approx 2$ and this phenomenon sets in can be estimated from (9):

$$E_k \sim \exp \{\mu \Delta N_1 / 2\sqrt{3}\pi a^2 \eta\}. \quad (10)$$

It must be noted, however, that it is not possible to estimate this value of the energy E_k at all precisely, since the coefficient of viscosity η enters into (10). The value of this coefficient can be estimated very roughly; at the same time E_k depends very strongly on it (exponentially). For example, if the ideal gas model is taken, then

$$\eta \approx \mu. \quad (11)$$

this value for η for a given density and temperature is an upper estimate.*

*Comparison of the kinetic coefficients of viscosity for gases and liquids shows that they are much smaller in liquids than in gases (see reference 4).

Consequently, by substituting (11) in (10), we obtain a reduced value of the critical energy $E_k \sim 10^{11}$ ev. Even if we take the coefficient of viscosity to be one third of this, then the corresponding value will be $E_k \sim 10^{14}$ ev.

These examples show that it is not possible to give a value for the critical energy E_k at the present time.

The calculations carried out above give grounds in support of the idea that the character of the elementary act must change with increase in energy. That is, beginning with a certain energy E_k, the effect of the reservation of a large fraction of the energy (~ 50 per cent) to a single particle[2] should no longer take place.

In conclusion, the authors extend their deep gratitude to G. A. Milekhin for fruitful discussions and a number of useful suggestions.

[1] N. M. Gerasimova and D. S. Chernavskiĭ, JETP **29**, 372 (1955), Soviet Phys. JETP **2**, 344 (1956).

[2] A. A. Emel'yanov, JETP **36**, 1550 (1959), Soviet Phys. JETP **9**, 1100 (1959).

[3] S. Z. Belen'kiĭ and L. D. Landau, Usp. Fiz. Nauk **56**, 309 (1955).

[4] L. D. Landau and E. M. Lifshitz, Механика сплошных сред (Mechanics of Continuous Media) (Gostekhizdat, 1953).

Translated by R. T. Beyer
206

SOME PROBLEMS OF THE DYNAMICS AND HEATING OF A CONDUCTING MEDIUM IN A MAGNETIC FIELD

G. S. GOLITSYN

Institute of Atmospheric Physics, Academy of Sciences, U.S.S.R.

Submitted to JETP editor May 16, 1959

J. Exptl. Theoret. Phys. (U.S.S.R.) 37, 1062-1067 (October, 1959)

One-dimensional motion of a perfectly conducting medium under the action of a magnetic field prescribed at the boundary is considered. Confinement of the plasma by a high frequency magnetic field is investigated. Some aspects of the problem of heating the plasma by magnetoacoustic waves are discussed.

IT is well known that a magnetic field acts on a perfectly conducting medium as a sort of piston. The peculiar feature of a magnetic piston compared to pistons encountered in ordinary gas dynamics is that at the boundary of the medium the pressure $H^2/8\pi$ is prescribed, while in gas-dynamic problems the speed of the piston is given.

If the magnetic field is specified at the initial moment inside the medium as well, then this extends the conditions of applicability of the theory under discussion to an actual hot plasma (for details see reference 1), in which in this case magneto-acoustic waves may occur,[2] while acoustic waves are not possible inside a plasma of finite dimensions without a field because of the large mean free path of the ions.

We shall assume that the field within the medium is perpendicular to the direction of motion. In such a case the hydrodynamic equations will hold also for a low-density plasma.[3] Moreover, this case is relatively simple analytically compared to the case of an arbitrary direction of the field. From a gas dynamic point of view the theory of magnetoacoustic waves of finite amplitude is completely analogous to the theory of Riemann waves in ordinary gas dynamics, and differs from it only by the greater complexity of the analytic expressions.[4]

1. MOTION UNDER THE ACTION OF A FIELD PRESCRIBED OVER THE BOUNDARY

The boundary condition at the surface of separation between the medium and the magnetic field may be easily established by choosing the system of coordinates in which this boundary is at rest. We assume that the medium is perfectly conducting, so that there is no flux of the field into the medium nor of the medium into the field. From the condition of the conservation of the normal component of the momentum flux we obtain at the boundary the equality of the total pressures

$$H_e^2/8\pi = p + H_i^2/8\pi. \tag{1.1}$$

Here H_e is the intensity of the external field and H_i is the field inside the medium.

We first investigate isentropic motion, and for simplicity set $H_i = 0$. Then in the case of one-dimensional motion the pressure is determined by the following equation[5]

$$p = p_0[1 \pm (\gamma - 1)\, u/2c_0]^{2\gamma/(\gamma-1)}, \tag{1.2}$$

where u is the velocity of the medium, and c is the velocity of sound. The subscript 0 denotes quantities defined at points where the gas is at rest. From (1.1) and (1.2) we obtain the following boundary condition:

$$H_e^2/8\pi = p_0[1 \pm (\gamma - 1)\, U/2c_0]^{2\gamma/(\gamma-1)}. \tag{1.3}$$

Here $U = dx/dt$ is the velocity of the boundary corresponding to given values of the external field and of the pressure of the medium. If the pressure is larger than $H_e^2/8\pi$, then the medium will expand, and a rarefaction wave will travel through it, while when $H_e^2/8\pi$ is greater than the pressure the gas will be compressed. From (1.3) we obtain the differential equation for the motion of the boundary of separation (the magnetic piston):

$$\frac{dx}{dt} = \frac{2c_0}{\gamma - 1}\left(\eta_e^{(\gamma-1)/2\gamma} - 1\right), \tag{1.4}$$

where $\eta_e = H_e^2/8\pi p_0$ is a given function of t and, perhaps, also of x. The system of coordinates is chosen in such a way that at the initial time the medium is situated at $x \geq 0$. When motion occurs in the direction $x > 0$ we have $U > 0$. On inte-

grating (1.4) we obtain the law of motion for the piston (for the separating boundary).

By utilizing results obtained earlier,[4] we obtain in exactly the same manner the corresponding equation for the case $H_i \neq 0$ ($\gamma = 5/3$), which, unfortunately, is not solved with respect to the derivative

$$\eta_e = y^3\left(y^2 + \frac{5}{6}\eta_i\right),$$

$$y = \frac{c}{c_0} = \frac{1}{\eta_i}\left\{\left[(1+\eta_i)^{5/2} \pm \frac{\eta_i}{2c_0}\frac{dx}{dt}\right]^{2/5} - 1\right\}. \quad (1.4')$$

Here $\eta_i = H_{i0}^2/4\pi\rho_0 c_0^2 = \text{const}$; η_e has its former meaning. If we know the law of motion for the piston we can in principle completely describe the isentropic motion of the gas by determining the velocity in the resulting simple wave in parametric form (cf. reference 5, section 94, problem 2). Generalization to the case $H_i \neq 0$ presents no difficulties.

Let us examine several examples. Let $\eta_e = \text{const} < 1$. Then the gas will expand into a vacuum, where there is a magnetic field. The limiting expansion velocity will be constant and in absolute value will be equal to

$$u_{max} = (1 - \eta_e^{(\gamma-1)/2\gamma})\, 2c_0/(\gamma - 1). \quad (1.5)$$

A wave of rarefaction will travel through the gas, as in the case of motion of a real piston with a speed $U = u_{max}$.

Now let $\eta_e = \text{const} > 1$. Then a shock wave will travel through the gas, compressing the gas to a pressure $p_2 = H_e^2/8\pi$. The boundary of separation will start moving with the velocity of the stream behind the front of the wave determined by the Huygens condition at the discontinuity.

2. ON THE CONFINEMENT OF PLASMA BY A RAPIDLY VARYING MAGNETIC FIELD AND ON THE HEATING OF PLASMA BY ACOUSTIC WAVES

The problem of the confinement of plasma by high frequency fields has been investigated by a number of authors.[1,6,9] Let us consider the one-dimensional problem of the motion of plasma (which we shall describe by means of the equations of magnetohydrodynamics) under the action of a magnetic field at the boundary which varies according to $H_e = H_0 \sin \omega t$. The field should not penetrate deeply into the medium, and this imposes the first condition on the frequency:

$$\omega \gg c^2/4\pi\sigma L^2, \quad (2.1)$$

where $\sigma \approx 2 \times 10^{13} T^{3/2}$ (the temperature is given in ev) is the conductivity of the medium, and L is a characteristic dimension of the system. When $L = 10^2$ cm, $T = 100$ ev, condition (2.1) yields $f = \omega/2\pi \gg 0.1$ cps. A much more difficult condition from a technical point of view is the second one: the deviations of the separation boundary from its average position must be small in comparison with L, and this can be written in the form

$$c_0/\omega \ll L, \quad (2.2)$$

where c_0 is the velocity of sound in the medium. When $T = 100$ ev the velocity of sound in a deuterium plasma is of the order of 5×10^6 cm/sec, which in the case of $L = 10^2$ cm yields $f \gg 10^4$ cps.

The pressure of the magnetic field must balance the time average of the plasma pressure. The problem consists of determining the amplitude of the balancing field, and of making more precise the condition (2.2).

For the sake of simplicity we consider first the case when there is no field within the medium. In this case the motion of the boundary is described by (1.4). We introduce the dimensionless variables: $\omega t = \tau$; $(\gamma - 1)\,\omega x/2c_0 = \xi$. Then (1.4) takes the form

$$d\xi/d\tau = \eta^{(\gamma-1)/2\gamma} - 1, \quad (A)$$

from which we obtain for the case of a sinusoidal field under the condition $\xi = 0$ at $\tau = 0$

$$\xi(\tau) = \int_0^{\tau} (H_0^2 \sin^2\tau/8\pi p_0)^{(\gamma-1)/2\gamma} d\tau - \tau. \quad (2.3)$$

We require that the average position of the boundary remain unaltered, and for this it is necessary that the equality $\xi(\pi) = 0$ should hold (since the pressure of the field is proportional to the square of H, the period of pressure oscillation at the boundary is equal to π). Due to the fact that the field appears nonlinearly in (2.3) there is no guarantee that the amplitude H_0 is determined by the seemingly obvious condition

$$\overline{H^2}/8\pi = \overline{H_0^2 \sin^2\tau}/8\pi = H_0^2/16\pi = p_0. \quad (B)$$

We therefore write $H_0 = \alpha_\gamma (8\pi p_0)^{1/2}$ and we determine the factor α_γ from the condition $\xi(\pi) = 0$. From this condition, and from (2.3) we obtain

$$\alpha_\gamma = \left[\frac{1}{\pi}\int_0^{\pi} (\sin\tau)^{(\gamma-1)/\gamma}\, d\tau\right]^{-\gamma/(\gamma-1)}$$

$$= \left[\frac{\sqrt{\pi}\,\Gamma(1 + (\gamma-1)/2\gamma)}{\Gamma(1/2 + (\gamma-1)/2\gamma)}\right]^{\gamma/(\gamma-1)}. \quad (2.4)$$

The factor α_γ depends on the properties of the

gas, but only to a very small extent. We present a small table which shows this dependence for different values of the adiabatic exponent γ:

$\gamma =$	1	$^7/_5$	$^5/_3$	2	3	∞
$\alpha_\gamma =$	2	1.81	1.76	1.72	1.66	1.57

It turns out that the amplitude of the external confining field must be larger by 20 — 30% than one might have supposed on the basis of elementary considerations without a detailed analysis of the motion of the boundary.

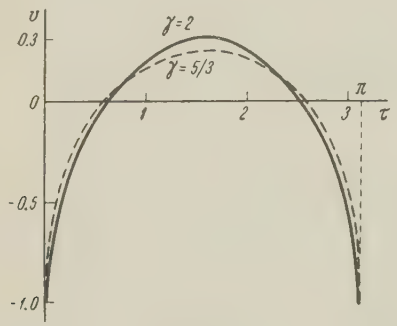

FIG. 1

Figures 1 and 2 give the results of numerical integration leading to the determination of the time dependence of the velocity $v = (\gamma - 1)/2c_0(dx/dt)$, and of the position of the separating boundary for the cases $\gamma = {}^5/_3$ and $\gamma = 2$. The maximum variation in the amplitude of oscillation $\Delta\xi_{max} = \xi_{max} - \xi_{min}$ is in the first case equal to 0.332, and in the second case to 0.396; corresponding to this Δx_{max} is respectively equal to $0.996\, c_0/\omega$ and $0.792\, c_0/\omega$.

Let us now consider the case when a magnetic field parallel to the boundary exists within the medium. In this case one must use Eq. (1.4'), which is quite awkward. However, a simple approximate analysis is possible. In order to utilize it, the actual adiabat of the gas $p = c\rho^\gamma$ must be approximated by the adiabat $p = c_1\rho^2$. This approximation will increase in accuracy as the field within the medium increases, simply because the relative role played by the thermodynamic pressure becomes less important.* In this case the whole of magnetohydrodynamics reduces to ordinary gas dynamics, provided we interpret the pressure to mean the total pressure $p^* = p + H^2/8\pi$, while the velocity of sound is interpreted to mean the velocity of propagation of magnetoacoustic waves $c_m = (c_0^2 + H^2/4\pi\rho)^{1/2}$.

Were a constant magnetic field H_{0i} to exist within the medium, it would apparently be natural to assume the external confining field to have a constant component equal to H_{0i}, and a variable

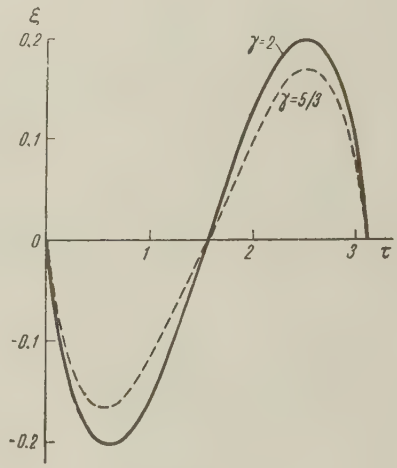

FIG. 2

component which on the average balances the gas pressure of the plasma. Let us investigate the same problem as before. In the case when the field has a constant component the period of pressure oscillation at the boundary will be 2π, and the conditions that the boundary should return to its initial position will be altered: we now must have $\xi(2\pi) = 0$. In the case $\gamma = 2$ this condition as applied to (2.3) may be brought into the form

$$I(a;\ \beta) = 2\pi(1+\beta)^{1/4} = \int_0^{2\pi} (|1 + a\sin\tau|)^{1/4}\, d\tau,$$

$$\beta = 8\pi p_0 / H_{0i}^2, \qquad a = \alpha\sqrt{\beta}; \tag{2.5}$$

where the factor α is introduced for the same purpose as in the preceding case. In the case of large β (small H_{0i}) we can obtain a correction to the value of α_2 obtained in the preceding case: $\alpha = \alpha_2 + 1.45\,\beta^{-1/2}$. Thus, if the external field has a constant component, the amplitude of the variable field must be larger; this is due to the fact that during the time $\pi < \tau < 2\pi$ the constant and the variable field have opposite signs, and the pressure due to the field during this half period decreases. In the limit of small β (large fields) we obtain by constructing the function $I(a;\beta)$ the limiting value $a = 7.3$, for which we still have

*As is well known,[3] the motion of a low-density plasma across a strong magnetic field is described by hydrodynamic equations with exponent $\gamma = 2$. This result is also obtained in magnetic gas dynamics for adiabatic motion in the case $\eta = H^2/8\pi\, p \to \infty$ (cf., for example, a number of problems solved in references 4 and 7). However, this does not hold, for example, in the case of shock waves. If the pressure discontinuity across the front is so large that the conditions $p_2/p_1 \gg \eta \gg 1$ hold, then the limiting density discontinuity will be determined by the properties of the gas itself,[4] i.e., by its own value of the exponent γ.

$I(a;0) = 2\pi$. In this case the external field is given by $H_e = H_0(1+7.3 \sin \omega t)$. These calculations show that it is not advantageous to have a constant component in the confining field, but that it is more convenient to have it wholly variable.

Let us discuss the limits of applicability of these results. Rarefaction and compression waves leave alternately the oscillating boundary, with the latter waves eventually turning into shock waves. At the point where the shock wave is formed a discontinuity in entropy also appears, and separates the region of the gas beyond the shock wave from the simple wave directly adjacent to the boundary. Since the discontinuity in the entropy is not displaced with respect to the medium, it will not approach the boundary (except for special values of the piston velocity,[8] where the motion must be accelerated in order that the discontinuity would be formed immediately at the boundary, whereas in our case the motion is periodic). Therefore the basic equation (1.4) will correctly describe the behavior of the boundary until a reflected shock wave arrives at that point. Then the gas compressed by the shock wave will begin to expand, a rarefaction wave will travel through the gas and equalize the pressure, and the oscillations of the boundary will stabilize around some new coordinate. Generally speaking, during the heating process the amplitude of the field must increase, but the ratio between $H_0^2/8\pi$ and p_0 must remain the same as found earlier.

The waves leaving the boundary will carry away a large amount of power, amounting to tens of kilowatts (cf. reference 6). The problem of the heating of plasma by acoustic waves has already been considered previously,[6,9] but without introducing a specific dissipation mechanism. In our case the formation of discontinuities in acoustic (magnetoacoustic) waves will be a more powerful loss mechanism than viscous, thermal, and Joule losses. Since the amplitude of pressure oscillations is great, the discontinuity will be formed already in the first wave. If condition (2.2) holds, we have many waves with shock discontinuities in a length L, and therefore the dissipation is great.

Let us check as to what will be the Larmor frequency of the ions in this case, since magnetoacoustic waves can exist only at frequencies much lower than the ion Larmor frequencies.[2] In the case of deuterium this is equivalent to the inequality

$$f \ll f_L = eH/2\pi mc = 7.65 \cdot 10^3 H, \qquad (2.6)$$

where H is given in oersteds. The inequalities (2.6) and (2.2) are contradictory (in the case $H_{0i} \neq 0$ we should interpret c_0 in (2.2) as c_m), but the technically important range of their simultaneous validity does exist. Apparently the optimum variant from the point of view of satisfying these two inequalities is the case $\eta = 1$.

For the purpose of heating the plasma by a pulsating magnetic field we should investigate the case when the field oscillates in phase at both ends of a plasma region of length 2L. If the amplitudes of the fields are the same, then the picture will be completely symmetric with respect to the central plane, where collision of waves will occur which, in view of the symmetry, can be regarded as reflection from a perfectly rigid wall. The collision of shock waves has also been investigated in magnetohydrodynamics.[4] In this case additional heating and an increase in entropy also take place.

The first shock wave after reflection from the wall and amplification will return, and collide with the shock wave following behind it. In this case the collision will no longer by symmetric, but amplification of both waves will in any case occur, although not to such a degree as in the case of the first collision. In the case of continuous motion of the piston at the boundary a stationary picture for strongly nonlinear waves is apparently impossible. In any case this question requires a separate detailed investigation. Probably one can assert that a standing wave is formed for the fundamental harmonic of the nonlinear waves, while the remaining harmonics will exist in the form of traveling waves. However, in all circumstances it is clear that in such a system the dissipation of energy will be very great (cf., for example, reference 5, section 95, problem 1).

In conclusion I wish to thank K. P. Stanyukovich and K. B. Pavlov for a number of useful discussions.

[1] A. I. Morozov, In the collection of articles, Физика плазмы и проблема управляемых термоядерных реакций (Plasma Physics and the Problem of Controlled Thermonuclear Reactions) **4**, U.S.S.R. Academy of Sciences, 1958, p. 331.

[2] S. I. Braginskiĭ and A. P. Kazantsev, ibid. **4**, p. 24.

[3] Chew, Goldberger, and Low, Proc. Roy. Soc. **A236**, 112 (1956).

[4] G. S. Golitsyn, JETP **35**, 776 (1958), Soviet Phys. JETP **8**, 538 (1959).

[5] L. D. Landau and E. M. Lifshitz, Механика сплошных сред (Mechanics of Continuous Media), GITTL, 1954, Ch. X.

[6] B. A. Trubnikov, loc. cit. in reference 2, p. 309.

[7] G. S. Golitsyn, JETP **34**, 688 (1958), Soviet Phys. JETP **7**, 473 (1958).

[8] K. P. Stanyukovich, Неустановившееся движение сплошной среды. (Unsteady Motion of Continuous Media), GITTL, 1955, Ch. 4.

[9] Gerger, Newcomb, Dawson, Frieman, Kulsrud, and Lenard, Phys. Fluids **1**, 308 (1958).

Translated by G. Volkoff
207

USE OF SLOW MOLECULES IN A MASER

N. G. BASOV and A. N. ORAEVSKIĬ

Submitted to JETP editor May 18, 1959

J. Exptl. Theoret. Phys. (U.S.S.R.) 37, 1068-1071 (October, 1959)

Several methods for improving the absolute frequency stability of a maser are considered; these methods are based on the use of molecular beams in which the mean velocity is much lower than the thermal velocity at room temperature.

IT has been shown experimentally[1] that a maser can have a frequency stability as high as 10^{-13} — 10^{-14} for a period of several seconds and 10^{-11} — 5×10^{-12} for a time of the order of thirty minutes. However, when a conventional system (ammonia inversion line, J = 3, K = 3) is used as an absolute standard of frequency the accuracy is 10^{-9} — 5×10^{-10}, a figure which is appreciably lower than the relative stability.[2-4] For this reason it is desirable to investigate the possibility of building a system with an absolute stability of the order of 10^{-11}, even if it could not provide prolonged operation. A system of this kind could provide intermittent frequency control of an ordinary maser which would operate for extended periods; in this way it might be possible to maintain the frequency for appreciable periods of time, because of the high relative stability.

The theory of the maser[5,6] indicates that the absolute frequency stability is inversely proportional to the line width and that the generated frequency does not differ from the frequency of the line by more than several percent of the line width. This deviation is determined by the accuracy with which the cavity is tuned to the frequency of the line, the dependence of line shape on external parameters, the line shape and so on.[7] In particular, the better the adjustment of the cavity to the line frequency, the higher the absolute stability of the system.

In this paper we report on a new method of increasing absolute stability in which the line is narrowed by the use of "slow molecules." Three methods of obtaining slow molecules are considered: 1) removal of high-velocity molecules from the beam, i.e., a high velocity "cutoff"; 2) retardation of the molecules by an external field; 3) reduction of the temperature of the molecular beam.

1. A high velocity cutoff can be imposed on the beam by reflecting the ammonia molecules from a potential barrier. An inhomogeneous electric field serves as a convenient potential barrier. The interaction of the ammonia molecules with the field is such that the energy of molecules in the upper inversion state is increased while the energy of molecules in the lower inversion state is reduced. Hence, if an ammonia molecule encounters a potential barrier in the form of an electric field it is reflected from the barrier if it is in the upper state and passes through the barrier if it is in the lower state.

Reflection from a barrier is an effective means of separating molecules. The potential barrier can be chosen in such a way that only low-velocity molecules are reflected, since the velocity of the reflected molecules must satisfy the relation

$$\tfrac{1}{2} m (\mathbf{vn})^2 \leqslant W, \qquad (1)$$

where $\mathbf{n}$ is a unit vector in the direction of grad W. In this case the field must be such that the isoenergetic surfaces $W(\mathbf{r}) = \text{const}$. act as focusing surfaces. By placing the source at the focus it is then possible to obtain a reflected beam with a small aperture, starting with an incident beam of large aperture.

A maser of this type can be realized most easily with deuterated ammonia (ND_3) because in this case the input aperture in the cavity can be large.[8] A potential barrier of the type discussed above can be produced by means of two flat plates, one of which has an aperture (fig. 1). The plates are arranged so that optimum focusing is achieved. A rough calculation, in which ideal reflection is assumed, indicates that when deuterated ammonia is used the excitation factor remains the same as in

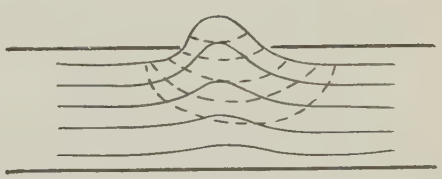

FIG. 1. The solid lines are equipotentials of the fields. The dashed lines are lines of equal potential energy for the interaction of molecules with the field.

a conventional system[8] if the mean velocity of the molecules in the beam is reduced by a factor of 10.

2. A potential barrier can also be used to retard molecules. If a molecule in the upper inversion state enters an electric field in which the interaction energy is W, then its velocity is reduced from v_0 to v so that the total energy is conserved,

$$\tfrac{1}{2} m v_0^2 = \tfrac{1}{2} m v^2 + W. \qquad (2)$$

The maximum possible number of molecules is obtained if molecules whose velocities are close to the most probable velocity are slowed down. This velocity is given approximately by $(kT/m)^{1/2}$. But electric fields which can be realized in practice are such that $W_{max} = 0.01\,kT$ for $T \approx 300°K$. Hence, a single retardation interaction does not reduce the velocity of the molecules appreciably. However, it is possible to use a multiple retardation system, in which regions of electric field are separated by regions of zero field. A molecule in the upper inversion state is decelerated on entering the field. On leaving the field it is accelerated to its original velocity. If, however, the molecule is caused to make a transition to the lower state by means of external radiation while it is in the field, it is again decelerated when it leaves the field. An external radiation field can then be used to raise the molecule to the upper level again and the process can be repeated.

If the frequency of the molecular transition is the same as the frequency of the external radiation, then the probability w of a transition from the upper level to the lower level (which is equal to the probability in the reverse direction) is given by[5]

$$w = \sin^2(\gamma \tau_v/2), \qquad \gamma = |d_{12}| E/\hbar, \qquad (3)$$

where τ_v is the time of flight of a molecule with velocity v and E is the amplitude of the external radiation. Hence, the total number of retarded molecules at the output of the system is given by

$$N = N_0 \int_{v_0-\Delta}^{v_0+\Delta} \left(\prod_{k=1}^{n} \sin^2 \frac{\gamma_k \tau_{vk}}{2} \right) F(v)\, dv \Big/ \int_0^\infty F(v)\, dv, \qquad (4)$$

where F(v) is the velocity distribution of the molecules, v_0 is the most probable velocity in F(v), 2Δ is the velocity range of the retarded molecules and N_0 is the original number of molecules.

If we wish to make the mean velocity in the retarded beam one-tenth the mean thermal velocity (roughly v_0), $\Delta/v_0 \approx 0.1$. In order to achieve this reduction it is necessary to have approximately fifty retardation sections, since $n \approx 100$. If the amplitude of the auxiliary field is chosen to make $\sin^2(\gamma_k \tau_{vk}/2) = 1$ for the mean velocity (which varies from section to section because of the retardation effect), a calculation of the integral in Eq. (4) with an electronic computer (Maxwellian velocity distribution) indicates that $N \approx 0.01\, N_0$. The use of retarding sections with uniform fields (parallel plates) is not desirable because these reduce the velocity component perpendicular to the plane of the plate and defocus the molecular beam itself. However, if the retarding sections are spherical mirrors, the system can be set up in such a way as to focus the beam, as can be seen from Fig. 2.

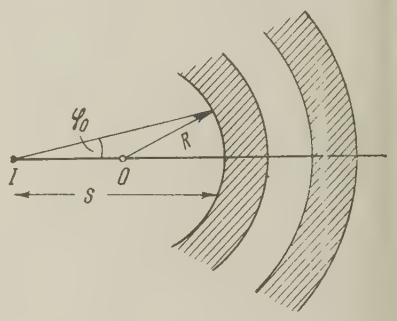

FIG. 2. To obtain focusing the distance S must be larger than the distance R. The point denoted by O is the center of the spherical focusing mirrors; I is the source of the molecular beam and regions with electric field are denoted by cross-hatching.

In this system the initial flight angle φ_0 is changed to $\pi - \varphi_0$ according to the retardation. As soon as the exit angle became equal to $\pi - \varphi_0$ the retardation process must be repeated identically if the first retardation is inadequate.

3. We now consider a method for reducing the temperature of the molecular beam. It is not feasible to reduce the temperature by cooling the source because a small reduction in source temperature has very little effect (the velocity is proportional to $T^{1/2}$). On the other hand, a large reduction in the source temperature causes the ammonia to freeze. It is possible, however, to reduce the ammonia temperature by allowing the ammonia molecules to collide with a cold gas. If the ammonia interacts with the cold gas solely through collisions the kinetic energy of the ammonia molecules is gradually reduced to that of the cold gas. Helium at a few degrees Kelvin serves as a convenient cooling gas. In order for a system of this kind to operate effectively, the following conditions must be satisfied: a) the time in which equilibrium is established in the helium-ammonia mixture must be shorter than the time between collisions of the ammonia molecules or collisions of the ammonia molecules with the walls; b) an effective means of heat removal must be provided so that the temperature of the helium does not rise.

Condition a) implies the relation

$$N_A\sigma_{A-A}/\sqrt{m_A} \ll N_H\sigma_{A-H}/\sqrt{2\mu_{A-H}}, \quad (5)$$

where σ_{A-A} is the cross section for a collision between ammonia molecules, σ_{A-H} is the cross section for a collision between an ammonia molecule and a helium molecule, m_A is the mass of the ammonia molecule, μ_{A-H} is the reduced mass of the system, consisting of the ammonia molecule and the helium molecule, and N_A and N_H are the ammonia and helium densities respectively. From the conditions for thermal equilibrium we can obtain the temperature of the mixture:

$$T = T_H + T_A N_A / N_H, \quad (6)$$

where T_H is the initial temperature of the helium and T_A is the initial temperature of the ammonia. Condition b) requires that the increment in the helium temperature be small ($\sim 1°K$). Both of these conditions can be satisfied if N_A/N_H is about 1/100.

One important point should be noted. If the ammonia molecules are in thermodynamic equilibrium at $4-5°K$ they are practically all in the ground state ($J = 0$, $K = 0$); this state cannot be used for generation since the dipole-moment matrix element for this state is zero. However, this situation is alleviated by the fact that the equilibrium time for the rotational energy is much greater than the equilibrium time for the translational motion because transitions with $\Delta K \neq 0$ are highly forbidden, even in collisions between molecules.[9]

Removal of slow molecules from the beam by a cutoff technique or retardation by external fields disturbs the molecular velocity distribution and this effect causes a change in the line shape. Since the frequency depends on the line shape, at first glance it might be supposed that these methods of obtaining slow molecules are not very useful. An analysis of this aspect of the problem indicates, however, that, in both cases considered above the absolute frequency stability increases for a given excitation factor linearly with the mean time spent by molecules in the cavity.

It should be noted that all these methods of obtaining slow molecules imply an appreciable loss in the number of useful molecules and a consequent reduction in power. Thermal noise in the maser is characterized by a frequency spectrum whose width is inversely proportional to power.[10] An appreciable loss of power can lead to a marked increase in the relative effect of this noise; hence, for effective operation the cavity should be cooled. If the mean time of flight is increased by a factor of ten through the use of a velocity cutoff the thermal noise at room temperature remains unimportant ($\Delta\omega/\omega \approx 10^{-14}$).

The considerations given above indicate that it may be possible to build a maser with an absolute stability of $10^{-11} - 10^{-12}$.

[1] N. G. Basov and A. P. Petrov, Радиотехника и электроника (Radio Engineering and Electronics) **3**, 298 (1958).

[2] Gordon, Zeiger, and Townes, Phys. Rev. **99**, 1264 (1955).

[3] N. G. Basov, Радиотехника и электроника (Radio Engineering and Electronics) **1**, 51 (1956).

[4] N. G. Basov, Приборы и техника эксперимента (Instruments and Measurement Engineering) **1**, 71 (1957).

[5] N. G. Basov and A. M. Prokhorov, Usp. Fiz. Nauk **57**, 485 (1955).

[6] Schimoda, Wang, and Townes, Phys. Rev. **102**, 1308 (1958).

[7] N. G. Basov and A. N. Oraevskiĭ, Радиотехника и электроника (Radio Engineering and Electronics) **4**, 1185 (1959).

[8] N. G. Basov, and K. K. Svidzinskiĭ, Изв. высш. учебн. завед., Радиофизика (News of the Institutions of Higher Learning, Radiophysics) **1**, 89 (1958).

[9] P. W. Anderson, Phys. Rev. **76**, 647 (1949).

[10] V. S. Troitskiĭ, JETP **34**, 390 (1958), Soviet Phys. JETP **7**, 271 (1958).

Translated by H. Lashinsky
208

EMISSION OF NEUTRINO PAIRS BY ELECTRONS AND THE ROLE PLAYED BY IT IN STARS

G. M. GANDEL' MAN and V. S. PINAEV

Submitted to JETP editor May 18, 1959

J. Exptl. Theoret. Phys. (U.S.S.R.) 37, 1072-1078 (October, 1959)

Bremsstrahlung emission of neutrino pairs by a nondegenerate gas is investigated. In a certain range of high densities and temperatures the energy loss by bremsstrahlung emission of neutrino pairs becomes greater than the loss due to radiative thermal conductivity. The inclusion of the energy loss due to neutrino pair emission may turn out to be significant, and in some cases even of decisive importance, for the theory of white dwarfs and stellar evolution, particularly for the dynamics of supernova explosions. The process under consideration leads to even greater energy losses than the process of neutrino pair formation in reaction (1) proposed by Gamow and Schoenberg in 1941.

1. INTRODUCTION

FEYNMAN and Gell-Mann[1] have assumed that all weak interactions arise as a result of the current

$$I_\mu = (\bar{\psi}_p \gamma_\mu a \psi_n) + (\bar{\psi}_\nu \gamma_\mu a \psi_e) + (\bar{\psi}_\nu \gamma_\mu a \psi_\mu) + \ldots$$

interacting with itself. Their theory has been brilliantly confirmed in β decay and in the decay of the μ meson, i.e., for the interactions $(\bar{p}n)(\bar{e}\nu)$ and $(\bar{\nu}\mu)(\bar{e}\nu)$. The theory yields the possibility of new direct interactions, in particular $(\bar{e}\nu)(\bar{\nu}e)$. Such an interaction results first of all in direct neutrino-electron scattering.[1]

B. M. Pontecorvo has drawn attention to the fact that in the case of this interaction there also exists the possibility of formation of neutrino pairs in the collision of electrons with nuclei. He noted that the bremsstrahlung "emission" of neutrino pairs might serve as an additional mechanism for energy loss from stars.[2] The probability of creation of neutrino pairs is considerably smaller than the probability of bremsstrahlung emission of photons. However, a neutrino that interacts weakly with matter has a mean free path which exceeds by a large factor the dimensions of the star, while under the same conditions a photon has a very much smaller mean free path. Because of this the losses of energy from stars as a result of the creation of neutrino pairs may, within a certain range of densities and temperatures, turn out to be comparable to, or even greater than, the losses of energy by photon emission. At large densities ρ and for large Z the creation of neutrino pairs becomes more probable, and the photon mean free path becomes smaller.

As early as 1941 Gamow and Schoenberg[3] have indicated a mechanism for the loss of energy from stars by neutrino emission

$$_ZN^A + e^- = {}_{Z-1}N^A + \nu, \qquad {}_{Z-1}N^A = {}_ZN^A + e^- + \bar{\nu}. \quad (1)$$

This process is possible when the temperature and the density in the interior of the star are both large. However, its intensity depends on the presence of nuclei with a low threshold.

In this paper we calculate the cross section for the creation of neutrino pairs in the collision of electrons with nuclei and the effective slowing down; in view of the intended astrophysical application the calculation is carried out in the nonrelativistic case.

2. CROSS SECTION FOR THE CREATION OF NEUTRINO PAIRS. EFFECTIVE SLOWING DOWN

For the evaluation of the matrix element we make use of the universal four-fermion interaction

$$\sqrt{8}\, G \left[\bar{e} \tfrac{1}{2} \gamma_\mu (1 - i\gamma_5) \nu\right] \left[\bar{\nu} \tfrac{1}{2} \gamma_\mu (1 - i\gamma_5) e\right].$$

Two Feynman diagrams for the process under consideration are shown in Fig. 1.

The matrix element for the creation of a neutrino pair in the collision of an electron with a nucleus has the form

$$M = \sqrt{8}\, eG \left\{\left[\bar{\nu}_{\mathbf{n}} \tfrac{1}{2} \gamma_\mu (1 - i\gamma_5) \frac{\hat{a}_q}{\hat{p} - \hat{m}} e_i\right] \left[\bar{e}_f \tfrac{1}{2} \gamma_\mu (1 - i\gamma_5) \nu_a\right] + \left[\bar{e}_f \frac{\hat{a}_q}{\hat{p}' - m} \tfrac{1}{2} \gamma_\mu (1 - i\gamma_5) \nu_a\right] \left[\bar{\nu}_{\mathbf{n}} \tfrac{1}{2} \gamma_\mu (1 - i\gamma_5) e_i\right]\right\}. \quad (2)$$

Here $p_1 (p_{10}, \mathbf{p}_1)$ and $p_2 (p_{20}, \mathbf{p}_2)$ are the four-momenta of the electron in the initial and final

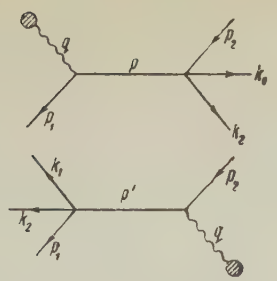

FIG. 1

stages respectively; k_1 (k_{10}, $\mathbf{k}_1$) and k_2 (k_{20}, $\mathbf{k}_2$) are the four-momenta of the neutrino and the antineutrino respectively; the subscript n denotes a neutrino, while the subscript a denotes an antineutrino;

$$a_q = \int A e^{-iqx} d^4x = 2\pi i a_q^0 \delta(E_1 - E_2 - k_{10} - k_{20}),$$
$$a_q^0 = \int A_0 e^{-i\mathbf{qr}}\, d\mathbf{r}; \qquad (3)$$

and q is the four-momentum transferred to the nucleus. The nucleus is taken to be at rest and the effect due to it is regarded as the action of an external static field, so that $q_0 = 0$. For the case of the Coulomb field of a nucleus of charge Ze we have:

$$a_q^0 = Ze/q^2. \qquad (4)$$

From the conservation laws we have

$$p = p_2 + k_1 + k_2, \quad p' = p_1 - k_1 - k_2,$$
$$q = p_2 + k_1 + k_2 - p_1, \quad q = p - p_1 = p_2 - p'.$$

We substitute (3) and (4) into (2). In order to simplify the calculation we reduce the matrix element to the form $(\bar{e}O_1 e)(\bar{\nu}O_2\nu)$ (the Fierz transformation). We then obtain

$$M = 2\pi\sqrt{8}\frac{Ze^2}{q^2} G \left\{\bar{e}_f \left[\frac{1}{2}\gamma_\mu(1 - i\gamma_5)\frac{1}{\hat{p} - m}\gamma_0 + \gamma_0 \frac{1}{\hat{p}' - m}\frac{1}{2}\gamma_\mu(1 - i\gamma_5)\right] e_i\right\}$$
$$\times \left[\bar{\nu}_n \frac{1}{2}\gamma_\mu(1 - i\gamma_5)\nu_a\right]\delta(E_1 - E_2 - k_{10} - k_{20}).$$

We introduce the notation

$$c_\mu = \left[\bar{\nu}_n \tfrac{1}{2}\gamma_\mu(1 - i\gamma_5)\nu_a\right]$$

and we make use of c_μ inside the figure brackets. By utilizing the Dirac equation $(\hat{p}_1 - m)e_i = 0$ and $\bar{e}_f(\hat{p}_2 - m) = 0$, we bring the matrix element into the form

$$M = 2\pi\sqrt{8}\frac{Ze^2}{q^2} \times G\bar{e}_f\left[\hat{c}\,\frac{1}{2}(1 - i\gamma_5)\frac{\hat{q}\gamma_0 + 2p_{10}}{p^2 - m^2} + \frac{2p_{20} - \gamma_0\hat{q}}{p'^2 - m^2}\,\hat{c}\,\frac{1}{2}(1 - i\gamma_5)\right] e_i. \qquad (5)$$

The evaluation of the square of the matrix element (5) is fairly complicated, but in the nonrelativistic approximation the form of (5) is considerably simplified. In this case we have

$$p_{10} \sim m, \quad p_{20} \sim m, \quad |\mathbf{p}| \ll m, \quad |k_0| \ll m.$$

Taking this into account, we have

$$p^2 - m^2 \sim 2m(k_{10} + k_{20}),$$
$$p'^2 - m^2 \sim -2m(k_{10} + k_{20}), \quad \mathbf{q} = \mathbf{p}_2 - \mathbf{p}_1.$$

On averaging the square of the matrix element over the initial polarizations of the electron, and on summing over the final polarizations of the electron and of the emitted neutrino and antineutrino, we obtain

$$\Sigma|M|^2 = 4\pi \frac{Z^2e^4G^2}{q^4m^2(k_{10} + k_{20})^2}[k_{10}k_{20}\mathbf{q}^2 + (\mathbf{qk}_1)(\mathbf{qk}_2)]$$
$$\times \delta(E_1 - E_2 - k_{10} - k_{20}).$$

The differential cross section of the process under consideration has the form

$$d\sigma = \Sigma|M|^2(2\pi)^{-9}\frac{p_2^2 dp_2 k_1^2 dk_1 k_2^2 dk_2}{dE_f}\frac{m}{E_2 k_{01} k_{02} J}$$
$$\times \delta(E_1 - E_2 - k_{10} - k_{20}) dE_f d\Omega_\nu d\Omega_{\bar{\nu}} d\Omega_e. \qquad (6)$$

Here $J = p_1/m$ is the flux density of incident electrons. By integrating (6) over the energy of the final state E_f and over the direction and the momentum of the neutrino we obtain:

$$d\sigma = \frac{1}{15\pi^4} Z^2 r_0^2 g^2 \frac{p_2}{p_1}(E_1 - E_2)^3 \frac{dE_2}{(p_2 - p_1)^2} d\Omega_e, \qquad (7)$$

where $g = G/mc^2(\hbar/mc)^3 = 3 \times 10^{-12}$ for $G = 1.41 \times 10^{-49}$ erg-cm^3, and r_0 is the classical electron radius. The energy and the momentum are expressed in units of mc^2 and mc respectively.

The total effective cross section for the creation of a neutrino pair is obtained by integrating (7) over the direction and the energy of the final electron

$$\sigma = (8Z^2/525\pi^3) r_0^2 g^2 E_1^3 = \sigma_0 Z^2 E_1^3,$$
$$\sigma_0 = 8r_0^2 g^2/525\pi^3 = 3.52 \cdot 10^{-52}\ \text{cm}^2.$$

The energy transferred by the electrons to the neutrino pairs, i.e., the effective slowing down κ, is equal to:

$$\varkappa = \int_0^{E_1} (E_1 - E_2)\, d\sigma = \tfrac{32}{45}\sigma_0 Z^2 E_1^4.$$

In ordinary units we have

$$\varkappa = (32/45)\sigma_0 Z^2 E_1 (E_1/mc^2)^3 = 2.5 \cdot 10^{-52} Z^2 E_1 (E_1/mc^2)^3. \qquad (8)$$

3. CREATION OF NEUTRINO PAIRS IN STARS

Let us evaluate the energy q_ν given up by the electrons to neutrino pairs per cm^3 per sec. If we assume that the electrons have a Maxwellian distribution we obtain

$$q_\nu = \int \varkappa v n_{nuc}\, dn_e = 2.5\cdot 10^{-52} 5!2 \sqrt{2/\pi}\, n_{nuc}\, n_e Z^2 mc^3 (T/mc^2)^{9/2}, \quad (9)$$

n_e and n_{nuc} are the numbers of electrons and of nuclei per cm^3. If the substance has a density ρ and consists of a mixture of atoms which are completely ionized, then

$$n_e = 6\cdot 10^{23}\rho/\mu_e, \text{ where } 1/\mu_e = \sum_i C_i Z_i/A_i;$$

C_i is the concentration of the element by weight:

$$\Sigma n_{nuc\,i} Z_i^2 = 6\cdot 10^{23}\rho/\nu, \qquad 1/\nu = \sum_i C_i Z_i^2/A_i.$$

On substituting these expressions into (9) we obtain*

$$q_\nu = 2.75\cdot 10^{-10}(\rho^2/\nu\mu_e)\, T^{9/2} \text{erg/cm}^3\text{-sec}, \quad (10)$$

where T is measured in kev.

It can be easily shown that in the case of a hydrogen star q_ν is smaller than the rate of liberation of energy in hydrogen reactions by a factor of $\sim 10^7$. Therefore the process under consideration may play a role only for large Z, when the thermonuclear reaction proceeds much more slowly.

It is of interest to compare q_ν with the rate of liberation of energy w by means of neutrino emission in the Gamow and Schoenberg process. The latter depends in an essential manner on the threshold Q for e^--capture; for large values of Q it falls off exponentially $\sim \exp(-Q/T)$ and has a maximum at $Q \sim 2T$. If we take the matrix element for the β process equal to 1, and the concentration of the element equal to 100%, then in the characteristic range $\rho \sim 10^5$ and $T < 100$ kev the maximum value w_{max} at a given temperature exceeds q_ν by a factor of approximately $10^6/A$. Moreover, both w_{max} and q_ν are proportional to $T^{4.5}$. The isotopes which are most important for the Gamow-Schoenberg process are (cf. reference 4) the elements with a low threshold Q:

Cl^{35} (threshold $Q = 170$ kev), N^{14} ($Q = 155$ kev), Sc^{45} ($Q = 212$ kev), Ga^{72} ($Q = 300$ kev), Ni^{60} ($Q = 300$ kev).

It turns out that C^{14} which is formed from the abundant element N^{14} has an anomalously small matrix element, so that $w = 2.3 \times 10^7$ erg/cm^3 sec for $T = 50$ kev, $\rho = 10^5$ even at a concentration of 100%, while

$$q_\nu = 3.6\cdot 10^8 \quad \text{at} \quad T = 50 \text{ kev}, \quad \rho = 10^5.$$

In the case of Cl^{35}: $w = 0.8 \times 10^{11}$ for $T = 50$ kev, but its concentration is $< 5 \times 10^{-4}$. The remaining elements (Sc^{45}, Ga^{72}, Ni^{60}) also lead to $w \ll q_\nu$ as a result of their low abundance.

It is therefore possible to assert that even though we have $w \sim g^2$ in the Gamow-Schoenberg process, while in our case we have $w \sim g^2 e^4$, nevertheless, owing to the low abundance of elements with a low threshold Q and to the anomalously long lifetime of certain nuclei, the effect under consideration is considerably larger for $T < 100$ kev.

4. COMPARISON OF THE NEUTRINO AND THE PHOTON LUMINOSITY OF STARS

Let us compare the energy carried away by neutrino pairs from the stars (the "neutrino" luminosity L_ν), with the ordinary photon luminosity L_γ. We examine the ratio of these two quantities for all possible stellar configurations, utilizing as independent variables the density ρ_c and the temperature T_c at the center of the star.

The neutrino and the photon luminosities have a different dependence on the stellar radius:

$$L_\nu \sim R^3, \qquad L_\gamma \sim R^2 \partial T^4/\partial R \sim R.$$

However, for a given ρ_c and T_c the radius R and the mass M are determined in terms of them by the conditions of mechanical equilibrium. In what follows we consider the regime in which the electrons are nondegenerate and the radiation pressure can be neglected. For such stars the expressions for the radius and for the mass in terms of ρ_c and T_c depend neither on the mechanism of energy liberation in nuclear reactions, nor on the mechanism of energy loss.

The equation for the equilibrium of a star has the form

$$dP/dr = -\rho G M_r/r^2, \qquad P = a\rho T/\mu,$$
$$dM_r/dr = 4\pi r^2 \rho, \quad (11)$$

where $1/\mu = \Sigma_i C_i (Z_i + 1)/A_i$.

By utilizing a similarity transformation we obtain from the system (11)

$$M \sim R^3 \rho_c, \quad R^2 \sim aT/G\mu\rho_c. \quad (12)$$

The total luminosity of the star is determined

*In the case that the electrons have a Fermi-Dirac distribution and are nearly degenerate, we have:

$q_\nu = 0.82\cdot 10^{-7}(\rho/\nu)T^6 \ln(0.89\, E_0/T)$, $E_0/mc^2 = 5.07\cdot 10^{-5}(\rho/\mu e)^{2/3}$ (T in kev)

by

$$L_\gamma = -4\pi r^2 \frac{lc}{3}\frac{d}{dr}(\sigma T^4). \quad (13)$$

The photon mean free path l deep within the star is determined primarily by the photoeffect. According to Kramers' formula we have

$$l = bT^{3.5}/\rho^2. \quad (14)$$

On substituting (12) and (14) into (13) we obtain on the basis of considerations of similarity the following expression for the photon luminosity of the star

$$L_\gamma = \text{const}\cdot B\sqrt{\frac{a}{G}}\,T_c^8/\rho_c^{2.5}\mu^{0.5}, \text{ where } B = 16\pi\sigma cb/3\cdot 7.5, \quad (15)$$

where the value of the constant can be obtained on the basis of a definite stellar model. For the model with a homogeneous distribution of energy we have: const = 9.6; for the point source model we have:[5] const = 3.37. Other models yield intermediate results.

For making further estimates we shall utilize the point source model since we are interested in the case when the star consists of heavy elements. In this case the rate of a nuclear reaction depends on a high power of the temperature, and falls off rapidly as the distance from the center increases.

On substituting the numerical coefficients into (15) we obtain

$$L_\gamma = 0.98\cdot 10^3 bT_c^8/\mu^{0.5}\rho_c^{2.5}. \quad (16)$$

Here T_c is in kev, L_γ is in solar units ($L_\odot = 3.78\times 10^{33}$ erg/sec), ρ_c is in g/cm^3.

Let us obtain the expression for the neutrino luminosity:

$$L_\nu = \int q_\nu dV = 2.75\cdot 10^{-10}\frac{1}{\mu_e^\nu}4\pi\int_0^R \rho^2 T^{9/2} r^2 dr. \quad (17)$$

We take the temperature and density distributions from the same point source model. Since in this case the convective core has a small radius (0.169 R) we take the temperature and the density to be constant within it and equal to T_c and ρ_c. Within the bulk of the stellar mass we have

$$T = T_c\frac{R/r-1}{1/\xi-1}, \qquad \rho = \rho_c\left(\frac{R/r-1}{1/\xi-1}\right)^{3.25}$$

where[6] $\xi = 0.169$. Integration yields:

$$\int_0^R \rho^2 T^{4.5} r^2 dr = 2.07\cdot 10^{-3} R^3 T_c^{4.5}\rho_c^2.$$

In our case we have[5] $T_c = 0.7\times 10^{-22}\mu M/R$, $\rho_c = 37\bar{\rho} = 111\, M/4\pi R^3$. If we solve these expressions for R in terms of ρ_c and T_c and substitute it into L_ν, we shall obtain the final formula for the neutrino luminosity of the star

$$L_\nu = 0.9\cdot 10^{-10}(T_c^6/\mu_e(\mu^{1.5}\nu)\rho_c^{0.5}. \quad (18)$$

We compare the photon and the neutrino luminosities expressed in terms of ρ_c and T_c:

$$L_\nu/L_\gamma = (0.92\cdot 10^{-13}/b\mu\mu_e\nu)\rho_c^3/T_c^2. \quad (19)$$

The cross section for the creation of neutrino pairs and for bremsstrahlung is proportional to Z^2/A, but $L_\gamma \sim 1/\sigma_{brems} \sim A/Z^2$, i.e.,

$$L_\nu/L_\gamma \sim Z^4/A^2 \sim Z^2.$$

It may be easily seen from (19) that the neutrino luminosity can produce an appreciable effect only in stars of high density.

According to modern views[7] very dense stars of low luminosity consist largely of heavy elements such as magnesium. Moreover, in the central regions of the star the temperature and the density are very high, but degeneracy does not yet occur.

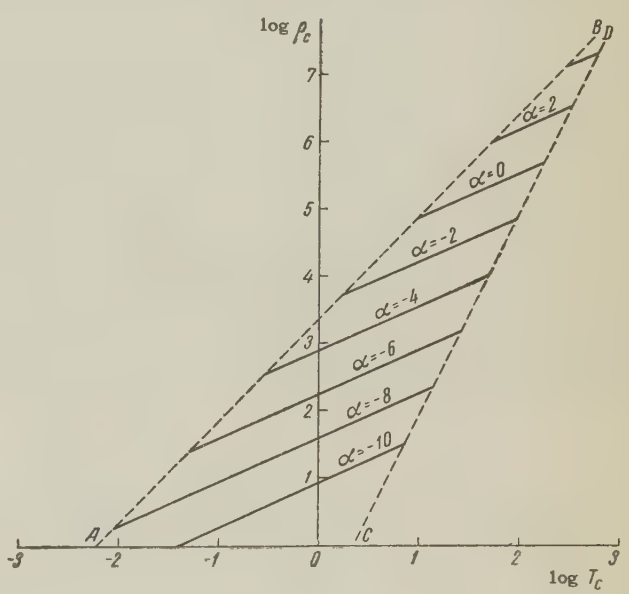

FIG. 2

Figure 2 shows the lines $L_\nu/L_\gamma = 10^\alpha$ for Mg ($\mu = \mu_e = 2$, $\nu = 2/Z = 1/6$, $b = 1$) on a logarithmic scale. The line AB in Fig. 2 is the boundary for degeneracy ($T = E_0/3$, E_0 is the limiting Fermi energy). The line CD is the boundary of the region to the right of which the radiation pressure is greater than the material pressure. We see, for example, that for $\rho = 10^5$, $T = 11$ kev: $L_\nu/L_\gamma = 1$; for $\rho = 2\times 10^6$, $T = 100$ kev: $L_\nu/L_\gamma = 100$.

At high densities the above results must be made more precise. On the one hand the effect of the screening of nuclei by electrons, the collective interaction of nuclei will lead to a change in the cross section for creation of neutrino pairs; on the other hand the inclusion of these phenomena

will also lead to a change in the photon mean free path.

We have not investigated the transition of an electron from a free state into a bound one accompanied by the creation of a neutrino pair. This is justified for $\rho > 10^4$ g/cm^3, because in this case the electron has no bound levels, since the atomic radius is of the order of the Bohr radius.

Among the observed stars the neutrino effect may play a significant role in white dwarfs which have in their central parts $\rho \sim 10^5$, and also in the process of stellar evolution.

We have not investigated the regime of the degenerate equation of state, however, from qualitative considerations we may conclude that the neutrino effect may play a role here only at still higher densities than in the nondegenerate regime. At a given temperature T degeneracy diminishes L_ν and increases L_γ.

It should be emphasized that in the development of the theory of white dwarfs and of stellar evolution, particularly in the dynamics of supernova explosions, the inclusion of the energy loss due to neutrinos may turn out to be significant, and in some cases even dominant.

In conclusion we express our sincere gratitude to Ya. B. Zel'dovich for valuable advice and discussions, and to B. M. Pontecorvo and D. A. Frank-Kamenetskiĭ for interesting discussions.

Note added in proof (September 16, 1959). Another form of radiation which interacts weakly with matter is gravitational radiation originating in the collision of particles. It can be easily evaluated by analogy with the quadrupole electromagnetic radiation [L. D. Landau and E. M. Lifshitz, Теория поля (Field Theory), p. 218]. The gravitational radiation plays its most important role in the case of Coulomb scattering of electrons, in this case calculation yields the value $q = 5.3 \times 10^{-20} \rho^2 T_{kev}^2$ erg/cm^3 sec, so that it is smaller than the neutrino radiation by a factor of 10^{10}.

[1] R. Feynman and M. Gell-Mann, Phys. Rev. **109**, 193 (1958).

[2] B. M. Pontecorvo, JETP **36**, 1615 (1959), Soviet Phys. JETP **9**, 1148 (1959).

[3] G. Gamow and M. Schoenberg, Phys. Rev. **59**, 539 (1941).

[4] G. Gamow, Phys. Rev. **59**, 617 (1941).

[5] L. H. Aller, Astrophysics, Roland Press, N.Y. 1953 (Russ. Transl. IIL, 1957).

[6] S. Chandrasekhar, Introduction to the Study of Stellar Structure (Russ. Transl. IIL, 1950).

[7] E. I. Epic, In the collection of articles Ядерные процессы в звездах (Nuclear Processes in Stars), IIL, 1957.

Translated by G. Volkoff
209

SIMPLE METHOD FOR COMPUTING THE MEAN RANGE OF RADIATION IN IONIZED GASES AT HIGH TEMPERATURES

Yu. P. RAĬZER

Submitted to JETP editor May 18, 1959

J. Exptl. Theoret. Phys. (U.S.S.R.) 37, 1079-1083 (October, 1959)

The optical absorption coefficients for multiply-ionized high-temperature gases are considered. A simple method is given by which it is possible to approximate rapidly the range of radiation averaged over the optical spectrum. This range determines the radiative thermal conductivity and emissivity of a gas at different temperatures and densities.

1. In the analysis of high-temperature phenomena it is usually necessary to consider the roles of radiative heat exchange and general radiation loss in determining the energy balance of a heated body. To determine these quantities, the mean range of the radiation must be known.

When the density of the gas is not too high the optical photons are generally absorbed in bound-free transitions of electrons from ground and excited states of ions (and atoms) and in free-free transitions. Bound-free transitions are not important energetically because of their small line widths.

At temperatures of the order of tens of thousands of degrees and higher, when the atoms are multiply ionized, the absorption is due to ions of different kinds. Hence, in computing the range for a given temperature and density it is necessary to determine the concentrations of various ions; this procedure involves the solution of a system of algebraic equations for ionization equilibrium, a task which is rather laborious. The labor involved is clearly not justified when one considers the fact that the "hydrogenic" approximation is generally used for establishing the effective absorption cross sections in complicated ions (and atoms); this approximation gives results which are probably never better than to within an order of magnitude.

Below we present a simple, rapid approximation method which can be used to estimate the mean range of radiation in any gas.

2. The total absorption factor for optical radiation of frequency ν by atoms which are ionized m times (m-ions) (bound-free) and by the field of (m+1)-ions (free-free) is[1]

$$\varkappa_{\nu m} = aN_m (m+1)^2 T^{-2} e^{-x_{1m}} F_m(x), \qquad (1)$$

where

$$a = (16\pi^2/3\sqrt{3})\, e^6/chk = 0.96\cdot 10^{-7}\ \text{cm}^2\text{-deg}^2, \qquad (2)$$

$$x = h\nu/kT, \quad x_{1m} = I_{m+1}/kT, \qquad (3)$$

I_{m+1} is the ionization potential of the m-ion and N_m is the number of m-ions in one cubic centimeter. The frequency dependence is given by the factor

$$F_m(x) = x^{-3}\left[2x_{1m}\sum_n n^{-3}\exp(x_{1m}/n^2) + 1\right]. \qquad (4)$$

The summation is taken over all levels with principle quantum number n from which a photon $h\nu$ can eject an electron, i.e., $x_{1m}/n^2 < x$.

As has been indicated by Unsöld,[1] because the field in non-hydrogenic atoms and ions is not a true Coulomb field, each level characterized by the number n is split into $2n^2$ levels. For this reason we can replace the summation over n by integration from the lower limit $x = x_{1m}/n^2$:

$$F_m(x) \approx x^{-3}e^x, \quad x < x_{1m}. \qquad (5)$$

Equation (5) does not hold when $x > x_{1m}$, because all levels contribute to the absorption and the summation in (4) yields a constant. The dominant role in this case is played by the ground level n = 1; hence we can write

$$F_m(x) \approx 2x_{1m}x^{-3}e^{x_{1m}}, \quad x > x_{1m}. \qquad (6)$$

The total absorption factor $\varkappa_\nu$ is obtained if we sum $\varkappa_{\nu m}$ over all ions, i.e., over m (for simplicity we assume that the gas consists of atoms of one element only).

The radiative thermal conductivity is determined from the Rosseland mean-free path defined by

$$l = \int_0^\infty \frac{G(x)\,dx}{\varkappa_\nu (1 - e^{-x})}, \quad G(x) = \frac{15}{4\pi^4}\,\frac{x^4 e^{-x}}{(1-e^{-x})^2}. \qquad (7)$$

The integrated emissivity of the gas is determined from the mean absorption coefficient

$$\varkappa_1 = 1/l_1 = \int_0^\infty \varkappa_\nu (1 - e^{-x})\, G_1(x)\,dx,$$

$$G_1(x) = 15\pi^{-4}x^3/(e^x - 1) \qquad (8)$$

3. Substituting κ_ν from (5) and (6) in (8) and computing the integral, we have

$$\varkappa_1 = 1/l_1 = (45a/\pi^4T^2)\sum_m N_m (m+1)^2 x_{1m} e^{-x_{1m}}. \quad (9)$$

In the expression for the Rosseland mean free path in (7) we have

$$l = \frac{T^2}{a}\int_0^\infty \frac{G(x)(1-e^{-x})^{-1}\,dx}{\sum_m N_m (m+1)^2 e^{-x_{1m}} F_m(x)}. \quad (10)$$

We cannot avoid integration over the spectrum, as in the case of κ_1, since here we do not average the absorption coefficient itself, but its reciprocal.

According to (5), all ions have the same absorption in their transmission bands, [for $x < x_{1m}$ ($h\nu < I_{m+1}$)]. The upper limit on the integral in (10) is the lowest transmission limit associated with ions which are present in sufficient number to make an important contribution in the summation over m.

At a given temperature and density the gas contains appreciable numbers of ions of two or three kinds. If the densities are not too high these ions have ionization potentials which are much higher than kT, so that their transmission limits x_{1m} are at the limits of the region of the spectrum which gives the main contribution in the integral in (10) [the maximum of the weighting function G(x) occurs at $x \approx 4$].

For this reason, as an approximation we can neglect the dependence of $F_m(x)$ on m, the charge of the ion, and take this function out from under the summation in (10); also, we can extend the expression in (5) to the region $x > x_{1m}$ (the integral still converges rapidly). The integral which results has been computed by Unsöld[1] and its value is 0.87. We have

$$l = (0.87T^2/a)\left\{\sum_m N_m (m+1)^2 e^{-x_{1m}}\right\}^{-1}. \quad (11)$$

4. The summations over m in (9) and (11) are carried out by a method which has been used earlier.[2]

We regard the ion concentration N_m and the ionization potential I_m as continuous functions of the number m and replace the summation in (9) and (11) by integration.*

The ion distribution function N(m) has a narrow peak whose skirts fall off more rapidly than the quantity $\exp\{-x_1(m)\}$ increases with decreasing m (cf. Appendix). Hence we can take out the mean value of the factors as averaged over the distribution function N(m). Then

$$l_1 = (\pi^4/45a)(T^2/N)\exp(\bar{x}_1)/(\bar{m}+1)^2\bar{x}_1,$$
$$l = (0.87/a)(T^2/N)\exp(\bar{x}_1)/(\bar{m}+1)^2, \quad (12)$$

where $N = \sum_m N_m$ is the number of original atoms per cubic centimeter. The mean charge $\bar{m}$ (obviously equal to the number of free electrons in the atom) and the potential $\bar{x}_1$ are determined in the same approximation from the Saha equations for N_m. As has been shown in reference 2, $\bar{m}$ can be found from the elementary transcendental equation

$$\bar{x}_1 = I(\bar{m}+1/2)/kT = \ln(AT^{3/2}/N\bar{m}),$$
$$A = 2(2\pi m_e k/h^2)^{3/2} = 4.8\cdot 10^{15}\ \mathrm{cm^{-3}\,deg^{-3/2}}. \quad (13)$$

Substituting (13) in (12) and introducing the numerical values of the constants, we obtain the final formulas for the mean ranges:

$$l_1 = 1.1\cdot 10^{23}T^{7/2}/N^2\bar{m}(\bar{m}+1)^2 x_1\ \mathrm{cm},$$
$$l = 4.4\cdot 10^{22}T^{7/2}/N^2\bar{m}(\bar{m}+1)^2\ \mathrm{cm}. \quad (14)$$

5. An idea of the numerical values of the ranges and the mean values of the ion charges and potentials, can be obtained from the Table, which shows

T, deg		N/N_{norm} = 1	10^{-1}	10^{-2}
50 000	$\bar{m}$	1.4	1.85	2.35
	$\bar{x}_1$	6.65	8.6	10.7
	l, cm	0.0053	0.28	17
	l_1, cm	0.002	0.08	3.9
100 000	$\bar{m}$	2.72	3.47	4.1
	$\bar{x}_1$	6.52	8.85	10.7
	l, cm	0.013	0.7	47
	l_1, cm	0.005	0.2	11

the results of a calculation for air.* In the region of T and N being considered the dependence of range on these quantities is given roughly by the relations

$$l \sim T^{1.35}N^{-1.80}, \qquad l_1 \sim T^{1.35}N^{-1.68}.$$

As an example of an emissivity calculation we find the radiative cooling rate of transparent (in the sense that $R \ll l_1$) air at $T = 50{,}000°$ and density $N/N_{norm} = 10^{-2}$. We have $j = 4\sigma T^4/l_1 = 3.6\times 10^{14}$ erg/cm^3·sec. The internal energy under these conditions is $\epsilon = 83$ ev/atom,[2] so that the initial cooling rate is $\epsilon/j = 1.9\times 10^{-7}$ sec.

*The function I(m) is plotted graphically by drawing a continuous curve through the discrete points (I_m) taken from appropriate tables.[3] The curves meet at the point I(0) = 0 [the ionization potential of the neutral atom is denoted by $I_1 = I(1)$].

*The ionization potentials for oxygen and nitrogen are taken as averages corresponding to the percentage content of these components.

The error introduced by the approximation used in calculating the summations in (9) and (11), as can be seen by comparison with the exact values computed from the data of Selivanov and Shlyapintokh[4] on ionization equilibrium in air, is found to be very small. In any case this error is much smaller than the possible errors which arise because of the "hydrogenic" approximation.

I wish to express my gratitude to Ya. B. Zel'dovich for his interest in this work and to V. S. Imshennik for a discussion of the results.

APPENDIX

ION CHARGE DISTRIBUTION IN MULTIPLE IONIZATION

Assuming for simplicity that the ratio of the statistical weights of the electronic states of the ions in the Saha formulas is unity we have

$$N_{m+1}N_e/N_m = 2(2\pi m_e kT/h^2)^{3/2}\exp\{-I_{m+1}/kT\}.$$

Combining the equations for different values of m = 0, 1, 2, ... and using the definition of the "average potential" (13), we have ($\bar{m} = N_e/N$)

$$N_{m+n}/N_m = \exp\left[-\sum_{l=1}^{n}(I_{m+l}-\bar{I})/kT\right],$$

$$N_{m-n}/N_m = \exp\left[-\sum_{l=0}^{n}(\bar{I}-I_{m-l})/kT\right], \qquad (15)$$

where n = 1, 2, 3, ... We take the value of m for which N_m is a maximum. $\bar{I}$ corresponds approximately to the potential of the same atoms so that all the terms in the summations are positive and the ion concentration falls off on both sides of the maximum.

In Eq. (15) we convert to the continuous functions N(m) and I(m) and write as an approximation:

$$I(m) \approx \bar{I} + (dI/dm)_{\bar{m}+1/2}(m-\bar{m}),$$

obtaining the Gaussian distribution

$$N(m) = N_{max}\exp\left[-\left(\frac{m-\bar{m}}{\Delta}\right)^2\right],$$

$$\Delta = [2kT/(dI/dm)_{\bar{m}+1/2}]^{1/2} < (2kT\bar{m}/\bar{I})^{1/2} = (2\bar{m}/\bar{x}_1)^{1/2}, \qquad (16)$$

if it is assumed that on the average dI/dm > I/m.

Taking the quantities $\bar{m}$ and $\bar{x}_1$ from the table, we see that the half width of the peak $\Delta \lesssim 1$, i.e., the peak is actually quite narrow.

[1] A. Unsöld, Physics of the Stellar Atmospheres, IIL (1949) (Russ. Transl.).

[2] Yu. P. Raĭzer, JETP **36**, 1583 (1959); Soviet Phys. JETP **9**, 1124 (1959).

[3] Kaye and Laby, Tables of Physical and Chemical Constants, Longmans, N.Y. 1948, (Russ. Transl. IIL 1949).

[4] V. V. Selivanov, and I. Ya. Shlyapintokh, J. Chem. Phys. (U.S.S.R.) **32**, 670 (1958).

Translated by H. Lashinsky
210

RADIATIVE CAPTURE OF NEUTRONS

D. F. ZARETSKIĬ

Submitted to JETP editor May 19, 1959

J. Exptl. Theoret. Phys. (U.S.S.R.) **37**, 1084-1087 (October, 1959)

An expression for the partial width of the radiative capture of neutrons in states described by shell model wave functions is derived. It is shown that in the case of s neutrons this width is proportional to the reduced neutron width for these neutrons. The relative probabilities for transitions to the $2p_{1/2}$ and $2p_{3/2}$ shell model states are calculated for a number of nuclei. The intensity ratios thus obtained are in good agreement with experiment.

THE spectrum of the γ quanta resulting from the capture of thermal neutrons by nuclei has some characteristic features, which were noticed by Groshev and collaborators.[1,2] For a number of light nuclei and nuclei of intermediate atomic weight intensive single lines are observed, which are mainly due to electric dipole transitions into the shell model states $2p_{1/2}$ and $2p_{3/2}$. The above-mentioned authors also measured the intensity ratios for the transitions into these states.

We shall give below an interpretation of these transitions in terms of the model of Lane, Thomas, and Wigner.[3] The wave function of the compound nucleus for excitation energies of the order of the neutron binding energy can be written in the form (for A nucleons)

$$\psi_\lambda = \sum_{c,\,k} C^\lambda_{c,\,k}\varphi_c u_k(\mathbf{r}_A), \tag{1}$$

where $\varphi_c(\mathbf{r}_1, \ldots, \mathbf{r}_{A-1})$ is a complete system of residual nucleus wave functions, and $u_k(\mathbf{r}_A)$ is a complete system of wave functions for a single nucleon in the self-consistent field of the nucleus.

We further assume that the wave function of the final state of the nucleus can be written in the form

$$\psi_0 = \varphi_0 u_p(\mathbf{r}_A), \tag{2}$$

where $\varphi_0(\mathbf{r}_1, \ldots, \mathbf{r}_{A-1})$ is the wave function corresponding to the unexcited residual nucleus, and $u_p(\mathbf{r}_A)$ is the wave function of the nucleon in the final state.

The dipole transition operator for a system of A nucleons with account of the effective charge of the neutrons and protons, arising as a result of the separation of the motion of the center of mass of the system, has the form[4]

$$Q_{1m} = \sum_{n=1}^{A} Q^{(n)}_{1m}, \qquad Q^{(n)}_{1m} = e_{eff} r_n Y^*_{1m}(\theta_n, \varphi_n), \tag{3}$$

where $Q^{(n)}_{1m}$ is the dipole transition operator for the n-th nucleon.

Let us now calculate the matrix element for the transition from the initial into the final state, $M_{1m} = \langle\lambda|Q_{1m}|0\rangle$. For this purpose we separate out of the expansion (1) the wave function corresponding to the incoming channel,

$$\psi_\lambda = C^\lambda_{0s}\varphi_0 u_s(\mathbf{r}) + \sum_{c,k}{}' C^\lambda_{ck}\varphi_c u_k(\mathbf{r}), \tag{4}$$

where the prime on the summation sign denotes the exclusion of the state corresponding to the incoming channel. It is then easily seen that

$$M_{1m} = \sum_{c,k}{}' C^\lambda_{ck}\langle\varphi_c u_k \left| \sum_{n=1}^{A-1} Q^{(n)}_{1m} \right| \varphi_0 u_p\rangle + C^\lambda_{0s}\langle u_s|Q^{(A)}_{1m}|u_p\rangle + \sum_{c,k}{}' C^\lambda_{ck}\langle\varphi_c u_k|Q^{(A)}_{1m}|\varphi_0 u_p\rangle. \tag{5}$$

The level width of the k-th single nucleon state, W_k, resulting from the transition of the whole system into a compound nucleus state, can be determined from the formula

$$W^2_k = \sum_\lambda (E_\lambda - E_{ck})^2 |C^\lambda_{ck}|^2 = \langle c, k|v^2|c, k\rangle, \tag{6}$$

where v is the operator of the potential energy of the interaction of a given nucleon with all the others Let us consider the case

$$\overline{D}_\lambda \ll W_k \ll \Delta E_k, \tag{7}$$

where $\overline{D}_\lambda$ is the average distance between the compound nucleus levels, and ΔE_k is the distance between the single particle levels in the self-consistent field of the nucleus. It is shown in the paper of Lane, Thomas, and Wigner that in this case

$$W^2_k = B^2/\zeta^2_k, \qquad B^2 = \int (E_\lambda - E_{ck})^2 S^{(k)}_\lambda dE_\lambda,$$

$$S^{(k)}_\lambda = \gamma^2_{\lambda,k}/\overline{D}_\lambda, \qquad \zeta^2_k = (a\hbar^2/2M) R^2_k(a), \tag{8}$$

where $S^{(k)}_\lambda$ is the strength function, $\gamma^2_{\lambda,k}$ is the reduced neutron width, ζ^2_k is the reduced single particle width, a is the radius of the nucleus,

$R_k(a)$ is the value of the radial nucleon wave function on the surface of the nucleus, and M is the mass of the nucleon.

For the nuclei of interest to us we have $\zeta^2 \sim 1$ Mev. The energy width of the strength function for s neutrons is, according to experiment, of the order of several Mev. The width of interest to us, W_s, is therefore also of the order of a few Mev. With the help of these estimates we can now draw conclusions as to which of the terms in expression (5) plays the most important role.

It should be noted, first of all, that we can neglect the contribution to the sum (5) of all single particle states with an energy separation $\Delta E_k \gg W_k$. If the wave function $u_p(r)$ corresponds to a p state, then we should keep only s states in the last term.* The energy separation between s levels with different principal quantum numbers is of the order ~ 15 Mev. We can therefore neglect the contribution of s states with principal quantum numbers different from that of the incoming channel.

Only the terms with index k = p should be kept in the first sum in (5). However, if the spacing between adjacent s and p single-nucleon levels is $\Delta E_{sp} \gg W_s$, the whole first sum can be neglected. If all the above-mentioned conditions are fulfilled, we get the result

$$|M_{1m}|^2 = |C_{0s}^{\lambda}|^2 |\langle u_s | Q_{1m}^{(A)} | u_p \rangle|^2. \quad (9)$$

The coefficient $|C_{0s}^{\lambda}|^2$ is simply related to the reduced neutron width, which can be determined from experiment:

$$\gamma_{\lambda,s}^2 = (a\hbar^2/2M)|C_{0s}^{\lambda}|^2 R_s^2(a) = |C_{0s}^{\lambda}|^2 \zeta_s^2. \quad (10)$$

Let us estimate the order of magnitude of the matrix element (9). For this purpose we consider the normalization condition

$$\sum_{\lambda} |C_{0s}^{\lambda}|^2 = 1. \quad (11)$$

The terms of the summation are significantly different from zero in the interval $\Delta E_\lambda \sim W_s$. Therefore

$$\overline{|C_{0s}^{\lambda}|^2} \approx 1/\rho_0 W_s,$$

where ρ_0 is the level density of the compound nucleus with a given value for the nuclear moment, corresponding to the capture of a thermal neutron. As a result we find for the partial width for the transition under consideration

$$\Gamma_p \approx \Gamma_{single}/\rho_0 W_s, \quad (12)$$

where Γ_{single} is the width for a single-particle transition in the self-consistent nuclear field with neglect of compound nucleus formation. In those cases where Γ_p is known (Si^{29}, S^{33}), relation (12) is confirmed by the experimental data. At the same time we find that $W_s \sim 1$ Mev.

Let us now calculate the ratio of the transition probabilities to the states $2p_{1/2}$ and $2p_{3/2}$. The wave function of the initial state can in this case be written in the form

$$u_s = R_s(r)\chi_{1/2,m_s}/\sqrt{4\pi}, \quad (13)$$

where $R_s(r)$ satisfies the boundary condition[4]

$$a(\partial R_s/\partial r)/R_s|_{r=a} = ik_s a, \quad (14)$$

where k_s is the wave number of the neutron outside the nucleus, corresponding to the energy at which the maximum of the strength function S_λ is observed; $\chi_{1/2,m_s}$ is the spin function.

The wave function of the final state has the form

$$u_p(r) = R_p^j(r) Y_{j,m_j},$$

$$Y_{j,m_j} = \sum_{m_s m} (1/2\,1 m_s m | j m_j 1/2\,1) Y_{1m}(\theta,\varphi)\chi_{1/2,m_s}, \quad (15)$$

where R_p^j is the radial wave function of the p state of the nucleon with total angular momentum $j = 1/2$ and $j = 3/2$. Using the wave functions (13) and (15), we obtain the ratio of the partial widths for transitions to states with different values j in the form

$$\frac{\Gamma_\gamma^{(3/2)}}{\Gamma_\gamma^{(1/2)}} = 2\left(\frac{\omega_{3/2}}{\omega_{1/2}}\right)^3 \left|\int_0^\infty R_p^{(3/2)} R_s r^3 dr\right|^2 \Big/ \left|\int_0^\infty R_p^{(1/2)} R_s r^3 dr\right|^2, \quad (16)$$

where $\omega_{3/2}$ and $\omega_{1/2}$ are the frequencies for the corresponding transitions.

The matrix elements in (14) can be calculated with the help of the known matrix relations

$$\langle\alpha|\ddot{r}|\beta\rangle = -\omega_{\alpha,\beta}^2\langle\alpha|r|\beta\rangle = -\frac{1}{M}\left\langle\alpha\left|\frac{\partial U}{\partial r}\right|\beta\right\rangle, \quad (17)$$

where U(r) is the self-consistent nuclear potential; $\partial U/\partial r$ is different from zero only near the surface of the nucleus. Let us estimate the magnitude of the logarithmic derivative $f_p^j = (\partial R_p^j/\partial r)/R_p^j\big|_{r=a}$. If $\kappa_j a \gg 1$, we have

$$f_p' = \varkappa_j \equiv \sqrt{2ME_j}/\hbar, \quad (18)$$

where E_j is the binding energy for the given level. If the neutron is captured by a nucleus for which S_λ is close to the maximum, we have $k_s \ll \kappa_j$. In this case

$$\frac{\Gamma_\gamma^{(3/2)}}{\Gamma_\gamma^{(1/2)}} = 2\left(\frac{\omega_{1/2}}{\omega_{3/2}}\right)\left|\int_0^\infty R_p^{(3/2)}\frac{\partial U}{\partial r} r^2 dr\right|^2 \Big/ \left|\int_0^\infty R_p^{(1/2)}\frac{\partial U}{\partial r} r^2 dr\right|^2. \quad (19)$$

To calculate the value of the ratio (19) we used

*d states do not give a contribution, since they can, in our case, combine only with excited states of the residual nucleus.

a potential U(r) of the form

$$U(r) = V(0)/[1 + e^{\alpha(r-r_0)}], \quad \alpha = \sqrt{2MV(0)}/\hbar. \qquad (20)$$

The wave functions for the single-particle $2p_{1/2}$ and $2p_{3/2}$ states and the parameters V(0) and r_0 were taken from Nemirovskiĭ:[5]

$$V(0) = 50\,\text{MeV}, \quad \alpha r_0 = 1.98\,A^{1/3}\,[1 - 0.5\,(0.5 - Z/A)]. \qquad (21)$$

In the table we compare the results of our calculations with the measured ratios (19) for those nuclei in which the $2p_{1/2}$ and $2p_{3/2}$ levels are identified. For the nuclei listed in the table, the single-particle 3s resonance occurs near the neutron binding energy.

Value of $\Gamma_\gamma^{(3/2)}/\Gamma_\gamma^{(1/2)}$

Nucleus	Experiment	By formula (19)	By formula (22)
Si^{29}	3	4.0	10
S^{33}	3.5	3.7	12
Ca^{41}	2	3.5	6
Ni^{59}	2.7	3.0	4.6

In the last column of the table we give the ratios of the widths as computed by the Weisskopf formula[4]

$$\Gamma_\gamma^{(3/2)}/\Gamma_\gamma^{(1/2)} = 2\,(\omega_{3/2}/\omega_{1/2})^3. \qquad (22)$$

It is seen from the table that our estimate is in satisfactory agreement with experiment, while formula (22) gives too high values for the ratio of the corresponding intensities.

In conclusion the author expresses his gratitude to P. É. Nemiroskiĭ for providing the tabulated values of the wave functions and also to L. V. Groshev and A. M. Demidov for an evaluation of the experimental data.

[1] L. V. Groshev and A. M. Demidov, Атомная энергия (Atomic Energy) **3**, 91 (1957).

[2] Groshev, Demidov, Lutsenko, and Pelekhov, Report at the Second Geneva Conference on the Peaceful Use of Atomic Energy, P/2029 (1958).

[3] Lane, Thomas, and Wigner, Phys. Rev. **98**, 693 (1955).

[4] J. Blatt and V. Weisskopf, Theoretical Nuclear Physics, J. Wiley and Sons, N.Y. (1952) (Russ. Transl., IIL, 1954).

[5] P. É. Nemirovskiĭ, JETP **36**, 588 (1959), Soviet Phys. JETP **9**, 408 (1959). Report at the Ninth All-Union Conference on Nuclear Spectroscopy, January, 1959.

Translated by R. Lipperheide
211

EQUILIBRIUM OF A PLASMA TOROID IN A MAGNETIC FIELD

V. D. SHAFRANOV

Submitted to JETP editor, May 19, 1959

J. Exptl. Theoret. Phys. (U.S.S.R.) **37**, 1088-1095 (October, 1959)

The equilibrium conditions for a plasma toroid with a distributed current in a magnetic field are obtained.

1. INTRODUCTION

In the present work we derive exact solutions for the equilibrium of a toroidal pinch with axial symmetry. As has been shown earlier,[1] a bound, axially symmetric, plasma configuration can be in equilibrium in a magnetic field only if there is a nonvanishing azimuthal current component j_φ. It has also been shown that for equilibrium to obtain the current density j_φ must be of the form

$$j_\varphi(r, z) = Ar + B/r, \tag{1}$$

where r is the distance from the axis of symmetry and A and B are arbitrary functions which are constant over surfaces of equal plasma pressure. The plasma pressure p and the functions

$$\psi = \int_0^r H_z 2\pi r dr, \qquad I = \int_0^r j_z 2\pi r dr = crH_\varphi/2, \tag{2}$$

through which the r and z components of the magnetic field and current are expressed, are interdependent. The functions A and B are expressed in terms of ψ and I in the following way:

$$A(\psi) = 2\pi c \frac{dp(\psi)}{d\psi}, \qquad B(\psi) = \frac{1}{c}\frac{dI^2(\psi)}{d\psi}. \tag{3}$$

The function ψ, which is related to the azimuthal component of the vector potential of the magnetic field A_φ, is given by the following equation (in cylindrical coordinates):

$$\frac{\partial^2\psi}{\partial r^2} - \frac{1}{r}\frac{\partial\psi}{\partial r} + \frac{\partial^2\psi}{\partial z^2} = -\frac{8\pi^2}{c} r j_\varphi = -\frac{8\pi^2}{c}[A(\psi) r^2 + B(\psi)]. \tag{4}$$

Given the actual form of the functions $A(\psi)$ and $B(\psi)$, it is possible in principle to solve this equation and then, knowing $\psi(r, z)$, to find the distribution of all quantities which characterize equilibrium. In this case, if the geometric configuration is given the conditions at infinity (or at external conductors) cannot be chosen arbitrarily since they are determined by the solutions of the problem. On the other hand, if the conditions at infinity or at the external conductors are given the geometric configuration is no longer arbitrary. In practice, it is obviously more convenient to assign the cross section of the pinch in the r-z plane and to use the coordinate system most convenient for solution of the problem. Below we consider a pinch of circular cross section with fixed values of A and B.

2. TOROIDAL COORDINATES

The most convenient coordinate system is the usual toroidal coordinate system, defined by ϑ, ω, and φ:

$$r = R_0 \sinh\vartheta/(\cosh\vartheta - \cos\omega),$$

$$z = R_0 \sin\omega/(\cosh\vartheta - \cos\omega). \tag{5}$$

Here $\vartheta = \vartheta_0$ defines the cross section of the toroidal pinch. The small and large radii of the toroid are then

$$a = R_0/\sinh\vartheta_0, \qquad R = R_0 \coth\vartheta_0. \tag{6}$$

Values for which $\vartheta > \vartheta_0$ correspond to the inner part of the toroid while values for which $\vartheta < \vartheta_0$ correspond to the outer part. In toroidal coordinates the components of the magnetic field are expressed in terms of ψ as follows:

$$H_\vartheta = \frac{(\cosh\vartheta - \cos\omega)^2}{2\pi R_0^2 \sinh\vartheta}\frac{\partial\psi}{\partial\omega}, \qquad H_\omega = -\frac{(\cosh\vartheta - \cos\omega)^2}{2\pi R_0^2 \sinh\vartheta}\frac{\partial\psi}{\partial\vartheta}. \tag{7}$$

The current density components j_ϑ, j_ω are expressed in terms of $I(\vartheta, \omega)$ in similar fashion.

As Fock has shown,[2] the variables can be separated in the homogeneous equation for the vector potential. Thus Eq. (4) can be solved easily if the right-hand side is independent of ψ, i.e., if

$$A = \text{const}, \qquad B = \text{const}. \tag{8}$$

This simple case is the one which is considered in the present paper.

If A and B are constant the particular solution of the inhomogeneous equation (4) is

$$\psi_1 = -(4\pi^2/c)(Ar^2 + B)z^2. \tag{9}$$

In order to find the general solution of the corre-

sponding homogeneous equation, following Fock we introduce the auxiliary function $F(\vartheta, \omega)$ which is related to $\psi(\vartheta, \omega)$ by the expression

$$\psi(\vartheta, \omega) = F(\vartheta, \omega)/\sqrt{2(\coth\vartheta - \cos\omega)}. \quad (10)$$

In toroidal coordinates, Eq. (4) for the function F becomes

$$\frac{\partial^2 F}{\partial\vartheta^2} + \frac{\partial^2 F}{\partial\omega^2} - \coth\vartheta\frac{\partial F}{\partial\vartheta} + \frac{1}{4}F = -\frac{32\pi^2 R_0^2}{c\,[2(\cosh\vartheta - \cos\omega)]^{5/2}}$$

$$\times\left[\frac{4AR_0^2\sinh^2\vartheta}{[2(\cosh\vartheta - \cos\omega)]^2} + B\right]. \quad (11)$$

The solution can be written as a Fourier series in ω:

$$F = F_0(\vartheta) + 2\sum_{n=1}^{\infty} F_n(\vartheta)\cos n\omega. \quad (12)$$

Following Fock we take the linearly independent solutions of the homogeneous equation for F to be*

$$g_n(\vartheta)\cos n\omega, \qquad f_n(\vartheta)\cos n\omega, \quad (13)$$

$$g_n(\vartheta) = \frac{1}{2\pi}\int_0^{2\pi}\sqrt{2(\cosh\vartheta - \cos\omega)}\cos n\omega\, d\omega.$$

$$f_n(\vartheta) = \frac{1}{2\pi}\int_{-\vartheta}^{\vartheta}\sqrt{2(\cosh\vartheta - \cosh t)}\cosh nt\, dt. \quad (15)$$

The Wronskian is

$$f_n\frac{dg_n}{d\vartheta} - g_n\frac{df_n}{d\vartheta} = \frac{\sinh\vartheta}{\pi(n^2 - 1/4)}. \quad (16)$$

The equation by which the functions f_n and g_n are obtained is

$$\frac{d^2 g_n}{d\vartheta^2} - \coth\vartheta\frac{dg_n}{d\vartheta} - \left(n^2 - \frac{1}{4}\right)g_n = 0. \quad (17)$$

The function $f_n(\vartheta)$ becomes infinite at the center of the toroid $\vartheta = \infty$, but is finite (as are its derivatives) in the outer region. Hence, we cannot use the function $g_n(\vartheta)$ in the inner region. Since it is impossible to satisfy the condition that the field vanish at infinity for the outer problem, we must use both linearly independent solutions.

We note that the particular solution for ψ in (9) corresponds to the following particular solution for F:

$$F_1 = -\frac{16\pi^2 R_0^2}{c}\frac{\sinh^2\omega}{[2(\cosh\vartheta - \cos\omega)]^{5/2}}$$

$$\times\left[4AR_0^2\frac{\sinh^2\vartheta}{[2(\cosh\vartheta - \cos\omega)]^{5/2}} + B\right]. \quad (18)$$

*These functions are related to the Legendre functions $P_{n-1/2}$, $Q_{n-1/2}$ by the following expressions (cf. reference 2):

$$(n^2 - 1/4)f_n(\vartheta) = \sinh\vartheta\, dP_{n-1/2}(\cosh\vartheta)/d\vartheta,$$

$$(n^2 - 1/4)g_n(\vartheta) = \sinh\vartheta\, dQ_{n-1/2}(\cosh\vartheta)/d\vartheta.$$

We expand this solution in a Fourier series

$$-F_1 = \gamma_0(\vartheta) + 2\sum_{n=1}^{\infty}\gamma_n(\vartheta)\cos n\omega. \quad (19)$$

In place of the constants A and B, which determine the current density j_φ, we introduce the total volume current J_φ through the cross section $\vartheta > \vartheta_0$, and the partial current J_p:

$$J_\varphi = \int_{\vartheta>\vartheta_0} j_\varphi dr dz = \int_{\vartheta>\vartheta_0}(Ar + B/r)\, dr dz \quad (20)$$

$$= J_p + 2\pi BR_0/e^{\vartheta_0}\sinh\vartheta_0,$$

$$J_p = \int_{\vartheta>\vartheta_0} A r dr dz = \pi AR_0^3\cosh\vartheta_0/\sinh^3\vartheta_0. \quad (21)$$

The Fourier coefficients $\gamma_n(\vartheta)$ in (19) are written in the form

$$\gamma_n(\vartheta) = \frac{8\pi}{c}R_0 J_p\frac{\sinh^3\vartheta_0}{\cosh\vartheta_0}\left[8\alpha_n(\vartheta) - \frac{\cosh\vartheta_0 e^{\vartheta_0}}{\sinh\vartheta_0}\beta_n(\vartheta)\right]$$

$$+\frac{8\pi}{c}R_0 J_\varphi\sinh\vartheta_0 e^{\vartheta_0}\beta_n(\vartheta), \quad (22)$$

where

$$\beta_n(\vartheta) = \frac{1}{2\pi}\int_0^{2\pi}\frac{\sin^2\omega\cos n\omega\, d\omega}{[2(\cosh\vartheta - \cos\omega)]^{5/2}}$$

$$= \coth\vartheta\frac{dg_n(\vartheta)}{d\vartheta} + \left(n^2 - \frac{1}{4}\right)g_n(\vartheta), \quad (23)$$

$$\alpha_n(\vartheta) = \frac{1}{2\pi}\int_0^{2\pi}\frac{\sin^2\omega\sinh^2\vartheta}{[2(\cosh\vartheta - \cos\omega)]^{5/2}}\cos n\omega\, d\omega$$

$$= \frac{1}{15}\left[\frac{d^2\beta_n(\vartheta)}{d\vartheta^2} - \frac{d\beta_n(\vartheta)}{d\vartheta}\coth\vartheta\right].$$

The latter expressions for α_n and β_n are easily obtained by differentiating (14) with respect to ϑ, using Eq. (17).

3. GENERAL SOLUTION

In accordance with (10) – (12), the solution for ψ can be written in the form

$$\psi = [2(\cosh\vartheta - \cos\omega)]^{-1/2}\left[F_0(\vartheta) + 2\sum_{n=1}^{\infty}F_n(\vartheta)\cos n\omega\right]. \quad (25)$$

The plasma pressure vanishes at the surface of the toroid $\vartheta = \vartheta_0$ (or is constant); consequently the function $\psi(\vartheta_0, \omega)$ can be taken as a constant. We can set this constant equal to zero so that

$$\psi(\vartheta_0, \omega) = 0. \quad (26)$$

The expansion coefficients $F_n(\vartheta)$ which satisfy Eq. (26) for the inner and outer regions are

$$F_{in} = \frac{\gamma_n(\vartheta_0)}{g_n(\vartheta_0)} g_n(\vartheta) - \gamma_n(\vartheta), \tag{27}$$

$$F_{en} = C_n \left[g_n(\vartheta) - \frac{g_n(\vartheta_0)}{f_n(\vartheta_0)} f_n(\vartheta) \right]. \tag{28}$$

We assume that outside the volume current there is an azimuthal surface current J_S whose density is constant at equilibrium $j_S = \frac{\sinh \vartheta_0}{2\pi R_0} J_S$ = const; this azimuthal current component is equal to the current discontinuity in the tangential component of the magnetic field H_ω:

$$\frac{4\pi}{c} j_S = \frac{2J_S}{cR_0} \sinh \vartheta_0 = \{H_\omega\} = \frac{[2(\cosh\vartheta_0 - \cos\omega)]^{3/2}}{8\pi R_0^2 \sinh\vartheta_0} \left\{\frac{\partial F}{\partial \vartheta}\right\}, \tag{29}$$

where the symbol $\{\ldots\}$ denotes the discontinuity in the corresponding quantity at the point ϑ_0. We write this condition, which serves for determining the constant C_n, in another form:

$$\left\{\frac{\partial F}{\partial \vartheta}\right\} = 8\pi R_0^2 \frac{2J_S}{cR_0} \frac{\sinh^2\vartheta_0}{[2(\cosh\vartheta_0 - \cos\omega)]^{3/2}}$$

$$= \frac{16\pi R_0 J_S}{c} \left[\delta_0(\vartheta_0) + 2\sum_{n=1}^{\infty} \delta_n(\vartheta_0) \cos n\omega \right]. \tag{30}$$

Here

$$\delta_n(\vartheta) = \frac{1}{2\pi} \int_0^{2\pi} \frac{\sinh^2\vartheta}{[2(\cosh\vartheta - \cos\omega)]^{3/2}} \cos n\omega d\omega$$

$$= -\left(n^2 - \frac{1}{4}\right) g_n(\vartheta) \tag{31}$$

[the integral is easily expressed in terms of $g_n(\vartheta)$ by means of (14) and (17)].

Substituting the derivatives of F_{in} and F_{en} in Eq. (30) we determine the coefficients C_n:

$$C_n = -\frac{\pi(n^2 - 1/4) f_n(\vartheta_0)}{\sinh\vartheta_0} \left\{ \gamma_n'(\vartheta_0) - \gamma_n(\vartheta_0) \frac{g_n'(\vartheta_0)}{g_n(\vartheta_0)} + \frac{16\pi R_0 J_S}{c} \left(n^2 - \frac{1}{4}\right) g_n(\vartheta_0) \right\}. \tag{32}$$

The general solution is given by Eqs. (25), (27), (28), and (32). The magnetic field outside the toroid is determined in terms of ψ_e by means of Eq. (7). The field, currents and pressure inside the toroid are determined in terms of ψ_i. In accordance with Eqs. (3), (8), (20), and (21), the pressure p and the function $I = crH_\varphi/2$ are given by the formulas

$$p = \frac{J_p}{2\pi^2 c R_0^3} \frac{\sinh^2\vartheta_0}{\cosh\vartheta_0} \psi_i(\vartheta, \omega) + \frac{J_S^2 + 2J_\varphi J_S}{2\pi c^2 R_0^2} \sinh^2\vartheta_0, \tag{33}$$

$$I^2 = c \frac{e^{\vartheta_0} \sinh\vartheta_0}{2\pi R_0} (J_\varphi - J_p) \psi_i(\vartheta, \omega) + I_e^2. \tag{34}$$

The second term in p takes account of the discontinuity in the pressure due to the surface current and I_e is the current which produces the external longitudinal field.

4. EXTERNAL FIELD

To determine the field, produced by the external conductors in order to contain the plasma in equilibrium, from the total field determined by the function $\psi_e(\vartheta, \omega)$ it is necessary to subtract off the self-field of the current which flows in the toroid. To find the self-field, once again it is necessary to solve (11), but this time with different boundary conditions. In particular, in place of the requirement that ψ and j_S be constant at the surface of the toroid we impose the condition that the field must vanish at infinity. This means that the solution in the external region is composed only of the functions $f_n(\vartheta) \cos n\omega$. We write the final result:

$$F_{ni}^{self} = \left\{ \frac{\pi}{4\sinh\vartheta_0} (4n^2 - 1) \times [\gamma_n'(\vartheta_0) f_n(\vartheta_0) - \gamma_n(\vartheta_0) f_n'(\vartheta_0)] + \frac{1}{c} LJ_S \right\} \times g_n(\vartheta) - \gamma_n(\vartheta), \tag{35}$$

$$F_{ne}^{self} = \left\{ \frac{\pi(4n^2 - 1)}{4\sinh\vartheta_0} \frac{g_n(\vartheta_0)}{f_n(\vartheta_0)} [\gamma_n'(\vartheta_0) f_n(\vartheta_0) - \gamma_n(\vartheta_0) f_n'(\vartheta_0)] - \frac{\gamma_n(\vartheta_0)}{f_n(\vartheta_0)} + \frac{1}{c} LJ_S \frac{g_n(\vartheta_0)}{f_n(\vartheta_0)} \right\} f_n(\vartheta). \tag{36}$$

Here L is the self induction of a toroid with a strong skin effect:[2]

$$\frac{1}{L} = \frac{1}{2\pi^2 R_0} \left\{ \frac{g_0(\vartheta_0)}{f_0(\vartheta_0)} - 2\sum_{n=1}^{\infty} \frac{1}{4n^2 - 1} \frac{g_n(\vartheta_0)}{f_n(\vartheta_0)} \right\}. \tag{37}$$

Subtracting (36) from (28) we find the coefficients $F_n(\vartheta)$ which determine the external field required for equilibrium. We write the values at infinity, where the functions $f_n(\vartheta)$ vanish:

$$F_{ne}^{ext} = -\left\{ \frac{\pi^2 R_0 J_S}{c \sinh\vartheta_0} \left(n^2 - \frac{1}{4}\right)^2 g_n(\vartheta_0) f_n(\vartheta_0) + \frac{\pi(4n^2 - 1)}{4\sinh\vartheta_0} \times \left[\gamma_n'(\vartheta_0) - \gamma_n(\vartheta_0) \frac{g_n'(\vartheta_0)}{g_n(\vartheta_0)} \right] f_n(\vartheta_0) \right\} g_n(\vartheta). \tag{38}$$

In principle the formulas which have been obtained allow us to compute the magnetic field configuration required for containing a plasma toroid of arbitrary cross section radius a in equilibrium. The corresponding equilibrium conditions for the limiting case $a/R_0 \to 0$ have been obtained by Osovets[3] who equilibrated the expansion forces of the circular current $(J_\varphi^2/2c^2)\partial L/\partial R$ to the contraction forces of the ring in the perpendicular magnetic field $2\pi RJH/c$.

5. CASE OF SMALL CURVATURE

In order to obtain a general idea of the nature of the solutions which have been obtained we consider the case of small curvature $a/R_0 \ll 1$, i.e., $e^{\vartheta_0} \gg 1$. A detailed examination of the functions $g_n(\vartheta)$ and $f_n(\vartheta)$ has been given by Fock.[2] In the limit, when $\vartheta \to \infty$ we find $(n \geq 2)$

$$g_0 = e^{\vartheta/2}, \quad g_1 = -\frac{1}{2} e^{-\vartheta/2}, \quad g_n = -\frac{(2n-3)!!}{n!\,2^n} e^{-(n-1/2)\vartheta},$$

$$f_0 = \frac{2}{\pi} e^{\vartheta/2}(\vartheta + 2\ln 2 - 2), \quad f_1 = \frac{2}{3\pi} e^{3\vartheta/2},$$

$$f_n = \frac{2^n}{\pi} \frac{(n-1)!}{(2n+1)!!} e^{(n+1/2)\vartheta}. \tag{39}$$

Correspondingly, from (22) – (24) we have

$$\alpha_0 = \frac{1}{8} e^{-3\vartheta/2}, \quad \beta_0 = \frac{1}{2} e^{-3\vartheta/2}, \quad \gamma_0 = \frac{2\pi R_0 J_\varphi}{c} e^{2\vartheta_0 - 3\vartheta/2},$$

$$\alpha_1 = \frac{7}{32} e^{-5\vartheta/2}, \quad \beta_1 = \frac{3}{8} e^{-5\vartheta/2},$$

$$\gamma_1 = \frac{2\pi R_0}{c}\left(J_p + \frac{3}{4} J_\varphi\right) e^{2\vartheta_0 - 5\vartheta/2}. \tag{40}$$

We write all solutions, limiting ourselves to two terms in the Fourier expansion for F.

a) Self-field of the current:

$$\psi_e^{\text{self}} = [2(\cosh\vartheta - \cos\omega)]^{-1}\{(2\pi^2 R_0/c)(J_\varphi + J_S) f_0(\vartheta)$$
$$+ (6\pi^2 R_0/c) e^{-2\vartheta_0}[(J_p + {}^3/_4 J_\varphi)$$
$$- (\vartheta_0 + 2\ln 2 - 2) J_S] f_1(\vartheta)\cos\omega\}. \tag{41}$$

When $\vartheta_0 = \infty$ only the first term remains; this represents the field of a linear circular current. When $e^{\vartheta} \ll 1$ we obtain the approximation formula

$$\psi_e^{\text{self}} = (4\pi R_0/c)(J_\varphi + J_S)(\vartheta + 2\ln 2 - 2)$$
$$+ (4\pi R_0/c)\{(J_\varphi + J_S)(\vartheta + 2\ln 2 - 2) e^{-\vartheta}$$
$$+ [J_p + {}^3/_4 J_\varphi - (\vartheta_0 + 2\ln 2 - 2) J_S] e^{-2\vartheta_0 + \vartheta}\}\cos\omega. \tag{42}$$

b) The equilibrium field (38) can be expressed conveniently in polar coordinates. In the approximation being used here $e^{-\vartheta}\cos\omega = (r - R_0)/2R_0$ and ψ^{ext} is of the form

$$\psi^{\text{ext}} = -(4\pi R_0/c)(J_S + J_\varphi)(\vartheta_0 + 2\ln 2 - 2)$$
$$- \{(2\pi/c)(J_S + J_\varphi)(\vartheta_0 + 2\ln 2 - 2)$$
$$+ (3\pi/c)[J_S + {}^2/_3(J_p + {}^3/_4 J_\varphi)]\}(r - R_0). \tag{43}$$

The magnetic field is determined by the formulas

$$H_r = -\frac{1}{2\pi r}\frac{\partial\psi}{\partial z} = 0,$$

$$H_z = \frac{1}{2\pi r}\frac{\partial\psi}{\partial r} = -\frac{J_S}{cR_0}\left(\vartheta_0 + 2\ln 2 - \frac{1}{2}\right)$$
$$- \frac{J_\varphi}{cR_0}\left(\vartheta_0 + 2\ln 2 - \frac{5}{4}\right) - \frac{J_p}{cR_0}, \tag{44}$$

where $\vartheta_0 = \ln(2R_0/a)$. When $J_\varphi = J_p = 0$, Eq. (44) coincides with the results obtained in references 1 and 4, and when $J_S = 0$, $J_\varphi = J_p$ (no longitudinal field), (44) coincides with the results obtained in reference 1.

c) We now find the equilibrium distributions of various quantities:

$$\psi_i = (2\pi R_0 J_\varphi/c)(1 - e^{2\vartheta_0 - 2\vartheta})$$
$$+ (4\pi R_0/c)(J_p + {}^5/_4 J_\varphi) e^{-\vartheta}(1 - e^{2\vartheta_0 - 2\vartheta})\cos\omega,$$

$$\psi_e \approx -(4\pi R_0/c)(J_\varphi + J_S)(\vartheta_0 - \vartheta)$$
$$- (4\pi R_0/c) e^{-\vartheta}\{(\vartheta_0 - \vartheta)(J_\varphi + J_S)$$
$$+ (J_p + {}^3/_4 J_\varphi + {}^3/_2 J_S)(1 - e^{2\vartheta - 2\vartheta_0})\}\cos\omega \tag{45}$$

The quantities p and I, given by (33) and (34), can be expressed conveniently in a local polar coordinate system ρ, ω, and φ, defined by the relations

$$r = R_0 + \rho\cos\omega, \quad z = \rho\sin\omega. \tag{46}$$

We write the values of p, I, H_ω in the absence of a surface current:

$$p = \frac{J_\varphi J_p}{\pi c^2 a^2}\left(1 - \frac{\rho^2}{a^2}\right) + \frac{J_p(J_p + {}^5/_4 J_\varphi)}{\pi c^2 a^2}\frac{a}{R_0}\frac{\rho}{a}\left(1 - \frac{\rho^2}{a^2}\right)\cos\omega,$$

$$I^2 - I_e^2 = 2\pi c^2 R_0^2 \frac{J_\varphi - J_p}{J_p}\, p(\rho, \omega),$$

$$H_\omega = -\frac{2J_\varphi}{ca}\frac{\rho}{a} + \frac{J_p}{cR_0}\left(1 - \frac{3\rho^2}{a^2}\right)\cos\omega$$
$$+ \frac{5}{4}\frac{J_\varphi}{cR_0}\left(1 + \frac{\rho^2}{5a^2}\right)\cos\omega. \tag{47}$$

1. If $J_\varphi J_p < 0$, this configuration is possible only in the presence of an external pressure p_e. We limit ourselves to the first term in p:

$$p = p_e - \frac{|J_\varphi J_p|}{\pi c^2 a^2}\left(1 - \frac{\rho^2}{a^2}\right). \tag{48}$$

Since $J_\varphi(J_\varphi - J_p) > 0$, the longitudinal magnetic field inside the toroid is larger than the applied field. A configuration of this kind can be in equilibrium without external fields.[1] It follows from Eq. (44) that this case is possible for a distributed current if $J_p = -J_\varphi[\ln(8R_0/a) - {}^5/_4]$.

In this case

$$I^2 = 2J_\varphi^2 \frac{R_0^2}{a^2}\left(\ln\frac{8R_0}{a} - \frac{1}{4}\right)\left(1 - \frac{\rho^2}{a^2}\right). \qquad (49)$$

2. The case $J_\varphi = 0$ is also only possible when $p_e \neq 0$ and, furthermore, if $I_e \neq 0$:

$$p = p_e + \frac{J_p^2}{\pi c^2 a^2}\frac{a}{R_0}\frac{\rho}{a}\left(1 - \frac{\rho^2}{a^2}\right)\cos\omega,$$

$$I^2 = I_e^2 - 2J_p^2\frac{R_0}{a}\frac{\rho}{a}\left(1 - \frac{\rho^2}{a^2}\right)\cos\omega. \qquad (50)$$

The pressure in the inner part of the toroid is smaller, and in the outer part is larger, than the external pressure. The currents in these two sections flows in opposite directions.

3. When $J_\varphi J_p > 0$, it is possible to have a configuration which is bounded by a vacuum. The internal longitudinal magnetic field can either be larger than the external field $I^2 > I_e^2$ if $|J_\varphi| > |J_p|$, or smaller than the external field ($|J_p| > |J_\varphi|$). The first case corresponds to a "paramagnetic" pinch and the second to a "diamagnetic" pinch. The distribution inside the pinch is given by (47).

4. When $J_p = 0$ we have the force-free field $p = \text{const}$. The internal longitudinal field is larger than the external field:

$$I^2 - I_e^2 = \frac{2R_0^2}{a^2}J_\varphi^2\left(1 - \frac{\rho^2}{a^2}\right) + \frac{5}{2}\frac{R_0}{a}J_\varphi^2\frac{\rho}{a}\left(1 - \frac{\rho^2}{a^2}\right)\cos\omega. \qquad (51)$$

In conclusion we compare the distribution in the toroid with the distribution in a cylinder. The quantities j_φ, H_φ, ψ, and H_ω in the toroid correspond to j_z, H_z, A_z, and H_φ in a straight cylinder with axis along the z-axis. The equilibrium equation for a cylindrical pinch [$j_z H_\varphi = j_\varphi H_z - c\,dp/dr$,] taking account of the relations $H_\varphi = -dA_z/dr$, $j_\varphi = -(c/4\pi)\,dH_z/dr$, can be written in the form

$$j_z = cdp/dA_z + (c/8\pi)\,dH_z^2/dA_z. \qquad (52)$$

This equation is the analog of (1) and (3). The analog of (4) is the equation $r^{-1}d(rH_\varphi)/dr = (4\pi/c)j_z$ or

$$\frac{1}{r}\frac{d}{dr}\left(r\frac{dA_z}{dr}\right) = -4\pi\frac{dp}{dA_z} - \frac{1}{2}\frac{dH_z^2}{dA_z}. \qquad (53)$$

The conditions in (8), $A = \text{const}$ and $B = \text{const}$, correspond to the relations $p = \text{const}\cdot A_z$ and $H_z^2 = \text{const}\cdot A_z$ in the case of the cylinder. In this case $j_z = \text{const}$ and, consequently, p, A_z and H_z^2 have parabolic distributions.

APPENDIX

For the convenience of the reader we give the expansion of the functions $f_n(\vartheta)$ and $g_n(\vartheta)$ from Fock[2]

$$g_n(\vartheta) = \frac{\Gamma(n-1/2)}{\Gamma(-1/2)\Gamma(n+1)}e^{-(n-1/2)\vartheta}(1-e^{-2\vartheta})^2 \times F(n+3/2,\ 3/2,\ n+1,\ e^{-2\vartheta}),$$

$$f_n(\vartheta) = \tfrac{1}{8}e^{-(n-1/2)\vartheta}(1-e^{-2\vartheta})^2 F(n+3/2,\ 3/2,\ 3,\ 1-e^{-2\vartheta})$$

$$= \frac{2}{\pi}\frac{\Gamma(n-1/2)}{\Gamma(-1/2)\Gamma(n+1)}e^{-(n-1/2)\vartheta} \times (1-e^{-2\vartheta})^2[-f_n^{(1)}(\vartheta) + f_n^{(2)}(\vartheta)].$$

Here F is the hypergeometric function:

$$F(n+3/2,\ 3/2,\ n+1,\ e^{-2\vartheta}) = 1 + \frac{(2n+3)3}{(2n+2)2}e^{-2\vartheta} + \frac{(2n+3)(2n+5)\cdot 3\cdot 5}{(2n+2)(2n+4)\cdot 2\cdot 4}e^{-4\vartheta} + \ldots,$$

$f_n^{(1)}$ is the finite series

$$f_n^{(1)}(\vartheta) = \frac{2n}{2n+1} \times \left\{e^{2\vartheta} + \frac{(2n-2)2}{(2n-1)1}e^{4\vartheta} + \frac{(2n-2)(2n-4)\cdot 2\cdot 4}{(2n-1)(2n-3)\cdot 1\cdot 3}e^{6\vartheta} + \ldots\right\},$$

$f_n^{(2)}$ is the infinite series

$$f_n^{(2)}(\vartheta) = \vartheta + 2\ln 2 - a_0 - a_n + \frac{(2n+3)3}{(2n+2)2}e^{-2\vartheta}(\vartheta + 2\ln 2 - a_1 - a_{n+1}) + \frac{(2n+3)(2n+5)\cdot 3\cdot 5}{(2n+2)(2n+4)\cdot 2\cdot 4} \times e^{-4\vartheta}(\vartheta + 2\ln 2 - a_2 - a_{n+2}) + \ldots,$$

where

$$a_0 = 1,\ a_s = a_{s-1} - \frac{1}{2s(2s+1)} = 1 - \frac{1}{2} + \frac{1}{3} \ldots - \frac{1}{2s} + \frac{1}{2s+1}.$$

[1] V. D. Shafranov, JETP **33**, 710 (1957); Soviet Phys. JETP **6**, 545 (1958).

[2] V. A. Fock, Жур. Русск. Физ.-Хим. Об-ва (J. Russ. Phys.-Chem. Soc.) **62**, 218 (1930); Physik Z. Sowjetunion **1**, 215 (1932).

[3] S. M. Osovets, Физика плазмы и проблемы управляемых термоядерных реакций (Plasma Physics and the Problem of a Controlled Thermonuclear Reaction, U.S.S.R. Academy of Sciences, 1958, Vol. 2, p. 238.

[4] Biermann, Hain, Jörgens, and Lüst, Z. Naturforsch **12**, 826 (1957).

Translated by H. Lashinsky
212

CONVECTIVE PINCH INSTABILITY

B. B. KADOMTSEV

Submitted to JETP editor May 19, 1959

J. Exptl. Theoret. Phys. (U.S.S.R.) **37**, 1096-1101 (October, 1959)

An investigation is made of the stability with respect to axially symmetric perturbations, including entropy-wave perturbations, of a pinch with a distributed current.

IT is well known that plasma configurations with closed lines of force are particularly susceptible to convection or transposition instabilities, corresponding to the transposition of neighboring lines of force.[1] In this report we investigate the simplest configuration of this type: a straight, axially symmetric pinch which is contained by the magnetic field produced by the current through the pinch. We are interested chiefly in perturbations of the convection type, i.e., perturbations that are constant along the lines of force. The equilibrium velocity distribution is assumed to be Maxwellian; this assumption is valid if the time during which equilibrium is maintained in the pinch exceeds the time between collisions. The conductivity of the plasma is assumed to be infinite.

1. HYDRODYNAMIC APPROXIMATION

As has been shown in references 2 and 3, the magnetohydrodynamic equations for small oscillations reduce to a single self-adjoint equation for the displacement from equilibrium $\eta(\mathbf{r},t)$. This equation can be obtained[2,3] by means of a variational principle and it is found that a necessary and sufficient condition for stability is that the potential energy of the small oscillations be positive.

We assume that the plasma is inside a conducting wall and that the radial component η_r vanishes at the interface. In this case the potential energy is

$$V=\frac{1}{2}\int\Big\{\gamma p\,(\operatorname{div}\eta)^2+\frac{1}{4\pi}\,(\operatorname{curl}[\eta\times\mathbf{H}])^2 + \eta\nabla p\operatorname{div}\eta-\frac{1}{4\pi}[\eta\operatorname{rot}\times\operatorname{curl}\mathbf{H}]\operatorname{curl}[\eta\times\mathbf{H}]\Big\}d\mathbf{r}, \quad (1)$$

where the displacement along the field due to the last two terms in (1) vanishes because the equation is self-adjoint. In Eq. (1) p and H are the equilibrium pressure and magnetic field and $\gamma = 5/3$ is the exponent of the adiabat.

In the case being considered ($H_z = 0$) the potential energy (1) for axially symmetric perturbations is a quadratic form in the two independent variables η_r and div η. The condition which must be satisfied if this form is to be positive definite is

$$-d\ln p/d\ln r<4\gamma/(2+\gamma\varepsilon), \quad (2)$$

where $\epsilon = 8\pi p/H^2$. It is apparent that this condition also follows from one of the two conditions for convection stability.[1]

We now consider perturbations that depend on azimuth φ. Without loss of generality this dependence can be written in the form

$$\eta_r=\eta_r(r,z)\cos m\varphi,\qquad \eta_\varphi=\eta_\varphi(r,z)\sin m\varphi,$$
$$\eta_z=\eta_z(r,z)\sin m\varphi.$$

In this case, the factors $\cos^2 m\varphi$ and $\sin^2 m\varphi$ appear in Eq. (1); when averages are taken these terms yield $\frac{1}{2}$. Varying Eq. (1) with respect to η_φ gives div $\eta = 0$, whence

$$V=\frac{1}{4}\int\Big\{\frac{1}{4\pi}\frac{m^2H^2}{r^2}(\eta_r^2+\eta_z^2)+\frac{1}{4\pi}\Big[H\frac{\partial\eta_z}{\partial z}+\frac{\partial}{\partial r}(H\eta_r)\Big]^2 + \eta_r\frac{dp}{dr}\Big[\frac{1}{r}\frac{\partial}{\partial r}(r\eta_r)+\frac{\partial\eta_z}{\partial z}\Big] + \eta_r\Big[\frac{\partial\eta_z}{\partial z}+\frac{1}{H}\frac{\partial}{\partial r}(H\eta_r)\Big]\frac{dp}{dr}\Big\}d\mathbf{r}. \quad (3)$$

Equation (3) is a quadratic form in η_r, η_z and $\partial\eta_r/\partial r + \partial\eta_z/\partial z$. If this form is to be positive definite the following condition must be satisfied*

$$-d\ln p/d\ln r<m^2/\varepsilon. \quad (4)$$

If $\epsilon < \frac{2}{3}\gamma$, the condition in (2) is stronger; if $\epsilon > \frac{2}{3}\gamma$ the condition in (4) is stronger (with m = 1). It is interesting to note that in the many photographs of contracting pinches it is possible to distinguish two regions clearly: an inner region where twist perturbations develop (m = 1), and an outer region where the perturbations are essentially axially symmetric. This behavior is in complete agreement with the conditions given in (2) and (4).

Writing

$$\frac{d\ln p}{d\ln r}=\begin{cases}-1/\varepsilon & \text{for}\quad \varepsilon>\frac{2}{3}\gamma\\ -4\gamma/(2+\gamma\varepsilon) & \text{for}\quad \varepsilon<\frac{2}{3}\gamma\end{cases} \quad (5)$$

*This relation is given in a different form in reference 4.

and taking account of the equilibrium condition, which can be written in the form

$$\frac{d\ln p}{d\ln r} = \frac{1}{1+\varepsilon}\left(\frac{d\ln \varepsilon}{d\ln r} - 2\right), \tag{6}$$

it is easy to obtain the limiting stable pressure distribution. When $\gamma = 5/3$ this distribution is of the form

$$p = p_0 \frac{\varepsilon}{1-\varepsilon}, \quad r = a(1-\varepsilon) \quad \text{for } \varepsilon > 0.4,$$

$$p = 18.1\, p_0 \left(\frac{\varepsilon}{1+{}^5/_4\,\varepsilon}\right)^{5/2}, \quad r = 3.94a\,\frac{1+{}^5/_4\,\varepsilon}{\varepsilon^{3/4}} \quad \text{for } \varepsilon < 0.4, \tag{7}$$

where p_0 and a are constants of integration. This distribution has a singularity as $r \to 0$ and cannot be obtained experimentally. However, if there is a current carrying metal conductor along the z axis it is possible to produce a situation in which the plasma is stable close to the axis. In this case, as follows from (2), (4) and (6), the quantity ϵ must be smaller than unity everywhere and the rate at which the plasma pressure falls off in the radial direction must be small.

2. KINETIC ANALYSIS

In a high-temperature plasma the collision time may become extremely large; in this case the hydrodynamic approximation no longer applies. In a strong magnetic field it is possible to use the drift-approximation equations; these are the hydrodynamic equations for motion transverse to the field lines, and the kinetic equation for the longitudinal motion.[5] In the case of axial symmetry these equations are of the form

$$Mn\frac{\partial^2 \eta}{\partial t^2} = -\nabla p'_\perp - \frac{r}{r^2}(p'_\parallel - p'_\perp) + \frac{1}{4\pi}\,\mathrm{curl\,curl}\,[\eta\times\mathbf{H}]\times\mathbf{H}] + \frac{1}{4\pi}\,\mathrm{curl}\,\mathbf{H}\times\mathrm{curl}\,[\eta\times\mathbf{H}]], \tag{8}$$

$$\frac{\partial f'}{\partial t} + \frac{u}{r}\frac{\partial f'}{\partial \varphi} + \frac{\partial \eta}{\partial t}\nabla f_0 + \frac{u}{r}\frac{\partial \eta}{\partial \varphi}\nabla f_0 - \left\{\frac{u}{T}eE'_\varphi - \frac{Mu^2}{T}\frac{1}{r}\frac{\partial \eta_r}{\partial t} + \frac{Mw^2}{2T}\,\mathrm{div}\,\frac{\partial \eta}{\partial t} - \frac{Mw^2}{2T}\frac{1}{r}\frac{\partial \eta_r}{\partial t}\right\} \tag{9}$$

Here f_0 is the ion Maxwellian equilibrium distribution function, T is the temperature, E_φ is the azimuthal component of the electric field, f′ is the perturbation on the distribution function, $p'_\perp$ and $p'_\parallel$ are the perturbations of the transverse and longitudinal pressures respectively. M is the mass, n is the ion density, u is the longitudinal ion velocity, and w is the transverse ion velocity.

We consider perturbations whose aximuthal dependence is of the form $e^{im\varphi}$ $(m \neq 0)$ and assume that the oscillation frequency satisfies the condition $\omega \ll v_T/r$, where v_T is the mean ion thermal velocity. Under these conditions we can neglect the time derivatives in Eq. (9) and

$$f' = -\eta\nabla f_0 - ireE'_\varphi f_0/MT.$$

Similar considerations apply for the electrons. The field E'_φ is found from the charge neutralization condition; it is apparent, that $E'_\varphi = 0$. Thus, $f' = -\eta\nabla f_0$, whence $p'_\parallel = p'_\perp = -\eta\nabla p_0$. If this relation is substituted in Eq. (8) we obtain an equation which coincides exactly with the magnetohydrodynamic equation with $\mathrm{div}\,\eta = 0$, i.e., the stability criterion is (4), the same as in the hydrodynamic approximation.[4]

We now consider perturbations with axial symmetry $(m=0)$. In this case Eq. (9) can be integrated with respect to time and we obtain the relations

$$p'_\perp = -\eta_r dp/dr - 2p\,\mathrm{div}\,\eta + p\eta_r/r,$$
$$p'_\parallel = -\eta_r dp/dr - p\,\mathrm{div}\,\eta - 2p\eta_r/r, \tag{10}$$

which coincide with the adiabatic relations obtained by Chew, Goldberger, and Low.[6] As has been shown in reference 3, hydrodynamic equations with this kind of pressure anisotropy can also be obtained by means of a variational principle for the potential energy which, in the present case, is

$$V_k = \frac{1}{2}\int\left\{\eta_r\,\mathrm{div}\,\eta\frac{dp}{dr} + 2p(\mathrm{div}\,\eta)^2 - \frac{2p}{r}\eta_r\,\mathrm{div}\,\eta + 3p\frac{\eta_r^2}{r^2} + \frac{1}{4\pi}\left[H\frac{\partial \eta_z}{\partial z} + \frac{\partial}{\partial r}(H\eta_r)\right]^2 + \frac{1}{H}\frac{dp}{dr}\eta_r\left[H\frac{\partial \eta_z}{\partial z} + \frac{\partial}{\partial r}(H\eta_r)\right]\right\}dr. \tag{11}$$

The condition that the quadratic form in η_r and $\mathrm{div}\,\eta$ (11) be positive definite is

$$-\frac{d\ln p}{d\ln r} < \frac{{}^7/_2 + 5\varepsilon/4}{1+\varepsilon}. \tag{12}$$

This condition is somewhat weaker than (2). For this reason it is of interest to delineate the effect of collisions between particles which lead to equilibration of the longitudinal and transverse pressures. In order to avoid complications we neglect the difference between the equilibration times for the electron and ion pressures and introduce an average relaxation time τ. If we assume that the total energy of the particles is conserved in collisions it is apparent that the pressure relaxation is described by the relations

$$-\frac{\partial p'_\perp}{\partial t} = -\frac{1}{3\tau}(p'_\perp - p'_\parallel), \quad \frac{\partial p'_\parallel}{\partial t} = -\frac{2}{3\tau}(p'_\parallel - p'_\perp). \tag{13}$$

We assume that all quantities have time factors of the form $e^{\lambda t}$. Then, taking account of collisions

we can write Eq. (10) in the form

$$p'_\perp + \frac{1}{3\lambda\tau}(p'_\perp - p'_\parallel) = -\eta_r \frac{dp}{dr} - 2p \operatorname{div}\eta + \frac{p}{r}\eta_r ,$$
$$p'_\parallel + \frac{2}{3\lambda\tau}(p'_\parallel - p'_\perp) = -\eta_r \frac{dp}{dr} - p \operatorname{div}\eta - \frac{2p}{r}\eta_r . \quad (14)$$

If the quantities $p'_\parallel$ and $p'_\perp$ are determined in this way and substituted in Eq. (8), neglecting the inertia term on the left side we obtain an equation which can be regarded as the Euler equation for the variational problem $\delta(V_k + V/\lambda\tau) = 0$, with a characteristic value of zero, i.e., the solution satisfies the equation

$$V_k + V/\lambda\tau = 0 . \quad (15)$$

Here V_k is given by Eq. (11) and V is given by Eq. (1). It follows from Eq. (15) that $\lambda\tau$ is real.

Now suppose that the energy V_k is positive, that is to say, the plasma is stable in the absence of collisions. Then, if V is positive, (15) has only the damped solution with $\lambda < 0$; if V is negative, of the extremum values of the functional $F = V_k + V/\lambda\tau$ there is one which vanishes when the parameter $\lambda\tau$ changes from 0 to ∞. This means that Eq. (15) has a solution with the increment $\lambda \sim 1/\tau > 0$. Thus, the two modes (the dynamic mode and the one associated with collisions) given by the kinetic equations for the small oscillations yield a stability condition which is exactly the same as the hydrodynamic stability condition.

3. DRIFT INSTABILITY OF A PINCH

Tserkovnikov[7] has shown that under certain conditions there can be an increasing solution for oscillations whose phase velocity is of the order of the drift velocity of the particles. Since it is difficult to delineate the physical significance of the drift instability in the kinetic analysis given by this author, we consider the problem here by means of the hydrodynamic equations, in which quantities of order ρ/r are retained, where ρ is the ion Larmor radius. Thus, in the heat transfer equations we introduce the thermal drift of the electrons ($\alpha = e$) and ions ($\alpha = i$)[8]

$$\mathbf{q}_\alpha = -(5n_\alpha T_\alpha / 2e_\alpha H^2)[\mathbf{H}\nabla T_\alpha] ,$$

but neglect the usual thermal conductivity and viscosity, assuming that the frequency of collisions between particles is much lower than the cyclotron frequency of the ions and that the wavelength of the perturbations is much larger than ρ. We also assume that the Debye radius is much smaller than all the characteristic lengths so that the charge neutralization condition is satisfied ($n_i = n_e = n$). We also assume that all quantities vary as $\exp(-i\omega t + ikz)$ so that the linearized equations of continuity are written in the form

$$n' = -\operatorname{div}(\eta n) = -\operatorname{div}(n\xi) + (kv_0/\omega)n' . \quad (16)$$

Here n' is the perturbed density, η is the ion displacement, ξ is the displacement of the electrons from the equilibrium position

$$v_0 = (c/eHn)\,dp/dr$$

and the equilibrium drift velocity of the electrons results in a current flow along the axis of the pinch.

The equations of motion are the Euler equation

$$-\omega^2 nM\eta + \nabla p' = \frac{1}{4\pi}[\operatorname{curl}\mathbf{H}'\times\mathbf{H}] + \frac{1}{4\pi}[\operatorname{curl}\mathbf{H}\times\mathbf{H}'] \quad (17)$$

and the equation of momentum transfer for the electrons, in which we neglect the inertia term is:

$$\frac{1}{n}\nabla p'_e - \frac{n'}{2n^2}\nabla p = -e\mathbf{E}' - \frac{e}{c}[\mathbf{v}_0\times\mathbf{H}'] + \frac{i\omega e}{c}[\xi\times\mathbf{H}]. \quad (18)$$

The linearized heat transfer equations are[8]

$$\omega\left(T'_e + \xi_r\frac{dT}{dr} + \frac{2}{3}T\operatorname{div}\xi\right) - kv_0T'_e + \frac{i}{2\tau}(T'_e - T'_i)$$
$$= -\frac{5}{3}\frac{kT'_e}{n}\frac{1}{r}\frac{d}{dr}\left(\frac{rncT}{eH}\right)$$
$$+ \frac{5}{3}\frac{kcT}{eH}\frac{dT}{dr}\left(\frac{n'}{n} + \frac{T'_e}{T} - \frac{H'}{H}\right), \quad (19)$$

$$\omega\left(T'_i + \eta_r\frac{dT}{dr} + \frac{2}{3}T\operatorname{div}\eta\right) + \frac{i}{2\tau}(T'_i - T'_e)$$
$$= \frac{5}{3}\frac{kT'_i}{n}\frac{1}{r}\frac{d}{dr}\left(\frac{rncT}{eH}\right) - \frac{5}{3}\frac{kcT}{eH}\frac{dT}{dr}\left(\frac{n'}{n} + \frac{T'_i}{T} - \frac{H'}{H}\right). \quad (20)$$

Here the last term on the left side takes account of the heat exchange between electrons and ions and τ is the characteristic time for temperature equilibration.

Equations (16) — (20), together with Maxwell's equations

$$\operatorname{curl}\mathbf{H}' = (4\pi e/c)\{-n'\mathbf{v}_0 + i\omega(\xi - \eta)n\} , \quad (21)$$

$$\operatorname{curl}\mathbf{E}' = (i\omega/c)\mathbf{H}' \quad (22)$$

represent the complete system of equations for the small oscillations.

If we neglect the magnetoacoustic oscillations the inertia term in the z component of (17) can be neglected so that

$$p' + H'H/4\pi = 0 . \quad (23)$$

Equation (23) and the radial component of (17) yield

$$\eta_r = -2p'/\omega^2 Mrn . \quad (24)$$

From (21), taking account of (16) and (23), we

have

$$\xi_r - \eta_r = \frac{kc}{e\omega nH} p',$$

$$\operatorname{div}(\xi - \eta) = \frac{kv_0}{\omega}\frac{n'}{n} - \frac{kc}{\omega eHn^2}\frac{dn}{dr} p'. \qquad (25)$$

Using (23) — (25), we reduce the remaining equations to a system of three algebraic equations

$$(\nu - q)\frac{T'}{T} + \left\{2 + \left(\frac{2}{5} + \frac{\varepsilon}{2}\right)q - s\right\}\frac{\theta}{T} + \left\{-\frac{2}{5}\nu + s + \frac{4}{\nu k^2\rho^2}\left(\frac{2}{5}q - s\right)\right\}\frac{p'}{p} = 0; \qquad (26)$$

$$\frac{5}{2}\left(2 + \frac{\varepsilon}{2}q\right)\frac{T'}{T} + \left(\nu + \frac{i}{\tau^*} - q\right)\frac{\theta}{T} - \frac{5}{3}\frac{\varepsilon}{2}s\frac{p'}{p} = 0; \qquad (27)$$

$$(\nu - q)\frac{T'}{T} + (q - s)\frac{\theta}{T} + \left\{-\nu\left(1 + \frac{\varepsilon}{2}\right) - 4 + \varepsilon + \frac{4}{\nu k^2\rho^2}\left[2 + \left(1 + \frac{\varepsilon}{2}\right)q - s\right]\right\}\frac{p'}{p} = 0. \qquad (28)$$

Here

$$T' = (T_e' + T_i')/T, \quad \theta = (T_e' - T_i')/T, \quad q = d\ln p/d\ln r,$$

$$s = d\ln T/d\ln r, \quad \nu = \omega eHr/kcT,$$

$$\tau^* = \tau kcT/eHr, \quad \rho = \sqrt{TMc^2/e^2H^2},$$

and ρ is the mean ion Larmor radius. Equation (26) is half the sum, and (27) is half the difference, of the heat transfer equations (19) and (20). Equation (28) is obtained from (22) by substitution of the electric field from (18). The requirement that the determinant of the system (26) — (28) must vanish gives a dispersion equation of the fourth degree. Since the coefficients of this equation are functions of r while the frequency can be considered independent of r, the perturbations must be localized with respect to r; strictly speaking they are δ-functions. We assume that the wavelength of the perturbation is much smaller than the ion Larmor radius $k\rho \ll 1$; thus in the dispersion equation there is a large coefficient $1/k^2\rho^2$. In this case the two roots are large (of order $\nu \sim 1/k\rho$), and we obtain the values

$$\omega^2 = \frac{2p}{Mnr}\left\{\frac{d\ln p}{d\ln r} + \frac{4\gamma}{2 + \gamma\varepsilon}\right\}, \qquad (29)$$

where $\gamma = 5/3$. This is obviously the frequency of the convection oscillations and the condition $\omega^2 > 0$ coincides exactly with (2).

The other two roots are of order unity and are determined by the equation

$$(\nu - q + \frac{i}{\tau^*})(\nu - q) = \gamma^2\frac{(4 + \varepsilon q)^2}{4\gamma + q(2 + \gamma\varepsilon)} \times \left\{1 + \left(\frac{7}{10} + \frac{\varepsilon}{4}\right)q - s\right\}. \qquad (30)$$

If (2) is satisfied, the following condition must be satisfied if the imaginary parts of the roots of (3) are to be positive:

$$d\ln T/d\ln r < 1 + (7/10 + \varepsilon/4)\, d\ln p/d\ln r. \qquad (31)$$

In the case of small curvature ($r \to \infty$) this condition becomes the condition $d\ln T/d\ln p < 7/10 + \varepsilon/4$, which has been obtained earlier by Tserkovnikov and represents the hydrodynamic analog of one of the conditions obtained in reference 7 by means of the kinetic equation. The condition in (31) shows that for a given value of $d\ln p/d\ln r$, the temperature cannot increase too rapidly with r and that for a given temperature gradient the pressure must not fall off too rapidly with r.

It is interesting to note that when $d\ln T/d\ln r = 0$, the condition in (31) becomes (2) (with $\gamma = 5/7$). Thus, the drift thermal conductivity leads to a more stringent stability condition than the usual condition; when this is taken into account we arrive at (2) with, $\gamma = 1$ (the isothermal condition).

According to (26) — (28), when $\nu \sim 1$ we have $p'/p \sim (k\rho)^2 T'/T \ll T'/T \sim \theta T$, i.e., the oscillations represent entropy waves, or a perturbation of the temperatures T_e and T_i at constant pressure. Because of the particle drift these waves propagate along the axis of the pinch and the plasma, in accordance with Eqs. (24) and (25), executes radial oscillations $\eta_r \approx \xi_r \sim rT'/T$ which compensate for the change in pressure by virtue of the drift thermal conductivity.

If (31) is not satisfied these oscillations increase without limit and this causes heat transfer along the radius until the temperature gradient is reduced to values given by (31).

It should be noted that the temperature difference between the electron temperature and ion temperature is of importance in these oscillations because $\theta \to 0$ when $\tau^* \to 0$ and (30) has only one root beside the real root $\nu = q$.

[1] B. B. Kadomtsev, Coll. Физика плазмы (Plasma Physics) **4**, (1958), p. 370.

[2] Hain, Lüst, and Shlüter, Z. Naturforschung, **12a**, 833 (1957).

[3] Bernstein, Frieman, Kruskal, and Kulsrud, Proc. Roy. Soc., **A244**, 17 (1958).

[4] R. Tayler, Proc. Phys. Soc. **B70**, 1049 (1957).

[5] B. B. Kadomtsev. Coll. Физика плазмы (Plasma Physics) **4**, (1958) p. 380

[6] Chew, Goldberger and Low, Proc. Roy. Soc. **A236**, 112 (1956).

[7] Yu. A. Tserkovnikov, JETP **32**, 67 (1957), Soviet Phys. JETP **5**, 58 (1957).

[8] S. I. Braginskiĭ, JETP **33**, 459 (1957); Soviet Phys. JETP **6**, 358 (1958).

Translated by H. Lashinsky
213

ON ELECTROMAGNETIC CORRECTIONS IN μ-e DECAY

V. P. KUZNETSOV

Moscow Physico-Technical Institute

Submitted to JETP editor May 21, 1959

J. Exptl. Theoret. Phys. (U.S.S.R.) **37**, 1102-1105 (October, 1959)

Electromagnetic corrections to the electron angular distribution have been obtained for the V-A theory of μ-e decay.

BEHRENDS, Finkelstein, and Sirlin[1] have calculated the electromagnetic corrections to the electron spectrum in the μ-e decay. The electron angular distribution in the decay of a polarized μ meson has been obtained by Kinoshita and Sirlin.[2] However, as was shown by Berman,[3] the infrared divergence was removed by the above-mentioned authors[1,2] incorrectly; Berman also gives the corrected energy spectrum of the decay electrons. In the present paper the corrected electron angular distribution is calculated.

We start from the interaction Lagrangian introduced by Feynman and Gell-Mann[4] (we use units such that $\hbar = c = 1$) with an additional term describing the interaction with the electromagnetic field:

$$L_{int} = 2G\,(\bar\psi_2\gamma_\mu \tfrac{1}{2}(1+\gamma_5)\psi_1)\,(\bar\psi_3\gamma_\mu \tfrac{1}{2}(1+\gamma_5)\psi_4) - ie\,(\bar\psi_1\hat A\psi_1) - ie(\bar\psi_2\hat A\psi_2) + \text{Herm. conj.} \qquad (1)$$

(the subscripts 1, 2, 3, 4, refer to the μ meson, electron and the two neutrinos respectively).

The electromagnetic corrections consist of coherent radiative corrections and corrections to the μ-e decay with the emission of a photon (internal bremsstrahlung, see Fig. 1). The radiative corrections consist of corrections to the vertex part and the proper self energy part of the electron and μ meson. The contribution of the vertex part has the form

$$\begin{aligned}\Lambda_\rho = 2G\,\frac{\alpha}{2\pi}\Big\{&\tfrac{1}{2}\gamma_\rho(1+\gamma_5)\,A(\theta,\omega) + \tfrac{1}{2}\gamma_\rho(1-\gamma_5)\frac{\theta}{\sinh\theta}\\ &+\tfrac{1}{2}(1+\gamma_5)\frac{i}{4m_1}\Big[P_\rho\Big(\frac{\theta}{\sinh\theta}-\frac{2}{\sinh\theta}F_2(\theta,\omega)\Big)\\ &+2q_\rho\Big(\frac{\theta}{\sinh\theta}-3\frac{F_2(\theta,\omega)}{\sinh\theta}+(\cosh\omega-\cosh\theta)^{-1}\\ &\times\Big(1-\frac{\sinh\omega}{\sinh\theta}F_2(\theta,\omega)-F_3(\theta,\omega)\Big)\Big)\Big]\\ &+\tfrac{1}{2}(1-\gamma_5)\frac{i}{4m_2}\Big[P_\rho\Big(\frac{\theta}{\sinh\theta}+\frac{2}{\sinh\theta}F_2(\theta,\omega)\Big)\\ &-2q_\rho\Big(\frac{\theta}{\sinh\theta}+3\frac{F_2(\theta,\omega)}{\sinh\theta}+(\cosh\omega-\cosh\theta)^{-1}\\ &\times\Big(1-\frac{\sinh\omega}{\sinh\theta}F_2(\theta,\omega)-F_3(\theta,\omega)\Big)\Big)\Big]\Big\}. \qquad (2)\end{aligned}$$

Here we used the convenient abbreviations introduced by Behrends et al[1]

$$\coth\theta = -(p_1p_2)/m_1m_2, \qquad \omega = \ln(m_1/m_2),$$

$$\omega_> = \ln(L/m_2), \qquad \omega_< = \ln(\lambda/m_2),$$

$$P = p_1 + p_2, \qquad q = p_1 - p_2,$$

where m_1 and m_2 are the masses of the μ meson and electron, L is the upper cutoff on the momentum of the virtual photon and λ is the photon mass. The functions $A(\theta,\omega)$ and $F_i(\theta,\omega)$ are

$$A(\theta,\omega) = (\theta - F_1(\theta,\omega))\coth\theta + (1-\theta\coth\theta)(\omega - 2\omega_<) + F_3(\theta,\omega) + r_\Lambda,$$

where

$$r_\Lambda = -\tfrac{3}{2}\omega + \tfrac{1}{4} + 2\omega_< + \omega_>; \qquad (3)$$

$$F_1(\theta,\omega) = L\left(\frac{2\sinh\theta}{e^\omega - e^{-\theta}}\right) - L\left(\frac{2\sinh\theta}{e^\theta - e^{-\omega}}\right) + (\omega-\theta)\ln\frac{\sinh\left[\frac{(\omega-\theta)}{2}\right]}{\sinh\left[\frac{(\omega+\theta)}{2}\right]},$$

$$F_2(\theta,\omega) = \frac{\omega\sinh\theta - \theta\sinh\omega}{2(\cosh\omega - \cosh\theta)},$$

$$F_3(\theta,\omega) = \frac{\omega\sinh\omega - \theta\sinh\theta}{2(\cosh\omega - \cosh\theta)},$$

$$L(x) = \int_0^x \frac{\ln(1-t)}{t}\,dt = -\sum_{k=1}^{\infty}\frac{x^k}{k^2}. \qquad (4)$$

The terms $\sim\gamma_\rho$, 1 in (2) correspond to the vector and the terms $\sim\gamma_\rho\gamma_5$, γ_5 correspond to the axial vector interactions.

After mass renormalization the radiative corrections corresponding to the electron and μ meson self energies give a contribution equal to

$$\Sigma_1 + \Sigma_2 = (G\alpha/2\pi)\,\gamma_\rho(1+\gamma_5)\,(\tfrac{3}{2}\omega - \tfrac{9}{4} - \omega_> - 2\omega_<). \qquad (5)$$

In the absence of transitions ($\theta = \omega = 0$) the complete matrix element for radiative corrections

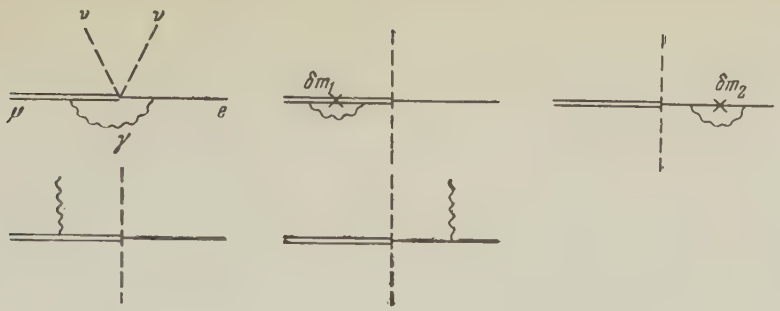

FIG. 1

should vanish. This is the case for the vector interaction. For the axial vector interaction there is a finite remainder $-(\alpha G/2\pi)\gamma_\rho\gamma_5$. It may be interpreted as a change in the axial vector coupling constant. It is of order $\alpha/2\pi$, i.e., 0.1%. Consequently second order radiative corrections leave the ratio of coupling constants in the V-A theory practically unchanged.

Second-order electromagnetic corrections, accurate to terms of order $\alpha/2\pi$, turn out to be equal for the V and A interactions in the approximation $m_2/m_1 \ll 1$. The infrared divergence in the radiative corrections is compensated by the infrared divergence in the internal bremsstrahlung. The probability per unit time for decay with the emission of a photon of a polarized μ meson (with polarization four-vector a satisfying $a \cdot p_1 = 0$) is given by

$$\frac{dw}{dt} = \frac{\alpha G^2}{3(2\pi)^5}\frac{d^3p_2}{\varepsilon_1\varepsilon_2}\frac{d^3k}{\varepsilon_\gamma}$$
$$\times\left\{\left[\frac{1}{2}(m_1^2-m_2^2)-Q^2\left(Q^2+\frac{1}{2}(m_1^2-m_2^2)\right)\right]\Phi\right.$$
$$-4Q^2+\frac{(kQ)^2}{(p_1k)(p_2k)}(m_1^2+m_2^2-2Q^2)$$
$$-m_1\left[(m_1^2-m_2^2+2Q^2)\left[\Phi(ap_2)+\frac{(kQ)}{(p_1k)(p_2k)}\right.\right.$$
$$\times\left[\frac{1}{2}(m_1^2+m_2^2+Q^2)\frac{(ka)}{(kp_1)}-(ap_2)\right]$$
$$\left.\left.-\frac{(ka)}{(kp_1)}\frac{m_2^2(kQ)}{(kp_2)^2}\right]-4Q^2\frac{(ka)}{(kp_1)}\right]\Bigg\}, \qquad (6)$$

where k and ϵ_γ are the four-momentum and energy of the photon and

$$\Phi = [p_{2\rho}/(p_2k) - p_{1\rho}/(p_1k)]^2, \qquad Q = p_1 - p_2 - k.$$

For $a = 0$, (6) goes over into Eq. (17) of Behrends et al.[1]

Integrating (6) over d^3k (with $k^2 = -\lambda^2$ taken into account) and combining the result with the radiative corrections we finally obtain the following expression for the spectrum and angular distribution of electrons from the decay of a polarized μ meson (with a polarization vector ξ in the μ-meson rest system for $m_2/m_1 \ll 1$):

$$dN(\varepsilon, \varphi, \xi) = \tfrac{1}{12}G^2m_1^5(2\pi)^{-3}\{3-2\varepsilon+(\alpha/2\pi)f(\varepsilon)$$
$$-\xi\cos\varphi[2\varepsilon-1+(\alpha/2\pi)h(\varepsilon)]$$
$$+6\zeta(m_2/m_1)(1-\varepsilon)/\varepsilon\}\varepsilon^2d\varepsilon d\Omega/4\pi. \qquad (7)$$

Here φ is the angle between the direction of electron emission and of the μ-meson spin vector, $\epsilon = \epsilon_2/\epsilon_{2\max}$;

$$\xi = \frac{2\,\mathrm{Re}\,g_V^*g_A}{|g_V|^2+|g_A|^2},$$
$$\zeta = \frac{|g_A|^2-|g_V|^2}{|g_V|^2+|g_A|^2}, \qquad |\zeta| \leqslant (1-\xi^2)^{1/2}, \qquad (8)$$

g_V and g_A are the vector and axial vector coupling constants, ξ is a measure of the relative contributions of the V and A couplings;

$$f(\varepsilon) = 2(3-2\varepsilon)u(\varepsilon) + 6(1-\varepsilon)\ln\varepsilon$$
$$+\tfrac{1}{3}\varepsilon^{-2}(1-\varepsilon)[(5+17\varepsilon-34\varepsilon^2)(\omega+\ln\varepsilon)-22\varepsilon+34\varepsilon^2],$$
$$h(\varepsilon) = 2(2\varepsilon-1)u(\varepsilon)+(6\varepsilon-2)\ln\varepsilon$$
$$+\tfrac{1}{3}\varepsilon^{-2}(1-\varepsilon)[(1+\varepsilon+34\varepsilon^2)(\omega+\ln\varepsilon)$$
$$+3-7\varepsilon-32\varepsilon^2-4\varepsilon^{-1}(1-\varepsilon)^2\ln(1-\varepsilon)],$$
$$u(\varepsilon) = 2\sum_{k=1}^{\infty}\frac{\varepsilon^k}{k^2}-\frac{\pi^2}{3}+\frac{3}{2}\omega-2+\ln\varepsilon\{3\ln(1-\varepsilon)$$
$$-2\ln\varepsilon-2\omega+1\}+(2\omega-1-\tfrac{1}{\varepsilon})\ln(1-\varepsilon). \qquad (9)$$

These expressions are a good approximation to the spectrum from $\epsilon \sim 0.1$ on. (For smaller values of ϵ the corrections become very large and it becomes necessary to consider higher order approximations in the electromagnetic field.) At the end of the spectrum (at $\epsilon = 1$) $f(\epsilon)$ and $h(\epsilon)$ diverge. This divergence may be removed by introducing an experimental energy interval $\Delta\epsilon$.[1] The function $(\alpha/2\pi)f(\epsilon)/(3-2\epsilon)$ was tabulated by Berman.[3] We give a table of values of $(\alpha/2\pi) \times h(\epsilon)$. In the absence of electromagnetic correc-

The correction function to the angular distribution ($\Delta\epsilon = 0$)

ε	$\frac{\alpha}{2\pi} h(\varepsilon)$	ε	$\frac{\alpha}{2\pi} h(\varepsilon)$
0.1	0.077	0.7	0.016
0.2	0.038	0.8	0.0033
0.3	0.031	0.9	—0.018
0.4	0.030	0.095	—0.038
0.5	0.027	0.099	—0.076
0.6	0.023		

tions the spectrum and angular distribution may be expressed as follows

$$dN(\varepsilon, \varphi, \xi) = \tfrac{1}{12} G^2 m_1^5 (2\pi)^{-3} [6(1-\varepsilon) + \tfrac{4}{3}\rho_M(4\varepsilon - 3) - \xi\cos\varphi(2(1-\varepsilon) + \tfrac{4}{3}\delta_M(4\varepsilon-3)) + 6\zeta(m_2/m_1)\varepsilon^{-1}(1-\varepsilon)]\varepsilon^2 d\varepsilon d\Omega/4\pi, \quad (10)$$

where ρ_M is the parameter introduced by Michel and δ_M is the δ of Kinoshita and Sirlin.[2]

Conclusions may be drawn from a comparison of (7) and (10) about the effect of electromagnetic corrections on the μ-e decay. The mean μ-meson lifetime (τ) is reduced by 0.42%. The constants introduced[1] to characterize the electromagnetic corrections are equal to $\Lambda_1 = 0.13$, $\Lambda_2 = -0.022$ (for an experimental interval $\Delta\epsilon = 0$). Thus we find for the ρ-parameter $\rho = \frac{3}{4}(1 - 0.0042) = 0.747$ (defined in reference 1 as $\rho = 3\tau/4\tau_0$ where τ_0 is the mean lifetime in the absence of electromagnetic corrections). The ρ introduced in this manner depends only weakly on the magnitude of the electromagnetic corrections to the spectrum since even if the spectrum should change significantly the area under the spectral curve, which is equal to the mean lifetime, may remain unchanged as it did in the present case. Since the spectrum, including electromagnetic corrections, when divided by ϵ^2 may be approximated by a straight line for ϵ in the range $0.3 \lesssim \epsilon \lesssim 0.95$, another means of introducing ρ is made possible by relating ρ to the tangent of the angle of inclination of this line: $\tan\alpha = 6 + 16\rho/3$ (see reference 2). This yields $\rho = 0.70$. For this definition of ρ the comparison with experiment should be made only in the middle part of the spectrum, whereas with the previous definition the comparison is possible over the entire spectrum (see Rosenson[5]). For the angular part we similarly approximate the quantity $2\epsilon - 1 + (\alpha/2\pi)h(\epsilon)$ by a straight line and obtain $\delta = 0.74$ (in the absence of electromagnetic correction $\delta_M = \frac{3}{4}$).

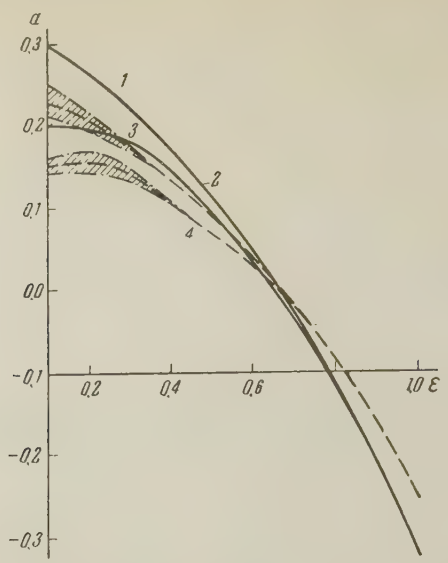

FIG. 2. Curves 1 and 2 give the asymmetry coefficient $a(\epsilon, \xi, \zeta)$ (introduced in reference 2) without electromagnetic corrections for $\xi = -1$ and $\xi = -0.76$; curves 3 and 4 – the same but including electromagnetic corrections. The shaded area indicates possible deviation from the equality $\zeta = 0$, i.e. from $|g_A| = |g_V|$ (for $\xi = -0.76$; $|\zeta| \leqslant 0.65$).

The values of the asymmetry coefficient introduced by Kinoshita and Sirlin,[2] including corrections resulting from the covariant method of elimination of the infrared divergence, are shown in Fig. 2.

In conclusion I am grateful to Professor V. B. Berestetskiĭ for guidance in this work and to Academician L. D. Landau for an interesting discussion.

Note added in proof (August 31, 1959). The question of electromagnetic corrections is also studied in the recent paper by Kinoshita and Sirlin.[6]

[1] Behrends, Finkelstein, and Sirlin, Phys. Rev. **101**, 866 (1956).

[2] T. Kinoshita and A. Sirlin, Phys. Rev. **107**, 593, 638 (1957).

[3] S. M. Berman, Phys. Rev. **112**, 267 (1958).

[4] R. P. Feynman and M. Gell-Mann, Phys. Rev. **109**, 193 (1958).

[5] L. Rosenson, Phys. Rev. **109**, 958 (1958).

[6] T. Kinoshita and A. Sirlin, Phys. Rev. **113**, 1652 (1959).

Translated by A. M. Bincer
214

TRANSITION RADIATION IN WAVEGUIDES

K. A. BARSUKOV

P. N. Lebedev Physics Institute, Academy of Sciences, U.S.S.R.

Submitted to JETP editor May 25, 1959

J. Exptl. Theoret. Phys. (U.S.S.R.) **37**, 1106-1109 (October, 1959)

We examine the radiation produced in a waveguide when a charged particle passes through the boundary between two media. It is shown that at ultrarelativistic charge velocities the radiation is mainly in the forward direction and its magnitude is proportional to the particle energy. Formulas are derived for the radiation energy and for its spectral distribution.

TRANSITION radiation[1-3] may in the near future find extensive application in fast-particle counters and in ultrashort-wave generators. The question of transition radiation in a waveguide is therefore of interest.

1. Let us consider an arbitrary cylindrical waveguide with perfectly conducting walls, filled with two homogeneous dielectrics, the constants of which are ϵ_1 and ϵ_2 for $z < 0$ and $z > 0$ respectively. A charged particle moves parallel to the axis of the waveguide from the negative z direction towards the separation boundary with velocity v. The field in the waveguide is described by a vector potential $\mathbf{A}(0, 0, A)$, the Fourier representation of which satisfies the equation

$$\nabla^2 A_{\omega i} + \frac{\varepsilon_i \omega^2}{c^2} A_{\omega i} = -\frac{4\pi}{c} j_\omega, \qquad i = 1, 2, \qquad (1.1)$$

where j_ω is the Fourier component of the particle current. The field vectors are obtained from the relations

$$\mathbf{E}_\omega = -\frac{i\omega}{c}\mathbf{A}_\omega + \frac{c}{i\omega\varepsilon}\operatorname{grad}\operatorname{div}\mathbf{A}_\omega, \quad \mathbf{H}_\omega = \operatorname{curl}\mathbf{A}_\omega, \qquad (1.2)$$

with $A_\omega = 0$ on the surface of the waveguide.

The solution of (1.1) is represented in the form of a field connected with the particle, and a free field, which is a "flash" of transition radiation, occurring during the reshaping of the particle field at the instant when it passes from one medium to another. The first field has the form

$$A^0_{\omega 1} = \frac{2e}{c} e^{-i\omega z/v} \sum_{n=1}^{\infty} \frac{\psi_n(M_0)\,\psi_n(M)}{\lambda_n^2 + (\omega/v)^2(1-\beta^2\varepsilon_1)},$$

$$A^0_{\omega 2} = \frac{2e}{c} e^{-i\omega z/v} \sum_{n=1}^{\infty} \frac{\psi_n(M_0)\,\psi_n(M)}{\lambda_n^2 + (\omega/v)^2(1-\beta^2\varepsilon_2)}, \qquad (1.3)$$

where $\psi_n(M)$ and λ_n are the normalized eigenfunction and eigenvalue of the first boundary problem for the transverse section of the waveguide:

$$\nabla^2\psi_n + \lambda_n^2\psi_n = 0 \qquad (1.4)$$

with $\psi_n = 0$ on the surface of the waveguide, and M_0 is the point of intersection of the trajectory of the charge with the transverse section.

The free field is written in the form of a system of propagating waves

$$A'_{\omega 1} = \frac{2e}{c}\sum_{n=1}^{\infty} A_n\psi_n(M_0)\,\psi_n(M)\,e^{i\Gamma_n z},$$

$$A'_{\omega 2} = \frac{2e}{c}\sum_{n=1}^{\infty} B_n\psi_n(M_0)\,\psi_n(M)\,e^{-i\gamma_n z}, \qquad (1.5)$$

with

$$\Gamma_n = \sqrt{\omega^2\varepsilon_1/c^2 - \lambda_n^2}, \quad \gamma_n = \sqrt{\omega^2\varepsilon_2/c^2 - \lambda_n^2},$$

$$\operatorname{Im}\Gamma_n < 0, \quad \operatorname{Im}\gamma_n < 0,$$

for $\omega > 0$, and a complex-conjugate expression for $\omega < 0$. The unknown coefficients are found from the condition of continuity of the tangential components of the vectors at $z = 0$:

$$A_n = \frac{1}{\varepsilon_1\Gamma_n + \varepsilon_2\gamma_n}\left[\frac{\varepsilon_2\omega/v - \varepsilon_1\gamma_n}{\lambda_n^2 + (\omega/v)^2(1-\beta^2\varepsilon_1)} - \frac{\varepsilon_1\omega/v - \varepsilon_1\gamma_n}{\lambda_n^2 + (\omega/v)^2(1-\beta^2\varepsilon_2)}\right],$$

$$B_n = \frac{1}{\varepsilon_1\Gamma_n + \varepsilon_2\gamma_n}\left[\frac{\varepsilon_2\Gamma_n + \omega\varepsilon_2/v}{\lambda_n^2 + (\omega/v)^2(1-\beta^2\varepsilon_1)} - \frac{\varepsilon_2\Gamma_n + \omega\varepsilon_1/v}{\lambda_n^2 + (\omega/v^2)(1-\beta^2\varepsilon_2)}\right]. \qquad (1.6)$$

Equations (1.2), (1.5), and (1.6) fully determine the field in the waveguide.

2. From the formulas just obtained it is easy to calculate the flux of the Poynting vector due to the free field. Using the orthogonality of the eigenfunctions and going over to integration over positive frequencies, we obtain

$$S^{\pm} = 4e^2\sum_{n=1}^{\infty}\lambda_n^2|\psi_n(M_0)|^2\operatorname{Re}\int_0^{\infty}\frac{|A_n|^2\Gamma_n}{\varepsilon_{1,2}\omega}\,d\omega, \qquad (2.1)$$

where the symbol ± indicates the direction of wave propagation.

It is known, however, that in the waveguide there can exist, at certain frequencies, damped waves which, generally speaking, can produce in our case a unique "blocked" field at the separation boundary, i.e., a field consisting of standing exponentially-damped waves, the lifetime of which is determined by the time of dissipation of the electromagnetic energy in the substance. To clarify the physical aspect of this problem, let us compare the work performed by the electromagnetic field on the particle with the energy flux of this field through a waveguide section located at infinity (we disregard the Cerenkov radiation of the charge). For this purpose we use the Poynting theorem

$$W_\infty - W_{-\infty} = \int_{-\infty}^{\infty} dt \int \mathbf{E}\mathbf{j}\, dV - \frac{c}{4\pi} \int_{-\infty}^{\infty} dt \int [\mathbf{E}\times\mathbf{H}]_n\, dS, \quad (2.2)$$

where the surface integral extends over the waveguide section at infinity, and the volume integral over the waveguide segment between them. From (1.2) and (1.6) we can calculate the first term in (2.2), which represents the work done by the field on the particle

$$\int_{-\infty}^{\infty} dt \int \mathbf{E}\mathbf{j}\, dV = S^+ + S^- - \frac{4e^2}{v} \sum_{n=1}^{\infty} \lambda_n^2 |\psi_n(M_0)|^2 \times \int_0^{\infty} \frac{(\varepsilon_1 - \varepsilon_2)\,[\lambda_n^2 + (\omega^2/v^2)\,(1 - \beta^2\,(\varepsilon_1 + \varepsilon_2))]\, d\omega}{\varepsilon_1\varepsilon_2\,[\lambda_n^2 + (\omega^2/v^2)\,(1 - \beta^2\varepsilon_1)]^2\,[\lambda_n^2 + (\omega^2/v^2)\,(1 - \beta^2\varepsilon_2)]^2}. \quad (2.3)$$

It can be readily shown that the sum in (2.3) represents the energy flux due to the field connected with the particle. Furthermore, (2.2) contains terms for the energy flux due to interference between the field of the particle proper and the radiation field. These terms have the form

$$\int_0^{\infty} \Phi_1(\omega) \exp\{i\,(\omega/v + \Gamma_n)\, z\}\, d\omega,$$

$$\int_0^{\infty} \Phi_2(\omega) \exp\{i\,(\omega/v - \gamma_n)\, z\}\, d\omega. \quad (2.4)$$

An estimate of these integrals at large z, for example by the well-known stationary-phase method, shows that the first of these terms diminishes exponentially with increasing $|z|$, while the second diminishes as $z^{-1/2}$. This result is physically understandable, since in the former case the particle field has practically all passed into the second medium, while in the latter case the radiation and the particle move in one direction and interfere intensely over a certain distance, until the field overtakes the particle. This distance is the characteristic zone of formation of transition radiation. More detailed estimates will be given below.

The foregoing leads to the conclusion that all the particle losses (we do not consider polarization losses) go into production of traveling waves. There is no localized field in the direct vicinity of the separation boundary. It must be recalled, however, that in transition radiation in a slab, this field, generally speaking, exists and must be taken into account.

3. Let us consider radiation for ultrarelativistic incident particles and for the simplest dependence of ϵ_i on the frequency, of the form $\epsilon_1 = 1$ and $\epsilon_2 = 1 - (\omega_0/\omega)^2$, where $\omega_0 = \sqrt{4\pi e^2 N/m}$ is the plasma frequency of the medium.

We estimate first the dimensions of the zone of formation of the transition radiation. The particle field will interact for the longest time with that group of frequencies, the wave packet of which moves at a group velocity v. The center of this packet is at the frequency

$$\omega_n = c\sqrt{(\lambda_n^2 + \omega_0^2/c^2)/(1 - \beta^2)}.$$

The interaction time $\Delta\tau_n$ is determined by the time of dissolution of this packet by dispersion in the waveguide; its order of magnitude is

$$\Delta\tau_n = 1/c\sqrt{(1 - \beta^2)\,(\lambda_n^2 + \omega_0^2/c^2)},$$

and therefore the dimensions of the effective zone of formation of transition radiation are given by

$$l_n \approx 1/\sqrt{(1 - \beta^2)\,(\lambda_n^2 + \omega_0^2/c^2)}. \quad (3.1)$$

The same result is obtained when the method of stationary phase is applied to (2.4).

Equation (3.1) determines the dimensions of the zone in which the motion of the particle cannot be distrubed. For example, we can draw from this the qualitative conclusion that to obtain a maximum effect in a slab (i.e., in order for the effects on the front and rear sides to add up) it is necessary to have a slab of thickness $\delta \gg l_1$.

In this case we can also calculate the total radiation energy. Integrating with respect to ω in (2.1) we obtain

$$S^- \approx 0,$$

$$S^+ = \frac{e^2\pi}{\sqrt{1 - \beta^2}} \sum_{n=1}^{\infty} |\psi_n(M_0)|^2 \times \left[\frac{1}{\lambda_n} + \frac{\lambda_n^2}{(\lambda_n^2 + k_0^2)^{3/2}} - \frac{4\lambda_n^2}{k_0^2}\left(\frac{1}{\lambda_n} - \frac{1}{\sqrt{\lambda_n^2 + k_0^2}}\right)\right], \quad (3.2)$$

where $k_0 = \omega_0/c$.

It is seen from (3.2) that the principal radiation is along the motion of the particle and is proportional to its energy. This circumstance was pointed out by Garibyan.[3]

Going to the limit in (3.2), by increasing the transverse dimensions of the waveguide without bounds, the sum becomes an integral, evaluation of which leads to

$$S^+ = e^2\omega_0 / 3c\sqrt{1-\beta^2}, \qquad (3.3)$$

which coincides with Garibyan's formula.[3]

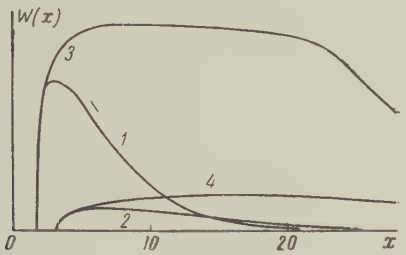

Radiation energy density as a function of a dimensionless parameter. $1-E_{01}$ mode and $2-E_{02}$ mode at 5 Mev particle energy, $3-E_{01}$ and $4-E_{02}$ mode at 50 Mev particle energy.

The diagram shows, on an arbitrary scale, curves for the radiation energy density W_n vs. the dimensionless parameter $x = \omega/\omega_0$ for a round waveguide, at $n = 1$ and 2 (E_{01} and E_{02} modes) and $\omega_0 r_0/c = 1.85$ (r_0 is the waveguide radius), for incident particles with energies on the order of 5 and 50 Mev. A comparison of the curves shows that the E_{02} mode is vanishingly small compared with the E_{01} mode (the scale of E_{02} is magnified ten times in the figure).

The radiation is essentially concentrated in the region of frequencies of order

$$c\sqrt{(\lambda_n^2 + k_0^2)/(1-\beta^2)};$$

while the magnitude of the radiated energy at a fixed frequency depends relatively little on the particle energy.

The result obtained shows that transition radiation can apparently be used to measure the energy of ultrafast particles. Bearing in mind the possibility of the use of transition radiation to generate millimeter waves, it becomes necessary, if noticeable radiation power is to be obtained, to use particle bunches whose dimensions are much less than the radiated wavelength (see reference 4 and the literature therein).

Assume for example, $\nu = 6 \times 10^9$ particles in the bunch, a bunch repetition rate 10^7/sec ($J = 10$ ma), $\omega \simeq 7.8 \times 10^{11}$ sec^{-1}, and $\Delta\omega/\omega \approx 0.1$. Then at particle energies on the order of 5 Mev the power radiated in the E_{01} mode is on the order of 15 watts. We also note that to increase the radiation efficiency it is advisable to use a series of alternating dielectric plates.

In conclusion, the author expresses his gratitude to B. M. Bolotovskiĭ and G. M. Garibyan for discussions.

[1] V. L. Ginzburg and I. M. Frank, JETP **16**, 15 (1945).

[2] G. M. Garibyan, JETP **33**, 1403 (1957), Soviet Phys. JETP **6**, 1079 (1958).

[3] G. M. Garibyan, JETP **37**, 527 (1959), Soviet Phys. JETP **10**, 372 (1960).

[4] G. A. Askar'yan, JETP **30**, 584 (1956), Soviet Phys. JETP **3**, 613 (1956).

Translated by J. G. Adashko
215

THEORY OF THE STABILITY OF MAGNETIC STATES OF FERROMAGNETIC MATERIALS IN THE MAGNETIZATION PROCESS

E. I. KONDORSKIĬ

Moscow State University

Submitted to JETP editor May 27, 1959

J. Exptl. Theoret. Phys. (U.S.S.R.) **37**, 1110-1115 (October, 1959)

The physical principles that determine the stability of magnetic states of a ferromagnetic monocrystal, with respect to external magnetic fields and to elastic forces, are considered. A formula is derived for the minimum value of magnetic fields and stresses at which the equilibrium of a domain wall passing near a nonmagnetic inclusion is destroyed, and at which an irreversible change of magnetization occurs. On this basis an explanation is given for the phenomenon, familiar experimentally, of strong magnetization of ferromagnets in weak magnetic fields by shocks or blows, and formulas are derived for estimating the irreversible changes of magnetization produced by elastic stresses. An explanation is given for the observed stability, with respect to elastic forces, of magnetic states corresponding to the ideal magnetization curve.

THE magnetic moment and mean magnetization of a ferromagnetic body are, as is known, not single-valued functions of the magnetic field intensity H, the temperature T, and the components σ_{ik} of the stress tensor that represents the effect of external forces. The magnetic moment can assume a value other than the original one when the values of H, T, or σ_{ik}, undergoing some kind of fluctuation, return to their original values (magnetic, thermomagnetic, and magnetoelastic hysteresis); it can also change with time though the values of these quantities remain constant (magnetic after-effect).

The present work deals with the physical principles that determine the stability of magnetic states of a ferromagnetic monocrystal with respect to elastic forces. An explanation is given for the observed stability of magnetic states corresponding to the ideal magnetization curve.

1. EFFECT OF EXTERNAL STRESSES ON THE COERCIVE FORCE AND MAGNETIZATION OF MONOCRYSTALS

The coercive force of a ferromagnetic monocrystal, magnetized along an axis of easy magnetization, depends on a number of factors and is usually a sum of several terms, for example

$$H_c = H_\sigma + H_d, \qquad (1)$$

where the first term is connected with the effect of inhomogeneous internal stresses, the second with the effect of inclusions on the movement of walls between domains. If the magnetic anisotropy constant $K >> \lambda_s \sigma_i$ (where λ_s is the saturation magnetostriction and σ_i the mean magnitude of the internal stresses), then the second term plays the fundamental role in magnetization processes.

In works of Néel[1] and the author[2] it has been shown that 180° walls are attracted by secondary domains toward inclusions; when no external magnetic field is present, these walls pass through inclusions[3] or are located in regions of greatest inclusion concentration. The first of these deductions was confirmed experimentally by observation of powder figures on the surfaces of monocrystals of silicon iron.[4] In these investigations it was also shown that in a magnetic field the walls begin to move, and thereupon the secondary domains that are produced around an inclusion become extended in a direction at an angle of 45° to the plane of the wall, forming a connection between the wall and the inclusion (cf. the figure). H_d represents the field intensity at which the wall breaks away from the secondary domain and an irreversible jump of magnetization occurs.

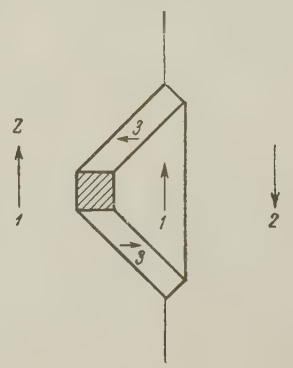

The surface and volume energies of domains depend, as is known, on the components of the strain tensor. It follows that external stresses should have an effect on the energy of secondary domains and thus should affect the value of H_d. The magnetic state of a crystal in a field H will be stable with respect to the elastic forces if the change of H_d due to these forces is such that the difference $H_d - H$ does not become zero. In the contrary case, a crystal in a magnetic field, under the influence of elastic stresses, will undergo irreversible changes of magnetization.

Calculations of H_d for various cases have already been made,[1-3] but the effect of elastic stresses on H_d has so far not been considered. Furthermore, in the calculation of H_d no attention has been paid to the elastic energy of secondary domains, an energy due to magnetostriction. In the present work, in calculating the H_d of a strained crystal, we shall restrict ourselves to consideration of the case in which a tensile or compressive force acts along the direction of a cube edge parallel to the magnetization of the primary domains of the crystal, such as domains 1 and 2 in the figure. Furthermore, following the method used by E. M. Lifshitz[5] in calculating the domain structure of an iron crystal, we shall suppose that the strain tensor is constant within the crystal, since the volume occupied by the secondary domains 3, formed around the inclusion, is small in comparison with the volume of the primary domains magnetized parallel or antiparallel to the z axis. In this case the difference of the strain tensor components is

$$\tau_{zz} - \tfrac{1}{2}(\tau_{xx} + \tau_{yy}) = \tau_{zz} - \tau_{xx} = \tfrac{3}{2}\lambda_{100} + \sigma / 2C_2, \qquad (2)$$

where λ_{100} is a magnetostriction constant, C_2 is an elastic modulus of the crystal, and σ is the value of the external tensile stress; hence the free-energy density of the secondary domains is

$$F = 3\lambda_{100}C_2(\tau_{zz} - \tau_{xx}) = \tfrac{9}{2}\lambda_{100}^2 C_2 + \tfrac{3}{2}\lambda_{100}\sigma. \qquad (3)$$

The change $\Delta\Phi$ in the thermodynamic potential $\Phi = F - HI$, referred to unit area of the wall, upon displacement of the latter through Δx in a constant field H, is

$$\Delta\Phi = \left[-2HI_s\left(1 - \tfrac{1}{2}a_2 v^{2/3}\right) + a_1\gamma_\sigma v^{2/3}/d + \tfrac{3}{2}a_2\lambda_{100}(3\lambda_{100}C_2 + \sigma)\, v^{2/3}\right]\Delta x, \qquad (4)$$

$$\gamma_\sigma = \gamma\left[1 + 3\lambda_{100}\sigma / 2(K + 3\lambda_{100}^2 C_2)\right]^{1/2}, \qquad (4')$$

where γ is the surface energy of the wall at $\sigma = 0$, d is the mean diameter of the inclusions, v is their volume concentration, K is the anisotropy constant, and a_1 and a_2 are dimensionless coefficients of order unity, dependent on the form of the inclusions. The mean number of inclusions per unit area of the wall is $v^{2/3}/d^2$. Formula (3) is valid under the conditions $v \ll 1$ and $d > \delta$, where $\delta = \pi\sqrt{J/Ka_0}$ is the so-called wall thickness, J is the exchange integral, and a_0 is the lattice parameter; for an iron crystal, $\delta \approx 10^{-5}$ cm.

The first term in square brackets in (4) is the change of magnetic energy of the volume in the crystal that reverses its magnetization on displacement of the wall through Δx (the term $a_2 v^{2/3}/2$ is a small correction for the volume of the secondary domains); the second term gives the change of surface energy, and the third the change of volume energy, of the secondary domains. The minimum values of field, $H = H_d$, and of external stress σ for which the wall can break away from the inclusion correspond to $\Delta\Phi = 0$. Hence, discarding the small term $a_2 v^{2/3}/2$, we get*

$$H_d = a_1\gamma_\sigma v^{2/3} / 2I_s d + (3a_2\lambda_{100} / 4I_s)(3\lambda_{100}C_2 + \sigma)\, v^{2/3}. \qquad (5)$$

For $|\lambda_{100}\sigma| << |K|$, the value of γ_σ is $\approx \gamma$, and (5) can be rewritten in the following form:

$$H_d = H_{d0}\left(1 + \frac{3a_2}{2a_1}\frac{\lambda_{100}}{\gamma / d + (9a_2 / 2a_1)\lambda_{100}^2 C_2}\sigma\right), \qquad (6)$$

where

$$H_{d0} = a_1\frac{\gamma v^{2/3}}{2I_s d}\left(1 + \frac{9}{2}\frac{a_2}{a_1}\frac{\lambda_{100}^2 C_2}{\gamma / d}\right). \qquad (7)$$

The second term in parentheses in (7) represents a correction connected with the magnetostrictive energy of the secondary domains. For iron crystals, $\tfrac{9}{2}\lambda_{100}^2 C_2 \approx 10^3$ erg/cm^3, $\gamma = 1.8$ erg/cm^2. Thus for $d \approx 10^{-4}$ cm, this correction amounts to about 10%, and for $d \approx 10^{-5}$ it is practically negligible. The size of the second term in parentheses in expression (6) depends on σ. For $\sigma = 10^9$ cgs units = 10 kg/mm^2, we get $\tfrac{3}{2}\lambda_{100}\sigma \approx 3 \times 10^4$ erg/cm^3. In this case, for d $\approx 10^{-4}$ to 10^{-5} cm we get $3\lambda_{100}\sigma d/2\gamma \approx 1$. It follows that H_d can, in accordance with the sign of $\lambda_{100}\sigma$, be several times larger or smaller than H_{d0}. On passage through the crystal of an elastic wave with amplitude of order 10^9 cgs units or more, H_d will periodically become zero; this will cause an increase of magnetization even for insignificantly small external fields H. Thus it is evidently possible to explain the phenomenon, well known from experiment, of strong magnetization of ferromagnetic bodies in very weak magnetic

*The first term of formula (5) was obtained by the author earlier[2] by a similar method.

fields under the influence of shocks or blows. It must be emphasized that, as follows from formula (6), the application of external stresses substantially affects the stability of 180° walls, despite the still prevalent opinion that elastic stresses for $H \neq 0$ can produce only motion of walls between domains magnetized at an angle different from 180° (for example, 90° walls).

In polycrystalline ferromagnets, besides the reasons indicated above for an effect of external stresses on coercive force, there are a number of others, connected with conditions on grain boundaries and with the effect of external stress on the orientation of axes of easy magnetization. We shall not be concerned with these topics here; to some extent they have already been treated in the literature.[6-8]

If, as is usual, irreversible changes of magnetization occur in some field interval, then the increase of the irreversible part of the magnetization takes the form $\Delta I_{ir} = \kappa_{ir}\Delta H$, where ΔH is the increase in the effective field. From (6) it follows that application of a stress σ is equivalent to change of the field by $\Delta H_\sigma = H_{d0} - H_d$. For $H \neq 0$ and $\Delta H_\sigma > 0$, this leads to an irreversible change of magnetization

$$\Delta I_{ir} = \varkappa_{ir}(H_{d0} - H_d). \tag{8}$$

If $H \approx H_d$ and if $\lambda\sigma \ll K$, then according to (2) — (5)

$$\Delta I_{ir} = \varkappa_{ir} v^{2/3} \lambda\sigma / I_s \approx \varkappa_{ir} H_d \sigma\lambda d / \gamma. \tag{9}$$

Formula (9) permits approximate estimation of the irreversible changes of magnetization that occur under the influence of external elastic stresses.

In the most general case, with an arbitrary mechanism for the effect of external stresses on irreversible changes of magnetization (we considered above only one of the possible mechanisms for such an effect), the condition for stability of 180° walls with respect to a change of stress is the vanishing of the field H_i that acts on the wall. This field is connected with the external field H and with the magnetization by the known relation

$$H_i = H - \nu_e I, \tag{10}$$

where ν_e is the local demagnetizing factor, dependent on the shape of the body and on its structure, in particular on the shape and concentration of the inclusions; in the general case ν_e is a function of the coordinates of points within the body.

Apart from the trivial case in which $I = 0$ at $H = 0$ (the demagnetized state), vanishing of the effective field H_i occurs in states for which $H = \nu_e I$. Thus the states that have greatest stability with respect to σ are those with mean magnetization

$$I = H / \nu, \tag{11}$$

where ν is the mean demagnetizing factor of the body.

Experiment shows that in bodies with a sufficiently large shape demagnetizing factor N_0, so that $\nu \approx N_0$, the stable states described by Eq. (11) can be obtained by means of the magnetic treatment that leads to "ideal" magnetization. It will be shown below that this result follows from modern theoretical ideas.

2. INITIAL MAGNETIC SUSCEPTIBILITY OF THE IDEAL CURVE, AND THE DEMAGNETIZING FACTOR

We consider the processes that take place in a ferromagnetic monocrystal during ideal magnetization. Let the values of the coercive forces in different regions of the monocrystal be included within narrow limits $H_{c\,min} \leq H_c \leq H_{c\,max}$. Upon the monocrystal, with an internal demagnetizing factor, let there act a constant field $H \leq \nu I_S$ and a slowly decreasing alternating field with amplitude h_0, directed along an axis of easy magnetization; and let the frequency of the alternating field be so low that its amplitude and phase are approximately the same at all points of the monocrystal.

In the time interval during which the amplitude of the alternating field, h_0, exceeds $H_{c\,max} + H + \nu I_S$, domain walls move back and forth past an inclusion, executing oscillations at frequency ω. In this process the mean magnetization of the monocrystal is zero, and the resultant field H_i changes, with cyclic magnetization reversal, between the limits $h_0 + H - \nu I_S$ and $-h_0 + H + \nu I_S$. At the instant when h_0 becomes less than $H_{c\,max} + H + \nu I_S$, and consequently the absolute value of the lower limit of H_i becomes less than $H_{c\,max}$, a part of the walls can no longer move past inclusions; there comes into existence a constant component I_0 of magnetization, directed along H, and there appears an additional constant component of field, equal to $-\nu I_0$. From this instant on, as long as the upper limit remains equal to I_S, the magnetization changes from I_S to $-I_S + 2I_0$ and the resultant field H_i accordingly from H_{i1} to $-H_{i2}$, where

$$-H_{i2} = -h_0 + H + \nu(I_s - 2I_0) \leqslant H_i \leqslant h_0 + H - \nu I_s = H_{i1}. \tag{12}$$

Under these conditions the various regions of the

monocrystal can be divided into two groups: 1) regions in which H_c lies within the limits

$$H_{c\,min} \leqslant H_c \leqslant H_{i2}; \tag{13}$$

2) regions in which

$$H_{i2} < H_c \leqslant H_{c\,max}. \tag{14}$$

In regions of the first group, walls move past inclusions twice during each period of alternation of h, i.e., even when h is directed opposite to the constant field H. These regions obviously make no contribution to I_0. In regions of the second group, whose coercive force is larger than the lower limit H_{i2} of the resultant field, walls cannot move past inclusions when the alternating field is directed opposite to the constant field. The magnetization of these regions remains parallel to the constant field, since, under the conditions assumed for the upper limit of the resultant field, saturation is attained (the upper limit of the magnetization is equal to I_S).

From (12) it is evident that as long as the upper limit of the magnetization is equal to I_S, the difference between the absolute values of the upper and lower limits of the resultant field is

$$H_{i1} - H_{i2} = 2(H - \nu I_0). \tag{15}$$

It is easy to demonstrate that (15) remains valid as long as $H > \nu I_0$, i.e., $H_{i1} > H_{i2}$. In fact, while the last inequality is satisfied, H_{i1} according to (13) is always larger than the largest of the coercive forces of regions of the first group; this guarantees attainment of saturation at field H_{i1}, i.e., attainment of the upper limit of the magnetization, equal to I_S.

With decrease of h_0, the number of regions falling in the second group increases, the number of regions remaining in the first decreases, and the constant component I_0 increases. Since, in the case we are considering, $H < \nu I_S$, there comes in the process of increase of I_0 an instant when $H - \nu I_0$ vanishes or changes sign, and when the upper limit of H_i becomes equal to the absolute value of the lower limit (or becomes less than the absolute value of the lower limit). Let this instant come at $H_{i2} = H_{C0}$. From this instant on, in the process of extinction of h, each successive value of the amplitude of H_i will be less in absolute value than the preceding (regardless of the sign of H_i). Therefore in only about half of the regions with coercive forces $H_C < H_{C0}$ will the magnetization, on transition from the first group to the second, remain parallel to the field H. In the other half of the regions, which pass from the first group to the second when $|H_{i2}| > H_{i1}$, the magnetization will remain antiparallel to the field. Thanks to this, at the instant when H_{i1} and H_{i2} become less than H_{C0}, the increase of the constant component I_0 will cease, and the upper limit of the magnetization will become less than I_S.

Thus in the process of decrease of the alternating field, the value of I_0 reaches a limiting value I_{0m}, which according to (15) is equal to

$$I_{0m} = H/\nu. \tag{16}$$

Comparison of (16) and (11) shows that states corresponding to points on the ideal curve actually are the most stable with respect to the effects of external stresses.

[1] L. Néel, Cahiers de Physique **25**, 21 (1944).

[2] E. I. Kondorskiĭ, Dokl. Akad. Nauk SSSR **68**, 37 (1949).

[3] M. Kersten, Grundlagen einer Theorie der ferromagnetischen Hysterese und der Koerzitivkraft (S. Hirzel, Leipzig, 1943; J. W. Edwards, Ann Arbor, 1946).

[4] Williams, Bozorth, and Shockley, Phys. Rev. **75**, 155 (1949); H. J. Williams and W. Shockley, Phys. Rev. **75**, 178 (1949).

[5] E. M. Lifshitz, JETP **15**, 97 (1945).

[6] E. I. Kondorskiĭ, JETP **10**, 420 (1940).

[7] J. Goodenough, Phys. Rev. **95**, 917 (1954).

[8] H. Dietrich and E. Kneller, Z. Metallkunde **47**, 716 (1956).

Translated by W. F. Brown, Jr.
216

ON THE THEORY OF THE RELATIVISTIC TRANSFORMATIONS OF THE WAVE FUNCTIONS AND DENSITY MATRIX OF PARTICLES WITH SPIN

V. S. POPOV

Submitted to JETP editor May 28, 1959

J. Exptl. Theoret. Phys. (U.S.S.R.) **37**, 1116-1126 (October, 1959)

Expansions are obtained for the wave functions of a particle with spin s and for those of a system of two particles with arbitrary spins s_1 and s_2, in terms of the irreducible representations of the homogeneous Lorentz group; this makes possible a relativistically invariant classification of the states. For the invariant description of the polarization of free particles an expansion of the density matrix is found in terms of the irreducible representations of the Lorentz group.

1. The finite-dimensional representations (tensor and spinor representations) of the Lorentz group are widely used in quantum field theory. Since, however, the Lorentz group is not compact, there exists for it an entirely different class of representations, namely the infinite-dimensional representations. The application of the infinite-dimensional representations in the theory of elementary particles was first achieved in a paper by Ginzburg and Tamm.[1]

The unitary representations of the Lorentz group were discovered almost simultaneously by several authors — Gel'fand and Naĭmark,[2] Dirac,[3] and Harish-Chandra[4] — but did not find any applications in physics for a long time thereafter.

In 1955 Shapiro[5] proposed and treated the problem of the expansion of the wave function of a free particle in terms of the irreducible representations of the Lorentz group. Such an expansion makes possible a relativistically invariant classification of the states of the particle in terms of the eigenvalues of the invariants of the homogeneous group: the scalar $\hat{F} = \frac{1}{2} M_{\mu\nu}M_{\mu\nu}$ and the pseudoscalar $\hat{G} = \frac{1}{16}\epsilon_{\mu\nu\rho\sigma}M_{\mu\nu}M_{\rho\sigma}$, where $M_{\mu\nu}$ is the four-dimensional angular-momentum tensor:

$$M_{\mu\nu} = -i(p_\mu \partial/\partial p_\nu - p_\nu \partial/\partial p_\mu) + S_{\mu\nu}.$$

$S_{\mu\nu}$ is the spin part of the four-dimensional angular momentum. Dolginov[6] also treated this problem by another method.

Later Chou Kuang-Chao and Zastavenko[7] made improvements in Shapiro's expansion for particles with nonzero spin. It must be remarked, however, that the method they used involves extremely cumbersome calculations, since they did not use to its full extent the theory of the representations of the Lorentz group.

From the mathematical point of view the formulas obtained in references 5 and 7 make up an integral transformation, which, following reference 7, we shall call the "Shapiro transformation." In the present paper we begin with a simpler derivation of the Shapiro transformation for a free particle with arbitrary spin s; we then use an analogous method to study a system of two interacting particles. In the concluding part of the paper an expansion in irreducible parts is carried out for the density matrix of the free particle and the system of two particles; this is of importance for the description of polarization in the relativistic case.

2. Let us consider a free particle with arbitrary spin s and mass κ ($\kappa \neq 0$). The amplitude of the one-particle state (after second quantization) has the form

$$\Phi_1 = \int \frac{\varkappa d^3p}{p_0} \sum_{\sigma=-s}^{s} \varphi_\sigma(\mathbf{p})\, a_\sigma^+(\mathbf{p})\, \Phi_0, \qquad (1)$$

where, as usual, $a_\sigma^+(\mathbf{p})$ is the operator for creation of a particle with momentum p and spin component σ along the z axis, Φ_0 is the vacuum amplitude, and $\varphi_\sigma(\mathbf{p})$ are the corresponding Fock amplitudes. Here we must be exact about what we mean by the spin: for example, for particles with spin $\frac{1}{2}$ that obey the Dirac equation the spin operator is ordinarily taken to be $\frac{1}{2}\sigma$.[8] But then there do not exist states with prescribed momentum p and definite spin component in any direction in space, unless the direction is that of the momentum itself. It will be more convenient for us to go over to the spin in the rest system, i.e., to introduce the operator $\hat{S}_i = L(\mathbf{p})\, S_i^0 L^{-1}(\mathbf{p})$, where $\hat{S}_i^0$ is the spin operator in the rest system, which has the same properties as the spin in the nonrelativistic theory,

and $L(p)$ is the pure Lorentz transformation* that gives the change from the rest system of the particle to the reference system in which it has the momentum p: $L(p)p_0 = p$, $p_0 = (0, 0, 0, \kappa)$. It is obvious that in the rest system the spin of the particle can be oriented in an arbitrary direction, and there exist states with momentum p and the spin component σ along the z axis:

$$\psi_{p\sigma}(x) = (2\pi)^{-3/2} v_\sigma(p) e^{i(px)}, \quad v_\sigma(p) = L(p) v_\sigma(0), \quad (2)$$

where $v_\sigma(0)$ is the eigenfunction of the ordinary operator $\hat{S}^0_z$ in the rest system: $\hat{S}^0_z v_\sigma(0) = \sigma v_\sigma(0)$. The field operator $\psi(x)$ is expanded in terms of the system of functions $\psi_{p\sigma}(x)$, $\psi^*_{p\sigma}(x)$:

$$\psi(x) = \int \frac{\varkappa d^3p}{p_0} \sum_{\sigma=-s}^{s} (a_\sigma(p)\psi_{p\sigma}(x) + b^+_\sigma(p)\psi^*_{p\sigma}(x)),$$

after which we can find the operators of the dynamical variables: the energy and momentum, and the angular momentum. Comparing them with the usual expressions, we find the commutation rule of the operators $a_\sigma(p)$:

$$[a_\sigma(p),\ a^+_{\sigma'}(p')] = \varkappa^{-1} p_0 \delta_{\sigma\sigma'} \delta(p - p') \quad (3)$$

(the left member must be the commutator for an integer spin s and the anticommutator for half-integral s).

We need to find the law of transformation of the Fock amplitudes $\varphi_\sigma(p)$. For this purpose we apply an arbitrary transformation g of the proper Lorentz group to the probability amplitude for finding the particle at the point x

$$f(x) = (\Phi_0, \psi(x)\Phi_1) = (2\pi)^{-3/2} \int \frac{\varkappa d^3p}{p_0} \sum_\sigma \varphi_\sigma(p) v_\sigma(p) e^{i(px)}. \quad (4)$$

We here take into account the fact that $v_\sigma(p)$ transforms according to a finite-dimensional representation τ_{s0} ($P = s$, $Q = 0$; for the notation see reference 9):

$$T_g v_\sigma(p) = T_g \tau_{s0}(L_p) v_\sigma(0) = \tau_{s0}(gL_p) v_\sigma(0)$$

$$= \tau_{s0}(L_{gp}) \tau_{s0}(R(g, p)) v_\sigma(0) = \sum_{\sigma'=-s}^{s} D^{(s)}_{\sigma\sigma'} \{R(g, p)\} v_{\sigma'}(gp),$$

where we have introduced the rotation $R(g, p)$:

$$gL_p = L_{gp} R(g, p) \quad (5)$$

(this is the so-called Thomas precession, if g itself is a pure Lorentz transformation), and where we use the condition that under rotations in the rest system the wave functions $v_\sigma(0)$ transform according to the irreducible representation of weight s of the rotation group (fundamental property of the spin s). From this we find how the Fock amplitudes transform:*

$$T_g \varphi_\sigma(p) = \sum_{\sigma'=-s}^{s} D^{(s)}_{\sigma\sigma'} \{R(g, g^{-1}p)\} \varphi_{\sigma'}(g^{-1}p). \quad (6)$$

It is clear from physical considerations that Eq. (6) must be a representation of the Lorentz group; formally this follows from the group property of the rotations R:

$$R(g_1, g_1^{-1}p) R(g_2, (g_1g_2)^{-1}p) = R(g_1g_2, (g_1g_2)^{-1}p). \quad (7)$$

It is also obvious that Eq. (6) is a unitary representation, because there is conservation of the total number of particles

$$\int \frac{\varkappa d^3p}{p_0} \sum_{\sigma=-s}^{s} |\varphi_\sigma(p)|^2;$$

therefore it can be expanded in terms of the unitary irreducible representations of the Lorentz group, which are all infinite-dimensional[10,11] and are characterized by two numbers m, ρ, which are connected with the eigenvalues of the invariants: $\hat{F} = -[1 + \frac{1}{4}(\rho^2 - m^2)]$, $\hat{G} = -\frac{1}{4} im\rho$. To find this expansion, let us go over from the wave function $\varphi_\sigma(p)$ to a new function $\chi_\sigma(g)$ of the Lorentz transformation g:

$$\chi_\sigma(g) = \sum_{\sigma'=-s}^{s} D^{(s)}_{\sigma\sigma'} \{R(g, p)\} \varphi_{\sigma'}(p), \quad (8)$$

where

$$p = g^{-1}p_0, \ p_0 = (0, 0, 0, \varkappa).$$

It follows from (6) that $\chi_\sigma(g)$ transforms by the regular representation of the Lorentz group:

$$T_{g_0} \chi_\sigma(g) = \chi_\sigma(gg_0) \quad (9)$$

(Here T_{g_0} denotes the operator that acts on the function $\chi_\sigma(g)$ when the Lorentz transformation g_0 is applied to the coordinates), and the expansion of the regular representation in terms of the irreducible representations is known.[10] Let us now find how $\chi_\sigma(g)$ depends on the left unitary operator. Since an arbitrary spatial rotation does not change the momentum in the rest system ($up_0 = p_0$), it follows from (7) that

$$R(ug, (ug)^{-1}p_0) = R(u, p_0) R(g, g^{-1}p_0);$$

the rotation $R(u, p_0)$ is determined from the equation $uL_{p_0} = L_{up_0} R(u, p_0)$, and since $up_0 = p_0$, $L_{p_0} = 1$, we have $R(u, p_0) = u$. Using the definition (8), we get

*Every transformation of the proper Lorentz group can be represented in the form $g = u_2 \epsilon u_1$, where u_2 and u_1 are spatial rotations and ϵ is the change to a reference system moving along the z axis. If $u_2 = u_1^{-1}$ we call g a pure Lorentz transformation.

*This formula was given without proof in reference 7.

$$\chi_\sigma(ug) = \sum_{\sigma'=-s}^{s} D^{(s)}_{\sigma\sigma'}\{R(ug, (ug)^{-1}p_0)\}\,\varphi_{\sigma'}(p)$$

$$= \sum_{\sigma'=-s}^{s} D^{(s)}_{\sigma\sigma'}(u)\,\chi_{\sigma'}(g). \qquad (10)$$

The properties (9) and (10) are sufficient for the expansion of $\chi_\sigma(g)$ in terms of irreducible representations. To accomplish it we use the analog of Plancherel's formula from reference 10. If $x(g)$ is the regular representation of the Lorentz group, its expansion in terms of irreducible representations has the form

$$K_{m\rho}(z_1, z_2) = \int x(z_1^{-1}kz_2)\,\alpha^*_{m\rho}(k)\,d\mu_l(k),$$

$$x(g) = (2\pi)^{-4} \sum_{m=-\infty}^{\infty} \int_0^\infty d\rho\,(m^2+\rho^2) \int d\mu(z)\,K_{m\rho}(z, z_1)\,\alpha_{m\rho}(k),$$

where $zg = kz_1$; here (and often in what follows) g denotes both some transformation of the proper Lorentz group and also the corresponding two-rowed matrix b of its spinor representation; $\alpha_{m\rho}(b)$ is a function defined on the group of two-rowed matrices b:

$$\alpha_{m\rho}(b) = |b_{22}|^{m+i\rho-2} b_{22}^{-m},$$

$$\text{for } b = \begin{pmatrix} b_{11} & b_{12} \\ b_{21} & b_{22} \end{pmatrix}, \quad \det b = 1.$$

Under transformations of the Lorentz group the function $K_{m\rho}(z_1, z_2)$ transforms by the irreducible $(m\rho)$ representation with respect to its first argument z_2, and its first argument z_1 remains unchanged [the space of the representations consists of the functions on the group of matrices $z = \begin{pmatrix} 1 & 0 \\ z & 1 \end{pmatrix}$; for further details see references 5, 11]. The representations (m, ρ) and $(-m, -\rho)$ are equivalent, and therefore the expansion of $x(g)$ involves only one of them $(\rho > 0)$. It will be more convenient for us to take as the space of the representation the manifold of functions on the unitary group u; for this purpose let us introduce the matrices u_1, u_2 by the formula* $z_1 = k_1u_1$, $z_2 = k_2u_2$, and the new function

$$\hat{K}_{m\rho}(u_1, u_2) = \pi\alpha^*_{m\rho}(u_1)\,\alpha_{m\rho}(u_2)\,K_{m\rho}(z_1, z_2)$$

$$= \pi \int x(u_1^{-1}ku_2)\,\alpha^*_{m\rho}(k)\,d\mu_l(k).$$

It transforms in the following way:

$$T_{g_0}\hat{K}_{m\rho}(u_1, u) = \alpha_{m\rho}(k)\,\hat{K}_{m\rho}(u_1, u'), \qquad ug_0 = ku'. \qquad (11)$$

This indeed means that $\hat{K}_{m\rho}(u_1, u)$ transforms by the irreducible representation $(m\rho)$ (with respect to its argument u). The expansion of the regular representation takes the form

$$\hat{K}_{m\rho}(u_1, u) = \pi \int x(u_1^{-1}ku)\,\alpha^*_{m\rho}(k)\,d\mu_l(k),$$

$$x(g) = \sum_{m=-\infty}^{\infty} \int_0^\infty d\rho\,\frac{m^2+\rho^2}{(2\pi)^4} \int du_1\,\hat{K}_{m\rho}(u_1, u)\,\alpha_{m\rho}(k), \qquad (12)$$

where $u_1g = ku$. Let us now substitute in (12) the function $\chi_\sigma(g)$ instead of $x(g)$ [cf. Eq. (8)]. It is well known that every matrix of the type k can be represented in the form $k = \gamma\epsilon\zeta$ (for further details see reference 5), where

$$\gamma = \begin{pmatrix} e^{-i\gamma/2} & 0 \\ 0 & e^{i\gamma/2} \end{pmatrix}, \quad \varepsilon = \begin{pmatrix} \lambda^{-1} & 0 \\ 0 & \lambda \end{pmatrix}, \quad \zeta = \begin{pmatrix} 1 & \zeta \\ 0 & 1 \end{pmatrix}$$

(in the spinor representation γ corresponds to a rotation through the angle γ around the z axis, and ϵ to a Lorentz transformation along the z axis). Furthermore $d\mu_l(k) = 2\pi d\mu(\gamma)\,d\mu(\epsilon)\,d\zeta$, where $d\mu_l(k)$, $d\mu(\gamma)$, $d\mu(\epsilon)$, $d\zeta$ are invariant measures* on the groups of matrices k, γ, ϵ, ζ. Substituting this in Eq. (12), we get

$$\hat{K}_{m\rho}(u_1\ u;\ \sigma) = 2\pi^2 \int \chi_\sigma(u^{-1}\gamma\varepsilon\zeta u)\alpha^*_{m\rho}(\gamma\varepsilon\zeta)\,d\mu(\gamma)\,d\mu(\varepsilon)\,d\zeta$$

$$= \pi^2 \sum_{\sigma'} \int d\mu(\gamma)\,D^{(s)}_{\sigma\sigma'}(u_1^{-1}\gamma)\,\alpha^*_{m\rho}(\gamma) \int \chi_{\sigma'}(\varepsilon\zeta u)\,\alpha^*_{m\rho}(\varepsilon)\,d\mu(\varepsilon)\,d\zeta.$$

Since $\alpha^*_{m\rho}(\gamma) = \exp\{im\gamma/2\}$, the integration over $d\mu(\gamma)$ gives $\delta_{\sigma', m/2} D^{(s)}_{\sigma, m/2}(u_1^{-1})$, from which there follows the selection rule: the wave function of a particle with spin s has as its components the irreducible representations (m, ρ) in which $m = -2s, -2s+2, \ldots, 2s-2, 2s$. In the remaining integral we transform $d\mu(\epsilon)\,d\zeta$.

---

*Here k is a triangular matrix of the type

$$\begin{pmatrix} k_{11} & k_{12} \\ 0 & k_{22} \end{pmatrix}, \quad \det k = k_{11}k_{22} = 1;$$

u is a unitary matrix:

$$u = \begin{pmatrix} \alpha & \beta \\ -\bar{\beta} & \bar{\alpha} \end{pmatrix}, \quad |\alpha|^2 + |\beta|^2 = 1.$$

*Let $k = \begin{pmatrix} \lambda^{-1} & \mu \\ 0 & \lambda \end{pmatrix}$, where λ, μ are arbitrary complex numbers; let us set $\lambda = \lambda' + i\lambda''$, $\mu = \mu' + i\mu''$, where λ', λ'', μ', μ'' are real. A left invariant measure on the subgroup of matrices k is an expression

$$d\mu_l(k) = \omega(\lambda, \mu)\,d\lambda'd\lambda''d\mu'd\mu'',$$

that satisfies the condition

$$\int f(k)\,d\mu_l(k) = \int f(k_0k)d\mu_l(k)$$

for any function f(k) that is integrable on the group of matrices k, and any fixed matrix k_0. Right invariant measure is defined analogously. It can be shown[11] that $d\mu_l(k) = d\lambda'd\lambda''d\mu'd\mu''$. For the subgroups γ, ϵ, ζ the left and right invariant measures are the same. We define them as follows:

$$d\mu(\gamma) = \frac{d\varphi}{2\pi} \text{ for } \gamma = \begin{pmatrix} e^{-i\varphi/2} & 0 \\ 0 & e^{i\varphi/2} \end{pmatrix},$$

$$d\mu(\varepsilon) = \frac{d\lambda}{\lambda} \text{ for } \varepsilon = \begin{pmatrix} 1/\lambda & 0 \\ 0 & \lambda \end{pmatrix},$$

$$d\zeta = d\zeta'd\zeta'' \text{ for } \zeta = \begin{pmatrix} 1 & \zeta \\ 0 & 1 \end{pmatrix},\ \zeta = \zeta' + i\zeta''.$$

Here λ is a real number, and ζ means simultaneously a definite type of two-rowed matrix and the complex number appearing in such a matrix.

To do so we set $p = (\epsilon\xi u)^{-1} p_0$; by a change of variables it can be shown that $d\mu(\epsilon)\, d\xi = (\lambda^4/2\kappa^2) \times d^3p/p_0$, where $\lambda = \epsilon_{22}$. Since $\alpha^*_{m\rho}(\epsilon) = \lambda^{-i\rho-2}$, we must express λ in terms of $\mathbf{p}$ and the parameters of the rotation u. It is easy to verify that for an arbitrary two-rowed matrix b of the spinor representation we have: $|k_{22}|^2 = |b_{21}|^2 + |b_{22}|^2$, if $b = ku$. Let us introduce a vector n_0 of zero length with its space part directed along the z axis, $n_0 = (0, 0, 1, 1)$, and calculate the scalar product:

$$(n_0,\ gp_0) = (gp_0)_3 - (gp_0)_0 = \varkappa (g_{30} - g_{00}),$$

since $p_0 = (0, 0, 0, \kappa)$. The elements of the matrix g are expressed in a known way in terms of the parameters of the corresponding matrix b of the spinor representation (see reference 11):

$$g_{30} = \tfrac{1}{2}(|b_{11}|^2 + |b_{12}|^2 - |b_{21}|^2 - |b_{22}|^2),$$

$$g_{00} = \tfrac{1}{2}(|b_{11}|^2 + |b_{12}|^2 + |b_{21}|^2 + |b_{22}|^2),$$

from which we get

$$|b_{21}|^2 + |b_{22}|^2 = -\varkappa^{-1}(n_0,\ gp_0) = |k_{22}|^2.$$

In our case $b = uL_p$, $k = (\epsilon\xi)^{-1}$, from which we have $k_{22} = \lambda^{-1}$. Therefore $\lambda^{-2} = -\kappa^{-1}(n_0, uL_p p_0) = -\kappa^{-1}(u^{-1}n_0, p) = \kappa^{-1}[p_0 - (\mathbf{p}\cdot\mathbf{n})]$. Here the three-dimensional vector $\mathbf{n} = u^{-1}\mathbf{n}_0$ has been introduced. We still have to express the auxiliary function $\chi_{\sigma'}(\epsilon\xi u)$ in terms of the Fock amplitude $\varphi_\sigma(\mathbf{p})$. For this purpose let us determine the rotation u from the condition $uL_p = (\epsilon\xi)^{-1}\tilde{u}$. It is well known that the representation of an arbitrary matrix b of the spinor representation in the form $b = ku$ is ambiguous (see references 5 and 11). In the present case, however, $\arg\{(\epsilon\xi)^{-1}\}_{22} = 0$ independently of the complex number ξ, and the rotation $\tilde{u}$ is determined uniquely. $\chi_{\sigma'}(\epsilon\xi u)$ is connected with $\varphi_\sigma(\mathbf{p})$ by the formula (8), in which $R(g, g^{-1}p_0)$ appears, with $g = \epsilon\xi u$. We have:

$$g^{-1}p_0 = (\varepsilon\zeta u)^{-1}p_0 = p, \qquad gL_p = \varepsilon\zeta u L_p = \tilde{u},$$

that is,

$$R(\varepsilon\zeta u,\ (\varepsilon\zeta u)^{-1}p_0) = \tilde{u}$$

and

$$\chi_{\sigma'}(\varepsilon\zeta u) = \sum_{\sigma=-s}^{s} D^{(s)}_{\sigma'\sigma}(\tilde{u})\, \varphi_\sigma(\mathbf{p}).$$

As the result we get the following formula:

$$\hat{K}_{m\rho}(u_1,\ u;\ \sigma) = \frac{\pi^2}{\varkappa^2} D^{(s)}_{\sigma, m/2}(u_1^{-1}) \times \sum_{\sigma'=-s}^{s} \int \frac{d^3p}{p_0} \left(\frac{p_0 - (\mathbf{pn})}{\varkappa}\right)^{-1+i\rho/2} D^{(s)}_{m/2,\sigma'}(\tilde{u})\, \varphi_{\sigma'}(\mathbf{p}).$$

Since u_1 does not change under Lorentz transformations, instead of $\hat{K}_{m\rho}(u_1, u;\ \sigma)$ we can introduce a function of only one argument u, which transforms according to the irreducible representation $(m\rho)$:

$$\hat{K}_{m\rho}(u_1,\ u;\ \sigma) = \frac{4\pi^3}{\varkappa} D^{(s)}_{\sigma, m/2}(u_1^{-1})\, c_{m\rho}(u),$$

$$c_{m\rho}(u) = \frac{1}{4\pi\varkappa} \sum_{\sigma=-s}^{s} \int \frac{d^3p}{p_0} \left(\frac{p_0 - (\mathbf{pn})}{\varkappa}\right)^{-1+i\rho/2} D^{(s)}_{m/2,\sigma}(\tilde{u})\, \varphi_\sigma(\mathbf{p}). \tag{13}$$

To find the inverse transformation we use the second of the equations (12)

$$\chi_\sigma(g) = (2\pi)^{-4} \sum_{m=-\infty}^{\infty} \int_0^\infty d\rho\,(m^2+\rho^2) \int du_1 \hat{K}_{m\rho}(u_1, u;\ \sigma)\, \alpha_{m\rho}(k)$$

$$= \frac{1}{4\pi\varkappa} \sum_{m=-\infty}^{\infty} \int_0^\infty d\rho\,(m^2+\rho^2) \int du\, c_{m\rho}(u)\, D^{(s)*}_{m/2,\sigma}(u_1)\, \alpha^*_{m\rho}(k).$$

Here we have gone over from integration over du_1 to integration over du $(ug^{-1} = ku_1)$; using (8), we easily get the final formula:

$$\varphi_\sigma(\mathbf{p}) = \frac{1}{4\pi\varkappa} \sum_{m=-\infty}^{\infty} \int_0^\infty d\rho\,(m^2+\rho^2) \times \int du \left(\frac{p_0 - (\mathbf{pn})}{\varkappa}\right)^{-1-i\rho/2} D^{(s)*}_{m/2,\sigma}(\tilde{u})\, c_{m\rho}(u). \tag{14}$$

Equations (13) and (14) give the Shapiro transformation for the wave function of a free particle with spin s. Conservation of the norm also follows from (13) and (14):

$$\sum_{\sigma=-s}^{s} \int \frac{d^3p}{p_0} |\varphi_\sigma(\mathbf{p})|^2 = \sum_{m=-\infty}^{\infty} \int_0^\infty d\rho\,(m^2+\rho^2) \int du\, |c_{m\rho}(u)|^2. \tag{15}$$

The rotation $\tilde{u}$ that appears in (13) and (14) is defined by

$$uL_p = k\tilde{u}, \quad \arg k_{22} = 0. \tag{16}$$

(in the spinor representation). It is clear that $\tilde{u}$ is a function of u and $\mathbf{p}$. Formulas for the explicit expression of $\tilde{u}$ in terms of u and $\mathbf{p}$ are given in the Appendix.

3. Let us go on to the treatment of a system of two particles with spins s_1 and s_2, which can interact with each other in some way. The Fock expansion of the state amplitude contains terms describing the motion of an arbitrary number of free particles. We consider only the very first of these (as to number of particles):

$$\Phi_{11} = \int \frac{\varkappa_1 d^3p_1}{E_1} \frac{\varkappa_2 d^3p_2}{E_2} \sum_{\sigma_1\sigma_2} \varphi_{s_1s_2}(\mathbf{p}_1\sigma_1,\ \mathbf{p}_2\sigma_2)\, a^+_{\sigma_1}(\mathbf{p}_1)\, a^+_{\sigma_2}(\mathbf{p}_2)\, \Phi_0.$$

By the same method as in Sec. 2, we find the transformation law of the two-particle amplitude $\varphi_{s_1s_2}$:

$$T_g \varphi_{s_1s_2}(\mathbf{p}_1\sigma_1; \mathbf{p}_2\sigma_2) = \sum_{\sigma_1'\sigma_2'} D^{(s_1)}_{\sigma_1\sigma_1'}\{R(g, g^{-1}p_1)\}\, D^{(s_2)}_{\sigma_2\sigma_2'}\{R(g, g^{-1}p_2)\} \times \varphi_{s_1s_2}(g^{-1}p_1, \sigma_1';\ g^{-1}p_2, \sigma_2'). \tag{17}$$

It is clear that (17) is a unitary transformation of the Lorentz group. We shall expand it in terms of irreducible representations, and thus obtain a relativistically invariant classification of the states of a system of two particles.

Let us go over from the momenta p_1, p_2 of the individual particles to new variables:

$$p = p_1 + p_2, \quad q = (\varkappa_2 p_1 - \varkappa_1 p_2)/(\varkappa_1 + \varkappa_2).$$

The vector p is timelike, and in the case of two free particles is the energy-momentum of the center of mass. As an invariant variable we introduce $\kappa^2 = p^2 = (p_1 + p_2)^2$; κ is the total mass in the center-of-mass system. Since the masses $\varkappa_1$ and $\varkappa_2$ of the particles are fixed, the wave function $\varphi_{s_1 s_2}(\mathbf{p}_1\sigma_1, \mathbf{p}_2\sigma_2)$ depends on six variables: $\mathbf{p}_1$, $\mathbf{p}_2$. Instead of them let us introduce the following six independent variables: $\mathbf{p} = \mathbf{p}_1 + \mathbf{p}_2$, κ, $\nu = \mathbf{q}/|\mathbf{q}|$ (unit vector). Thus $\varphi_{s_1 s_2}$ is converted into a function of p, κ, ν:

$$\varphi_{s_1 s_2}(\mathbf{p}_1\sigma_1, \mathbf{p}_2\sigma_2) = \Phi_{s_1 s_2}(\mathbf{p}, \varkappa, \nu, \sigma_1, \sigma_2), \tag{18}$$

and

$$\int \frac{\varkappa_1 d^3p_1}{E_1}\frac{\varkappa_2 d^3p_2}{E_2}\sum_{\sigma_1\sigma_2}|\varphi_{s_1 s_2}(\mathbf{p}_1\sigma_1, \mathbf{p}_2\sigma_2)|^2$$

$$= \int_{\varkappa_1+\varkappa_2}^{\infty} a(\varkappa)\, d\varkappa \int \frac{\varkappa d^3p}{E}\int d\Omega_\nu \sum_{\sigma_1\sigma_2}|\Phi_{s_1 s_2}(\mathbf{p}, \varkappa, \nu, \sigma_1, \sigma_2)|^2, \tag{19}$$

where

$$a(\varkappa) = \frac{\varkappa_1^2+\varkappa_2^2}{4(\varkappa_1+\varkappa_2)^2\varkappa^2}[\varkappa^2 - (\varkappa_1+\varkappa_2)^2]^{3/2}[\varkappa^2 - (\varkappa_1-\varkappa_2)^2]^{1/2},$$

$$E = \sqrt{p^2 + \varkappa^2}.$$

Now let us use the same approach as in Sec. 2. Instead of $\varphi_{s_1 s_2}(\mathbf{p}, \kappa, \nu, \sigma_1, \sigma_2)$ we introduce a function on the Lorentz group g:

$$\chi_{s_1 s_2}(g, \varkappa, \nu, \sigma_1, \sigma_2) = \sum_{\sigma_1'\sigma_2'} D^{(s_1)}_{\sigma_1\sigma_1'}\{R(g, g^{-1}p_{1c})\}$$

$$\times D^{(s_2)}_{\sigma_2\sigma_2'}\{R(g, g^{-1}p_{2c})\}\,\Phi_{s_1 s_2}(\mathbf{p}, \varkappa, \nu, \sigma_1, \sigma_2). \tag{20}$$

Here $p = g^{-1}p_0$; $p_0 = (0, 0, 0, \kappa)$; p_{1c} and p_{2c} are the momenta of the first and second particles in the center-of-mass system:

$$p_{1c} = [p_c\nu, (\varkappa^2 + \varkappa_1^2 - \varkappa_2^2)/2\varkappa], \quad p_{2c} = [-p_c\nu, (\varkappa^2 - \varkappa_1^2 + \varkappa_2^2)/2\varkappa],$$

$$p_c = \tfrac{1}{2}\varkappa^{-1}[\varkappa^2 - (\varkappa_1+\varkappa_2)^2]^{1/2}[\varkappa^2 - (\varkappa_1-\varkappa_2)^2]^{1/2},$$

p_{1c} and p_{2c} are completely determined if κ and ν are given. From (17) we find that $\chi_{s_1 s_2}$ transforms by the regular representation:

$$T_{g_0}\chi_{s_1 s_2}(g, \varkappa, \nu, \sigma_1, \sigma_2) = \chi_{s_1 s_2}(gg_0, \varkappa, \nu, \sigma_1, \sigma_2). \tag{21}$$

We can also determine how $\chi_{s_1 s_2}$ depends on a left unitary factor in g:

$$\chi_{s_1 s_2}(ug, \varkappa, \nu, \sigma_1, \sigma_2)$$

$$= \sum_{\sigma_1'\sigma_2'} D^{(s_1)}_{\sigma_1\sigma_1'}(u)\, D^{(s_2)}_{\sigma_2\sigma_2'}(u)\,\chi_{s_1 s_2}(g, \varkappa, u^{-1}\nu, \sigma_1', \sigma_2'). \tag{22}$$

The properties (21) and (22) are sufficient for the expansion in irreducible representations. The calculations are again based on the Plancherel formula (12), and are analogous to those carried out in Sec. 2, though more cumbersome. We give only the final formulas:

$$c_{n\varkappa}(m\rho u) = \sum_{\substack{M\mu\sigma\\ \sigma_1\sigma_1'\sigma_2\sigma_2'}} \int \frac{d^3p}{E} Y_J(m\rho u; \mathbf{p}, \varkappa, M)\, C^{JM}_{l\mu;s\sigma} C^{s\sigma}_{s_1\sigma_1;s_2\sigma_2}$$

$$\times \int d\Omega_\nu Y^*_{l\mu}(\nu)\, D^{(s_1)}_{\sigma_1\sigma_1'}\{R(L_p^{-1}, L_p p_{1c})\}\, D^{(s_2)}_{\sigma_2\sigma_2'}\{R(L_p^{-1}, L_p p_{2c})\}$$

$$\times \Phi_{s_1 s_2}(\mathbf{p}, \varkappa, \nu, \sigma_1', \sigma_2'),$$

$$\Phi_{s_1 s_2}(\mathbf{p}, \varkappa, \nu, \sigma_1, \sigma_2) = \sum_{\substack{nM\mu\sigma\\ \sigma_1'\sigma_2'}} D^{(s_1)}_{\sigma_1\sigma_1'}\{R(L_p^{-1}, L_p p_{1c})\}\, D^{(s_2)}_{\sigma_2\sigma_2'}$$

$$\times \{R(L_p^{-1}, L_p p_{2c})\}\, C^{JM}_{l\mu;s\sigma} C^{s\sigma}_{s_1\sigma_1';s_2\sigma_2'} Y_{l\mu}(\nu)$$

$$\times \sum_{m=-\infty}^{\infty}\int_0^{\infty} d\rho\,(m^2+\rho^2)\int du Y^*_J(m\rho u; \mathbf{p}, \varkappa, M)\, c_{n\varkappa}(m\rho u). \tag{23}$$

Here the index n on $c_{n\kappa}(m\rho u)$ denotes a set of invariants: $n = (l, s, J)$; l is the orbital angular momentum in the center-of-mass system, s is the total spin, and J is the total angular momentum in this same system. $C^{JM}_{l\mu;s\sigma}$, etc., are Clebsch-Gordan coefficients; $D^{(s)}_{\sigma\sigma'}(u)$, as usual, are the matrices of the irreducible representation of weight s of the three-dimensional rotation group; and finally,

$$Y_J(m\rho u; \mathbf{p}, \varkappa, M) = \frac{1}{4\pi\varkappa}\left(\frac{E - (p\nu)}{\varkappa}\right)^{-1+i\rho/2} D^{(J)}_{m/2,M}(\tilde{u}),$$

where $\tilde{u}$ is defined by (16) and $E = (p^2 + \kappa^2)^{1/2}$. Besides m and ρ, κ, l, s, and J are also invariants of the Lorentz group. We note that if the Fock amplitude $\varphi_{s_1 s_2}$ describes a system of two free particles with definite momenta $\mathbf{p}_1$ and $\mathbf{p}_2$, then the center-of-mass system exists and the quantities l, s, and J refer just to it. In the general case there does not exist a reference system such that in it the total momentum of the two particles is zero, because generally speaking $\varphi_{s_1 s_2}$ is different from zero in the entire momentum space. Therefore we cannot indicate a reference system in which l, s, and J have intuitive physical meaning, and must simply regard them as invariant variables.

4. Let us now go on to the description of polarization. We recall that in nonrelativistic quantum mechanics the state of polarization of a particle is

completely described by the spin density matrix. It is convenient to take as the parameters characterizing the polarization the coefficients in the expansion of the density matrix in terms of tensor operators that are multipole moments of various ranks and transform according to the irreducible representations of the three-dimensional rotation group.[12,13] We wish to introduce quantities that describe the polarization but transform according to irreducible representations of the Lorentz group. For one free particle it is natural to define the multipole-moment operator by the relation

$$T_{JM}=\int\frac{\varkappa d^3p}{p_0}\sum_{\sigma\sigma'}\sqrt{2J+1}\,C^{s\sigma}_{s\sigma';JM}\,a^{+}_{\sigma}(\mathbf{p})\,a_{\sigma'}(\mathbf{p}).$$

The polarization of a beam of free particles is determined by the average values of these operators for the one-particle state (1):

$$\xi_{JM}=(\Phi_1,\ T_{JM}\Phi_1)=\int\frac{\varkappa d^3p}{p_0}\sum_{\sigma\sigma'}\sqrt{2J+1}\,C^{s\sigma}_{s\sigma';JM}\,\varphi^{*}_{\sigma}(\mathbf{p})\,\varphi_{\sigma'}(\mathbf{p}). \tag{24}$$

It is obvious that the quantity

$$\zeta_{JM}(\mathbf{p})=\sum_{\sigma\sigma'}\sqrt{2J+1}\,C^{s\sigma}_{s\sigma';\,JM}\varphi^{*}_{\sigma}(\mathbf{p})\,\varphi_{\sigma'}(\mathbf{p})$$

is the density of the multipole moment of rank J. The transformation law of ξ_{JM} follows from Eq. (6):

$$T_{g_0}\zeta_{JM}(\mathbf{p})=\sum_{M=-J}^{J}D^{(J)*}_{MM'}\{R(g_0,\ g_0^{-1}p)\}\,\zeta_{JM'}(g_0^{-1}p). \tag{25}$$

From this formula it can be seen that under the Lorentz transformation g_0 all the multipole moments $\xi_{JM}(\mathbf{p})$ of a free particle with momentum $\mathbf{p}$ undergo the same rotation $R(g_0, p)$. Recalling that $\varphi_\sigma(\mathbf{p})$ is the amplitude of the state with momentum p and spin projection σ along the z axis in the rest system, we easily find that the rotation of the polarization vector relative to the momentum $\mathbf{p}$ is determined by the rotation

$$\tilde{R}(g_0,\ p)=R^{-1}(\mathbf{p}'/p')\,R(g_0,\ p)\,R(\mathbf{p}/p),\quad p'=gp,$$

where $R(\mathbf{n})\,\mathbf{n}_0=\mathbf{n}$. From this it follows that for $g_0=u$, $\tilde{R}(u, p)=1$, i.e., under space rotations the spin turns along with the momentum; if, on the other hand, $g_0=L_{p'}$, the angle of rotation of the polarization vector relative to the momentum is given by

$$\tan\theta=\frac{(u_0u_0'+1+uu'\cos\alpha)\,u'\sin\alpha}{uu_0'(u_0u_0'+1)+u'[u_0'(u_0^2+u^2)+u_0]\cos\alpha+uu_0u'^2\cos^2\alpha}, \tag{26}$$

where $(\mathbf{u}, u_0)=(\mathbf{v}(1-v^2)^{-1/2},\ (1-v^2)^{-1/2})$, with $\mathbf{v}$ the original velocity of the particle; u', u_0' are expressed in an analogous way in terms of $\mathbf{v}'$, the speed of the new reference system relative to the original system; α is the angle between $\mathbf{v}$ and $\mathbf{v}'$. For $\alpha=\pi/2$, $\tan\theta=(v'/v)(1-v^2)^{1/2}$ (cf. Wigner's article[14]). It also follows from Eq. (26) that if the original velocity v = 1 (i.e., is equal to the velocity of light), then $\theta=0$, and a longitudinal polarization remains longitudinal after an arbitrary Lorentz transformation.

The tensor $\xi_{JM}=\int\varkappa p_0^{-1}d^3p\,\xi_{JM}(\mathbf{p})$ does not transform in terms of itself, except in the case in which the particle has a definite momentum $\mathbf{p}$; in this case ξ_{JM} also transforms by Eq. (25), as was already pointed out in a paper by Shirokov.[15] The representation of the Lorentz group given by (25) is, however, reducible; namely, it is the complex conjugate of the representation (6) with s replaced by J. We cannot, however, apply the expansion in irreducible representations given by (13) and (14), since in the general case $\int\varkappa p_0^{-1}d^3p\times\sum_M|\xi_{JM}(\mathbf{p})|^2$ does not have to be bounded.

Furthermore, we shall not assume that the particle has a wave function, and shall treat the general case, in which the density matrix is given in the $|\mathbf{p}\sigma>$ representation: $\rho(\mathbf{p}\sigma;\ \mathbf{p}'\sigma')$. The density matrix transforms like the product of two wave functions $\varphi_S(\mathbf{p}\sigma)\,\varphi_S^{*}(\mathbf{p}'\sigma')$, so that by means of (13) we can change from the momentum to the $(m\rho)$ representation:

$$\rho(m\rho u;\ m'\rho'u')=\sum_{\sigma\sigma'}\int\frac{d^3p}{p_0}\frac{d^3p'}{p_0'}\,Y_s(m\rho u;\ \mathbf{p}\sigma)$$
$$\times Y_s^{*}(m'\rho'u';\ \mathbf{p}'\sigma')\,\rho(\mathbf{p}\sigma;\ \mathbf{p}'\sigma'). \tag{27}$$

The Y_S have been defined above.

The matrix ρ transforms by the direct product $\gamma_{m_1\rho_1}\times\gamma^{*}_{m_2\rho_2}$ of two irreducible representations of the Lorentz group. It is easy to show that $\gamma^{*}_{m\rho}$ is equivalent to the representation $\gamma_{-m,-\rho}$. For the final expansion of the density matrix we need the expansion of the direct product of two unitary representations $\gamma_{m_1\rho_1}\times\gamma_{-m_2-\rho_2}$ in terms of irreducible representations. This problem has been solved by Naĭmark.[16] We use his result and get

$$c_{m\rho}(u)=\int du_1du_2\rho(m_1\rho_1u_1;\ m_2\rho_2u_2)$$
$$\times T(m_1\rho_1u_1;-m_2,-\rho_2,u_2;m\rho u), \tag{28}$$

where T is the kernel of this integral transformation:

$$T(m_1\rho_1u_1;-m_2,-\rho_2,\ u_2;m\rho u)$$
$$=\pi^{3/2}\gamma_{n\sigma}(u_1u_2^{-1})\,\gamma_{n_1\sigma_1}(u_1u^{-1})\,\gamma_{n_2\sigma_2}(u_2u^{-1}),$$
$$n=-\tfrac{1}{2}(m+m_1-m_2),\qquad n_1=\tfrac{1}{2}(m-m_1-m_2),$$
$$n_2=\tfrac{1}{2}(m+m_1+m_2),\qquad \sigma=-\tfrac{1}{2}(\rho+\rho_1-\rho_2),$$
$$\sigma_1=\tfrac{1}{2}(\rho-\rho_1-\rho_2),\qquad \sigma_2=\tfrac{1}{2}(\rho+\rho_1+\rho_2),$$

and $\gamma_{n\sigma}(u)$ is the following function on the unitary group of matrices u:

$$\gamma_{n\sigma}(u) = |u_{21}|^{n-1+i\sigma} u_{21}^{-n} = |u_{21}|^{-1+i\sigma} \exp\{-in \arg u_{21}\}. \quad (29)$$

In Eq. (28) m runs through all the integral values for which n, n_1, and n_2 are integers. Thus the expansion of the density matrix ρ in terms of irreducible unitary representations of the Lorentz group is accomplished in two steps:

$$\rho(p\sigma;\ p'\sigma') \to \rho(m_1\rho_1 u_1;\ m_2\rho_2 u_2) \to c_{m\rho}(u).$$

Each of the steps here is reversible. The transformation inverse to the first step is obtained from (14). We write out only the inverse transformation for the second step:

$$\rho(m_1\rho_1 u_1;\ m_2\rho_2 u_2) = (2\pi)^{-4} \sum_m \int_{-\infty}^{\infty} d\rho\,(m^2+\rho^2) \int du c_{m\rho}(u) \times T^*(m_1\rho_1 u_1; -m_2, -\rho_2, u_2; m\rho u). \quad (28a)$$

We remark that in the general case the system of two particles also does not have a definite wave function and is characterized by a density matrix $\rho(p_1\sigma_1, p_2\sigma_2; p_1'\sigma_1', p_2'\sigma_2')$, which transforms like the product of two Fock amplitudes $\varphi_{s_1s_2}(p_1\sigma_1, p_2\sigma_2)\varphi^*_{s_1s_2}(p_1'\sigma_1', p_2'\sigma_2')$. To expand it in irreducible parts one must first change the density matrix ρ from the momentum representation $|p\sigma>$ into the representation $|m\rho u>$ by means of the transformation (23), and then apply the expansion (28) — (28a). Because of their cumbersomeness we shall not present the final formulas, and shall only remark that the function $c_{m\rho}(u)$ finally obtained, which transforms by the irreducible representation $(m\rho)$, is characterized by specifying, in addition to m and ρ, the following invariants: $m_1\rho_1 l_1 s_1 J_1$ and $m_2\rho_2 l_2 s_2 J_2$.

The writer is deeply grateful to I. S. Shapiro for suggesting this subject and for his constant interest in the work.

APPENDIX

The rotation $\tilde{u}$ is determined from the condition (16)

$$uL_p = \tilde{k}\tilde{u},\ \arg k_{22} = 0 \quad (A.1)$$

and is thus a function of u and p. Let us set $\tilde{u} = u_1 u$; then $uL_p u^{-1} = ku_1$. It is clear that $uL_p u^{-1}$ is a pure Lorentz transformation: $uL_p u^{-1} = L_{p'}$. We find the corresponding momentum p' from the equation $p' = L_{p'}p_0 = uL_p u^{-1}p_0 = up$. There remains for us to find the rotation u_1 such that

$$L_{p'} = ku_1, \quad \arg k_{22} = 0. \quad (A.2)$$

Substituting here the explicit form of $L_{p'}$ in the spinor representation, $L_{p'} = (p_0 + \kappa + (p\cdot\sigma))/\sqrt{2\kappa(p_0'+\kappa)}$, and making some simple calculations, we get

$$u_1 = u_z(\psi_1)\,u_x(\theta_1)\,u_z(\varphi_1), \quad \psi_1 = -\varphi_1 = \pi/2 + \tan^{-1}(p_y'/p_x'),$$

$$\tan(\theta_1/2) = \sqrt{p_x'^2 + p_y'^2}/(p_0' + \varkappa - p_z'). \quad (A.3)$$

Since the rotation u_1 depends on two independent variables, it is completely determined when the unit vector $n_1 = u_1^{-1}n_0$, $n_0 = (0, 0, 1)$, is prescribed. It can be shown that

$$u^{-1}n_1 = \frac{\varkappa(p_0+\varkappa)\,n - [p_0+\varkappa-(pn)]\,p}{(p_0+\varkappa)(p-(pn))}, \quad (A.4)$$

where $n = u^{-1}n_0$.

[1] V. L. Ginzburg and I. E. Tamm, JETP **17**, 227 (1947).

[2] I. M. Gel'fand and M. A. Naĭmark, J. Phys. U.S.S.R. **10**, 93 (1946).

[3] P. A. M. Dirac, Proc. Roy. Soc. **A183**, 284 (1945).

[4] Harish-Chandra, Proc. Roy. Soc. **A189**, 372 (1947).

[5] I. S. Shapiro, Dissertation, Moscow State University, 1955; Dokl. Akad. Nauk SSSR **106**, 647 (1956), Soviet Phys.-Doklady **1**, 91 (1956).

[6] A. Z. Dolginov, JETP **30**, 746 (1956), Soviet Phys. JETP **3**, 589 (1956).

[7] Chou Kuang-Chao and L. G. Zastavenko, JETP **35**, 1417 (1958), Soviet Phys. JETP **8**, 990 (1959).

[8] A. I. Akhiezer and V. B. Berestetskiĭ, Квантовая электродинамика (Quantum Electrodynamics), Gostekhizdat, Moscow-Leningrad, 1953, (AEC Tr. 2876).

[9] G. Ya. Lyubarskiĭ, Теория групп и ее применение в физике (Group Theory and its Application in Physics), Gostekhizdat, Moscow, 1957.

[10] I. M. Gel'fand and M. A. Naĭmark, Izv. Akad. Nauk SSSR, Ser. Mat. **11**, 411 (1947).

[11] M. A. Naĭmark, Usp. Mat. Nauk **9**, No. 4, 19 (1954).

[12] A. Simon, Phys. Rev. **92**, 1050 (1953).

[13] U. Fano, Revs. Modern Phys. **29**, 74 (1957).

[14] E. P. Wigner, Revs. Modern Phys. **29**, 255 (1957).

[15] Yu. M. Shirokov, JETP **35**, 1005 (1958), Soviet Phys. JETP **8**, 703 (1959).

[16] M. A. Naĭmark, Dokl. Akad. Nauk SSSR **119**, 872 (1958).

Translated by W. H. Furry
217

ON THE THEORY OF THE TEMPERATURE DEPENDENCE OF FERROMAGNETIC ANISOTROPY

E. A. TUROV and A. I. MITSEK

Institute for Metal Physics, Academy of Sciences, U.S.S.R.

Submitted to JETP editor May 30, 1959

J. Exptl. Theoret. Phys. (U.S.S.R.) **37**, 1127-1132 (October, 1959)

We have used the phenomenological spin wave theory to evaluate the temperature dependence of the magnetic anisotropy free energy in ferromagnets in the low temperature region. It is shown that if we use the usual expressions for this free energy, the temperature dependence of the anisotropy constant of N-th order may depend substantially on the magnitude of the ratio at 0° K of the subsequent constants to the one given. The mixing of anisotropy constants of different orders in the equations for their temperature dependence disappears only when the anisotropy energy is written in the form of an expansion in homogeneous harmonic polynomials (in the direction cosines of the magnetization vector relative to the crystal axes). It then turns out that in the low temperature region the temperature dependence (1) of the anisotropy constants, established theoretically by Zener,[1] is only approximately valid.

1. In recent years there have appeared a number of theoretical papers[1-7] devoted to the evaluation of the temperature dependence of the constants of magnetic crystallographic anisotropy of ferromagnetic single crystals. The interest in this problem is enhanced, in particular, by the large part played by the magnetic anisotropy in ferromagnetic resonance phenomena.

Zener[1] developed a classical theory of the change with temperature of the anisotropy constants; this theory was independent of the type of binding between the magnetic atoms. He started from the assumption that one can separate off in the crystal a short-range order region of spins around each atom, inside which the local anisotropy constants are temperature independent. Assuming also that the distribution of the spin oscillations between such regions would be a random one, Zener obtained, after averaging the local anisotropy energy over all directions of the short-range order, the following result for the macroscopic anisotropy constant of N-th order*

$$K_N(T)/K_N(0) = [M(T)/M(0)]^{N(2N+1)}. \qquad (1)$$

Here $K_N(T)$ and $K_N(0)$ are anisotropy constants and $M(T)$ and $M(0)$ the spontaneous magnetization at a temperature T and at the absolute zero, respectively. Carr[2] has shown that one can obtain essentially the same result in the molecular-field approximation. It follows, in particular from Eq. (1), that for cubic crystals ($N = 2$) we have for the first anisotropy constant $K_2 \sim M^{10}$. This last relation was already obtained in 1936 by Akulov[8] from theoretical considerations similar to Zener's.

The papers by Tyablikov and Gusev,[3] Pal,[4] Keffer,[5] Kasuya,[6] and Potapkov[7] used spin-wave theory to discuss the temperature dependence of the anisotropy constants. The results of these papers also agreed approximately with Eq. (1) for the first and second anisotropy constants of uniaxial and cubic crystals. Experiments, however, did not confirm such a simple and universal temperature dependence of those constants K_N which are usually used for a theoretical analysis. The constants K_2, for instance, change in a number of ferrites appreciably less with temperature than would follow from Eq. (1).* On the other hand, K_2 for nickel increases appreciably faster with decreasing temperature than according to the "M^{10}-law."

In the papers quoted,[3-7] the authors use as a rule, various microscopic models, which are based upon a number of often very arbitrary assumptions about the interaction mechanism that leads to the ferromagnetic anisotropy, and also upon assumptions about the nominal value of the spontaneous

*Since the anisotropy energy must be an even function of the magnetization M, it is convenient to define as the order of the constant not the degree of the invariant of the components of M which multiplies the constant, but one half of this degree. This we shall do throughout the whole of the paper.

*It was thought for a long time that the $K_2 \sim M^{10}$ law was well satisfied for iron. Recent experimental work,[9] however, led to a completely different result: $K_2 \sim M^4$ or M^5.

magnetization at 0°K.* It is thus of interest to evaluate the temperature dependence of the magnetic anisotropy constants of ferromagnetics in the low-temperature region using the phenomenological spin-wave theory,[10] which is based solely on symmetry considerations and is free from a number of restrictions inherent in the microscopic models. This calculation will be given in a general form which is independent of the type of symmetry of the crystal.

2. The phenomenological Hamiltonian of a ferromagnet can in the general case be written in the form[10]

$$\mathcal{H} = \int \mathcal{H}(\mathbf{r})\, d\mathbf{r},$$

$$\mathcal{H}(\mathbf{r}) = A_{ij}\frac{\partial m_k}{\partial r_i}\frac{\partial m_k}{\partial r_j} + K_{n_1n_2n_3} m_x^{n_1} m_y^{n_2} m_z^{n_3} - \frac{1}{2} M_0^2 \mathbf{m}\nabla \int \frac{\operatorname{div} \mathbf{m}(\mathbf{r}')\, d\mathbf{r}'}{|\mathbf{r} - \mathbf{r}'|} - M_0 \mathbf{m}\mathbf{H}. \quad (2)$$

Here $\mathbf{m}(\mathbf{r}) = \mathbf{M}(\mathbf{r})/M_0$ is the unit vector of the local magnetization; i, j, k = x, y, z; n_1, n_2, n_3 are integers such that $n_1+n_2+n_3 = 2N$ is an even number; repeated indices imply summation. The first term in (2) is that part of the exchange energy which is connected with the inhomogeneities of $\mathbf{m}(\mathbf{r})$ and is characterized by the parameters A_{ij}. The second term gives the energy of the magnetic crystallographic anisotropy written in the form of an expansion in increasing powers of the magnetization components; the set of non-vanishing anisotropy constants $K_{n_1n_2n_3}$ of order $N = \frac{1}{2}(n_1 + n_2 + n_3)$ (and also the number of different parameters A_{ij}) is determined by the crystal symmetry.† The third term describes the magnetostatic energy caused by the inhomogeneities of the magnetization and the last term, finally, is the energy of the ferromagnetic in an external field H.

We choose a system of coordinates (ξ, η, ζ) with a ζ axis along the classical equilibrium (at 0°K) magnetization vector $\mathbf{m}_0 = \boldsymbol{\alpha}$. The components of $\boldsymbol{\alpha}$ in the x, y, z system will then be equal to $\alpha_x = \sin\theta\cos\varphi$, $\alpha_y = \sin\theta\sin\varphi$, and $\alpha_z = \cos\theta$, where θ and φ are respectively the polar and azimuthal angles of the vector $\boldsymbol{\alpha}$ with respect to the x, y, z axes. Restricting ourselves to the low-temperature case, we shall consider only small oscillations of the vector $\mathbf{m}$ about the direction of $\boldsymbol{\alpha}$. These oscillations can be approximately expressed in terms of the Bose amplitudes $b_{\mathbf{r}}$ and $b_{\mathbf{r}}^+$ using the relations[10]

$$m_\xi = (\mu/2M_0)^{1/2}(b_{\mathbf{r}} + b_{\mathbf{r}}^+), \qquad m_\eta = i(\mu/2M_0)^{1/2}(b_{\mathbf{r}} - b_{\mathbf{r}}^+),$$
$$m_\zeta = 1 - \mu b_{\mathbf{r}}^+ b_{\mathbf{r}}/M_0, \quad (3)$$

where $\mu = ge\hbar/2mc$ and g is the Landé factor.

The changeover from (3) to m_x, m_y, and m_z is through the transformation formulae

$$m_x = m_\xi\cos\theta\cos\varphi - m_\eta\sin\varphi + m_\zeta\sin\theta\cos\varphi,$$
$$m_y = m_\xi\cos\theta\sin\varphi + m_\eta\cos\varphi + m_\zeta\sin\theta\sin\varphi,$$
$$m_z = -m_\xi\sin\theta + m_\zeta\cos\theta. \quad (4)$$

Substituting (3) into (4) and after that into the Hamiltonian (2), and segregating the quadratic expression in the operators $b_{\mathbf{r}}$ and $b_{\mathbf{r}}^+$, we obtain, after the usual transformations that bring this expression to diagonal form, the spectrum of the energy eigenvalues of the system

$$\mathcal{H} = \mathcal{H}_0 + \sum_{\mathbf{k}} \varepsilon_{\mathbf{k}} N_{\mathbf{k}}.$$

Here

$$\mathcal{H}_0 = K_{n_1n_2n_3}\alpha_x^{n_1}\alpha_y^{n_2}\alpha_z^{n_3} - M_0(\boldsymbol{\alpha}\mathbf{H}) \quad (5)$$

gives us, after minimizing with respect to $\boldsymbol{\alpha}$, the ground state of the system;* $\epsilon_{\mathbf{k}}$ is the energy of a spin wave with wave vector $\mathbf{k}$, and $N_{\mathbf{k}}$ the number of spin waves with that wave vector.

We shall restrict our considerations to the temperature range for which

$$\varkappa T \gg 2\pi\mu M_0, \ \mu K_N/M_0 \quad (6)$$

($\varkappa$ is Boltzmann's constant); the energy of the spin waves that influence the thermodynamic behavior of the system can then approximately be written in the form

$$\varepsilon_{\mathbf{k}} = (\mu/M_0)\{2A_{ij}k_ik_j + M_0(\boldsymbol{\alpha}\mathbf{H}) + 2\pi M_0^2\sin^2\theta_{\mathbf{k}} - {}^1/_2\sum_N [2N(2N+1) - \nabla_\alpha^2] f_N(0)\}, \quad (7)$$

where $\theta_{\mathbf{k}}$ is the angle between the vectors $\mathbf{k}$ and $\boldsymbol{\alpha}$, ∇_α^2 is the Laplacian in terms of the variables α_x, α_y, α_z, and $f_N(0)$ denotes the homogeneous polynomial of degree 2N

*References 3 and 7 are least encumbered by these deficiencies.

† In view of the condition $m_x^2 + m_y^2 + m_z^2 \approx 1$, different invariants permitted by the symmetry turn out to be linearly dependent. We shall assume that the expansion given contains already only independent invariants. The choice of these invariants and of the constants K_N is, finally, not unique. One can, however, always perform the transformation from one set of constants to another one.

*That is, the equilibrium orientation of the vector $\boldsymbol{\alpha}$, determined by the simultaneous action of the external field and the internal anistropy forces.

$$f_N(0) = \sum_{(n_1+n_2+n_3=2N)} K_{n_1 n_2 n_3} \alpha_x^{n_1} \alpha_y^{n_2} \alpha_z^{n_3}. \quad (8)$$

The first term in (5), which is just the anisotropy energy at 0°K, can be rewritten in terms of $f_N(0)$ in the form

$$F_A(0) = \sum_N f_N(0). \quad (9)$$

The spin wave energy consists according to (7) of the following successive four parts: the exchange energy, the energy in the external magnetic field, the magnetostatic energy, and, finally, the energy connected with the internal magnetic-anisotropy forces. Condition (6) means in fact that our results will only be valid in that temperature range where the first (exchange) term in (7) is large compared to the third and fourth terms. We shall exclude these latter from our consideration of the region of very low temperatures, near absolute zero ($T \lesssim 0.1$ to 1°K).

Knowing the energy spectrum of the system (7) we can evaluate its thermodynamic potential

$$\Omega = \mathcal{H}_0 + \varkappa T \sum_{\mathbf{k}} \ln(1 - e^{-\varepsilon_{\mathbf{k}}/\varkappa T}).$$

Separating in Ω the part that depends on the direction of $\boldsymbol{\alpha}$ relative to the crystallographic axes, and taking Eq. (6) into account, we get, for sufficiently large external fields H so that there is saturation ($\boldsymbol{\alpha} \cdot \mathbf{H} \approx H$), the free energy of anisotropy at temperature T:

$$F_A(T) = \sum_N \left\{1 - \frac{\Delta M(T)}{2M_0}[2N(2N+1) - \nabla_\alpha^2]\right\} f_N(0). \quad (10)$$

In this formula we have expressed that part of the anisotropy free energy which depends on the temperature through the temperature variation of the magnetization $\Delta M(T) = M_0 - M(T)$, taking into account that

$$M(T) = -\partial\Omega/\partial H = M_0 - \mu \sum_{\mathbf{k}} (e^{\varepsilon_{\mathbf{k}}/\varkappa T} - 1)^{-1}.$$

3. Expression (10) for the free energy of magnetic anisotropy can be simplified considerably if the homogeneous polynomials f_N, in which F_A is expanded, satisfy the Laplace equation

$$\nabla_\alpha^2 f_N = 0,$$

i.e., are harmonic polynomials. In that case we have instead of (10)

$$F_A(T) = \sum_N f_N(T), \quad (9')$$

where

$$f_N(T) = f_N(0)[1 - (\Delta M/M_0) N(2N+1)]. \quad (11)$$

The temperature dependence of any anisotropy constant which is one of the expansion coefficients of the free energy of anisotropy in terms of invariants written in the form of homogeneous harmonic polynomials ("harmonic invariants") satisfies thus, according to (9), (9'), and (11), a general law which is independent of the type of the crystal symmetry and which is determined solely by the degree 2N of the corresponding polynomial f_N. Indeed, if

$$f_N = \sum_n K_N^{(n)} W_{N,n}(\alpha_x, \alpha_y, \alpha_z),$$

where $W_{N,n}(\alpha_x, \alpha_y, \alpha_z)$ are independent harmonic invariants* of degree 2N, then

$$K_N^{(n)}(T) = K_N^{(n)}(0)[1 - N(2N+1)\Delta M/M_0], \quad (12)$$

or

$$(K_N^{(n)}(0) - K_N^{(n)}(T))/K_N^{(n)}(0) = P_N(M(0) - M(T))/M(0), \quad (13)$$

where $M(0) \equiv M_0$ and

$$P_N = N(2N+1). \quad (14)$$

This relation is approximately the same as Eq. (1) at low temperatures (i.e., for $\Delta M \ll M_0$), but with one reservation, namely that it must be applied to the constants in front of harmonic invariants.

Relation (13) remains formally the same in the case of the customary "non-harmonic" form of writing the anisotropy free energy. The coefficient P_N in it will, however, be essentially different: it will depend not only on the order N of the corresponding constant K_N, but also on the magnitude of the ratio at 0°K of the next constants to the one given. The coefficient P_N in Eq. (13) will, for instance, take on the following form for the case of the first constants in hexagonal (N=1) and in cubic (N=2) crystals, respectively, if one uses the standard form for the anisotropy energy[11]

$$P_1 = 3 - \frac{6K_2(0) + \cdots}{K_1(0)}, \qquad P_2 = 10 - \frac{K_3(0) + 8K_4(0) + \cdots}{K_2(0)}, \quad (15)$$

while if we use the harmonic expression for F_A we would have according to (14) $P_1 = 3$ and $P_2 = 10$.

*The index n is introduced for the case where the number of independent invariants of degree 2N is larger than 1.

It is well known that even at room temperature the first and second anisotropy constants in ferromagnets are often of the same order of magnitude (see Bozorth's book[12]), and with decreasing temperature the second constant usually increases faster than the first one.* There are also indications in the literature that constants of higher order are also by no means small compared with the first constants.[14] This fact enables us to explain in principle why, for instance, for cubic crystals the following rule which follows from Eq. (1)

$$\Delta K_2(T)/K_2(0) = 10\Delta M(T)/M(0) \qquad (16)$$

is not satisfied experimentally even in the low temperature region. It is clear from the second equation in (15) that in the case where F_A is written in the conventional way the numerical coefficient on the right hand side of (16) may be either less or more than 10, depending on the relative signs and on the ratio of the magnitudes at 0°K of the later constants and of the first constant.† The rule expressed by (16) needs only be satisfied when the anisotropy energy is analyzed using its harmonic representation.

4. We shall, in conclusion, give the general expansion of F_A in terms of harmonic invariants for cubic and uniaxial crystals.

For crystals of cubic symmetry we have (up to terms of the eighth power in the α_i)

$$\begin{aligned} F_A = {} & K_2[\alpha_x^4+\alpha_y^4+\alpha_z^4-{}^1/_3(\alpha_x^2\alpha_y^2+\alpha_x^2\alpha_z^2+\alpha_y^2\alpha_z^2)] \\ & + K_3[\alpha_x^6+\alpha_y^6+\alpha_z^6-{}^{15}/_2(\alpha_x^4\alpha_y^2+\alpha_x^2\alpha_y^4+\alpha_x^4\alpha_z^2 \\ & + \alpha_x^2\alpha_z^4+\alpha_y^4\alpha_z^2+\alpha_y^2\alpha_z^4)+90\alpha_x^2\alpha_y^2\alpha_z^2]+K_4[\alpha_x^8+\alpha_y^8+\alpha_z^8 \\ & - 14(\alpha_x^6\alpha_y^2+\alpha_x^2\alpha_y^6+\alpha_x^6\alpha_z^2+\alpha_x^2\alpha_z^6+\alpha_y^6\alpha_z^2+\alpha_y^2\alpha_z^6) \\ & + 35(\alpha_x^4\alpha_y^4+\alpha_x^4\alpha_z^4+\alpha_y^4\alpha_z^4)]. \end{aligned} \qquad (17)$$

For uniaxial crystals we have (up to terms of the fourth power and not taking the anisotropy in the basal plane into account)

$$\begin{aligned} F_A = {} & K_1(\alpha_x^2+\alpha_y^2-2\alpha_z^2) \\ & + K_2\left[(\alpha_x^2+\alpha_y^2)^2-8(\alpha_x^2+\alpha_y^2)\alpha_z^2+\frac{8}{3}\alpha_z^4\right]. \end{aligned} \qquad (18)$$

It is necessary to add to this last expression for the case of tetragonal crystals a term of the form

$$K_2'[\alpha_x^4+\alpha_y^4-6\alpha_x^2\alpha_y^2], \qquad (19)$$

which describes the anisotropy in the basal plane. The harmonic invariants of the fourth and sixth degree when the anisotropy in the basal plane is taken into account are, for instance, given for rhombohedral and hexagonal crystals by Landau and Lifshitz.[15]

The temperature dependence of the constants K_N entering into Eqs. (17) – (19) is described by the general Eq. (13). Since there is no mixing of constants of different order in this formula, we may expect the treatment of the experimental temperature dependence of the magnetic-anisotropy energy and of its theoretical analysis to be facilitated by precisely this formulation of F_A.

Accurate experimental studies of the temperature dependence of the anisotropy constants accompanied by a simultaneous measurement of the magnetization in order to verify the theoretical Eq. (13) would at this moment be of great importance, since they would enable us to verify the basic ideas and methods of contemporary ferromagnetic theory.

The authors express their deep gratitude to S. V. Vonsovskiĭ for discussing the present paper and for valuable advice.

*An indication that subsequent anistropy constants might influence the temperature dependence of earlier ones was already given in Zener's paper[1] and also in references 2 and 13.

†It has already been shown that both these cases ($P_2 < 10$ and $P_2 > 10$) occur experimentally.

[1] C. Zener, Phys. Rev. **96**, 1335 (1954).
[2] W. J. Carr Jr., Phys. Rev. **109**, 1971 (1958).
[3] S. V. Tyablikov, JETP **20**, 661 (1950); S. V. Tyablikov and A. A. Gusev, Физика металлов и металловедение (Physics of Metals and Metallography) **2**, 385 (1956).
[4] L. Pal, Acta Phys. Hung. **3**, 287 (1954).
[5] F. Keffer, Phys. Rev. **100**, 1692 (1955).
[6] T. Kasuya, J. Phys. Soc. Japan **11**, 944 (1956).
[7] N. A. Potapkov, Dokl. Akad. Nauk SSSR **118**, 269 (1958), Soviet Phys.–Doklady **3**, 89 (1958).
[8] N. Akulov, Z. Physik **100**, 197 (1936); Ферромагнетизм (Ferromagnetism), M.-L., 1939.
[9] C. D. Graham Jr., Phys. Rev. **112**, 1117 (1958).
[10] E. A. Turov and V. G. Shavrov, Тр. Ин-та физики металлов АН СССР (Proc. Inst. Metals Acad. Sc. U.S.S.R.) No. 20, 101 (1958); Izv. Akad. Nauk SSSR, Ser. Fiz. **22**, 1168 (1958), Columbia Tech. Transl. p. 1158.
[11] S. V. Vonsovskiĭ and Ya. S. Shur, Ферромагнетизм (Ferromagnetism), Gostekhizdat, 1948, pp. 268 and 272.
[12] R. Bozorth, Ferromagnetism (Russ. Transl.), IIL, 1956, p. 453 [Van Nastrand, N.Y. 1951].
[13] H. Sato and B. S. Chandrasekhar, J. Phys. Chem. Solids **1**, 228 (1957).

[14] Kirenskiĭ, Nosova, and Reshetnikova, Izv. Akad. Nauk SSSR, Ser. Fiz. 21, 1105 (1957), Columbia Tech. Transl. p. 1093.

[15] L. D. Landau and E. M. Lifshitz, Электродинамика сплошных сред (Electrodynamics of Continuous Media), Gostekhizdat, 1957, p. 200. Translated by D. ter Haar 218

Letters to the Editor

GAMMA RAYS FROM A Po-O^{18} *NEUTRON SOURCE*

É. M. TSENTER, A. G. KHABAKHPASHEV, and I. A. PIRKIN

Submitted to JETP editor May 26, 1959

J. Exptl. Theoret. Phys. (U.S.S.R.) **37**, 1133-1134 (October, 1959)

IN a previous paper[1] it has been shown that in a Po-O neutron source the (α, n) reaction operates on the isotope O^{18}. The neutrons yielded by the reaction $O^{18}(\alpha, n)Ne^{21}$ are accompanied by 0.35 Mev γ rays with a relative intensity of $30 \pm 10\%$.

A neutron source of 120,000 n/sec intensity was used in the present measurements. The source was a solution of Po^{210} nitrate in water enriched with O^{18} to 24%. A single-crystal scintillation spectrometer and n-γ and γ-γ coincidence circuits were used to investigate the gamma spectra. A 40×40 mm crystal of NaI(Tl) was used in the spectrometer. The resolution of the Cs^{137} γ line was 12%.

Figure 1 shows the γ spectrum of Po-O^{18}, taken up to 1.6 Mev. The 0.35-Mev γ line corresponds[2] to the first excited level of Ne^{21}. The 1.38-Mev γ line corresponds to the transition from the second excited level to the first excited level. The 0.803-Mev γ line accompanies the decay of Po^{210}.

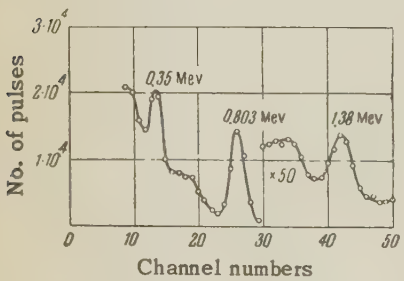

FIG. 1. Gamma spectrum of Po-O^{18} source.

The Po-O^{18} spectrum contains a certain number of pulses with energies up to 2.8 Mev. Some of these are evidently due to neutrons registered by the NaI(Tl) crystal. Others are possibly due to hard γ rays which could not be detected in the course of these measurements because of low intensity.

The intensities of the 0.35-Mev and 1.38-Mev γ lines were determined from the areas under the full energy peaks (photopeaks). The crystal counting efficiency and the ratio of the area under a photopeak to that under the entire spectral curve were taken from other references.[3,4]

The intensity of the 0.35-Mev line, relative to the neutron yield, was found to be $45 \pm 5\%$. To determine this particular intensity, the gamma spectrum was measured separately, at a high amplification factor. The intensity of the 1.38-Mev line was $10 \pm 2\%$. Upper limits for the relative intensities of the 1.73-Mev γ line (direct transition from the second level of Ne^{21} to the ground level) and of the 2.84-Mev line (direct transition from the third level) were determined from the complete gamma spectrum of the Po-O^{18} source. The upper limit was 1% for the 1.73 Mev line and 2% for the 2.84 Mev line.

To verify the results obtained with the single-crystal spectrometer, the Po-O^{18} γ spectrum was measured with the use of neutron coincidences. A tolane crystal with 20 mm of lead shielding was used to count the neutrons. The coincidence circuit had a resolving time of 6×10^{-9} seconds.

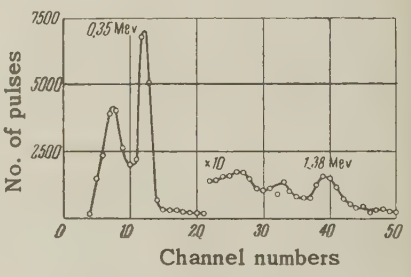

FIG. 2. Gamma spectrum of Po-O^{18} source, taken with neutron coincidence.

Figure 2 shows the γ-ray spectrum taken with neutron coincidence. The 0.35- and 1.38-Mev lines are also seen here. The sharp Compton-scattering cutoff of the 0.35-Mev line is associated with the sensitivity threshold of the coincidence circuit. The presence of the 1.38 — 0.35 Mev cascade transition was also confirmed by γ-γ coincidence measurements.

Thus, it is possible to establish from these $O^{18}(\alpha, n)Ne^{21}$ γ-ray measurements that the decay of the intermediate nucleus Ne^{22} proceeds 55% to the ground level of Ne^{21}, 35% to the first excited level, and 10% to the second excited level. The Ne^{21} nucleus undergoes transition from the second excited level at 1.73 Mev to the ground state by γ cascade, releasing 1.38-Mev and 0.35-Mev γ rays. The probability of direct transition is at least tenfold smaller.

[1] Serdyukova, Khabakhpashev, and Tsenter, Izv. Akad. Nauk SSR, Ser. Fiz. **21**, 1017 (1957), Columbia Tech. Transl. p. 1018.

[2] F. Ajzenberg and T. Lauritsen, Revs. Modern Phys. **27**, 77 (1955).

[3] Miller, Reynolds, and Snow, Rev. Sci. Instr. **28**, 717 (1957).
[4] A. Stanford and W. Rivers, Rev. Sci. Instr. **29**, 406 (1958).

Translated by D. A. Kellogg
219

ON THE ROTATIONAL LEVELS OF Li^7

V. I. MAMASAKHLISOV and T. I. KOPALEĬSHVILI

Physics Institute, Academy of Sciences, Georgian S.S.R.

Submitted to JETP editor June 6, 1959

J. Exptl. Theoret. Phys. (U.S.S.R.) **37**, 1134-1136 (October, 1959)

THE conjecture that structural subgroups consisting of two, three, and four nucleons can be formed within light nuclei has been made by many authors.[1-4] In references 5 and 6, the disintegration of Li^7 into an α particle and a triton as a result of Coulomb excitation and of scattering of a heavy nucleus has been treated in terms of the α-triton model. One can easily see that such a model will lead to rotational levels in Li^7. The axis of symmetry will be given by the line connecting the centers of mass of the α particle and of the triton while the axis of rotation will be perpendicular to the symmetry axis and will go through the center of mass of the system.

Recently Blair and Henley[7] have shown that several levels of Be can be interpreted as rotational states if this nucleus is visualized as consisting of two separate α particles oscillating along an axis connecting their centers of gravity. In the present paper it will be shown that one can also interpret some levels of Li^7 as having rotational character if one assumes the α-triton model.

As is well known, the ground-state spin of Li^7 differs from zero ($J_0 = 3/2$). Taking further into account that the present model has just an axis of symmetry (not a center of symmetry) one deduces that the rotational spectrum will have angular momenta $J = J_0,\ J_0 + 1,\ J_0 + 2, \ldots$ while the parities will coincide with the ground-state parity ($3/2^-$). The energies of the levels are given by the expression

$$E_J = (\hbar^2/2I)]\, J\,(J+1) - J_0\,(J_0+1)], \qquad I = \mu\overline{r^2}, \qquad (1)$$

where μ is the reduced mass of the (α+t) system, and r is the distance between α and t. It follows from (1) that the ratios of the excitation energies of the rotational levels are

$$E_{5/2} : E_{7/2} : E_{9/2} \ldots = 1 : 2.40 : 4.20 \ldots .$$

Amongst the levels of Li^7 there exists[8] one 7.46-Mev level with spin $5/2^-$. Taking this to be the first rotational level, we see that the 17.5-Mev level can be assumed to be the next rotational level with spin $7/2^-$ since the experimental ratio 2.35 of the energies is close enough to the theoretical ratio 2.40.

To verify our treatment we must obtain the right value for the energy of the first level, viz. 7.46 Mev. To that end we utilize the rms value 2.71×10^{-13} cm obtained by Hofstadter[9] for the charge radius of the Li^7 nucleus. Assuming that the mean distance between the α particle and the triton equals roughly the charge radius, we obtain from (1) a value 8.22 Mev, which is close enough to the experimental value of 7.46 Mev. If we require that the energy of the first level coincide exactly with the experimental value, we obtain for the rms distance a value 2.85×10^{-13} cm. This value is somewhat larger than the charge radius. However, as is known the nuclear radius always turns out larger than the charge radius.

The value obtained for $\overline{r^2}$ allows also the evaluation of the quadrupole moment of the Li^7 nucleus. Taking it into account that the quadrupole moments of He^4 and He^3 vanish, we obtain, in a coordinate system in which the origin coincides with the center of mass of the (α+t) system and where the z axis is oriented along the axis of symmetry of the nucleus, the following expression for the quadrupole moment operator;

$$\hat{Q} = (68/49)\,\sqrt{4\pi/5}\, r^2 Y_{20}(\vartheta). \qquad (2)$$

In our coordinate system the wave function of the (α+t) system will have the form

$$\psi = [\delta\,(\mathbf{r} - \mathbf{R}_0)]^{1/2}, \qquad \mathbf{R}_0 = (\sqrt{\overline{r^2}},\ 0,\ 0). \qquad (3)$$

Using this expression, we obtain for the intrinsic quadrupole moment of Li^7

$$Q_0 = 68\overline{r^2}/49 = 11 \cdot 10^{-26}\ \text{cm}^2.$$

This value is several times larger than the experimental value, 2×10^{-26} cm^2. However we have to consider the obtained value to be more or less acceptable when we recall that even the unified model which describes the nuclear states rather satisfactorily leads to too large a value for the quadrupole moment. Also, the hydrodynamic model (assuming that Li^7 is deformed in the sense of the unified model and utilizing the energy of the first rotational level) yields a value for the quadrupole mo-

ment which is an order of magnitude larger than the experimental value. As has been shown earlier[5] the present model of Li^7 leads to a good agreement also for the magnetic moment ($\mu_{theoret} = 3.56$; $\mu_{exp} = 3.25$).

We finally point out that the value for the distance between the α particle and the triton (2.8×10^{-13} cm) is larger than the particle size, $\sim 1.5 \times 10^{-13}$ cm. This indicates that the employed model is not self-contradictory.

In conclusion we express our gratitude to I. Sh. Vashakidze and G. A. Chilashvili for discussions.

[1] K. Wildermuth and Th. Kanellopoulos, Nucl. Phys. **7**, 150 (1958).

[2] V. I. Mamasakhlisov, JETP **24**, 190 (1953).

[3] P. Cüer and G. J. Combe, Compt. rend. **329**, 351 (1954).

[4] V. I. Mamasakhlisov, Тр. Ин-та физики АН Груз. ССР (Proc. Physics Inst. Acad. Sci. Georgian S.S.R.) **3**, 31 (1955).

[5] V. I. Mamasakhlisov and G. A. Chilashvili, JETP **32**, 806 (1957), Soviet Phys. JETP **5**, 661 (1957).

[6] A. G. Sitenko and Yu. A. Berezhnoĭ, JETP **35**, 1289 (1958), Soviet Phys. JETP **8**, 899 (1959).

[7] J. S. Blair and E. M. Henley, Phys. Rev. **112**, 2029 (1958).

[8] F. Ajzenberg and T. Lauritzen, Revs. Modern Phys. **27**, 77 (1955).

[9] R. Hofstadter, Revs. Modern Phys. **28**, 214 (1956).

Translated by M. Danos
220

ON THE THEORY OF THE NUCLEAR MOMENT OF INERTIA

Yu. K. KHOKHLOV

P. N. Lebedev Physics Institute, Academy of Sciences, U.S.S.R.

Submitted to JETP editor July 11, 1959

J. Exptl. Theoret. Phys. (U.S.S.R.) **37**, 1136-1137 (October, 1959)

THE aim of the present note is to establish a connection between the two ways of determining the nuclear moments of inertia which have been proposed by Inglis[1] and Bohr and Mottelson[2] on the one hand and by Villars[3] and Hayakawa and Marumori[4] on the other hand. To begin with we have to consider the formulation of the second of these approaches. Further, we are not interested in the original abstract formulation but in the one to which we must turn when actually performing a computation.

Let φ be the collective angular variable, given by the angle of rotation of the main axes of the nucleus in a plane perpendicular to the axis of rotation, Z:*

$$\varphi = {}^1/_2 \tan^{-1}\left[\sum 2mxy \Big/ \sum m(x^2 - y^2)\right]. \qquad (1)$$

The summation in (1) is over all nucleons; the indices showing the nucleon number have been omitted; m is the nucleon mass.

We note the important commutation relation: $i[M_Z, \varphi] = \hbar$ where M_Z is the projection of the angular momentum operator of the nucleus on the Z axis.

Let H_0 be a model Hamiltonian of the nucleus oriented in a given manner in the XY plane. The kinetic energy operator of such a Hamiltonian commutes with M_Z while the potential energy operator does not. We now define the quantities N_Z and I_0 by means of the relations

$$i\hbar^{-1}[H_0, \varphi] = -N_Z/I_0, \qquad -\hbar^{-2}[[H_0, \varphi], \varphi] = 1/I_0. \qquad (2)$$

The quantity $L_Z = M_Z + N_Z$ is the projection of the angular momentum on the Z axis in a coordinate system fixed with respect to the nuclear axes. It commutes both with φ and M_Z, while $i[N_Z, \varphi] = -\hbar$. The quantity I_0 is the so-called hydrodynamic moment of inertia. It is a continuous function of the coordinates and commutes with φ as well as with M_Z and N_Z. As a simplification we shall take I_0 to be a c-number, but as one can easily convince oneself the final result does not depend on this assumption.

According to the references 3 and 4 the nuclear moment of inertia is roughly given by

$$I = I_0 + 2\sum_{n\neq 0} |\langle \Phi_n, L_Z \Phi_0 \rangle|^2/(E_n - E_0). \qquad (3)$$

Here Φ_n and E_n are the eigenfunctions and eigenvalues of the Hamiltonian H_0 respectively.

On the other hand, according to references 1 and 2 the moment of inertia is given by

$$I = 2\sum_{n\neq 0} |\langle \Phi_n, M_Z \Phi_0 \rangle|^2/(E_n - E_0). \qquad (4)$$

We now compare these two expressions. First we note that in deriving (3) it is implicitly assumed that in a deformed nucleus the orientation of the main axes cannot deviate appreciably from the orientation of the self-consistent field. This implies in particular that the first of the relations (2) can be replaced by

$$i\hbar^{-1}(E_n - E_0)\langle\Phi_n, \varphi\Phi_0\rangle = -I_0^{-1}\langle\Phi_n, N_Z\Phi_0\rangle. \quad (5)$$

From (5) and from the commutation relations one can easily derive the expressions

$$2\sum_{n\neq 0}\frac{\langle\Phi_0, M_Z\Phi_n\rangle\langle\Phi_n, N_Z\Phi_0\rangle}{E_n - E_0} = -I_0,\ 2\sum_{n\neq 0}\frac{|\langle\Phi_n, N_Z\Phi_0\rangle|^2}{E_n - E_0} = I_0. \quad (6)$$

Exchanging L_Z by $M_Z + N_Z$ in (3) and applying (6) we immediately obtain (4).

Thus the expressions (3) and (4) are equivalent.

*Here and in the following we speak about a rotation of the nucleus around a fixed axis. Consideration of the rotation around a free axis will only introduce complications in the intermediate expressions and will not lead to any essential changes in the final results.

[1] D. R. Inglis, Phys. Rev. **96**, 1059 (1954).
[2] A. Bohr and B. Mottelson, Preprint (1958).
[3] F. Villars, Nucl. Phys. **3**, 240 (1957), Ann. of Phys. **5**, 224 (1958).
[4] S. Hayakawa and T. Marumori, Progr. Theor. Phys. **18**, 396 (1957).

Translated by M. Danos
221

EFFECT OF VACUUM FLUCTUATIONS ON THE POLARIZATION OF ELECTRONS MOVING IN A MAGNETIC FIELD

I. M. TERNOV and V. S. TUMANOV

Moscow State University

Submitted to JETP editor June 12, 1959

J. Exptl. Theoret. Phys. (U.S.S.R.) **37**, 1137-1139 (October, 1959)

OWING to the anomalous magnetic moment, the spin of an electron moving in a uniform magnetic field does not preserve its orientation along or opposite to the direction of motion, but precesses about the direction of the momentum. The quasiclassical interpretation of this effect was given by Mendlowitz and Case,[1] who obtained the equations of motion for the spin operator in the Heisenberg representation, from where they derived the precession. The corresponding experimental investigations have also been carried out.[2]

It seems useful to give a consistent quantum mechanical description of this effect which is valid for electrons with arbitrary energy. We start from the Dirac equation with radiative corrections taking into account the effects of the photon vacuum (see, for example, reference 3), which, in first approximation, has the form

$$(i\hat{\partial} + e\hat{A} - m)\psi(x) = -ie^2\int\gamma^\nu S^c(x, x')\gamma_\nu D^c(x - x')\psi(x')\,d^4x', \quad (1)$$

where D^c is the causal photon function, and S^c is the causal Green's function of the electron, expressed in terms of the exact solutions of the Dirac equation for an electron moving in a magnetic field. The time integration transforms (1) into

$$(E - \mathcal{H})\psi(\mathbf{r}) = \int K(\mathbf{r}, \mathbf{r}')\psi(\mathbf{r}')\,d\mathbf{r}', \quad (2)$$

where $\mathcal{H}$ is the Hamiltonian of the Dirac equation.

Each energy level is doubly degenerate with respect to the quantum number $s = \pm 1$ characterizing the projection of the spin on the direction of the momentum. The right hand side of (2) is a constant perturbation and causes periodic transitions between these states. Writing ψ as a superposition of ψ_1 and ψ_{-1}, multiplying (2) by ψ_s^+ and integrating over $\mathbf{r}$, we obtain a system of equations which determines the two energy values and the coefficients of the expansion. We introduce a time dependent wave function which satisfies the initial condition $\Psi(0) = \psi_1$, and find the following expression for the average value of the projection of the spin on the direction of the momentum:

$$\left\langle\frac{\sigma\mathbf{k}}{k}\right\rangle = \int\Psi^+(t)\frac{\sigma\mathbf{k}}{k}\Psi(t)\,d\mathbf{r} = \cos^2\delta t + \frac{1}{4}A^{-2}[(W_{1,1} - W_{-1,-1})^2 - 4W_{-1,1}^2]\sin^2\delta t, \quad (3)$$

where

$$A = {}^1/_2[(W_{1,1} - W_{-1,-1})^2 + 4W_{1,-1}W_{-1,1}]^{1/2}, \qquad \delta = A/\hbar,$$

$$W_{ss'} = \int\psi_s^+(\mathbf{r})K(\mathbf{r}, \mathbf{r}')\psi_{s'}(\mathbf{r}')\,d\mathbf{r}\,d\mathbf{r}'.$$

Expression (3) has no divergencies connected with the mass of the field. Only for the calculation of the energy of the interaction with the vacuum it becomes necessary to introduce the corresponding compensating term in (1). If the electron moves in the direction of the field, we find $W_{s,-s} = 0$ and $\langle\sigma\mathbf{k}/k\rangle = 1$, i.e., the spin of the electron preserves its initial orientation. In the other limiting case — motion in the plane perpendicular to the direction of the field — we have $W_{1,1} = W_{-1,-1}$ and (3) takes the form

$$\langle\sigma\,\mathbf{k}/k\rangle = \cos 2\delta t, \qquad \delta = |W_{1,-1}|/\hbar. \quad (4)$$

Also $\langle\sigma_Z\rangle = 0$. These relations can be interpreted as the precession of the spin in the plane

of the orbit. However, in view of the fact that only the projections of the spin on the direction of the momentum are integrals of the motion (± 1), it would be more consistent to avoid the term "precession" and to speak of the transition time between these states or of the transition probability per unit time.

With regard to the calculation of $W_{1,-1}$, the following should be noted. It is impossible to expand the Green's function in powers of the potential, since the potential of the uniform field is not a perturbation. Indeed, the vector potential depends on a coordinate which can become very large in the relativistic case (for example, in the relativistic case, $\langle e^2\hat{A}^2\rangle \sim e^2 \times H^2 \langle r^2\rangle \sim E^2$). Similarly, with any other method of expansion, one must guard against the appearance in the neglected terms of expressions which depend on coordinates which after integration could lead to large values. In our case the expansion in terms of H/H_0 ($H_0 = m^2c^3/e\hbar \sim 10^{13}$ oe) was introduced in the last phase of the calculations, after the integration over space and the summation over the virtual states. As a result we obtained in first approximation in H/H_0 the following value for $W_{1,-1}$, which is valid both in the relativistic and nonrelativistic regions:

$$W_{1,-1} = -(\alpha/2\pi)\mu H. \qquad (5)$$

This result could have been derived from the operator $(\alpha/2\pi)(\sigma H)\mu$, but the use of this operator in the relativistic region would, according to the considerations above, require a special justification.

The time for the spin-flip caused by the interaction of the electron with the photon vacuum is, therefore, equal to $\pi/2\delta = 2\pi^2 mc/\alpha eH$. The ratio of this over the period of rotation of the electron is equal to $(\pi/\alpha)\,mc^2/E \sim 450\ mc^2/E$. The last quantity decreases as the energy becomes larger, and reaches the value 1 at energies of ~ 200 Mev.

The authors thank Prof. A. A. Sokolov for a discussion of this work.

[1] H. Mendlowitz and K. M. Case, Phys. Rev. **97**, 33 (1955).

[2] Louisell, Pidd, and Crane, Phys. Rev. **94**, 7 (1954).

[3] N. N. Bogolyubov and D. V. Shirkov, Введение в теорию квантованных полей (Introduction to the Theory of Quantized Fields), Gostekhizdat, Sec. 38, 1957.

Translated by R. Lipperheide
222

MINIMAL ERROR IN THE EXPERIMENTAL OBSERVATION OF ASYMMETRY

N. P. KLEPIKOV

Joint Institute for Nuclear Research; Ain Shams University, Cairo, UAR

Submitted to JETP editor June 13, 1959

J. Exptl. Theoret. Phys. (U.S.S.R.) **37**, 1139-1142 (October, 1959)

MANY experiments with elementary particles, aimed at proving or disproving the conservation of spatial parity or proving the existence of spin in a particle, reduce to the observation of a definite asymmetry in the distribution of the particles, produced in a certain reaction. It becomes useful to estimate the probability of the error committed when conclusions concerning the presence or absence of asymmetry are drawn from such an experiment.

In the observation of asymmetry, all particles are separated (during the course of the experiment or during the data reduction) into two groups, such that in the absence of asymmetry of the observed process a particle can belong to either group with equal probability. Usually the probability of registration of each particle in one of the groups is independent of the number of particles already accumulated in these groups. Therefore, if the data are corrected for possible systematic errors, the number of particles in the two groups, n_+ and n_-, have Poisson distributions with mean values $\frac{1}{2}n(1 \pm F)$, where $n = n_+ + n_-$, and F is a constant that characterizes the force of the interaction that leads to violation of the symmetry.

It can be shown that for $n_+ > n_- \gg 1$ the relation

$$t = (n_+ - n_- - 1)/\sqrt{n} \qquad (1)$$

has a Student's t-distribution with f degrees of freedom, where

$$\frac{1}{f} = \left(\frac{n_+}{n}\right)^2 \frac{1}{n_+ - 1} + \left(\frac{n_-}{n}\right)^2 \frac{1}{n_- - 1} \approx \frac{1 + 2(n_+ - n_-)^2 n^{-3}}{n - 2}. \qquad (2)$$

When $n \gg 1$ the value of t tends to $F\sqrt{n}$.

When $F = 0$, relation (1) satisfies, with probability $1 - \alpha$, the inequality

$$t < t_{1-\alpha/2}(f), \qquad (3)$$

where $t_P(f)$ is the number that has the probability P of satisfying the inequality $t < t_P$. If the value obtained for t does not satisfy inequality

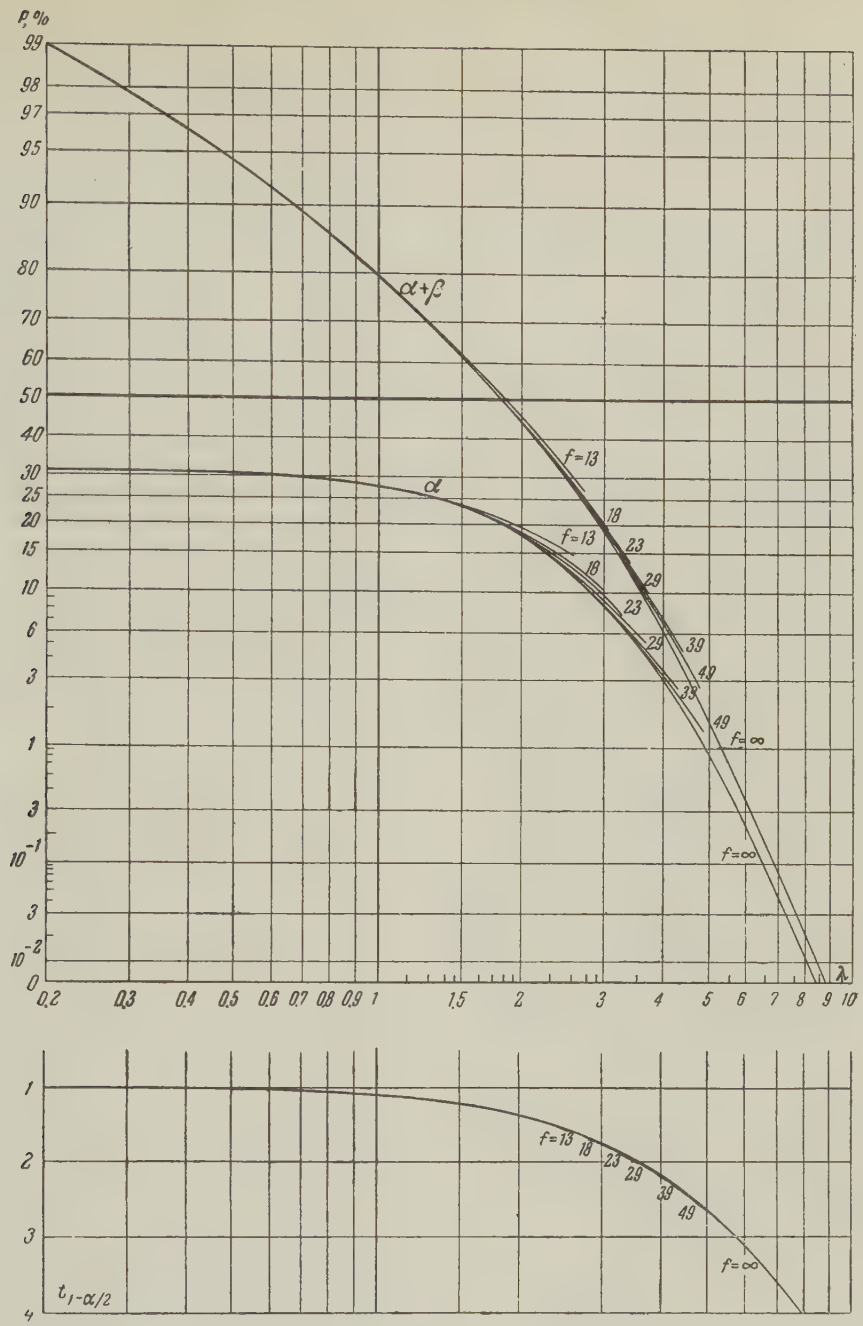

(3), the deviation of $\bar{F}$ from 0 is conceded to be significant and the hypothesis that the asymmetry is random is rejected.

The question arises, however, of the choice of the level of significance of α, equal to the probability of first-order error, when the random deviation of t from zero is assumed to be the deviation due to the fact that $F \neq 0$. To solve this problem it is necessary to take into account the probability of an error β of the second kind, when $F \neq 0$ but the small value of t is accepted as an indication that $F = 0$. The value of β is given in special tables.[1] When $f \gg 1$

$$\beta = 1 - \Phi\left[u_{\alpha/2} + \lambda\left(1 - \frac{1+u_{\alpha/2}^2}{4f}\right)\right] - \Phi\left[u_{\alpha/2} - \lambda\left(1 - \frac{1+u_{\alpha/2}^2}{4f}\right)\right], \quad (4)$$

where

$$\lambda = F\sqrt{n}, \qquad \Phi(x) = \frac{1}{\sqrt{2\pi}} \int_{-\infty}^{x} \exp\left\{-\frac{1}{2}u^2\right\} du.$$

We now choose α such that the sum of probabilities of errors of both kinds, $\alpha+\beta$, is a minimum. It can be readily verified that, for the approximation (4),

$$(\alpha+\beta)_{\min}=1-\Phi\left[u_{\alpha/2}+\lambda\left(1-\frac{1+u_{\alpha/2}^2}{4f}\right)\right]$$

$$-\Phi\left[u_{\alpha/2}-\lambda\left(1-\frac{1+u_{\alpha/2}^2}{4f}\right)\right]+2\Phi(u_{\alpha/2}), \quad (5)$$

where

$$u_{\alpha/2}=u+\frac{1}{4f}[u^3-u+\lambda(1+u^2)(1-e^{-\lambda^2})^{-1/2}],$$

$$u=-\frac{1}{\lambda}\cosh^{-1}e^{1/2\lambda^2}. \quad (6)$$

The last term in (5) equals the optimum value of α.

The upper half of the diagram shows the dependence of α and of $(\alpha+\beta)_{\min}$ on $\lambda = F\sqrt{n}$ and f, while the lower half shows the corresponding values of $t_{1-\alpha/2} = -t_{\alpha/2}$. With the aid of these curves we can determine the minimal value of the probability of first and second kind errors, provided n_+ and n_- are known. This probability is found to be a function of that value of F, which the experimenter undertakes to distinguish from the value F = 0. To the contrary, if a certain value of F is specified along with an upper limit of probable error, it is possible to find the number of observations $n = (\lambda/F)^2$ necessary to establish a deviation of F from 0.

Example: At n = 100 the value F = 0.1 is considered to be present when $t > 1.098$ and absent when $t < 1.098$, and the probability of error is 82%; at n = 6400, a value F = 0.1 is rejected when $t < 4.087$ and the probability of error is 0.018%. Another example: in order to clarify whether an asymmetrical interaction with intensity F = 0.01 exists, and in order to insure that the probability of the erroneous decision is less than 1%, it is necessary to carry out $n = (5.30/0.01)^2 = 280{,}000$ observations. Third example: an experiment yielded $n_+ = 5080$ and $n_- = 4920$; we then obtain $t = 1.59$ and $f = 9998 \gg 1$, from which we conclude that the values $F > 0.026$ are rejected, and the probability of error in stating the presence of F = 0.02 is 45%, that for the presence of F = 0.002 is 99.0%, and for the absence of F = 0.05 is 1.5%. If, on the other hand, $n_+ = 5200$ and $n_- = 4800$, then $t = 3.99$ and f = 9998; the values $F > 0.078$ are rejected, and the probable error in assuming that F = 0.07 is present, is 0.08%, while that of confirming the presence of F = 0.01 is 80%.

The author is grateful to R. M. Ryndin who called his attention to the usefulness of solving this problem.

[1] G. J. Resnikov and G. J. Lieberman, Tables of the Non-central t-distribution, Stanford, 1957.

Translated by J. G. Adashko
223

ENERGY LOST TO RADIATION IN A GAS-DISCHARGE PLASMA

V. D. KIRILLOV

Submitted to JETP editor June 22, 1959

J. Exptl. Theoret. Phys. (U.S.S.R.) 37, 1142-1144 (October, 1959)

IN all known experiments on the heating of a hydrogen plasma by Joule heat, only a small fraction of this heat serves to raise the plasma temperature.[1] It can be assumed that the energy is either carried away by the heated particles or is radiated. The present investigation was undertaken to clarify this problem.

The measurements were made with a cylindrical porcelain gas-discharge chamber (length L = 70 cm, diameter 22 cm) terminated on each end by copper electrodes 4 cm in diameter. The apparatus was evacuated to 10^{-5} mm mercury. The experiments were carried out at discharge currents of amplitude J_{max} = 13 to 45 kiloamp and half-period approximately 500 μsec. The initial deuterium pressures were 0.01—0.02 mm mercury and the intensity of the longitudinal magnetic field was H = 0 — 24,000 oe.

Under conditions satisfying the Shafranov stability criterion, we observed a plasma column with diameter $a \sim 6$ cm along the axis of the chamber.[2] We first describe briefly the probe measurements with the ionization chamber,* which have led us to attribute an important role to the radiation losses.

To count the charged particles that reached the wall of the discharge chamber, we used an instrument (Fig. 1) that combined an ordinary plane double probe (with electrodes A and B) and an ionization chamber B. From 20 to 70 volts were applied to the electrodes of the probe. The current in the probe circuit, a measure of the plasma den-

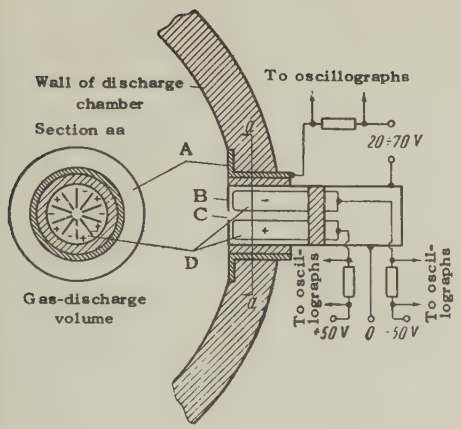

FIG. 1

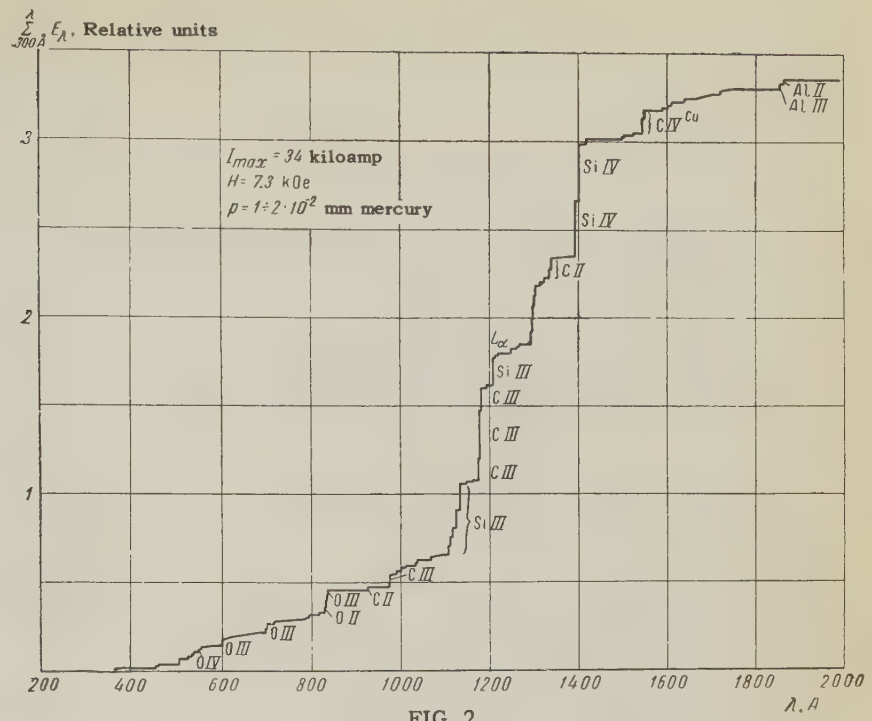

FIG. 2

sity at the wall, was registered with an oscillograph.

The ionization chamber comprised a metal container with a small (a fraction of a millimeter) opening C. The charged particles entered through the opening into the chamber and produced between two oppositely-charged groups of electrodes D a current which was registered by the oscillograph. The voltage between the electrodes (100 volts) was set to produce saturation current. The instrument was placed in the center of the discharge chamber. It was assumed that the current in the ionization chamber was proportional to the flow of the charged particles in the hole and consequently on the wall. Actually, at $H = 0$, when the discharge current flowed at random over the entire cross section of the chamber, good correlation was observed between the signals of the ionization chamber and of the double probe. Under stable conditions (at $H > 4LI_{max}/\pi ca^2$) the double-probe signal was increased by a factor of 10^5, while the current in the saturation chamber dropped only by a factor of $10 - 100$. In this case the ionization-chamber current was proportional at each instant of time, in first approximation, to the electric power liberated in the plasma, and was practically independent of the pressure and of the value of H.

Test experiments with filters and diaphragms of complex shapes have demonstrated that under stable conditions the ionization-chamber current is due to photoelectrons emitted by the walls and electrodes of the chamber under the influence of light penetrating from the discharge through the opening. Reduction of the data, based on a reasonable assumption of the quantum yield of the photoeffect (~ 0.02) and of the quantum energies (~ 10 ev) has shown that the light carries away a considerable portion of the energy delivered to the plasma. The assumption that this light was due to ultraviolet radiation by the impurities was corroborated by tentative computations[3] and confirmed by spectrograms plotted with a DFS-6 vacuum spectrograph. The spectrum was registered on photographic film sensitized with sodium salicylate. The spectrum lines were identified and photometrically analyzed, so that the energy E_λ carried by the individual lines was determined in arbitrary units.

Figure 2 is a plot of ΣE_λ in the range from 300 to 2000 A and shows that the greater part of the light energy is contained in the wavelength interval $1100 - 1400$ A (photon energy ~ 10 ev). The Lyman lines take a small fraction of the light energy (see table). The predominant portion is emitted by the ionized atoms of the carbon and the chamber wall material (silicon, oxygen, aluminum). The fraction of long-wave radiation ($\lambda > 2500 - 3000$ A) in the total light flux is also small, as found from experiments with a camera obscura, in which the film was placed either with the sensitized emulsion or with the backing side to the light. In the second case the film was not exposed.

The absolute light energy was measured with a thermoluminophor procedure. The thermoluminophor† was placed in a vacuum camera ob-

	Discharge conditions		Ratio
	I_{max} = 13.5 kiloamp, H = 7300 oe, $p = 1-2 \times 10^{-2}$ mm Hg	I_{max} = 34 kiloamp, H = 7300 oe, $p = 1-2 \times 10^{-2}$ mm Hg	
Total electric energy delivered to the plasma, kilojoules	2.8	11.9	4.3
Value of $\sum_{300\text{Å}}^{1900\text{Å}} E_\lambda$, arbitrary units	0.7	3.3	4.8
Fraction of light energy taken by the Lyman lines	1/180	1/580	
Fraction of the total energy (%) lost by radiation, based on measurements with thermoluminophor in three positions	65; 105; 65	80; –; 70	

scura at several distances from the small aperture (0.14 mm in diameter) so that various sections of the image of the plasma column were projected on it. The total energy losses were calculated with allowance for the energy distribution of the radiation and the spectral sensitivity of the thermoluminophor, known only up to $\lambda = 800$ A. The data were extrapolated to the shorter wavelengths. The estimated possible error in the determination of the absolute value of the light losses does not exceed 50%. The results of the measurements with the thermoluminophor are listed in the table. The results of all the measurements show that the greater part of the energy delivered to the plasma is lost by radiation from the impurities. In view of this, it is difficult to count on success in heating a deuterium plasma by Joule heat without eliminating the sources of contamination.

The author thanks L. A. Artsimovich and N. A. Yavlinskiĭ for help in the work.

*The construction of the ionization chamber was developed by V. S. Mukhovatov in his diploma project.

†The thermoluminophor, calibrated in absolute energy units, was graciously furnished us by V. A. Arkhangel'skaya and T. K. Razumova, to whom the author expresses his gratitude.

[1] Butt, Carruthers, Mitchell, Pease, Thonemann, Bird, Blears, and Hartill, Second UN Internat. Conf. on Peaceful Uses of Atomic Energy, Geneva, 1958, P/1519.

[2] Golovin, Ivanov, Kirillov, Petrov, Razumova, and Yavlinskiĭ, ibid. P/2226.

[3] V. I. Kogan, Dokl. Akad. Nauk SSSR **128**, No. 4, 1959, Soviet Phys.–Doklady, in press.

[4] Arkhangel'skaya, Vaĭnberg, and Razumova, Оптика и спектроскопия (Optics and Spectroscopy) **1**, 1018 (1956).

Translated by J. G. Adashko
224

ANTIFERROMAGNETISM IN NiF_2

R. A. ALIKHANOV

Institute of Physical Problems, Academy of Sciences, U.S.S.R.

Submitted to JETP editor June 25, 1959

J. Exptl. Theoret. Phys. (U.S.S.R.) **37**, 1145-1147 (October, 1959)

THE fluorides of the elements of the iron group (Mn, Fe, Co, and Ni) form an isomorphic series of compounds with a tetragonal lattice. Neutronographic studies of these compounds, conducted by Erickson,[1] show that they all have an antiferromagnetic structure at hydrogen temperatures. In the diffraction picture, at the locations of the reflections having indices (100), (111), (210), and (201), an increase of intensity over that of room temperature was observed. The absence of a (001) reflection for MnF_2, FeF_2, and CoF_2 indicates that the direction of the antiferromagnetic vector coincides with the tetragonal axis of the crystal. For nickel fluoride at 25° K some change of intensity in the region of the (001) reflection is noted. This is manifest by a small increase in the right arm of the (110) peak. On this basis, Erickson proposed a magnetic structure for NiF_2 somewhat different from that of the other fluorides. According to his data the spins are inclined at an angle of 10° from the tetragonal axis. The magnetic structure pro-

posed by Erickson is shown dashed in Fig. 1. Angle α, obtained from x-ray data,[2] is equal to 8° and was apparently taken as the direction of the spins. The angular half-width of the (110) diffraction maximum on the NiF_2 neutron-diffraction pattern is 1.5°, a fairly large value. The (110) nuclear reflection thus overlaps the (001) magnetic reflection and the precision with which a prediction regarding the magnetic structure can be made is limited.

Our neutron-diffraction studies of NiF_2 were made from patterns with diffraction maxima that had an angular half-width of 0.65°.[3] Our NiF_2 sample was prepared by the Technology Division of the Institute of Physical Problems, U.S.S.R. Academy of Sciences, by heating the aqueous salt for several hours in a current of hydrogen fluoride. This procedure produced a yellowish-green fine crystalline powder. The neutron-diffraction pattern of the sample at hydrogen temperature is shown in Fig. 2. Owing to good resolving power, the (001) and (100) reflections are separated.

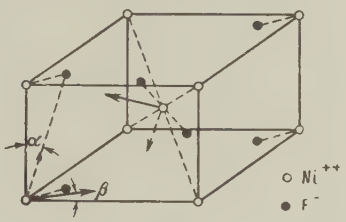

FIG. 1

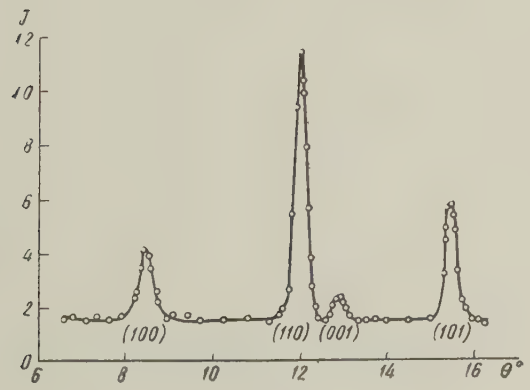

FIG. 2

The direction of the antiferromagnetism with respect to the crystallographic axes was determined from data on the ratio of the magnetic intensities J_{100}/J_{001}. Calculation shows that the antiferromagnetic moments lie in the (001) plane, perpendicular to the tetragonal axis (see Fig. 1). The possibility of such a structure was investigated earlier by Dzyaloshinskiĭ[4] on the basis of Landau's theory of phase transitions. This theory admits of three possible magnetic states. In the first state, the equal but oppositely oriented spins of the two metallic ions of the lattice are directed along the tetragonal axis. In the second state, II_1, the spins are directed along one of the equivalent [100] directions, which are rotated slightly toward one another about the crystal axis in the (001) plane, so that there results a spontaneous magnetic moment $\overline{m}$ directed along [100]. In the third possible state, II_2, the magnetic moments are directed along one of the [110] axes, but they are of different magnitudes. Moreover, within a very narrow temperature range, where mutual changes are possible between the above-mentioned magnetic states, the theory admits of the existence of two additional magnetic states. In the first of these, III_1, the spins lie in the (001) plane inclined at a small angle to the crystal axis, so that a spontaneous magnetic moment appears in the [100] direction. In state III_2, the spins and the moment $\overline{m}$ lie in the (110) plane. According to Erickson's data, the first magnetic state is found in MnF_2, FeF_2, and CoF_2. As present measurements have proved, the magnetic structure of NiF_2 corresponds to that of the second state. The weak ferromagnetism (presence of moment $\overline{m}$), characteristic of this state, should have made a magnetic contribution to the reflections with indices of even sum, particularly to the (110) reflection. A very small increase in the intensity of this reflection is actually observed upon changing from nitrogen temperature to that of hydrogen. In our experiments a change of intensity in the (110) maximum was constantly recorded upon cooling the sample from nitrogen to hydrogen temperature and upon heating the sample after vaporization of the hydrogen. A small change of intensity was observed in both cases: an increase in the former and a decrease in the latter. In the latter case, the intensity of the neutron beam was increased in order to increase the effect. Calculation shows that the observed effect, including the change of intensity with temperature, may be explained by a deflection of the moments of the sublattices from the (100) plane by an angle β not greater than 13° (see Fig. 1).

Matarresse and Stout,[5] in studying the twisting moment of a single crystal of NiF_2, discovered a weak ferromagnetism of this compound in the [100] direction. Its absolute value, equal to 350 ergs per gauss-mole, constitutes 3 percent of the saturation moment of the nickel ion, corresponding to an angle β of 2.5°. The experimental data obtained in this manner quite definitely establish a magnetic state II_1 for NiF_2. The possibility of

the existence of type III states was studied by measuring the temperature dependence of the intensity J of the (100) and (001) magnetic reflections (Fig. 3). The transition point, determined by extrapolating the curves, is at 78.5°K. According to specific-heat data, the transition point is at 73.2°K.[6] The curves are in general smooth. The difference $J_{He} - J_T$ varies approximately as T^2. The crystal does not change in magnetic structure as the temperature is reduced from T_N down to helium temperature. Had there been a change in magnetic structure, the temperature-dependence curve of J_{001} would have had a maximum.

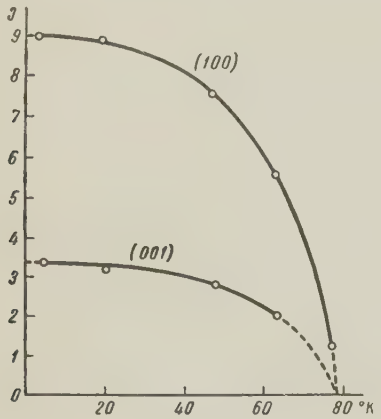

FIG. 3

I wish to thank Academician P. L. Kapitza for continuous interest in this work. I am grateful to A. S. Borovik-Romanov for much advice and to I. E. Dzyaloshinskiĭ for valuable discussion. I am indebted to Yu. G. Abov for his constant cooperation in the work. I also thank N. N. Mikhaĭlov for furnishing the sample.

[1] R. A. Erickson, Phys. Rev. **90**, 779 (1953).

[2] Haendler, Patterson, and Bernard, J. Amer. Chem. Soc. **74**, 3167 (1952).

[3] R. A. Alikhanov, JETP **36**, 1690 (1959), Soviet Phys. JETP **9**, 1204 (1959).

[4] I. E. Dzyaloshinskiĭ, JETP **33**, 1454 (1957), Soviet Phys. JETP **6**, 1120 (1958).

[5] L. M. Matarresse, J. W. Stout, Phys. Rev. **94**, 1792 (1954).

[6] E. Catalano and J. W. Stout, J. Chem. Phys. **23**, 1284 (1955).

Translated by G. F. Schultz
225

ON CERTAIN SINGULARITIES IN THE INTERACTION WITH LIGHT NUCLEI OF PARTICLES WITH ENERGIES $E \geq 2 \times 10^{12}$ ev

N. L. GRIGOROV and V. Ya. SHESTOPEROV

Nuclear Physics Institute, Moscow State University

Submitted to JETP editor June 30, 1959

J. Exptl. Theoret. Phys. (U.S.S.R.) **37**, 1147-1149 (October, 1959)

In a previous paper[1] we have shown, by assuming the existence of large fluctuations in the fraction of energy transferred to π mesons when a high-energy nucleon interacts with a light nucleus, that all the observed basic characteristics of extensive atmospheric showers can be easily explained without resorting to the hypothesis that the shower development is influenced by the nuclear cascade.[2] This paper presents experimental data demonstrating the existence of interactions in which the primary particle loses almost all its energy (to the production of π^0 mesons), and estimates the probability of this process.

The experimental array, shown schematically in Fig. 1, consisted of four mutually perpendicular rows of pulse ionization chambers. Each row contained 33 chambers 330 cm long and 10 cm in diameter. The effective area of the array was 10 m^2. Each of the 132 chambers was connected to its own amplifier, which measured the pulses with 300 to 400-fold range of amplitudes. Pulse registration occurred whenever the ionization in any two or more chamber rows exceeded a given value. Part of the time the array operated with a hodoscope of 250 counters located at various distances from the array. This work was performed in Moscow during 1959. E. S. Loskevich and A. A. Oles' took part in the task.

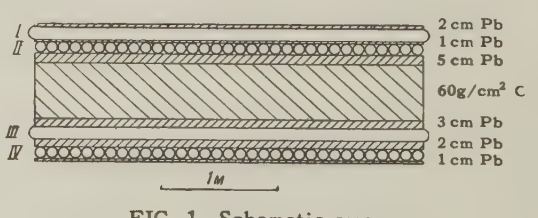

FIG. 1. Schematic array

During the operation of the array, there were observed in chamber rows I and II impulses for which almost all the ionization was confined to a circle of ~ 20 cm radius. In subsequent data processing, those events were selected in which more than 70% of all ionization was concentrated in not

more than four chambers (in a circle of 20 cm radius), and the energy of the soft component falling on the array was $E \geq 2 \times 10^{12}$ ev. The ionization distribution in one of these impulses is shown in Fig. 2. There were 27 such events recorded during 800 hours of array operation. Hence their frequency is $\sim 9 \times 10^{-11}\,cm^{-2}\,sec^{-1}$. If the integrated spectrum of these impulses is represented by an exponential function, the exponent is $\gamma = 1.5 \pm 0.5$.

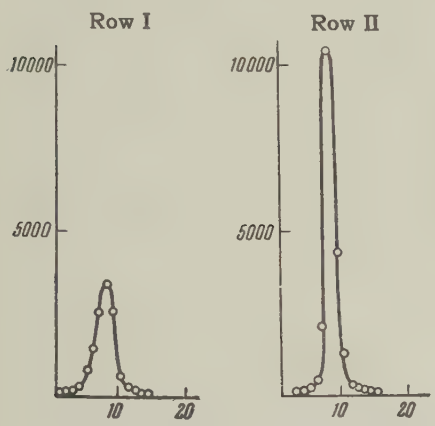

FIG. 2. Example of an event in which a newborn shower impinges on the array. Abscissa – chamber numbers; ordinate – ionization in each chamber, expressed in terms of the number of recorded particles.

It can easily be shown that μ mesons cannot contribute more than 10% of the selected events. One can therefore assert that those impulses, for which almost all the ionization occurring in the upper rows of chambers is concentrated within a circle of ~ 20 cm radius, are produced by newborn electron-photon showers generated by the interaction of particles of $E \geq 2 \times 10^{12}$ ev with the nuclei of atmospheric atoms located not far above the array. The concentration of 70% of the shower energy within a radius of 20 cm shows that shower generation occurs within an atmospheric layer ~ 100 g/cm^2 above the array. In those cases when the hodoscope was operating, the number of particles in the atmospheric shower accompanying such an impulse in the upper chamber rows comprised $\lesssim 5\%$ of the number of particles in an extensive atmospheric shower, for which the energy of the electron-photon component $\geq 2 \times 10^{12}$ ev was contained in a circle of 20 cm radius. This circumstance also furnishes direct proof that the recorded shower is newborn.

The two lower rows of chambers in the array permit determination of the energy of the nuclear-active particles accompanying newborn electron-photon showers. (Counting efficiency for individual nuclear-active particles was 70%.) According to the experimental data, impulses produced in the lower chamber rows III and IV, by nuclear-active interactions in the filtering array are observed in only 30% of the events (8 occurrences out of 27). During such occurrences, as a rule, not one but several nuclear-active particles fall on the array, generating impulses of commensurate magnitude (from which it follows that the counting efficiency of the nuclear-active component in the selected events approaches 100%). For the 30% of events in which newborn showers are accompanied by nuclear-active particles, the pulse amplitude in the lower rows averages 40% of the pulse amplitude in the upper rows. We conclude that in these events the energy of the nuclear-active particles equals the energy of the electron-photon component.

The fact that a significant fraction of the newborn showers, generated not far above the array, does not contain high-energy nuclear-active particles, indicates the existence of processes in which the primary particles transfer almost all their energy to the electron-photon component. If a given process in which 100% of the nuclear-active particle energy goes to the soft component occurs via π^0-meson production, then it follows from our data that the number of π^0 mesons thus created is small ($\ll 10$), and indeed it is possible that almost all the energy is transferred to a single π^0 meson.

The probability of such interactions, in which almost all the primary-particle energy is transferred to the soft component, can be determined by comparing our count of such events in an atmospheric layer ~ 100 g/cm^2 thick with the absolute flux of nuclear-active particles having $E \geq 2 \times 10^{12}$ ev (nuclear-active particle flux data were taken from reference 3). Comparison of the experimental data indicates that the probability of complete energy transfer to the soft component is $\sim 10\%$.

If one assumes that the basic characteristics of the interaction do not change materially as the particle energy increases to $10^{13} - 10^{14}$ ev, then it can be shown, from the frequency of newborn showers registered, that $25 - 50\%$ of the observed extensive atmospheric showers containing $10^4 - 10^5$ particles can be produced merely by those interactions in which almost all the primary-particle energy is transferred to the soft component. In these showers the energy of the nuclear-active component will be significantly lower than the energy of the electron-photon component.

Since as a rule a newborn shower is accompanied by a very weak atmospheric shower, it follows that nuclear-active particles with $E \geq 2 \times 10^{12}$ ev, which have interacted not far above the array, have passed through almost the entire atmosphere without taking part in any interactions involving

a large energy loss. Hence, along with the interactions associated with almost 100% energy loss, there must also be weak interactions which involve little energy loss, and which occur with significantly higher probability.

[1] Grigorov, Shestoperov, Sobinyakov, and Podgurskaya, JETP **33**, 1099 (1957), Soviet Phys. JETP **6**, 848 (1958).

[2] N. L. Grigorov and V. Ya. Shestoperov, JETP **34**, 1539 (1958), Soviet Phys. JETP **7**, 1061 (1958).

[3] Grigorov, Murzin, and Rapoport, JETP **36**, 1068 (1959), Soviet Phys. JETP **9**, 759 (1959).

Translated by D. A. Kellogg
226

PHOTOPRODUCTION OF π^0-MESONS FROM CARBON NEAR THRESHOLD

R. G. VASIL'KOV, B. B. GOVORKOV, and V. I. GOLDANSKIĬ

P. N. Lebedev Physics Institute, Academy of Sciences, U.S.S.R.

Submitted to JETP editor July 2, 1959

J. Exptl. Theoret. Phys. (U.S.S.R.) **37**, 1149-1151 (October, 1959)

IT has been shown[1,2] that in the photoproduction of π^0 mesons from helium at energies between threshold and ~ 200 Mev, the elastic production dominates. To investigate the role played by the elastic process in the photoproduction of π^0 mesons from more complex nuclei, we measured in the present work the ratios of the total cross sections for photoproduction from carbon and from hydrogen at primary photon energies of 160, 180, and 200 Mev. The geometry and the experimental method for the carbon measurements, which were made on the 265-Mev synchrotron of the P. N. Lebedev Physics Institute of the U.S.S.R. Academy of Sciences, are similar to those previously described[3] for hydrogen experiments.

Curves were obtained for the energy dependence of the emerging γ rays from the decay of the π^0 mesons from carbon, for three angles. The emerging decay γ rays were measured to within 1 or 2%. The energy dependence of the cross section for producing the decay γ rays was calculated by the method of "photon differences" from the corresponding measured energy-dependence curves. The angular distributions of the decay photons obtained in this way were then integrated to obtain the total cross sections for the photoproduction of π^0 mesons from carbon (σ_t^C) in relative units.

The ratios of the number of decay γ rays emerging from carbon and hydrogen at angles of less than 90°, obtained by measuring the counting rate of decay photons from hydrogen and styrofoam (C_8H_8) targets with the same geometry, were used to determined the ratio of the total cross sections σ_t^C/σ_t^H. The measured values of these ratios are shown in the figure.

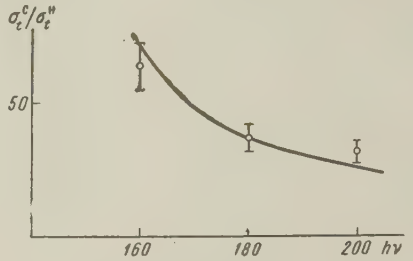

The results obtained were compared with the predictions of the theory of elastic photoproduction of π^0 mesons from nuclei.[1] According to the theory, the differential cross section for π^0-meson photoproduction from a nucleus with nucleon number A and spin zero can be expressed in the form

$$(d\sigma(k)/d\Omega)_A = A^2 (d\sigma(k)/d\Omega)_H F_A^2(qR)/F_H^2(q), \qquad (1)$$

where q is the nuclear recoil momentum, while $F_A^2(qR)$ and $F_H^2(q)$ are the nuclear and proton form factors; the second can be set equal to unity. From electron scattering experiments on carbon[4] it is known that the form factor for the carbon nucleus is expressed as follows

$$F_C^2(qR) = \left\{\left[1 - \frac{\alpha a^2 q^2}{2(2+3\alpha)}\right] e^{-q^2a^2/4}\right\}^2, \qquad (2)$$

where $\alpha = 4/3$, $a = 1.635 \times 10^{-13}$ cm, $(d\sigma(k)/d\Omega)_H$ is the spin-independent differential cross section for π^0-meson photoproduction from hydrogen. From the form of the matrix elements for π-meson photoproduction from nucleons one can easily get

$$(d\sigma(k)/d\Omega)_H = (3/8\pi)\,\sigma_t \sin^2\theta_\pi, \qquad (3)$$

where θ_π is the angle of emission of the π^0 meson in the center-of-mass system, and σ_t is the spin-independent part of the total cross section for π^0-meson photoproduction from protons.

Substituting (3) into (1) and integrating over the solid angle, we obtain

$$\sigma_t^C = 17.2 \cdot \sigma_t \int_0^\pi F_C^2(qR) \sin^3\theta_\pi \, d\theta_\pi.$$

The integrals on the right-hand side were computed graphically and then normalized by analytic evaluation of the integral for the threshold photon energy when $F_C^2(qR) = \text{const}$.

From the analysis of the experimental data[3] of π^0-meson photoproduction from protons,[5] it follows that within 10% accuracy, for the energy region of primary photons studied, one can neglect the contributions of the $M(\frac{1}{2})$, E1, and E2 photoproduction amplitudes to the total cross section σ_t^H. Hence taking into account only the amplitude $M(\frac{3}{2})$ in the total cross section for π^0-meson photoproduction from protons, we can easily determine that $\sigma_t = \frac{2}{3}\sigma_t^H$. To calculate σ_t we use the total cross section σ_t^H measured in reference 6. The calculated curve σ_t^C/σ_t^H is compared with the experimental points in the figure. Calculation of the contribution of the E1 amplitude makes a small reduction in the calculated magnitude of σ_t^C/σ_t^H for $h\nu = 160$ Mev; however this change lies within the limits of the statistical uncertainty of the experiments.

As can be seen from the figure, there is good agreement between theory and the observed experimental results. Therefore at primary photon energies of 160 to 200 Mev the elastic photoproduction of π^0 mesons from carbon dominates. At higher energies it seems that inelastic processes begin to appear in π^0-meson photoproduction which show up as small deviations of the experimental ratio σ_t^C/σ_t^H from that calculated theoretically. This is consistent with the conclusion recently given.[7]

Similar measurements we have made of the π^0-meson photoproduction cross section from beryllium nuclei do not show any significant differences between the energy dependence of the total cross section for π^0-meson photoproduction from carbon and beryllium.

The authors thank A. M. Baldin for valuable advice.

[1] G. de Saussure and L. Osborne, Phys. Rev. **99**, 843 (1955).

[2] E. Goldwasser and L. Koester, Nuovo cimento **4**, 950 (1956).

[3] Vasil'kov, Govorkov, and Goldanskiĭ, JETP **37**, 11 (1959), Soviet Phys. JETP **10**, 7 (1960); Vasil'kov, Govorkov, and Kutsenko, Приборы и техника эксперимента (Instrument and Meas. Engg.), in press.

[4] J. Fregan, Phys. Rev. **104**, 225 (1956).

[5] A. M. Baldin and B. B. Govorkov, Dokl. Akad. Nauk SSSR, in press.

[6] R. G. Vasil'kov and B. B. Govorkov, JETP **37**, 317 (1959), Soviet Phys. JETP **10**, 224 (1960).

[7] G. Leiss and R. Schrack, Revs. Modern Phys. **30**, 456 (1958); Goodwin, Anderson, and Kenney, Bull. Am. Phys. Soc. **3**, 421 (1959).

Translated by R. F. Peierls
227

CALCULATION OF ENERGY LEVELS OF Tl^{206} *AND* Bi^{210} *NUCLEI*

L. A. SLIV and Yu. I. KHARITONOV

Leningrad Physico-technical Institute, Academy of Sciences, U.S.S.R.

Submitted to JETP editor July 2, 1959

J. Exptl. Theoret. Phys. (U.S.S.R.) **37**, 1151-1153 (October, 1959)

1. To calculate the energy levels of the Tl^{206} and Bi^{210} nuclei we used the data of Sliv and Volchok[1] on the neighboring nuclei. The nucleus ${}_{81}Tl_{125}^{206}$ has one neutron hole and one proton hole. Using the single-particle neutron wave functions of Pb^{207} ($p_{1/2}$ — ground state, $f_{5/2}$ — 620 kev) and the proton wave functions of Tl^{207} ($s_{1/2}$ — ground state, $d_{3/2}$ — 350 kev), we can plot a zeroth-approximation level scheme for Tl^{206} up to 1 Mev. With the aid of these data for Tl^{206} we obtain the following multiplets with corresponding energies, spins, and parities: $(p_{1/2}s_{1/2})$, 0 kev, $I = 0^-, 1^-$; $(p_{1/2}d_{3/2})$, 350 kev, $I = 1^-, 2^-$; $(f_{5/2}s_{1/2})$, 620 kev, $I = 2^-, 3^-$; $(f_{5/2}d_{3/2})$, 970 kev, $I = 1^-, 2^-, 3^-, 4^-$. The problem is to determine the forces that split the levels belonging to individual multiplets. Such forces may be: 1) interaction with the surface of the nucleus, and 2) weak paired interaction of the neutron and proton holes, located in different shells. The interaction with the surface was computed in the weak-coupling approximation.[2] It was found significant that regardless of the choice of parameters, the interaction with the surface does not split the doublet levels, but shifts them as a whole. The magnitude of this shift is a function of the energy $\hbar\omega$ of the first vibration level and of the "hardness" C of the Tl^{206} nucleus. Calculation has shown that as C changes from 1000 to 1500 Mev, and as $\hbar\omega$ changes from 1 to 3 Mev, the relative distances between the doublets do not change substantially.

On the basis of our calculations we arrive at the following conclusions:

1. The transitions ($^3/_2 1 \rightarrow {}^1/_2$) and ($^5/_2 1 \rightarrow {}^1/_2$) [besides the transition ($^5/_2 3 \rightarrow {}^3/_2 2$)] have the greatest reduced probability among all the above-mentioned E2 transitions. This is in agreement with the experimental results on Coulomb excitation (for W^{183}, see reference 6). If the nuclear shape deviates strongly from the axially symmetric one, the transitions ($^3/_2 2 \rightarrow {}^3/_2 1$) and ($^5/_2 2 \rightarrow {}^5/_2 1$) also become pronounced.

2. If the nucleus deviates little from the axially symmetric shape, all M1 transitions between the rotational levels of the nucleus have small reduced probabilities. If, however, the nuclear shape is far from being axially symmetric, the transitions ($^5/_2 2 \rightarrow {}^5/_2 1$) and ($^5/_2 3 \rightarrow {}^3/_2 2$) become important.

3. It follows from (5) and (6) that all magnetic transitions to the ground state should be very weak as compared to the electric transitions.

4. According to Davydov,[1] we have $\gamma \approx 27°$ for the nucleus W^{183}. From Fig. 1 we then obtain for the ratio of the reduced transition probabilities for the transitions ($^1/_2 \rightarrow {}^5/_2 2$) and ($^1/_2 \rightarrow {}^3/_2 2$) the value (6/4)(4/2.3) = 2.6. This is in good agreement with the estimate based on the experimental results of Alder et al.[6]

The author expresses his sincere gratitude to Prof. A. S. Davydov for his interest in this work.

[1] A. S. Davydov, JETP **36**, 1555 (1959); Soviet Phys. JETP **9**, 1103 (1959).

[2] A. S. Davydov and G. F. Filippov, JETP **35**, 440 (1958), Soviet Phys. JETP **8**, 303 (1959).

[3] A. Bohr and B. Mottelson, Kgl. Danske Videnskab. Selskab, Mat.-fys. Medd. **27**, Nr. 16 (1953), Russ. Transl. Пробл. совр. физ. (Prob. Modern Phys.) **9**, 34 (1955).

[4] A. S. Davydov and G. F. Filippov, JETP **35**, 703 (1958), Soviet Phys. JETP **8**, 488 (1959).

[5] A. S. Davydov, Теория атомного ядра (Theory of the Atomic Nucleus) Fizmatgiz (1958).

[6] Alder, Bohr, Huus, Mottelson, and Winther, Revs. Modern Phys. **28**, 432 (1956).

Translated by R. Lipperheide
229

ALPHA DECAY OF Th^{229}. *INTERACTION OF NUCLEAR LEVELS*

L. L. GOL' DIN, G. I. NOVIKOVA, N. I. PIROGOVA, and E. F. TRET' YAKOV

Submitted to JETP editor July 4, 1959

J. Exptl. Theoret. Phys. (U.S.S.R.) **37**, 1155-1157 (October, 1959)

THE α decay of Th^{229} has not been investigated heretofore. Nor is anything known concerning the structure of the levels of the daughter nucleus Ra^{225}.

We have investigated the α decay of Th^{229} with a magnetic α spectrometer;[1] the spectra of conversion electrons of Ra^{225} accompanying the α decay of Th^{229} were investigated with a high-aperture toroidal β spectrometer[2] and an α-β coincidence circuit. The measurements were carried out with the isotope Th^{229}, obtained by chemical separation of thorium from U^{233} that was aged for a long time.

The investigation of the α spectrum of Th^{229} disclosed 12 α lines. The energies of the α lines and the intensities of the corresponding transitions are listed in the table, which contains also the hindrance coefficients (ratio of the transition intensity, calculated from the formula for even-even nuclei, to the observed intensity).

In the investigation of the spectrum of the conversion electrons we observed approximately 100 conversion lines that could not yet be fully interpreted. We separated reliably the γ transitions with energies 17.2, 42.8, 69.9, 75.5, 137.2, 156.6, 193.4, and 210.5 kev. The 29.1, 31.6, 56.8, 58.9, 85.0, 132.1, 154.4, 179.6, 242.0 kev and a few other transitions are less reliable.

A comparison of the data obtained with both instruments suggests the existence of a Ra^{225} level with excitation energy ~ 3 kev. Whether this level becomes populated in α decay of Th^{229} and at what probability is still unknown. Apparently the γ transitions from high levels occur mainly at this level rather than at the ground level of Ra^{225}.

The α decay to the ground state of Ra^{225} appears to be strongly forbidden ($\eta = 330$). The more likely transition is that to the 214.5-kev level ($\eta = 1.5$). The spin of this level should therefore equal the spin of the ground state of Th^{229}, i.e., $^5/_2$. Located above this level are several others, some of which have small η. The Ra^{225} nucleus lies in a region sufficiently far from closed shells. The investigated nuclei in this region are prolate. It is natural to assume that

α line	α-line energy, Mev	Transition intensity, percent	η	α line	α-line energy, Mev	Transition intensity, percent	η
α_0	5.048	6.7	330	α_{156}	4.894	10.7	25
α_{20}	5.028	~0.2	$\sim 10^4$	α_{214}	4.837	58.2	1.5
α_{45}	5.003	~0.1	$\sim 10^4$	α_{246}	4.806	11.4	7
α_{78}	4.971	3.4	200	α_{264}	4.788	1.0	40
α_{88}	4.961	6.0	100	α_{302}	4.751	1.5	20
α_{125}	4.925	0.25	$\sim 10^3$	α_{376}	4.678	0.4	25

Ra^{225} is also prolate, and its level spectrum should therefore contain rotation bands. Such bands are usually determined from the multipolarities of the γ transitions between levels and from the energy variation, described by the well known formula

$$E_{rot} = (\hbar^2/2J)\{I(I+1) - I_0(I_0+1)\}. \quad (1)$$

As already mentioned, we have not yet succeeded in interpreting the γ spectrum, and comparison with (1) does not enable us to separate a single rotation band in the Ra^{225} spectrum. One can assume that the interaction between levels of very high density has caused them to shift and to deviate from (1).

An important auxiliary method, which can be employed for the analysis of the problem, is to study the α decay intensities at the rotational levels. These intensities behave, generally speaking, in an irregular manner. For α transitions at the levels of the principal rotation band (the band beginning with the level for which $\eta \approx 1$) there exists, however, the well known formula of Ter-Martirosyan,[3] which has been experimentally confirmed with good accuracy (see, for example, reference 4).

The population of the level with energy 214.5 kev, the transition to which is facilitated, is 58.2% (see table). Assuming a value of 43 kev for the energy of the first rotational level of Ra^{225} (the energy value is taken from the level spectrum of Th^{229}, the daughter nucleus of U^{233}, and is characteristic of the entire adjacent region of nuclei) and putting $K = 5/2$ we find that the levels ($I = 7/2$; $K = 5/2$) and ($I = 9/2$; $K = 5/2$) should have populations ~10 and ~1.0% respectively.

It follows from the table that the required region contains only one level with a population of ~10%, α_{246}. Its excitation energy is, however, less than expected, merely 31.6 kev (relative to the α_{214} level).

The only possible level with $I = 9/2$ and $K = 5/2$ is α_{302}, with 1.5% population. The excitation energies of these two levels, however, do not fit the rotation formula (1).

We thus arrive at one of two possible conclusions:

1. The levels of the principal rotation band has an anomalously small population (smaller than theoretical by a factor of several times ten) and therefore do not appear in the α spectrum. This case appears to us, however, to be very unlikely, since no noticeable deviations from the Ter-Martirosyan formula have yet been observed. 2. The α_{246} level is shifted because of interaction with the α_{264} level.

As is known, interaction between levels should manifest itself particularly strongly only when their spins coincide and their K differ by unity. Since the spin of α_{246} is $7/2$, we must assume that the α_{264} level also has $I = 7/2$; inasmuch as this level is not a rotation satellite, its K also equals $7/2$. The selection rules with respect to K are thus automatically satisfied.

The "unshifted" position of the α_{246} level cannot exceed $(246+264)/2 = 255$ kev. Its excitation level lies in this case between 32 kev (observed value) and 41 kev. The upper value is in sensible agreement with the data for other nuclei.

The α_{302} level is apparently also shifted.

Let us indicate in conclusion that this interpretation raises a difficulty connected with a great difference in the α-populations of the interacting levels.

The investigation of the Ra^{225} levels will be continued by an improved procedure.

The authors are grateful to Academician L. D. Landau for a discussion of the results, to G. I. Grishuk, V. F. Konyaev, S. V. Kalashnikov and Yu. N. Chernov for help with the experiment, and to V. I. Krotkova for reduction of the photographic data.

[1] L. L. Gol'din and E. F. Tret'yakov, Izv. Akad. Nauk SSSR, Ser. Fiz. **20**, 859 (1956), Columbia Tech. Transl. p. 781.

[2] Tret'yakov, Gol'din, and Grishuk, Приборы и техника эксперимента (Instrum. and Meas. Engg.) No. 6, 22 (1957).

[3] Gol'din, Adel'son-Vel'skiĭ, Birzgal, Piliya, and Ter-Martirosyan, JETP **35**, 184 (1958), Soviet Phys. JETP **8**, 127 (1959).

[4] Gol'din, Novikova, and Tret'yakov, Izv. Akad. Nauk SSSR, Ser. Fiz. 20, 868 (1956), Columbia Tech. Transl. p. 789.

Translated by J. G. Adashko
230

ANGULAR DISTRIBUTION OF LONG-RANGE ALPHA PARTICLES, CONNECTED WITH THE FISSION PROCESS

N. A. PERFILOV and Z. I. SOLOV' EVA

Submitted to JETP editor June 8, 1959

J. Exptl. Theoret. Phys. (U.S.S.R.) 37, 1157-1159 (October, 1959)

We investigated the complex fission of U^{235} by thermal neutrons with thick photographic emulsions. In the experiments we used type P-8 photographic plates, prepared in our laboratory. The emulsion used had good discriminating ability with respect to tracks of fragments, α particles, and protons.

Cases in which a track of a long-range α particle was connected with the fission point were counted. We selected those cases, in which both the fragments and the α particle stopped in the emulsion. For approximately 600 such cases we calculated the ranges of all particles and the angles between the α particle and the fragments. The distribution of α particles by ranges, corrected for the probability of their exit from the emulsion, for the angular distribution of the α particles (Fig. 1), and for the asymmetry of fission were in good agreement with the results given in other papers.[1,2]

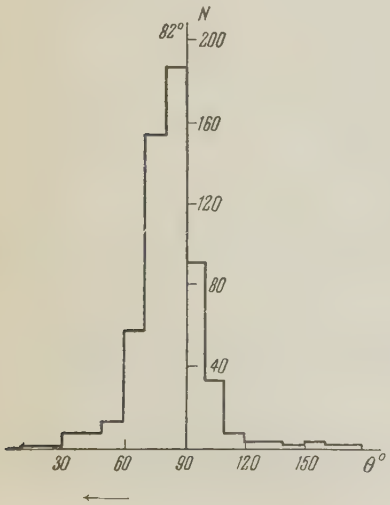

FIG. 1. Angular distribution of particles about the direction (shown by an arrow to the left) of light fission fragment.

Reference 1 proposes a mechanism whereby the production of a long-range α particle is considered as the scattering, under the influence of Coulomb forces, of three particles produced as the result of vibrations of a drop of nuclear liquid, in which the fourth harmonic, which is responsible for the triple fission, has a noticeable amplitude. Such a scheme explains satisfactorily the following: a) That the most probable angle of emission of an α particle deviates noticeably from 90° towards the lighter fragment. In fact, it is seen from Fig. 1 that the maximum in the angular distribution is located near 82° from the light fragment. b) That the energies of the α particles are close in order of magnitude to the total of the Coulomb barriers of the fragments.

Within the framework of this scheme, one would also expect the angle of emission of an α particle to be related to the asymmetry of the fragment, i.e., deviations from the most probable value in the angular distribution (82°) should result either from a more symmetrical fission (towards 90°), or a more asymmetric one (towards smaller angles). In addition, the angle of emission of the α particle should not be greater than 90° relative to the light fragment.

The experimental data,* however, indicate lack of agreement with the expected results.

1. There is a considerable number of cases when the α particle is emitted more than 90° from the track of the light fragment. Furthermore, it has been noted that the angular distribution broadens with increasing range of the α particle. If the graph shown in Fig. 1 is broken up into three parts for three α-particle ranges (up to 100 μ, from 100 to 200 μ, and above 200 μ of range in photographic emulsion), the graphs obtained (see Fig. 2) differ noticeably from each other. The half-width of the distribution curve increases with range, and at maximum range the angular distribution for the α particles becomes nearly isotropic. On the other hand, almost no angles greater than 90° are observed for α particles with ranges less than 100 μ. Thus, the greater the energy of the α particle, the more independent its behavior in the field of two heavy fragments.

2. To estimate the influence of the magnitude of the mass asymmetry on the α-particle emission angle we can employ, with a certain degree of approximation, the value of the asymmetry of the fragment ranges provided we neglect the difference in $v(R)$ of the light and heavy fragments. The mean values of R_L/R_H for α particles emitted at angles both greater and less than 82°

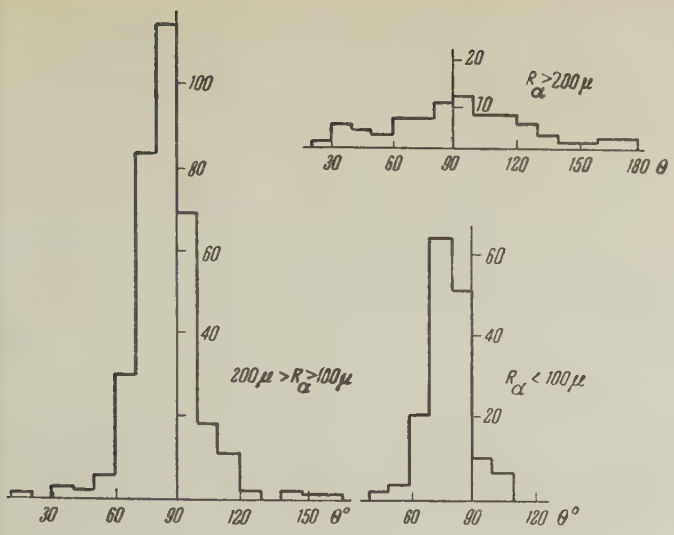

FIG. 2

(to the light fragment) were found to be approximately 1.3, i.e., the method of division of the uranium nucleus into two heavy fragments does not influence noticeably the deviation of the angle of emission of the α particle from its most probable value. Apparently the spread in the angles about the most probable value is caused by another circumstance.

On the basis of the present observations we can assume that at the instant of fission the α particle has a considerable velocity, the direction of which is equally probable relative to the line of fragment divergence. The presence of an initial velocity causes a spread in the angular distribution, the general character of which is established by the effect of the Coulomb fields of the fragments on the motion of the α particle. At high initial velocities the angle of emission of the α particle can deviate noticeably from the most probable value (82°), determined by the pattern of the scattering of the three particles at rest.

The existence of an α-particle initial velocity may serve as a confirmation of the existence of α complexes in heavy nuclei. If such a complex happens to be near the point of scission at the instant of fission, complex fission with a third long-range α particle will be observed.

*The preliminary data were reported by N. A. Perfilov at the Conference on Fission Physics in January, 1956.[3]

[1] Tsien, Chastel, Ho, and Vigneron, J. Phys. radium **8**, 165, 200 (1947).

[2] E. W. Titterton, Phys. Rev. **83**, 673 (1951).

[3] N. A. Perfilov, Supplement to Атомная энергия (Atomic Energy), No. 1, 1957.

Translated by J. G. Adashko
231

FEATURES OF MAGNETIC HYSTERESIS PHENOMENA IN THE SYSTEMS $Pr_2O_3 \cdot Fe_2O_3$ *AND* $La_2O_3 \cdot Fe_2O_3$

K. P. BELOV, M. A. ZAĬTSEVA, and A. M. KADOMTSEVA

Moscow State University

Submitted to JETP editor July 9, 1959

J. Exptl. Theoret. Phys. (U.S.S.R.) **37**, 1159-1161 (October, 1959)

FERRITES of rare-earth elements, with a general formula $M_2O_3 \cdot Fe_2O_3$ (where M is the rare-earth ion) have a perovskite structure. Although ferromagnetic, they exhibit weak ferromagnetic properties in a fixed temperature interval.[1-3] Many of them are characterized by so-called thermoremanence phenomena, whereby the magnetization temperature-dependence curves plotted during the initial heating differ from those obtained in the subsequent cooling. The curve obtained upon cooling in the field is always the upper one (thermoremanence effect). Figure 1 shows by way of an example the curves obtained in our measurements (in a 5500-oe field) for the ferrite $Pr_2O_3 \cdot Fe_2O_3$ (1 — heating, 2 — cooling).

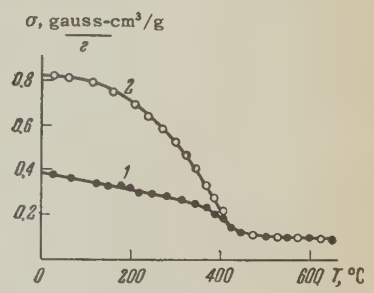

FIG. 1. Temperature dependence of specific magnetization of $Pr_2O_3 \cdot Fe_2O_3$ ferrite in a field of 5500 oe; 1 — heating, 2 — cooling.

In the present investigation we were interested in the unusual hysteresis in specimens of $Pr_2O_3 \cdot Fe_2O_3$ and $La_2O_3 \cdot Fe_2O_3$ both stoichiometric and with excess iron oxide. The specimens were prepared by the usual ceramic technology. The preliminary annealing was at a temperature of 900° C for 6 hours, after which the specimens were sintered four hours at 1300° C in air and slowly cooled in the furnace. The hysteresis curves were plotted by the ponderomotive method in fields up to 7500 oe for ferrite samples in the initial state and after cooling in the magnetic field from the Curie point. In all cases of cooling in the magnetic field from the Curie point, the hysteresis in the investigated specimens was highly asymmetric about the coordinate axes, the hysteresis curve being shifted upward along the magnetization axis (Fig. 2). It can be seen that this shift increases the closer the

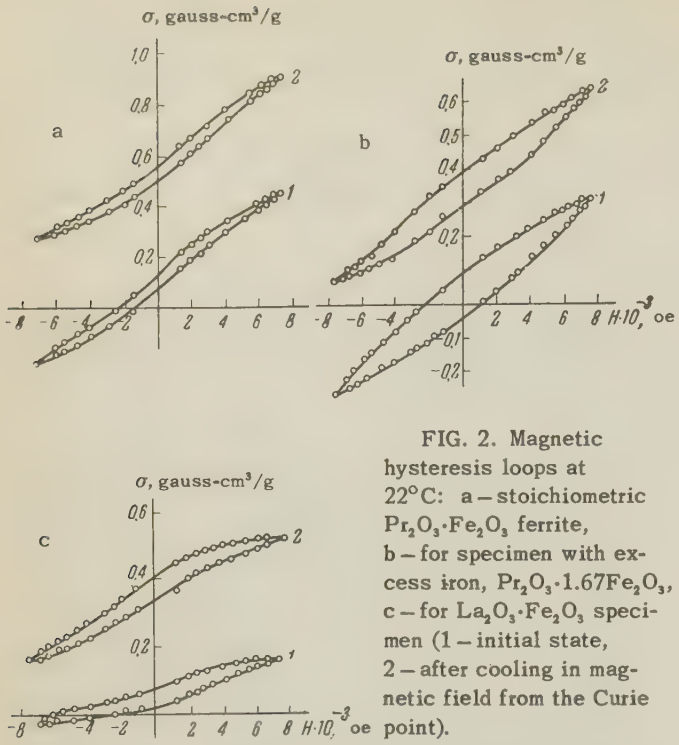

FIG. 2. Magnetic hysteresis loops at 22°C: a – stoichiometric $Pr_2O_3 \cdot Fe_2O_3$ ferrite, b – for specimen with excess iron, $Pr_2O_3 \cdot 1.67Fe_2O_3$, c – for $La_2O_3 \cdot Fe_2O_3$ specimen (1 – initial state, 2 – after cooling in magnetic field from the Curie point).

composition of the specimen to stoichiometric and decreases with increasing excess of Fe_2O_3. Analogous phenomena were recently observed by Watanabe[4] for $Nd_2O_3 \cdot Fe_2O_3$ and $La_2O_3 \cdot Fe_2O_3$.

It should be noted that the hysteresis loops shown in Fig. 2 are partial cycles, since the magnetization did not reach saturation in 7500-oe fields for any of the investigated ferrites. Nevertheless, the coercive force of the partial cycle is very large, on the order of 1000 oe. There are grounds for assuming that the total coercive force of the investigated ferrite samples is tremendous. This is apparently a common property of many rare-earth ferrites with perovskite structure, which are characterized, as indicated by Bozorth,[5] by a large magnetic anisotropy.

This explains the asymmetry of the hysteresis loop about the ordinate axis after cooling in the field. Upon cooling from the Curie point in a field, a residual magnetization corresponding to the total coercive force is produced (thermoremanence magnetization). This magnetization cannot be completely destroyed by a 7500-oe field. The "undestroyed" portion of the residual magnetization indeed shifts the partial hysteresis cycles of Fig. 2 along the magnetization axis. The presence of excess Fe_2O_3 in the ferrite apparently reduces the anisotropy of the perovskite-ferrite, and this leads in turn to a reduction in the effect of shifting the hysteresis loop along the magnetization axis.

[1] H. Forestier and G. Guiot-Guillain, Compt. rend. **230**, 1844 (1950).

[2] H. Forestier and G. Guiot-Guillain, Compt. rend. **235**, 48 (1952).

[3] G. Guiot-Guillain, Compt. rend. **237**, 1654 (1953).

[4] H. Watanabe, J. Phys. Soc. Japan **14**, 511 (1959).

[5] R. M. Bozorth, Phys. Rev. Lett. **1**, 362 (1958).

Translated by J. G. Adashko
232

USE OF DISPERSION RELATIONS FOR A TEST OF QUANTUM ELECTRODYNAMICS AT SMALL DISTANCES

I. S. ZLATEV and P. S. ISAEV

Joint Institute for Nuclear Research

Submitted to JETP editor July 9, 1959

J. Exptl. Theoret. Phys. (U.S.S.R.) **37**, 1161-1162 (October, 1959)

FOR electron and γ quantum energies higher than 150 Mev in bremsstrahlung and pair creation processes it is evidently necessary to consider not only the diagrams of the Bethe-Heitler type 1 and 2 (see the figure), but also the contributions from the generalized diagrams 3 and 4. These latter diagrams were not calculated in reference 1. However, their inclusion would make it possible to test quantum electrodynamics, in the spirit of the idea of Drell,[2] energies $\geq$ 500 to 600 Mev, as long as the higher order corrections in e do not become significant.

To compute the diagrams 3 and 4 we used the method of dispersion relations developed by Bogolyubov.[3] Starting from the existence proof of Vladimirov and Logunov[4] for the dispersion relations in the case of the virtual Compton effect, we obtained these relations in the center of mass system.[5] The first approximation of these dispersion relations allows us in a rigorous fashion to introduce form factors of the Hofstadter type at the nucleon vertex connected to the virtual γ quantum. The method of dispersion relations also makes it possible, in principle, to include the contributions from an arbitrary number of π-meson states.

We calculated, for the bremsstrahlung process, the diagrams of the type 1 (references 6 and 7), the one-nucleon approximation (diagram of the type 5), and the interference term. We also made an approximate estimate of the one-pion contribu-

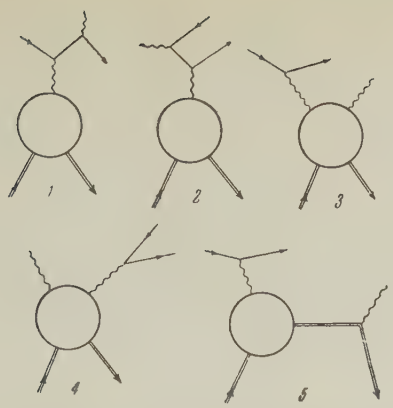

tion. The diagrams of the Bethe-Heitler type have been treated exactly. In the one-nucleon approximation we kept only the term proportional to the direct contribution from the electric charge, and the interference term contains only the contributions proportional to the electric charge and the first power of the anomalous magnetic moment. In general, such an approximation leads to an error $< 3\%$ for incident electron energies of ≈ 500 Mev and angles $\leq 90°$. The exact calculation of the one-pion approximation, which requires the knowledge of the amplitudes for the virtual photoproduction of π mesons, is possible in principle, but connected with great technical difficulties. For our purpose it is sufficient to make an approximate estimate of the one-pion contribution. If the length of the 4-vector of the virtual γ quantum, κ^2, is close to zero, we may regard the virtual Compton effect as a real one. We obtain the required estimate by comparing the contributions from the real Compton effect, calculated by the method of dispersion relations with account of the one-pion state,[8] with the one-nucleon approximation. The contribution from the one-pion state to the bremsstrahlung process for angles $< 30°$ is < 3 to 5%; it increases rapidly for angles $> 30°$, and at angles $\sim 90°$ it becomes of the order of magnitude of the Bethe-Heitler cross section. The multiple bremsstrahlung process gives a negligibly small contribution,[9] and the higher order corrections in the electric charge[10-11] become significant only in the region of large angles ($> 90°$) and high energies (> 500 Mev).

In this way we find that in the case of a bremsstrahlung process in which the momenta of the photon, the electron, and the proton in the final state lie in the same plane, for angles $\sim 30°$, with an initial electron energy 0.54 and photon energy 0.25 (in the units $\hbar = c = M = 1$, where M is the nucleon mass), quantum electrodynamics is valid for distances $\geq 3 \times 10^{-14}$ cm. Here we have assumed that the experimental accuracy is 10%.

It is interesting to note that, for those angles where $\kappa^2 \approx 0$, the one-nucleon and interference terms in the bremsstrahlung cross section have a sharp and high maximum which is 3 to 4 orders larger than the Bethe-Heitler cross section. As the energy of the γ quantum is decreased, the maximum becomes sharper.

In conclusion we express our deep gratitude to Academician N. N. Bogolyubov and A. A. Logunov for proposing this problem and useful advice, and also to D. V. Shirkov and A. N. Tavkhelidze for fruitful discussions.

[1] Bjorken, Drell, and Frautschi, Phys. Rev. **112**, 1409 (1958).

[2] S. D. Drell, Ann. Physik, **4**, 75 (1958).

[3] Bogolyubov, Medvedev, and Polivanov, Вопросы теории дисперсионных соотношений, (Problems of the Theory of Dispersion Relations), Gostekhizdat (1958). N. N. Bogolyubov and D. V. Shirkov, Введение в теорию квантованных полей, (Introduction to the Theory of Quantized Fields), Gostekhizdat, 1957.

[4] V. S. Vladimirov and A. A. Logunov, Izv. Akad. Nauk SSSR, Ser. Mat. (in press); preprint Joint Inst. Nuc. Res. R-260 (1958).

[5] I. S. Zlatev and P. S. Isaev, JETP **37**, 728 (1959), Soviet Phys. JETP **10**, 519 (1960), Preprint Joint Inst. Nuc. Res. P-321.

[6] I. S. Zlatev and P. S. Isaev, JETP **35**, 309 (1958), Soviet Phys. JETP **8**, 213 (1959).

[7] I. S. Zlatev and P. S. Isaev, Report at the All-Union Intercollegiate Conference on Quantum Field Theory and the Theory of Elementary Particles, Uzhgorod, October 2 to 6, 1958. Nuovo cimento **13**, 1 (1959).

[8] R. H. Capps, Phys. Rev. **108**, 1032 (1957).

[9] S. N. Gupta, Phys. Rev. **99**, 1015 (1955).

[10] P. I. Fomin, JETP **35**, 707 (1958), Soviet Phys. JETP **8**, 491 (1959).

[11] Mitra, Narayanaswamy, and Pande, Nucl. Phys. **10**, 629 (1959).

Translated by R. Lipperheide
233

ON POPOV'S RELATION BETWEEN THE SYMMETRY OF TRANSPORT COEFFICIENTS AND THERMODYNAMICS

R. DAVIES and F. GOODMAN

London University

Submitted to JETP editor December 16, 1958

J. Exptl. Theoret. Phys. (U.S.S.R.) **37**, 1163-1164 (October, 1959)

K. POPOV[1] tried to show that the Onsager relations

$$dx_i/dt = \sum_{k=1}^{n} L_{ik}X_k \qquad (i = 1, 2, \ldots n) \tag{1}$$

together with the symmetry properties

$$L_{ik} = L_{ki} \tag{2}$$

are connected with the existence of first integrals of a more general system of differential equations

$$d^2x_i/dt^2 = \ddot{x}_i = \sum_{j=1}^{n} g_{ij}x_j \tag{3}$$

if one assumes that the solution stays finite when $t \to +\infty$. According to Popov the g_{ij} are essentially thermodynamic quantities determined by the relation

$$\Delta S = -\tfrac{1}{2} \sum_{i,j=1}^{n} g_{ij}x_ix_j, \tag{4}$$

although they occur in the transport equation (3). We shall show in the following that this assumption (taken over and further developed by Karanikolov[2]) is not compatible with the theory of irreversible processes.

If we define the g-matrix using (4) and start with an equation of the form (3) one can, indeed, obtain relations which are similar in form to (1) and (2). One obtains, namely, ultimately a set of equations

$$\dot{x}_i + \sum_{j=1}^{n} \mathcal{L}_{ij}X_j = 0, \qquad \mathcal{L}_{ij} = \mathcal{L}_{ji}, \tag{5}$$

where the $\mathcal{L}$-matrix is completely determined by the g-matrix. Although Eq. (5) is formally similar to (1) and (2) the $\mathcal{L}$-matrix is not the matrix of the Onsager coefficients which we shall denote by L. Indeed, if $g^{1/2}$ is the positive definite square root of g one can easily show that $\mathcal{L} = g^{1/2}$. It is at the same time essential for the theory of irreversible processes that the Onsager coefficients are independent of the g-matrix and can therefore not determine the $\mathcal{L}$-matrix.

Moreover, starting from (3) Popov shows that the inverse relaxation time matrix τ^{-1} given by its values $-r_1, -r_2, \ldots, -r_n$ is given by the equation

$$\tau^{-1} = g^{1/2}. \tag{6}$$

In actual fact, however, it is well known from the theory of irreversible processes that the τ^{-1} matrix satisfies the relation

$$\tau^{-1} = Lg. \tag{7}$$

Equations (6) and (7) are only compatible if $L = g^{-1/2} = \tau$, which is clearly incorrect.

The source of the contradictions mentioned here lies in Popov's initial assumption (3). The assumption which establishes a connection between the transport properties of the system and the purely thermodynamic quantities is totally inadmissable and contradicts all we know about irreversible processes.

We shall briefly give an analysis of (3) starting from the usual equations of the thermodynamics of irreversible processes

$$X_i = \sum_{j=1}^{n} g_{ij}x_j. \tag{8}$$

The g-matrix is here defined according to (4) and in contradistinction to (3) it is assumed that

$$d^2x_i/dt^2 = \sum_{j=1}^{n} b_{ij}x_j, \tag{9}$$

where $b \neq g$. Putting afterwards $b = g$ we can see immediately that (5) follows from that.

Starting from (9) one shows easily that

$$\dot{x}_i + \sum_{k=1}^{n} K_{ik}x_k = 0, \tag{10}$$

where the K-matrix is symmetric; it is namely the positive definite square root of b, i.e.,

$$K_{ik} = K_{ki}, \tag{11}$$

$$K = b^{1/2}. \tag{12}$$

If we now substitute x from (8) into (10), we get

$$\dot{x}_i + \sum_{j=1}^{n} \mathcal{L}_{ij}X_j = 0, \text{ where } \mathcal{L}_{ij} = \sum_{k=1}^{n} K_{ik}g_{kj}^{-1}. \tag{13}$$

The $\mathcal{L}$-matrix is thus in the general case not at all symmetric, but if we take Popov's assumption that $b = g$ it follows from (12) and (13) that $\mathcal{L}_{ij} = g_{ij}^{-1/2} = K_{ij}^{-1}$. This matrix is symmetric according to (11). This is just the basis on which Popov constructed the derivation of the symmetry relations,

starting from second order equations.

The assumption b = g is, however, as we have already seen, totally unjustified.

[1] K. Popov, JETP **28**, 257 (1955), Soviet Phys. JETP **1**, 336 (1955).

[2] Kh. Karanikolov, JETP **28**, 283 (1955), Soviet Phys. JETP **1**, 265 (1955).

Translated by D. ter Haar
234

TWO-PARTICLE EXCITATIONS OF SUPERFLUID FERMI-SYSTEMS

Yu. V. TSEKHMISTRENKO

Institute of Physics, Academy of Sciences, Ukrainian S.S.R.

Submitted to JETP editor June 11, 1959

J. Exptl. Theoret. Phys. (U.S.S.R.) **37**, 1164-1166 (October, 1959)

It was shown in a paper by Ch'en Ch'un-Hsien[1] that the superfluidity of a gas of weakly interacting Fermi-particles can easily be explained if one "uncouples" the infinite set of coupled Schwinger equations for the Green functions, reducing it to a second order system. The characteristic spectrum of elementary excitations is determined in this way. Up to now there are, however, no prescriptions for the "uncoupling" when one studies more complicated problems, for instance, to find the two-particle excitation spectrum. In the following we state a method of obtaining a complete set of equations to determine the two-particle Green function using the formalism, proposed by Bogolyubov,[2] the u, v-transformation. Although the u, v-transformation does not contain the total number of particles, there are grounds for believing that the results obtained with it are the same as the results of a different consideration, but in a higher approximation.[3]

We shall consider a system of nonrelativistic Fermi particles, the Lagrangian density function of which has the form

$$L = \sum_s \psi_s^+(x)\,[-i\partial/\partial t + \nabla^2/2M + E_F]\,\psi_s(x) + L_{\text{int}},$$

$$L_{\text{int}} = (g^2/2)\sum_{ss'} \psi_s^+(x)\,\psi_{s'}^+(x)\,\psi_{s'}(x)\,\psi_s(x). \qquad (1)$$

(the interaction is, as usual, localized in a spherical shell $E_F - \omega < E < E_F + \omega$). We shall determine the time dependent functions ψ and ψ^+ in the interaction representation

$$\psi(\mathbf{x}, t) = e^{iH_0 t}\,\psi(\mathbf{x}, 0)\,e^{-iH_0 t};\quad \psi^+(\mathbf{x}, t) = e^{-iH_0 t}\psi^+(\mathbf{x}, 0)\,e^{iH_0 t},$$

$$H_0 = \int \psi^+(\mathbf{x}, 0)\,[-\nabla^2/2M - E_F]\,\psi(\mathbf{x}, 0)\,dx. \qquad (2)$$

We shall consider two functions

$$F = \langle T(\psi\psi\psi^+\psi^+ S)\rangle / \langle TS\rangle, \quad \Phi = \langle T(\psi\psi^+\psi^+\psi^+ S)\rangle / \langle TS\rangle,$$

where $S = \exp\{i\int L_{\text{int}}\,dx\}$; the averaging is over the state determined by the vector C. If C is the wave-function of the ground state of the system C_V, $\Phi = 0$, and F is the exact two-particle Green function. Our approximate method consists in approximating the exact ground state function C_V by the function of the "vacuum without interaction," introduced by N. N. Bogolyubov.[2] Expanding

$$\psi_s = \frac{1}{\sqrt{V}}\sum_{\mathbf{k}} a_{\mathbf{k}s}\exp\left\{i\mathbf{kx} - i\left(\frac{k^2}{2M} - E_F\right)\right\},$$

we determine the new Fermi amplitudes $\alpha_{\mathbf{k}s}$ which are connected with the old $a_{\mathbf{k}s}$ through the u, v-transformation. The normalized function C satisfies the relation $\alpha_{\mathbf{k}s}C = 0$, and u and v must be found from the condition that the average energy value of the system be a minimum.

We shall construct the equations for F and Φ in the weak coupling approximation using the generalized Wick theorem[4] and the following rules: a) the system of equations must be complete, b) the spin dependence of F and Φ and also the additional time dependence of Φ must be the same as for $g^2 = 0$, c) the integral kernels in the equations must be of the kind $\langle T(\psi\psi^+ S)\rangle/\langle TS\rangle$ (up to terms of order g^2) which corresponds to taking into account a number of terms of second order in g^2. Determining these integral kernels, going over to Fourier components for all functions and throwing away terms described by unconnected diagrams we obtain after a number of transformations a system of equations for the Fourier components of F and Φ which are integrated over the relative four-momentum (K is the total four-momentum)

$$A(K)\,F(K) + B(K)\,\Phi(K) = F_0(K);$$

$$C(K)\,F(K) + D(K)\,\Phi(K) = \Phi_0(K); \qquad (3)$$

A, B, C, D, F_0, and Φ_0 are some complicated functions.

The energies E_2 of the two-particle excitations are defined as the zeroes of the determinant $\begin{vmatrix} A & B \\ C & D \end{vmatrix}$ relative to the fourth component of the vector K. The coefficients A, B, C, D must be determined

for small $C = \omega e^{-1/\rho}$, $|K|/C$, E_2/C ($\rho = g^2 \times (dn/dE)_{E=E_F}$). The secular equation becomes in that case of the form

$$(E_2^2 - s^2|K|^2/3) + \rho(s|K|/C)^2 f(E_2/s|K|) = 0. \quad (4)$$

In zeroth approximation

$$E_2 = s|K|/\sqrt{3}; \quad s = k_F/M, \quad (5)$$

which agrees with the result of Bogolyubov[2] and Galitskiĭ.[5] It is necessary to note that these authors found the energy E_2 by studying a model but not the true Hamiltonian. Such a procedure leads as a matter of principle to difficulties when one tries to determine corrections to E_2. Among other things, the approximate method stated in the foregoing enables us in principle to increase the accuracy of determining E_2 by improving the approximation in the wave function (and apart from this, of course, by calculating terms of higher order in g^2). In the framework of this method one can completely analogously study also more complicated than two-body excitations of Fermi-systems.

In conclusion I express my gratitude to Academician N. N. Bogolyubov for suggesting this work and to D. V. Shirkov for useful discussions.

[1] Ch'en Ch'un-Hsien, Dokl. Akad. Nauk SSSR **125**, 1238 (1959), Soviet Phys. Doklady **4**, 413 (1959).

[2] Bogolyubov, Tolmachev, and Shirkov, Новый метод в теории сверхпроводимости (A New Method in the Theory of Superconductivity), M., Acad. Sci. U.S.S.R., 1958, Fortschr. Physik **6**, 605 (1958).

[3] N. N. Bogolyubov, Usp. Fiz. Nauk **67**, 549 (1959), Soviet Phys. Uspekhi **2**, 236 (1959).

[4] N. N. Bogolyubov and D. V. Shirkov, Introduction into the Theory of Quantum Fields, Interscience, 1959.

[5] V. M. Galitskiĭ, JETP **34**, 1011 (1958), Soviet Phys. JETP **7**, 698 (1958).

Translated by D. ter Haar
235

ON THE INFLUENCE OF THE PAULI PRINCIPLE AND OF SHORT-RANGE NUCLEAR FORCES ON THE ABSORPTION OF PHOTONS BY NUCLEI IN THE OSCILLATOR MODEL

V. A. ÉL' TEKOV

Institute for Nuclear Physics, Moscow State University

Submitted to JETP editor June 8, 1959

J. Exptl. Theoret. Phys. (U.S.S.R.) **37**, 1166-1168 (October, 1959)

As has been shown by Brink,[1] the collective[2] and the independent-particle[3] descriptions are identical in the case of the oscillator potential. This is due to the circumstance that the Schrödinger equation is separable in this case both in the single-particle and the Jacobi coordinates. In particular one can take for one of the Jacobi coordinates the difference of the coordinates of one proton and one neutron. Thus in this case the two-nucleon (quasi-deuteron) mechanism[4] will also be identical with the previous two.

This equivalence is violated on going over to a real nucleus, mainly because of the short range of the nuclear forces and because of the Pauli principle.

The influence of the short-range forces can be estimated taking for the zeroth approximation the oscillator Hamiltonian H_{osc} and considering $H - H_{osc}$ as a perturbation. In the zeroth order the nuclear wave function is a product wave function. In first order this multiplicative character will be violated. The separability of a particular coordinate (i.e., the degree of applicability of the corresponding mechanism) can reasonably be indicated by the integral $N_{\sigma_0\tau_0}$ of the square of the modulus of the nonfactorizable part of the wave function:

$$N_{\sigma_0\tau_0} = \sum_{\sigma,\tau}{}' \left\{ \frac{\langle f_\sigma \varphi_\tau | H - H_{osc} | f_{\sigma_0}\varphi_{\tau_0}\rangle}{E_{\sigma\tau} - E_{\sigma_0\tau_0}} \right\}^2. \quad (1)$$

Here f_σ and φ_τ are the zeroth-approximation oscillator functions corresponding to the factorized coordinate and the remaining variables respectively; the indices zero indicate the ground state. The function $N_{\sigma_0\tau_0}$ equals zero for a function factorizable in the coordinate singled out and equals unity for a function containing no factorizable part. The evaluation of (1) requires the application of the Talmi transformation[5] and is in general very involved.

The quantity $N_{\sigma_0\tau_0}$ was calculated for the ground state of He^4 with a two-body potential which has oscillator character at short distances and equals zero at distances larger than 1.7×10^{-12} cm. Taking as a first approximation only the lowest states in the sum (1), we find that $N_{\sigma_0\tau_0}$ equals 0.015 for the collective, 0.014 for the single-particle, and 0.011 for the two-particle coordinates respectively. Thus we find that for the α particle either of these mechanisms can be applied with sufficient accuracy.

However, one can expect that for heavier nuclei the collective model will yield rather larger values for $N_{\sigma_0\tau_0}$ than the other models. Because of the short range of the nuclear forces, collective oscillations of many nucleons will be more difficult to establish than oscillations of individual nucleons. Even a rough estimate of the magnitude of $N_{\sigma_0\tau_0}$ as a function of the atomic number would be of interest.

The influence of the Pauli principle reduces to the circumstance that, for example in the excitation of the collective oscillation, the more tightly bound nucleons cannot be excited since those states are already occupied by other nucleons. This will also result in excitation of other degrees of freedom simultaneously with the excitation of the collective coordinate. One can take for a measure of the forbiddenness of collective transitions the quantity $Q = 1 - w_1/w_2$ where w_1 and w_2 are the probabilities of the collective dipole transition calculated with and without the Pauli principle respectively. In the oscillator model we have $Q = 9/25$ for O^{16} and $Q = 5/9$ for Ca^{40}.

As can be seen the Pauli principle will also lead to quenching of the collective degrees of freedom.

Thus the collective model of the electric dipole excitation can be applied only for the lightest nuclei. For heavier nuclei the single and the two-particle mechanisms will play the more important role.

[1] D. M. Brink, Nucl. Phys. **4**, 215 (1957).
[2] A. B. Migdal, JETP **15**, 81 (1945), M. Goldhaber and E. Teller, Phys. Rev. **74**, 1046 (1948).
[3] D. H. Wilkinson, Physica **22**, 1039 (1956).
[4] J. S. Levinger, Phys. Rev. **84**, 43 (1951). Yu. K. Khokhlov, JETP **23**, 241 (1952). V. V. Daragan and Yu. M. Shirokov, Тр. Всесоюзной конференции 1957 г. по ядерным реакциям при малых и средних энергиях, (Proceedings of the All-Union Conference on Nuclear Reactions at Low and Medium Energies, 1957) U.S.S.R. Acad. Sci. (1958), p. 472
[5] I. Talmi, Helv. Phys. Acta **25**, 185 (1952).

Translated by M. Danos
236

MEASUREMENT OF THE DEGREE OF LONGITUDINAL POLARIZATION OF BETA PARTICLES

L. A. MIKAÉLYAN and P. E. SPIVAK

Submitted to JETP editor August 6, 1959

J. Exptl. Theoret. Phys. (U.S.S.R.) **37**, 1168-1170 (October, 1959)

MEASUREMENTS of the degree of longitudinal polarization of β electrons have been made by many authors (cf. for example the survey of Smorodinskiĭ[1]).

In the present work the longitudinal polarization was converted to transverse by passing the electrons through crossed magnetic and electric fields. After emerging from the field region, the electrons passed through a system of diaphragms and impinged on a thin gold scatterer. Electrons scattered through an angle of 120° were recorded by Geiger counters. In the experiment we measured the magnitude of the left-right scattering asymmetry, which is a measure of the polarization of the electrons.

The length of the field region, l, was 300 mm, and the gap between the plates to which the high voltage was applied was 14 mm. The size of the magnetic field H and electric field E needed to rotate the spin of electrons with momentum p through angle φ was found from the relation

$$\varphi = eHl\sqrt{1-\beta^2}/pc; \quad E = \beta H.$$

The absolute values of the applied fields were found to an accuracy of about 1% from conversion lines of known energy. The measurements were carried out for an electron energy of 340 kev and an angle φ equal to 90°.

The end points of the spectra of the isotopes studied differed very much, which could result in

Nucleus	P^{32}	Sm^{153}	Lu^{177}	Ho^{166}	In^{114}
Relative value of the polarization	1.047±0.012	1.00	0.945±0.012	0.930±0.012	0.965±0.030
Absolute value (error = ±4%)	0.94	0.90	0.85	0.84	0.86

errors which are very difficult to evaluate. In order to have the same conditions of measurement for all substances, we made a preliminary energy separation of the electrons. The spectrum of the electrons entering the region of action of the crossed fields extended from ~250 to 450 kev.

The work can be divided into two parts. The first consisted in a comparison of the polarization of electrons from P^{32}, In^{114}, Lu^{177}, Sm^{153}, and Ho^{166}. After making the relative measurements, the absolute value of the polarization of the Sm^{153} β particles was measured.

The relative measurements were made by measuring, under identical conditions, the left-right asymmetry in the scattering of β particles of the isotopes enumerated above by gold of thickness 0.55 mg/cm^2.

In making relative measurements of polarization, it is not necessary to know the apparatus asymmetry. All that is necessary is that the apparatus asymmetry be small and remain constant. For this reason, the apparatus asymmetry was not determined in these measurements. Instead, we repeatedly measured the asymmetry in scattering of β particles from Sm^{153} by gold. This source had sufficient intensity so that we could get a statistical accuracy better than one percent in a relatively short time. Numerous measurements of the asymmetry for Sm^{153} showed that the spread in values of the apparatus asymmetry did not exceed 0.5%. As an additional check, we made some special experiments in which the source was moved in various directions from its working position, and also in which the applied fields were changed by an amount 2 or 3 times as great as the error in their setting when making the relative measurements. In these control experiments, to an accuracy of one percent, we noted no dependence of the results on these factors.

We used sources with a mean thickness of 0.6 to 0.9 mg/cm^2. To determine the depolarization in the source, we did an experiment in which we compared the asymmetry for a Sm source of thickness 0.8 mg/cm^2 with the asymmetry when the same source was covered by a layer of inactive Sm of the same thickness deposited on an aluminum foil of thickness 0.8 mg/cm^2, so that the average path of electrons in the source material was increased by a factor of three. From this experiment we found that the depolarization in the source of thickness 0.8 mg/cm^2 for an electron energy of 340 kev is (0.6 ± 1.2)%. Considering that the upper limit for this effect does not exceed 1.8%, we find that the spread in values for the depolarization correction for different sources does not exceed 0.6%.

The results of the relative measurements of polarization of β particles are given in the top line of the table. The polarization of the Sm^{153} betas is arbitrarily set equal to unity. From the results given, it is clear that the degree of longitudinal polarization is different for different isotopes. It is interesting to note that the polarizations in the case of P^{32} and In^{114}, both of which are allowed Gamow-Teller transitions, differ by (8 ± 4)%.

Absolute measurements of the degree of polarization of the electrons were made for the most intense β emitter, Sm^{153}.

The apparatus asymmetry was measured by using thin aluminum scatterers (thicknesses 4 and 8 μ). The scattering asymmetry was measured using gold scatterers with thicknesses 0.55, 0.36, and 0.18 mg/cm^2. The thicknesses of the gold scatterers were determined by weighing to relatively low accuracy. However, for a correct extrapolation to zero thickness with good accuracy, it is necessary to know only the relative values of the weights. These relative values were found from the counting rates for scattered electrons.

As already stated, in our experiments the spin was rotated through 90°. Under these conditions, even a relatively large error in determining the angle of rotation (for example 10%) cannot lead to any significant error in the measurements. Special experiments, in which the electron spins were turned through 75, 90, and 115°, confirmed this to a high degree of accuracy.

From the measurement and extrapolation to zero thickness, we obtained a value of the asymmetry corresponding to a degree of longitudinal polarization of $-0.85 \pm 3\%$ (in units of v/c). Correc-

tions were made to this value to take account of the following effects: 1) depolarization in the source (0.6 ± 1.2%); 2) scattering of electrons from the diaphragms, 0.5%; 3) scattering of electrons from the backing on which the gold was deposited, 0.6%; 4) arrival at the counters of electrons multiply scattered in the chamber in which the gold scatterers were placed, (3 ± 1.5%); 5) the finite range of angles and energies of the electrons which were recorded, 0.3%; 6) a coefficient for the apparatus asymmetry, 1.00 ± 0.02.

The total of all these corrections to the experimental value of the polarization does not exceed 5%. Introducing these corrections gives a value of the polarization for Sm^{153} equal to 0.90 ± 4%.

The absolute values for the degree of polarization of the other nuclei which were investigated were found from the relative measurements, and are shown in the lower line of the table.

From the table we see that we succeeded in making the relative measurements to sufficiently high accuracy. It should be noted that the accuracy achieved by us in the absolute measurements is clearly insufficient. It is probable that we can improve it significantly in the near future. We also propose to make an absolute calibration of the apparatus using a beam of accelerated electrons, polarized by single scattering on gold.

[1] Ya. A. Smorodinskiĭ, Usp. Fiz. Nauk 67, 43 (1959), Soviet Phys.–Uspekhi 2, 1 (1959).

Translated by M. Hamermesh
237

POSSIBILITY OF INVESTIGATING THE LEVELS OF THE COMPOUND NUCLEUS PRODUCED BY INTERACTION BETWEEN SLOW NEUTRONS AND ISOMERS

Yu. V. PETROV

Leningrad Physico-technical Institute, Academy of Sciences, U.S.S.R.

Submitted to JETP editor May 27, 1959; resubmitted July 29, 1959

J. Exptl. Theoret. Phys. (U.S.S.R.) 37, 1170-1172 (October, 1959)

AN investigation of the interaction between slow neutrons with energy $E < 1$ kev and unexcited heavy nuclei disclosed the resonant structure of the cross section and yielded the parameters of the levels of the compound nucleus. There are no similar data in the 10 or 100 kev range, since the experimentally-measured cross sections are averaged over many resonances, owing to the insufficient resolving power of the apparatus as well as to the Doppler broadening.

To obtain information on the levels of the compound nucleus at high excitation energies, use can be made of the interaction between neutrons and isomers. If a nucleus in an excited isomer state is bombarded with slow neutrons, a group of levels will be excited tens or hundreds of kev above the levels of the compound nucleus that results when the unexcited target nucleus is bombarded with slow neutrons. Such an experiment would help explain how the widths and densities of levels change in a nucleus of given Z and A when the excitation energy is shifted by several tens or hundreds of kev. The spins of the two level groups should be different, since the spins of the isomer and ground states differ by several units.

It is easy to estimate very roughly the number of isomer nuclei, necessary for such an experiment, in the following manner. Let a beam of monoenergetic neutrons pass through a target of area $S \sim 1$ cm^2. Then the necessary number of isomer nuclei is $N \sim S/\sigma$, where σ is the cross section in the neighborhoods of resonance. Assume $\sigma \sim 10^3$ barns. Then the necessary number of nuclei amounts to 10^{21} or several tenths of a gram. The isomers can be accumulated by activation in a nuclear reactor, separated from fission fragments, or produced in accelerators. In a modern reactor with a neutron flux $\Phi \sim 10^{14}$ at an activation cross section $\sigma_a \sim 1$ barn, it is possible to accumulate within several months $\sigma_a \Phi t$ long-lived isomer nuclei, or 10^{-3} times the number of the nuclei in the original isotope. The fractions of several isomers in fission fragments are of the same order. Thus, an accumulation of enough isomer nuclei for the experiment is quite feasible.

The spin of the compound nucleus can be determined for many isomer nuclei.

In interactions between slow neutrons and isomers it is possible to have, along with elastic scattering (n, n) and radiation capture (n, γ), also inelastic scattering with emission of a fast neutron (n, n'), when the emitted neutron carries away the excitation energy of the isomer. When the isomer is bombarded by thermal or epithermal neutrons, the resultant fast neutrons should be highly monoenergetic. For isomers with excitation energy on the order of 100 kev, owing to the small density of the initial states and the high density of the final states, the cross section for such

a reaction of inelastic "acceleration" in the region up to 100 ev is $10^3 - 10^6$ times greater than the cross section of the inverse reaction — the excitation of the isomer state by a fast neutron.

Naturally, one must expect the cross section to obey the 1/v law at small energies, if there is no resonant level in the vicinity.

For a rough estimate of the ratio of the widths of the reactions (n, n′) and (n, γ) we assume[1] that for nuclei with A > 80 the neutron and radiation widths become equalized at ~ 1 kev. Since the escaping neutron has a large momentum l, then for nuclei with kR < 1 (see reference 1)

$$\Gamma_{n'}/\Gamma_\gamma \approx \sqrt{E'}\,(E'A^{2/3}\cdot 10^{-4})^l/[(2l-1)!!]^2, \qquad (1)$$

where E is the energy of the emitted neutron in kev.

Isomer	T	I_m	I	E', kev	$10^3\,\frac{\Gamma_{n'}}{\Gamma_\gamma}$
$_{41}Nb^{91m}$	64 d	1/2−	9/2+	104	0.4
$_{43}Tc^{97m}$	91 d	1/2−	9/2+	99.2	0.4
$_{47}Ag^{110m}$	270 d	6−	2+	116	0.9
$_{48}Cd^{113m}$	5.11 yr	11/2−	1/2+	265	$2\cdot10^{-3}$
$_{52}Te^{125m}$	58 d	11/2−	3/2+	110	1

For certain long-lived isomers[2] the table lists the lifetimes T, the spins I and I_m and the parities of the final and initial states, the transition energy E′, and also the ratio $\Gamma_{n'}/\Gamma_\gamma$, estimated from formula (1). For all the isomers given, with the exception of Cd^{113m}, the (n, n′) reaction is accompanied by spin flip, since ΔI = 4, and the parities of the initial and final states are opposite. The table lists the values of $\Gamma_{n'}/\Gamma_\gamma$, for $l = 3$. For $l = 5$ these values are $10^4 - 10^5$ times smaller. Thus, given the intensity of the fast neutrons produced in the (n, n′) reaction, we can determine the spin of the compound nucleus for these isomers.

In conclusion, I express my gratitude to V. N. Gribov, A. D. Piliya, and M. I. Pevzner for discussion of our work.

[1] J. M. Blatt and V. M. Weisskopf, Theoretical Nuclear Physics, Wiley, N.Y. 1952, Russ. Transl. IIL, 1954.

[2] B. S. Dzhelepov and L. K. Pekar, Схемы распада радиоактивных ядер (Decay Schemes of Radioactive Nuclei), U.S.S.R. Acad. Sci., 1958.

Translated by J. G. Adashko
238

ON THE INCLUSION OF EXCHANGE IN THE THEORY OF COLLISIONS

R. K. PETERKOP

Latvian State University

Submitted to JETP editor December 6, 1958

J. Exptl. Theoret. Phys. (U.S.S.R.) **37**, 1172-1173 (October, 1959)

THE formulation of the problem of scattering of electrons by atoms, which has been given by Drukarev,[1] reduces in the case of the hydrogen atom to the solution of the system of integro-differential equations

$$(\Delta_1 + k_\alpha^2)\,F_\alpha^\pm(\mathbf{r}_1) = \sum_\beta F_\beta^\pm(\mathbf{r}_1)\,2\int\psi_\alpha^*(\mathbf{r}_2)\left(\frac{1}{r_{12}} - \frac{1}{r_1}\right)\psi_\beta(\mathbf{r}_2)\,d\mathbf{r}_2 \pm A_\alpha^\pm(\mathbf{r}_1), \qquad (1a)$$

with boundary conditions

$$F^\pm(\mathbf{r}) \underset{r\to\infty}{\sim} \delta_{\alpha 0}\exp(ik_\alpha z) + a_\alpha^\pm(\theta,\varphi)\,r^{-1}\exp(ik_\alpha r), \qquad (1b)$$

where α and β denote the sets of quantum numbers characterizing the hydrogen atomic states, for example (nlm) or (klm); $\sum$ denotes summation over the discrete and integration over the continuous spectrum; $k_\alpha^2 = 2(E - \epsilon_\alpha)$, where ϵ_α are the energy levels of the hydrogen atom;

$$A_\alpha^\pm(\mathbf{r}_1) = \sum_\beta \psi_\beta(\mathbf{r}_1)\,2\int\psi_\alpha^*(\mathbf{r}_2)\left(\frac{1}{r_{12}} + \varepsilon_\beta - \frac{1}{2}k_\alpha^2\right)F_\beta^\pm(\mathbf{r}_2)\,d\mathbf{r}_2$$

$$= \int\psi_\alpha^*(\mathbf{r}_2)\,(H - E)\sum_\beta\psi_\beta(\mathbf{r}_1)\,F_\beta^\pm(\mathbf{r}_2)\,d\mathbf{r}_2, \qquad (2)$$

$$H = -\tfrac{1}{2}\Delta_1 - \tfrac{1}{2}\Delta_2 - 1/r_1 - 1/r_2 + 1/r_{12}. \qquad (3)$$

For a unique solution the function $\Phi^\pm(\mathbf{r}_1, \mathbf{r}_2) = \sum_\alpha [F_\alpha^\pm(\mathbf{r}_1)\,\psi_\alpha(\mathbf{r}_2) \pm F_\alpha^\pm(\mathbf{r}_2)\,\psi_\alpha(\mathbf{r}_1)]$ must be required to have the asymptotic form*

$$\Phi^\pm(\mathbf{r}_1, \mathbf{r}_2) \underset{r_1\to\infty}{\sim} \sum_\alpha \psi_\alpha(\mathbf{r}_2)\,[\delta_{\alpha 0}\exp(ik_\alpha z_1) + a_\alpha'^\pm(\theta_1,\varphi_1)\,r_1^{-1}\exp(ik_\alpha r_1)]. \qquad (1c)$$

For practical calculations, we solve instead of the infinite system (1a) a reduced system consisting, for example, of one or two equations. In this case one obtains appreciable differences between a_α^+ and a_α^-.

It is not always sufficiently clearly recognized that for an accurate solution of the infinite system the relation

$$a_\alpha^+ = a_\alpha^- \qquad (4)$$

must be satisfied.

To prove this it is sufficient to show that there is a solution for which $A_\alpha^\pm = 0$. But this property describes the solution which is distinguished by the

absence of $A_\alpha^\pm$ in (1a) [because the function $\Phi(r_1, r_2) = \sum_\alpha \psi_\alpha(r_1) F_\alpha(r_2)$ satisfies the Schrödinger equation $(H - E)\Phi(r_1, r_2) = 0$].

The equality (4) becomes nearly obvious if we note that the exact solution of the Schrödinger equation need not be sought in an explicitly symmetric form but may be found first as an asymmetric solution and then symmetrized.

Further, if we calculate the cross sections using only $a_\alpha^\pm$,[1] they will be the same for both signs. However one cannot agree with such a definition. Indeed, if the wave function of the two electrons has the form $\Phi^\pm(r_1, r_2) = \sum_\alpha [F_\alpha(r_1) \times \psi_\alpha(r_2) \pm F_\alpha(r_2)\psi_\alpha(r_1)]$, we obtain the following expression for the radial component of the scattered flux:

$$j^\pm(r) = 2\,\mathrm{Im}\left\{\sum_\alpha f_\alpha^*(r)\frac{\partial}{\partial r}f_\alpha(r) + \sum_{\alpha\beta}\psi_\alpha^*(r)\frac{\partial}{\partial r}\psi_\beta(r)\int f_\alpha^*(r')\right.$$
$$\times f_\beta(r')\,dr' \pm \sum_{\alpha\beta}\left[\psi_\alpha^*(r)\frac{\partial}{\partial r}f_\beta(r)\int f_\alpha^*(r')\psi_\beta(r')\,dr'\right.$$
$$\left.\left. + f_\alpha^*(r)\frac{\partial}{\partial r}\psi_\beta(r)\int \psi_\alpha^*(r')f_\beta(r')\,dr'\right]\right\}, \qquad (5)$$

where the f_α differ from the F_α by the absence of incident waves.

Hence we can see that the difference between the cross sections must appear not because of the inequality of a_α^+ and a_α^- but because of the exchange term in the flux, which Drukarev ignores, since he does not consider the flux produced by the functions ψ_α of the continuous spectra. Taking account of the exchange according to references 2 and 3 is simply taking account of the flux of atomic electrons excited to corresponding levels of the continuous spectrum.

*It should be remarked that Eqs. (1b) and (1c) are not wholly accurate in the case of ionization, in which case the asymptotic form of the wave function of one electron cannot be given independently of the other electron.

[1] G. F. Drukarev, JETP **31**, 288 (1956), Soviet Phys. JETP **4**, 309 (1957).

[2] N. Mott and H. Massey, Theory of Atomic Collisions, Oxford 1949; Russ. Trans. M., 1951; ch. 8 Sec. 4.

[3] H. Massey, Revs. Modern Phys. **28**, 199 (1956); Russ. Trans. Usp. Fiz. Nauk **64**, 589 (1958).

Translated by R. F. Peierls
239

ON THE PAPER OF V. A. BELOKON': "THE PERMANENT STRUCTURE OF SHOCK WAVES WITH JOULE DISSIPATION"

A. G. KULIKOVSKIĬ and G. A. LYUBIMOV

Submitted to JETP editor June 23, 1959

J. Exptl. Theoret. Phys. (U.S.S.R.) **37**, 1173-1174 (October, 1959)

In his discussion of the magnetohydrodynamic shock wave, V. A. Belokon'[1] writes down equations for the momenta and for the heat flow for the one-dimensional stationary motion of a non-viscous, non-heat-conducting, but electrically conducting gas. It is asserted that this system of equations leads, on the one hand, to the necessity of the existence of a maximum of the entropy inside the region of flow, and on the other hand, to the impossibility of a decrease in the entropy. On the basis of these facts, the author comes to the following conclusion: "In view of the absurdity of a continuous solution, we consider it unavoidable to postulate a Riemann isentropic discontinuity in the flow parameters within a compression wave of any amplitude, by analogy with the isothermal discontinuity for purely heat-conducting gases." The magnetic field at this discontinuity is considered continuous.

We cannot agree with this basic postulate. Indeed, if the magnetic field is continuous in the passage through the discontinuity and the gas is considered non-viscous and non-heat-conducting before and after the discontinuity, then this is a gas-dynamical discontinuity which always leads to an increase in the entropy.

The same kind of problem concerning the structure of the shock wave was considered earlier by Burgers.[2] He showed that two cases are possible: a) in strong magnetic fields all parameters inside the region of flow, including the entropy, change monotonically. The entropy reaches its maximum value at the point corresponding to $x = +\infty$; b) in weak magnetic fields the region of flow consists of two parts, the region of continuous variation of the parameters, at the end of which the entropy reaches some value $S^* \neq S_\infty$, and a compression discontinuity with a constant field, at which the entropy increases from S^* to S_∞.

The problem proposed by Belokon', therefore, has a complete solution without any additional postulates, and the postulate put forward in his paper is incorrect.

It is furthermore impossible to accept the following assertion of the author with respect to the

effect of viscosity on the structure of the shock wave:

"If dissipation occurs by way of viscosity in addition to Joule heating, then the isentropic discontinuity mentioned above will be smoothed out for all amplitudes, since for vanishing viscosity the curves for continuous evolution of the flow parameters pass arbitrarily close to the isentropic line S_{max}, coinciding with it only in a single point, at $+\infty$."

The problem of the family of integral curves for the one-dimensional stationary flow of a viscous and electrically conducting gas, corresponding to the problem of the structure of the magnetohydrodynamic shock wave, was discussed in detail by Ludford.[3] He showed that in the case of vanishing viscosity the corresponding curve approaches the curve obtained by Burgers.

[1] V. A. Belokon', JETP **36**, 1316 (1959), Soviet Phys. JETP **9**, 932 (1959).

[2] J. M. Burgers, Penetration of a Shock Wave into a Magnetic Field. Magnetohydrodynamics, Ed. R. K. M. Landshoff, Stanford (1957) (Russ. Transl., Atomizdat, 1958).

[3] C. S. S. Ludford, J. Fluid Mechanics **5**, 67 (1959).

Translated by R. Lipperheide
240

ON THE PHASE OF THE SCATTERED WAVE (A REPLY TO V. V. MALYAROV)

F. S. LOS'

Submitted to JETP editor June 3, 1958

J. Exptl. Theoret. Phys. (U.S.S.R.) **37**, 1174-1175 (October, 1959)

THE possibility of determining the phase of the scattered wave by numerical methods with the help of the differential equation for the phase

$$d\delta/d\rho = -[l(l+1)/\rho^2 + U(\rho)]\sin^2(\rho+\delta) \qquad (1)$$

was discussed in reference 1, and it was shown that it is necessary in this case to find the solution which satisfies the condition

$$\sin(\rho+\delta) = \rho/(l+1) \text{ for } \rho \to 0. \qquad (2)$$

V. V. Malyarov[2] correctly observed that one and the same symbol is used in reference 1 to denote two proportional constants, and also that the condition $\int_0^\infty U(\rho)\,d\rho < C$ should be replaced by $\int_0^\infty |U(\rho)|\,d\rho < C$.

Then V. V. Malyarov proposes, incorrectly, to obtain the second term in the expansion for $\delta(\rho)$ from the expression for $\delta(\rho)$ of reference 1, overlooking the fact that this expression was formally obtained from (1) and (2). Actually this term can be obtained by substituting the series

$$\delta(\rho) = -l\rho/(l+1) - a_2\rho^2 - a_3\rho^3 - \ldots$$

in (1). We then obtain for $\delta(\rho)$ the expansion

$$\delta(\rho) = -l\rho/(l+1) - \gamma_0\rho^2/2(l+1)^3 - \ldots, \qquad (3)$$

while the method of V. V. Malyarov would lead to the incorrect expression

$$\delta(\rho) = -l\rho/(l+1) - \gamma_0\rho^2/2(l+1)^2.$$

Finally, V. V. Malyarov alleges that the note[1] "...is of no interest for scattering theory and can lead the reader into error," and he bases this assertion on the following argument: "The use of the additional condition (5) is justified for $\rho \to \infty$, when $A(\rho) \to$ const and $\delta(\rho) \to$ const. For $\rho \to 0$, however, any other supplementary condition could be used instead of (5). Different additional conditions correspond to different phases $\delta(\rho)$. The problem is indeterminate. It follows from the definition of the phase of the scattered wave that the phase $\delta(\rho)$ obtained with the help of such a supplementary condition is not the phase of the scattered wave."

This remark of V. V. Malyarov cannot be applied to the contents of our note, because there we obtained (6) and (7) by using the classical method of variation of the arbitrary Lagrange constants, and we were concerned with the determination of the phase of the scattered wave at infinity [i.e., finding the limit of $\delta(\rho)$ for $\rho \to \infty$].

Applying (1) and (7) of reference 1 to the known cases where the scattering problem can be solved exactly, one easily sees that this phase is indeed the phase of the scattered wave, according to the interpretation of scattering theory.

The remarks of V. V. Malyarov concerning the note[1] are therefore without substance.

[1] F. S. Los', On the Phase of the Scattered Wave, JETP **33**, 273 (1957); Soviet Phys. JETP **6**, 211 (1958).

[2] V. V. Malyarov, JETP **34**, 1039 (1958); Soviet Phys. JETP **7**, 719 (1958).

Translated by R. Lipperheide
241